Trends in Radiopharmaceuticals (ISTR-2005)

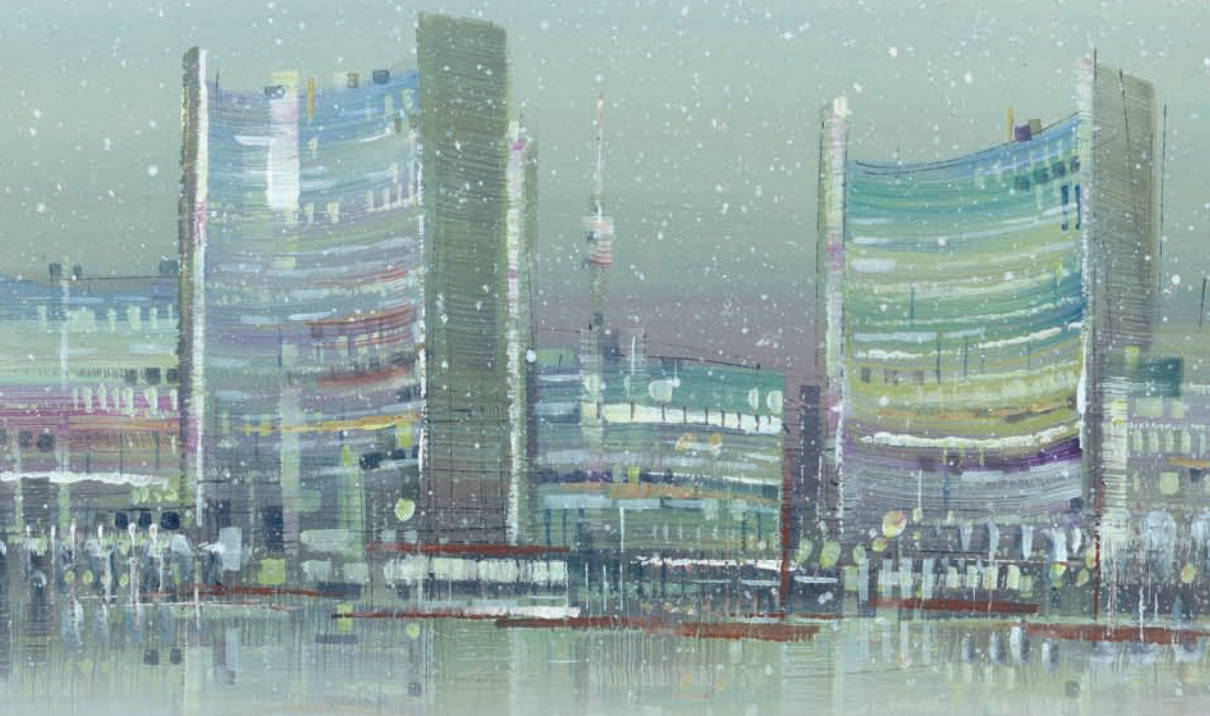

Proceedings of an International Symposium
Vienna, 14–18 November 2005

Vol. 2

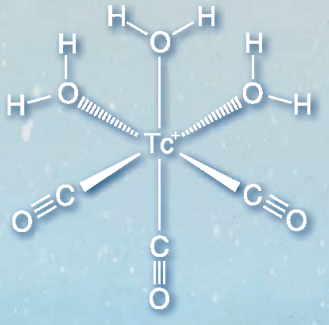

IAEA
International Atomic Energy Agency

TRENDS IN RADIOPHARMACEUTICALS (ISTR-2005)

VOLUME 2

The following States are Members of the International Atomic Energy Agency:

AFGHANISTAN
ALBANIA
ALGERIA
ANGOLA
ARGENTINA
ARMENIA
AUSTRALIA
AUSTRIA
AZERBAIJAN
BANGLADESH
BELARUS
BELGIUM
BELIZE
BENIN
BOLIVIA
BOSNIA AND HERZEGOVINA
BOTSWANA
BRAZIL
BULGARIA
BURKINA FASO
CAMEROON
CANADA
CENTRAL AFRICAN REPUBLIC
CHAD
CHILE
CHINA
COLOMBIA
COSTA RICA
CÔTE D'IVOIRE
CROATIA
CUBA
CYPRUS
CZECH REPUBLIC
DEMOCRATIC REPUBLIC OF THE CONGO
DENMARK
DOMINICAN REPUBLIC
ECUADOR
EGYPT
EL SALVADOR
ERITREA
ESTONIA
ETHIOPIA
FINLAND
FRANCE
GABON
GEORGIA
GERMANY
GHANA
GREECE
GUATEMALA
HAITI
HOLY SEE
HONDURAS
HUNGARY
ICELAND
INDIA
INDONESIA
IRAN, ISLAMIC REPUBLIC OF
IRAQ
IRELAND
ISRAEL
ITALY
JAMAICA
JAPAN
JORDAN
KAZAKHSTAN
KENYA
KOREA, REPUBLIC OF
KUWAIT
KYRGYZSTAN
LATVIA
LEBANON
LIBERIA
LIBYAN ARAB JAMAHIRIYA
LIECHTENSTEIN
LITHUANIA
LUXEMBOURG
MADAGASCAR
MALAWI
MALAYSIA
MALI
MALTA
MARSHALL ISLANDS
MAURITANIA
MAURITIUS
MEXICO
MONACO
MONGOLIA
MONTENEGRO
MOROCCO
MOZAMBIQUE
MYANMAR
NAMIBIA
NETHERLANDS
NEW ZEALAND
NICARAGUA
NIGER
NIGERIA
NORWAY
PAKISTAN
PALAU
PANAMA
PARAGUAY
PERU
PHILIPPINES
POLAND
PORTUGAL
QATAR
REPUBLIC OF MOLDOVA
ROMANIA
RUSSIAN FEDERATION
SAUDI ARABIA
SENEGAL
SERBIA
SEYCHELLES
SIERRA LEONE
SINGAPORE
SLOVAKIA
SLOVENIA
SOUTH AFRICA
SPAIN
SRI LANKA
SUDAN
SWEDEN
SWITZERLAND
SYRIAN ARAB REPUBLIC
TAJIKISTAN
THAILAND
THE FORMER YUGOSLAV REPUBLIC OF MACEDONIA
TUNISIA
TURKEY
UGANDA
UKRAINE
UNITED ARAB EMIRATES
UNITED KINGDOM OF GREAT BRITAIN AND NORTHERN IRELAND
UNITED REPUBLIC OF TANZANIA
UNITED STATES OF AMERICA
URUGUAY
UZBEKISTAN
VENEZUELA
VIETNAM
YEMEN
ZAMBIA
ZIMBABWE

The Agency's Statute was approved on 23 October 1956 by the Conference on the Statute of the IAEA held at United Nations Headquarters, New York; it entered into force on 29 July 1957. The Headquarters of the Agency are situated in Vienna. Its principal objective is "to accelerate and enlarge the contribution of atomic energy to peace, health and prosperity throughout the world".

PROCEEDINGS SERIES

TRENDS IN RADIOPHARMACEUTICALS (ISTR-2005)

PROCEEDINGS OF AN INTERNATIONAL SYMPOSIUM
ORGANIZED BY THE INTERNATIONAL ATOMIC ENERGY AGENCY
AND HELD IN VIENNA, 14–18 NOVEMBER 2005

In two volumes

VOLUME 2

INTERNATIONAL ATOMIC ENERGY AGENCY
VIENNA, 2007

COPYRIGHT NOTICE

Sales and Promotion, Publishing Section
International Atomic Energy Agency
Wagramer Strasse 5
P.O. Box 100
1400 Vienna, Austria
fax: +43 1 2600 29302
tel.: +43 1 2600 22417
email: sales.publications@iaea.org
http://www.iaea.org/books

Printed by the IAEA in Austria
November 2007
STI/PUB/1294

IAEA Library Cataloguing in Publication Data

International Symposium on Trends in Radiopharmaceuticals (2005 : Vienna, Austria)
Trends in radiopharmaceuticals : ISTR-2005 : proceedings of an international symposium / organized by the International Atomic Energy Agency and held in Vienna, 14–18 November, 2005. — Vienna : IAEA, 2007.
p. ; 24 cm. (Proceedings series, ISSN 0074–1884)
STI/PUB/1294
ISBN 92–0–101707–3
Includes bibliographical references.

1. Radiopharmaceuticals — Congresses. 2. Nuclear medicine — Congresses. I. International Atomic Energy Agency. II. Series: Proceedings series (International Atomic Energy Agency).

IAEAL 07–00497

FOREWORD

The growth of nuclear medicine depends on advances in radiopharmaceutical development and discovery, as well as improvements in instrumentation. The field of radiopharmaceuticals has witnessed continuous evolution thanks to the contributions of scientists from diverse disciplines such as chemistry, physiology and pharmacology. The IAEA has been supporting activities in the field of radiopharmaceuticals, which has resulted in significant capacity building in the above fields in Member States. Many Member States have developed manufacturing facilities through technical cooperation projects for the large scale production of radiopharmaceuticals which helped the growth of nuclear medicine in those countries. IAEA efforts through coordinated research projects have also helped in advancing research activities in the development and utilization of new products in many Member States.

The International Symposium on Trends in Radiopharmaceuticals (ISTR-2005) was organized in order to provide scientists and professionals from 70 countries working in the field of radiopharmaceuticals and related sciences with the opportunity to present their research to an international audience. Sessions covered the most relevant topics of radiopharmaceuticals chemistry, including radionuclide production, radiochemical processing, manufacturing and quality control, quality assurance, latest advances in radiopharmaceuticals research, good manufacturing practices and regulatory aspects. On the basis of the invited presentations, papers and panel discussions during ISTR-2005, several areas of possible future international cooperation were identified.

This publication comprises two volumes and constitutes a record of the symposium and includes a summary as well as invited papers presented. A CD-ROM containing the unedited contributed papers which were presented in the two poster sessions of the symposium is included in volume 2.

The IAEA gratefully acknowledges the contribution made by the various participants to the success of this symposium, in particular to M.M. Vora for his technical editing of the papers.

EDITORIAL NOTE

The Proceedings have been edited by the editorial staff of the IAEA to the extent considered necessary for the reader's assistance. The views expressed remain, however, the responsibility of the named authors or participants. In addition, the views are not necessarily those of the governments of the nominating Member States or of the nominating organizations.

Although great care has been taken to maintain the accuracy of information contained in this publication, neither the IAEA nor its Member States assume any responsibility for consequences which may arise from its use.

The use of particular designations of countries or territories does not imply any judgement by the publisher, the IAEA, as to the legal status of such countries or territories, of their authorities and institutions or of the delimitation of their boundaries.

The mention of names of specific companies or products (whether or not indicated as registered) does not imply any intention to infringe proprietary rights, nor should it be construed as an endorsement or recommendation on the part of the IAEA.

The authors are responsible for having obtained the necessary permission for the IAEA to reproduce, translate or use material from sources already protected by copyrights.

CONTENTS OF VOLUME 2

PET RADIOPHARMACEUTICALS (SESSION 10)

RADIOIODINE RADIOPHARMACEUTICALS (SESSION 11)

^{18}F RADIOPHARMACEUTICALS AND AUTOMATION OF SYNTHESIS (SESSION 12)

CYCLOTRON BASED RADIONUCLIDES AND GENERATORS (SESSION 13)

PHARMACOLOGY AND THERAPEUTIC RADIOPHARMACEUTICALS

(Session 8)

Chairpersons

C. DECRISTOFORO
Austria

K.K. SOLANKI
IAEA

BIOLOGICAL AND CHEMICAL EVALUATION OF VARIOUS RADIOCOLLOIDS USED FOR CLINICAL RADIOSYNOVECTOMY

G.A. JÁNOKI, L. BALOGH, A. POLYÁK, D. MÁTHÉ, L. KŐRÖSI, R. KIRÁLY
"Fodor József" National Centre of Public Health, "FJC" National Research Institute for Radiobiology and Radiohygiene,
Budapest, Hungary
Email: janoki@hp.osski.hu

Abstract

Radiopharmaceuticals used for radiosynovectomy are the following: ^{90}Y-citrate colloid, ^{90}Y-silicate colloid, ^{169}Er-citrate colloid, ^{166}Ho-phytate and ^{188}Re-tin colloid. Radiochemical purity and stability in all cases were higher than 99.0%. The particle sizes of the radiocolloids were different; the mean values were as follows: ^{90}Y-citrate colloid: 3.1 μm, ^{90}Y-silicate colloid: 0.9 μm, ^{167}Er-citrate colloid: 1.1 μm, ^{166}Ho-phytate: 0.66 μm, ^{188}Re-tin colloid: 0.6 μm. During biodistribution studies in rabbits the activity values in various organs (liver, blood, spleen, kidneys, lymph nodes, skeleton) outside of the injected knee ranged up to 10% of injected dose (ID) even after 14 days since injection. Activity values retained in the knee were in the range 95–87% of ID. Activity recoveries during animal studies were also high during the initial time period (90–95%) and a week after injection only dropped slightly below 90%. Owing to the favourable intra-articular retention and very low leakage values in all cases, the calculated absorbed dose showed high values in the target synovial surface (~40 Gy), low effective dose (5.3 mGy) and also low whole body absorbed dose (1.9 mGy) values. According to preclinical data obtained during this study, the authors concluded that all the colloid radiopharmaceuticals tested showed very low leakage and that organs only accumulate insignificant amounts of radioactivity. This leads to very favourable dosimetric calculations.

1. INTRODUCTION

Radiation synovectomy is a technique whereby a beta emitting radiopharmaceutical is delivered into the affected synovial compartment in order to treat rheumatoid arthritis. Beta emitting radiocolloids are widely used for this purpose. The ideal radionuclide would possess beta emission with sufficient energy for a maxiumum tissue penetration of 5–10 mm, gamma emission suitable for gamma camera imaging, a short half-life and ready availability. An

^{198}Au colloid was first used for radiocolloid synovectomy and this isotope has been continously investigated. The main drawbacks of an ^{198}Au colloid are the 411 keV gamma emission which creates an unnecessary radiation hazard, the small particle size, which results in excessive loss from the joint space by lymphatic drainage, and the high radiation doses to the proximal lymph nodes.

Other radiopharmaceuticals [1–17] that have been developed, studied and registered for human use are listed in Table 1. The different radiation properties of each therapeutic isotope determine their respective use regarding the joint size. The authors studied the preparation and biological use of colloids labelled with isotopes ^{90}Y, ^{166}Ho, ^{169}Er and ^{188}Re which are applicable for treating the various joints for radiosynoviorthesis.

TABLE 1. RADIONUCLIDE USED FOR RADIATION SYNOVECTOMY

Radionuclide and pharmaceutical form	$T_{½}$ (d)	Max.β^- energy (MeV)	Γ energy (KeV)	Tissue penetration depth (mm)	
				Max:	Min:
^{32}P colloid	14.4	1.71		7.9	2.6
^{198}Au colloid	2.7	0.96	411	3.9	1.2
^{165}Dy-FHMA	0.1	1.29	95	5.7	1.3
^{90}Y-Ca-oxalate ferric hydroxide citrate colloid silicate	2.7	2.26		11.0	3.6
^{166}Ho-hydroxyapatite -FHM-phytate	1.2	1.85	81	8.5	2.1
^{153}Sm-hydroxy MA	1.9	0.811	103	3.1	0.7
^{169}Er-citrate colloid	9.4	0.35		1.0	0.3
^{186}Re colloid -rhenium sulphide	3.7	1.07	137	3.6	1.2
^{188}Re-tin colloid -sulphur colloid -microsphere	0.7	2.12	155	11.0	2.1

2. MATERIALS AND METHODS

Compounds tested during this study were as follows:

^{90}Y-citrate colloid (CIS bio YMM-1), ^{90}Y-silicate colloid (GE Amersham Health YAS-2P), ^{169}Er-citrate colloid (CIS bio ERMM-1) and ^{188}Re-tin colloid were prepared in the "Fodor József" laboratory using methods published previously [3], ^{166}Ho-phytate suspension was the test compound obtained from the Isotope Institute Ltd (Hungary).

2.1. Methods for determination of activity ratio bound to colloid form

In the case of the ^{90}Y-citrate-silicate colloid, the TLC method was used to determine colloid bound activity. Merck Silicagel 5553 layer, solvent containing 64 mL n-Propanol, 16 mL water, 20 mL methanol and 1 g of tartaric acid were used and 1–5 µL volume of sample was deposited.

The R_f value of radiocolloids was zero. For in vivo stability study 100 µL of radiocolloid was inoculated in 3 mL of rabbit synovial fluid at 37ºC for 24 h and 5 d. After inoculation, colloid bound activity ratios were determined by using the same TLC method used earlier.

2.2. Methods used for particle size determination of various radiocolloids

The analytical instrument (DynaPro) used in the authors' experiments is a product of Proteinsolutions Inc. (United States of America). The sample is illuminated by a semiconductor laser of ~830 nm wavelength. The light scattered by the sample in the cell is collected and guided via a fibre optic cable to an actively quenched, solid state single photon counting module. The photons are then converted to electrical pulses and correlated. The DynaPro analyses the timescale of the scattered light intensity fluctuations by a mathematical process called autocorrelation. The translational diffusion coefficient of the molecules in the sample cell is determined from the decay of the intensity autocorrelation data. The hydrodynamic radius of the sample is then derived from the translational diffusion coefficient, using the Stokes-Einstein equation.

In the authors' experiments, 160 nm and 240 nm polystyrene calibration standards (Bangs Laboratories Inc., Serial No. 5692) were measured in parallel with the samples.

2.3. Biodistribution study

New Zealand white male laboratory rabbits weighing 2–3 kg were purchased. Rabbits were individually housed in 60 cm × 80 cm × 80 cm metal

cages. Environmental conditions in the animal room were maintained at an average temperature of 20.5ºC (ranging from 18.6–23.8ºC), an average relative humidity of 55% (ranging from 32% to 66%), and a 12 h light/12 h dark photoperiod. The rabbits had ad libitum access to fresh standard rodent feed manufactured and purchased by Biofarm Kft., Hungary. The rabbits had ad libitum access to fresh tap water, provided daily in glass bottles with stainless steel sipper tubes. Feed certification was performed by the manufacturer. Water analysis was performed by the "Fodor József" National Centre for Public Health, National Institute of Public Health Water Laboratories (Budapest, Hungary) and included dissolved solids, conductivity, microbial content (heterotrophic plate count) and heavy metals. The animals were acclimatized for a minimum of 5 d. General health status was monitored by the veterinarian in charge.

Cage side observation of general health, behaviour and appearance was made at least once daily. The rabbits were under continuous observation for any clinical signs for at least 1 h after dosing. Any clinical signs were recorded. The animals were weighed at receipt, before dosing and before being sacrificed.

The animals used for the study were received in good health and were clinically free from any apparent abnormalities or disease. A veterinarian examined the animals within 24 h of receipt and deemed them healthy and free of gross abnormalities.

Prior to dose administration, the animals were weighed and anaesthetized by intramuscular administration of 100 mg ketamine hydrochloride/kg b.w. (SBH-Ketamin, SBH Kft., Hungary) and 2 mg xylazine/kg b.w. (Primazin, Alfasan B.V., Netherlands). This resulted in an anaesthetic and immobile state of at least 30 min.

To assess the needle positioning during the injections, some rabbits were checked by X ray (BV 22, Müller Co., Germany) and ultrasound (SpinelVET 2000, Echoson Ltd, Poland) imaging. The needle was found to be correctly positioned in the knee joint cavity with the proposed injection method as described in Section 2.4.

2.4. Dose administration

An aliquot of 100 µL of the supplied test article suspensions was injected into the knee joint cavity. After induction of general anaesthesia, the hair above the knee joint was shaved and the skin cleaned and disinfected with iodine spray. The knee joints were punctured in slight flexion through the first third of the median patellar ligament with an analytical syringe with fixed needle (Hamilton Corp., USA) under aseptic conditions. The rabbits received

an activity in the range 105–500 μCi (5.6–18.5 MBq)/100 μL of the test article into their knee joint randomly selected.

As previous experiments in the NRIRR have shown, in the case of gamma camera (Nucline X-Ring/R, Mediso Ltd, Hungary) imaging of ^{90}Y bremsstrahlung in a fully open energy window centred at 140 keV, a vial with 0.55 MBq and a vial containing 25 MBq of activity placed at the same detector can be distinguished visually by the operator. Thus, correctness of the injections was controlled with the use of a gamma camera, the exclusion criterion being the appearance of a second spot of activity near the injection site. Immediately after dosing, the animal was placed in the ventrodorsal position above the detector and the scintigraphic image was checked. In the case of two or more spots appearing on screen, the fact was recorded and the animal was discarded from the experiment. If the activity spot was unique and in the region of the knee, the injection was deemed to be correct. Figure 1 shows an example of correct injection.

2.5. Sample collection, processing and analysis

At the end of the study, the rabbits were anaesthetized again by intramuscular administration of 100 mg ketamine/kg b.w. (SBH-Ketamin, SBH Kft., Hungary) and 2 mg xylazine/kg b.w. (Primazin, Alfasav B.V., Netherlands). The animals were sacrificed 5–10 min after anaesthesia induction by intracardial injection of 0.5 mL/kg b.w. of a specific veterinary drug for euthanasia, T 61® ad

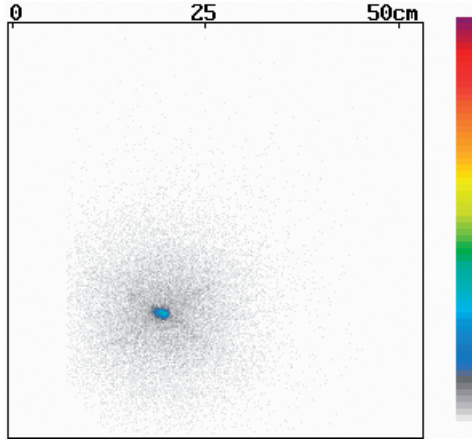

FIG. 1. Ventrodorsal whole body scintillation image of a correctly injected rabbit. The only spot appearing corresponds to the injection site at the knee.

us. vet. (Intervet B.V., Netherlands). All the animal handling methods used in the study were in compliance with all applicable sections of the Hungarian Laws No. XXVIII/1998 and LXVII/2002 on the protection and welfare of animals.

Animals were sacrificed at 6, 24 and 48 h and 5 d post-injection. The samples of the injected knees (with 1 cm of femoral and tibial bone outside the capsule) were collected. The samples were washed in physiological saline, dried with absorbent paper and weighed after collection. Samples were collected in containers labelled according to animal identification, organ, collection time points and date.

Samples were placed in individually identified porcelain crucibles. The wet net weight of the samples was calculated from weight measurements made on the empty crucible and containing the sample. Samples were desiccated in a thermodryer at 200°C for 24 h and ashed in a laboratory furnace (OH-63, OMSZOV, Hungary) at 600°C for 12 h. The net weight of each ash sample was determined by measuring the crucibles with and without ashes with an analytical balance to four digits.

Concentrated HNO_3 was added to the ash samples and the solution of each sample was brought to a fixed 10 mL volume. This solution was incubated for at least 12 h at room temperature and homogenized by a Vortex mixer several times during dissolution. Immediately after the last homogenization, 1 mL aliquots of the sample solutions were transferred to plastic measurement test tubes in triplicate.

2.6. Immobilization of the injected knee

After the dose administration and a 30 min totally immobile period due to general anaesthesia, the injected knee of the rabbits in the immobilized group was held by a PVC plastic splint formed individually for the animals and fixed by tape and bandage to hold the knee at semi-flexion, to facilitate the keeping of a natural seated position of the rabbit in the cage. This immobilization splint was kept on the knees for 24 h to ensure proper and indulgent immobilization of the joint, as demonstrated by preliminary experiments at the NRIRR.

2.7. Radioactivity measurements

Before sample measurements, the device, a NaI(Tl) crystal gamma scintillation counter with automatic sample changer and multichannel signal amplifier–analyser (NZ-310, Gamma, Hungary), was checked for linearity of bremsstrahlung measurements and sensitivity. Radioactivity was determined in

triplicate sample solutions. It was found that the device measurements are linear in the range of 750–2694 kBq for 1 mL sample volumes and 60 s measurements.

2.8. Statistical methods for data analysis

Standard deviations (SD) of data were calculated using n-1 as the degree of freedom for multiplying n in the divider of the appropriate formula. Comparison of the groups was performed using the two-tailed Student's t-test and the Mann-Whitney U-test. ANOVA calculations were made to compare the different organ uptake values at the different time points. On the basis of biodistribution data, retention times, pharmacokinetic curves and the absorbed doses were calculated using Prism 4.0 and MIRDOSE 3.1 softwares.

3. RESULTS

3.1. Radiochemical purity study

The results of radiochemical purity and stability data of the five compounds studied are given in Table 2.

3.2. Particle size determination

A summary of particle size determinations are given in Figs 2 and 3. The results for standard colloids are also shown.

TABLE 2. COLLOID BOUND ACTIVITY OF RADIOPHARMACEUTICALS USED FOR RADIOSYNOVECTOMY

Compounds	Colloid bound activity (%)	
	in saline	in synovial fluid
^{90}Y-citrate colloid	99.2	99.8
^{90}Y-silicate	99.7	99.2
^{167}Er-citrate colloid	99.3	99.5
^{166}Ho-phytate	99.2	
^{188}Re-tin colloid	97.3	

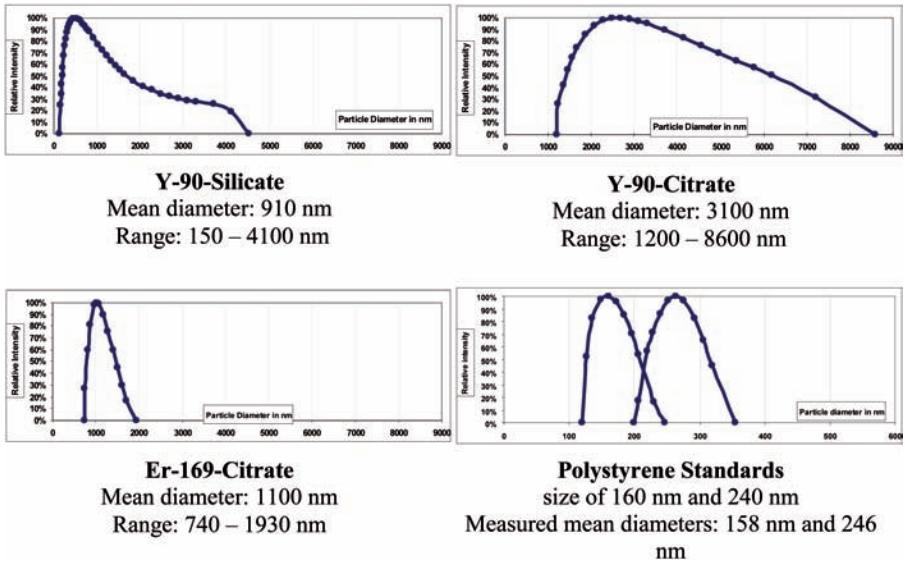

FIG. 2. Colloid size distribution of registered radiopharmaceuticals available for radiosynovectomy.

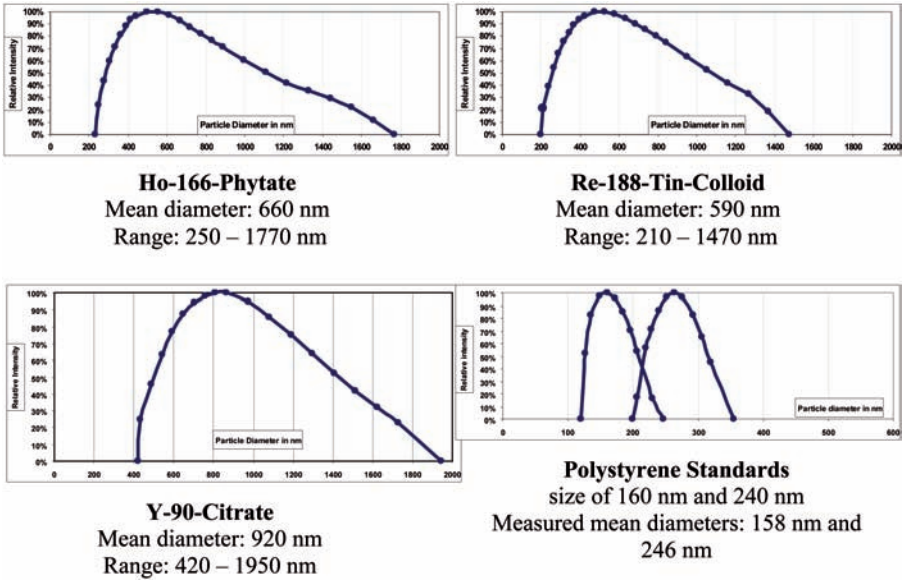

FIG. 3. Colloid size distribution of research radiopharmaceuticals used for radiosynovectomy.

4. BIODISTRIBUTION STUDY

4.1. ^{90}Y-citrate/silicate colloid

Biodistribution of these two ^{90}Y labelled colloids are seen in Tables 3 and 4.

4.2. ^{167}Er-citrate colloid

In the present study, the remaining activity in rabbit knee after intra-articularly injected ^{167}Er-citrate colloid suspension was determined. At three different time points (6 h, 2d, 8 d) knee, bone and blood were sampled and measured by liquid scintillation techniques. Radiochemical purity of the filtered batch used in the present work was high throughout the study (>99%).

Activity values retained in the knee as injected dose per cent were as follows:

6 h: 90.8 ± 0.36%; 2 d: 87.2 ± 0.05%; 8 d: 80.07 ± 0.04%.

TABLE 3. SUMMARY OF DISPOSITION OF ^{90}Y-CITRATE COLLOID AT DIFFERENT TIME POINTS IN ORGANS AFTER INTRA-ARTICULAR INJECTION
(%ID/whole organ)

Time point	6 h		24 h		5 d		8 d		13 d	
Dose % in whole organ	Ave.	± SD	Ave.	± SD	Ave.	± SD	Ave.	± SD	Ave.	± SD
Blood	0.158	0.386	0.083	0.120	1.454	2.606	0.885	2.168	0.018	0.030
Liver	0.318	0.307	0.301	0.437	0.749	1.009	0.272	0.196	0.082	0.183
Spleen	0.014	0.017	0.029	0.030	0.050	0.043	0.099	0.051	0.046	0.048
Kidney	0.120	0.106	0.061	0.047	0.205	0.095	0.248	0.372	0.082	0.077
Testes	0.006	0.010	0.029	0.032	0.008	0.008	0.055	0.069	0.000	0.000
Ing. lymph node	0.006	0.008	0.015	0.016	0.000	0.001	0.075	0.064	0.059	0.081
Whole skeleton	1.396	2.495	0.050	0.050	3.252	1.023	6.300	2.969	0.150	0.196
Knee	95.984	2.479	94.265	1.733	91.282	2.721	88.116	4.851	87.600	2.074

TABLE 4. SUMMARY OF DISPOSITION OF ^{90}Y-SILICATE COLLOID AT DIFFERENT TIME POINTS IN ORGANS AFTER INTRA-ARTICULAR INJECTION
(%ID/whole organ)

Time point	6 h		24 h		48 h		5 d	
Dose % in whole organ	Ave.	± SD	Ave.	± SD	Ave.	± SD	Ave.	± SD
Blood	0.025	0.030	0.277	0.379	0.008	0.011	0.076	0.155
Liver	0.033	0.026	0.012	0.005	0.005	0.010	0.064	0.066
Popl. lymph. node	0.085	0.194	0.002	0.005	0.001	0.001	0.003	0.005
Ing. lymph node	0.010	0.006	0.007	0.006	0.000	0.001	0.006	0.010
Whole skeleton	2.673	0.946	1.814	0.782	0.368	0.122	5.013	2.615
Knee	100.106	10.978	91.480	8.592	84.451	13.522	78.894	13.320

Low level leakage was documented also with the very low blood activity which was always less than 0.01%ID and with the low whole skeleton uptake which ranged 1.7–4.3%ID.

None of the rabbits used in this experiment showed any chemical or radiation toxicity signs, including any local intolerance.

4.3. ^{188}Re-tin colloid

Retention of ^{188}Re-tin colloid in the synovial space of the rabbits was observed up to 72 h.

No leakage to the inguinal lymph node (the predilection site of the accumulated outflow of radioactivity) or other lymph nodes could be observed. Figure 4 presents static scintigraphic images of the knee regions of a rabbit at 3, 24, 48 and 72 h after injection into the knee. The knee:knee radiopharmaceutical uptake ratios were stable over time. In whole body scans, no other activity accumulation was seen anywhere in the body (e.g. in the predilection sites such as the thyroid gland and the gastric mucosa). The scans of healthy rabbits receiving only intra-articular ^{188}Re perrhenate solution revealed uptake in the predilection sites — stomach mucosa and thyroid gland were visualized in the images, most prominently 3 h after injection (Fig. 5). Later, healthy rabbit scans

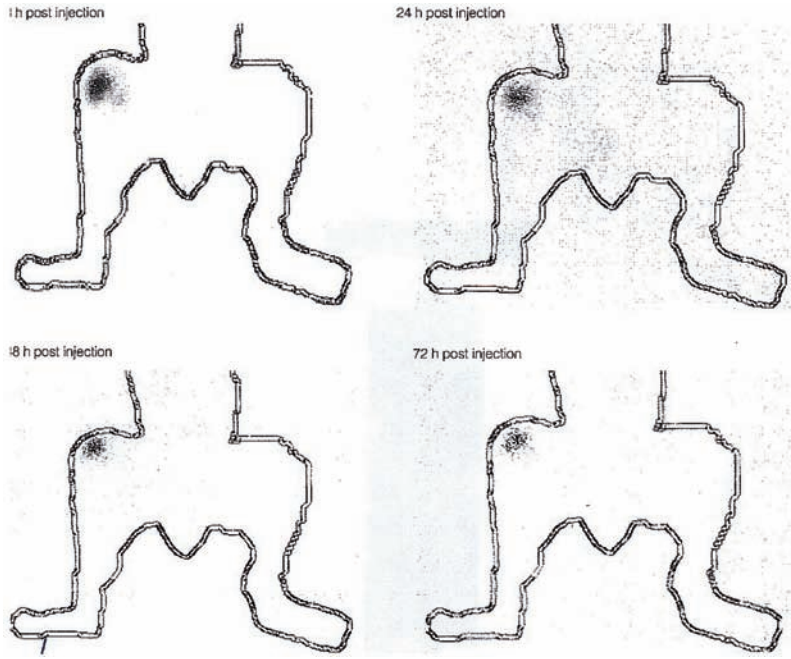

FIG. 4. Static images of the knee of a rabbit taken at 3, 24, 48 and 72 h after injection. Differences in background are due to the automatic cut-off level setting of the camera software. Rabbit contours were generated from the acquisition data by using the Inter-View© software.

demonstrated a very fast excretion of perrhenate via the kidneys and bladder 48 and 72 h post-injection; only background activity could be observed in healthy rabbits receiving perrhenate eluate only.

4.4. ^{166}Ho-phytate biodistribution

The intra-articularly injected 37 MBq/0.1 mL ^{166}Ho-phytate solution is retained at the injection site. Results 6, 24, 72 and 168 h after injection showed that 88.5–98.5% of injected dose remains in the knee sample. Leakage was in the range 1.5–11.5%. Only liver, kidney, lung and blood samples contained low amounts of activity. Because no lymph nodes contained measurable activity the authors conclude that only low levels of leakage occurred by the hematogene process. Figure 6 shows ^{166}Ho-phytate biodistribution 48 h after injection.

Even after 168 h of injection the levels were: knee: 92%; liver: 2.8% and kidney: 1.5%; with cummulative activities: urine 1.19% and faeces 2.23%.

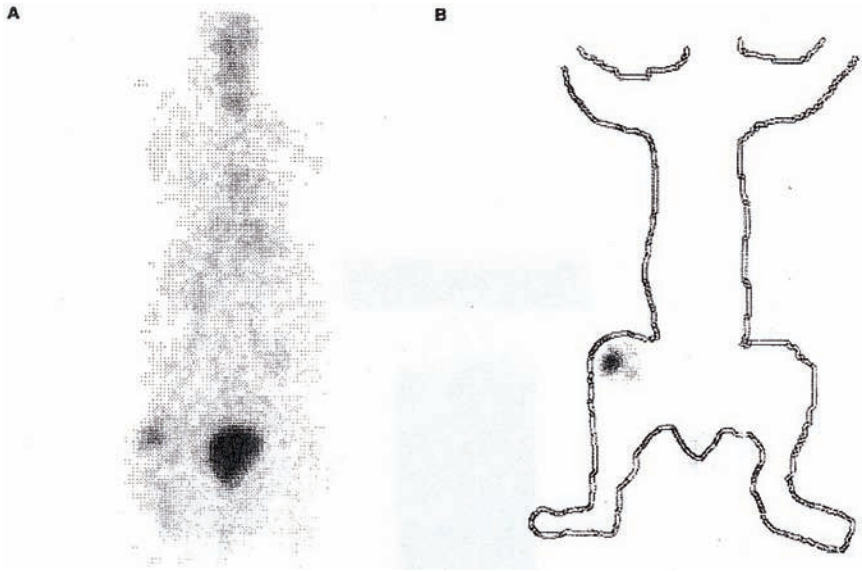

FIG. 5. Comparison of biodistributions of the same amount and activity of intra-articular perrhenate eluate (A) and ^{188}Re-tin colloid solution (B) in rabbit, 3 h post-injection.

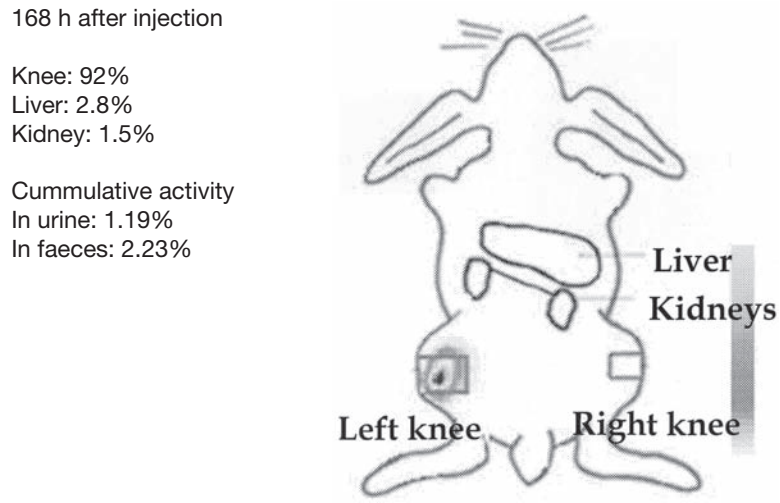

FIG. 6. ^{166}Ho-phytate distribution in rabbit 48 h after intra-articulation injection.

4.5. Dosimetric evaluation

The residence time of various radiocolloids tested are shown in Table 5. The doses delivered to the knee are summarized in Table 6. The knee doses were calculated with the MIRD unit density spheres method (the authors considered the adult knee a 300 g sphere of 8.19 cm diameter). Absorbed radiation dose of various organs by the MIRD method is presented in Table 7.

The dose calculations were performed using the standard MIRD method (MIRD pamphlet no.1 Society of Nuclear Medicine, 1976) and Olinda 1.0 software.

TABLE 5. RESIDENCE TIMES IN THE KNEE FOR DIFFERENT COLLOID RADIOPHARMCEUTICALS

	^{90}Y-citrate	^{90}Y-citrate	^{90}Y-silicate	^{169}Er-citrate	^{188}Re-tin	^{166}Ho-phytate
Observation time	13 d	5 d	5 d	19 d	3 d	7 d
$T_{1/2}$	2.67 d	2.67 d	2.67 d	9.4 d	0.71 d	1.12 d
Residence time (h)						
Knee	282.072	112.081	103.152	395.042	10.647	157.380

TABLE 6. SUMMARY OF KNEE DOSES AFTER INTRA-ARTICULAR APPLICATION OF DIFFERENT RADIOCOLLOIDS

Target organ	^{90}Y-citrate colloid (13 d) (Gy/MBq)	^{90}Y-citrate colloid (5 d) (Gy/MBq)	^{90}Y-silicate colloid (5 d) (Gy/MBq)	^{169}Er-citrate colloid (19 d) (Gy/MBq)	^{188}Re-tin colloid (3 d) (Gy/MBq)	^{166}Ho-phytate colloid (7 d) (Gy/MBq)
Knee	0.487	0.194	0.178	0.0778	0.0156	0.206

TABLE 7. ESTIMATED ABSORBED RADIATION DOSE INTRA-ARTICULAR APPLICATION
(phantom: 70 kg adult)

Target organ	^{90}Y-citrate colloid (13 d) (μSv/MBq)	^{90}Y-citrate colloid (5 d) (μSv/MBq)	90Y-silicate colloid (5 d) (μSv/MBq)	^{169}Er-citrate colloid (19 d) (μSv/MBq)	^{188}Re-tin colloid (3 d) (μSv/MBq)	^{166}Ho-phytate colloid (7 d) (μSv/MBq)
Adrenals	11.800	5.580	0.796	0.119	7.720	8.680
Brain	11.800	5.580	0.796	0.119	7.680	7.640
Breasts	11.800	5.580	0.796	0.119	7.390	7.520
Gall bladder wall	11.800	5.580	0.796	0.119	7.550	9.290
LLI wall	11.800	5.580	0.796	0.119	7.630	7.530
Small intestine	11.800	5.580	0.796	0.119	7.580	7.690
Stomach wall	11.800	5.580	0.796	0.119	7.500	7.720
ULI wall	11.800	5.580	0.796	0.119	7.550	7.820
Heart wall	11.800	5.580	0.796	0.119	7.560	87.400
Kidney	890.000	5.580	0.796	0.119	7.570	243.000
Liver	323.000	160.000	8.800	0.119	7.520	552.000
Lungs	11.800	5.580	0.796	0.119	7.550	126.000
Muscle	11.800	5.580	0.796	0.119	7.560	7.660
Ovaries	11.800	5.580	0.796	0.119	7.610	7.540
Pancreas	11.800	5.580	0.796	0.119	7.610	8.320
Red marrow	636.000	125.000	187.000	111.000	119.000	226.000
Osteogeniccells	1280.000	252.000	374.000	991.000	259.000	595.000
Skin	11.800	5.580	0.796	0.119	7.430	7.440
Spleen	521.000	5.580	0.796	0.119	7.530	7.680
Testes	11.800	5.580	0.796	0.119	7.460	7.330
Thymus	11.800	5.580	0.796	0.119	7.500	7.630
Thyroid	11.800	5.580	0.796	0.119	7.590	7.520
Urinary bladder wall	11.800	5.580	0.796	0.119	7.520	7.390
Uterus	11.800	5.580	0.796	0.119	7.570	7.470
Total body	91.500	22.600	20.700	16.700	19.700	49.100
Effective dose equivalents (μSv/MBq))	227.000	36.600	34.800	43.100	28.500	117.000
Effective dose (μSv/MBq))	121.000	29.900	27.200	23.300	23.000	82.000

5. DISCUSSION

5.1. Discussion of literature data

Synovectomy by intra-articular application of β emitting radioisotopes (radiation synovectomy) was introduced in 1952 by Fellinger et al. [18] for treatment of an inflamed synovial membrane. Since that time a number of radiopharmaceuticals have been studied [19–23]. In Europe recently, the following compounds are registered and used to treat various sized joints: ^{90}Y-silicate, ^{90}Y-citrate colloids, ^{186}Re-sulphide and ^{169}Er-citrate. Today, radiosynoviorthesis is an alternative or even supplementary therapeutic approach to pharmacotherapy for the treatment of patients suffering from painful, inflammatory or severe degenerative joint diseases [24–28].

After intra-articular injection, radiocolloids are phagocytosed by the superficial synovial cells. Owing to irradiation, necrosis of the superficial synovial layer is observed from the first day on. Early animal studies in rabbits demonstrated the uptake of the radiocolloid by the synovial membranes and homogenous distribution throughout the entire tissue by autoradiography.

After injection of 0.59 MBq (16 μCi) of ^{88}Y (the isotope chosen for its gamma radiation which increases counting precision), a study reported that 87–100% of the injected yttrium is recovered in the articulation after 7 d. Another study showed that 24 h after intra-articular injection of 3.7–37 MBq of ^{90}Y-citrate colloid, 0.2% of the activity is recovered in the blood and 0.4% and 0.13% in urine and faeces respectively. The problem of radioactivity leakage from the joint was experienced during the human clinical practice. Several studies have suggested that particle size is critical in limiting the leakage of radiocolloids from the synovial joint [7, 12, 27]. Attempts to quantify the amount of leakage have given values of 5–10% at 24 h after administration and between 15–25% of injected dose at 5 d after application of small-sized (10–100 nm) ^{90}Y-silicate particles. Even from moderate leakage, the radiation absorbed dose to normal organ (e.g. liver, regional lymph nodes) has raised the level of concern because of the unnecessary radiation burden.

There have been only a few animal studies to determine the amount of leakage occurring during radiation synovectomy using ^{90}Y colloids or other radiopharmaceutical products [7, 12, 29–31].

Dedicated animal studies to determine all factors affecting the amount of leakage, stability of colloid in vitro and in synovium, including particle size and size distribution of colloid, biodistribution after intra-articulation injection in a large number of animals at different time points and presented as ID% in whole organ (lymph node, skeleton, blood, liver and knee) have not been published until now. The authors' designed studies allowed monitoring and

comparison of extra-articular leakage and biodistribution of different registered and experimental products. Their experimental works were based on detailed protocol which covered all aspects of the work dealing with experimental animal testing, biodistribution of radiopharmaceuticals and, finally, handling of low level radioactive waste.

During housing, anaesthesia and sacrifice of experimental animals, current laws on protection and welfare of animals were followed. Activity measuring devices and other tools used during experiments were calibrated and proven to be sensitive and precise. For each animal, the quality (success) of intra-articular administration was followed and documented by gamma camera scintigraphy, X ray or ultrasound image.

Immobilization of the group of animals was also managed. PVC plastic splints were formed individually for each animal and fixed by tape and bindings to hold the knee of the rabbits in a semi-flexed position.

The testing facility at the "Fodor József" National Centre of Public Health, "Frederic Joliot-Curie" National Research Institute for Radiobiology and Radiohygiene, the Diagnostic and Therapeutic Isotope Laboratory, has no GLP status but during the experiments and reports the GLP rules were followed.

The compiled study set-up allowed determination of the volume of leakage and the amounts of various organ uptake, if any occurred.

5.2. Discussion of the authors experiments

The radiochemical purity and stability studies (in vitro and in synovial fluid) of different radiocolloids showed very uniform results. In all cases, the rate of colloid bound activity always exceeded 99% throughout the whole experiment. The mean particle size of this colloid was 0.6–3.1 μm and after intra-articular injection into 149 rabbits the animals showed no sign of chemical or radiation toxicity. No local intolerance was reported. The injection technique developed and practiced was controlled by XR, US and scintigraphy and allowed personnel to control any leakage relating to the incorrectly positioned needle in the knee joint cavity.

The distribution of injected activity in various organs outside the knee (this value is equivalent to leakage activity) such as the liver, spleen, kidneys, testes, blood, lymph nodes and skeleton was very low; in most cases it was around 1% ID during the whole study.

The long stability of radiocolloids is exemplified by ^{90}Y-citrate colloid where applied activity values retained in the knee between 6 h and 13 d ranged from 93.61 ± 1.67% to 86.80 ± 1.59% of injected activity in the non-immobilized group and 95.10 ± 0.91% to 87.68 ± 2.26% in the immobilized

group of animals. The non-significant difference occurring between the immobilized and non-immobilized groups can be explained by the influence of anaesthesia and animal movement behaviour. The anaesthetic state in both groups was at least 30 min. This is generally followed by a reconvalescent period, usually connected to restricted moving. This can be a time long enough for the colloid to bind into the joints. The higher blood perfusion of the joints in rabbits can account for a shortened leakage time window than in humans. Owing to behavioural characteristics, rabbits tend to redistribute their weight onto the untreated legs after any treatment. This means that in any case, an animal will move and charge less its treated leg and will rather use the remaining three limbs. The self-restriction of movement in the treated leg will be present in all animal models of joint treatment. The moving space available for a rabbit in a standard 60 cm × 80 cm × 80 cm cage is enough to provide for the habitual moving needs of the animal. However, these natural movements are restricted in a small space with a lower amplitude of movement. The lack of higher angle flexion and extension of the joint can result in a normal blood perfusion. There is no increased blood flow (consequently the lymph flow also remains normal) that could lead to higher leakage. The investigators found no activity in the splints, thus there is no evidence of misinjection or increased pressure in the joint space.

The activity recovery during studies was also high at early time points (90–95%); only 13 d after injection did it drop slightly below 90%.

On the basis of the favourable intra-articular retention and very low leakage values, the calculated absorbed dose showed high values in the target synovial surface (~40 Gy) and low effective dose (5.3 mGy) and also low whole body absorbed dose (1.9 mGy) values.

In the scientific literature, Noble et al. [8] and Davis et al. [11] reported studies about the animal evaluation of various radiocolloid agents. They determined the leakage of radioactivity from the rabbit synovial pouch and found that it is dependent on the size and resistance to degradation of the various colloids (e.g. ^{99m}Tc-FeHMAA, MAA, phytate, ^{90}YCa-oxalate, ^{90}Y-ferric hydroxide). In their work, Noble et al. [8] reported leakage values of 0.3–65% ID after 24 h of intra-articular injection of ^{99m}Tc labelled diagnostic radiopharmaceuticals. Davis et. al [11] published results that showed that their in-house prepared ^{90}Y-oxalate and ^{90}Y-ferric hydroxide macro-aggregates were sized in the range 1–10 μm, and therefore the leakage was less, 5 ± 2%.

6. CONCLUSION

In their review article, Kampen et al. [24] reported a literature compilation about the leakages of different radiopharmaceuticals. The reviewed literature showed the leakage value for small-sized colloids (<30 nm), as ^{198}Au colloid, is up to 48% of ID, leading to a 50–150 Gy radiation dose to the involved regional lymph nodes.

In the case of ^{90}Y, they also report a radiation dose of more than 100 Gy to regional lymph nodes. They explained that, owing to a lack of strict size control of the colloidal radionuclide, some very small particles (fines) seem to leave the joint and lead to this excessive leakage.

Moreover, a colloidal solution of ^{90}Y of pH<6 may contain free ^{90}Y ions which can be easily drained from the treated joint. In these cases, besides the problem of whole body (non-target) radiation burden, leakage of radionuclide out of the treated joint will lead to a significant reduction of the radiation dose imported to the synovial surface, which may fall to 60% and thus constitutes a drop in the probability of clinical success.

If one summarizes literature information about the 'ideal' radiopharmaceutical for radiosynovectomy, the following have to be mentioned:

(a) The energy of the ß$^-$ particles must be high enough to penetrate the whole depth of the inflamed synovial membrane.
(b) The colloid particle size should be between 1 and 5 μm.
(c) The hardness of particles (resistance to in vivo dissolution, enzymatic action or mechanical stress) are also important.

In the light of literature to date, the evaluated ^{90}Y-citrate/silicate colloid, ^{169}Er-citrate colloid, ^{166}Ho-phytate and ^{188}Re-tin colloid possess features that are very close to literature advice. The leakage activity value of up to 2 weeks is around 10% ID, and organs accumulate only insignificant amounts of radioactivity and this leads to very favourable dosimetric calculations. The authors believe that the reported data of this lege artis developed and evaluated preclinical studies proved and support the efficient and safe use of radiocolloid injection in humans.

ACKNOWLEDGEMENTS

The authors would like to thank M. Pállai, Z. Suhajda, K. Haller and N. Fésüs for technical assistence and M. Kovács for preparation of the manuscript.

REFERENCES

[1] WEBB, F.W.S., LOWE, J., BLUESTONE, R., Uptake of colloidal radioactive Yttrium by synovial membrane, Ann. Rheum. Dis., 28: p. 300, (1969).

[2] HUŠÁK, V., WIEDERMANN, M., KRÁL, M., Absorbed dose due to beta-rays from radioactive colloids in radiation synovectomy, Phys. Med. Biol.,. Vol. 18, No. 6, pp. 848-854, (1973).

[3] OKA, M., Radiation synovectomy of the rheumatoid knee with Yttrium-90, Annals of Clinical Research 7: pp. 205 – 210, (1975).

[4] BOWRING, C.S., KEELING, D.H., Absorbed radiation dose in radiation synovectomy, British Journal of Radiology, 51, pp. 836 – 837, (1978).

[5] McCOY, J.M., Radioactive Yttrium-90: intra-articularly for the treatment of rheumatoid arthritis, Journal of MAG Vol. 67, pp. 361 – 365, May (1978).

[6] DUNSCOMBE, P.B., RAMSEY, N.W., Radioactivity studies on 2 synovial specimens after radiation synovectomy with Yttrium-90 Silicate, Annals of the Rheumatic Diseases, 39: pp. 87 – 89, (1980).

[7] BEATSON, T.R., Radiation synovectomy (synoviorthesis) for rheumatoid arthritis in the Isle of Man, Gerontology 28: pp. 258 – 264, (1982).

[8] NOBLE, J., et al., Leakage of radioactive particle systems from a synovial joint studied with a gamma camera, The Journal of Bone and Joint Surgery, Incorporated, Vol. 65-A, No. 3, March, (1983).

[9] ZALUTSKY, M.R., et al., Radiation synovectomy with 165DY-FHMA: lymph node uptake and radiation dosimetry calculations, Int. J. Nucl. Med. Biol. Vol. 12, No. 6. pp. 457 – 465, (1986).

[10] ZALUTSKY, M.R., NOSKA, M.A., GALLAGHER, P.W., SHORTKROFF, S., SLEDGE, C.B., Use of liposomes as carriers for radiation synovectomy, Nucl. Med. Biol. Vol. 15, No. 2. pp. 151 – 156, (1988).

[11] DAVIS, M.A., CHINOL, M., Radiopharmaceuticals for radiation synovectomy: evaluation of two Yttrium-90 particulate agents, J. Nucl. Med. Vol. 30: No. 6, pp. 1047 – 1055, June (1989).

[12] MYERS, S.L., SLOWMAN, S.D., BRANDT, K.D., Radiation synovectomy stimulates glicosaminoglycan synthesis by normal articular cartilage, J. Lab. Clinik Meg. pp. 28 – 35, (1989).

[13] CHINOL, M., VALLABHAJOSULA, S., ZUCKERMAN, J.D., GOLDSMITH, S.J., In vivo stability of ferric hydroxide macroaggregates (FHMA). Is it a suitable carrier for radionuclides used in synovectomy?, Nucl. Med. Biol. Vol. 17, No. 5. pp. 479 – 486, (1990).

[14] JOHNSON, L.S., YANCH, J.C., Absorbed dose profiles for radionuclides of frequent use in radiation synovectomy, arthritis and rheumatism, Vol. 34, No.12, December, (1991).

[15] VAN KASTEREN, M.E.E., NOVÁKOVÁ, I.R.O., BOERBOOMS, A.M.T., LEMMENS, J.A.M., Long term follow up of radiosynovectomy with Yttrium-90 silicate in haemophilic haemarthrosis, Ann Rheum Dis 52: 548 – 550, (1993).

[16] STUCKI, G., BOZZONE, P., TREUER, E., WASSMER, P., FELKER, M., Efficacy and safety of radiation synovectomy with Yttrium-90: a retrospective long-term analysis of 164 applications in 82 patients, British Journal of Rheumatology 32: 383 – 386, (1993).
[17] EDMONDS, J., et al., A comparative study of the safety and efficacy of dysprosium-165 hydroxide macro-aggregate and Yttrium-90 silicate colloid in radiation synovectomy–a multicentre double blind clinical trial, British Journal of Rheumatology 33: pp. 947 – 953, (1994).
[18] FELLINGER, K., SCHMIDT, J., Wien Z. Inn. Med., 33, 351 (1952).
[19] CLUNIE, G., PETER, J., A survey of radiation synovectomy in Europe, 1991 – 1993, European Journal of Nuclear Medicine Vol.22, No. 9, September, (1995).
[20] OHASHI, F., et al., The production os arthritis in beagles by an immunological reaction to bovine serum albumin, Exp. Anim. 45 (4), pp. 299 – 307, (1996).
[21] JAHANGIER, Z.N., JACOBS, J.W.G., VAN ISSELT, J.W., BIJLSMA, W.J., Persistent synovitis treated with radiation synovectomy using Yttrium-90: a retrospective evaluation of 83 procedures for 45 patients, British Journal of Rheumatology 36: pp. 861 – 869, (1997).
[22] WUNDERLICH, G., et al., Preparation and biodistribution of Rhenium-188 labeled albumin microspheres b 20: a promising new agent for radiotherapy, Applied Radiation and Isotopes 52: pp. 63 – 68, (2000).
[23] HEUFT-DORENBOSCH, L.L.J., DE VET, H.C.W., VAN DER LINDEN, S., Yttrium radiosynoviortheses in the treatment of knee arthritis in rheumatoid arthritis: A systematic review, Ann. Rheum. Diss. 59 (2000) 583–586.
[24] KAMPEN, W.U., BRENNER, W., CZECH, N., HENZE, E., Intraarticular application of unsealed beta-emitting radionuclides in the treatment course of inflammatory joint diseases, Curr. Med. Chem. Anti-inflamatory & Anti-allergy Agents 1 (2002) 77–87.
[25] VUORELA, J., SOKKA, T., PUKKALA, E., HANNONEN, P., Does Yttrium radiosynovectomy increase the risk of cancer in patients with rheumatoid arthritis?, Ann. Rheum. Dis. 62: pp. 251 – 253, (2003).
[26] EUROPEAN ASSOCIATION OF NUCLEAR MEDICINE, EANM procedure guidelines for radiosynovectomy, Eur. J. Nucl. Med. BP12 – PB16 Vol . 30, No. 3, March (2003).
[27] ERSELCAN, T., et al., Lypoma arborescens; successfully treated by Yttrium-90 radiosynovectomy, Annals of Nuclear Medicine, Vol. 17, No. 7, pp. 593 – 596, (2003).
[28] SILVA, M., LUCK, J.V., LLINÁS, A., Chronic hemophilic synovitis: the role of radiosynovectomy, Treatment of Hemophilia, 33, April (2004).
[29] MÄKELÄLA, O., et al., Experimental radiation synovectomy in rabbit knee with holmium-166 ferric hydroxide macroaggregate, Nucl. Med. Biol. 29 (2002) 593–598.
[30] WANG, S.-J., et al., Histologic study of effects of radiation synovectomy with rhenium-188 microsphere, Nucl. Med. Biol. 28 (2001) 727–732.

[31] UNNI, P.R., CHAUDHARI, P.R., VENKATESH, M., RAMAMOORTHY, N., PILLAI, M.R.A., Preparation and bioevaluation of ^{166}Ho labelled hydroxyapatite (HA) particles for radiosynovectomy, Nucl. Med. Biol. 29 (2002) 199–209.

[32] MÁTHÉ, D., et al., Preliminary studies with 188Rhenium-tin colloid for radiation synovectomy: preparation, size determination, in-vivo distribution, effects and dosimetry studies, Nuclear Medicine Review Vol 5., No 2., (2002)

TARGETED RADIOTHERAPY WITH ALPHA PARTICLE EMITTING RADIONUCLIDES

M.R. ZALUTSKY, O.R. POZZI, G. VAIDYANATHAN
Department of Radiology, Duke University Medical Center,
Durham, North Carolina,
United States of America
Email: zalut001@mc.duke.edu

Abstract

One of the most important considerations in the development of radiopharmaceuticals for the targeted radiotherapy of cancers is the selection of the type of radiation emitted during the decay of the radionuclide. Alpha particle emitters have emerged as a promising approach for certain clinical applications such as compartmentally spread disease and neoplasms present in the blood. An attractive feature of radionuclides decaying by the emission of α particles is that they offer the prospect of matching the cell specific reactivity of targeting vehicles, such as receptor avid peptides and monoclonal antibodies, with radiation with a range of only a few cell diameters. In addition, α particles have important radiobiological advantages when compared with conventional external beam radiotherapy and β particles including a more potent cytotoxic effectiveness, with sterilizing potential nearly independent of oxygen concentration, dose rate and cell cycle position. This review summarizes the current status of targeted radiotherapy with α particle emitting radionuclides. Because they have reached the stage of clinical investigation, monoclonal antibodies labelled with the promising α particle emitting radionuclides ^{213}Bi, ^{225}Ac and ^{211}At will be highlighted.

1. INTRODUCTION

Targeted radiotherapy involves the use of a molecular carrier such as a receptor avid compound or an antibody to deliver a radionuclide to malignant cell populations. This emerging therapeutic strategy has a number of potential advantages that compensate for its relatively complex nature. Compared with conventional external beam radiation treatment, targeted radionuclide therapy offers the prospect of delivering lethal radiation doses to tumour cells more selectively while leaving neighbouring normal cells intact. Unlike conceptually similar targeted therapeutics employing toxins or chemotherapeutics as the cytotoxic agent, radionuclides do not require intracellular localization to be effective. Indeed, one of the attractions of radionuclide therapy is the existence

of radiation with quite different dimensions of effectiveness, ranging from subcellular (Auger electrons) to hundreds of cell diameters (β particles). One of the attractive features of α particles for targeted radiotherapy is their intermediate tissue range equivalent to only a few cell diameters. As a consquence of this property, as well as the radiobiological advantages discussed in the next section, interest in the utilization of α particle emitters for targeted radiotherapy has blossomed [1, 2].

Although the potential utility of α particle emitters for targeted radiotherapy has been appreciated for many years, translation of this concept into the clinical domain has been slow. Many of the reasons for this are in the realm of radiopharmaceutical chemistry. One problem has been the poor availability of α particle emitters with radionuclide decay and chemical properties that have practical potential for cancer treatment. Another is the need for labelling methods that provide sufficient stability in the in vivo environment to be suitable for patient studies. This is a major challenge for radionuclides with multiple α particle emitting progeny because each has its own chemical behaviour. Finally, an important consideration for therapeutic radiopharmaceutical chemistry that is particularly relevant for α particle emitters is the potentially deleterious effects of radiolysis on both labelling chemistry and product stability.

2. RATIONALE FOR ALPHA EMITTERS

The best utilization of targeted radionuclide therapy is problably not for the treatment of large tumours, which might be best treated by conventional approaches, but rather, in minimal residual disease settings in which cancerous deposits are small, perhaps even subclinical [3]. For this reason, radiations which are well matched to the dimensions of micrometastatic disease might be of particular value. In that regard, Humm [4] compared the fraction of decay energy that would be deposited in spherical tumours for a high energy β emitter (^{90}Y), a low energy β emitter (^{131}I) and an β emitter (^{211}At). In 1000 μm diameter tumours, the calculated absorbed fractions were 0.097, 0.54 and ~0.9, for the particulate emissions of ^{90}Y, ^{131}I and ^{211}At, respectively; for 200 μm diameter lesions, absorbed fractions of 0.015, 0.17 and ~0.5 were calculated. Extrapolating to single cell conditions, which are found in diseases such as neoplastic meningitis, the calculated energy deposition advantage for ^{211}At compared with ^{90}Y is about one thousand [5].

An important consequence of the relatively short range of α particles is that this characteristic, in combination with their high energy (4–9 MeV for the radionuclides of interest for targeted radiotherapy), imparts a high linear

energy transfer (LET) quality to this radiation. Yttrium-90 emits high energy β particles that have a mean LET of about 0.2 keV/μm; in comparison, the LET of clinically relevant α particle emitters is several orders of magnitude higher, about 100 keV/μm. The radiobiological implications of high LET radiation are perhaps the most compelling rationale for pursuing α particle emitters for therapy [6]. Of primary importance is the fact that the relative biological effectiveness of high LET α particles is considerably higher than β particles or standard external beam radiation. Radiation at 100 keV/μm is particularly cytotoxic because the distance between ionizing events at this LET is nearly identical to that between DNA strands, increasing the probability of creating highly cytotoxic double DNA strand breaks. The predicted exquisite cytotoxicity of targeted α particle emitting radiopharmaceuticals has been validated experimentally with a variety of radionuclides, carrier molecules and human cancer cell lines [7]. In addition, the conditions under which high LET radiation is maximally effective are relatively wide ranging, not being compromised by a lack of oxygen, cell cycle stage or dose rate.

3. ALPHA PARTICLE EMITTING RADIONUCLIDES

Even though more than 100 α particle emitting radionuclides exist, to date, less than 10 of them have received serious attention for targeted radiotherapy applications. This can be attributed in part to the fact that most α particle emitters are part of natural decay chains with multiple progeny radionuclides, necessitating the development of strategies that can compensate for the often divergent chemical behaviour of the radioactive parent and progeny. To date, the α particle emitters that have been utilized for clinical investigations include 45.6 min ^{213}Bi, 7.2 h ^{211}At and 11.4 d ^{223}Ra, while 61 min ^{212}Bi, 4.2 h ^{149}Tb and 10 d ^{225}Ac have been explored in cell culture and animal models of human cancer, and clinical studies with ^{225}Ac are commencing. The physical properties of these radionuclides and their radioactive progeny are summarized in Table 1.

The α particle emitters under investigation fall into two general groups – those with half-lives of about 1–7 h and emitting about 1 α particle per decay (^{213}Bi, ^{211}At, ^{212}Bi and ^{149}Tb) and those which are part of natural decay chains with half-lives of about 10 d and emitting multiple α particles per decay (^{223}Ra and ^{225}Ac). The first group presents practical problems with regard to radionuclide supply to locations distant from the site of production, time available for radiopharmaceutical synthesis and adaptability to the exigencies of administering therapeutics to cancer patients. The main problem with the second group is in devising strategies that will maximize the probability that all of the

TABLE 1. ALPHA PARTICLE EMITTING RADIONUCLIDES FOR TARGETED RADIOTHERAPY

Radionuclide	Progeny	Half-life	α particle energy (MeV)	Yield per 100 decays
^{149}Tb		4.15 h	3.97	17
^{211}At		7.21 h	5.87	42
	^{211}Po	516 msec	7.44	58
^{212}Bi		61 min	6.05	36
	^{212}Po	298 nsec	8.78	64
^{213}Bi		45.6 min	5.84	36
	^{213}Po	4.2 μsec	8.38	64
^{225}Ac		10 d	5.75	100
	^{221}Fr	4.9 min	6.36	100
	^{217} At	32.3 msec	7.07	100
	^{213}Bi	45.6 min	5.84	2
	^{213}Po	4.2 μsec	8.38	98
^{223}Ra		11.4 d	5.64	100
	^{219}Rn	4.0 sec	6.75	100
	^{215}Po	1.78 msec	7.39	100
	^{211}Pb	36.1 min	1.37(â)	
	^{211}Bi	2.17 min	6.55	100

radionuclide progeny decay in close proximity to the originally targeted tumour cells and do not migrate to normal organs, causing significant toxicities.

A wide variety of molecular carriers have been investigated for use in tandem with α particle emitting radionuclides, including monoclonal antibodies, peptides, bone seeking complexes as well as receptor and transporter avid molecules. As with all types of radiopharmaceutical development, the selection of the radionuclide must take into account the pharmacokinetics of the carrier molecule. Monoclonal antibodies have been the most widely investigated tumour targeting vehicle; however, as noted above, none of the α particle emitters currently under investigation has a half-life in the range of 1–2 d, which would be best suited to the pharmacokinetics of antibody molecules. As noted below, this has lead investigators to focus on clinical settings, such as compartmental administration or tumours in the blood, where more rapid delivery of the labelled antibody to malignant cells can be accomplished.

4. TERBIUM-149

One of the least explored α particle emitting radionuclides is ^{149}Tb, which was first proposed for therapeutic applications by Allen and Blagojevic 10 years ago [8]. A significant limitation of this 4.15 h half-life radiolanthanide is that α particle emission is associated with only 17% of its decays. A potential problem is that with such a low α particle yield, effective killing of cancer cells will require the targeting of a molecule expressed at a high density because of limitations in the specific activity of the labelled molecule that can be produced by current chemistries.

An additional shortcoming of ^{149}Tb for targeted radiotherapy is limited radionuclide availabilty. Terbium-149 has been produced at the ISOLDE isotope separator facility at CERN using a tantalum foil target irradiated with 1.0 or 1.4 GeV protons [9]. After surface ionization and collection of the A = 149 isobars, the ^{149}Tb was isolated in nearly 100% radionuclidic purity. A variety of antibodies has been labelled successfully in high yield with ^{149}Tb using the SCN-CHX-A'-DTPA bifunctional chelate via procedures adapted from those originally developed for other radiometals and these immunoconjugates have been shown to be cytotoxic to human cancer cells in vitro [2].

Two recent papers have explored the therapeutic potential of ^{149}Tb labelled mAbs in both cell culture and murine models of human cancers. The first involved labelling of a truly tumour specific antibody, d9, which binds specifically to the mutated delta form of the E-cadherin molecule [10]. This mutated molecular target is found only on cancer cells such as diffuse type gastric cancers but not on normal tissues. The d9 mAb was labelled with ^{149}Tb via SCN-CHX-A'-DTPA in nearly quantitative yield with an immunoreactive fraction of about 30% and a specific activity of about 100 MBq per mg. The ^{149}Tb labelled d9 immunoconjugate was able to inhibit the proliferation by 50% of tumour cells expressing the d9 mutant target at an activity concentration of 444 kBq/mL. However, there were two negative aspects to this study. Killing of cells expressing the wild type E-cadherin molecule (i.e. those not expressing the d9 molecular target) were killed just as efficiently, suggesting that the cytotoxic effect was non-specific. Furthermore, even with high activity concentrations of ^{149}Tb labelled d9 mAb, cell survival could not be reduced below about 20% suggesting that antigen saturation occurred prior to the achievement of total cell kill.

The therapeutic potential of ^{149}Tb labelled Rituximab® has also been evaluated. This is the same anti-CD20 chimeric mAb that when labelled with ^{90}Y is utilized for the treatment of patients with lymphoma. Groups of SCID mice (n = 4–9) received 5×10^6 Daudi leukemia cells and only 2 d later were treated with: 5 µg Rituximab, 300 µg Rituximab, 5 µg Rituximab labelled with

5.55 MBq ^{149}Tb, or saline control [11]. At 120 d, tumour free survival was observed in all but one animal receiving the labelled mAb but none of the animals receiving cold mAb or vehicle alone. Although these results at first glance appear to be encouraging, this interpretation must be made with caution. Treatment only two days after injection of tumour cells presents a rather favourable model in which problems related to homogeneous delivery of radionuclide are minimized. Additionally, particularly for a model of this type, the most critical control was not performed, namely, a ^{149}Tb labelled non-specific control mAb.

In summary, the principal attractions of ^{149}Tb as an α particle emitter for targeted radiotherapy are its 4.15 h half-life, which could be a good match for smaller molecular weight tumour avid compounds, as well as its adaptability to radiochemistries already developed for other radiometals such as ^{90}Y and ^{177}Lu. On the other hand, the limited availablity of ^{149}Tb and its low α particle abundance are signficant disadvantages. Finally, the lack of compelling evidence that specific and selective tumour cell kill can be achieved with a ^{149}Tb labelled molecule is also of concern.

5. RADIUM-223

Radium-223 is a naturally occurring radionuclide that is derived from the decay of ^{235}U. The decay properties of 11.4 d half-life ^{223}Ra as well as those of its principal progeny are summarized in Table 1. From a commercial perspective, the long half-life of ^{223}Ra is a significant advantage because it facilitates distribution and, provided radiolysis associated problems can be avoided, allows for a longer product shelf life. However, it presents a major challenge to the radiopharmaceutical chemist because strategies must be devised to trap the ^{223}Ra labelled therapeutic and its radioactive progeny at the tumour site for prolonged time periods in order to maximize tumour dose and minimize toxicity to normal tissues.

For radiopharmaceutical purposes, the optimal method of supplying ^{223}Ra is from a generator with 21.8 y ^{227}Ac serving as the radionuclide parent. The ^{227}Ac is produced in a reactor by irradiation of ^{226}Ra, which produces ^{227}Ra, which in turn decays to the desired ^{227}Ac. The ^{227}Ac undergoes β decay to 18.7 d ^{227}Th, which decays by α particle emission to ^{223}Ra. An efficient generator system has been developed by Algeta (Oslo, Norway) [12]. The ^{227}Ac and ^{227}Th are immobilized on an actinide selective resin and the ^{223}Ra is isolated as $^{223}RaCl_2$.

With the exception of a study using sterically stabilized liposomes as a carrier system for entrapping ^{223}Ra [13], the main focus of endoradiothera-

peutic efforts with ^{223}Ra has involved exploiting the natural affinity of radium for bone for the treatment of skeletal metastases. An α emitter could be ideal for this type of clinical application because the shorter particle range, compared with β emitters, should greatly increase the capability of delivering high radiation doses to bone metastases while minimizing excessive dose to radiation sensitive bone marrow, which otherwise could be dose limiting.

Because ^{89}Sr was used routinely in the past as a bone seeking radiopharmaceutical, the biodistribution and radiation dosimetry of ^{223}Ra has been compared to that of ^{89}Sr, with both being administered as their chloride salts [14]. The uptake of ^{223}Ra in the bone was significantly higher than that of ^{89}Sr, reaching a level of 40% injected dose per gram in the femur at 24 h post-injection. Importantly, no significant decline in bone retention was seen over the course of the 14 d experiment and redistribution of progeny from the bone was quite small. Accumulation of ^{223}Ra was also observed in soft tissues, particularly the spleen and the kidneys. However, femur:soft tissue radiation dose ratios were extremely favourable, generally greater than 1000:1. Dosimetry calculations modelled dose to bone and bone marrow and indicated that ^{223}Ra should offer significant advantages compared with ^{89}Sr with regard to minimizing bone marrow radiation dose.

Preclinical evaluation of ^{223}Ra has also been performed in rats including those with skeletal metastases [15]. Initital studies confirmed the bone seeking properties of the radiopharmaceutical, with femur:kidney, femur:liver and femur:spleen ratios of 590:1, 620:1 and 810:1 observed 24 h after injection. The femur:bone marrow ratio increased from 6.5:1 at 24 h to >15:1 at 14 d. For the therapy studies, rats were injected with 1×10^6 MT-1 human breast cancer cells into the left ventricle and then treated one week later. Control animals had to be killed 20–30 d later because of tumour induced paralysis while 36 or 40% of rats receiving 10 or 11 kBq ^{223}Ra had significantly longer symptom free survival over the 67 d follow-up period. No sign of bone marrow toxicity was observed, indicating that this radiopharmaceutical warranted evaluation as an endoradiotherapeutic in cancer patients.

Recently, the results of the first clinical trial of ^{223}Ra in patients with skeletal metastases were reported [16]. In this phase I trial, 25 patients (10 breast cancer, 15 prostate cancer) were treated in cohorts of five patients at doses of 46, 93, 163, 213 or 250 kBq per kg body weight. The labelled compound was well tolerated with myelosuppression being mild and reversible. No dose limiting toxicites were observed at any dose level. Median survival for the 25 patients was greater than 20 months which is encouraging; however, the lack of a control group makes it difficult to draw meaningful conclusions about the survival benefit of this treatment. Such a comparison will be done in due

course, in a phase II randomized trial in prostate cancer patients with bone metastases [16].

6. BISMUTH-213

Bismuth-213 has a 45.6 min half-life and α particle emission is associated with each of its decays, either directly to 2.2 min ^{209}Tl (2%) or after β decay to 4.2 μsec ^{213}Po (98%), followed by α emission to 3.25 h ^{209}Pb. A radionuclide generator system for supplying ^{213}Bi has been developed using 10 d ^{225}Ac as the parent. The system has been scaled up and optimized so that it is capable of providing clinical dose levels of ^{213}Bi [17, 18]. The generator is based on an AGMP-50 column that is eluted with 0.1M HCl/NaI and is a reasonable source of ^{213}Bi provided that the ^{225}Ac parent is available at a reasonable cost.

A variety of tumour specific mAbs and fragments have been labelled with ^{213}Bi, with the labelling most frequently being accomplished via the bifunctional *trans*-cyclohexyldiethlenetriaminepentaacetic acid SCN-CHXA'-DTPA chelator. For example, the anti-prostate specific membrane antigen (PSMA) mAb J591 was labelled with ^{213}Bi and demonstrated to be highly effective in killing human prostate carcinoma cells grown in culture, as tumour spheroids and as subcutaneous tumour xenografts grown in athymic mice [19, 20]. Intraperitoneal injection of a ^{213}Bi labelled mAb reactive with a tumour specific mutant E-cadherin molecule was reported to be effective in treating a peritoneally spread gastric cancer in mice [21]. Other types of application involving ^{213}Bi labelled antibodies or fragments have been directed at fungal infections [22] and bone marrow conditioning prior to transplantation [23, 24]. Strategies to compensate for the short half-life of this radionuclide are vital to the use of ^{213}Bi and in that regard, pretargeting [25] and use of small scFv fragments [26] have been investigated.

The first α emitting radiotherapeutic to be evaluated in a clinical trial was ^{213}Bi labelled HuM195, a humanized mAb that binds to the anti-CD33 antigen that is over expressed on human leukemia cells [27]. Gamma camera imaging documented the rapid uptake of ^{213}Bi activity in liver and spleen, which also express the target antigen. A phase I trial was performed on 18 patients with relapsed and refractory acute myelogenous leukemia or chronic myelomonocytic leukemia. The patients received 3–7 doses of ^{213}Bi labelled HuM195 at total administered activities ranging from 602 to 3515 MBq [28]. The ratios of radiation absorbed dose to potential sites of tumour (bone marrow, liver and spleen) and whole body were about three orders of magnitude higher than those observed in previous trials when β emitting radionuclides were used. Large leukemia volume reductions were achieved in many patients; however,

no complete remissions were observed. Nonetheless, this study demonstrated that α particle endoradiotherapy in patients is a feasible treatment approach.

7. ACTINIUM-225

A number of significant problems result from the short half-life of ^{213}Bi and these have decreased enthusiasm for using this radionuclide for targeted radiotherapy. First, delivery of the ^{213}Bi labelled radiopharmaceutical to the tumour must be accomplished very rapidly in order to achieve acceptable tumour-to-normal organ radiation absorbed dose ratios. Second, decay during radionuclide purification, radiopharmaceutical synthesis and transport of the labelled compound to the clinic drastically decreases the activity available for use. This has lead investigators to seek alternative radiometal α particle emitting radionuclides and 10 d ^{225}Ac has emerged as a promising α emitter for radioimmunotherapeutic applications. A radionuclide generator has been developed for supplying ^{225}Ac from a ^{229}Th parent following a two column based purification procedure [29].

As shown in Table 1, four α particles are produced as a consequence of each ^{225}Ac decay, which could lead to very effective cell killing, provided that all of the decays occurred within the tumour. However, accomplishing this will be a formidable challenge because of the different chemical characteristics of all the ^{225}Ac progeny. A ligand system that can be utilized to form actinium mAb complexes that are stable under in vivo conditions has yet to be identified [30–32]. Furthermore, the ligand must form chemically stable complexes with all of the ^{225}Ac progeny [33], which include radionuclides of francium, astatine and bismuth — elements with diverse chemistries. An additional daunting problem is that the energy of the α particle recoil nuclei is sufficient to break chemical bonds in the progeny radionuclide complexes, releasing these radionuclides into the circulation.

An innovative tactic for minimizing the problems noted above relies on the use of receptor or antigens that are rapidly internalized into tumour cells as molecular targets for ^{225}Ac labelled radiopharmaceuticals [34, 35]. With this strategy, the egress of the progeny radionuclides from the initial site of ^{225}Ac localization might be reduced because even if they dissociated from the chelate, they could be trapped within the tumour cell because of their charge. Using a DOTA bifunctional macrocycle to accomplish initial ^{225}Ac labelling, promising therapeutic responses have been obtained with several internalizing mAbs in various murine xenograft models.

Concern exists about utilization of this strategy in patients because in most cases only a small fraction (<5%) of the injected dose of radiopharmaceu-

tical localizes in tumour. Thus, release and redistribution of progeny radionuclides could occur after the vast majority of ^{225}Ac decays which do not take place inside cancer cells. Recently, the toxicity and pharmacokinetics of ^{225}Ac labelled Hu195, an mAb reactive with the CD33 molecule found on human leukemias, were evaluated in cynomolgus monkeys [36]. The main toxic effect that was observed was damage to the renal tubules and the labelled mAb was deemed to be safe at a dose of 28 kBq/kg. Investigational new drug approval was obtained by the Sloan Kettering group for a phase I clinical trial of ^{225}Ac labelled Hu195 in patients with leukemia.

8. ASTATINE-211

Astatine-211 has many attractive characteristics for targeted α particle radiotherapy and has been the radionuclide of choice for this purpose in the authors' laboratory. Their rationale for this perspective is that ^{211}At has a half-life (7.2 h) that is long enough for multistep synthetic procedures and is also compatible with the pharmacokinetics of a wide range of molecules, including peptides, mAbs and small organic molecules. Each decay of ^{211}At yields an α particle, either by direct α emission to ^{207}Bi (42%), or by electron capture decay to 520 msec ^{211}Po (58%) followed by α emission (Table 1). An important practical consequence of the electron capture branch, which results in the emission of 77–92 keV polonium X rays, is that ^{211}At distribution can be determined in animals or patients using either conventional nuclear medicine planar or single photon emission tomographic imaging devices [37, 38].

Astatine-211 is most frequently produced by cyclotron bombardment of natural bismuth metal targets with α particles via the ^{209}Bi(α,2n)^{211}At reaction. Particularly for clinical radiotherapy applications, it is critical to utilize an incident α particle energy that minimizes the production of 8.1 h ^{210}At, a radionuclide that decays to ^{210}Po, a 138 d α emitter that could cause bone marrow toxicity. For this reason, incident beam energies for ^{211}At production are generally kept below 29 MeV. Separation of ^{211}At from the bismuth metal target is generally accomplished using a variety of modifications of the dry distillation procedure described by Friedman et al. [39]. Internal cyclotron target systems have been developed that permit the production of clinically useful levels of ^{211}At [40]. Using this type of target, the authors have been able to produce 6.6 GBq of ^{211}At after a 4 h irradiation with a 55 μA beam of 28 MeV α particles [41].

Because astatine is a halogen, radioiodination methods can often be adapted for use with ^{211}At; however, an important exception is protein and peptide labelling by electrophilic radiohalogenation of constituent tyrosine

residues. The most common tactic for labelling biomolecules with ^{211}At is via an astatodemetallation reaction and a wide variety of ^{211}At labelled molecules have been synthesized and evaluated as potential targeted radiotherapeutics [7]. The authors' own efforts in the small molecule arena have included ^{211}At labelled *meta*-iodobenzylguanidine analogues, biotin conjugates, peptides, bisphosphonates and thymidine analogues [7]. By far the most active area of research both at the authors' institution and elsewhere has been in evaluation of ^{211}At labelled mAbs and mAb fragments as α particle emitting targeted radiotherapeutics. Promising results have been obtained with ^{211}At labelled immunoconjugates directed at many types of cancer including brain, ovarian, osteosarcoma, melanoma and non-Hodgkins lymphoma [42–48]. A clinical trial of ^{211}At labelled chimeric 81C6 mAb administered directly into surgically created tumour resection cavities is currently under way at the authors' institution and the results thus far have been very encouraging [49].

9. CONCLUSIONS

Targeted radiotherapy with α particle emitting radionuclides is an attractive approach for cancer therapy. Recent studies at several institutions have documented the feasibility of this approach in patients. Ongoing research in radionuclide production and radiochemistry, as well as in tumour and molecular biology, should further advance the field and perhaps ultimately lead to radiopharmaceuticals that are both highly effective and practical.

ACKNOWLEDGEMENTS

Work performed in the authors' laboratory was supported by grants from the National Institutes of Health and the US Department of Energy.

REFERENCES

[1] MCDEVITT, M.R., et al., Radioimmunotherapy with alpha-emitting nuclides. Eur. J. Nucl. Med. **25** (1998) 1341.

[2] BEYER, G.J., et al., In vitro and preclinical targeted alpha therapy for melanoma, breast, prostate and colorectal cancers. Critical Rev. Oncol. Hematol. **39** (2001) 139.

[3] SAUTTER-BIHL, M.-L., et al., Minimal residual disease: a target for radioimmunotherapy with ^{131}I-labeled monoclonal antibodies? Some dosimetric considerations. Recent Results Cancer Res. **141** (1996) 67

[4] HUMM, J.L., Dosimetric aspects of radiolabeled antibodies for tumor therapy. J. Nucl. Med. **27** (1986) 1490

[5] HUMM, J.L., A microdosimetric model of astatine-211 labeled antibodies for radioimmunotherapy. Int. J. Radiat. Oncol. Biol. Phys. **13** (1987) 1767.

[6] HALL, E.J., Radiobiology for the Radiologist 5th edition. J. B. Lippincott, Williams, and Wilkins, Philadelphia (2000).

[7] ZALUTSKY, M.R., VAIDYANATHAN, G. Astatine-211-labeled radiotherapeutics: an emerging approach to targeted alpha particle therapy. Current Pharm. Design 6 (2000) 1433.

[8] ALLEN, B.J., BLAGOJEVIC, N., Alpha and beta emitting radiolanthanides in targeted cancer therapy: the potential tole of Terbium-149. Nucl. Med. Comm. **17** (1996) 40.

[9] BEYER, G.J., Radioactive ion beams for biomedical research and application. Hyperfine Interact. **129** (2000) 529.

[10] MIEDERER, M., et al., Comparison of the radiotoxicity of two alpha-particle-emitting immunoconjugates, terbium-149 and bismuth-214, directed against a tumor-specific, exon 9 deleted (d9) E-cadherin adhesion protein. Radiation Res. **159** (2003) 612.

[11] BEYER, G.J., et al., Targeted alpha particle therapy in vivo: direct evidence for single cancer cell kill using ^{149}Tb-rituximab. Eur. J. Nucl. Med. Mol. Imaging **31** (2004) 547.

[12] HENRIKSEN, G., et al., ^{223}Ra for endoradiotherapeutic applications prepared from an immobilized ^{227}Ac/^{227}Th source. Radiochim. Acta **89** (2001) 66.

[13] HENRIKSEN, G., et al., Sterically stabilized liposomes as a carrier for α-emitting radium and actinium radionuclides. Nucl. Med. Biol. **31** (2004) 441.

[14] HENRIKSEN, G., et al., Targeting of osseous sites with α-emitting ^{223}Ra: comparison with the β-emitter ^{89}Sr in mice. J. Nucl. Med. **44** (2003) 252.

[15] HENRIKSEN, G., et al., Significant antitumor effect from bone-seeking α-particle-emitting ^{223}Ra demonstrated in an experimental skeletal metastases model. Cancer Res. **62** (2002) 3120.

[16] NILSSON, S., et al., First clinical experience with α-emitting radium-223 in the treatment of skeletal metastases. Clin. Cancer Res. **11** (2005) 4451.

[17] MCDEVITT, M.R., et al., Preparation of α-emitting ^{213}Bi-labeled antibody constructs for clinical use. J. Nucl. Med. **40** (1999) 1722.

[18] MA, D., et al., Breakthrough of ^{225}Ac and its radionuclide daughters from an ^{225}Ac/^{213}Bi generator: development of new methods, quantitative characterization, and implications for clinical use. Appl. Radiat. Isotop. **55** (2001) 667.

[19] MCDEVITT, M.R., et al., An alpha-particle emitting antibody ([^{213}Bi]J591) for radioimmunotherapy of prostate cancer. Cancer Res. **60** (2000) 6095.

[20] BALLANGRUD, A.M., et al., Response of LNCaP spheroids after treatment with an α-particle emitter (^{213}Bi)-labeled anti-prostate-specific membrane antigen antibody (J591). Cancer Res. **61** (2001) 2008.

[21] SENEKOWITSCH-SCHMIDTKE, R., et al., Highly specific tumor binding of a ^{213}Bi-labeled monoclonal antibody against mutant E-cadherin suggests its usefulness for locoregional alpha-radioimmunotherapy of diffuse-type gastric cancer. Cancer Res. **61** (2001) 2804.

[22] DADACHOVA, E., et al., Ionizing radiation delivered by specific antibody is therapeutic against a fungal infection. Proc. Natl. Acad. Sci. USA **100** (2003) 10942.

[23] BETHGE, W.A., et al., Selective T-cell ablation with bismuth-213-labeled anti-TCRalphabeta as nonmyeloablative conditioning for allogeneic canine marrow transplantation. Blood **101** (2003) 5068.

[24] SANDMAIER, B.M., et al., Bismuth 213-labeled anti-CD45 radioimmunoconjugate to condition dogs for nonmyeloablative allogeneic marrow grafts. Blood **100 (**2002) 318.

[25] ZHANG, M., et al., Pretargeting radioimmunotherapy of a murine model of adult T-cell leukemia with the alpha-emitting radionuclide, bismuth 213. Blood **100 (**2002) 208.

[26] ADAMS, G.P., et al., Delivery of the alpha-emitting radioisotope bismuth-213 to solid tumors via single-chain Fv and diabody molecules. Nucl. Med. Biol. **27** (2000) 339.

[27] SGOUROS, G., et al., Pharmacokinetics and dosimetry of an alpha-particle emitter labeled antibody: ^{213}Bi-HuM195 (anti-CD33) in patients with leukemia. J. Nucl. Med. **40** (1999) 1935.

[28] JURCIC, J.G., et al., Targeted alpha particle immunotherapy for myeloid leukemia. Blood **100** (2002) 1233.

[29] GEERLINGS, M.W., et al., The feasibility of ^{225}Ac as a source of alpha-particles in radioimmunotherapy. Nucl. Med. Comm. **14** (1993) 121.

[30] DAVIS, I.A., et al., Comparison of ^{225}actinium chelates: tissue distribution and radiotoxicity. Nucl. Med. Biol. **26** (1999) 581.

[31] CHAPPELL, L.L., et al., Synthesis, conjugation, and radiolabeling of a novel bifunctional chelating agent for ^{225}Ac radioimmunotherapy applications. Bioconj. Chem. **11** (2000) 510.

[32] KENNEL, S.J., et al., Evaluation of ^{225}Ac for vascular targeted radioimmunotherapy of lung tumors. Cancer Biother. Radiopharm. **15** (2000) 235.

[33] KENNEL, S.J., et al., Actinium-225 conjugates of MAb CC49 and humanized delta CH2CC49. Cancer Biother. Radiopharm. **17** (2002) 219.

[34] MCDEVITT, M.R., et al., Tumor therapy with targeted atomic nanogenerators. Science **294** (2001) 1537.

[35] BORCHARDT, P.E., et al., Targeted actinium-225 in vivo generators for therapy of ovarian cancer. Cancer Res. 6**3** (2003) 5084.

[36] MIEDERER, M., et al., Pharmacokinetics, dosimetry, and toxicity of the targetable atomic generator, ^{225}Ac-HuM195, in nonhuman primates. J. Nucl. Med. **45** (2004) 129.
[37] TURKINGTON, T.G., et al., Measuring astatine-211 distributions with SPECT. Phys. Med. Biol. **38** (1993) 1121.
[38] JOHNSON, E.L., et al., Quantitation of ^{211}At in small volumes for evaluation of targeted radiotherapy in animal models. Nucl. Med. Biol. **22** (1995) 45.
[39] FRIEDMAN, A.M., et al., Preparation of a biologically stable and immunogenically competent astatinated protein. Int. J. Nucl. Med. Biol. **4** (1977) 219.
[40] LARSEN, R.H., et al., Evaluation of an internal cyclotron target for the production of astatine-211 via the ^{209}Bi(α,2n)^{211}At reaction. Appl. Radiat. Isotop. **47** (1996) 135.
[41] ZALUTSKY, M.R., et al., High-level production of alpha-particle-emitting ^{211}At and preparation of ^{211}At-labeled antibodies for clinical use. J. Nucl. Med. **42** (2001) 1508.
[42] YORDANOV, A.T., et al., Preparation and in vivo evaluation of linkers for ^{211}At labeling of humanized anti-Tac. Nucl. Med. Biol. **28** (2001) 845.
[43] AURLIEN, E., et al., Radiation doses to non-Hodgkin's lymphoma cells and normal bone marrow exposed in vitro. Comparison of an alpha-emitting radioimmunoconjugate and external gamma-irradiation. Int. J. Radiat. Biol. **78** (2002) 133.
[44] AURLIEN, E., et al., Exposure of human osteosarcoma and bone marrow cells to tumour-targeted alpha-particles and gamma-irradiation: analysis of cell survival and microdosimetry. Int. J. Radiat. Biol. **76** (2000) 1129.
[45] LARSEN, R.H., et al., The cytotoxicity and microdosimetry of astatine-211-labeled chimeric monoclonal antibodies in human glioma and melanoma cells in vitro. Radiat. Res. **149** (1998) 155.
[46] ANDERSSON, H., et al., Astatine-211-labeled antibodies for treatment of disseminated ovarian cancer: an overview of results in an ovarian tumor model. Clin. Cancer Res. **9** (suppl) (2003) 3914S.
[47] KENNEL, S.J., et al., Vascular-targeted radioimmunotherapy with the alpha-particle emitter ^{211}At. Radiat. Res. **157** (2002) 633.
[48] AKABANI, G., et al., Vascular targeted endoradiotherapy using alpha-particle emitting compounds: theoretical analysis. Int. J. Radiat. Oncol. Biol. Phys. **54** (2002) 1259.
[49] ZALUTSKY, M.R., et al., Astatine-211 labeled human/mouse chimeric anti-tenascin monoclonal antibody via surgically created resection cavities for patients with recurrent glioma: Phase I study. Neuro-Oncol. **4** (2002) S103 (abstract).

DOTA-TYR3-OCTREOTATE LABELLED WITH ^{177}Lu AND ^{131}I
A comparative evaluation

V. LUNGU*, D. NICULAE*, D. CHIPER*, M. RADU**

*Radiopharmaceuticals and Labelled Compounds Department
Email: vlungu2000@yahoo.com

** Nuclear Medicine Department
"Horia Hulubei" National Institute for Physics and Nuclear Engineering

Bucharest, Romania

Abstract

The chemical structure of somatostatin receptor ligand 1,4,7,10-tetraazacyclododecane-N,N',N'',N'''-tetraacetic acid-Tyr3-octreotate (DOTA-Tyr3-TATE), provides the means for radiolabelling with halogen, by electrophilic substitution, to the Tyr3 residue and with metal, by a coordination mechanism, to the DOTA chelator. In this study, the DOTA-Tyr3-TATE was radiolabelled with ^{177}Lu and ^{131}I of high radiochemical purity and specific activity. The in vitro study regarding the competitive and the saturation binding assays were performed using rat brain cortex membrane. The IC_{50} value was determined as 4.74nM for ^{nat}Lu-DOTA-Tyr3-TATE and the K_d value was 142.8pM for ^{177}Lu-DOTA-Tyr3-TATE. The biodistribution data of ^{177}Lu-DOTA-Tyr3-TATE and DOTA-^{131}I-Tyr3-TATE in HRS1 (hepato-colangiom carcinomas) tumour bearing rats, show that the ^{177}Lu-DOTA-Tyr3-TATE is more stable and has better uptake than DOTA-^{131}I-Tyr3-TATE. Furthermore, the competitive localization index of ^{177}Lu-DOTA-Tyr3-TATE is three times higher than that obtained for DOTA-^{131}I -Tyr3-TATE. The results of work based on comparative experiments suggest that ^{177}Lu-DOTA-Tyr3-TATE could be an effective targeted radiotherapy agent of SSTR tumours.

1. INTRODUCTION

There is a great interest in the radiolabelling of somatostatin analogues or their bioconjugates with the aim of developing new radiopharmaceuticals for targeted diagnosis [1–3] and therapy [4–8] of cancer as well as in vitro radioassays of somatostatin receptors. In the authors' experiments, the biological and pharmacological properties of the receptor binding sequence of

DOTA-Tyr3-TATE, after radiolabelling with ^{131}I and ^{177}Lu, were investigated. The DOTA-^{131}I-Tyr3-TATE and ^{177}Lu-DOTA-Tyr3-TATE products were studied individually and in competition.

2. MATERIALS AND METHODS

2.1. Materials

All chemicals were purchased from Fluka Chemical and Sigma Aldrich.

The $^{177}LuCl_3$ and $Na^{131}I$, with specific activities of 45 Ci/mg and 1600 Ci/mg respectively, were purchased from Nordion Canada.

DOTA-Tyr3-TATE and Sandostatin were obtained from the IAEA and from Pichem Austria.

Wistar rats (150–200 g) were used for the preparation of cortex membranes and Lewis rats were used for biodistribution studies. The HRS1 tumour bearing rats were prepared in the Institute of Oncology Bucharest, Romania.

Radioactive samples were counted on Robotron and Spectroscaler gamma counters.

2.2. Methods

2.2.1. Preparation of DOTA-^{131}I-Tyr3-TATE

Experiments were performed taking into account the regularly used therapeutic dose of 100 mCi ^{131}I and 100 μg DOTA-Tyr3-TATE; the molar ratios of DOTA-Tyr3-TATE to ^{131}I and DOTA-Tyr3-TATE to chloramine-T being 1.7 and 0.09, respectively.

The samples of DOTA-^{131}I-Tyr3-TATE with the activity of 10 mCi were prepared. The synthesis method was as follows. A solution (5–10 μL) of $Na^{131}I$ (10 mCi) was added to a solution containing 10 μg DOTA-Tyr3-TATE in 50 μL 0.01M PBS, pH7.4. To this reaction mixture 19.7 μg of chloramine-T in 20 μL 0.1M PBS were added, followed by 1–3 min stirring at room temperature. The reaction was stopped by the addition of 39.8 μg sodium methabisulphite dissolved in 10 μL 0.1M PBS. 5 mg of 3-hydroxy-4-aminobenzoic acid (HABA), for each 10 mCi DOTA-^{131}I-Tyr3-TATE, were added for mixture stabilization.

The RCP was estimated by PC and ITLC using BuOH:acetic acid:water (5:2:1) as solvent; the R_f of DOTA-^{131}I-Tyr3-TATE is 0.65–0.70, while the R_f of I^+ is 0 and R_f of I^- is 0.9–1.0. The addition of 5 mg HABA to DOTA-^{131}I-Tyr3-TATE has a scavenger effect, maintaining a high radiochemical purity of the radiocompound at 4–8ºC, up to 6 d.

2.2.2. Preparation of ^{177}Lu-DOTA-Tyr3-TATE

54 mCi $^{177}LuCl_3$ in 0.05N HCl, 45 Ci/mg specific activity, was diluted to 100 µL with 0.05N HCl .

The samples consisting of 10 µg DOTA-Tyr3-TATE in 50 µL acetate buffer 0.4M, pH4.5, were labelled with 10 mCi $^{177}LuCl_3$ in 20 µL 0.05N HCl. The vials containing the reaction mixture were incubated for 30 min at 80°C. After incubation and cooling, 5 mg of HABA, as radiolytic stabilizer, was added. The stabilizer was added after the radiolabelling process because it is subjected to a certain degree of thermal decomposition. The concentration of the stabilizer is calculated for 10 mCi ^{177}Lu-DOTA-Tyr3-TATE.

The RCP of ^{177}Lu-DOTA-Tyr3-TATE was checked by PC and ITLC using different solvents: in the 0.1M Na-citrate, pH5, the labelled peptide migrated from the origin with $R_f = 0.67$, while the free radionuclide migrated with the solvent front ($R_f = 1$); in other solvent, 10% NH_4COOCH_3:MeOH (30:70), the labelled peptide migrated to R_f 0.76–0.80 while free radionuclide remains at the origin.

2.2.3. Preparation of SST membrane receptor from rat brain cortex

Rat brain cortex membranes were prepared according to a published method [10].

2.2.4. Competition binding assays of DOTA-^{131}I-Tyr3-TATE

The competition binding assay was performed using rat brain cortex membrane (50 µg protein). 35 000–40 000 counts/min of ^{125}I-Tyr^3-octreotide (970 Ci/mM) were added in each test tube in the presence of increasing concentration of DOTA-^{nat}I-Tyr3-TATE (synthesized in the same conditions as DOTA-^{131}I-Tyr3-TATE): 0.06; 0.13; 0.34; 0.68; 1.00; 2.72; 10.00; 57.80; 100nM in total volume of 300 µL 50mM HEPES (pH7.6, 0.3% BSA, 5mM $MgCl_2$, 10µM bacitracin). The samples were incubated for 2 h at room temperature; the incubation was stopped by addition of ice cold buffer (1 mL, 10mM HEPES, 150mM NaCl, pH7.6).

The suspension was rapidly filtered over glass fibre filters (Whatman GF/B) presoaked in binding buffer using a Millipore multifiltration apparatus. The filters were rinsed with buffer (4 × 2 mL) and filter activity was measured on a NaI(Tl) gamma counter.

2.2.5. Competition binding assays of ^{177}Lu-DOTA-Tyr3-TATE

The binding affinity of ^{nat}Lu-DOTA-Tyr3-TATE was measured in rat brain cortex membrane. 20 000 counts/min of ^{125}I-Tyr^3-octreotide was displaced with the following increasing concentrations of ^{nat}Lu-DOTA-Tyr3-TATE (synthesized under the same conditions as ^{177}Lu-DOTA-Tyr3-TATE): 0.03; 0.14; 0.45; 0.70; 3.80; 12.80; 30.80; 170; 500nM. The obtained samples were processed using the same procedure (Section 2.2.4).

2.2.6. Saturation binding assays of DOTA-^{131}I-Tyr3-TATE

The saturation binding experiments of *DOTA-^{131}I-Tyr3-TATE* were performed using rat brain cortex membrane. For total binding assay, the following concentrations of DOTA-^{131}I-Tyr3-TATE were prepared: 0.06; 0.13; 0.34; 0.68; 1.00; 2.72; 10.00; 57.80; 100nM in 50 µL binding buffer, 50 µL radioligand solution of corresponding concentration and 200 µL rat brain cortex membrane homogenate containing 40 µg protein. For the non-specific series, the authors used 20 µL binding buffer plus 30 µL of unlabelled peptide as competitor (Sandostatin) (1µM in the reaction vial), instead of 50 µL buffer. The tubes were incubated for 2 h at room temperature and then binding was interrupted by rapid filtration through a glass fibre filter presoaked with the binding buffer. Filters were washed with binding buffer, dried and counted using a NaI(Tl) gamma counter.

2.2.7. Saturation binding assays of ^{177}Lu-DOTA-Tyr3-TATE

A similar method (Section 2.2.6) was used. For the experiments regarding saturation binding assay of ^{177}Lu-DOTA-Tyr3-TATE, the following concentrations of ^{177}Lu-DOTA-TATE were prepared: 0.05; 0.15; 4.5; 13.5; 40.5; 120.5; 361.5nM for total and non-specific binding assay. A method similar to that described in Section 2.2.6 was used for the processing of the obtained samples and acquisition of data.

2.2.8. Experimental animal models

The hepatom RS1 (HRS1), hepato colangiom carcinoma, was obtained as a cell culture from the Institute of Oncology, Bucharest. The solid tumour was obtained by subcutaneous injection of 10^7 cells into 5 week old female Lewis rats (150–200 g). Once the tumours had grown to ~1 cm^3, they were serially propagated by subcutaneous injection of 0.2 mL of a 20% (w/v) tumour

suspension, prepared by mincing tumours in 0.9% NaCl. Ten days prior to radiobiological studies, the following lots of HRS1 bearing rats were prepared:

(a) Lot for the biodistribution studies of ^{177}Lu- DOTA-Tyr3-TATE;
(b) Lot for the biodistribution studies of DOTA-^{131}I-Tyr3-TATE;
(c) Lot for the biodistribution competitive studies of ^{177}Lu- DOTA-Tyr3-TATE and DOTA-^{131}I-Tyr3-TATE;
(d) Lot for the biodistribution experiments of ^{177}Lu-DOTA-Tyr3-TATE and DOTA-^{131}I-Tyr3-TATE in the presence of SSTR blocking agent.

2.2.9. Biodistribution experiments of ^{177}Lu- DOTA-Tyr3-TATE and DOTA-^{131}I-Tyr3-TATE either alone or in competition

For individual biodistribution studies of ^{177}Lu- DOTA-Tyr3-TATE and DOTA-^{131}I-Tyr3-TATE, tumour bearing rats from lots (a) and (b) were IV injected with 0.2 mL radioactive solutions containing 50 µCi ^{177}Lu-DOTA-Tyr3-TATE and DOTA-^{131}I-Tyr3-TATE, respectively, corresponding to approximately 0.68 µg DOTA-Tyr3-TATE. The tumour bearing rats from lot (c), for competitive biodistribution studies, were IV injected with 35 µCi ^{177}Lu-DOTA-Tyr3-TATE and 15 µCi DOTA-^{131}I-Tyr3-TATE as a cocktail solution containing 0.68 µg DOTA-Tyr3-TATE, 0.2 mL.

At specific time points, the tumours as well as various tissues (blood, liver, spleen, kidney, stomach, small intestine, large intestine, adrenals, pancreas, thyroid, pituitary gland, bone and lung) were removed, weighed and their radioactivity determined.

The tumour bearing rats from lot (d), for biodistribution of ^{177}Lu-DOTA-Tyr3-TATE and DOTA-^{131}I-Tyr3-TATE in the presence of SSTR blocking agent, 0.2 mL containing 50 µCi ^{177}Lu-DOTA-Tyr3-TATE and DOTA-^{131}I-Tyr3-TATE, were IV injected, corresponding to 0.68 µg DOTA-Tyr3-TATE and 150 µg Sandostatin as blocking agent. After 1 h post-injection, the tumours and SSTR expressive tissues were removed, weighed and their radioactivity determined.

3. RESULTS AND DISCUSSION

3.1. In vitro binding assay

The experimental results regarding the SSTR receptor binding assays of the prepared radiopeptides indicate the biological properties of the receptor binding sequence of DOTA-Tyr3-TATE after radiolabelling with ^{131}I and ^{177}Lu.

3.1.1. Competition binding assays of DOTA-^{131}I-Tyr3-TATE and ^{177}Lu-DOTA-Tyr3-TATE

The competition binding data obtained from the experiments (Sections 2.2.4 and 2.2.5) using rat brain cortex membranes were analysed using the Prism-2 program (GraphPad software). The representative competition curves are shown in Figs 1 and 2. The IC_{50} values were determined to be 1.28nM for DOTA-^{nat}I-Tyr3-TATE and 4.74nM for ^{nat}Lu-DOTA-Tyr3-TATE.

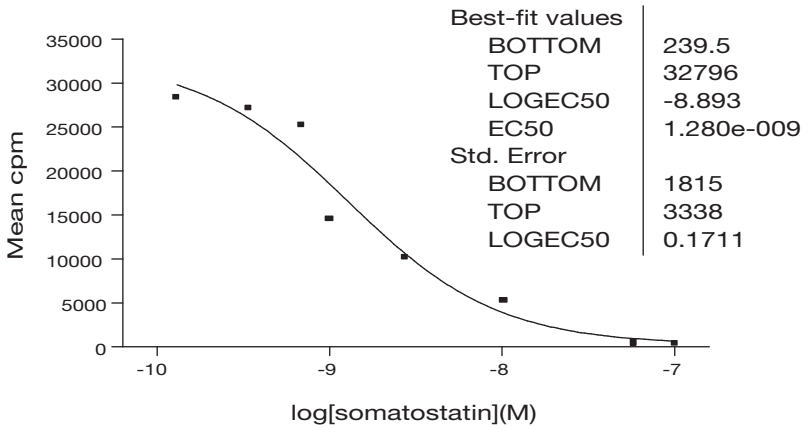

FIG. 1. Competitive binding curve of DOTA-^{nat}I-Tyr3-TATE.

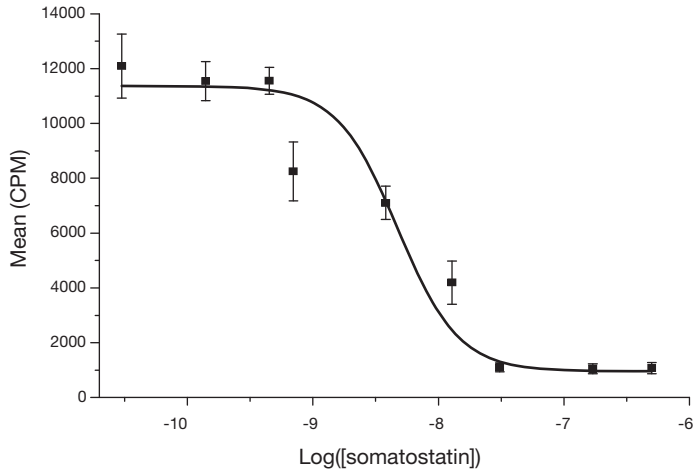

FIG. 2. Competitive binding curve of ^{nat}Lu-DOTA-Tyr3-TATE.

3.1.2. Saturation binding assays of DOTA-^{131}I-Tyr3-TATE and ^{177}Lu-DOTA-Tyr3-TATE

Radioactive measurements for total and non-specific binding were made experimentally (Sections 2.2.6 and 2.2.7) and were analysed using the Prism-2 program for determination of the equilibrium dissociation constant, K_d, for both DOTA-^{131}I-Tyr3-TATE and ^{177}Lu-DOTA-Tyr3-TATE as shown in Figs 3 and 4.

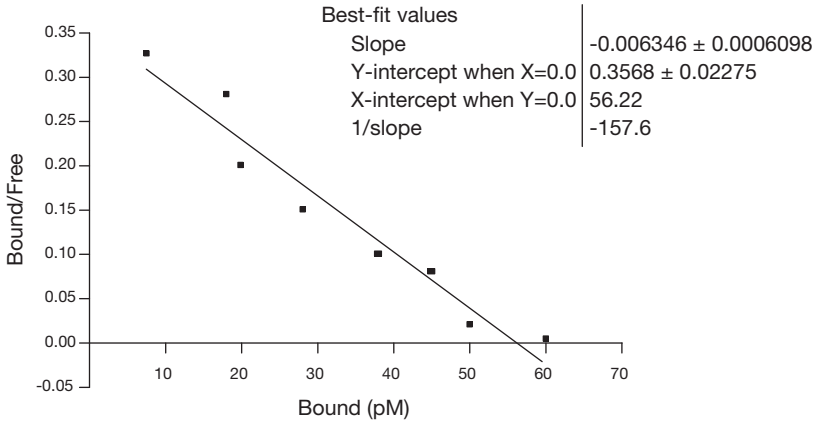

FIG. 3. Saturation binding curve of DOTA-^{131}I-Tyr3-TATE.

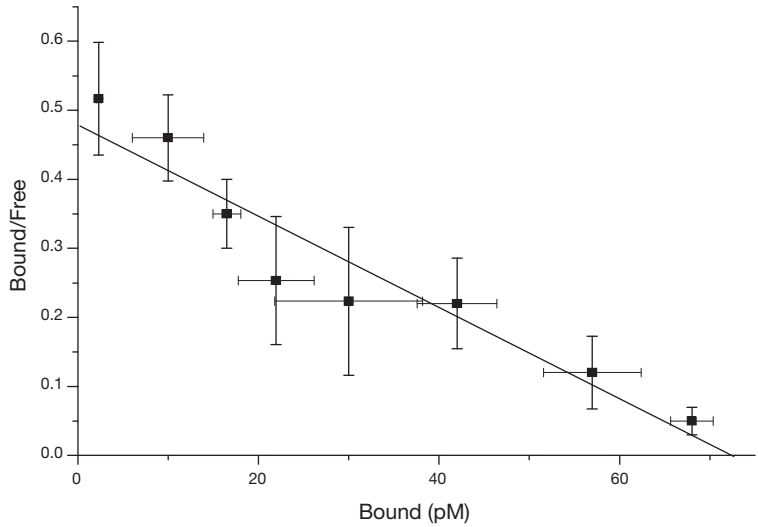

FIG. 4. Saturation binding curve of ^{177}Lu-DOTA-Tyr3-TATE. Fit line: y = A + Bx: A = 0.48 ± 0.03; B = -0.007 ± 0.0008 pM.

The K_d values of radiopeptides were found to be 157.6 for DOTA-^{131}I-Tyr3-TATE and 142.8 for ^{177}Lu-DOTA-Tyr3-TATE.

3.2. Biodistribution studies

3.2.1. Biodistribution of ^{177}Lu-DOTA-Tyr3-TATE in HRS1 tumour bearing rats

In Table 1 are presented the biodistribution data of ^{177}Lu-DOTA-Tyr3-TATE for all studied time points. The blood clearance is fast. The uptake of ^{177}Lu-DOTA-TATE in SSTR expressed tissues is high up to 24 h and decreases with each time point of the investigation. The uptake of ^{177}Lu-DOTA-Tyr3-TATE in tumour increases between 24–72 h post-injection.

Figure 5 shows the decreasing biodistribution of ^{177}Lu-DOTA-Tyr3-TATE in SSTR expressed normal tissues and increasing, with a maximum in the 24–72 h time range of biodistribution of ^{177}Lu-DOTA-Tyr3-TATE in HRS1 tumour. The bone uptake of ^{177}Lu-DOTA-Tyr3-TATE was high but shows a linear decrease, indicating the possibility of decomposition after IV injection, with delivery of free ^{177}Lu. With this view, the biodistribution of $^{177}LuCl_3$ in

TABLE 1. BIODISTRIBUTION OF ^{177}Lu-DOTA-Tyr3-TATE IN SELECTED ORGANS EXPRESSED IN %ID/g

Organ	3 h	24 h	48 h	72 h	168 h
Blood	0.72 ± 0.47	0.04 ± 0.03	0.04 ± 0.01	0.03 ± 0.01	0.03 ± 0.00
Liver	0.68 ± 0.15	0.44 ± 0.11	0.40 ± 0.05	0.28 ± 0.13	0.18 ± 0.01
Spleen	0.20 ± 0.11	0.14 ± 0.05	0.07 ± 0.01	0.03 ± 0.05	0.03 ± 0.00
Kidney	2.12 ± 0.23	1.90 ± 0.78	1.55 ± 0.82	1.56 ± 0.02	1.23 ± 0.05
Stomach	1.95 ± 0.42	1.25 ± 0.03	1.08 ± 0.32	0.94 ± 0.08	0.79 ± 0.01
Small intestine	0.92 ± 0.37	0.89 ± 0.13	0.57 ± 0.22	0.30 ± 0.10	0.17 ± 0.01
Large intestine	2.66 ± 0.14	2.02 ± 0.10	1.73 ± 0.10	1.99 ± 0.21	0.73 ± 0.02
Adrenal	0.71 ± 0.32	0.76 ± 0.51	0.75 ± 0.16	0.50 ± 0.11	0.35 ± 0.01
Pancreas	7.79 ± 0.08	4.10 ± 0.92	3.67 ± 0.67	2.01 ± 0.31	1.50 ± 0.02
Thyroid	1.92 ± 0.21	2.09 ± 0.14	0.82 ± 0.13	0.97 ± 0.08	0.73 ± 0.10
Pituitary	0.37 ± 0.13	0.57 ± 0.17	0.39 ± 0.11	0.34 ± 0.02	0.12 ± 0.01
Bone	9.54 ± 0.27	5.40 ± 0.72	2.79 ± 0.53	1.72 ± 0.31	1.05 ± 0.15
Lung	0.24 ± 0.11	0.17 ± 0.08	0.12 ± 0.05	0.05 ± 0.01	0.02 ± 0.01
Tumour	3.22 ± 2.15	6.31 ± 3.02	4.18 ± 3.42	4.07 ± 2.58	0.61 ± 0.29

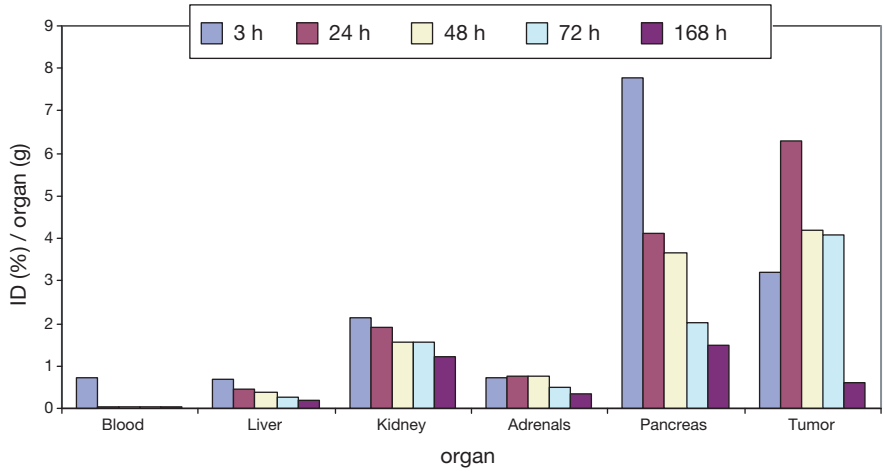

FIG. 5. Biodistribution of ^{177}Lu-DOTA-Tyr3-TATE in SSTR2 expressed tissues (adrenals, pancreas and tumour) in comparison with the biodistribution of ^{177}Lu-DOTA-Tyr3-TATE in transport, metabolic and elimination tissues.

bone was tested. The results (see Fig. 6.) show a progressive accumulation of ^{177}Lu, with the maximum value in the 4–24 h range. The high level of radioactivity was maintained for the duration of the experiment; the kinetics of $^{177}LuCl_3$ appear different from those obtained for ^{177}Lu-DOTA-Tyr3-TATE.

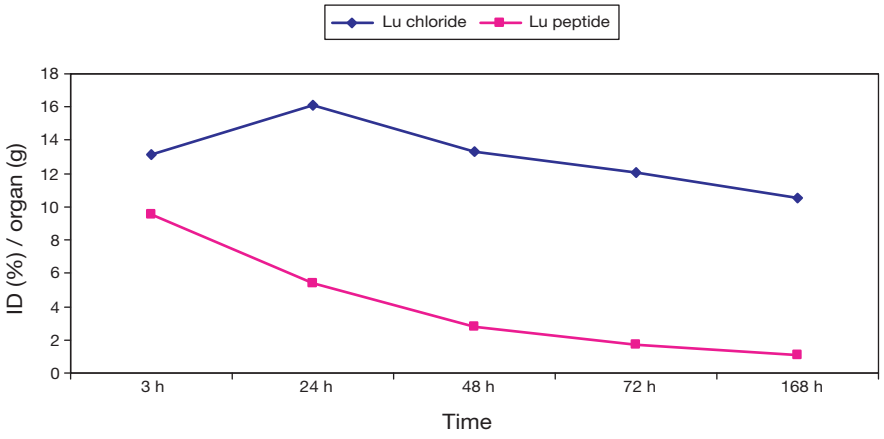

FIG. 6. Bone uptake of ^{177}Lu-DOTA-Tyr3-TATE and ^{177}LuCl.

3.2.2. Competitive biodistribution studies of ^{177}Lu-DOTA-Tyr3-TATE and DOTA-^{131}I-Tyr3-TATE

Because the uptake in the non-tumour tissues and the clearance of ^{177}Lu- and ^{131}I-DOTA-TATE were similar, the present study examines whether one radioproduct is more stable and has more uptake than the other in tumour bearing rats co-injected with ^{177}Lu-DOTA-TATE and ^{131}I-DOTA-TATE.

The competitive localization index (CLI) was defined:

$$^{177}\text{Lu-CLI} = \frac{\%\text{ID/g}\ ^{177}\text{Lu-DOTA-TATE in tumour}}{\%\text{ID/g}\ ^{177}\text{Lu-DOTA-TATE in blood}}$$

$$^{131}\text{I-CLI} = \frac{\%\text{ID/g}\ ^{131}\text{I-DOTA-TATE in tumour}}{\%\text{ID/g}\ ^{131}\text{I-DOTA-TATE in blood}}$$

The results (see Table 2 and Fig. 7) show that ^{177}Lu-CLI is higher than ^{131}I-CLI (~3 times).

TABLE 2. COMPETITIVE LOCALIZATION INDEX OF ^{177}Lu-DOTA-Tyr3-TATE AND DOTA-^{131}I-Tyr3-TATE IN TUMOUR

CLI	3 h	24 h	48 h	72 h	168 h
^{177}Lu-CLI	4.87	157.75	104.50	69	20.38
^{131}I-CLI	1.42	103.00	29.81	6.38	3.08

3.2.3. Biodistribution of ^{177}Lu-DOTA-TATE and DOTA-^{131}I-Tyr3-TATE in HRS1 tumour bearing rats with and without co-administration of SSTR2 blocking agent

The results show a smaller uptake of the radiopeptides in SSTR expressed tissues and tumour in rats injected with a blocking agent than in those animals where a blocking agent was absent (see Table 3).

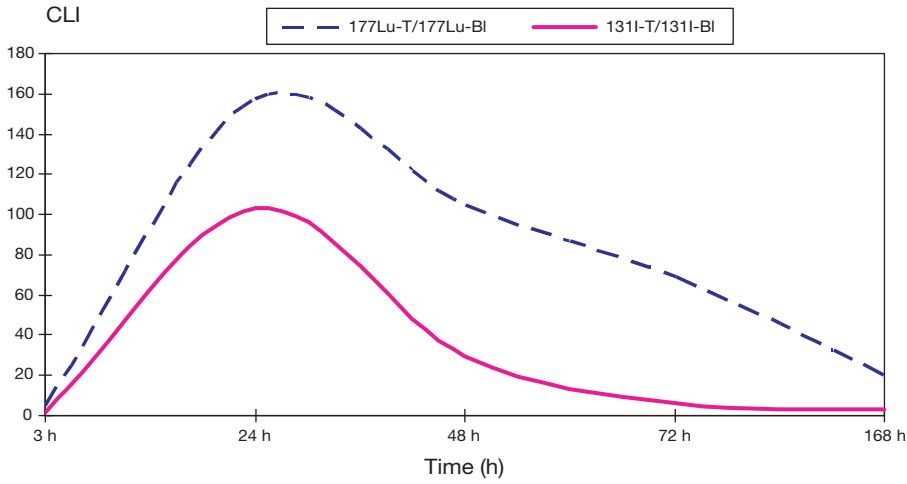

FIG. 7. Competitive uptake of ^{177}Lu-DOTA-Tyr3-TATE and DOTA-^{131}I-Tyr3-TATE.

TABLE 3. BIODISTRIBUTION OF ^{177}Lu-DOTA-Tyr3-TATE AND DOTA-^{131}I-Tyr3-TATE IN HRS1 TUMOUR BEARING RATS WITH AND WITHOUT A BLOCKING AGENT

Organ	^{177}Lu	^{177}Lu, block	^{131}I	^{131}I, block
Blood	0.96 ± 0.05	1.12 ± 0.04	1.02 ± 0.03	1.35 ± 0.01
Liver	0.82 ± 0.01	0.98 ± 0.05	0.38 ± 0.07	0.42 ± 0.03
Kidney	2.91 ± 0.03	3.41 ± 0.06	8.63 ± 0.01	9.37 ± 0.03
Pituitary	0.93 ± 0.15	0.38 ± 0.02	2.12 ± 0.12	0.51 ± 0.34
Adrenal	0.89 ± 0.32	0.12 ± 0.10	3.42 ± 0.24	0.48 ± 0.61
Pancreas	3.72 ± 0.33	0.95 ± 0.12	2.66 ± 0.04	0.62 ± 0.10
Tumour	3.01 ± 0.15	0.72 ± 0.04	2.24 ± 0.05	1.98 ± 0.32

4. CONCLUSIONS

The authors' studies demonstrate that the DOTA-Tyr3-TATE can be labelled with both ^{131}I and ^{177}Lu. The IC_{50} and K_d values for DOTA-^{131}I-Tyr3-TATE and ^{177}Lu-DOTA-Tyr3-TATE places these products in the range of radiopeptides with high binding affinity for somatostatin expressive receptors.

The biodistribution data show that the ^{177}Lu-DOTA-Tyr3-TATE is more stable and has higher uptake than DOTA-^{131}I-Tyr3-TATE and the CLI of ^{177}Lu DOTA-Tyr3-TATE is threefold higher than that obtained for DOTA-^{131}I-Tyr3-TATE. The results of work based on the comparative experiments suggest that the ^{177}Lu-DOTA-Tyr3-TATE could be an effective targeted radiotherapy agent for SSTR tumours.

ACKNOWLEDGEMENTS

This work was financially supported by the National Research Programme of Health VIASAN, Project No. 367/2004 and by the IAEA through the Coordination Research Programme on Comparative Evaluation of Therapeutic Radiopharmaceuticals (contract no. 12122/R0).

REFERENCES

[1] WEN, PING LI, et al., DOTA-D-Tyr – Octreotate: A Somatostatine analogue for labeling with metal and halogen radionuclides for cancer imaging and therapy, Bioconjugate Chem. **13** (2002) 721-728.

[2] BAKKER, W.H., et al., Iodine-131 labelled octreotide: not an option for somatostatine receptor therapy, Eur. J. Nucl. Med. **23** 7 (1996) 775-781.

[3] MAINA, T., et al., [^{99m}Tc] Demotate, a new ^{99m}Tc-based [Tyr^3] octreotate analogue for the detection of somatostatine receptor – positive tumours: synthesis and preclinical results, Eur. J. Nucl. Med. **29** 6 (2002) 742-753.

[4] KWEKKEBOOM, D.J., et al., [^{177}Lu-DOTA^0,Tyr^3] octreotate: comparison with [^{111}In-DTPA^0]octreotide in patients, Eur. J. Nucl. Med. **28** 9(2001) 1319-1325.

[5] LEWIS, J.S., et al., Toxicity and dosimetry of ^{177}Lu-DOTA-Y3-octreotate in a rat model, Int. J. Cancer 94 (2001) 873-877.

[6] LEWIS, J.S., et al., Radiotherapy and dosimetry of ^{64}Cu-TETA-Tyr^3 -Octreotate in a somatostative receptor-positive, tumor-bearing rat model, Clinical Cancer Research **5** (1999) 3608-3616.

[7] VALKEMA, R., et al., Long-term folow-up of renal function after peptide receptor radiation therapy with ^{90}Y-DOTA^0, Tyr^3 – Octreotide and ^{177}Lu-DOTA^0, Tyr^3 -Octreotate, J. Nucl. Med. **46** 1 (2005) 995-1065.

[8] KWEKKEBOOM, D.J., et al., Overview of results of peptide receptor radionuclide therapy with 3 radiolabeled somatostatin analogs, J. Nucl. Med. **45** 11 (2004) 1-5.

[9] RAYNOR, K., REISINE, T., Analogs of somatostatin selectively label distinct serbtypes of somatostatin receptor in ratbrain, J. Pharmacol Exp. Ther. 251 (1989) 510-517.

^{177}Lu LABELLED NITROIMADZOLES AND NITROTRIAZOLES FOR POSSIBLE USE IN TARGETED THERAPY OF HYPOXIC TUMOURS

T. DAS*, S. CHAKRABORTY*, A. MUKHERJEE*, S. BANERJEE*, G. SAMUEL*, H.D. SARMA**, M. VENKATESH*

*Radiopharmaceuticals Division
Email: meerav@apsara.barc.ernet.in

** Radiation Biology and Health Sciences Division

Bhabha Atomic Research Centre,
Mumbai, India

Abstract

In the authors' attempt at the development of potential therapeutic agents for targeting hypoxic tumours, two potent tumour avid substrates, metronidazole (a 5-nitroimadazole) and sanazole (a nitrotriazole derivative), were radiolabelled with ^{177}Lu after their conjugation with suitable bifunctional chelating agents. Lutetium-177 is presently being considered as an excellent radionuclide for the development of targeted agents for tumour therapy owing to its suitable nuclear decay characteristics and the possibility of its production with reasonably high specific activity and high radionuclidic purity using moderate flux reactors. In both cases, radiolabelling yields of >95% were achieved under optimized reaction conditions and the radiolabelled conjugates showed excellent stability at room temperature. Biodistribution studies carried out in Swiss mice bearing fibrosarcoma tumours showed selective accumulation of activity in tumour with high tumour/blood and tumour/muscle ratios within 1 h post-injection. No accumulation of injected activity was observed in any of the vital organs/tissues of the animals.

1. INTRODUCTION

The presence of hypoxic cells in tumours is considered to be a major factor limiting the efficacy of tumour diagnosis and radiotherapy [1]. The interesting observation that nitroimidazole derivatives have a tendency to be accumulated in the hypoxic regions led to the possibility of these compounds being considered for use as hypoxia markers [2, 3]. In the authors' attempt to develop a potential agent for targeted tumour therapy, metronidazole, a 5-nitroimadazole, and sanazole, a nitrotriazole derivative, documented earlier

as potent tumour avid substrates, are chosen as the carrier molecules [4, 5]. Lutetium-177, which is fast emerging as a promising radionuclide for targeted therapy owing to its suitable decay characteristics ($T_{1/2}$ = 6.73 d, $E_{\beta(max)}$ = 497 keV and E_{γ} = 113 keV (6.4%), 208 keV (11%)) and favourable production logistics (σ = 2100 b for $^{176}Lu(n,\gamma)^{177}Lu$), was identified as the radioisotope of choice [6]. The relatively longer half-life of ^{177}Lu provides logistical advantages for facilitating supply to places far away from the reactors and assumes significance for those countries having limited reactor facilities for isotope production. Moreover, ^{177}Lu can be produced in adequate specific activity for in vivo targeted therapy applications by a simple (n,γ) process using an enriched ^{176}Lu target due to its very high neutron capture cross-section (σ = 2100 b) [6, 7]. Since direct incorporation of ^{177}Lu in either of the aforementioned nitroimidazole or nitrotriazole moiety is not feasible, indirect incorporation of ^{177}Lu through a suitable bifunctional chelating agent (BFCA) was envisaged. As it is well documented that the lanthanide complexes of polyazamacrocycles exhibit very high thermodynamic stability and excellent kinetic inertness, it is quite logical to choose those ligands as the BFCAs of choice [8]. For the present study, metronidazole was coupled with para-aminobenzyl-1,4,7,10-tetraazacyclododecane-1,4,7,10-tetraacetic acid (*p*-amino-benzyl-DOTA) while the sanazole derivative [(N-2'(carboxyethyl)-2-(3'-nitro-1'-triazolyl)acetamide] was conjugated with 1,4,7,10-tetraaza-1-(4'-aminobenzyl-acetamido)-cyclododecane-4,7,10-triacetic acid (*p*-amino-DOTA-anilide). The present paper describes the radiolabelling of both the conjugates with ^{177}Lu in high yields and the pharmacokinetic behaviour of the developed radiochemical agents in suitable tumour bearing animal models.

2. EXPERIMENTAL

2.1. Materials

Metronidazole was obtained as a gift from a local pharmacy college. Sanazole derivative [(N-2'(carboxyethyl)-2-(3'-nitro-1'-triazolyl)acetamide] was obtained from the Radiation Biology and Health Sciences Division of the Bhabha Atomic Research Centre. The *p*-amino-benzyl-DOTA and *p*-amino-DOTA-anilide were procured from Macrocyclics (United States of America). Dicyclohexylcarbodiimide was purchased from Aldrich chemical company (USA). Dioxane was distilled and dried as per reported procedure [9]. All the other chemicals were purchased from reputable local manufacturers and were of analytical grade. The Lu_2O_3 (60.6% enriched in ^{176}Lu) powder used as the target for irradiation was procured from Isoflex (Russian Federation).

The radionuclidic purity of ^{177}Lu produced was determined by recording gamma ray spectra using a HPGe detector (EGG Ortec/Canbera detector) coupled to a 4K multichannel analyser system. A ^{152}Eu reference source, obtained from Amersham Inc., USA, was used for both energy and efficiency calibration of the detector. All other radioactivity measurements were carried out using a well-type NaI(Tl) scintillation counter unless otherwise mentioned, keeping the base line at 150 keV and a window of 100 keV, thereby utilizing the 208 keV gamma photon of ^{177}Lu.

Flexible silica gel plates used for carrying out thin layer chromatography (TLC) studies were obtained from Bakerflex Chemical Co., Germany. Whatman 3 MM chromatography paper (United Kingdom) was used for paper chromatography (PC) studies. The high performance liquid chromatography (HPLC) system used was obtained from JASCO, Japan (PU 1580). All the solvents used for HPLC studies were of HPLC grade and purchased from reputable local manufacturers. The solvents were degassed and filtered prior to use. Fourier transform infrared (FT-IR) spectra were recorded by using a Jasco FT/IR-420 spectrophotometer. Proton NMR spectra were recorded on 300 MHz Varian VXR 300S spectrometer.

2.2. Production of ^{177}Lu

Lutetium-177 was produced by thermal neutron bombardment of an isotopically enriched (60.6% in ^{176}Lu) Lu_2O_3 target at a thermal neutron flux of 3×10^{13} n·cm^{-2}·s^{-1} for 14 d. Following irradiation, the target was dissolved in 1M HCl by gentle warming. The resultant solution was evaporated to near dryness and reconstituted in double distilled water. The assay of the activity as well as the determination of specific activity and radionuclidic purity of the ^{177}Lu produced was carried out by recording gamma ray spectra using a HPGe detector coupled to a 4K multichannel analyser system. Energy and efficiency calibrations of the detector were carried out using a standard ^{152}Eu source.

2.3. Synthesis of the conjugates

2.3.1. Metronidazole-p-amino-benzyl-DOTA

The metronidazole-*p*-amino-benzyl-DOTA conjugate was synthesized by a two-step reaction. Metronidazole was first converted to its carboxylic acid derivative by oxidation using alkaline $KMnO_4$. To a solution of metronidazole (500 mg, 2.92mM) in 5 mL 10% aqueous Na_2CO_3, $KMnO_4$ (580 mg, 3.67mM) dissolved in 10 mL of double distilled water was added slowly under constant stirring at 4–5°C. The reaction was continued for another 4 h at 4–5°C and then

left overnight at room temperature (25°C). The reaction mixture was filtered and the filtrate was acidified and extracted in diethyl ether. The oxidized product, 2-[N-(2'-methyl-5'-nitro)imidazolyl]ethanoic acid, was obtained by evaporating the solvent under vacuum. In the second step, 2-[N-(2'-methyl-5'-nitro)imidazolyl]ethanoic acid (3 mg, 0.0162mM), *p*-NH_2-benzyl-DOTA.4HCl (10 mg, 0.0152mM) and DCC (3 mg, 0.0146mM) were stirred in dioxan for 20 h at room temperature to obtain the desired conjugate. After the completion of reaction, the reaction mixture was filtered and the filtrate was evaporated. The crude product thus obtained was purified by preparative TLC using 3% ammonium hydroxide in methanol as the eluting solvent.

2.3.2. Sanazole-p-amino-DOTA-anilide

The coupling between sanazole derivative [(N-2'(carboxyethyl)-2-(3'-nitro-1'-triazolyl)acetamide] and *p*-amino-DOTA-anilide was achieved by a single step procedure. In a typical reaction, the sanazole derivative (5 mg, 0.0205mM), *p*-amino-DOTA-anilide (13 mg, 0.0203mM) and DCC (5 mg, 0.0243mM) were dissolved in 2–3 mL of dry dioxane and the resulting mixture was stirred at room temperature for 24 h. After completion of the reaction, the precipitate was separated from the supernatant liquid by filtration and dried. The crude product thus obtained was purified by preparative TLC using 2% ammonium hydroxide in methanol as the eluting solvent. Both the conjugates were characterized by FT-IR and proton NMR spectroscopy.

2.4. Preparation of ^{177}Lu labelled conjugates

For preparation of the ^{177}Lu complexes of the synthesized conjugates, a stock solution of the conjugate was prepared in 0.1M NH_4Ac buffer (pH~5). Then, 20 μL of $^{177}LuCl_3$ (~25 MBq of ^{177}Lu, 0.2 μg Lu) was added to 100 μL of the stock solution of the conjugate (containing 100 μg sanazole-*p*-amino-DOTA-anilide or 25 μg metronidazole-*p*-amino-benzyl-DOTA conjugate) and the volume of the reaction mixture was made up to 200 μL by addition of 0.1M NH_4Ac buffer (pH~5). The reaction mixture was incubated at 50°C for 1 h maintaining its pH at ~5. Various reaction parameters, such as ligand concentration, pH, incubation time and temperature were optimized in order to obtain maximum radiolabelling yield.

2.5. Characterization of ^{177}Lu labelled conjugates

The radiolabelled conjugates were characterized by PC using 50% aqueous acetonitrile and TLC using 10% ammonium acetate:methanol (1:1, v/v)

as the eluting solvents. The radiolabelled conjugates were further purified by HPLC (C-18 reversed phase column (25 cm × 0.46 cm)) using water (A) acetonitrile (B) with 0.1% trifluoroacetic acid as the mobile phase and employing a gradient elution technique (0–4 min: 95% A, 4–6 min: 95–80% A, 6–9 min: 80–40% A, 9–12 min: 40% A, 12–18 min: 5% A). The flow rate was maintained at 1 mL/min and the elution was monitored by detecting the radioactivity signal using a NaI(Tl) detector.

2.6. Biodistribution studies

The in vivo biological evaluations of ^{177}Lu labelled conjugates were carried out on Swiss mice bearing fibrosarcoma tumours. Fibrosarcoma cells were prepared in normal saline (10^6 cells/mL) and 200 μL of the cell suspension was injected subcutaneously into each Swiss mouse, the weight of which varied around 20–25 g. The animals were observed for visible tumours. At the end of two weeks, tumours of ~1 cm diameter were observable. The radiolabelled conjugates (~100 μL, 7–8 MBq) were injected into the tumour bearing animals through the tail vein. The animals were sacrificed by cardiac puncture post-anesthesia at 1 h, 3 h and 24 h post-injection. Various organs and tumours were excised following sacrifice and the radioactivity associated with each organ/tissue was measured using a flat type NaI(Tl) counter. The percentage of injected dose (%ID) in various organs/tissues and tumours was calculated from the above data and expressed as percentage injected dose per gram (%ID/g) of organ/tissue. The activity excreted was indirectly determined from the difference between ID and the %ID accounted for in all the organs. All the animal experiments were carried out in strict compliance with the relevant national laws relating to the conduct of animal experimentation.

3. RESULTS AND DISCUSSION

3.1. Production of ^{177}Lu

Approximately 185 TBq/g (5×10^3 Ci/g) of ^{177}Lu activity was obtained at 6 h post-end of bombardment when a 60.6% enriched Lu_2O_3 target was irradiated at a thermal neutron flux of 3×10^{13} n·cm^{-2}·s^{-1} for 14 d. The radionuclidic purity of ^{177}Lu produced was 99.985% as estimated by analysing the gamma ray spectrum; ^{177m}Lu ($T_{1/2}$ = 160.5 d) being the sole radionuclidic impurity detected. The major gamma peaks were observed at 72, 113, 208, 250 and 321 keV, all of which correspond to the photopeaks of ^{177}Lu [6]. For determining the radionuclidic impurity burden in the ^{177}Lu produced due to

^{177m}Lu, the activity of ^{177}Lu was allowed to decay completely (45–65 d, ~8–10 half-lives of ^{177}Lu) and the gamma ray spectrum was recorded. The average level of radionuclidic impurity burden was found to be 150 nCi of ^{177m}Lu /1 mCi of ^{177}Lu (5.5 kBq /37 MBq) at end of bombardment.

3.2. Characterization of the conjugates

The conjugates were characterized by FT-IR and proton NMR spectroscopy.

3.2.1. Metronidazole-p-amino-benzyl-DOTA

FT-IR (KBr, *ν cm^{-1})*: 3425, 2925, 2849, 1733, 1692, 1514, 1469, 1385.

^{1}H-NMR, CD$_3$OD *(δ ppm)*: 1.29 [3H, s, metronidazole C<u>H</u>$_3$], 3.56-3.63 [15H, m, DOTA cyclic C<u>H</u>$_2$], 3.67-3.74 [8H, m, N(DOTA)-C<u>H</u>$_2$-COOH], 4.08-4.20 [2H, m, CH(DOTA)-C<u>H</u>$_2$-Ph], 4.94 [2H, s, N(metronidazole)-C<u>H</u>$_2$-CO], 7.44-7.49 [2H, m, *p*-amino-benzyl-DOTA Ar<u>H</u>], 7.58-7.62 [2H, m, *p*-amino-benzyl-DOTA Ar<u>H</u>], 8.03 [1H, s, metronidazole <u>H</u>].

The peak positions and integrations observed in the ^{1}H-NMR spectrum of the conjugate were consistent with the structure of the expected compound. In addition to the protons assignable to the DOTA moiety, the presence of the peaks at δ = 1.29 and 4.94 corresponding to the protons of the metronidazole moiety and the deshielded proton of the imidazole ring of metronidazole observable at δ = 8.03 provided further evidence towards the desired derivatization.

3.2.2. Sanazole-p-amino-DOTA-anilide

FT-IR (KBr, *ν cm^{-1})*: 3443, 3096, 2966, 2853, 1682, 1631, 1555.

^{1}H-NMR (CD$_3$OD, *δ ppm)*: 3.40-3.78 [16H, m, cyclic C<u>H</u>$_2$], 4.11-4.24 [6H, m, N(DOTA)-C<u>H</u>$_2$-COOH] 4.30-4.38 [2H, m, N(DOTA)-C<u>H</u>$_2$-CO-NH], 4.76 [2H, dd, J = 2.2 Hz & 14.3 Hz, sanazole-N-C<u>H</u>$_2$-CO], 5.11 [4H, dd, J = 9.9 Hz & 23 Hz, -CO-C<u>H</u>$_2$-C<u>H</u>$_2$-CO], 8.07 [2H, bs, CONH-aromatic <u>H</u>], 8.09 [1H, s, sanazole <u>H</u>], 8.11-8.13 [2H, m, CONH-aromatic <u>H</u>].

The peak positions, multiplicities and integrations observed in the high resolution ^{1}H-NMR spectrum of the conjugate were consistent with the structure of the expected compound. Appearance of the peaks at δ = 5.11 and 4.76 corresponding to the protons of the sanazole moiety indicates the desired conjugation. The deshielded proton of the triazole ring of sanazole observable at δ = 8.09 provides further evidence towards the desired derivatization.

3.3. Characterization of ^{177}Lu complexes

The radiolabelled conjugates were characterized by a combination of PC and TLC systems. In PC using 50% aqueous acetonitrile as the eluting solvent, it was observed that both ^{177}Lu labelled conjugate and ^{177}Lu labelled BFCA exhibited R_f = 0.7–0.8, while uncomplexed ^{177}Lu remained at the point of spotting (R_f = 0). Therefore, this technique could be used to determine the percentage radioactivity due to uncomplexed ^{177}Lu in the reaction mixture. On the other hand, in TLC and 10% ammonium acetate:methanol (1:1, v/v), it was observed that only ^{177}Lu labelled BFCA moved towards the solvent front with R_f = 0.7, while both the uncomplexed ^{177}Lu as well as the ^{177}Lu labelled conjugate did not show any appreciable movement from the point of spotting (R_f = 0 and 0–0.1, respectively). The percentage radioactivity due to the ^{177}Lu labelled BFCA in the reaction mixture could therefore be determined by employing this technique. Hence, a combination of PC and TLC techniques enabled the determination of the radiolabelling yield.

Determination of the accurate radiochemical purities of the ^{177}Lu labelled conjugates was achieved by employing HPLC. The ^{177}Lu labelled metronidazole-BFCA conjugate exhibited a retention time of 675 s while the uncomplexed ^{177}Lu and ^{177}Lu-BFCA complex were eluted out with retention times of 184 s and 250 s, respectively. On the other hand, ^{177}Lu labelled sanazole-BFCA conjugate exhibited a retention time of 420 s while ^{177}Lu labelled BFCA eluted out in 330 s under identical conditions. The HPLC chromatograms of the radiolabelled conjugates are shown in Fig. 1 (a) and (b).

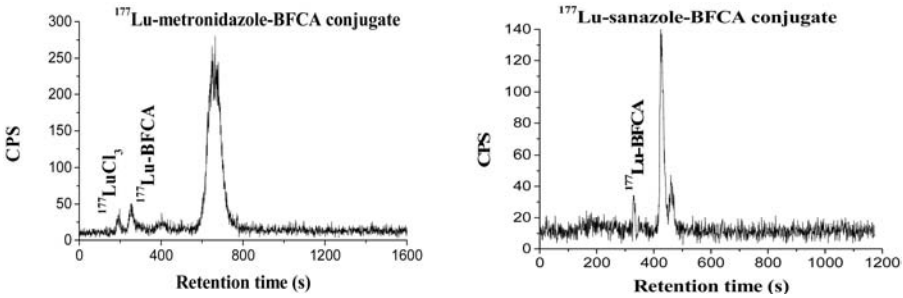

FIG. 1. (a) HPLC pattern of ^{177}Lu labelled metronidazole-BFCA conjugate, (b) HPLC pattern of ^{177}Lu labelled sanazole-BFCA conjugate.

3.4. Optimization of the complexation yield

Several reaction parameters, such as concentration of the conjugates, pH of the reaction mixture, incubation time and temperature, were varied extensively in order to maximize the complexation yield. A maximum complexation of ~97% was obtained when 25 μg of the metronidazole-BFCA conjugate was incubated at 50°C for a period of 1 h at pH~5, while ~98% complexation was obtained using 100 μg of the sanazole-BFCA conjugate under identical conditions.

3.5. Stability of the ^{177}Lu labelled conjugates

The stability of the ^{177}Lu labelled conjugates was studied by incubating the radiolabelled conjugates prepared under optimized conditions, employing the standard quality control techniques mentioned earlier. It was observed that both radiolabelled conjugates exhibited excellent stability as the radiochemical purities of the complexes remained unaltered for 7 d at room temperature.

3.6. Biodistribution studies

To determine the tumour specificity of the ^{177}Lu labelled conjugates, the radiolabelled preparations were injected in Swiss mice bearing fibrosarcoma tumours. The results of the biodistribution studies for ^{177}Lu labelled metronidazole-BFCA conjugate and sanazole-BFCA conjugate are tabulated in Tables 1 and 2, respectively. The results show moderate tumour uptake of 0.73–0.88% of the injected activity per gram (ID/g) within 1 h post-injection. Around 90% of the injected activity was observed to clear via the renal route with insignificant accumulation in other major organs/tissues except the liver at this time point. Clearance of the activity from all the organs at 24 h post-injection is evident from the >98% excretion observed at this time point. The tumour uptake was observed to decrease gradually over time and at 24 h post-injection, 0.18–0.45% of the injected activity was retained in the tumour. However, as the activity cleared out rapidly from all the non-target organs, the tumour to blood (4.0–5.2 at 1 h post-injection and 18.0–22.5 at 24 h post-injection) and tumour to muscle (4.6–12.2 at 1 h post-injection and 15.0–18.0 at 24 h post-injection) ratios at all the time points studied (1–24 h) were observed to be quite high.

Though imaging hypoxia using diagnostic radiopharmaceuticals is a quite well explored field, reports describing therapeutic agents making use of nitroimidazoles as hypoxia markers are not well documented. Therefore, it is

TABLE 1. BIODISTRIBUTION PATTERN OF ^{177}Lu LABELLED METRONIDAZOLE-*P*-AMINO-BENZYL-DOTA CONJUGATE IN SWISS MICE BEARING FIBROSARCOMA TUMOUR

Organ	%ID/g		
	1 h	3 h	24 h
Blood	0.14 (0.03)	0.02 (0.00)	0.02 (0.01)
Liver	0.52 (0.01)	0.18 (0.09)	0.07 (0.03)
Intestine	0.57 (0.04)	0.59 (0.13)	0.07 (0.01)
Kidney	1.72 (0.45)	0.56 (0.13)	0.61 (0.06)
Stomach	0.15 (0.05)	0.04 (0.03)	0.03 (0.01)
Heart	0.09 (0.05)	0.02 (0.02)	0.01 (0.01)
Lung	0.26 (0.14)	0.05 (0.03)	0.04 (0.03)
Muscle	0.06 (0.05)	0.04 (0.02)	0.06 (0.03)
Bone	0.16 (0.07)	0.13 (0.06)	0.08 (0.02)
Spleen	0.13 (0.08)	0.09 (0.04)	0.02 (0.01)
Tumour	0.73 (0.13)	0.56 (0.27)	0.45 (0.02)
Excretion	96.38 (0.90)	97.63 (0.68)	98.95 (0.28)

Note: Figures in parentheses show standard deviations. Three animals were used for each time point studied.

pertinent to draw a comparison with respect to the tumour uptake and target to non-target ratios of the radiolabelled conjugates described in the present paper with a few standard agents intended for use in hypoxia imaging, such as ^{99m}Tc-BMS181321 [10] and ^{99m}Tc-BRU59-21 [11], which indicates that the developed agents exhibit superior tumour to blood and tumour to muscle ratios at the time points studied.

4. CONCLUSION

The preparation and preliminary biodistribution studies of two tumour avid ^{177}Lu labelled conjugates are described in the present paper. Lutetium-177 was produced in ~185 Tbq/g (~5×10^3 Ci/g) specific activity and excellent radionuclidic purity in moderate thermal neutron flux using an enriched (60.6% in ^{176}Lu) Lu_2O_3 target. Metronidazole and sanazole were successfully coupled with polyazamacrocyclic BFCAs and subsequently radiolabelled with ^{177}Lu of

TABLE 2. BIODISTRIBUTION PATTERN OF ^{177}Lu LABELLED SANAZOLE-*P*-AMINO-DOTA-ANILIDE CONJUGATE IN SWISS MICE BEARING FIBROSARCOMA TUMOUR

Organ	%ID/g		
	1 h	3 h	24 h
Blood	0.22 (0.10)	0.10 (0.04)	0.01 (0.00)
Liver	1.34 (1.05)	1.34 (0.13)	0.38 (0.03)
Intestine	0.36 (0.03)	0.26 (0.09)	0.17 (0.15)
Kidney	2.76 (0.62)	1.33 (0.31)	1.01 (0.12)
Stomach	0.30 (0.08)	0.20 (0.10)	0.06 (0.05)
Heart	0.22 (0.09)	0.04 (0.04)	0.03 (0.02)
Lung	0.50 (0.19)	0.13 (0.06)	0.03 (0.01)
Muscle	0.19 (0.14)	0.04 (0.00)	0.01 (0.00)
Spleen	0.24 (0.07)	0.09 (0.02)	0.07 (0.03)
Tumour	0.88 (0.20)	0.43 (0.12)	0.18 (0.02)
Excretion	89.55 (2.32)	94.77 (1.64)	97.69 (0.98)

Note: Figures in parentheses show standard deviations. Three animals were used for each time point studied.

high radiochemical purity (>95%). The radiolabelled conjugates exhibited excellent stability in storage at room temperature for up to 7 d. Biodistribution studies carried out in Swiss mice bearing fibrosarcoma tumours revealed good tumour uptake (0.73–0.88% ID/g at 1 h post-injection) with favourable tumour to blood (4.0–5.2 at 1 h post-injection and 18.0–22.5 at 24 h post-injection) and tumour to muscle (4.6–12.2 at 1 h post-injection and 15.0–18.0 at 24 h post-injection) ratios.

ACKNOWLEDGEMENTS

The authors gratefully acknowledge V. Venugopal, Director, Radiochemistry and Isotope Group for his keen interest and constant encouragement. The authors are grateful to C.K.K. Nair, Radiation Biology and Health Sciences Division, BARC and to V.T. Kagiya, Health Research Foundation, Kyoto, Japan for the kind gift of sanazole. The authors acknowledge the help received from the staff members of the Animal

Experimentation Facility during animal experiments. The authors are grateful to S.V. Thakare and K.C. Jagadeesan for their valuable help in carrying out the irradiations of Lu targets.

REFERENCES

[1] NUNN, A., LINDER, K., STRAUSS, H.W., Nitroimidazoles and imaging hypoxia, Eur. J. Nucl. Med. **22** (1995) 265.

[2] BROWN, J.M., Hypoxic cell radiosensitizers: What next?, Int. J. Radiat. Oncol. Biol. Phys. **16** (1989), 987.

[3] CHAPMAN, J.D., Hypoxic sensitizers: Implications for radiation therapy, N. Engl. J. Med. **301** (1979) 1429.

[4] DAS, T., et al., ^{99m}Tc-labeled modified metronidazole: A potential agent for imaging hypoxia, Nucl. Med. Biol. **30** (2003) 127.

[5] SHIBAMOTO, Y., et al., Evaluation of various types of new hypoxic cell sensitizers using the EMT6 single cell-spheroid-solid tumor system. Int. J. Radiat. Biol. **52** (1987) 347.

[6] FIRESTONE, R., Table of isotopes (Shirley, V.S., Ed.), John Wiley and Sons, New York (1996).

[7] PILLAI, M.R.A., CHAKRABORTY, S., DAS, T., VENKATESH, M., RAMAMOORTHY, N., Production logistics of ^{177}Lu for radionuclide therapy. Appl. Radiat. Isot. **59** (2003)109.

[8] LIU, S., EDWARDS, D.S., Bifunctional chelators for therapeutic lanthanide radiopharmaceuticals, Bioconj. Chem. **12** (2001) 7.

[9] VOGEL, A.I., Textbook of practical organic chemistry, Longman Scientific Group, London (1994).

[10] BALLINGER, J.R., MIN-KEE, J.W., RAUTH, A.M., *In vitro* and *in vivo* evaluation of a technetium-99m labeled 2-nitroimidazole (BMS 181321) as marker of tumor hypoxia, J. Nucl. Med. **37** (1996) 1023.

[11] MELO, T., DUNCAN, J., BALLINGER, J.R., RAUTH, A.M., BRU59-21, a second-generation ^{99m}Tc-labeled 2-nitroimidazole for imaging hypoxia in tumors, J. Nucl. Med. **41** (2000)169.

LABELLING AND BIOLOGICAL EVALUATION OF ANTI-CD20 FOR TREATMENT OF NON-HODGKIN'S LYMPHOMA

P. OLIVER, A. ROBLES, V. TRINDADE, P. CABRAL,
V. TORTAROLO, A. NAPPA, G. RODRIGUEZ, H. BALTER
Radiopharmacy Department, Nuclear Research Center,
Faculty of Sciences,
Montevideo, Uruguay
Email: poliver@cin.edu.uy

Abstract

A radiopharmaceutical based on the use of Mab anti-CD20 labelled with ^{131}I and ^{188}Re is proposed for the treatment of non-Hodgkin's lymphoma. The antibody has been successfully used alone as well as associated with cytotoxic drugs, therefore encouraging the present research. The radionuclides were chosen on the basis of their decay properties and availability. Labelling techniques employed were previously used with other monoclonals. Oxidation with chloramine-T was used for ^{131}I labelling and $SnF_2 \cdot 2H_2O$ as the reducing agent for ^{188}Re. Non-specific precipitation and Sephadex purification were used for primary control and extraction. Quality control procedures including thin layer as well as high performance liquid chromatography were undertaken. Biodistribution in mice as well as affinity characteristics in a source rich in CD20 antigens were also studied. Stability over time was estimated. It was concluded that the labelling of anti-CD20 with ß emitters of therapeutic interest, in this case ^{131}I and ^{188}Re, gave reliable results by simple and efficient methodologies, yielding products compatible with clinical radioimmunotherapy. Quality control methods for the evaluation of radiochemical purity showed good reproducibility with short bench time. Immunoaffinity studies showed binding dependency on membrane antigen concentration and good specificity of binding was demonstrated by inhibition with unlabelled anti-CD20. Use of membranes, stable at -80ºC for more than 6 months instead of concentrated short lived leucocytes, has shown excellent reproducibility and therefore they are convenient at production centres distant from blood banks. Biodistributions were useful to determine the normal pattern and kinetics of uptake and excretion.

1. INTRODUCTION

The CD20 antigen is a non-glycosilated transmembrane phosphoprotein 35-37kD, expressed on the cell surface of normal B and pre-B but not in differentiated normal plasma cells. It is overexpressed in neoplastic B cells; it then being a good target for the therapeutical use of mab anti-CD20.

The anti-CD20 monoclonal chimeric humanized murine antibody (Rituximab) has been successfully applied for the treatment of non-Hodgkin's lymphoma. However, upon labelling of the mab anti-CD20 with ß emitters such as ^{90}Y or ^{131}I, the therapeutic efficacy is significantly increased due to the radiological effects of ionizing radiation [1].

The authors' objective was to develop reliable and efficient methods for labelling anti-CD20 with ß emitters of therapeutic interest, and simple and rugged quality control methods to evaluate radiochemical purity, biological performance and immunoaffinity assessment.

Iodine-131 and ^{188}Re have been used for the labelling of anti-CD20 as two attractive alternatives due to their decay properties and availability (^{131}I: $E_{ßmax}$ = 0.63 MeV, Eγ = 0.364 MeV, $T_{1/2}$ = 8 d; ^{188}Re: $E_{ßmax}$ = 2.2 MeV, Eγ = 0.155 MeV, $T_{1/2}$ = 17 h, generator produced). Labelling of anti-CD20 was optimized following the oxidation procedure of chloramine-T in the case of ^{131}I [2] and the synthesis of ^{188}Re(IV) complex with the previously reduced monoclonal antibody [3]. Quality control of the species obtained was done by physico-chemical methods, including ITLC-SG and HPLC, non-specifc protein precipitation, biological distribution in normal mice and immunoaffinity studies with membrane antigens extracted from isolated leucocytes.

2. MATERIALS

Monoclonal antibody anti-CD20, 10 mg/mL, (Rituximab, Mabthera) from Roche. $Na^{131}I$, pH7–11, highly concentrated >100 mCi/mL (>3.7 GBq/mL) from Tecnonuclear, Argentina. $Na^{188}ReO_4$ from ^{188}W–^{188}Re alumina generator system with 24 h since previous elution, 500 mCi (18.5 GBq) from Oak Ridge National Laboratory, ARCAL LII Programme.

Protein pak column SW300 (Waters). Gel permeation Sephadex G25 fine short column PD10 (Pharmacia). Chloramine-T, phosphate buffer, BSA, NaCl, methyl ethyl ketone, sodium tartrate, stannous fluoride, gentisic acid, ITLC-SG, ammonia, ethanol, water.

Oven, magnetic stirrer, homogenizer, ionizing chamber calibrator (Capintec CRC-7, United States of America), solid crystal NaI(Tl) low efficiency gamma counter (ORTEC, USA), coaxial NaI(Tl) automatic high efficiency gamma counter (Compac-120, Picker, USA), HPLC system with radiometric and UV detectors (Varian Associates, model 5000), refrigerated high speed and low speed centrifuges (Heraeus, Kendro, Germany and IEC-CENTRA 8, USA).

3. METHODOLOGY

3.1. Labelling with iodine

The $^{131}I^-$ was introduced in one tyrosyl residue of the protein chain by adding 28 MBq to 20 µg of anti-CD20 at pH7.4 and 10 µL of chloramine-T (0.13 µg/µL). After 1 min reaction time at room temperature, the yield was determined by protein precipitation with trichloroacetic acid solution (10%) and purification was done by gel permeation with Sephadex G-25 eluting with phosphate saline buffer 50mM, 0.2% BSA. Specific activity and iodine incorporation were determined.

3.2. Labelling with rhenium

For the labelling with ^{188}Re, anti-CD20 was first reduced by incubation with 2-mercaptoethanol to expose sulphydril groups and then purified by gel permeation over a PD10 column. Fractions of reduced antibody were pooled and formulated as kit for instant labelling. Each kit contained 1 mg anti-CD20; 82.8 mg of sodium tartrate; 1.67 mg of stannous fluoride and 0.25 mg gentisic acid. For the labelling, sodium perrhenate (1.5–1.9 GBq), previously acidified, was added to the kit and then incubated for 1 h at room temperature. The radiochemical purity of ^{188}Re-anti-CD20 was evaluated by ITLC-SG using MEK and saline as solvents and by saturated ITLC-SG strips (BSA 5%) using EtOH-NH_4OH-H_2O (2:1:5). It was also evaluated by HPLC using an SW300 protein Pak column and eluting with phosphate buffer 0.01M, pH7.4 at 1.0 mL/min. Specific activity was determined.

3.3. Affinity studies

Affinity studies were performed on leucocytes and on extracted membrane antigens. Isolated CD20 antigen membrane preparations were developed using a pool of concentrated leucocytes from the blood bank. After initial centrifugation at 500g for 10 min at 4°C, the supernatant yellow layer containing the leucocytes was separated, homogenized and centrifuged again at 500g to eliminate debris in the precipitate from the supernatant CD20 activity. Isolation of membrane antigens was achieved by centrifugation at 26 800g for 60 min. Final protein concentration was determined by Lowry. The recovered pool was aliquoted and stored at –80°C. Immunoaffinity was evaluated by specific binding of tracer to membrane preparations ranging from 0.25 mg/mL to 30 mg/mL, using an excess of (1.5×10^4 and 1×10^5) unlabelled monoclonal anti-CD20 as two levels of non-specific binding, followed by calculating the

maximum binding capacity. Inhibition studies were conducted by incubating a fixed membrane concentration of 1 and 4 mg/mL for ^{188}Re-anti-CD20 and ^{131}I-anti-CD20 respectively, with increasing concentrations of unlabelled anti-CD20 (0.3–3 mg/mL) and 250 Bq of tracer. All incubations of membrane assays were done overnight at 4°C. For assays of intact leucocytes, 1×10^6 and 2.5×10^6 cells per tube were incubated with a similar amount of tracer and unlabelled antibody for 1 h at 37°C. Data were analysed and fitted by Prisma GraphPad software.

3.4. Biological studies

Biodistribution studies at 4, 18 and 24 h post-injection were carried out in CD1 normal mice by intravenous administration of 9.3–55.5 MBq of ^{188}Re-anti-CD20. Organs and tissues of interest were removed and weighed and the radioactivity counted. Results were expressed as per cent injected dose per organ (%ID).

4. RESULTS

Radioiodination yields of anti-CD20 ranged from 43% to 82% and specific activity was over 30 μCi/μg (1.11 MBq/μg), depending upon the amount of monoclonal and the activity concentration of the radionuclide. The best results were obtained when excess monoclonal and high concentrations of activity were present. Figure 1 shows the typical purification profile.

The labelling with ^{188}Re gave a radiochemical purity higher than 95% for up to 3 h elapsed time and a specific activity of 40–50 μCi/μg (1.48–1.85 MBq/μg).

HPLC analysis revealed an R_t of 8.2 ± 0.3 min for the native mab anti-CD20, while for $^{188}ReO_4^-$ it was 10.6 ± 1 min.

Specific binding of ^{131}I-anti-CD20 to membrane antigens increased as a function of membrane concentration and reached 20.2 ± 0.5% for a total protein content of 16.5 mg/mL (Fig. 2). Maximum binding capacity was 15 ± 2% (n = 3). Inhibition of binding to membranes (4 mg/mL) was 67.2 ± 1% when 290 μg (5.22μM) of unlabelled anti-CD20 was added (Fig. 3). The IC_{50} value was 12.7nM.

Specific binding of ^{188}Re-anti-CD20 to membranes reached 46 ± 1% for a protein content of 33 mg/mL (Fig. 4). Maximum binding capacity was 17 ± 2% (n = 3). Inhibition of binding to membranes (1 mg/mL) was 66 ± 5% when 12.6 μM (700 μg) of unlabelled anti-CD20 was added (Fig. 5). The IC_{50} was determined as 13.3nM.

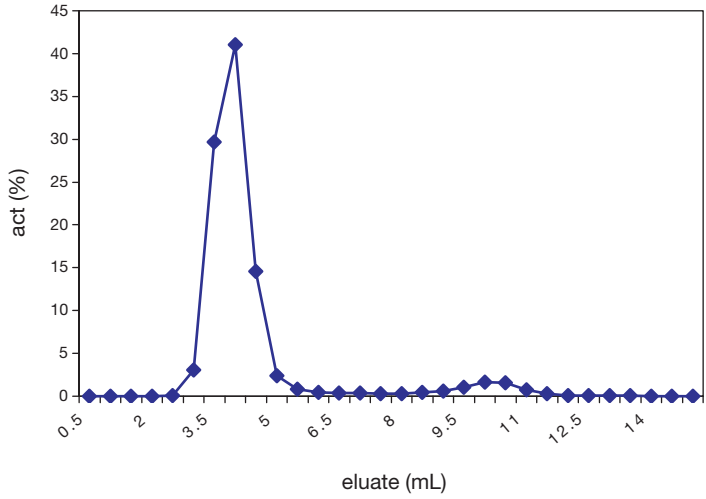

FIG. 1. Purification profile of mab anti-CD20 labelled with ^{131}I on PD10 columns.

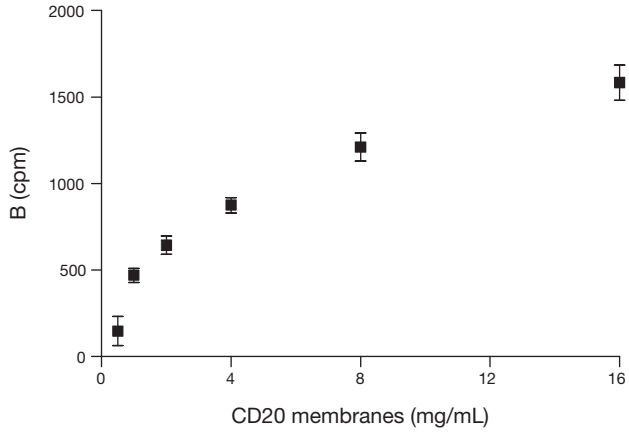

FIG. 2. Binding of ^{131}I anti-CD20 to increasing amounts of membrane antigens isolated from leucocytes.

The biological distribution showed high urinary elimination at 24 h (59%) while intestinal excretion was 10%. Negligible uptake by thyroid and stomach (less than 0.7% and 1.9%, respectively) was observed.

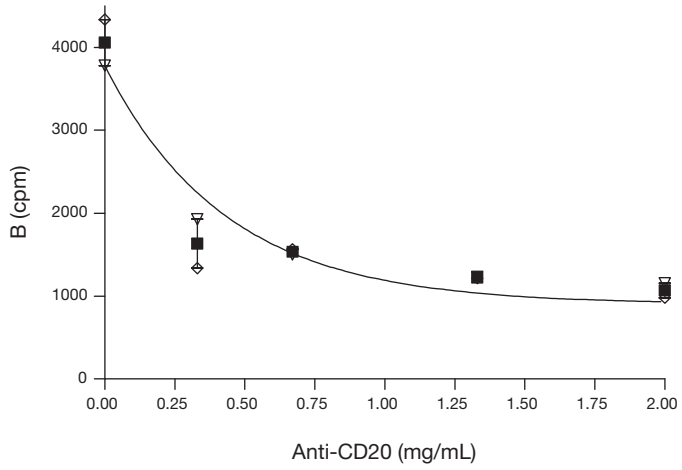

FIG. 3. Inhibition of the binding of ^{131}I-anti-CD20 to membrane antigens by unlabelled anti-CD20.

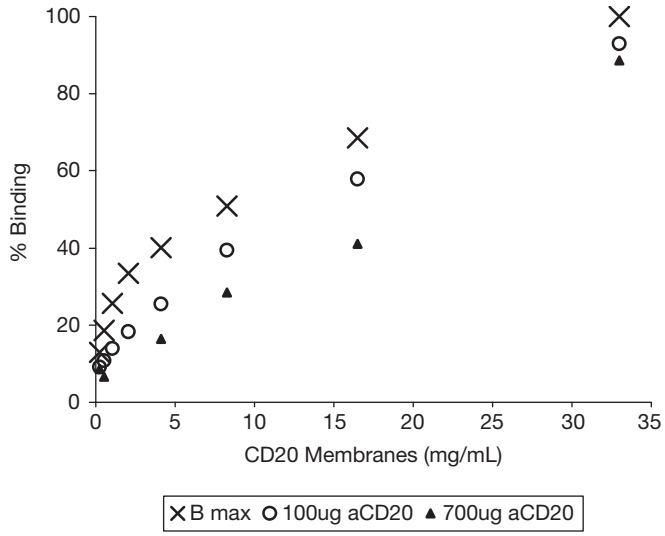

FIG. 4. ^{188}Re-anti-CD20 binding to increasing amounts of membrane antigens isolated from leucocytes.

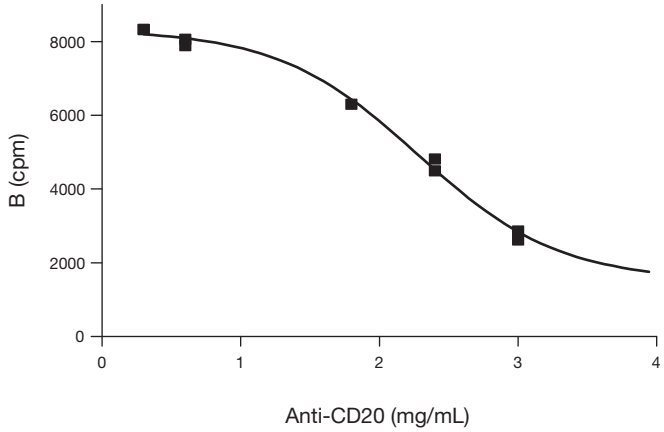

FIG. 5. Inhibition of the binding of ^{188}Re-anti-CD20 to membrane antigens by unlabelled anti-CD20.

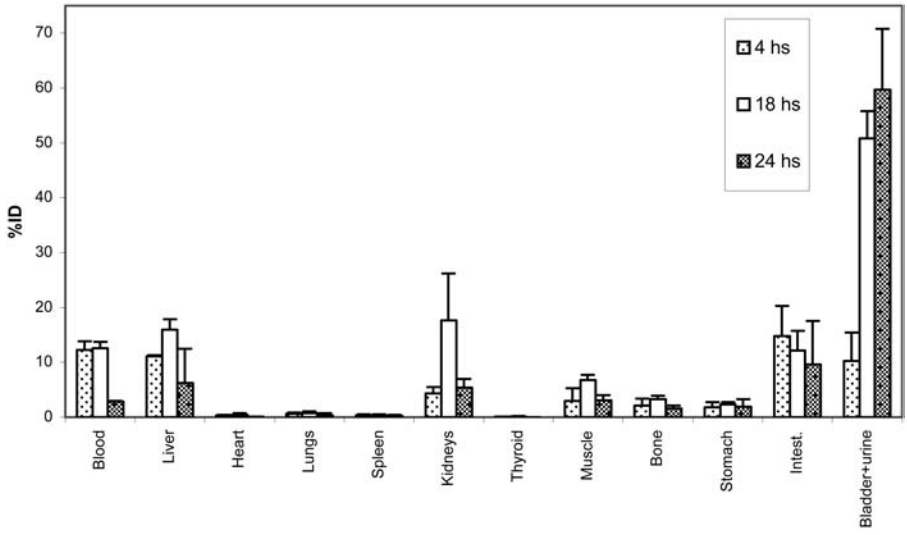

FIG. 6. Per cent injected dose of ^{188}Re-anti-CD20 in CD1 mice at 4, 18 and 24 h.

5. CONCLUSIONS

The labelling of anti-CD20 with ß emitters of therapeutic interest, in this case ^{131}I and ^{188}Re, gave reliable results by simple and efficient methodologies yielding products compatible with clinical radioimmunotherapy. In particular, the radioiodination results were satisfactory even though purification was always needed. Quality control methods for evaluation of radiochemical purity showed good reproducibility with short bench time.

Immunoaffinity studies showed binding dependency to membrane antigen concentration and good specificity of binding demonstrated by inhibition with unlabelled anti-CD20.

Both tracers displayed high affinity in their binding to antigen membranes with better results in the case of ^{188}Re owing to its higher specific activity. Nevertheless, it is considered that with a better quality and higher specific activity of ^{131}I than the one used in the present work, both tracers would be equivalent.

Use of membranes, stable at -80ºC for more than 6 months instead of concentrated short lived leucocytes, has shown excellent reproducibility and therefore they are convenient at production centres distant from blood banks.

ACKNOWLEDGEMENTS

Partially supported by the IAEA, Arcal LII, and PEDECIBA Quimica.

REFERENCES

[1] JUWEID, M.E., Radioimmunotherapy of B cell Non-Hodgkin's lymphoma: from clinical trials to clinical practice, J Nucl Med (2002) 43:1507-1529.

[2] ROBLES, A.M., BALTER, H., OLIVER, P., WELLING, M., PAUWELS, E.K.J., Improved Radioiodination of biomolecules using exhaustive chloramine-T oxidation, Nucl. Med. Biol. (2001) 28:999-1008.

[3] OLIVER, P., et al., Anti-CD20-188Re: Labelling and biological performance, Nucl. Med. Review (2005) 8: 19-20.

THERAPEUTIC RADIOPHARMACEUTICALS

(Session 9)

Chairpersons

J. HARVEY TURNER
Australia

M. DONDI
IAEA

^{177}Lu-DOTA-J591 MONOCLONAL ANTIBODY: CHEMISTRY, TOXICITY, DOSIMETRY AND CLINICAL EFFICACY

RIT of prostate cancer using ^{177}Lu-J591 anti-PSMA antibody

S.J. GOLDSMITH, S. VALLABHAJOSULA, M.I. MILOWSKY, D.M. NANUS, N.H. BANDER
Department of Radiology, Medicine and Urology,
New York Presbyterian Hospital and Weill Cornell Medical College of Cornell University,
New York, United States of America
Email: svallabh@med.cornell.edu

Abstract

Prostate specific membrane antigen (PSMA) is a transmembrane antigen virtually restricted to prostate tissue and the expression of which is increased in prostate carcinoma. Indium-111 capromab pendetide (ProstaScint®) is an antibody specific to the intracellular epitope of PSMA. For the past several years, the authors have been engaged in the development and evaluation of a radiolabelled humanized monoclonal antibody, J591, specific to an extracellular epitope of PSMA. After demonstrating that J591 is internalized, the authors developed ^{90}Y and ^{177}Lu labelled DOTA-J591 for radioimmunotherapy of prostate cancer. These radiometals remain localized in tumour foci (as well as other tissues including non-specific hepatic uptake) compared to ^{131}I labelled proteins. In contrast to ^{90}Y, ^{177}Lu is a radiometal with a low energy β^- emission as well as a γ photon emission that makes it convenient to demonstrate localization and quantify biodistribution and turnover externally. Metastatic prostate carcinoma, in particular, is an ideal target for radioimmunotherapy since chemotherapeutic or other medical therapies are not ideal or appropriate. All human studies were approved by the institutional IRB and were performed as a phase I dose escalation study under an IND. Initially, different doses of J591 were used to assess the influence of total protein content on biodistribution. From these studies, it was determined that 10 mg/m^2 total protein per patient was sufficient to reduce non-specific organ uptake, potentially optimizing tumour access to labelled antibody. With ^{177}Lu-J591, dose limiting haematological toxicity was observed at 2590 MBq/m^2. In 35 patients, the appearance and severity of myelotoxicity correlated with the calculated bone marrow radiation absorbed dose. Response in terms of significant decreases in PSA, bone flare phenomena followed by improvement in bone scan findings have been observed but only in a single dose trial; relapse has occurred suggesting that further evaluation with multidose administration at $\leq$MTD or therapy in combination with radiosensitizing chemotherapy may be necessary.

1. INTRODUCTION

In the last 10 years, among a number of radionuclides emitting β^- particles, ^{131}I and ^{90}Y have emerged as the primary choices for developing radiopharmaceuticals for therapy. Both of these nuclides, however, have advantages and disadvantages [1]. Iodine-131 has lower energy β^- particles and longer physical half-life compared to ^{90}Y. The radioiodinated molecules are dehalogenated in vivo and the free radioiodide and the iodinated peptide fragments are washed out of tissues and excreted in the urine. In contrast, when ^{90}Y is bound to peptides and proteins via a bifunctional chelate, the radiolabelled complex is stable in vivo and ^{90}Y is trapped within the cell, leading to higher accretion and retention by the tumour. Iodine-131 has γ photons (0.364 MeV) useful for biodistribution and dosimetry studies. Since ^{90}Y does not emit γ photons, ^{111}In labelled antibodies are generally used as chemical and biological surrogates to study biodistribution and estimate radiation dosimetry of ^{90}Y labelled antibodies. Some recent studies, however, have shown that there are significant differences in biodistribution between ^{111}In and ^{90}Y labelled agents.

1.1. ^{177}Lu for therapy

In recent years, ^{177}Lu, a β^- emitting lanthanide radiometal with excellent physical properties (Table 1), has emerged as an ideal and appropriate radionuclide for therapy [2]. Unlike ^{90}Y, ^{177}Lu has gamma photons that are useful for biodistribution and dosimetry studies. Chemically, yttrium and lutetium metals favour the +3 oxidation state, similar to indium, but there are minor differences in the solution and coordination chemistries among these metals.

The theoretical maximum specific activity of ^{177}Lu is 4070 GBq/mg (110 Ci/mg). At present, ^{177}Lu is produced in reactors by neutron capture on natural Lu or enriched ^{176}Lu (direct method) and ^{176}Yb (indirect method).

TABLE 1. RADIONUCLIDES FOR THERAPY

Nuclide	Half-life (d)	β^- energy (MeV)		γ energy	Range in tissue (mm)	
		Max.	Ave.	(MeV)	Max.	Ave.
^{90}Y	2.67	2.28	0.935	No γ	12.0	2.76
^{177}Lu	6.7	0.497	0.133	208 (11%)		
^{131}I	8.04	0.61	0.20	364 (81%)	2.4	0.40

The maximum achievable specific activity of ^{177}Lu produced via neutron irradiation of ^{176}Yb strongly depends on the percentage of ^{175}Lu, ^{176}Lu and ^{174}Yb stable isotopes in the material to be irradiated. The 'indirect' route could provide no carrier added ^{177}Lu free of ^{177m}Lu ($T_{½}$ = 160 d) radionuclidic contaminant. Processing and dispensing of ^{177}Lu from the 'direct' route is straightforward and efficient, while processing and purification from the indirect route is time consuming and expensive [3].

The ^{177}Lu (specific activity = 740–1110 GBq/mg) used in the authors' J591 antibody studies was produced using the direct method at the Missouri University Research Reactor facility. Radionuclide purity was evaluated by gamma spectroscopy to determine the amount of ^{177}Lu present in the samples. A typical sample of ^{177}Lu contains 59–64 ppm of ^{177m}Lu, which corresponds to approximately 0.006% [4].

1.2. Prostate specific membrane antigen (PSMA)

In prostate cancer, the most well-established, cell surface antigen yet identified is PSMA [5, 6]. Since it is not secreted into the blood stream, PSMA is an ideal antigen for targeted therapy. PSMA is a highly prostate restricted type II integral membrane cell surface glycoprotein expressed by all prostate cancers and expression levels progressively increase in more poorly differentiated, metastatic and hormone refractory cancers [7–10]. PSMA was originally thought to be prostate specific, but recent studies have shown that it is also expressed by small intestine epithelial (brush border) cells, proximal renal tubule cells and salivary glands [11] and the level of expression in these normal tissues, however, is 100–1000 fold less than in prostate tissue. Immunohistochemical studies have shown that PSMA is also expressed by vascular endothelial cells of numerous solid tumour malignancies. However, PSMA is not expressed by normal vascular endothelium in benign tissues or in neoplastic epithelial cells of non-prostate malignancies [12, 13]. These data suggest that metastatic prostate carcinoma, in particular, is an ideal target for radioimmunotherapy because of the restricted expression of PSMA, the pattern of metastatic involvement often involving micrometastases in lymph nodes and bone marrow and the general lack of suitable chemotherapeutic or other medical therapy [14].

PSMA is a 100 000 kDa molecular weight protein that spans the cell membrane [5, 15]. The first 19 amino acids (from the N-terminus) lie within the cytoplasm, followed by a membrane spanning domain of 24 amino acids, in turn followed by a large extracellular domain of 707 amino acids [15].

1.3. Anti-PSMA monoclonal antibodies (mAb)

A murine mAb, 7E11 that binds to an intracellular epitope of the PSMA protein [16] labelled with ^{111}In (Capromab pendetide or ProstaScint®) is an FDA approved imaging agent for identification of soft tissue metastases in patients with prostate cancer [17, 18]. Owing to its intracellular binding site, however, 7E11 binds only dead or dying PC cells [19].

The J591 is an anti-PSMA mAb that binds with high affinity to the extracellular domain of $PSMA_{ext}$ and is rapidly internalized [12, 20]. The murine antibody J591 was de-immunized to allow for repeated dosing. J591 de-immunization involved genetic engineering into a human IgG1 with identical specificity and affinity as its murine counterpart with the added capability to induce ADCC with human immune effector cells [21, 22].

1.4. ^{177}Lu-DOTA-J591

The clinical grade de-immunized J591 mAb was produced under GMP conditions at Lonza Biologics (Slough, United Kingdom) and supplied in 5 mL of phosphate buffer, pH7.0 containing 5 mg/mL of antibody. The J591 antibody was covalently linked with the chelating agent, 1,4,7,10-tetraazacyclododecane-N,N',N'',N'''-tetraacetic acid (DOTA) (Goodwin Biotech, Plantation, United States of America) as previously reported [22]. The sterile pyrogen free clinical material, DOTA-J591 mAb in 0.3M ammonium acetate buffer, pH7.0 (8 mg/mL) was provided by BZL Biologics (Framingham, USA).

The DOTA-J591 mAb was labelled by incubating the antibody in an ammonium acetate buffer (1M, pH7.0) with ^{177}Lu chloride as previously described [23]. ^{177}Lu-DOTA-J591 mAb (^{177}Lu-J591) was purified by gel filtration and sterilized by membrane (0.2 μm) filtration prior to administration into patients. Labelling efficiency and radiochemical purity were determined using ITLC SG and 5mM DTPA solution as solvent. Immunoreactivity of ^{177}Lu-J591 was determined by the Lindmo method using PSMA positive LNCaP tumour cells [24, 25]. Immunoreactivity was well preserved, even at 0.5–0.7 GBq/mg of specific activity.

2. CLINICAL STUDIES

2.1. Patient population

Eligible patients had a prior histological diagnosis of prostate cancer with evidence of recurrent or metastatic disease as defined by a rising prostate

specific antigen (PSA) and/or abnormal radiological studies including bone scan, computed axial tomography and/or magnetic resonance imaging. Patients were required to have a PSA ≥1.0 at the time of entry with three consecutive rising PSA values over a period of ≥2 weeks. Additional requirements included: platelet count ≥150 000/mm^3 and neutrophil count ≥2000/mm^3; a bone marrow biopsy demonstrating ≤10% replacement by tumour on a unilateral sample or a mean of ≤25% replacement by tumour on bilateral samples. A total of 35 patients received ^{177}Lu treatment; 19 patients received a single dose while 16 patients received 2–3 doses.

2.2. Dose escalation

In a dose escalation phase I clinical, patients received ^{177}Lu activity in the range 370–2775 MBq/m^2 (10–75 mCi/m^2). Additional unconjugated, cold J591 antibody was added to give a constant protein dose of 10 mg/m^2 with the ^{177}Lu dose. The final radiolabelled J591 mAb was diluted to 20 mL with physiological saline solution and was infused intravenously over a period of 5 min.

2.2.1. Retreatment

Patients were considered eligible for up to 2 or 3 retreatments with ^{177}Lu-J591 at 6 week intervals if their platelet and neutrophil count recovery was satisfactory (platelet count ≥70% of the baseline platelet count of the prior treatment cycle with a minimum recovery to at least 75×10^9/L and ANC ≥80% of the baseline ANC of the prior treatment cycle with a minimum recovery to 1.3×10^9/L). Patients who experienced any grade ≥3 non-haematological toxicity in a prior treatment cycle were ineligible for retreatment. Retreatment consisted of patients receiving the same ^{177}Lu dose as their initial cycle.

2.3. Imaging studies: Tumour targeting of ^{177}Lu-J591

In order to determine the plasma clearance kinetics following infusion of ^{177}Lu-J591, 8–10 venous blood samples were obtained over a period of 12–14 d. To assess the biodistribution, total body images were obtained within 1 h post-infusion (day 0) and again at 4 additional time points over the next 2 weeks (e.g. 1, 3, 6–9 and 13–14 d). The gamma camera images were obtained using a dual head ADAC (ADAC, Milpitas, USA) or GE gamma camera (GE, Milwaukee, USA) fitted with an appropriate collimator. All 5 scans for each patient were obtained with the same gamma camera. SPECT studies of the abdomen, pelvis and/or areas of suspected metastatic lesions were performed on days 2–3 and/or 6–7 in selected patients.

2.4. Toxicity evaluation

Dose limiting toxicity (DLT) was defined as the following: haematological toxicity consisting of grade 4 thrombocytopenia (platelet $<10 \times 10^9$/L) and/or grade 4 neutropenia (ANC $<0.5 \times 10^9$) lasting >5 d; and other toxicity consisting of any grade ≥3 non-haematological toxicity attributable to ^{177}Lu or ^{90}Y labelled J591. The NCI CTEP Common Toxicity Criteria, version 2.0, was utilized. The maximum tolerated dose (MTD) was defined as the dose level at which 0/6 or 1/6 patients experience a DLT with the next higher dose level having ≥2 patients experiencing DLT. Once the MTD was reached, at least 6 patients were to be evaluated at that dose level. The stopping point for single doses and the subsequent doses were the same. DLT and MTD were determined with multiple doses using the same criteria that were used for single doses.

3. PHARMACOKINETICS AND RADIATION DOSIMETRY

Following intravenous administration of ^{177}Lu-J591, there is a bi-exponential plasma clearance; <20% of activity had a fast component with a $T_{½}$ of <3 h. The remaining 80% cleared from plasma slowly with an average $T_{½}$ of 44 ± 15 h. The percentage of injected radioactivity in the total urine collected over a period of 3 d is 7.3 ± 2.8%.

Whole body gamma camera images showed that within 24 h post-injection, ^{177}Lu radioactivity was predominantly in the blood pool as seen by the increased activity in the heart and major blood vessels. Subsequently, there was a decrease in blood pool activity with a gradual accumulation of activity in liver, spleen, kidney and bone or bone marrow. Starting from day 2, there was some gastrointestinal activity. Images on days 6 and 7 clearly show that ^{177}Lu is very effective in identifying the metastatic lesions with a very high target/background contrast.

Radiation absorbed dose estimates (mGy/MBq) for a number of target organs from ^{177}Lu-J591 were estimated using the MIRD technique. The liver receives the highest dose followed by spleen and kidney. The liver is the critical organ, with a radiation absorbed dose of 2.10 ± 0.60 mGy/MBq. The dose to bone marrow is 0.32 ± 0.1 mGy/MBq.

4. ^{177}Lu-J591 TUMOUR TARGETING

Among the 35 patients receiving ^{177}Lu-J591 mAb, 30 (86%) had metastatic disease detected on imaging studies following administration of treatment dose. Specifically, 21 (60%) patients had bone only metastases, 6 (17%) had soft tissue only metastases and 3 (9%) had both bone and soft tissue disease. In all patients, all known sites of metastatic disease were successfully imaged by ^{177}Lu-J591 scintigraphy as shown in Fig. 1. Patients receiving multiple doses were imaged one week after dose 2 and, where applicable, dose 3. In all of these cases, tumour targeting was seen on serial images.

5. HAEMATOLOGICAL TOXICITY

Among patients receiving a single dose of ^{177}Lu-J591, thrombocytopenia and neutropenia were dose related and this is summarized in Table 2. One of the six patients at the 2590 MBq/m^2 dose level and one of the three patients at the 2775 MBq/m^2 dose level experienced dose limiting (grade 4) platelet toxicity.

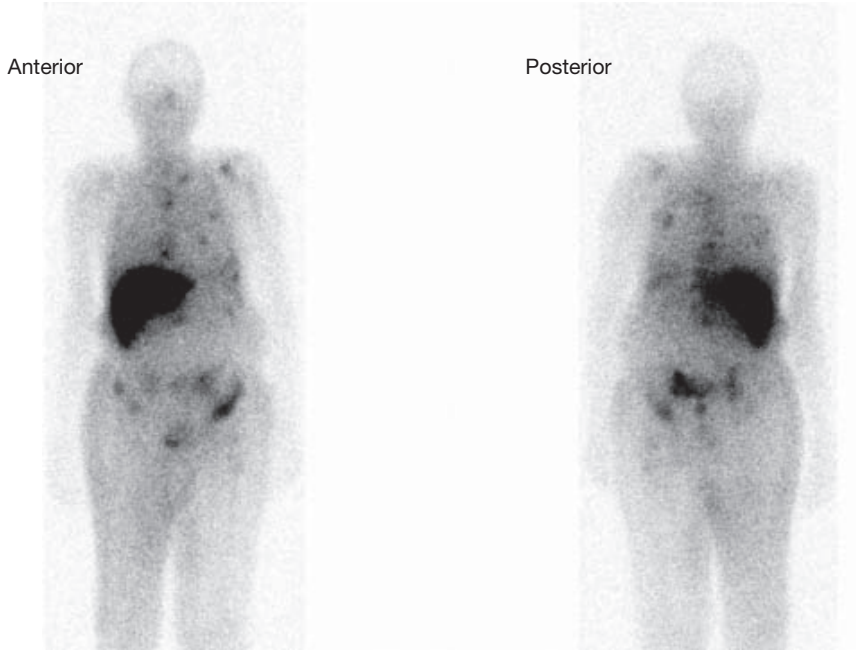

FIG. 1. Tumour localization of ^{177}Lu-J591 (on day 6) in a patient with prostate cancer.

TABLE 2. HAEMATOLOGICAL TOXICITY FOLLOWING ^{177}Lu-J591 ADMINISTRATION

Dose (MBq/m^2)	Pts (n)	Thrombocytopenia grade					Neutropenia grade				
		0	1	2	3	4	0	1	2	2	4
370	3	3					3				
555	3	2	1				3				
1110	5	2	2	1			2	2	1		
1665	5		1	3	1		2	1	2		
2220	3		1	1	1			1	2		
2590	6		1		4	1		1	2	1	2
2775	3				2	1				2	1

Most of the remaining patients at these two dose levels experienced grade 3 platelet toxicity. With the ^{177}Lu-J591 antibody, the 2590 MBq/m^2 dose level was determined to be the MTD. Post-treatment platelet counts decline generally at 2.5–3 weeks with platelet nadirs occurring at 4–5 weeks thereafter followed by a recovery phase. In all the three subjects, at 2775 MBq/m^2, the fractional decrease in platelets as a function of time (days) is shown in Fig. 2. The mean platelet counts returned to 80–90% of their pre-treatment values over 2–3 weeks.

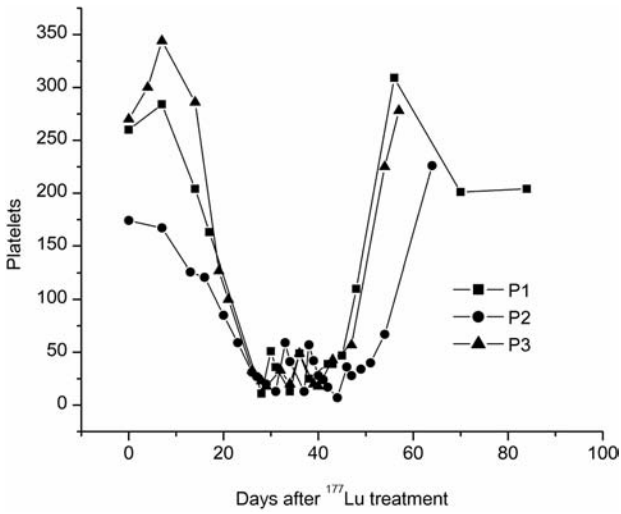

FIG. 2. Haematological toxicity (thrombocytopenia) in patients with prostate cancer (P1–P3) following treatment with a single dose (2775 MBq/m^2) of ^{177}Lu-J591.

5.1. Haematological toxicity following retreatment

Multiple doses of 1110 MBq/m^2 were well tolerated in 10 patients; 6 received 2 doses and 4 received 3 doses. The median time between doses 1 and 2 was 64 d (range 42–238 d) and between doses 2 and 3 was 53 d (range: 50–55 d). The 4 patients who received 3 doses totalling 3330 MBq/m^2 did so over a period of 98–126 d. The fractional decrease in platelets following the three doses at 1110 MBq/m^2 is shown in Fig. 3(a). The platelet recovery was very good in three patients while the fourth patient had grade 4 platelet toxicity and began a different therapy owing to disease progression, prior to being able to assess toxicity. At 1665 MBq/m^2, two of the three patients developed prolonged grade 3 platelet toxicity, each requiring three platelet transfusions after the second dose. Thrombocytopenia in one of the patients who received two doses is shown in Fig. 3(b).

5.2. Correlation of haematological toxicity with bone marrow radiation dose

With ^{177}Lu-J591, haematological toxicity increased directly with the dose of ^{177}Lu. Similarly, the fractional decrease in platelets also gradually increased as the ^{177}Lu dose is increased. However, with ANC, no dose–response relationship was seen in the range 370–1665 MBq/m^2. The fractional decrease in platelets following administration of ^{177}Lu-J591 correlated very well with

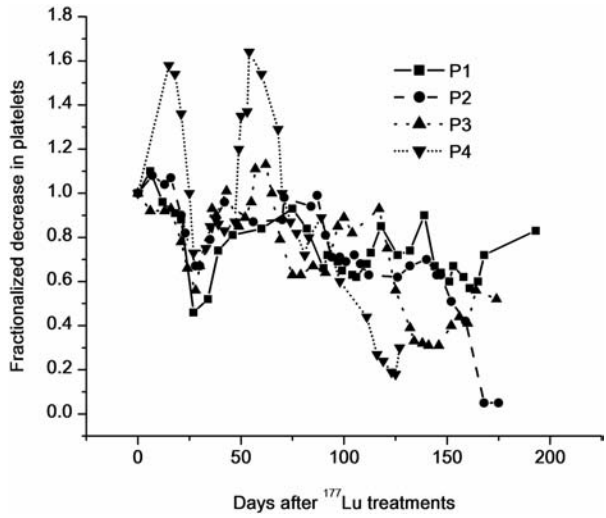

FIG. 3(a). Haematological toxicity (thrombocytopenia) in patients with prostate cancer (P1–P4) following treatment with three doses (1110 MBq/m^2) of ^{177}Lu-J591.

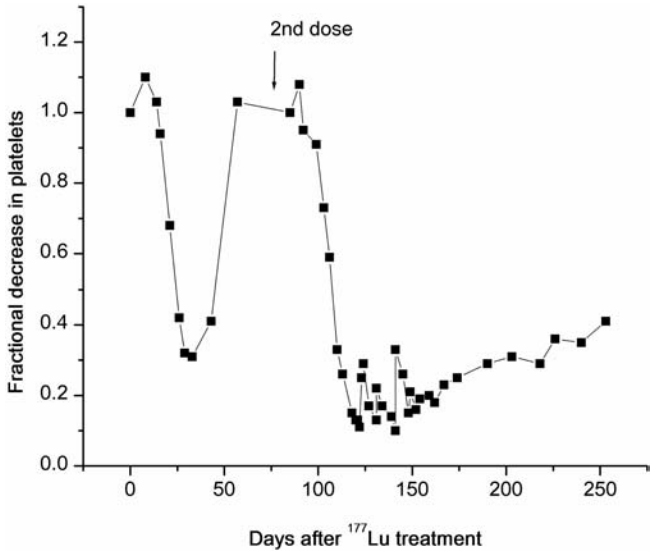

FIG. 3(b). Haematological toxicity (thrombocytopenia) in a patient with prostate cancer following treatment with two doses (1665 MBq/m^2 each) of ^{177}Lu-J591.

^{177}Lu dose (r = 0.88) and the bone marrow radiation dose based on blood radioactivity (Fig. 4 (a) and (b)).

6. FORMATION OF HUMAN ANTI-HUMAN ANTIBODIES

Human anti-human antibody assays were negative throughout the trial, including those patients receiving multiple doses. In the patients who received multiple doses, there was no change in the rate of drug clearance or tumour targeting on scans with sequential doses although, in some cases, it appeared that increased uptake and/or additional lesions were seen on the later antibody scan(s) consistent with disease progression (data not shown).

7. ANTI-TUMOUR RESPONSE

All 35 patients in this trial had abnormal, rising PSAs and 7 patients had measurable disease. None of the 7 patients with measurable disease had an objective tumour response nor a ≥50% PSA decline. On the basis of PSA, 14 patients demonstrated progressive disease (PSA increase of ≥25%) after

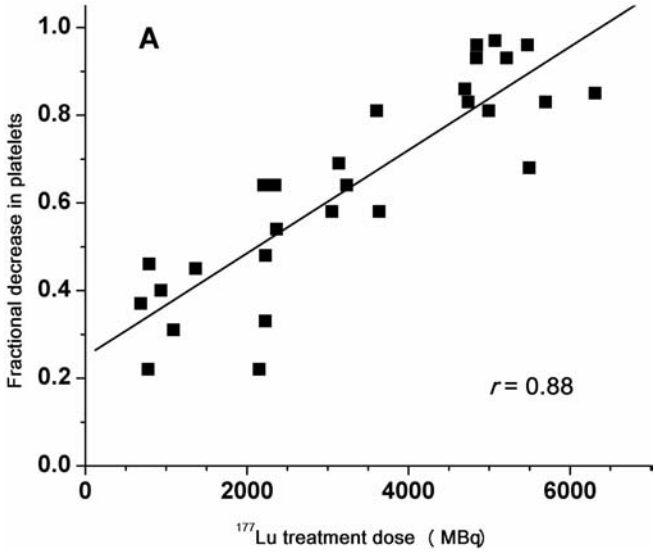

FIG. 4(a). Correlation of fractional decrease in platelets with the total treatment dose (MBq) of the ^{177}Lu-J591 antibody.

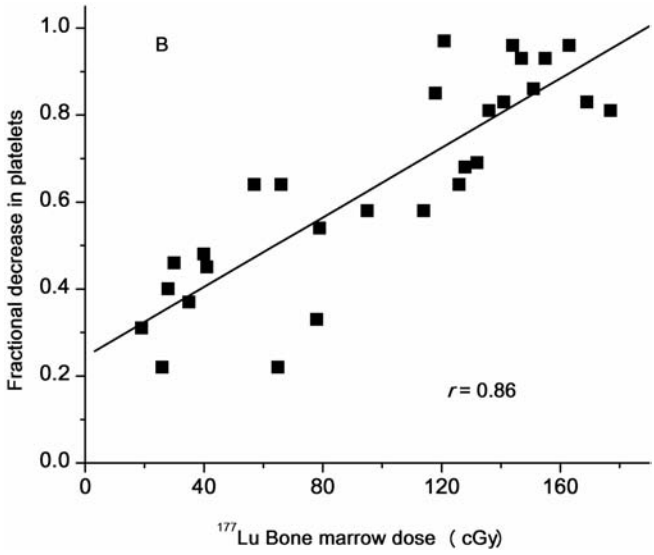

FIG. 4(b). Correlation of fractional decrease in platelets with bone marrow radiation absorbed dose (cGy) following treatment with the ^{177}Lu-J591 antibody.

treatment while 21 of the 35 patients had evidence of biological activity. Four patients had ≥50% PSA declines lasting 3+ to 8 months, and 16 patients had PSA stabilization (<25% increase from baseline) of ≥28 d. The median duration of PSA stabilization was 60 d with a range of 28–601+ d.

8. DISCUSSION

The de-immunized J591 mAb is the first radiolabelled antibody specific to the extracellular domain of PSMA to be tested as a radiotherapeutic in patients with prostate cancer. The authors have previously documented that radiolabelled J591 binds with high affinity (1nM) to PSMA and that the PSMA antibody complex is internalized, thereby delivering the radionuclide only to the interior of the targeted cancer cells [20, 22]. In nude mice bearing PSMA positive xenografts, the authors demonstrated the tumour specific localization of the J591 antibody labelled with ^{131}I and ^{111}In. Autoradiographic studies suggested that J591 preferentially accumulates in the areas of viable tumour [26]. In the same animal model, the authors have also compared the biodistribution of ^{111}In, ^{90}Y and ^{177}Lu labelled DOTA-J591 mAbs and reported that the biodistribution of ^{177}Lu and ^{90}Y-J591 were similar. However, the uptake and retention of ^{111}In activity in the liver and spleen were significantly higher [27]. In PSMA positive prostate cancer xenografts, RIT with single and multiple treatments demonstrated significant tumour reduction and prolongation of average life span with both ^{90}Y and ^{177}Lu labelled J591 antibodies [28].

In patients with prostate cancer, the authors have performed several phase I dose escalation studies to evaluate the safety and toxicity of RIT using ^{111}In, ^{90}Y and ^{177}Lu labelled de-immunized DOTA J591 mAb [6, 14, 29, 30]. Following intravenous administration of radiolabelled J591, the plasma clearance of ^{111}In-J591 (44.2 ± 14) and ^{177}Lu-J591 (43.6 ± 16) are quite similar [31]. Between these two tracers, statistically no significant differences were observed in biological half-life, area under the curve, maximum blood concentration at time zero, volume of distribution and clearance. The imaging studies, however, showed that there were minor differences in the biodistribution of ^{111}In and ^{177}Lu labelled J591 [31]. During the first week, both tracers showed a gradual accumulation in the liver and by day 6, the amount of ^{111}In activity was 25% higher compared to that with ^{177}Lu ($p < 0.05$). Radiation dosimetry estimates for ^{90}Y-J591 calculated from ^{111}In or ^{177}Lu data were mostly similar and show that the liver is the critical organ, followed by the spleen and kidney. The biodistribution studies in human subjects suggest that ^{177}Lu may be a potential alternative for estimating the pharmacokinetics and biodistribution of ^{90}Y labelled radiopharmaceuticals [31].

8.1. ^{177}Lu-J591 tumour targeting

The authors have previously published their experiences with regard to imaging studies using ^{111}In-J591, which clearly demonstrated excellent tumour targeting in PC patients without prior selection for PSMA expression [32]. In this trial, using the same preparation of DOTA-J591 and a similar patient population, the authors also studied the value of ^{177}Lu-J591 imaging studies to assess tumour targeting. The gamma emission from ^{177}Lu allows direct imaging and dosimetry determinations, thereby eliminating the need for a surrogate isotope such as ^{111}In for scintigraphy purposes. As in the authors' previous trials, patients in this trial were not pre-screened or selected for PSMA expression. Nevertheless, as previously observed with the J591 antibody, targeting in this trial was excellent, further confirming immunopathological studies indicating that all prostate cancers are PSMA positive and, therefore, potential candidates for J591 targeted monoclonal antibody vehicles. In this trial, all known lesions clinically defined on bone scan and computed tomography or magnetic resonance imaging were detectable on planar J591 images [30]. In at least three cases, bone lesions were apparent on the J591 scan prior to becoming evident on the conventional bone scan. Sequential imaging in patients who received multiple doses continued to localize in tumour sites with no change in pharmacokinetics or biodistribution, consistent with laboratory assays which demonstrated that the J591 antibody is not immunogenic and that human anti-human antibody development has not occurred.

8.2. ^{177}Lu-J591 toxicity

DLT in this trial, as in RIT trials in general, was limited to myelotoxicity. The MTD of a single dose of ^{177}Lu-J591 was 2590 MBq/m^2. This MTD is significantly higher than the MTD of 647.5 MBq/m^2 that the authors found with ^{90}Y using the same DOTA-J591 preparation in a similar patient population [29]. This finding likely relates to the lower energy and range of ^{177}Lu resulting in less bystander radiation to the marrow. The longer half-life, lower energy and shorter range of the beta emission of ^{177}Lu, relative to ^{90}Y, provide theoretical advantages in prostate cancer where the metastases tend to be small volume sites in marrow rather than bulky sites. Ultimately, of course, a higher MTD is irrelevant unless it results in an improved therapeutic ratio. There is limited prior experience with RIT in prostate cancer and no previous RIT trials have studied ^{177}Lu labelled antibodies in prostate cancer. The MTD of 2590 MBq/m^2, however, compares well with that of ^{131}I labelled mAbs in other RIT trials in prostate and other cancers. While ^{177}Lu and ^{131}I have similar decay

characteristics, use of the latter is compromised in this antigenic system as, after internalization, ^{131}I labelled antibody is rapidly dehalogenated and diffuses out of tumour cells while radiometals such as ^{177}Lu or ^{90}Y remain sequestered within the targeted tumour cells.

In this study, as in the authors' ^{90}Y-J591 trial, no clear relationship was found between toxicity and a history of prior chemotherapy treatment. Similarly, no correlation was found between toxicity and prior radiotherapy nor between toxicity and the extent of bone marrow involvement by cancer [30]. Similar observations in prostate cancer were made by Knox et al. [33] and O'Donnell et al. [34]. The non-haematological toxicity in RIT trials in general and in this ^{177}Lu-J591 trial was minimal and not dose limiting. Radiation dosimetry calculations indicate a radiation dose to liver is approximately 1088 cGy at the MTD of 2590 MBq/m^2. In addition, in this ^{177}Lu-J591 trial, no significant hepatotoxicity was seen in patients who received multiple doses, including 8 patients who received cumulative doses between 3330–4440 MBq/m^2. Radiation doses to kidney and spleen were also well within acceptable limits and no related organ toxicity was noted [31].

In patients who were treated with ^{177}Lu-J591, a strong correlation was observed between myelotoxicity and the amount of administered ^{177}Lu dose or the bone marrow absorbed radiation dose [35]. In contrast, the correlation between myelotoxicity and marrow radiation absorbed dose or the administered total MBq dose has been poor with ^{90}Y-J591. The similarly weak association between myelotoxicity and bone marrow radiation absorbed doses based on blood has been previously reported for both ^{131}I and ^{90}Y labelled mAbs. The authors believe that the demonstration of the predictability of myelotoxicity based on bone marrow radiation dose with ^{177}Lu, but not with the ^{90}Y radionuclide, may help us understand the importance of the energy of radiation and the relative in vivo stability of the radionuclide–antibody complex in the overall assessment of radiation dose and myelotoxicity.

8.3. ^{177}Lu-J591 retreatment

Sixteen of the 35 patients in ^{177}Lu trial received multiple doses. Two doses of 1665 or 2220 mCi/m^2, totalling 3330–4440 MBq/m^2, proved to be quite toxic, with 3 of 5 patients experiencing prolonged and incomplete platelet recovery. Two or more doses of 1110 MBq/m^2, however, were well tolerated and 4 patients received cumulative doses of 3330 MBq/m^2, almost 30% higher than the single dose MTD [30]. In this study, each dose was administered after allowing for haematological recovery from the prior dose. It therefore took 3–4 months to administer the three doses, resulting in a higher cumulative dose but lower dose rate. While there may be advantages to the higher cumulative

dose, the time required to deliver this dose using this regimen may be more than offset by unrelenting tumour progression. Given the kinetics of platelet decline and recovery, a dose interval of 14–17 d may allow a two dose regimen that might result in a higher cumulative dose than a single dose regimen to be given over a shorter period of time than attempted in this trial. Such a schedule would result in the onset of platelet recovery from the first dose coinciding with platelet decline from the second dose thereby resulting in a longer but shallower nadir than with a single MTD dose. Such a dose schedule remains to be explored.

9. CONCLUSION

The ^{177}Lu-J591 is well tolerated, non-immunogenic, can be administered in multiple doses and targets PC metastases with sensitivity and specificity. Having determined the single dose MTD of 2590 MBq/m^2 and the tolerability of multiple doses of ^{177}Lu-J591, phase 2 trials are being performed to assess anti-tumour activity in both the single and multiple dose formats. Although no patients in this trial had an objective measurable disease response (PR or CR), in the authors' ^{90}Y trial there was a correlation of PSA response with measurable disease response indicating that PSA was a reasonable measure of anti-tumour activity in the RIT setting. In the ^{177}Lu trial, 4 patients had PSA declines of ≥50% and 16 patients had PSA stabilization suggesting that ^{177}Lu-J591 may have biological activity. This merits exploration in a phase 2 trial. Additional studies can evaluate the combination of radiolabelled J591 plus chemotherapy, such as docetaxel, an agent active in prostate cancer and known to have radiosensitizing properties.

ACKNOWLEDGEMENTS

The following individuals are acknowledged for their substantial contribution to this trial: P.J. Kothari, K.A. Hamacher, M. Cobham, RN, F. Berger, RN, and M. Joyce, NP, and the technical staff in Nuclear Medicine and the General Clinical Research Center.

REFERENCES

[1] SURFACE, D., Promising isotopes - looking at lutetium-177 and other targeted radiotherapy isotopes, Radiology Today **5** (2004) 20.

[2] LEONARD, J.P., et al., Comparative physical and pharmacologic characteristics of iodine-131 and yttrium-90: Implications for radioimmunotherapy for patients with non-Hodgkin's lymphoma, Cancer Investigation **21** (2003) 241.

[3] KNAPP, F.F., et al., "Direct" production of lutetium-177 (Lu-177) from enriched Lu-176 in a high flux reactor - the only practical route to provide high multi curie levels of high specific activity Lu-177 required for routine clinical use. 5th Internation Conference of Isotopes, Brussels, Belgium, April 2005. Abstract book, page 11.

[4] CUTLER, C.S., Personal communication regarding specific activity of Lu-177, 2005.

[5] ISRAELI, R.S., et al., Expression of the prostate-specific membrane antigen, Cancer Res. **54** (1994) 1807.

[6] BANDER, N.H., et al., Targeted systemic therapy of prostate cancer with a monoclonal antibody to prostate specific membrane antigen (PSMA), Semin. Oncol. **30** (2003) 667.

[7] BOSTWICK, D.G., et al., Prostate specific membrane antigen expression in prostatic intra-epithelial neoplasia and adenocarcinoma: A study of 184 cases, Cancer **82** (1998) 2256.

[8] SILVER, D.A., et al., Prostate-specific membrane antigen expression in normal and malignant human tissues, Clin. Cancer. Res. **3** (1997) 81.

[9] WRIGHT, G.L., et al., Upregulation of prostate-specific membrane antigen after androgen-deprivation therapy, Urology **48** (1996) 326.

[10] SWEAT, S.D., et al., PSMA expression is greatest in prostate adenocarcinoma and lymph node metastases, Urology **52**, (1998) 637.

[11] TROYER, J.K., et al., Detection and characterization of the prostate-specific membrane antigen (PSMA) in tissue extracts and body fluids, Int. J. Cancer **62** (1995) 552.

[12] LIU, H., et al., Monoclonal antibodies to the extracellular domain of prostate specific membrane antigen also react with tumor endothelium, Cancer Res. **57** (1997) 3629.

[13] CHANG, S.S., et al., Five different anti-prostate-specific membrane antigen (PSMA) antibodies confirm PSMA expression in tumor-associated neovasculature, Cancer Res. **59** (1999) 3192.

[14] NANUS, D., et al., Clinical use of monoclonal antibody huJ591 therapy: Targeting prostate specific membrane ntigen, J.Urol. **170** (2003) S84.

[15] O'KEEFE, D.S., et al., Mapping, genomic organization and promotor analysis of the human prostate-specific membrane antigen gene, Biochim. Biophys. Acta. **144** (1998) 113.

[16] HOROSZEWICZ, J.S., et al., Monoclonal antibodies to a new antigenic marker in epithelial prostatic cells and serum of prostatic cancer patients, Anticancer Res. **7** (1987) 927.
[17] PETRONIS, J.D., et al., Indium-111 capromab pendetide (ProstaScint) imaging to detect recurrent and metastatic prostate cancer, Clin. Nucl. Med. **23** (1998) 672.
[18] ELGAMAL, A.A., et al., ProstaScint scan may enhance identification of prostate cancer recurrences after prostatectomy, radiation, or hormone therapy: analysis of 136 scans of 100 patients, Prostate **37** (1998) 261.
[19] TROYER, J.K., et al., Location of prostate-specific membrane antigen in the LNCaP prostate carcinoma cell line, Prostate **30** (1997), 232.
[20] LIU, H., et al., Constitutive and antibody-induced internalization of prostate-specific membrane antigen, Cancer Res. **58** (1998) 4055.
[21] HAMILTON, A., et al., A novel humanized antibody against prostate specific membrane antigen (PSMA) for *in vivo* targeting and therapy, Proc. Am. Assoc. Cancer Res. **39** (1998) 440.
[22] SMITH-JONES, P.M., et al., In vitro characterization of radiolabeled monoclonal antibodies specific for the extracellular domain of prostate specific membrane antigen, Cancer Res. **60** (2000) 5237.
[23] VALLABHAJOSULA, S., et al., Radiolabeled J591 antibody specific to prostate specific membrane antigen (PSMA): comparison of indium-111, yttrium-90 and lutetium-177, J. Label. Compd. Radiopharma., 46 (2003) S313.
[24] LINDMO, T., et al., Determination of the IF of radiolabeled monoclonal antibodies by linear extrapolation to binding at infinite antigen excess, J. Immunol. Methods **72** (1984) 77.
[25] KONISHI, S., et al., Determination of Immunoreactive Fraction of Radiolabeled MAbs: What is an Appropriate Method?, Cancer Biother. Radiopharmma. **19** (2004) 706.
[26] SMITH-JONES, P.M., et al., Radiolabeled monoclonal antibodies specific to the extracellular domain of prostate-specific membrane antigen: preclinical studies in nude mice bearing LNCaP human prostate tumor. J. Nucl. Med. **44** (2003) 610.
[27] SMITH-JONES, P.M., et al., Comparative biodistributions of ^{111}In-DOTA-J591 and ^{177}Lu-J591 in nude mice bearing LNCaP tumors, J. Nucl. Med. **42** (2001) 241.
[28] VALLABHAJOSULA, S., et al., Radioimmunotherapy of prostate cancer in human xenografts using monoclonal antibodies specific prostate specific membrane antigen (PSMA): Studies in nude mice, The prostate **58** (2004) 145.
[29] MILOWSKY, M.I., et al., Phase I trial of ^{90}Y-labeled anti-PSMA monoclonal antibody J591 for androgen-independent prostate cancer, J. Clin. Oncol. **22** (2004) 2522.
[30] BANDER, N.H., et al., Phase I trial of ^{177}Lutetium-labeled J591, a monoclonal antibody to prostate specific membrane antigen, in patients with androgen-independent prostate cancer, J. Clin. Oncol. **23** (2005) 4591.

[31] VALLABHAJOSULA, S., et al., Pharmacokinetics and biodistribution of ^{111}In and ^{177}Lu labeled J591 antibody specific to prostate specific membrane antigen: prediction of ^{90}Y-J591 radiation dosimetry based on ^{111}In or ^{177}Lu?, J. Nucl. Med. **46** (2005) 634.

[32] BANDER, N.H., et al., Targeting metastatic prostate cancer with radiolabeled monoclonal antibody J591 to the extracellular domain of prostate specific membrane antigen, J. Urology **170** (2003) 1717.

[33] KNOX, S.J., et al., Yttrium-90-labeled anti-CD20 monoclonal antibody therapy of recurrent B-cell lymphoma, Clin. Cancer Res. **2** (1996) 457.

[34] O'DONNELL, R.T., et al., Combined modality radioimmunotherapy for human prostate cancer xenografts with taxanes and ^{90}Yttrium-DOTA-peptide-ChL6, Prostate **50** (2002) 37.

[35] VALLABHAJOSULA, S., et al., Prediction of myelotoxicity based on bone marrow radiation absorbed dose: radioimmunotherapy studies using ^{90}Y and ^{177}Lu labeled J591 antibodies specific to prostate specific membrane antigen (PSMA), J. Nucl. Med. **46** (2005) 850.

RADIOLABELLED SOMATOSTATIN ANALOGUES FOR RADIONUCLIDE THERAPY OF TUMOURS

M. DE JONG, D. KWEKKEBOOM, R. VALKEMA, E. KRENNING
Department of Nuclear Medicine,
Erasmus MC,
Rotterdam, Netherlands
Email: m.hendriks-dejong@erasmusmc.nl

Abstract

Molecular imaging and therapy are rapidly developing and will become important topics in medicine in the 21st century. Radiolabelled peptides that bind to receptors form an important class of radiopharmaceuticals for tumour diagnosis and therapy. The specific receptor binding property of the peptide can be exploited by labelling with radionuclide and using the radiolabelled peptide as a vehicle to guide the radioactivity to tumours expressing a particular receptor. The high affinity of the peptide for the peptide–receptor complex facilitates high uptake of the radiolabel in receptor expressing tumours, while its relatively small size facilitates rapid clearance from blood, resulting in low background radioactivity. The use of radiolabelled peptides is growing rapidly due to these favourable characteristics, their low antigenicity and ease of production. Receptor binding peptides labelled with gamma radiation emitters or positron emitters enable non-evasive, whole body visualization. This process is referred to as peptide receptor scintigraphy and is being used to detect, stage and plan the therapy of receptor expressing tumours and also to follow tumours after therapy. In addition, labelled with a therapeutic beta emitter these peptide molecules have the potential to destroy receptor expressing tumours, an approach referred to as peptide receptor radionuclide therapy (PRRT). To date, five somatostatin receptor subtypes (sst_1–sst_5) have been identified and cloned. The diagnostic accuracy of ^{111}In labelled octreotide to visualize tumour lesions after intravenous injection has been determined in a large series of patients with sst_2 positive, mostly neuroendocrine tumours. Most interesting is the successful application of somatostatin analogues in PET, after labelling with positron emitters. The next logical step was to try to label these with therapeutic radionuclides and to treat receptor positive tumors with peptide receptor radionuclides. So far, ^{90}Y and ^{177}Lu are the most frequently used radionuclides in PRRT. The second generation somatostatin analogue DOTA-Tyr3-octreotide can form a stable complex with ^{90}Y. In rats with subcutaneous, CA20948 pancreatic tumours, ^{90}Y-DOTA-Tyr3-octreotide, effectively controlled tumour growth. Studies to determine the therapeutic efficacy of ^{90}Y-DOTA-Tyr3-octreotide in cancer patients are ongoing at various institutions and show most promising rates of complete plus partial remission. With the development of new somatostatin analogues that bind with high affinity receptors on

tumours, the available tools for radionuclide imaging and therapy of these tumours have increased significantly.

1. INTRODUCTION

The 14 amino acid peptide somatostatin plays an important role in the physiological regulation of hormones and organs in the body. Somatostatin effects are mediated by high affinity G-protein coupled membrane receptors, the integral membrane glycoproteins. Five different human somatostatin receptor subtypes have been cloned [1–3]. Somatostatin binds to all subtypes with high affinity.

The finding that somatostatin inhibits hormone secretion of various glands led to the use of somatostatin in the treatment of symptoms due to diseases with overproduction of hormones. The native peptide somatostatin is itself unsuitable for treatment, as after intravenous administration it has a very short half-life due to rapid enzymatic degradation. Therefore, somatostatin analogues that are more resistant to enzymatic degradation were synthesized. The molecule was modified in various ways with preservation of the biological activity of the original molecule, resulting in, for example, the 8 amino acids containing the somatostatin analogue octreotide, having a long and therapeutically useful plasma half-life. The affinity of the different somatostatin analogues for these subtypes differs considerably. Octreotide for example binds with high affinity to the somatostatin receptor subtype 2 (sst_2), and with lower affinities to sst_5 and sst_3. It shows no binding to sst_1 or sst_4 [2, 4].

Neuroendocrine gastro-entero-pancreatic (GEP) tumours, which comprise pancreatic islet cell tumours, non-functioning neuroendocrine pancreatic tumours and carcinoids are usually slow growing. When metastasized, the widely used treatment with stable somatostatin analogues results in reduced hormonal overproduction and symptomatic relief in most cases [5–8]. Treatment with somatostatin analogues, whether or not in combination with Interferon-alpha, is however seldom successful in terms of CT or MRI assessed tumour size reduction [9].

An interesting application of these peptides in nuclear medicine is the use of radiolabelled analogues for tumour scintigraphy after intravenous injection. The diagnostic peptide [^{111}In-DTPA]octreotide (OctreoScan, ^{111}In-pentetreotide) was approved by the FDA on 2 June 1994 for scintigraphy of patients with these somatostatin receptor positive tumours. As soon as the success of peptide receptor scintigraphy for tumour visualization became clear, the next logical step was to try to label these peptides with therapeutic radionuclides

and to perform peptide receptor radionuclide therapy (PRRT) of receptor positive GEP tumours.

2. [^{111}In-DTPA]OCTREOTIDE

The molecular basis for the use of radiolabelled octreotide in scintigraphy and radionuclide therapy is receptor mediated internalization and cellular retention of the radionuclide. Internalization of radiolabelled [DTPA]octreotide in somatostatin receptor positive tumours and tumour cell lines has been investigated [10–12]. It appeared that this process is receptor specific and temperature dependent. Receptor mediated internalization of [^{111}In-DTPA]octreotide results in degradation to the final radiolabelled metabolite, ^{111}In-DTPA-D-Phe, in the lysosomes [13]. This metabolite is not capable of passing the lysosomal and/or other cell membrane(s) and will therefore stay in the lysosomes, causing the long retention time of ^{111}In in sst_2 positive (tumour) cells. Internalization of [^{111}In-DTPA]octreotide is especially important for the radionuclide therapy of tumours when radionuclides emitting therapeutic particles with very short path lengths are used, such as those emitting Auger electrons. These electrons are only effective at a short distance of only a few nanometres up to micrometres from their target, the nuclear DNA. Recently, Hornick et al. [14] and Wang et al. [15] described in vitro cellular internalization, nuclear translocation and DNA binding of radiolabelled somatostatin analogues, which significantly increased after prolonged exposure. Indium-111 labelled peptides are therefore suitable for both scintigraphy and radionuclide therapy, all the more so as the decay of Auger electron emitters has recently been shown to lead to a 'bystander' effect, an in vivo, dose independent inhibition or retardation of tumour growth in non-radiotargeted cells by a signal produced in Auger electron labelled cells [16].

2.1. Clinical studies with [^{111}In-DTPA]octreotide

Initial studies with high dosages of [^{111}In-DTPA]octreotide in patients with metastasized neuroendocrine tumours were encouraging, although partial remissions were exceptional. Fifty patients with somatostatin receptor positive tumours, of which 26 had GEP tumours, were treated with multiple doses of [^{111}In-DTPA]octreotide in Rotterdam [17, 18]. Forty patients were evaluable after cumulative doses of at least 20 GBq up to 160 GBq. The therapeutic effects found in the patients with GEP tumours were no partial remissions, minor remissions (i.e. a decrease in tumour size of 25–50%, as measured on CT scans) in 5 patients, and stabilization of previously progressive tumours in

11 patients, underscoring the therapeutic potential of Auger emitting radiolabelled peptides. The toxicity was generally mild bone marrow toxicity. However, 3 out of the 6 patients who received more than 100 GBq developed a myelodysplastic syndrome or leukemia. Therefore, 100 GBq was considered the maximum tolerable dose. With a renal radiation dose of 0.45 mGy/MBq (based on previous studies), a cumulative dose of 100 GBq will lead to 45 Gy on the kidneys, twice the accepted limit for external beam radiation. However, no development of hypertension, proteinuria, or significant changes in serum creatinine or creatinine clearance were observed in the patients, including the 2 patients who received 106 and 113 GBq of [^{111}In-DTPA]octreotide without renal protection by infusion with amino acids (see further) over a follow-up period of 3 and 2 years, respectively. These findings show that the radiation of the short range Auger electrons originating from the cells of the proximal tubules is not harmful for the renal function. The decrease in serum inhibin B and concomitant increase of serum FSH levels in males indicate that spermatogenesis was impaired.

At the Louisiana State University Medical Center in New Orleans, a clinical trial was performed to determine the effectiveness and tolerability of therapeutic doses of [^{111}In-DTPA]octreotide in patients with GEP tumours [19–21]. GEP tumour patients who had failed all forms of conventional therapy, with worsening of tumour related signs and symptoms and/or radiographically documented progressive disease, an expected survival of less than 6 months and somatostatin receptor expression on the tumour as determined by the uptake on a 222 MBq [^{111}In-DTPA]octreotide scan, were treated with at least 2 monthly 6.6 GBq intravenous injections. Twenty-seven GEP (24 carcinoid neoplasms with carcinoid syndrome and 3 pancreatic islet cells) patients were accrued. Clinical benefit occurred in 16 (62%) patients. Objective partial responses on CT occurred in 2 (8%) patients. The following transient grades 3/4 side effects were observed, respectively: leucocytes: 1/1; platelets: 0/2; haemoglobin: 3/0; bilirubin: 1/3; creatinine: 1/0; neurological: 1/0. The renal insufficiency in one patient was probably not treatment related but due to pre-existent retroperitoneal fibrosis. Transient liver toxicity was observed in 3 patients with widespread liver metastases. Myeloproliferative disease and/or myelodysplastic syndrome had not been observed in the 6 patients followed up for 48+ months. It was concluded that two doses (6.6 GBq each) of [^{111}In-DTPA]octreotide were safe, well tolerated and improved symptoms in 62% of patients, with 8% partial radiographic responses and increased expected survival in GEP cancer patients with somatostatin receptor expressing tumours.

Both series had relatively high numbers of GEP cancer patients who were in a poor clinical condition upon study entry. Also, many had progressive

disease when entering the study. Although in both series favourable effects on symptomatology were reported, CT assessed tumour regression was only observed in rare cases.

Stokkel et al. [22] recently reported on a study that determined the effect of [^{111}In-DTPA]octreotide therapy in patients with progressive radioiodine non-responsive thyroid cancer. Therapeutic effects were determined in relation to [^{111}In-DTPA]octreotide uptake by tumour localizations assessed on pre-treatment diagnostic [^{111}In-DTPA]octreotide scans. Eleven patients, selected on positive pretreatment diagnostic scans, were treated with up to four fixed doses of 7400 MBq [^{111}In-DTPA]octreotide with an interval of 2–3 weeks between the doses. In 44% of the patients, stable disease was achieved up to 6 months after the first treatment. These four patients had relatively low pretreatment thyroglobulin values, representing limited metastasized disease. It was therefore concluded that treatment with high doses of [^{111}In-DTPA]octreotide in differentiated thyroid cancer can result in stable disease in a subgroup of patients, whereas low pretreatment thyroglobulin value, representing a small tumour load, might be a selection criterion for treatment.

It was concluded that ^{111}In coupled peptides are not ideal for PRRT because of the small particle range and therefore short tissue penetration. Consequently, various research groups have aimed to develop somatostatin analogues that can be linked via a chelator to a therapeutic radionuclide. DOTA is a universal chelator capable of forming stable complexes with such metals as ^{111}In, ^{67}Ga, ^{68}Ga, ^{86}Y and ^{64}Cu for imaging as well as with ^{90}Y and with radiolanthanides such as ^{177}Lu for receptor mediated radionuclide therapy [23–25]. In addition, new somatostatin analogues were synthesized to improve receptor affinity [4, 26].

3. OTHER SOMATOSTATIN ANALOGUES

After ^{111}In, the next radionuclide investigated for PRRT was ^{90}Y, emitting ß particles with a high maximum energy (2.27 MeV) and a long maximum particle range. The first somatostatin analogue radiolabelled with ^{90}Y and applied for PRRT in animals and patients was [^{90}Y-DOTA,Tyr^3]octreotide, in which, in comparison with octreotide, the phenylalanine residue at position 3 has been replaced with tyrosine; this makes the compound more hydrophilic and increases the affinity for sst_2, leading to higher uptake in sst_2 positive tumours both in preclinical studies and in patients [27, 28].

The next analogue investigated in preclinical radionuclide therapy studies was [^{177}Lu-DOTA,Tyr^3]octreotate. This somatostatin analogue has a very high affinity for sst_2 [4] and after radiolabelling with ^{177}Lu high tumour uptake was

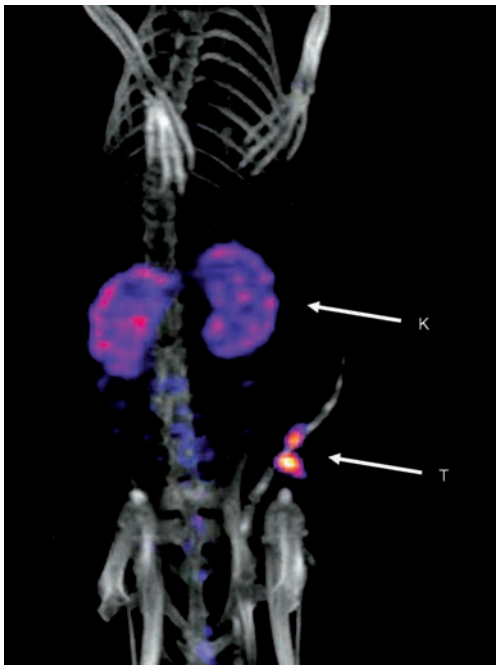

FIG. 1. SPECT/CT image (NanoSPECT, BioScan, United States of America) of a rat bearing small CA20948 tumours on flank and injected with [^{177}Lu-DOTA,Tyr^3]octreotide.

seen, even very small tumours could be visualized (Fig. 1) and very good anti-tumour effects were found in therapeutic studies in animal models [29–31]. Lutetium-177 emits gamma radiation with a suitable energy for imaging and therapeutic β particles with low to medium energy (maximum 0.50 MeV), so the same compound can be used for imaging and dosimetry and radionuclide therapy, thus obviating the need for a pretherapeutic dosimetric study. The approximate range of the β particles is 20 cell diameters, whereas the range of those emitted by ^{90}Y is 150 cell diameters. Less 'cross-fire' induced radiation damage in the radiosensitive renal glomeruli (see below) can therefore be expected with ^{177}Lu. Also, in comparison with ^{90}Y, a higher percentage of the ^{177}Lu radiation energy will be absorbed in very small tumours and (micro)metastases [24, 29, 32].

3.1. Reduction of renal uptake

One problem arising during radionuclide therapy may be caused by the uptake and retention of radioactivity in the radiosensitive kidneys; small

radiolabelled peptides in the blood plasma are filtered through the glomerular capillaries in the kidneys and subsequently partly reabsorbed by, and retained in, the proximal tubular cells, thereby reducing the scintigraphic sensitivity for detection of small tumours in the perirenal region and the possibilities for radionuclide therapy. It was shown that the renal uptake of radiolabelled octreotide in rats could be reduced by positively charged amino acids, such as lysine and arginine. About a 50% reduction could be obtained by single intravenous administration of 400 mg/kg of L- or D-lysine [33, 34]. Therefore, during PRRT, an infusion containing the positively charged amino acids L-lysine and L-arginine can be given during and after the infusion of the radiopharmaceutical, in order to reduce the kidney uptake. Various protocols have been described, resulting in up to a 55% reduction in renal uptake of radioactivity, thereby allowing a higher administered dose [35–38]. The authors' preferred protocol comprises a combination of lysine and arginine. Patients receive a 1 L infusion (500 mL of L-lysine HCl 5% plus 250 mL of L-arginine HCl 10% plus 250 mL saline, brought to pH7.4). This infusion lasts 4 h; it starts 30 min prior to the radiopeptide injection and a constant infusion rate is used throughout the infusion period [35].

3.2. Clinical studies with [^{90}Y-DOTA,Tyr^3]octreotide

Various multicentre phase 1 and phase 2 PRRT trials have been performed using these ^{90}Y and ^{177}Lu labelled somatostatin analogues. Otte et al. [39–41] and Waldherr et al. (University Hospital, Basel, Switzerland) reported different phase 1 and phase 2 studies in patients with neuroendocrine GEP tumours. Otte et al. [39–41] described a study in which patients received four or more single doses of [^{90}Y-DOTA,Tyr^3]octreotide with ascending activity at intervals of approximately 6 weeks (cumulative dose 6.12 ± 1.3 GBq/m^2) with the aim of performing an intra-patient dose escalation study. In total, 127 single treatments were given. In 8 of these 127 single treatments, total doses of ≥3.7 GBq were administered. In an effort to prevent renal toxicity, two patients received Hartmann-Hepa 8% amino acids (including lysine and arginine) solution during all therapy cycles, while 13 patients did so during some but not all therapy cycles; in 14 patients no solution was administered during the therapy cycles. Of the 29 patients, 24 showed no severe renal or haematological toxicity (toxicity ≤grade 2 according to the National Cancer Institute grading criteria). These 24 patients received a cumulative dose of ≤7.4 GBq/m^2. Five patients developed renal and/or haematological toxicity. All five patients received a cumulative dose of >7.4 GBq/m^2 and had received no Hartmann-Hepa 8% solution during the therapy cycles. Four of the five patients developed renal toxicity; two of these patients showed stable renal insufficiency

and two required haemodialysis. Two of the five patients exhibited anaemia (both grade 3) and thrombocytopenia (grades 2 and 4, respectively). Twenty of the 29 patients had disease stabilization, two a partial remission, four a reduction of tumour mass of <50% and three a progression of tumour growth.

Waldherr et al. reported several phase 2 studies in patients with neuroendocrine tumours [42–44]. The patients received four or more single doses of [^{90}Y-DOTA,Tyr^3]octreotide with ascending activity at intervals of approximately 6 weeks. Observed renal or haematological toxicity was ≤grade 2 according to the National Cancer Institute grading criteria. The cumulative dose was ≤7.4 GBq/m^2. Complete and partial responses obtained in different studies amounted to 24%. In addition, distinct protocols were compared: in the above mentioned studies, patients received four injections of 1.85 GBq/m^2 (at intervals of around 6 weeks), while in another study two injections of 3.7 GBq/m^2 were administered at an interval of 8 weeks. Interestingly, the results from the last study were the most impressive. A higher percentage of complete responses plus partial remissions (24% after four injections versus 33% after two injections) was found, while side effects were not significantly different [44]. It should be emphasized, however, that this was not a randomized trial comparing two dosing schemes.

Forrer et al. recently described the results of a study with [^{90}Y-DOTA,Tyr^3]octreotide in which 116 patients with metastatic neuroendocrine tumours were included [45]. All patients were pre-therapeutically staged with morphological imaging procedures and with somatostatin receptor scintigraphy. The scintigraphy was positive in all cases. The patients were treated with 6–7.4 GBq/m^2 body surface. In this study, complete remissions were found in 4%, partial remissions in 23%, stabilization in 62% and progressive disease in 11%. A significant reduction of symptoms was found in 83%. No serious adverse event occurred and the toxicity was acceptable [45].

Chinol et al. from the European Institute of Oncology (Milan, Italy) described dosimetric and dose finding studies with [^{90}Y-DOTA,Tyr^3]octreotide with and without the administration of kidney protecting agents [46]. No major acute reactions were observed up to an administered dose of 5.6 GBq per cycle. Reversible grade 3 haematological toxicity was found in patients injected with 5.2 GBq, which was defined as the maximum tolerated dose per cycle. None of the patients developed acute or delayed kidney nephropathy, although follow-up was short. Partial and complete remissions were reported by the same group in 28% of 87 patients with neuroendocrine tumours [47]. In more detailed publications from the same group, Bodei et al. [36, 38] report the results of a phase 1 study of 40 patients with somatostatin receptor positive tumours, of whom 21 had GEP tumours. Cumulative total treatment doses were in the range 5.9–11.1 GBq, given in two treatment cycles. Six of 21 (29%) patients had

tumour regression. Median duration of the response was 9 months. Bodei et al. also recently evaluated the efficacy of [^{90}Y-DOTA,Tyr^3]octreotide therapy in metastatic MTC patients with a positive [^{111}In-DTPA]octreotide scintigram, progressing after conventional treatments. Twenty-one patients were retrospectively evaluated after therapy, receiving 7.5–19.2 GBq in 2–8 cycles. Two patients (10%) obtained a CR, while stable disease was observed in 12 patients (57%); 7 patients (33%) did not respond to therapy. The duration of the response was in the range 3–40 months [38].

Another study with [^{90}Y-DOTA,Tyr^3]octreotide (OctreoTher, ^{90}Y-SMT-487) was the phase 1 Novartis study performed in Rotterdam, Brussels and Tampa, which aimed to define the maximum tolerated single and four cycle doses of [^{90}Y-DOTA,Tyr^3]octreotide and in which patients received escalating doses up to 14.8 GBq/m^2 in 4 cycles or up to a 9.3 GBq/m^2 single dose, without reaching the maximum tolerated single dose [18, 48, 49]. The cumulative radiation dose to kidneys was limited to 27 Gy. All patients received amino acids concomitant with [^{90}Y-DOTA,Tyr^3]octreotide for kidney protection. Three patients had dose limiting toxicity: 1 liver toxicity, 1 thrombocytopenia grade 4 ($<25 \times 10^9$/L) and 1 myelodysplastic syndrome. Four out of 54 (7%) patients who had received their maximum allowed dose had partial remission and 7 (13%) minor remission. The median time to progression in the 44 patients who had either stable disease, minor remission or partial remission was 30 months. An important observation in this study was a clear dose–response relation; the percentage reduction in tumour volume increased with increasing tumour radiation dose (up to about 600 Gy) [50]. Prior chemotherapy was predisposed to haematological toxicity. Renal toxicity was mild in these patients, with individualized dosimetry and amino acid infusion for kidney protection. Despite the differences in the protocols used, the rate of complete plus partial responses seen in the various aforementioned [^{90}Y-DOTA,Tyr^3]octreotide studies consistently exceeds that obtained with [^{111}In-DTPA]octreotide (see above).

3.3. Clinical studies with [^{177}Lu-DOTA,Tyr^3]octreotate

Most promising is the use of [^{177}Lu-DOTA,Tyr^3]octreotate. In patients, it was found that the uptake of radioactivity, expressed as a percentage of the injected dose of [^{177}Lu-DOTA,Tyr^3]octreotate was comparable to that of [^{111}In-DTPA^0]octreotide for kidneys, spleen and liver, but was three- to fourfold higher for 4 of 5 tumours [37]. Therefore, [^{177}Lu-DOTA,Tyr^3]octreotate potentially represents an important improvement because of the higher absorbed doses that can be achieved in most tumours with about equal doses to potentially dose limiting organs and because of the lower tissue penetration

range of ^{177}Lu when compared with ^{90}Y, which may be especially important for small tumours [24].

The first treatment effects of [^{177}Lu-DOTA,Tyr^3]octreotate therapy were described in 35 patients with neuroendocrine GEP tumours, who had a follow-up of 3–6 months after receiving their final dose [51]. Patients were treated with dosages of 3.7, 5.6, or 7.4 GBq [^{177}Lu-DOTA,Tyr^3]octreotate, up to a final cumulative dose of 22.2–29.6 GBq, with treatment intervals of 6–9 weeks. The effects of the therapy on tumour size were evaluable in 34 patients. Three months after the final administration a complete remission was found in one patient (3%), partial remission in 12 (35%), stable disease in 14 (41%) and progressive disease in 7 (21%), including 3 patients who died during the treatment period. The side effects of treatment with [^{177}Lu-DOTA,Tyr^3]octreotate were few and mostly transient, with mild bone marrow depression the most common finding. In a more recent update of this treatment in 76 patients with GEP tumours [52], complete remission was found in 1 patient (1%), partial remission in 22 (29%), minor remission in 9 (12%), stable disease in 30 (39%), and PD in 14 patients (18%). Six out of 32 patients who had initially stable disease or tumour regression after the therapy and who were also evaluated after 12 months (mean 18 months from therapy start) became progressive; in the other 26 the tumour response was unchanged. Median time to progression was not reached at 25 months from start of therapy. Serious side effects in the whole group of patients who had been treated or were being treated up to that moment consisted of myelodysplastic syndrome in a patient who had had chemotherapy with alkylating agents two years before entering the study and renal insufficiency in another patient who had had unexplained rises in serum creatinine concentrations in the year preceding the start of therapy and who had a urinary creatinine clearance of 41 mL/min when entering the study. Tumour regression was positively correlated with a high uptake on the [^{111}In-DTPA]octreotide scintigram, limited hepatic tumour mass and high Karnofsky performance score.

In patients with progressive metastatic (or recurrent) differentiated thyroid carcinoma (DTC) who do not respond to radioiodine therapy or do not show uptake on radioiodine scintigraphy, treatment options are few. As these tumours may express somatostatin receptors, PRRT using somatostatin analogues might be effective and therefore the authors evaluated the therapeutic efficacy of [^{177}Lu-DOTA,Tyr^3]octreotate in patients with DTC. In addition, the uptake of radioactivity in the tumours was studied in relation to treatment outcome. Five patients with DTC were treated with 22.4–30.1 GBq of [^{177}Lu-DOTA,Tyr^3]octreotate. Three patients had Hürthle cell thyroid carcinoma, one patient had papillary thyroid carcinoma and one had follicular thyroid carcinoma. The uptake on [^{177}Lu-DOTA,Tyr^3]octreotate scintigraphy

was compared with the uptake on the pre-therapy [^{111}In-DTPA]octreotide scintigram. After the last treatment with [^{177}Lu-DOTA,Tyr^3]octreotate, one patient had stable disease as the maximum response, whereas the other two patients had minor remission and partial remission, respectively. The response in papillary thyroid carcinoma and follicular thyroid carcinoma was stable disease and progressive disease, respectively. The patients with minor remission and partial remission had the highest [^{177}Lu-DOTA,Tyr^3]octreotate versus [^{111}In-DTPA]octreotide uptake ratios. The authors concluded that in patients with progressive DTC with no therapeutic option left and with sufficient uptake of [^{111}In-DTPA]octreotide in the tumour lesions, [^{177}Lu-DOTA,Tyr^3]octreotate therapy can be effective. This finding is especially important in patients with Hürthle cell thyroid carcinoma, as these patients cannot benefit from radioiodine therapy because of non-iodine avid lesions at diagnosis [53].

3.4. Comparison of the different treatments

Treatment with radiolabelled somatostatin analogues is a promising new tool in the management of patients with inoperable or metastasized neuroendocrine tumours. The results that were obtained with [^{90}Y-DOTA,Tyr^3]octreotide and [^{177}Lu-DOTA,Tyr^3]octreotate are very encouraging, although a direct, randomized comparison between the various treatments is lacking. Also, the reported percentages of tumour remission after [^{90}Y-DOTA,Tyr^3]octreotide treatment vary. This may be due to several causes: (i) the administered doses and dosing schemes differ; some studies use dose escalating schemes, whereas others use fixed doses; and (ii) there are several patient and tumour characteristics that determine treatment outcome, such as the amount of uptake on the [^{111}In-DTPA]octreotide scintigram, the estimated total tumour burden and the extent of liver involvement. Therefore, differences in patient selection may play an important role in determining treatment outcome. Other factors that can have contributed to the different results that were found in the different centres performing trials with the same compounds may be differences in tumour response criteria and centralized versus decentralized follow-up CT scoring. Therefore, in order to establish which treatment scheme and which radiolabelled somatostatin analogue or combination of analogues is optimal, randomized trials are needed.

3.5. [^{90}Y-DOTA]lanreotide

Virgolini et al. developed an ^{111}In–^{90}Y labelled somatostatin analogue, [DOTA]lanreotide, for tumour diagnosis and therapy [54–57]. They described

that ^{111}In labelled [DOTA]lanreotide bound with high affinity to $hsst_2$, $hsst_3$, $hsst_4$ and $hsst_5$ and with lower affinity to $hsst_1$ expressed on COS7 cells, making it a universal receptor binder [58]. However, Reubi et al. found in vitro in cell lines transfected with the different somatostatin receptor subtypes and that whereas [^{90}Y-DOTA]lanreotide had a good affinity for the sst_5, it had a low affinity for sst_3 (IC_{50} 290nM) and sst_4 (IC_{50} > 10 000nM) [4]. Froidevaux et al. [59] concluded from their comparison study of, among other things, [DOTA,Tyr^3]octreotide and [DOTA]lanreotide in rats that radiolabelled [DOTA,Tyr^3]octreotide has more potential for clinical application than [DOTA]lanreotide.

3.6. Clinical data with [^{90}Y-DOTA]lanreotide

Lanreotide labelled with ^{90}Y was the second analogue used for clinical PRRT studies at different centres in the MAURITIUS trial [56]. In this study, cumulative treatment doses of up to 8.58 GBq [^{90}Y-DOTA]lanreotide were given as a short term intravenous infusion. Treatment results in 154 patients indicated minor responses in 14%. No severe, acute or chronic haematological toxicity or changes in renal or liver function parameters due to [^{90}Y-DOTA]lanreotide were reported. In two-thirds of patients with neuroendocrine tumour lesions, [^{90}Y-DOTA,Tyr^3]octreotide showed a higher tumour uptake than [^{90}Y-DOTA]lanreotide, which can be explained by the lower affinity of [^{90}Y-DOTA]lanreotide for sst_2.

3.7. Patient characteristics

Despite differences in amounts and types of radioactivity that are administered, there are also shared patient and disease characteristics as well as similar exclusion and inclusion criteria between the various studies with radiolabelled somatostatin analogues.

Needless to say, all protocols share the feature that the patients' tumours have to show uptake on the diagnostic [^{111}In-DTPA]octreotide scintigram. In some studies, the amount of uptake has at least to equal that of normal liver tissue, in others it is required to be more than that. Most studies also require a patient life expectancy of at least 3–6 months, which makes sense if the administration of the total cumulative dose takes several months and one of the studies' objectives is to evaluate tumour response. Also, as in all studies with new treatment modalities, other, accepted, treatments have to be exhausted (i.e. in case of neuroendocrine GEP tumours) and that tumours have to be inoperable or metastasized. Because of the absorbed radiation doses, especially to the kidneys and the bone marrow, most studies require certain minimum

kidney function and haematological parameters for study entry and for each new administration. Lastly, the patients have to meet a minimum performance score as they are isolated in a nuclear medicine ward for a variable time, depending on national laws on radiation protection.

4. OPTIONS TO IMPROVE PRRT

From animal experiments it can be inferred that ^{90}Y labelled somatostatin analogues may be more effective for larger tumours, whereas ^{177}Lu labelled somatostatin analogues may be more effective for smaller tumours, but their combination may be the most effective [24]. Therefore, apart from comparisons between radiolabelled octreotate and octreotide, and between somatostatin analogues labelled with ^{90}Y or ^{177}Lu, PRRT with combinations of ^{90}Y and ^{177}Lu labelled analogues should also be evaluated. Apart from the combination of analogues labelled with different radionuclides, future efforts to improve this therapy will also mean increasing the somatostatin receptor number on the tumours, studying the effects of radiosensitizers as well as developing new peptide analogues. An interesting example is [DOTA, 1-Nal^3]octreotide, which has a high affinity for sst_2, sst_3 and sst_5 [60]. This compound may allow the PRRT of tumours which do not bind octreotide and octreotate with high affinity, i.e. sst_3 and sst_5 positive tumours.

5. CONCLUSION

Treatment with radiolabelled somatostatin analogues is a promising new tool in the management of patients with inoperable or metastasized (neuro)endocrine tumours. Symptomatic improvement may occur with all ^{111}In, ^{90}Y, or ^{177}Lu labelled somatostatin analogues that have been used for PRRT. In particular, the results that were obtained with [^{90}Y-DOTA,Tyr^3]octreotide and [^{177}Lu-DOTA,Tyr^3]octreotate are very encouraging in terms of tumour regression. Also, if kidney protective agents are used, the side effects of this therapy are few and mild and the duration of the therapy response for both radiopharmaceuticals is more than two years. These data compare favourably with the limited number of alternative treatment approaches.

REFERENCES

[1] PATEL, Y.C., et al., The somatostatin receptor family. Life Sci, 1995. 57(13): p. 1249-65.
[2] PATEL, Y.C., Somatostatin and its receptor family. Front Neuroendocrinol, 1999. 20(3): p. 157-98.
[3] SCHONBRUNN, A., Somatostatin receptors present knowledge and future directions. Ann Oncol, 1999. 10(Suppl 2): p. S17-21.
[4] REUBI, J.C., et al., Affinity profiles for human somatostatin receptor subtypes SST1-SST5 of somatostatin radiotracers selected for scintigraphic and radiotherapeutic use. Eur J Nucl Med, 2000. 27(3): p. 273-82.
[5] KVOLS, L.K., et al., Treatment of the malignant carcinoid syndrome. Evaluation of a long- acting somatostatin analogue. N Engl J Med, 1986. 315(11): p. 663-6.
[6] ERIKSSON, B., OBERG, K., Summing up 15 years of somatostatin analog therapy in neuroendocrine tumors: future outlook. Ann Oncol, 1999. 10(Suppl 2): p. S31-8.
[7] LAMBERTS, S.W., KRENNING, E.P., REUBI, J.C., The role of somatostatin and its analogs in the diagnosis and treatment of tumors. Endocr Rev, 1991. 12(4): p. 450-82.
[8] LAMBERTS, S.W., REUBI, J.C., KRENNING, E.P., Somatostatin analogs in the treatment of acromegaly. Endocrinol Metab Clin North Am, 1992. 21(3): p. 737-52.
[9] JANSON, E.T., OBERG, K., Long-term management of the carcinoid syndrome. Treatment with octreotide alone and in combination with alpha-interferon. Acta Oncol, 1993. 32(2): p. 225-9.
[10] ANDERSSON, P., et al., Internalization of indium-111 into human neuroendocrine tumor cells after incubation with indium-111-DTPA-D-Phe1-octreotide. J Nucl Med, 1996. 37(12): p. 2002-6.
[11] DE JONG, M., et al., Internalization of radiolabelled [DTPA0]octreotide and [DOTA0,Tyr3]octreotide: peptides for somatostatin receptor-targeted scintigraphy and radionuclide therapy. Nucl Med Commun, 1998. 19(3): p. 283-8.
[12] HOFLAND, L.J., VAN KOETSVELD, P.M., WAAIJERS, M., LAMBERTS, S.W., Internalisation of isotope-coupled somatostatin analogues. Digestion, 1996. 57(Suppl 1): p. 2-6.
[13] DUNCAN, J.R., STEPHENSON, M.T., WU, H.P., ANDERSON, C.J., Indium-111-diethylenetriaminepentaacetic acid-octreotide is delivered in vivo to pancreatic, tumor cell, renal, and hepatocyte lysosomes. Cancer Res, 1997. 57(4): p. 659-71.
[14] HORNIK, C.A., et al., Progressive nuclear translocation of somatostatin analogs. J Nucl Med, 2000. 41(7): p. 1256-63.
[15] WANG, M., et al., Subcellular localization of radiolabeled somatostatin analogues: implications for targeted radiotherapy of cancer. Cancer Res, 2003. 63(20): p. 6864-9.

[16] XUE, L.Y., BUTLER, N.J., MAKRIGIORGOS, G.M., ADELSTEIN, S.J., KASSIS, A.I., Bystander effect produced by radiolabeled tumor cells in vivo. Proc Natl Acad Sci U S A, 2002. 99(21): p. 13765-70.

[17] VALKEMA, R., et al., Phase I study of peptide receptor radionuclide therapy with [In- DTPA]octreotide: the Rotterdam experience. Semin Nucl Med, 2002. 32(2): p. 110-22.

[18] VALKEMA, R., et al., Long-term follow-up of a phase 1 study of peptide receptor radionuclide therapy (PRRT) with [90Y-DOTA0,Tyr3]octreotide in patients with somatostatin receptor positive tumours. Eur J Nucl Med Mol Imaging, 2003. 30: p. S232.

[19] ANTHONY, L.B., et al., Indium-111-pentetreotide prolongs survival in gastroenteropancreatic malignancies. Semin Nucl Med, 2002. 32(2): p. 123-32.

[20] McCARTHY, K.E., WOLTERING, E.A., ANTHONY, L.B., In situ radiotherapy with 111In-pentetreotide. State of the art and perspectives. Q J Nucl Med, 2000. 44(1): p. 88-95.

[21] McCARTHY, K.E., et al., In situ radiotherapy with 111In-pentetreotide: initial observations and future directions. Cancer J Sci Am, 1998. 4(2): p. 94-102.

[22] STOKKEL, M.P., VERKOOIJEN, R.B., BOUWSMA, H., SMIT, J.W., Six month follow-up after 111In-DTPA-octreotide therapy in patients with progressive radioiodine non-responsive thyroid cancer: a pilot study. Nucl Med Commun, 2004. 25(7): p. 683-90.

[23] BREEMAN, W.A., et al., Radiolabelling DOTA-peptides with (68)Ga. Eur J Nucl Med Mol Imaging, 2005.

[24] DE JONG, M., BREEMAN, W.A., VALKEMA, R., BERNARD, B.F., KRENNING, E.P., Combination radionuclide therapy using 177Lu- and 90Y-labeled somatostatin analogs. J Nucl Med, 2005. 46 Suppl 1: p. 13S-7S.

[25] BREEMAN, W.A., DE JONG, M., VISSER, T.J., ERION, J.L., KRENNING, E.P., Optimising conditions for radiolabelling of DOTA-peptides with 90Y, 111In and 177Lu at high specific activities. Eur J Nucl Med Mol Imaging, 2003. 30(6): p. 917-20.

[26] DE JONG, M., et al., Pre-clinical comparison of [DTPA0] octreotide, [DTPA0,Tyr3] octreotide and [DOTA0,Tyr3] octreotide as carriers for somatostatin receptor- targeted scintigraphy and radionuclide therapy. Int J Cancer, 1998. 75(3): p. 406-11.

[27] DE JONG, M., et al., Comparison of (111)In-labeled somatostatin analogues for tumor scintigraphy and radionuclide therapy. Cancer Res, 1998. 58(3): p. 437-41.

[28] KWEKKEBOOM, D.J., KOOIJ, P.P., BAKKER, W.H., MAECKE, H.R., KRENNING, E.P., Comparison of 111In-DOTA-Tyr3-octreotide and 111In-DTPA-octreotide in the same patients: biodistribution, kinetics, organ and tumor uptake. J Nucl Med, 1999. 40(5): p. 762-7.

[29] DE JONG, M., et al., [177Lu-DOTA(0),Tyr3] octreotate for somatostatin receptor-targeted radionuclide therapy. Int J Cancer, 2001. 92(5): p. 628-33.

[30] KOLBY, L., et al., Successful receptor-mediated radiation therapy of xenografted human midgut carcinoid tumour. Br J Cancer, 2005. 93(10): p. 1144-51.

[31] SCHMITT, A., et al., Radiation therapy of small cell lung cancer with 177Lu-DOTA-Tyr3-octreotate in an animal model. J Nucl Med, 2004. 45(9): p. 1542-8.
[32] DE JONG, M., et al., Tumor Response After [(90)Y-DOTA(0),Tyr(3)]Octreotide Radionuclide Therapy in a Transplantable Rat Tumor Model Is Dependent on Tumor Size. J Nucl Med, 2001. 42(12): p. 1841-6.
[33] DE JONG, M., et al., Inhibition of renal uptake of indium-111-DTPA-octreotide in vivo. J Nucl Med, 1996. 37(8): p. 1388-92.
[34] BERNARD, B.F., et al., D-lysine reduction of indium-111 octreotide and yttrium-90 octreotide renal uptake. J Nucl Med, 1997. 38(12): p. 1929-33.
[35] ROLLEMAN, E.J., VALKEMA, R., DE JONG, M., KOOIJ, P.P., KRENNING, E.P., Safe and effective inhibition of renal uptake of radiolabelled octreotide by a combination of lysine and arginine. Eur J Nucl Med Mol Imaging, 2003. 30(1): p. 9-15.
[36] BODEI, L., et al., Receptor-mediated radionuclide therapy with 90Y-DOTATOC in association with amino acid infusion: a phase I study. Eur J Nucl Med Mol Imaging, 2003. 30(2): p. 207-16.
[37] KWEKKEBOOM, D.J., et al., [^{177}Lu-DOTA^{0},Tyr^{3}]octreotate: comparison with [^{111}In-DTPA^{0}]octreotide in patients. Eur J Nucl Med, 2001. 28(9): p. 1319-1325.
[38] BODEI, L., et al., Receptor radionuclide therapy with 90Y-[DOTA]0-Tyr3-octreotide (90Y-DOTATOC) in neuroendocrine tumours. Eur J Nucl Med Mol Imaging, 2004. 31(7): p. 1038-46.
[39] OTTE, A., et al., Yttrium-90 DOTATOC: first clinical results. Eur J Nucl Med, 1999. 26(11): p. 1439-47.
[40] OTTE, A., HERRMANN, R., MAECKE, H.R., MUELLER-BRAND, J., [Yttrium 90 DOTATOC: a new somatostatin analog for cancer therapy of neuroendocrine tumors]. Schweiz Rundsch Med Prax, 1999. 88(31-32): p. 1263-8.
[41] OTTE, A., et al., Yttrium-90-labelled somatostatin-analogue for cancer treatment [letter]. Lancet, 1998. 351(9100): p. 417-8.
[42] WALDHERR, C., PLESS, M., MAECKE, H.R., HALDEMANN, A., MUELLER-BRAND, J., The clinical value of [90Y-DOTA]-D-Phe1-Tyr3-octreotide (90Y-DOTATOC) in the treatment of neuroendocrine tumours: a clinical phase II study. Ann Oncol, 2001. 12(7): p. 941-5.
[43] WALDHERR, C., et al., Tumor response and clinical benefit in neuroendocrine tumors after 7.4 GBq (90)Y-DOTATOC. J Nucl Med, 2002. 43(5): p. 610-6.
[44] WALDHERR, C., et al., Does tumor response depend on the number of treatment sessions at constant injected dose using 90Yttrium-DOTATOC in neuroendocrine tumors? Eur J Nucl Med, 2002. 29: p. S100.
[45] FORRER, F., WALDHERR, C., MAECKE, H.R., MUELLER-BRAND, J., Targeted radionuclide therapy with 90Y-DOTATOC in patients with neuroendocrine tumors. Anticancer Res, 2006. 26(1B): p. 703-7.
[46] CHINOL, M., BODEI, L., CREMONESI, M., PAGANELLI, G., Receptor-mediated radiotherapy with Y-DOTA-DPhe-Tyr-octreotide: the experience of the European Institute of Oncology Group. Semin Nucl Med, 2002. 32(2): p. 141-7.

[47] PAGANELLI, G., et al., 90Y-DOTA-D-Phe1-Try3-octreotide in therapy of neuroendocrine malignancies. Biopolymers, 2002. 66(6): p. 393-8.
[48] SMITH, M.C., et al., OctreoTher: ongoing early clinical development of a somatostatin- receptor-targeted radionuclide antineoplastic therapy. Digestion, 2000. 62(Suppl 1): p. 69-72.
[49] VALKEMA, R., et al., Phase 1 study of therapy with 90Y-SMT487 (OctreoTher) in patients with somatostatin receptor-positive tumors. J Nucl Med, 2002. 43(5): p. 33P.
[50] JONARD, P., et al., Tumor dosimetry based on PET ^{86}Y-DOTA-Tyr^{3}-octreotide (SMT487) and CT-scan predicts tumor response to ^{90}Y-SMT487 (OctreoTher). J Nucl Med, 2000. 41(5): p. 111P.
[51] KWEKKEBOOM, D.J., et al., Treatment of patients with gastro-entero-pancreatic (GEP) tumours with the novel radiolabelled somatostatin analogue [177Lu-DOTA(0),Tyr3]octreotate. Eur J Nucl Med Mol Imaging, 2003. 30(3): p. 417-22.
[52] KWEKKEBOOM, D.J., BAKKER, W.H., TEUNISSEN, J.J.M., KOOIJ, P.P., KRENNING, E.P., Treatment with Lu-177-DOTA-Tyr3-Octreotate in patients with neuroendocrine tumors: interim results. Eur J Nucl Med Mol Imaging, 2003. 30: p. S231.
[53] KWEKKEBOOM, D.J., et al., Overview of results of peptide receptor radionuclide therapy with 3 radiolabeled somatostatin analogs. J Nucl Med, 2005. 46 Suppl 1: p. 62S-6S.
[54] VIRGOLINI, I., et al., Experience with indium-111 and yttrium-90-labeled somatostatin analogs. Curr Pharm Des, 2002. 8(20): p. 1781-807.
[55] VIRGOLINI, I., et al., Indium-111-DOTA-lanreotide: biodistribution, safety and radiation absorbed dose in tumor patients. J Nucl Med, 1998. 39(11): p. 1928-36.
[56] VIRGOLINI, I., et al., In- and Y-DOTA-lanreotide: results and implications of the MAURITIUS trial. Semin Nucl Med, 2002. 32(2): p. 148-55.
[57] VIRGOLINI, I., et al., "MAURITIUS": tumour dose in patients with advanced carcinoma. Ital J Gastroenterol Hepatol, 1999. 31 Suppl 2: p. S227-30.
[58] SMITH-JONES, P.M., et al., DOTA-lanreotide: a novel somatostatin analog for tumor diagnosis and therapy. Endocrinology, 1999. 140(11): p. 5136-48.
[59] FROIDEVAUX, S., et al., Preclinical comparison in AR4-2J tumor-bearing mice of four radiolabeled 1,4,7,10-tetraazacyclododecane-1,4,7,10-tetraacetic acid-somatostatin analogs for tumor diagnosis and internal radiotherapy. Endocrinology, 2000. 141(9): p. 3304-12.
[60] SCHMITT, J.S., et al., DOTA-NOC, a high affinity ligand of the somatostatin receptor subtypes 2,3 and 5 for radiotherapy. J Labelled Cpd Radiopharm, 2001. 44: p. s697-s699.

IODINE WHOLE BODY SCAN, THYROGLOBULIN LEVELS, ^{99m}Tc MIBI SCAN AND COMPUTED TOMOGRAPHY

Results in patients with lung metastasis from differentiated thyroid cancer

N.Ö. KÜÇÜK, S.S. GÜLTEKIN, G. ARAS, E. İBIŞ
Department of Nuclear Medicine,
Ankara University Faculty of Medicine,
Ankara, Turkey
Email: n.ozlem.kucuk@medicine.ankara.edu.tr

Abstract

Correlation of the ^{131}I whole body scan (^{131}I WBS), ^{99m}Tc-sestamibi (Tc-MIBI) scans, computed tomography (CT) and the value of routine follow-up for ^{131}I WBS and thyroglobulin levels were assessed in patients with differentiated thyroid cancer (DTC) lung metastasis. Pulmonary metastasis was detected with ^{131}I WBS, increased thyroglobulin levels and/or other positive radiological findings in 32 patients out of 583 with DTC. Iodine-131 WBS, thyroglobulin level assessment and/or CT were performed in the diagnosis and follow-up of the patients with lung metastasis. A Tc-MIBI scan was performed on 19 randomly chosen patients. Nineteen out of 32 patients had lung metastasis before they received the first ^{131}I treatment. Pulmonary metastasis was observed in the first ^{131}I WBS of all the patients except one; whereas no pulmonary metastasis was detected in CT in 3/32. The final ^{131}I WBS became normal in 13/32. Thyroglobulin levels diminished in 21/32 and were elevated in 3/32. Iodine-131 WBS continued to be abnormal in 2 out of 3 patients with increased thyroglobulin levels but became normal in 1 patient whose CT still demonstrated macronodulary lesions. Thyroglobulin levels did not change significantly in 8/32. Iodine-131 WBS became normal in 5/8 and 4/5 showed micronodules in their CT scans. Metastasis was detected in 12/19 patients who had Tc-MIBI scans, 18/19 showed metastasis in ^{131}I WBS and 17/19 in CT. Of the 7 patients without the sign of metastasis in Tc-MIBI scintigraphy, 1 was negative in terms of metastasis in ^{131}I WBS and 1 in CT. Fibrosis was observed in 2/32 patients in CT. One patient developed dedifferentiation decided by negative ^{131}I WBS and positive CT. It was concluded that the ^{131}I WBS and thyroglobulin levels are the most important parameters in the evaluation of lung metastasis in DTC. CT is an additional effect to ^{131}I WBS and thyroglobulin level, on the other hand, MIBI imaging alone may not be enough to detect these metastases.

1. INTRODUCTION

Thyroid cancer represents 90% of all endocrine malignancy but it represents less than 1% of all malignancies. Metastatic disease develops in 7–23% of patients with differentiated thyroid carcinoma (DTC) [1, 2]. However, distant metastasis at the time of initial diagnosis is observed in only 1–4% [3]. Lungs are the most frequent distant localization of metastasis from DTC [4].

Complete surgical resection of the thyroid (total or near total thyroidectomy) and post-operative ablation therapy with ^{131}I involve routine treatment approaches for patients with DTC. The patients are followed up after thyroidectomy and radioiodine therapy by serial ^{131}I whole body scan (^{131}I WBS) and serum thyroglobulin measurements [5]. Technetium-99m-sestamibi whole body scan (Tc-MIBI WBS) is useful, especially for the evaluation of patients with negative ^{131}I WBS and elevated thyroglobulin levels (non-functional disease) in DTC. Furthermore, the Tc-MIBI scan has advantages over the ^{131}I scan, which are: (a) no necessity to discontinue hormonal therapy when performing scintigraphy (b) Tc-MIBI provides better quality images and (c) undertaking scintigraphic examination is easy and saves time. On the basis of these favourable considerations, the use of Tc-MIBI WBS has been suggested as an alternative to ^{131}I WBS for the evaluation of the metastatic disease in DTC patients [6–8].

This retrospective study researched the correlation and value of the ^{131}I WBS, Tc-MIBI scan, computed tomography (CT) and thyroglobulin levels in the assessment of the lung metastasis in patients with DTC. The use of routine thyroglobulin level measurements and ^{131}I WBS combined as a gold standard in the verification and follow-up of lung metastasis in patients without any distant organ metastasis after successful thyroid remnant ablation were evaluated.

2. MATERIALS AND METHODS

2.1. Patients

A total of 583 patients with DTC were admitted to the Department of Nuclear Medicine of Ankara University Medical School between 1985 and 2004 and these patients were examined retrospectively. They were evaluated by clinical examination and ^{99m}Tc pertechnetate thyroid scintigraphy. Routine nuclear medicine methods (^{131}I WBS, ^{201}Tl or ^{99m}Tc-MIBI scans, thyroid function tests) and when necessary some biochemical tests and radiological studies (chest X ray, neck USG, neck and thorax CT, etc.) were performed for

the evaluation and follow-up of patients. Of the patients, 32 had lung metastasis. Histopathologically, papillary carcinoma in 15/32 patients, follicular carcinoma in 13/32 patients and mixed type in 4/32 patients were observed. Ages at the first diagnosis of the 32 patients ranged from 22 to 79 years (mean: 58 ± 19 years, 15 female and 17 male). The duration of follow-up was in the range 36–240 months. Clinical, pathological and treatment related characteristics are presented in Table 1.

2.2. Surgery

All 32 patients except one underwent a total or near total thyroidectomy. Lymph node dissections at the initial surgery were performed for 12 patients. Nine patients underwent operations twice for an adequate operation.

TABLE 1. CLINICAL, PATHOLOGICAL AND TREATMENT RELATED CHARACTERISTICS OF THE PATIENTS WITH LUNG METASTASIS FROM DTC

Characteristic	n = 32	%
Gender		
Male	17	53.12
Female	15	46.87
Median age at the diagnosis (years) 58 ± 19		
Surgery		
None	1	3.12
Total or near total thyroidectomy	31	96.87
Lymph node dissection	12	37.50
Histology		
Papillary	15	46.87
Follicular	13	40.62
Mix type	4	12.50
Lung metastasis at the diagnosis		
Yes	19	59.37
No	13	40.62

2.3. The algorithm of treatment and follow-up

The patients with DTC who had undergone total thyroidectomy received a fixed dose of ^{131}I for the ablation of thyroid remnants. Post-treatment WBS (PTWBS) was performed six days after the ablation therapy. Periodical thyroglobulin measurement and DWBS were used for the follow-up of patients after successful ablation. Tellurium-201 or Tc-MIBI is used for diagnosis and follow-up in the case of negative DWBS and elevated thyroglobulin levels. The authors could not undertake F-18 FDG scanning of the patients owing to the absence of a PET camera in the department. The algorithm of treatment and follow-up used is given in Fig. 1.

2.4. ^{131}I therapy and PTWBS

The patients were given a high fixed ablative dose of ^{131}I. L-thyroxin replacement therapy withdrawal and low iodine diet protocols were applied for 4 weeks before the ^{131}I therapy. TSH levels were increased at least 30 ng/mL. A total of 100–1450 mCi (3.7–53.65 GBq) ^{131}I was given to each patient. In the presence of persistent functioning lung metastasis, radioiodine therapy was repeated periodically (at least 6 months after the therapy).

PTWBS planar and spot images were obtained in anterior and posterior projections. It was performed on the sixth post-treatment day using a large field of view gamma camera equipped with a high energy (peak energy centred on 360 keV with a 20% energy window) parallel hole collimator (GE 4000iXC-T/STARCAM, GE Medical Systems, Milwaukee, United States of America). PTWBS was used only for the purpose of verification of the metastatic disease. All the patients were researched about positive uptake on the PTWBS. These patients with increased pulmonary activity were referred to the Department of Thoracic Diseases and evaluated by bronchoscopy in order to confirm the metastasis.

2.5. Routine follow-up protocol

Suppressive hormonal therapy (L-thyroxin) was started 48–72 h after the radioiodine therapy. Diagnostic ^{131}I WBS (DWBS) and thyroglobulin level were obtained after the first treatment for the first follow-up in 6 months and both 3 and 6 months, respectively. Thyroid hormone withdrawal and low iodine diet protocols were applied for 4 weeks. The DWBS was performed with a 5 mCi (185 MBq) dose of ^{131}I. DWBS, planar and spot images were acquired with anterior and posterior projections at 24 and 72 h (early and late images) using a GE 4000iXC-T/STARCAM gamma camera equipped with a high

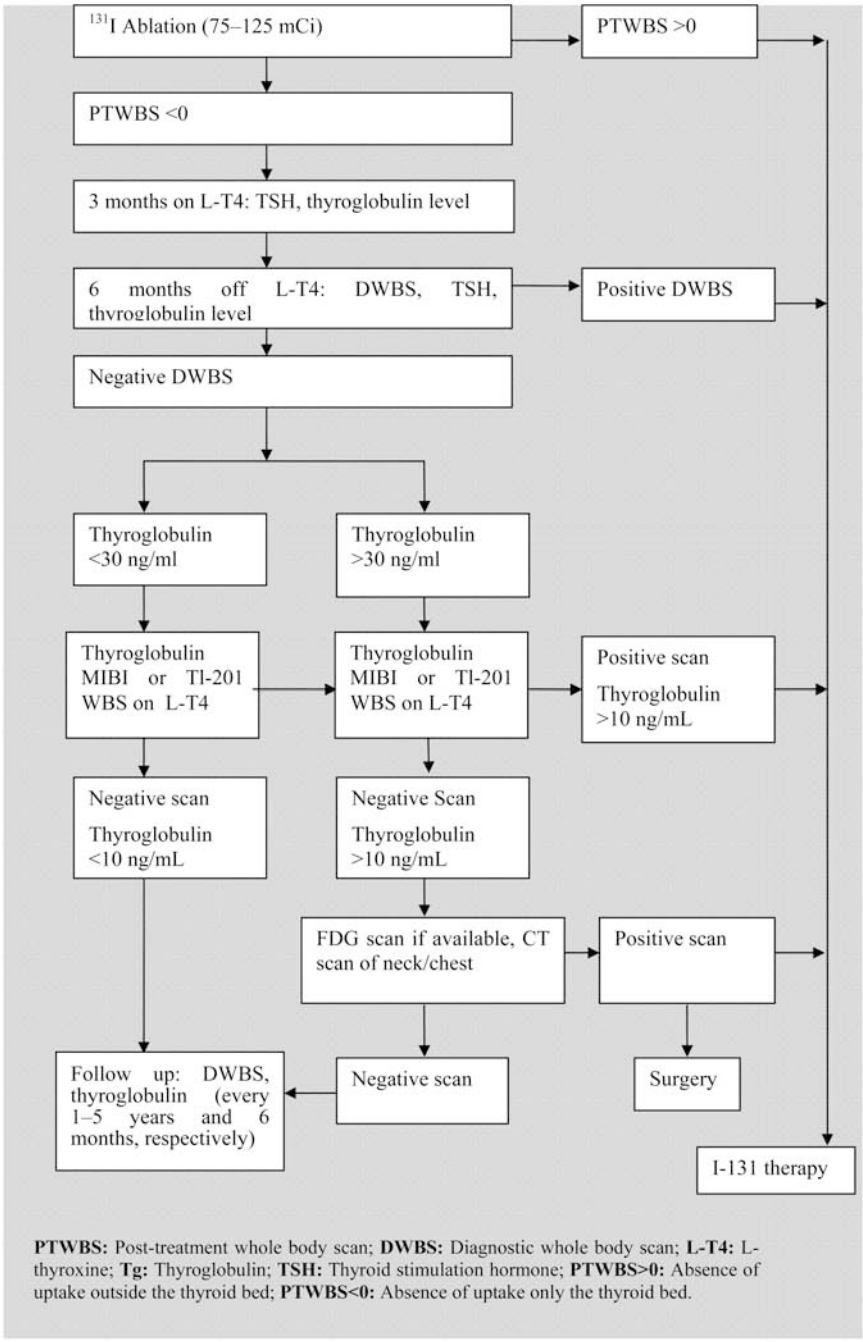

FIG. 1. The algorithm of treatment and follow-up.

energy collimator. Patients with normal DWBS were evaluated with periodic follow-up, at first once a year and then every two or three years within a ten year period. However, thyroglobulin levels of all the patients were obtained every sixth month. The thyroglobulin levels were measured by the immunoradiometric method over the period 1985–2000 and by the chemiluminescence method after 2000. Suppressive hormonal therapy was resumed after each ^{131}I WBS. All the patients were evaluated regarding positive pulmonary uptake on the DWBS.

2.6. Tc-MIBI scan

The Tc-MIBI WBS was carried out on 19 patients who were randomly chosen. The authors have used Tc-MIBI in since 1990 and it took a long time to start using it routinely for the patient group. Therefore, not all patients in the group have had Tc-MIBI scans. The authors performed the ^{201}Tl WBS on some patients but did not include them in this study because their number was small. A Tc-MIBI WBS was performed on the patients during suppressive hormonal therapy. Tc-MIBI (15–20 mCi (555–740 MBq), CARDIO-SPECT, Medi-Radiopharma Ltd, Hungary) was injected intravenously. Images were obtained 20–30 min later. MIBI WBS planar and spot images were obtained in anterior and posterior projections with a large field of view gamma camera equipped with a low energy (peak energy centred on 140 keV with a 15% energy window), high resolution collimator (Siemens ECAM Dual Head Variable Systems, Siemens Medical Solutions, Illinois, USA). The patients were examined for the similar positive pulmonary uptake regions in Tc-MIBI and ^{131}I WBS.

2.7. CT

CT was performed when pulmonary metastasis was detected by positive ^{131}I WBS and/or increasing thyroglobulin levels. In most of the patients, CT was not performed in order to follow up. All patients underwent conventional CT for the examination of metastatic lesions without the use of contrast media in order not to affect the radioiodine therapy. The CT equipment used did not have high resolution properties. The CT images were obtained with a 7 mm slice thickness starting from the apex of the lungs. All CT images were taken in the supine position. The patients were evaluated in terms of metastatic pulmonary lesions and the lesions were classified according to size (macronodule >10 mm).

3. RESULTS

Nineteen out of 32 patients had lung metastasis before the first ^{131}I treatment. Thirteen out of 32 patients exhibited lung metastasis during the follow-up period. All patients were given radioiodine therapy. Thyroid remnant ablation was successful in the first DWBS in 22/32 patients. Six out of 32 patients had other distant organ metastases than the lungs. Four of the 6 patients only had lung and bone metastases. Pulmonary metastasis was observed in the ^{131}I WBS of all the patients except one (31/32, 96.8%), whereas CT showed pulmonary metastasis to be absent in 3/32 patients.

The last DWBS was negative in 13/32 patients (40.6%). DWBS was positive in 19/32 patients. In their initial examination, 27/32 patients had thyroglobulin levels higher than 30 ng/mL (84.4%) and 5/32 patients had thyroglobulin lower than 30 ng/mL (15.6%). In their final examination, 20/32 patients had thyroglobulin levels higher than 30 ng/mL (62.5%) and 12/32 patients had thyroglobulin levels lower than 30 ng/mL. The final thyroglobulin levels began to change in 7/32 patients. In 8/32 patients the thyroglobulin level was lower than 30 ng/mL plus a negative ^{131}I WBS. However, one patient had thyroglobulin values higher than 30 ng/mL who had been negative for ^{131}I WBS. Four out of 32 patients had thyroglobulin levels less than 30 ng/mL (15.6%) and positive ^{131}I WBS. Thirteen out of 32 patients had negative ^{131}I WBS after a final diagnostic ^{131}I WBS. Thyroglobulin levels were lower in 21/32 and elevated in 3/32 patients. The ^{131}I WBS continued to be abnormal in 2 out of 3 patients with increased thyroglobulin levels but became normal in one patient whose CT still demonstrated macronodular lesions. Thyroglobulin levels did not change significantly in 8/32. Iodine-131 WBS became normal in 5/8 and 4/5 showed micronodules in their CTs. Fibrosis was observed in 2/32 patients in CT. One patient developed dedifferentiation with negative ^{131}I WBS and positive CT.

Metastasis was discerned in 12/19 patients who underwent Tc-MIBI WBS, 18/19 showed metastasis in ^{131}I WBS and 17/19 in CT (Table 2). Of the

TABLE 2. PATIENTS WITH SERUM THYROGLOBULIN LEVELS ≥30 ng/mL WITH RESPECT TO DIFFERENT MODALITIES

Finding	^{131}I WBS	Tc-MIBI scan	CT
Positive	18	12	17
Negative	1	7	2
%	94.7	63.1	89.4

seven patients showing no sign of metastasis in Tc-MIBI WBS, one was negative in terms of metastasis in ^{131}I WBS and one in CT. Of the 3/4 patients who had negative ^{131}I WBS and thyroglobulin levels higher than 30 ng/mL during last follow-up examination, scans were performed by Tc-MIBI WBS. Of the patients, two (2/3) had positive Tc-MIBI scans. In contrast, the patient who had negative ^{131}I WBS and a thyroglobulin level higher than 30 ng/mL during initial follow-up had a negative MIBI scan.

4. DISCUSSION

Lungs are the most frequent distant localization of metastasis due to DTC (1–4%) [4]. The ^{131}I WBS and thyroglobulin levels play an important diagnostic role in the evaluation of lung metastasis in DTC [9, 10]. Lung metastases were observed in the ^{131}I WBS of all the patients except one, who had a very high thyroglobulin level and a negative ^{131}I WBS.

Serum thyroglobulin level measurement is the most sensitive and specific marker of DTC patients, but increased thyroglobulin concentration alone is not enough when there is a large thyroid remnant. The thyroglobulin levels used in the retrospective study were measured by an immunoradiometric method over the period 1985–2000 and by chemiluminescence after 2000. The cut-off values were 30 ng/mL in the first period and 5 ng/mL in the second period and the values above these were considered for the assessment of metastatic disease. Although it is reported that the chemiluminescence method is more sensitive compared to the immunoradiometric method [19], a cut-off value of 30 ng/mL was selected in this retrospective study because both methods were used over the long duration of the analysis period.

Initial thyroglobulin concentrations determined after total thyroidectomy or near total thyroidectomy with lung metastasis in 32 patients off thyroxin and before ^{131}I therapy or scanning showed that 15.6% (5/32) of patients had initial levels less than 30 ng/mL and, in a contrary manner, 84.4% (27/32) had initial levels higher than 30 ng/mL. Filesi et al. [11] reported that in their series of patients, 66.7% of those with metastases had their initial thyroglobulin levels higher than 60 ng/mL. David et al. [7] reported that 46% of patients with thyroid remnants or metastases had their initial serum thyroglobulin values higher than 30 ng/mL. In the authors' group, 84.4% of patients with lung metastases had their initial thyroglobulin levels higher than 30 ng/mL. In addition, Filesi et al. reported metastases were observed in the initial ^{131}I WBS in 47.8% of patients with thyroglobulin values of less than 60 ng/mL; 61.3% of patients with the initial ^{131}I WBS negative for metastases had thyroglobulin levels greater than 60 ng/mL. In contrast to the finding, David et al. determined

only 2.7% of scan negative subjects had initial serum thyroglobulin levels higher than 30 ng/mL. The authors' retrospective findings suggested that 3.1% of patients had both ^{131}I WBS negative and thyroglobulin levels higher than 30 ng/mL. It might be associated with thyroid remnants and/or other distant metastases. Thyroid remnant ablation was successful in the first DWBS in 22/32 patients and 6/32 patients had other distant organ metastases out of lung in the study. In addition, the study showed that 16.5% of patients who had initial ^{131}I scan positive for metastases had thyroglobulin levels of less than 30 ng/mL. The authors consider that the thyroglobulin cut-off level must be reduced to below 30 ng/mL. David et al. reported that with ^{131}I ablation and long term thyroxin suppression, the level of thyroglobulin tended to fall. In the study, final thyroglobulin concentrations were determined in order to measure initial thyroglobulin concentrations under the same conditions. The authors observed that 37.5% (12/32) of patients had final thyroglobulin levels of less than 30 ng/mL and, conversely, 62.5% (20/32) had final thyroglobulin levels higher than 30 ng/mL. Initial thyroglobulin levels varied from 0.5 to 13 454 (average: 882.6) ng/mL. Final thyroglobulin levels were measured from 0.5 to 4795 (average: 519). Consequently, declining thyroglobulin levels were observed in 65.6% (21/32) of the patients. Furthermore, final thyroglobulin values had less than 30 ng/mL in 37.5% (12/32) of the patients (Fig. 2).

The combination of routine thyroglobulin measurement and ^{131}I WBS can be used as a gold standard in the diagnosis and follow-up of lung metastasis in DTC patients without any determined distant organ metastasis and after successful thyroid remnant ablation. Increased activity in the lung region in the

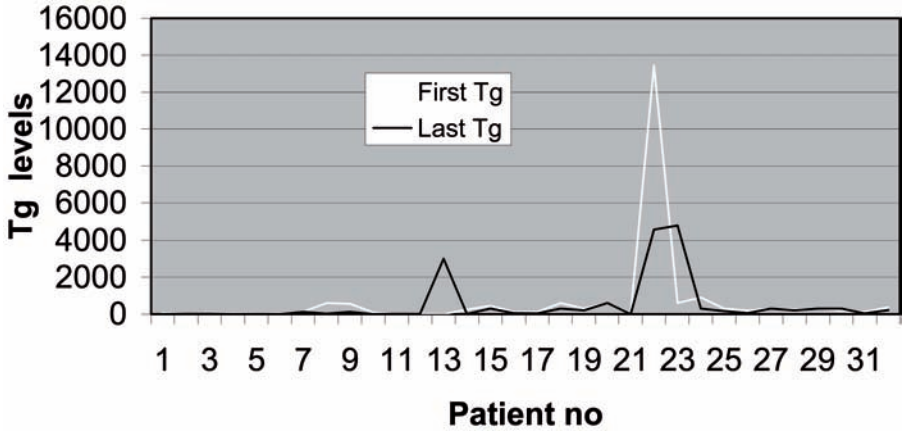

FIG. 2. Thyroglobulin levels are presented in 32 patients with lung metastases from DTC.

PTWBS is considered as pulmonary metastasis. These patients were referred to the Department of Thoracic Diseases and bronchoscopic methods were used to confirm the presence of metastatic disease. The patients were divided into two groups according to whether their thyroglobulin levels were higher or lower than 30 ng/mL after L-T4 replacement therapy had been stopped. It is thought that the group with thyroglobulin higher than 30 ng/mL can represent the high risk group for the effective treatment of the disease [1, 11]. By doing this the authors were able to evaluate how effective routine thyroglobulin determination can be in the follow-up of patients as a preparameter prior to the multistep, multiparameter evaluation of progression. At the beginning of the study there were 27 patients with thyroglobulin levels higher than 30 ng/mL and 5 patients with thyroglobulin levels of less than 30 ng/mL. In the last evaluation there were only 20 patients with thyroglobulin levels higher than 30 ng/mL. The last DWBS were negative in 13 of these 20 patients. DWBS was negative in 8 and positive in 4 of 12/32 patients with thyroglobulin less than 30 ng/mL in the final evaluation. In two of three patients with thyroglobulin progression, DWBS continued to be positive in the final evaluation. These results show that thyroglobulin measurement and ^{131}I WBS cannot yet be evaluated as a gold standard in the follow-up of DTC patients with pulmonary metastasis. However, depression of the serum thyroglobulin level can be considered as an obvious sign that the patient benefits from radioactive iodine therapy although selecting a lower cut-off value will increase the sensitivity and the chance of a better correlation. Although it was not easy to evaluate the efficacy of treatment, the authors were able to gather valuable information on deciding if the high dose cumulative radioactive iodine therapy would result in long term stability in the patient group by using thyroglobulin measurement and DWBS together.

The Tc-MIBI scan has been useful especially for the evaluation of patients with a negative ^{131}I scan and elevated thyroglobulin levels (non-functional disease) in DTC. Furthermore, the Tc-MIBI scan has advantages over the ^{131}I scan, these being (a) no necessity to discontinue hormonal therapy when performing scintigraphy (b) MIBI provides better quality images and (c) undertaking scintigraphic examination is easy and saves time.

On the basis of these favourable considerations, the use of Tc-MIBI WBS has been suggested as an alternative to ^{131}I WBS for the evaluation of the metastatic disease in DTC patients [6–8]. However, there are different opinions about the sensitivity of Tc-MIBI WBS in DTC. Sundram et al. showed Tc-MIBI WBS had a sensitivity comparable to ^{131}I WBS [12]. On the other hand,

Dadparvar et al. [13] found a poor sensitivity (36%) but a high specificity (89%) for Tc-MIBI WBS compared with ^{131}I WBS. Miyamoto et al. reported that Tc-MIBI WBS did not discern pulmonary metastases in more patients than the ^{131}I scan (75% and 85%, respectively). The authors' findings suggested that, compared with ^{131}I WBS, Tc-MIBI WBS was less sensitive (94.2% and 63.2%, respectively) in detecting lung metastasis with DTC patients.

It has been reported that the sensitivity of thoracic CT is about 80% [14]. To the contrary, some studies have shown that a CT scan can detect 3 mm peripheral and 6 mm central nodules, although it still fails to discern the diffuse interstitial type of lung metastases in patients with DTC [15]. The authors found that CT detected lung metastases in 29/32 patients (90.6%) in their series. Nevertheless, their findings suggest that, compared with ^{131}I WBS, CT was less sensitive in detecting lung metastasis with DTC patients. It may be difficult to interpret data in an area of the neck already submitted to surgery. However, the authors also found that fibrosis was observed in 2/32 patients in CT. Dedifferentiation was observed in one patient decided by negative ^{131}I WBS and positive CT, owing to the fact that CT was an additive effect to the ^{131}I WBS and the thyroglobulin level.

FDG PET scanning may be useful in localizing distant metastases, especially when there is no radioiodine uptake. These metastases may be located in the mediastinum or other distant areas [16, 17]. FDG uptake was also detected more frequently in patients with poor DTC, in whom no detectable ^{131}I uptake could be demonstrated. FDG PET cannot supersede the ^{131}I scan. However, several investigators reported that FDG PET and ^{131}I WBS played complementary roles in the detection of recurrent metastatic DTC [17]. The authors were not able to use PET scanning because this modality was not available in the department.

In their study, the authors chose to evaluate retrospective data with the help of previous data, instead of statistically assessing various parameters affecting the survival period. Their aim in doing so was to see if there was a treatment mode which would result in progress in the patients. Margo et al. analysed patient, tumour and treatment related factors and their relation to disease specific survival using statistical tests. They found that at the age of 45 years or more, a site other than lung only or bone only and symptoms at the time of diagnosis are associated with poorer outcomes [18]. In addition, Ronga et al. reported that a young age at diagnosis and radioiodine uptake by metastases are the most important factors positively affecting survival time. They found that radioiodine therapy, also with high cumulative radioiodine ^{131}I activity, can lead to longer survival time or complete recovery [4]. The authors found a prolongation of the disease free period and progress in the parameters followed in those of their patient group who showed radioactive iodine

accumulation and were younger than 45 years old at the first diagnosis. Six of 8/32 patients who showed progress in the parameters followed (DWBS, thyroglobulin level less than 30 ng/mL) were younger than 45 years old and needed fewer cumulative doses than the other two patients. The authors believe that radioactive iodine therapy should continue to be given to the patients because metastatic disease at least slows down the course of the disease, although it may not appear to cure the disease in persistent or recurrent cases.

5. CONCLUSION

For lung metastasis detection and follow-up after total thyroidectomy, the ^{131}I WBS and thyroglobulin levels were the most important parameters. CT has an additive effect to ^{131}I WBS. The authors' findings suggested that, compared with ^{131}I WBS, Tc-MIBI WBS was less sensitive (94.2% and 63.2%, respectively) in detecting lung metastasis with DTC patients. MIBI imaging alone might not be enough to detect these metastases.

REFERENCES

[1] SCHLUMBERGER, M., et al., Long-term results of treatment of 283 patients with lung and bone metastases from differentiated thyroid carcinoma. J Clin Endocrinol Metab 1986; 63:960–967.

[2] RUEGEMER, J.J., et al., Distant metastases in differentiated thyroid carcinoma: a multivariate analysis of prognostic variables. J Clin Endocrinol Metab 1988;67:501–507.

[3] HOIE, J., STENWIG, A.E., KULLMANN, G., LINDEGARD, M., Distant metastases in papillary thyroid cancer. A review of 91 patients. Cancer 1988;61:1–6.

[4] RONGA, G., et al., Lung metastases from differentiated thyroid carcinoma. Q j nucl med mol ımagıng 2004;48:12-9.

[5] OZATA, M., et al., Serum thyroglobulin in the follow-up of patients with treated differentiated thyroid cancer. J Clin Endocrinol Metab. 1994;79:98–105.

[6] NEMEC, J., et al., Positive thyroid cancer scintigraphy using technetium-99m methoxyisobutylisonitrile. Eur J Nucl Med. 1996;23:69–71.

[7] NG ENG, C.D., SUNDRAM, F.X., SIN, E.A., 99mTc-Sestamibi and 131I Whole-Body Scintigraphy and Initial Serum Thyroglobulin in the Management of Differentiated Thyroid Carcinoma. J Nucl Med 2000; 41:631–635.

[8] MIYAMOTO, S., KASAGI, K., MISAKI, T., ALAM, M.S., KONISHI, J., Evaluation of technetium- 99m-MIBI scintigraphy in metastatic differentiated thyroid carcinoma. *J Nucl Med*. 1997;38:352–356.

[9] MAZZAFERRI, E.L., MASSOLL, N., Management of papillary and follicular (differentiated) thyroid cancer: new paradigms using recombinant human thyrotropin. Endocrine-Related Cancer (2002) 9 227–247.

[10] PACINI, F., et al., Diagnostic 131-iodine whole-body scan may be avoided in thyroid cancer patients who have undetectable stimulated serum thyroglobulin levels after initial treatment. Journal of Clinical Endocrinology and Metabolism (2002) 87 1499–1501.

[11] FILESI, M., SIGNORE, A., VENTRONI, G., MELACRINIS, F.F., RONGA, G., Role of initial iodine-131 whole-body scan and serum thyroglobulin in differentiated thyroid carcinoma metastases. J Nucl Med. 1998;39:1542–1546.

[12] SUNDRAM, F.X., GOH, A.S.W., ANG, E.S., Role of technetium-99m sestamibi in localisation of thyroid cancer metastases. Ann Acad Med Singapore. 1993; 22:557–559.

[13] DADPARVAR, S., et al., Clinical utility of technetium-99m methoxisobutylisonitrile imaging in differentiated thyroid carcinoma: comparison with thallium-201 and iodine-131 scintigraphy and serum thyroglobulin quantitation. *Eur J Nucl Med*. 1995;22:1330– 1338.

[14] LORENZEN, J., et al., Chest X ray: routine indication in the follow-up of differentiated thyroid cancer? Nuklearmedizin 1998; 37:208–212.

[15] PIEKARSKI, J.D., et al., Chest computed tomography in patients with micronodular lung metastases of differentiated thyroid carcinoma. *Int J Radiat Oncol Biol Phys.* 1985;11(5):1023-7.

[16] WANG, W., et al., 18F-2-Floro-2-D-glucose positron emission tomography localizes residual thyroid cancer in patients with negative diagnostic 131I iodine whole body scans and elevated serum thyroglobulin levels. *J Clin Endocrinol Metab.* 1999;84(7):2291-302.

[17] SHIGA, T., et al., Comparison of (18)F-FDG, (131)I-Na, and (201)Tl in diagnosis of recurrent or metastatic thyroid carcinoma. *J Nucl Med.* 2001;42(3):414-9.

[18] SHOUP, M., et al., Prognostic indicators of outcomes in patients with distant metastases from differentiated thyroid carcinoma. *J Am Coll Surg.* 2003;197(2):191-7.

^{99m}Tc-MIBI AND ^{131}I SCINTIGRAPHY IN THE FOLLOW-UP OF DIFFERENTIATED THYROID CARCINOMA (DTC) PATIENTS AFTER SURGERY

S. SERGIEVA*, T. HADJIEVA**, V. BOTEV*, A. DUDOV*

*Sofia Cancer Centre
Email: sergieva_s@yahoo.com

**UH "Queen Giovanna"

Sofia, Bulgaria

Abstract

The MIBI scan has been reported to be a highly sensitive imaging technique for the detection of differentiated thyroid carcinoma (DTC) metastases that have lost the capability to uptake ^{131}I. The purpose of this study was to evaluate, retrospectively, the value of the ^{99m}Tc-MIBI scan and ^{131}I whole body scintigraphy using thyroglobulin (Tg) levels as a basis for comparison. A total of 84 patients with DTC (47 cases with papillary, 18 cases with follicular and 19 cases with papillary–follicular) were assessed. All of them had undergone total or near total thyroidectomy and received radioiodine treatment for ablation of post-surgical residual thyroid tissue. They were examined after 4 weeks L-thyroxin withdrawal in the follow-up of DTC. Planar and whole body images were acquired at 15 min and 180 min after IV application of ^{99m}Tc-MIBI (555–740 MBq) and at 48 h after post-operative administration of ^{131}I (111–185 MBq). Serum Tg assays were performed to clarify the presence of residual recurrent malignancy. The ^{131}I scan was positive in 55 patients, showing thyroid remnants in 31 cases, lymph node metastases in 24 cases, pulmonary metastases in 6 cases and bone lesions in 2 cases. In 18 patients the ^{131}I scan was negative, Tg was undetectable, and therefore the patients were considered tumour free. In 11 patients the ^{131}I scan was negative while serum Tg was increased. These false negative results were observed predominantly in cases with less differentiated metastatic cells, especially after several courses of high dose ^{131}I therapy. The ^{99m}Tc-MIBI scan revealed the presence of lymph node and/or lung metastases (non-functioning metastases) in 9 of them; false negative results were obtained in 2 cases. Serum Tg was increased in all patients with local lymph node and distant metastases, visualized by ^{131}I or by ^{99m}Tc-MIBI, but also in 18 patients with thyroid remnants only. Considering the ^{131}I scan as the most specific standard procedure the authors conclude that the combined ^{99m}Tc-MIBI scintigraphy and serum Tg assay appear to be an alternative to radioiodine diagnostic imaging to demonstrate the extent of the disease in cases with DTC and elevated Tg.

1. INTRODUCTION

It is widely accepted that the ^{131}I scan is the most specific diagnostic procedure, a 'gold standard' in follow-up of patients with differentiated thyroid carcinoma (DTC) after surgery. Depending on the histological type and tumour stage, local recurrence, lymph node metastases or distant metastases may be present or may develop during follow-up [1]. The most reliable parameter for tumour recurrence or metastatic disease is a raised thyroglobulin (Tg) level. With the introduction of lipophilic cationic tracers such as ^{99m}Tc–sestamibi (MIBI) and ^{99m}Tc-tetrofosmin and, especially, fluorine-18 fluorodeoxyglucose positron emission tomography (FDG PET) it has become obvious that the use of only whole body ^{131}I scintigraphy (^{131}I-WBS) leads to serious underestimation of the extent of disease in patients with DTC and elevated Tg [2–4].

The ^{99m}Tc-MIBI scan has been reported to be a highly sensitive imaging technique for detection of DTC metastases that have lost the capability to uptake ^{131}I [5–7].

The purpose of the present study was to evaluate, retrospectively, the value of the ^{99m}Tc-MIBI scan and ^{131}I-WBS using Tg levels as a basis for comparison.

2. MATERIALS AND METHODS

2.1. Patients

A group of 84 patients (63 females and 21 males) with an age range of 17–74 years (mean: 43.5 years) with DTC were assessed. Forty-seven cases exhibited the papillary variant of DTC, 18 cases had follicular and 19 cases had papillary–follicular cancer.

2.2. Methods

All of the patients had undergone total or near total thyroidectomy and received radioiodine treatment for ablation of post-surgical residual thyroid tissue, in a total activity range of 3.3–7.0 GBq (90–190 mCi).

Routine follow-up examination was conducted 6 months post-ablation therapy, after 4 weeks of L-thyroxin withdrawal. Serum Tg was measured. A serum level above 4 ng/mL was considered abnormal when the patients were in the hypothyroid state. All patients were asked to adhere to a low iodine diet until the study had been completed.

^{131}I-WBS images were acquired at 48 h after oral administration of 111–185 MBq radioiodine on Toshiba GCA gamma camera at a speed of 7.5 cm/min with a 1.024 × 512 matrix. Additional planar views from the neck, chest and abdominal regions were also acquired as necessary using a HEAP collimator. In 15 patients post-therapeutic ^{131}I-WBS was carried out 5 d after treatment with high dose radioiodine.

In 11 patients with a negative ^{131}I scan and increased level of serum Tg, additional ^{99m}Tc-MIBI scintigraphy was carried out. Planar images were performed at 15 min and 180 min after IV application of 555–740 MBq ^{99m}Tc-MIBI with a LEHR collimator.

All scintigraphy findings were compared to US, CT or MRT data.

3. RESULTS

The ^{131}I-WBS was positive in 55 patients. Scintigraphy data showed thyroid remnants in 31 cases. Thirteen patients had normal levels of Tg, but in another 18 cases serum Tg was increased before radioiodine treatment. Six months to one year after the ablation therapy of these patients ^{131}I-WBS revealed reduced or ablated remnant with a corresponding decrease in Tg level in all of them (Figs 1 and 2).

Lymph node metastases were visualized in 24 cases with elevated serum Tg levels (17 had hot spots in the neck region and 7 in the neck/upper mediastinum regions) (Fig. 3).

In 19 patients with positive ^{131}I-WBS for lymph node metastases, visualized by sonography, ^{131}I therapy was carried out (Fig. 4). In the other 5

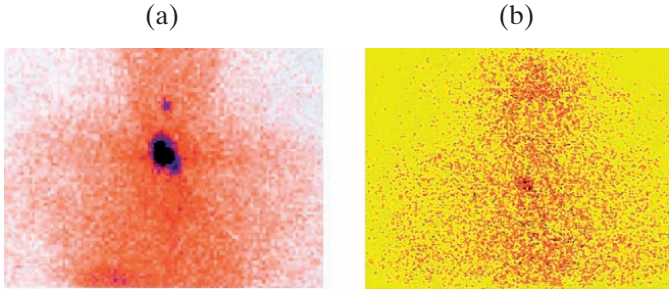

FIG. 1. A female patient (68 years) with the clinical diagnosis "Ca gl.thyreoideae. Status post-thyreoidectomiam et ^{131}I therapiam – pT4pNxM0"; Tg 11.55 ng/mL. (a) ^{131}I-WBS was positive for a remnant in the region of operative cicatrise. (b) After a second course of radioiodine therapy ^{131}I-WBS showed a reduced residual thyroid tissue; Tg 2.68 ng/mL.

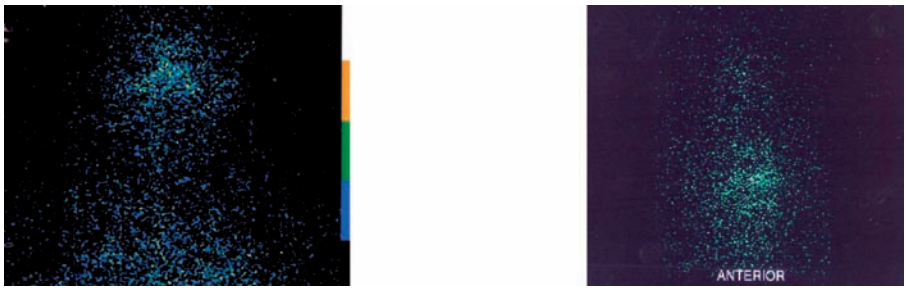

(a) (b)

FIG. 2. A female patient (76 years) with the clinical diagnosis "Ca gl.thyreoideae. Status post-thyreoidectomiam – pT1pN0M0. Status post-^{131}I therapiam"; Tg 2.05 ng/mL. (a) Planar and (b) ^{131}I-WBS showed totally ablated remnant after radioiodine treatment.

cases cervical lymph node dissection was performed with histological confirmation for metastatic infiltration (Fig. 5).

Six patients had positive ^{131}I-WBS for pulmonary metastases and 2 had bone lesions, confirmed by CT and/or MRI (Figs 6 and 7). After therapy with a high dose of radioiodine, a partial therapeutic response and decreased level of serum Tg were obtained during the follow-up in 5 of them with lung metastases.

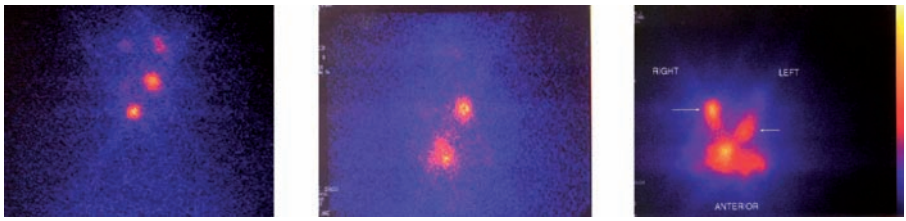

(a) (b) (c)

FIG. 3. (a) A female patient (33 years) with the clinical diagnosis "Ca gl.thyreoideae. Status post-thyreoidectomiam et ^{131}I therapiam – pT1pN1M0"; Tg 23.74 ng/mL. ^{131}I-WBS was positive for a remnant in the region of operative cicatrise and metastatic infiltration of left cervical lymph nodes. (b) A female patient (23 years) with the clinical diagnosis "Ca gl.thyreoideae. Status post-thyreoidectomiam et ^{131}I therapiam – pT4pN1M0"; Tg 115.32 ng/mL. ^{131}I-WBS was positive for metastatic process in the region of the left cervical lymph nodes and upper mediastinum. (c) A female patient (22 years) with the clinical diagnosis "Ca gl.thyreoideae. Status post-thyreoidectomiam et ^{131}I therapiam – pT2pN1bM0"; Tg 1548.0 ng/mL. ^{131}I-WBS was positive for a recurrence in the region of operative cicatrice and metastatic infiltration of left and right cervical lymph nodes.

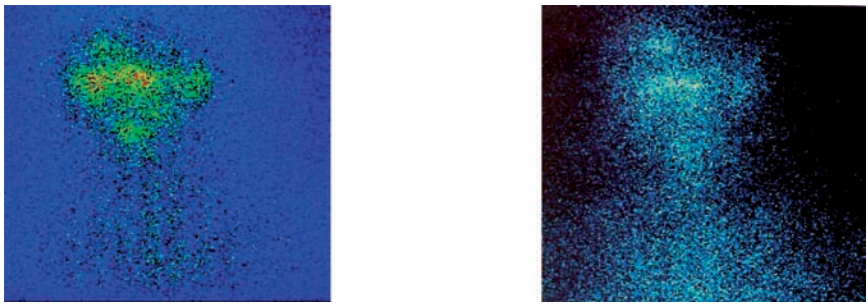

(a) (b)

FIG. 4. A male patient (38 years) with the clinical diagnosis "Ca gl.thyreoideae. Status post-thyreoidectomiam et ^{131}I therapiam – pT2pN1M0"; Tg 28.98 ng/mL. (a) ^{131}I-WBS was positive for a metastatic infiltration of right cervical lymph nodes. (b) After radioiodine therapy 6 months later ^{131}I-WBS was negative for lymph node metastases; Tg 4.05 ng/mL.

In 1 case with lung lesions and 2 with bone metastases, there was no answer to the therapy and they showed disease progression (Fig. 8).

In 11 patients, the ^{131}I scan was negative while the serum Tg was increased. These false negative results were observed predominantly in cases with lymph node and pulmonary metastases, especially after several courses of high dose ^{131}I therapy. The ^{99m}Tc-MIBI scan revealed the presence of lymph node and/or lung lesions, which have lost the capability to uptake ^{131}I in 9 of

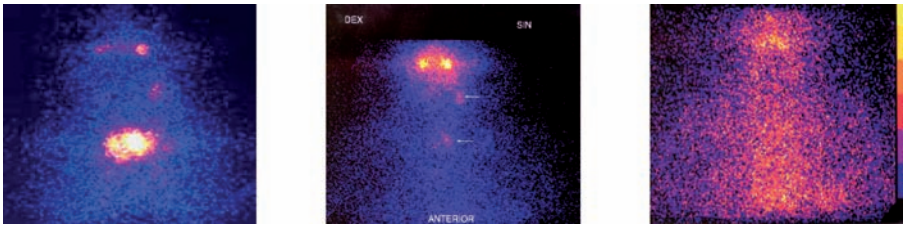

(a) (b) (c)

FIG. 5. A male patient (34 years) with the clinical diagnosis "Ca gl.thyreoideae. Status post-thyreoidectomiam et ^{131}I therapiam – pT4pN1M0". (a) First ^{131}I-WBS was positive for a remnant and metastatic infiltration of left cervical lymph nodes; Tg 19.36 ng/mL. (b) Second ^{131}I-WBS performed 6 months later was positive for a reduced remnant and persistence of metastatic infiltration of left cervical lymph nodes; Tg 9.23 ng/mL. (c) ^{131}I-WBS, performed after extirpation of metastatic cervical lymph node in the right and the third course of radioiodine therapy, showed background radioactivity in the neck.

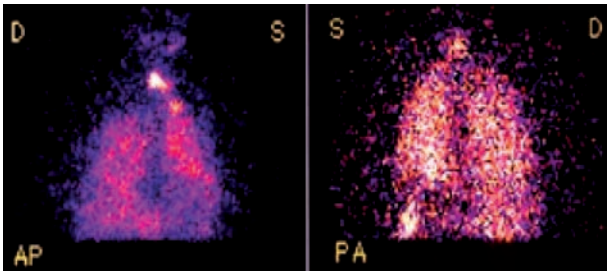

FIG. 6. A male patient (50 years) with the clinical diagnosis "Ca gl.thyreoideae. Status post-thyreoidectomiam et ^{131}I therapiam – pT4pN1M1"; Tg 1350 ng/mL. ^{131}I-WBS was positive for a recurrence and diffuse lung metastases.

these patients (Figs 9–11). In 2 cases with elevated Tg, the ^{99m}Tc-MIBI scan and the ^{131}I-WBS were negative.

Serum Tg was increased in all patients with local lymph node lesions and distant metastases, visualized either by ^{131}I or by ^{99m}Tc-MIBI, but also in 18 patients with thyroid remnants only (Figs 12 and 13).

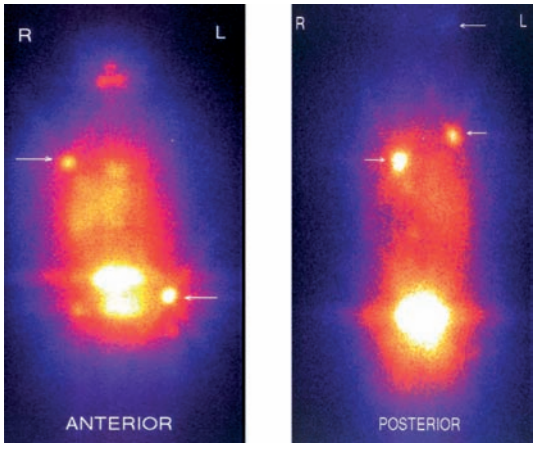

(a) (b)

FIG. 7. A female patient (50 years) with the clinical diagnosis "Ca gl.thyreoideae. Status post-thyreoidectomiam et ^{131}I therapiam – pT3pN1M1"; Tg 1341 ng/mL. ^{131}I-WBS was positive for multiple lung and bone metastases, visualized in anterior (a) and posterior (b) positions.

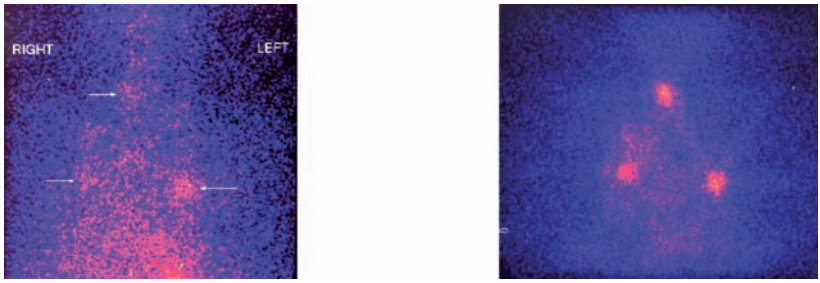

(a) (b)

FIG. 8. A female patient (70 years) with the clinical diagnosis "Ca gl.thyreoideae. Status post-thyreoidectomiam et ^{131}I therapiam – pT2pN0M0"; Tg 294 ng/mL. ^{131}I-WBS was positive for multiple lung metastases, visualized before application of high ^{131}I activity (a); Tg 194 ng/mL. There was no answer to the radioiodine treatment on the control ^{131}I-WBS (b); Tg 203.4 ng/mL.

In three cases, additional lymph node metastatic lesions were visualized on the ^{131}I-WBS performed 5 d after administration of a high therapeutic ^{131}I activity compared to the diagnostic imaging with a low ^{131}I dose (Fig. 14).

4. DISCUSSION

Accurate staging of local, regional and distant metastases is extremely important for treatment and prognosis of patients with thyroid cancer. Most of these lesions can be managed successfully by surgery and/or radioiodine

(a) (b)

FIG. 9. A female patient (54 years) with the clinical diagnosis "Ca gl.thyreoideae. Status post-thyreoidectomiam – pT3pN1aM0. Status post-^{131}I therapiam"; Tg 139.7 ng/mL. (a) ^{131}I-WBS showed background radioactivity in the neck. (b) ^{99m}Tc-MIBI showed an intensive uptake of the tracer in the region of left cervical lymph nodes, significant for metastatic infiltration.

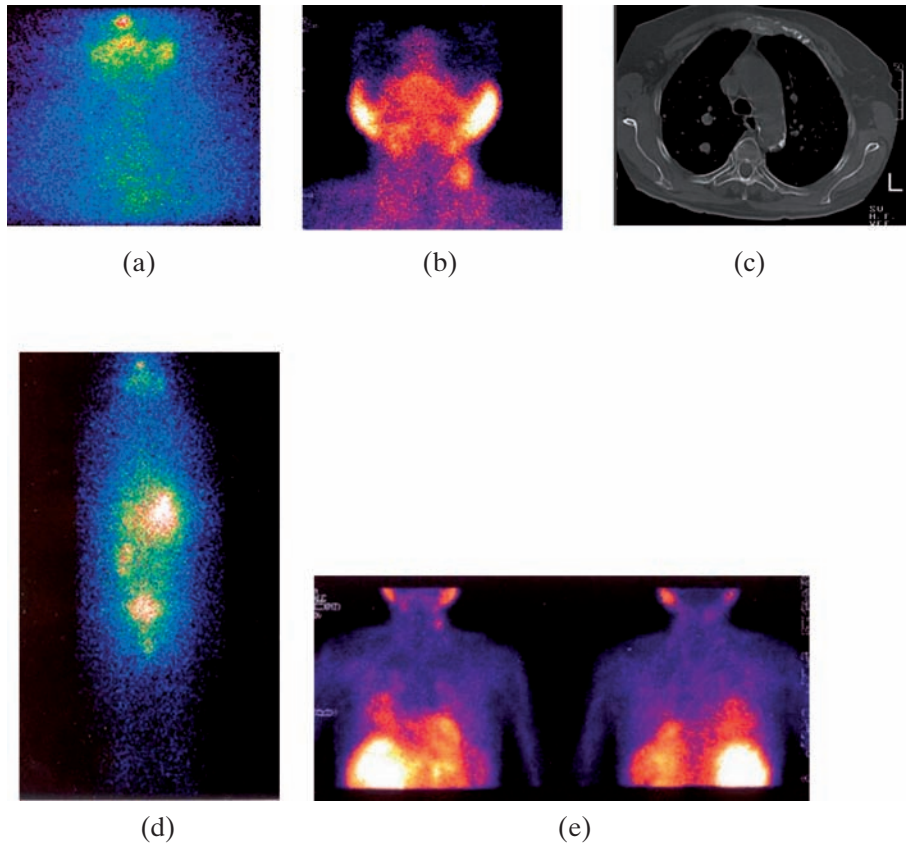

FIG. 10. A female patient (72 years) with the clinical diagnosis "Ca gl.thyreoideae. Status post-thyreoidectomiam et lymphadenectomiam – pT4pN2M0. Status post-^{131}I therapiam et TGT"; Tg 10.19 ng/mL. (a) ^{131}I scan showed background radioactivity in the neck region. (b) ^{99m}Tc-MIBI showed an intensive uptake of the tracer in the region of left cervical lymph nodes, significant for metastatic infiltration. (c) Pulmonary metastases, visualized in the CT. (d) ^{131}I-WBS showed a high level of background radioactivity in the gastric and intestinal regions. (e) ^{99m}Tc-MIBI showed intensive uptake of the tracer in the left and right lung, visualized in the anterior and posterior positions, significant for an active proliferation.

therapy, therefore, early detection of recurrent or metastatic events is critical [8].

As Tg is produced only by normal or malignant thyroid tissue, it should not be detectable in ablated patients [9]. An increase in the Tg level indicates the presence of neoplastic tissue. In order to decide upon the most appropriate therapeutic regimen in the case of elevated Tg, it is necessary to identify as

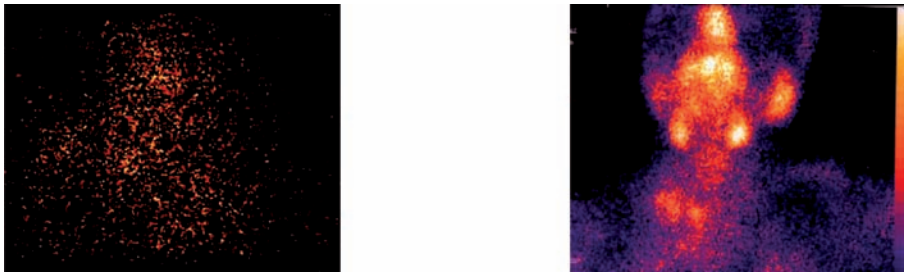

(a) (b)

FIG. 11. A female patient (70 years) with clinical diagnosis "Ca gl.thyreoideae. Status post-thyreoidectomiam et ^{131}I therapiam – pT1pN0M0. Lymph metastases colli dextra. Status post-extirpationem". (a) ^{131}I-WBS showed background radioactivity in the neck. (b) ^{99m}Tc-MIBI showed an intensive uptake of the tracer in the region of the right subclavicular and cervical lymph nodes, significant for metastatic infiltration; Tg 123.2 ng/mL.

many of the lesions as possible and to ascertain whether they have the capability ability to store iodine [3, 8, 9]. Negative ^{131}I-WBS in patients with elevated Tg may be explained by methodological difficulties or by the degree of differentiation of the neoplastic cells. These false negative results were observed predominantly in cases with less differentiated metastatic cells, especially after several courses of high dose ^{131}I therapy. The authors' results showed that ^{99m}Tc-MIBI scintigraphy has a high sensitivity in revealing metastatic lesions that have lost the capability to uptake radioiodine. Others reported that the ^{99m}Tc-MIBI scan has a higher sensitivity for detection of local recurrences, lymph nodes and bone metastases, but lower sensitivity in

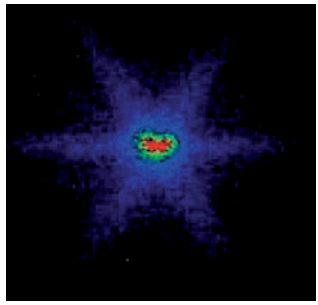

FIG. 12. A female patient (51 years) with the clinical diagnosis "Ca gl.thyreoideae. Status post-thyreoidectomiam et ^{131}I therapiam – pT4apN0M0"; Tg 14.05 ng/mL. ^{131}I-WBS was positive for a remnant in the region of operative cicatrice.

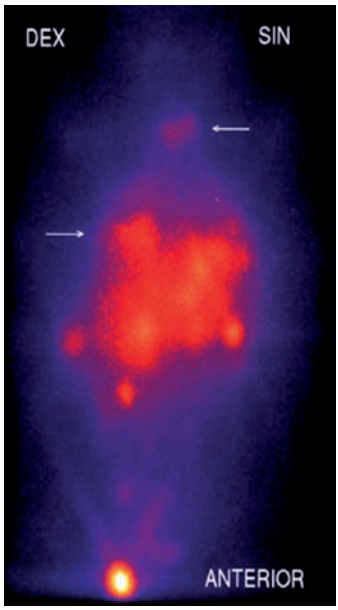

FIG. 13. A female patient (70 years) with the clinical diagnosis "Ca gl.thyreoideae. Status post thyreoidectomiam et ^{131}I therapiam – pT2pN0M0"; Tg 194 ng/mL. ^{131}I-WBS was positive for multiple lung and liver metastases.

revealing thyroid remnants and diffuse lung metastases as compared to the ^{131}I-WBS [10, 11].

By using the ^{99m}Tc-MIBI scan instead of the ^{131}I-WBS it is not necessary to stop thyroid replacement treatment. It is very important for patients who cannot tolerate the withdrawal of replacement therapy.

In three cases, additional metastatic lesions in the cervical region were visualized on the post-therapeutic ^{131}I-WBS compared to the diagnostic imaging obtained before radioiodine treatment. These data suggest that a negative diagnostic ^{131}I-WBS does not necessarily indicate a lesion lacking the capability to accumulate iodine [3, 12]. There is also evidence that 'blind' high dose administration of radioiodine has a beneficial therapeutic effect in these cases [8, 13]. Therapeutic effect of 'blind' radioiodine treatment is indicated by a significant reduction in the serum Tg level. On the other hand, this practice has been questioned by other groups, mainly due to a lack of long term randomized trials [14].

In conclusion, considering the ^{131}I scan as the most specific standard procedure, the combined ^{99m}Tc-MIBI scintigraphy and serum Tg assay appears

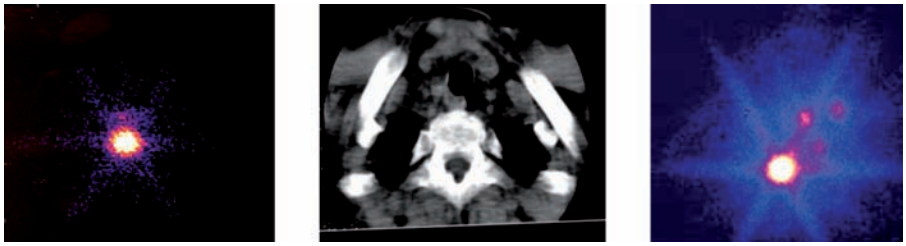

(a) (b) (c)

FIG. 14. A male patient (72 years) with the clinical diagnosis "Ca gl.thyreoideae. Status post-thyreoidectomiam et ^{131}I therapiam – pT4apN0M0"; Tg 75.15 ng/mL. (a) Diagnostic ^{131}I-WBS was positive for a recurrence in the region of operative cicatrice, visualized on the CT scan (b). In (c), ^{131}I-WBS performed 5 d after administration of a high dose of therapeutic radioiodine showed intensive uptake in the region of cervical lymph nodes significant for metastatic process.

to be an alternative substitute for radioiodine diagnostic imaging to demonstrate the extent of the disease in cases with DTC and elevated Tg.

REFERENCES

[1] LIND, P., I-131 whole-body scintigraphy in thyroid cancer patients, Q J Nucl Med 43 (1999) 188-194.

[2] PACINI, F., et al., Diagnostic 131-I whole-body scan may be avoided in thyroid cancer patients who have undetectable stimulated serum Tg levels after initial treatment, J Clin Endicrinol Metab 87 (2002) 1499-1501.

[3] LIND, P., Should high hTg levels in the absence of iodine uptake be treated? Eur J Nucl Med 30 (2003) 157-160.

[4] GROSSO, M., et al., Usefulness of 99mTc-Tetrofosmin scintigraphy and gamma-probe detection of node metastases of thyroid cancer, Eur J Nucl Med (2000) 27(8): Abstract PS-561, p1151.

[5] MAZZAFERRI, E.L., KLOOS, R.T., Current approaches to primary therapy for papillary and follicular thyroid cancer, J Clin Endocrinol Metab 89 (2001) 1447-1463.

[6] MALESEVIC, M., STEFANOVIC, L.J., Value of 99mTc-MIBI scintigraphy in the follow-up of patients confirmed thyroid carcinoma, Eur J Nucl Med (2000) 27(8): Abstract PS-560, p1150.

[7] CASARA, D., et al., Role of MIBI scan, neck us and s-Tg in clinical staging of differentiated thyroid carcinoma (DTC) patients after surgery, Eur J Nucl Med (2000) 27(8): Abstract PS-562, p1151.

[8] KABASAKAL, L., et al., Treatment of iodine-negative thyroglobuline-positive thyroid cancer: differences in outcome in patients with macrometastases and patients with micrometastases, Eur J Nucl Med Mol Imaging (2004) 31:1500-1504.
[9] SCHLUMBERGER, M., BAUDIN, E., Serum thyroglobulin determination in the follow-up of patients with differentiated thyroid carcinoma, Eur J Endocrinol (1998) 138: 249-252.
[10] RUBELLO, D., et al., The role of technetium-99m methoxyisobutylisonitrile scintigraphy in planning of therapy and follow-up of patients with differentiated thyroid carcinoma after surgery, Eur J Nucl Med 27 (2000) 431-440.
[11] TZONEVSKA, A., et al., Comparative assessment of 131I and 99mTc-MIBI imaging in the follow-up of patients with differentiated thyroid carcinoma after thyroidectimy, Hell J Nucl Med 4 (2001)165-168.
[12] WU, H.S., et al., Decreased uptake after fractionated ablative doses of iodine-131, Eur J Nucl Med Mol Omaging 32 (2005)167-173.
[13] PINEDA, J.D., et al., Iodine therapy for thyroid cancer patients with elevated thyroglobulin and negative diagnostic scan, J Clin Endocrinol Metab 80 (1995) 1488-1492.
[14] BIERMANN, M., SCHOBER, O., Should high hTg levels in the absence of iodine uptake be treated?- Aginst. Eur J Nucl Med 30 (2003) 160-163.

RESULTS OF KNEE RADIOSYNOVIORTHESIS IN HAEMOPHILIC AND RHEUMATOID ARTHRITIC PATIENTS WITH ^{32}P COLLOID OF LOCAL PRODUCTION

V.E. SOROA*,**, M.H. VELÁZQUEZ ESPECHE**, C. GIANNONE*,**, G. NASWETTER**, H. CAVIGLIA***, G. GALATROS***

*Centro de Medicina Nuclear,
Comisión Nacional de Energía Atómica
Email: soroa@cnea.gov.ar

** Hospital de Clínicas,
University of Buenos Aires

***Traumatology and Orthopedics,
Hospital Municipal J.A. Fernández, Hemophilic Foundation

Buenos Aires, Argentina

Abstract

The objective of this study was to assess the effects of radioactive treatment in knee joints with refractory synovitis in haemophilic patients, using a colloidal suspension of ^{32}P, a pure beta emitter, developed domestically. Results were then compared with those from chemical synovectomy. A population of rheumatoid arthritis (RA) patients was treated and compared against intra-articular steroids and systemic drugs. Fifty-eight male haemophilic patients, aged 4–52 years, were treated. Nine of them had re-injections (67 procedures). Adults received 37–74 MBq; children of 2–6 years received one third the adult's activity; 6–10 years received one half the activity, whereas 10–16 years were injected with three quarters the activity given to adults. Anti-haemophilic factors (AHF) therapy, clinical examination as well as a pre-3-phase MDP scan were registered and followed-up with MDP scans through 9 months. The intra-articular therapies for either ^{32}P in 44 patients or the antibiotic Rifampicin-^{99m}Tc macroaggregates in 14 patients were monitored in the gamma camera with ^{32}P bremsstrahlung emission, searching for leakage. Twelve RA patients were studied: six received ^{32}P and the others intra-articular corticoids. Comparison of RoIs in treated knees during soft tissue scintigraphies in pre- and post-third MDP control shows knee improvement. Joint motion increased. Bleeding episodes, as well as requirements of AHF in 80% of the radiosinovectomies, diminished. Intra-articular Rifampicin treatment requires several

injections. Outcomes in RA lasted 3 months and were less promising. Radiosinovectomy in haemophilic patients with one injection provides 3–6 months relief. The paediatric benefit from radiosinovectomy outweighs potential radiation hazards. Radiosinovectomy is a safe, cost effective alternative therapy in emerging nations, where availability of AHF is difficult and expensive.

1. INTRODUCTION

Haemophilia is a worldwide disease, affecting males including young children; management of the associated arthropathy is compromised in emerging countries by high cost (injection of anti-haemophilic factors (AHF)) and limited availability of specialized treatments. Intra-articular injections of chemicals (such as osmic acid) or of antibiotics (Rifampicin) have been applied to ameliorate haemophilic chronic recurrent synovitis and control joint bleeding [1]. If unsuccessful, an alternative could be surgical intervention with synovium removal. The latter is not an option in the haemophiliac patient, because of possible haemorrhage [2]. Moreover, requirements of AHF for haemostatic preparation rose to 100% during surgery. This elevates health costs and requires prolonged hospitalization and kinesic therapy for the intervened joint.

In rheumatoid arthritis (RA), an auto-immune disease, the compromised painful joints are predominantly small ones. Systemic treatment must be prescribed (aspirin, non-steroidal and steroidal anti-inflamatory anti-metabolites, penicillamine or tumour necrosis factor α blocker). Local intra-articular corticoid injections have also been used [2].

Radiosinovectomy is a procedure used to destroy the synovium with an intra-articular injection of appropriate β colloids. The physical characteristics of the β radiopharmaceutical will provide the indication of how to treat different types of joint. New developments of colloid particles such as hydroxide, citrates, silicates or macroaggregates of appropriate size, to be phagocytosized without signs of inflammation and labelled with different β emitters have reduced the unwanted joint leakage and the radiation exposure to different organs [3].

The aim of this study was to assess the effects of radioactive treatment in large joints, using a colloidal suspension of ^{32}P, a pure β emitter, developed domestically [4, 5]. The amelioration of synovial inflammation with radiosinovectomies was evaluated against the alternative treatments in the studied pathologies, also taking into account the cost–benefit ratio to justify the present option.

2. MATERIALS AND SUBJECTS

Characteristics of ^{32}P: $T_{1/2}$ 14.3 d; max. β energy 1.71 MeV; max. tissue penetration 7.9 mm (mean penetration 2.2 mm). The authors' local radiopharmacy, BACON Laboratories, supplied sterile ^{32}P enriched gelatine chromic phosphate colloid sized 100–200 nm, with 97% radiochemical purity and a specific activity of 20 μCi/mg ^{32}P [4, 6].

Radiosinovectomies were performed using ^{32}P colloid in 58 male haemophilic patients sent by the Hemophilic Foundation, aged 4–52 years. Nine of them had retreatments (67 procedures), either in the same or in the contralateral knee. The doses used were found to be safe and are based on the results of several trials [5, 7]. Adults were injected with 37–74 MBq; children of 2–6 years of age received one third the activity of the adult; 6–10 year olds received one half the activity of an adult, whereas 10–16 year olds were injected with three quarters the activity given to adults. When children were overweight by more than 20% from normal (for age and height), one quarter more activity from the adult dose was added. Informed consent from adults or from the children's parents was obtained.

Patients were included in this study only if several knee episodes had occurred. Exclusion criteria: large Bakers cysts, grades IV–V arthropaties, skin infections of the joint area and bleeding at the time of the radiosinovectomies [8]. Documentation of patients' haemophilic history (severity, haemophilia A or B), AHF therapy, number of bleedings, pain (visual analogue scale in 10 steps) range of articular movement and clinical examination were registered as well as a pre-3-phase MDP scan in case report forms (CRF). Patients were followed-up with the 3-phase bone scans through 1, 3, 6, 9 and 12 months. If required, joint aspiration was carried out. The puncture sites for intra-articular therapy for either the radiosinovectomies ^{32}P in 44 patients or the antibiotic Rifampicin–^{99m}Tc macroaggregates (4 MBq) in 14 patients were monitored with the gamma camera.

Twelve RA patients were studied: six received ^{32}P therapy and the other six intra-articular corticoids. Clinical, blind evaluation (state of joint involvement, pain, motility, requirements of AHF, corticoids or analgesics) was registered in follow-up charts. For intra-articular chemical or corticoid injection therapy, 4 MBq of ^{99m}Tc macroaggregates was added in order to obtain gamma camera images and to blind the evaluating team of which patient received radiotherapeutic treatment

To quantify the remission of the lesion over time, a remission rate index (RR) was defined as the rate of severity of the lesion at the baseline and at each control after treatment (months 3, 6, 9).

The severity at each control was defined as the product of the extension of the lesion (area of the lesion expressed in pixels) and the increase in count density at the lesion relative to a background normal area. This definition for the relative count density was a means to establish afterwards an RR independently of the acquisition parameters and the total activity applied at each study:

$$SI(t) = \{[dL(t) - dR(t)] / dR(t)\} \times N(t)$$

where for each planar image, SI(t) is the severity index at time t, with t = 0 (baseline), or month 3, or month 6 and so on, after treatment and:

N(t): area of the lesion [RoI in pixels] at time t.

dL(t): average counts/pixels in the lesion RoI at time t.

dR(t): average count density in the reference background selected in the same image at time t.

The RR at time t is defined as:

$$RR(t) = SI(t=0) / SI(t)$$

A successful treatment implies RR(t) >1 while RR(t) <1 implies disease progression.

A clinical criterion for recovery was considered based on the fall of lesion detectability with time for responders owing to lack of contrast, or in other words, an increasing standard error (inversely proportional to the square root of the count statistics at the lesion RoI). As a result, the authors accepted clinical recovery as RR(t) values >1.10 whereas RR(t) values less than 0.90 define disease progression. Between both limits, patients were considered as being without clinical improvement or non-responders.

2.1. Therapeutic protocol for haemophilia and RA

Procedure undertaken in a clean room. Intra-articular injection performed with sterile instruments. ^{32}P phosphate chromic colloid unit dose was drawn in a laminar flow hood. Intra-articular injection was in accordance to patient age, joint (volume) and body weight [4, 7]. Synovial or haematic content was previously evacuated from the compromised joint. The injection was performed under gamma camera control. Knee and large joints were the only ones that could be treated due to the characteristics of ^{32}P colloid [9].

Saline flushing was carried out before the needle was withdrawn. The treated joint was manipulated through a full range of motion to distribute the radio-colloid throughout the joint space [1, 6, 8]. ^{32}P bremsstrahlung emission in ^{201}Tl photopeak settings with a 25% window was used in the gamma camera for early and late 24–48 h imaging to monitor extra-articular leakage [6]. After the procedures, immobilization with a plaster and relative rest for 72 h followed [8, 10]. Twenty-four h urine collections were obtained from 3 haemophilic patients and counted in a β scintillation counter.

Figure 1 shows an example of a successfully treated haemophilic child with ^{32}P colloid injection in the left knee followed through 48 h images, to which ^{99m}Tc markers or flood sources were added in order to provide anatomical landmarks. Acquisition was obtained with bremsstrahlung emission.

2.2. Follow-up

CRF, with a similar set of questions as before treatment, entailed registering the number of subsequent episodes, diminished bleeding episodes, pain score, range of movement, joint circumference and AHF requirements. The MDP scan was obtained with an evaluation on the 2-phase at 1, 3, 6 and 12 months. In the pre-^{32}P and third bone scans, irregular/similar RoIs were drawn on the treated knee and in a background area over the contralateral thigh. The analyses took into account the background, density, counts and number of pixels, and then a formula was applied to obtain the severity index and the RR in the radiosinovectomy treated knee (see the example in Fig. 2), the location of RoIs in lesion and background, both in the baseline MDP scan and in the 3 month MDP images. If the RR was greater than unity, it was considered a treatment success [6].

3. RESULTS

For the haemophilic patients, there were neither local burns, systemic effects, nor leakage registered during ^{32}P treatment (see the example in Fig. 1). Intra-articular Rifampicin procedure required frequent injections (5–9) to obtain a similar outcome as with ^{32}P. Comparison of RoIs in treated knees during soft tissue scintigraphies in pre- and post-third MDP control showed knee improvement when the RR was >1. The follow-up evaluation demonstrated an increase in joint motion, between 10–30%, diminished articular volume and less requirement and frequency for the use of AHF in 80% of the

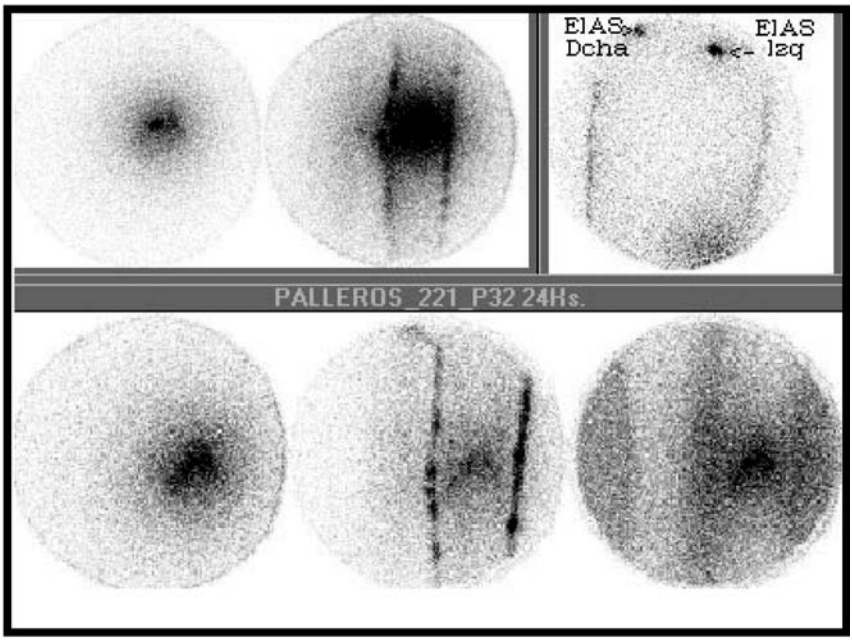

(a)

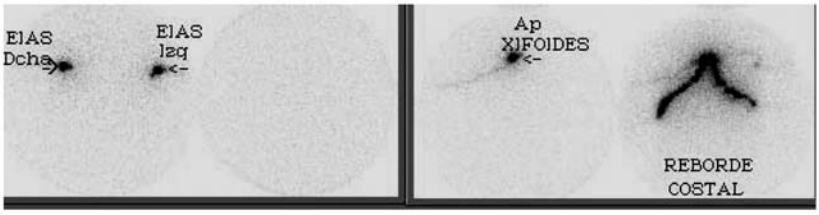

(b)

FIG. 1. Intra-articular ^{32}P colloid injection in the left knee of a haemophilic patient. (a) Upper quadrant of the gamma camera image at 4 h, to which a contour of a ^{99m}Tc marker was added around the left leg. The lower quadrant is the 24 h registration, plus a ^{99m}Tc flood source underneath the patient. (b) 48 h images with no leakage in the iliac fossa or thorax.

radiosynovectomies (54/67 procedures), thus lowering health costs dramatically. No ^{32}P counts were observed in the 24 h urine collections of the 3 patients.

Outcomes in RA lasted 2–3 months and were not so promising. In Fig. 2, the authors present an RA patient where the low RR obtained proves the unwanted outcome.

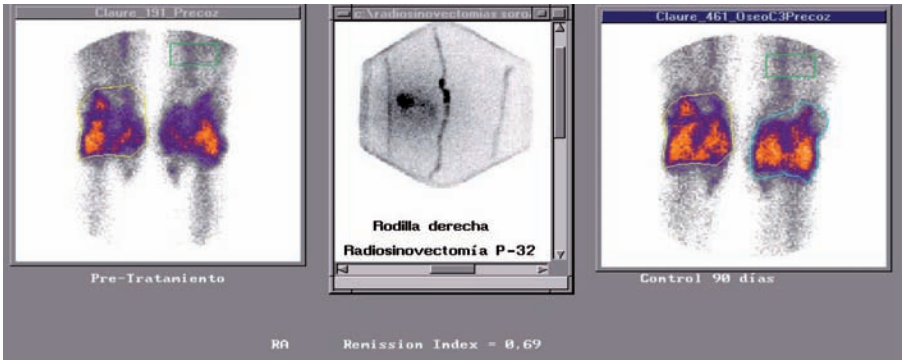

FIG. 2. An RA patient in which the RR = 0.69 proved an unsuccessful treatment.

Figure 3 shows plots of the RR of the haemophiliac knees treated with ^{32}P colloidal injection against the results of the Rifampicin injection. It clearly demonstrates that the RR exceeds 1.5 in more than 80% of the RS.

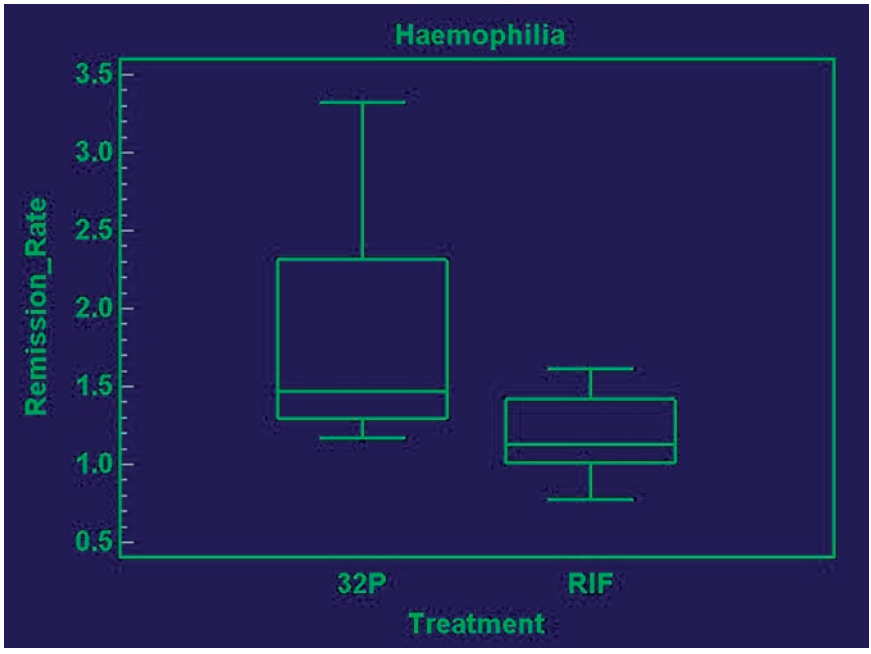

FIG. 3. Comparable RR of ^{32}P treatment with those from chemical synovitis in haemophilic patients.

4. CONCLUSIONS

One intra-articular knee RS in haemophilic patients provides around 3–6 months relief of symptoms after treatment with locally produced ^{32}P colloid. Bleeding episodes diminished in the RS treated knees and the range of movement increased [5–7]. Younger patients had a greater likelihood of successful outcome [11].

In RA, a maximum of a 3 month pain palliative effect was documented. RA is predominantly a pathology of small joints, but the high beta penetration of ^{32}P colloid allowed only the knees to be treated with this radiotherapeutic alternative, making its use less beneficial.

Extra-articular leakage was not detected in any of the RS procedures (67 in haemophilia plus 6 in RA).

RS turned out to be a safe, cost effective alternative outpatient therapy for use in emerging nations and could be considered as an initial procedure for haemophilic haemartrosis where AHF is not readily available or is expensive.

ACKNOWLEDGEMENTS

The authors wish to thank L.B. Questa and T. Bonavita providing gamma camera images, as well as N. Moretti in charge of the kinesic therapy and the coordination of all the haemophiliac patients received by the Hemophilic Foundation.

We thank R. Ughetti from the Radiopharmacist Section in BACON Laboratories S.A.I.C. for the provision of ^{32}P β colloid. This study was supported by the IAEA (CRP).

REFERENCES

[1] MOLHO, P., et al., A retropspective study on chemical and radioactive synovectomy in severe haemophilia patients with recurrent hemarthrosis, Hemophilia **5** (1999) 115-123.

[2] SCHNEIDER, P., FARAHATI, J., REINERS, C., Radiosynovectomy in Reumatology, Orthopedics, and Hemophilia, J. Nucl. Med. **46** (2005) 11 (Suppl.1) 48 S-54 S.

[3] CLUNIE, G., LUI, D., CULLUM, I., EDWARDS, J.C.W., ELL, P., Samarium-153-particulate hydroxyapatite radiation synovectomy: Biodistribution data for chronic knee synovitis, J. Nucl. Med. **36** (1995) 51-57.

[4] ANGHELERI, L.J., Rapid method for obtaining colloidal suspension of phosphorous-32 as chromic phosphate, Proc of 2nd Intl. Conf on Peaceful uses of Atomic Energy, UN, Geneva (1957).

[5] SOROA, V.E., Radiosynoviorthesis with P-32 colloid is still a helpful therapeutic practice in haemophilia, J. Nucl. Med. **45** (2004) Abstract Book Supplement abstract) 147.

[6] SOROA, V.E., et al., Effects of radiosynovectomy with P-32 colloid therapy in haemophilia and rheumatoid ar-thritis, Cancer Biotherapy & Radiopharmaceuticals **20** (2005) 3, 344-348.

[7] RIVARD, G.-E., et al., Synoviorthesis with colloidal Phosphorous-32 Chromic Phosphate for the Treatment of Hemophilic Arthropathy, JB & JS **76-A** (1994) 4, 482-488.

[8] CLUNIE, G., FISCHER, M., EANM Procedure Guidelines for Radiosynovectomy. Eur. J. Nucl. Med. **30** (2003) BP12-BP16.

[9] JOHNSON, L.S., YANCH, J.C., SHORTKOFF, C.L., BARNES, A.L., SLEDGE, C.B., Beta-particle dosimetry in radiation synovectomy, Eur. J. Nucl. Med. **22** (1995) 977-988.

[10] WINFIELD, J., CRAWLEY, J.C., HUDSON, E.A., FISHER, M., GUMPEL, J.M., Evaluation of two regimens to immobilise the knee after injections of ^{90}yttrium, British Med. J. **1**(1979) 986-987.

[11] SIEGEL, H.J., LUCK, J.V., SIEGEL, M., QUINONES, C., The clinical utilization of ^{32}Pchromic phosphate radiosynovectomy in Hemophilia outcome analysis of 125 procedures, Proc. Orthopedic Surgeon Annual Meeting (2000) Poster PE152 (abs).

PET RADIOPHARMACEUTICALS

(Session 10)

Chairpersons

H.-J. MACHULLA
Germany

M.C. LEE
Republic of Korea

ALTERNATIVE METHODS OF MAKING [^{11}C]AMIDES: APPLICATION TO THE PREPARATION OF 5-HT$_{1A}$ RECEPTOR RADIOLIGANDS

V.W. PIKE, S.Y. LU, J. HONG, J.L. MUSACHIO, J.A. McCARRON
Molecular Imaging Branch, National Institute of Mental Health,
National Institutes of Health,
Bethesda, Maryland,
United States of America
pikev@mail.nih.gov

Abstract

Many ligands for brain 5-HT$_{1A}$ receptors contain an amide group that is subject to hydrolysis in vivo. In the development of radioligands for use with positron emission tomography (PET), labelling in the carbonyl function of an amide group may be advantageous for avoiding radioactive metabolites that would readily enter the brain to confound PET receptor measurements. Several methods of labelling secondary and tertiary amides in their carbonyl functions with ^{11}C ($T_{1/2}$ = 20.4 min) have been developed over the past two decades or so. These methods include reaction of a [carbonyl-^{11}C]acid chloride, [carboxyl-^{11}C]magnesium halide carboxylate or [carboxyl-^{11}C]acid with an amine or reaction of [^{11}C]carbon monoxide with an amine plus an aryl halide, alkyl halide or aryl triflate. Some of these processes are successfully promoted with microwaves, palladium complexes, light or thermally intitated radicals. These methods are surveyed here and especially exemplified from research on the development of 5-HT$_{1A}$ receptor radioligands for brain imaging applications with PET.

1. INTRODUCTION

The amide group is widely found in drug-like ligands for neurotransmitter receptors from which radioligands [1, 2] are sometimes developed for imaging these receptors in the brain using positron emission tomography (PET), either in clinical research [3] or in drug development [4, 5]. An important consideration for radioligand development is the molecular position at which a positron emitting isotope, frequently ^{11}C ($T_{1/2}$ = 20.4 min), should be introduced. Careful choice of position may avoid radioactive metabolites that could enter the brain to confound PET measurements of radioligand binding to the target receptor. Amides are often metabolized in phase 1 by simple hydrolysis in the liver and/

or other organs to produce the parent amine and carboxylic acid in the blood. Generally, simple carboxylic acids, because they are ionized at physiological pH7.4, do not enter the brain to a great extent, whereas the brain penetration of amines, though subject to many factors, can be very appreciable. Hence, for a potential PET radioligand containing an amide linkage, introduction of the ^{11}C label on the carbonyl side of the amide group, and even in the carbonyl entity, may be advantageous. This is strikingly so [6, 7] for PET imaging of human brain 5-HT_{1A} receptors with ^{11}C labelled WAY-100635 (1), where labelling in the carbonyl function has been shown to provide a far more sensitive radioligand [8] than labelling in the methoxy group [9] (Fig. 1). Labelling in the methoxy group gives rise to a radioactive amine, ^{11}C labelled WAY-100634 (2) which readily enters the brain to bind both specifically and non-specifically, whereas labelling in the carbonyl function avoids this radioactive metabolite and instead gives rise to [^{11}C]cyclohexanecarboxylic acid which enters the brain only to a low and transient extent (Fig. 2). Such metabolic considerations create a need for effective methods of labelling amides in their carbonyl functions with cyclotron produced ^{11}C, which is nearly always produced from the $^{14}N(p,\alpha)^{11}C$ reaction as either [^{11}C]carbon dioxide or [^{11}C]methane [10].

Various methods of labelling secondary and tertiary amides in the carbonyl function with ^{11}C have been developed over the last two decades or so, and these methods are surveyed here. Although these methods have very wide applicability, they are mainly exemplified in this survey through their previous and ongoing applications in producing antagonist and agonist type

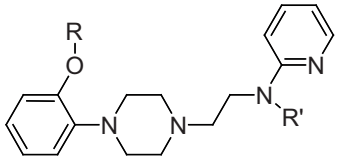

1, WAY-100635, R = Me, R' = *c*.hexyl-CO
2, WAY-100634, R = Me, R' = H
3, DWAY, R = H, R' = *c*.hexyl-CO
4, *p*-MMPF, R = Me, R' = 4-F-C_6H_4-CO

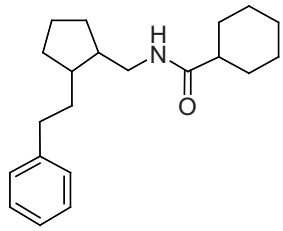

5, (-)-NPPC

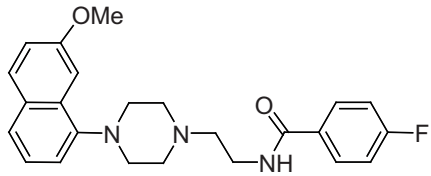

6, S14506

FIG. 1. Labelling with ^{11}C.

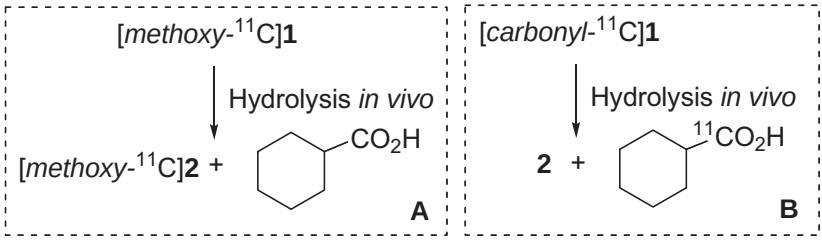

FIG. 2. The metabolic fate of [methoxy-^{11}C]1 (A) and [carbonyl-^{11}C]1 in humans (B).

PET radioligands for 5-HT_{1A} receptors. Key considerations with respect to the various methods to be discussed here are their isotope efficiency (i.e. radiochemical yields), speed and ability to deliver high specific radioactivity. If a radioligand is to be obtained in adequately high activity and specific radioactivity for PET investigations, then generally no more than two half-lives of ^{11}C (i.e. a total of 40 min) may be taken for radiosynthesis, purification and formulation. Useful labelling methods typically comply with this time constraint.

2. LABELLING VIA [CARBONYL-^{11}C]ACID CHLORIDES

A wide range of [carbonyl-^{11}C]acid chlorides has been prepared by the general method of carboxylation of a Grignard reagent (RMgX, X = halogen) with cyclotron produced [^{11}C]carbon dioxide followed by chlorination of the adduct (Fig. 3). The ^{11}C-carboxylation reaction has to be controlled in order to avoid further reaction of the adduct or acid with the Grignard reagent, which is necessarily present in excess. Judicious choice of the halogen in the Grignard reagent, reagent concentration, temperature and reaction time often result in efficient carboxylation to give the initial adduct. Chlorination with high boiling

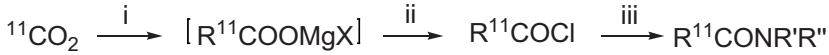

FIG. 3. Synthesis of [carbonyl-^{11}C]acid chlorides for conversion into [carbonyl-^{11}C]amides. Typical conditions: (i) RMgX (X = Cl or Br) in diethyl ether solution for R = lower alkyl or aryl, or immobilized in tube for R = aryl or c.Hex, RT, 2 min; (ii) phthaloyl dichloride and 2,6-di-t-butylpyridine for R = lower akyl or aryl, or thionyl chloride for R = aryl, c.Hex, heat, 5–8 min; (iii) primary or secondary amine (R'R"NH), solvent (e.g. THF, CH_2Cl_2), 0-37°C, 5–8 min. Reported specific radioactivity (exemplified by [carbonyl-^{11}C]3 [23, 24]): 74 GBq/μmol.

point phthalolyl dichloride in the presence of an involatile base allows volatile [^{11}C]acid chlorides (e.g. R^{11}COCl, R = Me, Et, Pr, *c.*Pr or *c.*Bu) to be transferred cleanly out of the heated reaction mixture in a nitrogen stream. The [^{11}C]acid chloride may then be trapped within an amine solution to generate the desired [carbonyl-^{11}C]amide, usually in a moderate decay corrected radiochemical yield (RCY) [11–12].

Where the required [^{11}C]acid chloride is not very volatile (e.g. R^{11}COCl, R = *c.*Hex, Ar), reaction with the amine partner may be performed in situ [13, 14]. However, this method may pose a severe separation challenge. Hence, an alternative technique has been devised to limit the amount of material that needs to be separated [15]. A narrow plastic (e.g. polypropylene) tube is coated with an almost dry film of the Grignard reagent. ^{11}C-carboxylation is achieved by controlled passage of the cyclotron produced [^{11}C]carbon dioxide into the tube and the generated adduct washed out with a solution of thionyl chloride into a solution of the amine partner. This method has been automated and applied routinely to the production of [carbonyl-^{11}C](1) ([^{11}C]WAY) from [carbonyl-^{11}C]cyclohexanecarbonyl chloride [16]. Some laboratories prefer to use the one pot process and this method has also been automated for the production of [^{11}C]WAY [17, 18]. Practical aspects with regard to the regular production of [^{11}C]WAY, by either the one pot or 'immobilized' Grignard reagent procedure, have been discussed in an EC sponsored workshop and the key conclusions published [19].

Desmethyl-WAY (DWAY, 3), may also be labelled in a similar manner to WAY without need for protection of the phenolic hydroxyl group [20]. In fact, [^{11}C]DWAY is superior to [^{11}C]WAY as a PET radioligand for 5-HT$_{1A}$ receptors in monkey and human subjects [21]. Several analogues of WAY have also been labelled similarly, either from [carbonyl-^{11}C]cyclohexanecarbonyl chloride [22–23] or one of the various [carbonyl-^{11}C]benzoyl chlorides [24]. These analogues include *p*-MPPF (4), which it may be noted has been exploited extensively as a 5-HT$_{1A}$ receptor radioligand in humans with a longer lived ^{18}F ($T_{1/2}$ = 109.7 min) radiolabel [25].

This method can deliver acceptably high specific radioactivities if care is taken to exclude atmospheric carbon dioxide during the preparation and use of the Grignard reagent.

3. LABELLING VIA [CARBONYL-^{11}C]MAGNESIUM HALIDE CARBOXYLATES

Aubert et al. [26] have reported the rapid one pot synthesis of aliphatic [carbonyl-^{11}C]amides in moderate RCYs (15–60%) by direct treatment of

FIG. 4. Preparation of aliphatic [carbonyl-^{11}C]amides by reaction of [carboxyl-^{11}C]magnesium halide carboxylates with amines. Typical conditions: (i) RMgX (R = lower alkyl; X = Cl or Br), THF or diethyl ether, 0°C, 3–8 min; (ii) R'R''NH (primary or secondary amine with R' and R''aliphatic or alicyclic, THF, 70°C, 1–10 min and then aq. HCl or aq. NH_4Cl at 0°C). Specific activity: no carrier added.

[^{11}C]magnesium halide carboxylates with amines in THF in the presence of 2.5 equivalents of alkylmagnesium halide (Fig. 4). The 5-HT_{1A} agonist (-)-NPCC (5) has been labelled succesfully with this type of procedure [Lu et al., unpublished results]. Aniline, however, failed to give a labelled amide by this route under thermal conditions [31].

With the application of microwaves, this approach has been extended to encompass the preparation of a [carbonyl-^{11}C]amide having a benzoyl moiety (4-F-$C_6H_4{}^{11}CO$) in up to 45% RCY in 10 min (Fig. 5) [27]. This method has been applied to label the 5-HT_{1A} receptor agonist, S14506 (6) in the carbonyl function with ^{11}C in 10–18% overall RCY [28].

4. LABELLING VIA [CARBOXYL-^{11}C]ACIDS

The controlled carboxylation of organometallic reagents, such as Grignard reagents or organolithiums, with [^{11}C]carbon dioxide followed by hydrolysis has been exploited for generally efficient radiosynthesis of a very wide range of aliphatic and aryl [carboxyl-^{11}C]acids [29]. In non-radioactive chemistry, many methods, aside from conversion into acid chlorides, are known for activating acids for amide formation. However, such methods have been adapted only sparsely for preparing [carbonyl-^{11}C]amides. Rogers et al. [30]

FIG. 5. Preparation of aryl [carbonyl-^{11}C]amides by reaction of [carboxyl-^{11}C]magnesium halide carboxylate with amine. Typical conditions: (i) 4-F-C_6H_4MgX, THF, RT, 6 min; (ii) R'R''NH (primary arylamine or primary or secondary aliphatic amine), THF, microwaves, 70–130°C, 2–10 min, and then aq. H_2SO_4. Specific radioactivity: no carrier added.

FIG. 6. Preparation of aryl [carbonyl-^{11}C]amides from a [carboxyl-^{11}C]benzoic acid by activation with carbonyldiimidazole. Typical conditions: (i) ArMgBr, 5 min; (ii) imidazole-HCl (Im HCl), 1 min; (iii) bromine, 2 min; (iv) carbonyldiimidazole, 5 min; (v) R'R''NH (e.g. piperidine), 5 min. Specific radioactivity: no carrier added.

demonstrated activation of [carboxyl-^{11}C]benzoic acids with carbonyldiimidazole for one pot amide synthesis (Fig. 6). As for many one pot radiosyntheses with ^{11}C, separation of the radioactive product from unused reagents and by-products was challenging. In this work, an aryl by-product was produced that was incompletely resolved from labelled amide during HPLC. This separation problem was circumvented by brominating the aryl byproduct with bromine, before activation of the labelled acid. The desired [carbonyl-^{11}C]amide was then obtained pure in >80% RCY in a preparation time of 22 min.

5. LABELLING VIA [^{11}C]CARBON MONOXIDE

5.1. Palladium mediated

Carbon monoxide has a versatile transition metal mediated chemistry for the introduction of the carbonyl function into organic compounds, including amides. [^{11}C]carbon monoxide of high specific activity may be produced efficiently from [^{11}C]carbon dioxide by on-line reduction over heated zinc [31] or molybdenum [32]. The low solubility of [^{11}C]carbon monoxide in organic solvents had impeded its application in radiosynthesis until techniques were developed quite recently to overcome this obstacle, including recirculation [33], the use of high pressure miniature autoclaves [34, 35] and reversible entrapment as a borane complex [36, 37]. Synthia Lab Systems AB (Uppsala, Sweden) has shown that its miniature high pressure apparatus may be automated for radiation safe radiosynthesis with [^{11}C]carbon monoxide.

5.1.1. From aryl halides

Kihlberg and Långström first demonstrated the potential of palladium mediated reactions of [^{11}C]carbon monoxide with aryl and benzyl halides and primary and secondary amines for the preparation of biologically active [carbonyl-^{11}C]amides in almost quantitative RCYs (Fig. 7) [38].

FIG. 7. Preparation of [carbonyl-^{11}C]amides from [^{11}C]carbon monoxide, aryl or benzyl halides halides and primary or secondary amines. Typical conditions: (i) aryl or benzyl halide, $Pd(PPh_3)_4$, 1,4-dioxane, primary or secondary alkyl amine, 130–150°C, 5 min. Reported specific activities: = 1000 GBq/μmol [43]; = 1250 GBq/μmol [45].

In an extension of this work, less reactive amines were activated with lithium *bis*(trimethylsilyl)amide, resulting in greatly improved RCYs over reactions conducted without activation [39]. Several analogues of (1) have been labelled in this manner [B. Långström, personal communication]. Alternatively, addition of 1,2,2,,6,6-pentamethylpiperidine to the reactions also increased RCYs for less reactive amines, such as methylamine [40].

5.1.2. From aryl triflates

Rahman et al. [41] have shown that aryl triflates may serve well in place of aryl halides in the palladium mediated radiosynthesis of [carbonyl-^{11}C]amides from [^{11}C]carbon monoxide. Lithium bromide facilitates the reactions which may be performed in the miniaturized autoclave described by Synthia AB. A variety of [carbonyl-^{11}C]amides was prepared from aryl triflates and primary or secondary aliphatic amines or aniline in RCYs of 2–63% from 5 min reaction times (Fig. 8).

This method has been applied successfully to the preparation of several candidate radioligands for the peripheral benzodiazepine receptor (PBR) in RCYs ranging from 10 to 55% and with high specific radioactivities (200–900 GBq/μmol) [42].

FIG. 8. Preparation of [carbonyl-^{11}C]amides from [^{11}C]carbon monoxide, aryl triflates and amines. Typical conditions: (i) $Pd(PPh_3)_4$, LiBr, THF, aryl triflate, primary or secondary alkyl amine or aniline, 150°C, 5 min. Reported specific radioactivity: 200–900 GBq/μmol [47].

FIG. 9. Preparation of [carbonyl-^{11}C]amides via photoinitiated carbonylation with [^{11}C]carbon monoxide using amines and alkyl iodides. Typical conditions: (i) N-methyl pyrolidinone, primary or secondary aliphatic amine or primary aromatic amine, alkyl bromide or iodide or aryl iodide, hv, 400 s. Reported specific activity: 192 GBq/μmol [48].

5.2. Radical carbonylation

5.2.1. Photoinitiation

The use of palladium to mediate the insertion of [^{11}C]carbon monoxide into amides and other carbonyl compounds is restricted when competing β-hydride elimination is possible in the electrophile. For this reason, this approach is inapplicable to the radiosynthesis of [^{11}C]WAY since an appropriate electrophile (cyclohexyl halide) would have a β-hydrogen. Recently, photoinitiated radical carbonylation was shown to be successful for the preparation of [carbonyl-^{11}C]amides and alkyl halides bearing β-hydrogens, such as ethyl iodide and cyclohexyl bromide, from [^{11}C]carbon monoxide, amines and alkyl halides [43] (Fig. 9). In particular examples, conversions of [^{11}C]carbon monoxide in fast reactions (e.g. 400 s) may reach up to 95%, with RCYs of labelled amides reaching 74%.

This method has been adapted to the one step synthesis of [^{11}C]WAY in 40–50% RCY in 30 min synthesis time (Fig. 10) [44].

5.2.2. Thermal initiation

Recently, it was briefly reported that the preparation of a [carbonyl-^{11}C]amide from [^{11}C]carbon monoxide, alkyl halide and amine may be achieved through thermal generation of free radicals [45]. In a preliminary finding, a 30% conversion of [^{11}C]carbon monoxide and a 19% RCY of [carbonyl-^{11}C]amide was achieved. Further development of this approach may provide practical advantages over the corresponding photoinitiated process, since these reactions may be conducted simply in a 'windowless' miniature autoclave.

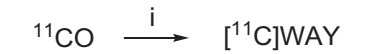

FIG. 10. One step preparation of [^{11}C]WAY from [^{11}C]carbon monoxide. Conditions: (i) WAY-100634 (2), base, c.hexyl iodide, hv, 5 min. Specific radioactivity: no carrier added.

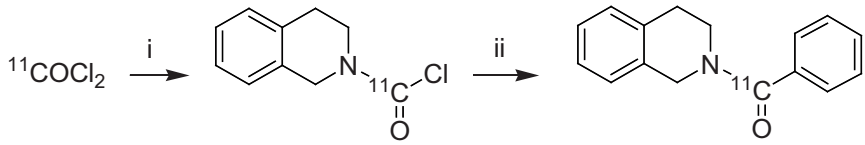

FIG. 11. Synthesis of a [carbonyl-^{11}C]amide via [^{11}C]phosgene and a [carbonyl-^{11}C]carbamoyl chloride. Sample conditions: (i) 2,4-dimethoxybenzyl-tetrahydroisoquinoline, dichloromethane, 20°C; (ii) $Ph_2CuMgBr.BrMgCN$, THF, -30°C, 5 min then sat. aq. NH_4Cl. Specific radioactivity: no carrier added.

6. LABELLING VIA [CARBONYL-^{11}C]CARBAMOYL CHLORIDES

[^{11}C]phosgene may be obtained by different methods from cyclotron produced ^{11}C. The most effective, especially with regard to achieving high specific radioactivity, is the conversion of cyclotron produced [^{11}C]methane into [^{11}C]carbon tetrachloride with subsequent oxidation [46]. Lemoucheux et al. [47] have shown that [^{11}C]carbamoyl chlorides can be formed efficiently (RCY = 76%) by reactions of tertiary amines with [^{11}C]phosgene and in one example (Fig. 11) that such a [^{11}C]carbamoyl chloride may be converted with high RCY (54%) into a [carbonyl-^{11}C]amide by treatment with an organometallic reagent (cyanocuprate, or a Grignard reagent in the presence of a nickel catalyst).

However, it is recognized that the two step catalyzed production of [^{11}C]phosgene requires a high level of skilled maintenance for reliability and hence this method is unlikely to supplant the simpler alternatives.

7. CONCLUSIONS

Several useful and alternative methods are now known for the versatile and efficient labelling of secondary and tertiary amides in their carbonyl functions with cyclotron produced ^{11}C and these are finding extensive application in the preparation of PET radioligands for 5-HT_{1A} receptors and other targets (e.g. opiate receptors [11, 17, 42], α_1-adrenoceptors [15], σ_1 receptors [42], CK receptors [42], PBR [47] and MAO [42]).

ACKNOWLEDGEMENTS

This work was supported by the Intramural Research Program of the National Institutes of Health (National Institute of Mental Health).

REFERENCES

[1] PIKE, V.W., Positron-emitting radioligands for studies in vivo — probes for human psychopharmacology, J. Psychopharmacology **7** (1993) 139–158.

[2] HALLDIN, C., GULYAS, B., LANGER, O., FARDE, L., Brain radioligands - state of the art and new trends, Q. J. Nucl. Med. **45** (2001) 139-152.

[3] SEDVALL, G., PET scanning as a tool in clinical psychopharmacology, Triangle **30** (1991) 11-20.

[4] FARDE, L., The advantage of using positron emission tomography in drug research, Trends Neurosci. **19** (1996) 211-214.

[5] BURNS, H.D., et al., Positron emisison tomography neuroreceptor imaging as a tool in drug discovery, research and development, Curr. Opinion Chem. Biol. **3** (1999) 388-394.

[6] OSMAN, S., et al., Characterization of the radioactive metabolites of the 5-HT_{1A} receptor radioligand, [*O-methyl*-^{11}C]WAY-100635, in monkey and human plasma by HPLC — comparison of the behaviour of an identified radioactive metabolite with parent radioligand in monkey using PET, Nucl. Med. Biol. **23** (1996) 627–634.

[7] OSMAN, S., et al., Characterisation of the appearance of radioactive metabolites in monkey and human plasma from the 5-HT_{1A} receptor radioligand, [*carbonyl*-^{11}C]WAY-100635 — explanation of high signal in PET and an aid to biomathematical modelling, Nucl. Med. Biol. **25** (1998) 215–223.

[8] PIKE, V.W., et al., Exquisite delineation of 5-HT_{1A} receptors in human brain with PET and [*carbonyl*-^{11}C]WAY-100635, Eur. J. Pharmacol. **301** (1996) R5–R7.

[9] PIKE, V.W., et al., First delineation of 5-HT_{1A} receptors in human brain with PET and [^{11}C]WAY-100635, Eur. J. Pharmacol. **283** (1995) R1–R3.

[10] QAIM, S.M., et al., PET radionuclide production, in Radiopharmaceuticals for Positron Emission Tomography, Stöcklin G., Pike V.W. (Eds), Kluwer Academic Publishers, the Nertherlands (1993) pp. 1-43.

[11] LUTHRA, S.K., PIKE, V.W., BRADY, F., The preparation of carbon-11 labelled diprenorphine: a new radioligand for the study of the opiate receptor system *in vivo*, J. Chem. Soc., Chem. Commun. (1985) 1423–1425.

[12] EHRIN, E., LUTHRA, S.K., CROUZEL, C., PIKE, V.W., Preparation of carbon-11 labeled prazosin, a potent and selective α1–adrenoceptor antagonist, J. Label. Compd. Radiopharm. 25 (1987) 177-183.

[13] PIKE, V.W., et al., Pre-clinical development of a radioligand for studies of central 5-HT_{1A} receptors *in vivo* — [^{11}C]WAY-100635, Med. Chem. Res. **5** (1995) 208–227.

[14] SCRIPKO, J.G., HUANG, C.C., KILBOURN, M.R., Synthesis of [carbonyl-11C]CI-99, a potent κ-opioid receptor agonist, J. Label. Compd. Radiopharm. 38 (1996) 141 (Abstract).

[15] MCCARRON, J.A., TURTON, D.R., PIKE, V.W., POOLE, K.G., Remotely-controlled production of the 5-HT_{1A} receptor radioligand, [*carbonyl*-^{11}C]WAY-100635, via ^{11}C-carboxylation of an immobilized Grignard reagent, J. Label. Compd. Radiopharm. **38** (1996) 941–953.

[16] TRUONG, P., KRASIKOVA, R.N., HALLDIN, C., A fully automated production of [carbonyl-11C]WAY-1000635 for clinical studies, J. Label Compd. Radiopharm. 46 (2003) S244 (Abstract).

[17] HWANG, D.R., SIMPSON, N.R., MONTOYA, J., MANN, J.J., LARUELLE, M., An improved one-pot procedure for the preparation of [^{11}C-*carbonyl*]-WAY100635. Nucl. Med. Biol. **26** (1999) 815-819.

[18] SHCHUKIN, E.V., KRASIKOVA, R.N., ANDERSSON, J., TRUONG, P., HALLDIN, C., A fully automated one-pot synthesis of [carbonyl-11C]WAY-100635: validation in routine PET studies, J. Label. Compd. Radiopharm. **48** (2005) S208 (Abstract).

[19] PIKE, V.W., European concerted action on "New radiotracers for quality assurance for nuclear medicine applications" Eur. J. Nucl. Med. **24** (1997) BP15–BP19.

[20] PIKE, V.W., et al., [*carbonyl*-^{11}C]Desmethyl-WAY-100635 (DWAY) is a potent and selective radioligand for central 5-HT_{1A} receptors *in vitro* and *in vivo*, Eur. J. Nucl. Med. **25** (1998) 338–346.

[21] ANDRÉE, B., et al., The PET radioligand [*carbonyl*-^{11}C]desmethyl-WAY-1000635 binds to 5-HT_{1A} receptors and provides a higher radioactive signal than [*carbonyl*-^{11}C]WAY-1000635 in the human brain, J. Nucl. Med. **43** (2002) 292-303.

[22] PIKE, V.W., et al., Radioligands for the study of brain 5-HT_{1A} receptors *in vivo* – development of some new analogues of WAY, Nucl. Med. Biol. (2000) **27**, 429–527.

[23] MCCARRON, J.A., et al., Two *C*-methyl derivatives of [^{11}C]WAY-100635 – effects of an amido α-methyl group on metabolism and brain 5-HT_{1A} receptor radioligand behavior in monkey, Mol. Imaging & Biol. **7** (2005) 209–219.

[24] MCCARRON, J.A., Development of radioligands for the study of brain 5-HT_{1A} and α_2-adrenoceptors with PET. PhD Thesis, University of London, U.K. (1998).

[25] SHIUE, C.Y., et al., *p*-[^{18}F]-MPPF: a potential radioligand for PET studies of 5-HT_{1A} receptors in humans, Synapse **25** (1997)147-154.

[26] AUBERT, C., HUARD-PERRIO, C., LASNE, M.-C., Rapid synthesis of aliphatic amides by reaction of carboxylic acids, Grignard reagent and amines: application to the preparation of [^{11}C]amides, J. Chem. Soc., Perkin Trans. 1 (1997) 2837-2842.

[27] LU, S.Y., HONG, J.S., PIKE, V.W., Synthesis of NCA [*carbonyl*-^{11}C]amides by direct reaction of in situ generated [^{11}C]carboxymagnesium halides with amines under microwave-enhanced conditions, J. Label. Compd. Radiopharm. **4**6 (2003) 1249–1259.

[28] LU, S.Y, et al., Alternative methods for labeling the 5-HT_{1A} receptor agonist, 1-[2-(4-fluorobenzoylamino)ethyl]-4-(7-methoxynaphthyl)piperazine (S14506), with carbon-11 or fluorine-18, J. Label. Compd. Radiopharm. **48** (2005), 971.

[29] WINSTEAD, M.B., LAMB, J.F., WINCHELL, H.S., Relationship of chemical structures to in vivo scintigraphic distribution patterns of ^{11}C-compounds. 1. ^{11}C-carboxylates, J. Nucl. Med. **14** (1973) 747-754.

[30] ROGERS, G.A., STONE-ELANDER, S., INGVAR, M., Rapid one-pot method for synthesizing substituted [^{11}C]amides, J. Label. Compd. Radiopharm. **25** (1994) 327 (Abstract).

[31] WELCH, M.J., TER-POGOSSIAN, M.M., The preparation of short-lived gases for medical studies, Radiat. Res. **36** (1968) 580–589.

[32] ZEISLER, S.K., NADER, M., THEOBALD, A., OBERDORFER, F., Conversion of no-carrier-added [^{11}C]carbon dioxide to [^{11}C]carbon monoxide on molybdenum for the synthesis of ^{11}C-labelled aromatic ketones, Appl. Radiat. Isot. **48** (1997) 1091-1095.

[33] LIDSTRÖM, P., KIHLBERG, T., LÅNGSTRÖM, B., [^{11}C]Carbon monoxide in the palladium-mediated synthesis of ^{11}C-labelled ketones, J. Chem. Soc. Perkin Trans. 1 (1997) 2701–2706.

[34] KIHLBERG, T., LÅNGSTRÖM, B., Method and apparatus for production and use of [^{11}C]carbon monoxide in labeling synthesis, PCT Int Appl. PCT/SE02/01222.

[35] HOSTETLER, E.D., BURNS, H.D., A remote-controlled high pressure reactor for radiotracer synthesis with [^{11}C]carbon monoxide, Nucl. Med. Biol. **29** (2002) 845-848.

[36] AUDRAIN, H., MARTARELLO, L., GEE, A., BENDER, D., A new method for trapping [^{11}C]carbon monoxide and its application for the synthesis of PET radiopharmaceuticals, J. Label. Compd. Radiopharm. **46** (2003) S77 (Abstract).

[37] AUDRAIN, H., MARTARELLO, L., GEE, A., BENDER, D., Utilisation of [^{11}C]-labelled boron carbonyl complexes in palladium carbonylation reaction, Chem. Commun. (2004) 558-559.

[38] KIHLBERG, T., LÅNGSTRÖM, B., Biologically active ^{11}C-labeled amides using palladium-mediated reactions with aryl halides and [^{11}C]carbon monoxide, J. Org. Chem. **64** (1999) 9201-9205.

[39] KARIMI, F., LÅNGSTRÖM, B., Synthesis of ^{11}C-amides using [^{11}C]carbon monoxide and in situ activated amines by palladium-mediated carboxaminations, Org. & Biomol. Chem. **1** (2003) 541-546.

[40] KARIMI, F., LÅNGSTRÖM, B., Synthesis of ^{11}C-labelled amides by palladium-mediated carboxamination using [^{11}C]carbon monoxide, in situ activated amines and 1,2,2,6,6-pentamethylpiperidine, Eur. J. Org. Chem. (2003) 2132-2137.

[41] RAHMAN, O., KIHLBERG, T., LÅNGSTRÖM, B., Aryl triflates and [^{11}C]/(^{13}C)carbon monoxide in the synthesis of ^{11}C-/^{13}C-amides, J. Org. Chem. **68** (2003) 3558-3562.

[42] RAHMAN, O., KIHLBERG, T., LÅNGSTRÖM, B., Synthesis of *N*-methyl-N-(1-methylpropyl)-1-(2-chlorophenyl)isoquinoline-3-[^{11}C]carboxamide ([^{11}C-carbonyl]PK11195) and some analogues using [^{11}C]carbon monoxide and 1-(2-chlorophenyl)isoquinolin-3-yl triflate, J. Chem. Soc., Perkin Trans 1 (2002) 2699-2703.

[43] ITSENKO, O., KIHLBERG, T., LÅNGSTRÖM, B., Photoinitiated carbonylation with [^{11}C]carbon monoxide using amines and alkyl iodides, J. Org. Chem. **69** (2004) 4356-4360.

[44] ITSENKO, O., KIHLBERG, T., BLOM, E., LÅNGSTRÖM, B., One step synthesis of [*carbonyl*-^{11}C]WAY-100635, J. Label. Compd. Radiopharm. **48** (2005) S135 (Abstract).

[45] ITSENKO, O., LÅNGSTRÖM, B., Labeling via free radical carbonylation using ^{11}CO. J. Label. Compd, Radiopharm. **48** (2005) S25 (Abstract).

[46] LANDAIS, P., CROUZEL, C., A new synthesis of of carbon-11 labeled phosgene, Appl. Radiat. Isot. **38** (1987) 297-300.

[47] LEMOUCHEUX, L., ROUDEN, J., IBAZIZENE, M., SOBRIO, F., LASNE, M.-C., Debenzylation of tertiary amines using phosgene or triphosgene: An efficient and rapid procedure for the preparation of carbamoyl chlorides and unsymmetrical ureas Application in carbon-11 chemistry, J. Org. Chem. **68** (2003) 7289-7297.

[^{18}F]FLUOROETHYLATED AND [^{11}C]METHYLATED PET TRACERS FOR RESEARCH AND ROUTINE DIAGNOSIS

M. MITTERHAUSER, W. WADSAK
Department for Nuclear Medicine, Medical University of Vienna, Vienna, Austria
Email: markus.mitterhauser@meduniwien.ac.at

Abstract

Development of new tracers for PET is a prerequisite for the success of this technique as a tool for routine diagnosis. Routine PET is mainly used for oncological, cardiological and neurological/psychiatric purposes. Two important characteristics of the radiotracers are specificity and selectivity, requiring strong focus on research in this field. Also necessary is a wide understanding of the mechanisms involved in the uptake process for the improvement of the status of existing radiotracers, with consideration given to saturation processes or whether there are enzymes or receptors involved as targets. Radiopharmacological aspects such as metabolic stability and the behaviour of these potential radioactive metabolites should also play a pivotal role in the design of the new radiotracers. Additionally, the feasibility of the preparation method should be considered for routine demands. There are few methods for the introduction of the ^{18}F into molecules, including electrophilic substitution, nucleophilic substitution and simple isotopic exchange. The preparations and formulations play a pivotal role in the selection of new radiotracers. Owing to the short half-lives of ^{18}F (~109 min) and ^{11}C (~20 min), only fast and reproducible methods can be used for these radiosyntheses. Additionally, the preparation method can significantly influence the stability of the radiotracer in vivo. The paper addresses aspects of the preparation and application of the newly developed radiopharmaceuticals and discusses differences and improvements, and also drawbacks to the routine tracers. Emphasis will be put on tracers for the dopamine transporter, for the GABA receptor, the serotonin receptor (5HT1A) and the μ-opioid receptor. Also, new attempts for the imaging of adrenocortical pathologies ([^{11}C]-MTO and [^{18}F]-FETO) will be discussed as examples for innovative oncological tracers.

1. HISTORICAL BACKGROUND

The history of radiopharmaceuticals is rather short, since radioactivity was not detected until the end of the 19th century. The first nuclear medical examinations of the thyroid were conducted in the 1940s and in 1958 the first clinical application of a positron emitting nuclide (i.e. ^{15}O) was described [1]. But only after considerable improvements in the instrumentation were

implemented did positron emission tomography (PET) become of interest as a diagnostic technique for use in the commuinity. Ido et al. presented the first synthesis of 2-[^{18}F]fluoro-2-deoxy-D-glucose (FDG) in 1978 [2] but it was the significant improvements made by Hamacher and Coenen at the research centre Juelich (Germany) [3] which led to the continued success of this compound. Even today, FDG is by far the most important PET radiopharmaceutical, accounting for approximately 90% of all clinical PET studies worldwide [4]. In recent years, more specific and selective tracers have been developed and labelled with different PET nuclides, which provides further insight into oncological, cardiological and neurological relationships.

2. PET NUCLIDES

Positron emitters can be found throughout the entire chart of nuclides but only few display suitable physical properties while being capable of being produced under simple conditions. The most important PET nuclides for clinical applications are summarized in Table 1. Fluorine-18 is the most widely used nuclide since it combines a relatively long half-life (109.7 min) with the possibility of production in a small, medical cyclotron.

3. LABELLING REACTIONS WITH ^{18}F

Figure 1 illustrates the labelling techniques possible with ^{18}F. Depending on the starting material, e.g. [^{18}F]fluoride or [^{18}F]F_2 gas, respectively,

TABLE 1. IMPORTANT PET NUCLIDES

Nuclide	Production	Half-life
F-18 (F^-)	^{18}O (p,n) ^{18}F	109.7 min
F-18 (F_2)	^{20}Ne (d,α) ^{18}F	109.7 min
C-11	^{14}N (p,α) ^{11}C	20.4 min
N-13	^{16}O (p,α) ^{13}N	10.0 min
O-15	^{14}N (d,n) ^{15}O	2.0 min
Cu-64	^{64}Ni (p,n) ^{64}Cu	12.7 h
Y-86	^{86}Sr (p,n) ^{86}Y	14.7 h
Br-76	^{76}Se (p,n) ^{76}Br	16.0 h
Ga-68	^{68}Ge/^{68}Ga generator	67.6 min

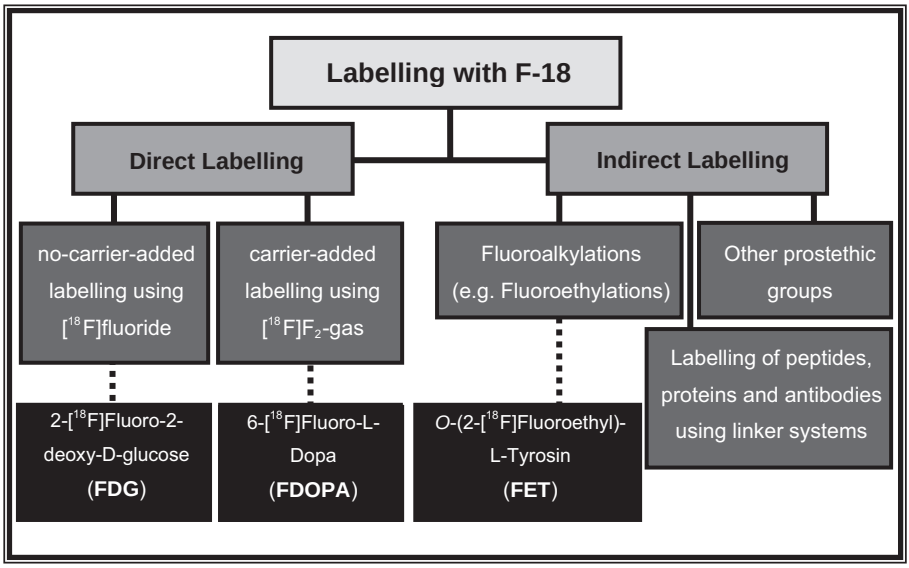

FIG. 1. Labelling with ^{18}F.

nucleophilic and electrophilic reactions are possible. Complementary to the direct radiofluorination reactions, fluorinated synthons can be produced which are subsequently bound to the target molecules. Fluoroalkylations – and especially fluoroethylations – represent the most important class for this indirect labelling technique. Important examples are given in the black boxes.

4. FLUORALKYLATIONS

Since many biologically active compounds contain alkylic side chains, e.g. methyl and ethyl groups, these structural units may be targets for the affixation of a radiolabel. In fact, many compounds have been labelled with a [^{11}C]methyl group for PET (vide infra). Thus, the development of [^{18}F]fluoroalkylated tracers was the logical consequence. A variety of different fluoroalkylating agents have been developed so far: [^{18}F]bromofluoromethane [5, 6], [^{18}F]fluoro-iodomethane [7], 2-[^{18}F]bromofluoroethane [8, 9], 2-[^{18}F]tosyloxyfluoroethane [10, 11], 3-[^{18}F]bromofluoropropane [12–14], 3-[^{18}F]fluoroiodopropane [14, 15]

and 3-[^{18}F]tosyloxyfluoropropane [16]. The thus labelled synthons are restricted to small alkyl chains to avoid too large a structural difference. The most important fluoroalkylated tracers, already introduced into clinical application, are [^{18}F]FET (O-(2-[^{18}F]fluorethyl)-l-tyrosin) [17] and [^{18}F]FP-CIT (2β-carbomethoxy-3β-(4-iodophenyl)-8-(3-[^{18}F]fluorpropyl)nortropan) [13, 18, 19].

5. FLUOROETHYLATIONS

Fluoroethylations represent the most important class amongst the fluoroalkylations since: (1) fluoroethylating agents can be easily produced from commercially available substances and (2) the fluoroethyl group is sterically close to methyl and ethyl groups. Targets for fluoroethylations are amine [20–25], hydroxylic [17, 26, 27], mercapto [28, 29] and carboxylic [30–35] moieties. 2-[^{18}F]tosyloxyfluoroethane is widely used since it is easy to prepare, very stable and suitable for a variety of compounds [36]. On the other hand, it is: (1) not as reactive as 2-[^{18}F]fluoroethyltriflate [37, 38]; (2) sensitive to some solvents and bases [37]; (3) not a selective agent [39]; and (4) complex to purify – a semi-preparative HPLC is unavoidable. Hence, microwave enhanced conditions were proposed that increased the selectivity and the radiochemical yields [40].

2-[^{18}F]bromofluoroethane can also be produced rapidly. Thus, a lot of effort was put into investigations to optimize the yields and quality of this intermediate compound by addition of sodium iodide and application of solid phase extraction for purification [38, 41, 42].

6. LABELLING REACTIONS WITH ^{11}C

Carbon-11 is commonly prepared as carbon dioxide in the cyclotron. Subsequently, this active precursor is converted into: (1) methyl iodide for methylations; (2) [^{11}C]HCN, [^{11}C]$COCl_2$ or [^{11}C]CHO for special applications; or (3) it is used directly for the synthesis of carbonyls or carboxyls via corresponding Grignard reactions. The major radiosynthetic pathways are illustrated in Fig. 2.

6.1. Methylations

[^{11}C]methyl iodide may be prepared from [^{11}C]carbon dioxide by reduction to [^{11}C]methanol and then treatment with a source of HI. The reduction is carried out either by catalytic hydrogenation or more often by

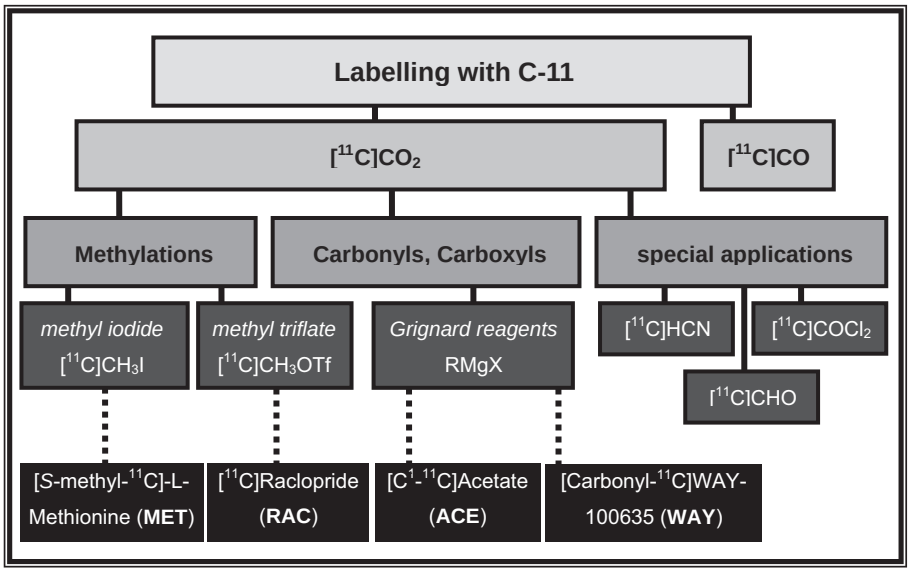

FIG. 2. Labelling with ^{11}C.

lithium aluminium hydride ($LiAlH_4$). As the carbon dioxide, methanol and methyl halide are all volatile, separation from non-volatile impurities is easily achieved by distillation or gas chromatography. [^{11}C]methyl iodide has also been prepared (60 ± 10% radiochemical yield) from [^{11}C]methane through substitution by iodine [43]. Larsen et al. [44] have reported the automated on-line preparation of [^{11}C]methyl iodide in 1.0 Ci quantities. [^{11}C]methane and iodine in helium were recirculated through a tube at 700–750°C, removing the iodomethane being formed. Methyl triflate has been introduced as an even faster methylating agent [45–47]. As mentioned earlier, radiolabelled methyl triflate is generally obtained by the reaction of methyl halide with silver triflate; for example, a gas stream containing [^{11}C]methyl iodide impinges upon silver triflate absorbed upon graphite at loadings as high as 50% at 170–200°C.

Recently, an excellent review on this topic was presented by Bolton [48]. In Table 2, an overview of the most commonly used [^{11}C]methylated PET radiopharmaceuticals is given. In the following section, a more detailed insight into four applications of the authors' fluoroethylation concept is given.

6.2. [^{18}F]FE@CIT

In the last decade, radiolabelled cocaine analogues based on ß-CIT have proven indispensable for the imaging of the dopamine transporter (DAT).

TABLE 2. IMPORTANT [^{11}C]METHYLATED PET RADIOPHARMACEUTICALS

Tracer	Abbreviation	Application	References
[*S*-methyl-^{11}C]-L-methionine	MET	Brain tumours	69, 70
[^{11}C]metomidate	MTO	11ß-hydroxylase (adrenal cortex)	58–60
[^{11}C]flumazenil	FMZ, Ro 15-1788	Central benzodiazepine receptors ($GABA_A$)	52–54
(R)-[*N*-methyl-^{11}C-]PK11195	PK11195	Peripheral benzodiazepine receptor	71, 72
[^{11}C]Patrick-Emond-substance 2I	PE2I	Dopamine transporter	73
[^{11}C]raclopride	RAC	D_2 receptor	74
[^{11}C]FLB 457	FLB 457	D_2 receptor	75, 76
[^{11}C]*N,N*-Dimethyl-2-(2-amino-4-cyanophenylthio)-benzylamine	DASB	Serotonin transporter	77, 78
[^{11}C]carfentanyl	CFN	μ-opioid receptor	63–65
[*N*-Methyl-^{11}C]-6-OH-BTA-1	PIB	ß-amyloid plaques (AD)	79

Alterations of the DAT can be associated with neurodegenerative and neuropsychiatric disorders, including Parkinson's disease, depression, attention deficit hyperactivity disorder, Huntington's chorea and schizophrenia. A multitude of cocaine analogues have been synthesized to date [9, 13, 30, 48–51]. Among these the so-called WIN compounds exhibit a 2–200-fold higher affinity for the DAT than cocaine. Some of these compounds have been labelled with ^{11}C or ^{18}F and were used for PET. However, further improvements in their pharmacodynamic and pharmacokinetic features are desirable. An important improvement, yielding in higher affinity to the DAT versus serotonin transporter (SERT) can be achieved by a simple replacement of the carboxylic methyl ester group in ß-CIT by a fluoroethyl ester [48, 49]. The preparation and ex vivo evaluation of this new ß-CIT-analogue – [^{18}F]FE@CIT – is discussed. Precursor and standard were prepared from ß-CIT and analysed by spectroscopic methods. Yields of precursor and standard preparation were 61% and 42%, respectively. [^{18}F]FE@CIT was prepared by distillation of [^{18}F]bromofluoroethane ([^{18}F]BFE) and reaction with (1R-2-exo-3-exo)8-methyl-3-(4-iodo-phenyl)-8-azabicyclo[3.2.1]octane-2-carboxylic

acid. After 10 min at 150°C, the product was purified using a C-18 SepPak. The radiosynthesis evinced radiochemical yields of >90% (based on [^{18}F]BFE), the specific radioactivity was >416 GBq/μmol. An average 30 μA·h cyclotron irradiation yielded more than 2.5 GBq [^{18}F]FE@CIT (Figs 3–5).

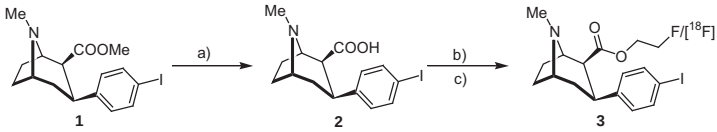

FIG. 3. A scheme for the synthesis of FE@CIT and [^{18}F]FE@CIT. Reagents and conditions: (a) 6N HCl, reflux; (b) standard synthesis: 2-fluoroethanol, DMAP, EDCI, dichloromethane; (c) radiosynthesis: TBAH, DMF, [^{18}F]BFE, 150°C.

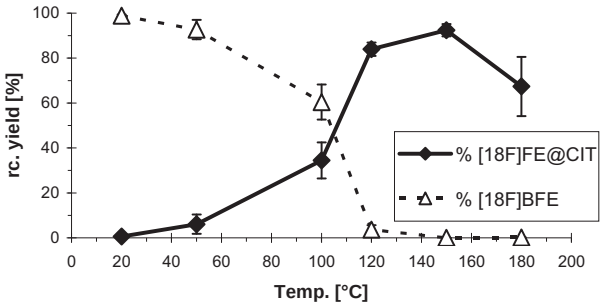

FIG. 4. Showing the dependence of the radiochemical yield of [^{18}F]FE@CIT and [^{18}F]BFE on reaction temperature (5mM, 20 min, means ± SD; n = 4; P = 0.95).

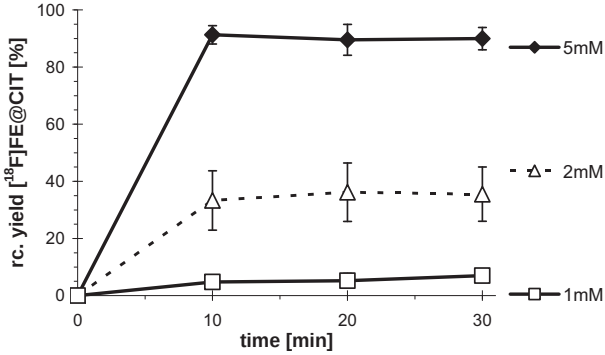

FIG. 5. Showing the dependence of the radiochemical yield of [^{18}F]FE@CIT on the amount of precursor (150°C; means ± SD; n = 4; P = 0.95).

For the ex vivo bioevaluation, 20 male Sprague-Dawley rats were sacrificed at 5, 15, 30, 60 and 120 min after infection. Organs were removed, weighed and counted. For autoradiographic experiments, transversal brain slices of about 100 µm were prepared. The ex vivo evaluation showed the highest brain uptake in striatal regions followed by the thalamus and cerebellum. The highest striatum to cerebellum ratio was 3.73 and the highest thalamus to cerebellum ratio was 1.65. Autoradiographic images showed good and differentiated uptake in striatal regions with a good target to background ratio (Fig. 6).

In conclusion, [^{18}F]FE@CIT was prepared via the well-established distillation method and followed the expected biodistribution routes. Precursor and standard syntheses were fast and simple with good yields. Optimum reaction conditions are 10 min at a temperature of 150°C with a precursor concentration of ≥5mM. Uptake in DAT rich regions was high with striatum to thalamus/hypothalamus ratios in the upper range of comparable DAT tracers. Ex vivo bioevaluation together with ex vivo autoradiographic findings support the further evaluation of [^{18}F]FE@CIT for DAT-PET.

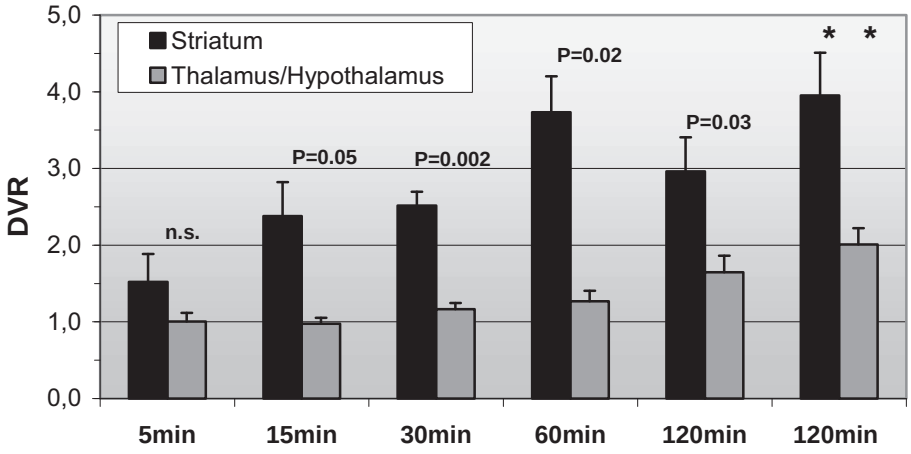

*FIG. 6. Showing distribution volume ratios (DVR) representing tissue to cerebellum ratios at various time points (%ID/g; means ± SD; n = 4; P = 0.95). The * denotes values for [^{123}I]FP-CIT for reasons of comparison. Statistical P-values are given for DVR (striatum) versus DVR (thalamus/hypothalamus) and were determined via t-test for comparison of two means from independent (unpaired) samples with α = 0.05.*

6.3. [^{18}F]FE@FMZ

Benzodiazepines are used as sedative, anxiolytic, hypnotic, anti-convulsant and muscle relaxant drugs. These drugs evolve their action via a special binding pocket on the central GABA receptor (CBR). Various diseases, such as epilepsy, Huntington's disease, Alzheimer's disease or schizophrenia can be caused by alterations of the CBR. Thus, imaging and quantification of CBRs with PET can be helpful for the diagnosis of neurological and psychiatric diseases. [^{11}C]flumazenil, a highly selective benzodiazepine antagonist is the most extensively used $GABA_A$ ligand for PET so far [52–54] (Fig. 7).

To overcome half-life disadvantages of ^{11}C, a [^{18}F] labelled flumazenil derivative, 2´-[^{18}F]fluoroflumazenil, was developed and biologically evaluated with respect to the $GABA_A$ receptor. In contrast to the presented analogue FEFMZ [21, 55, 56], FE@FMZ is radiolabelled at the original ethylester group and the radiosynthesis followed the distillation method. FE@FMZ was also presented by a group of Korean scientists, in a one pot reaction with direct [^{18}F] fluorination of the tosylated ethylester precursor [57].

The organ with the highest uptake was the pituitary gland. Brain uptake was high and followed the order cortex>thalamus>cerebellum>rest of brain. Fluoroflumazenil displaced [^{3}H]flumazenil binding from membrane $GABA_A$

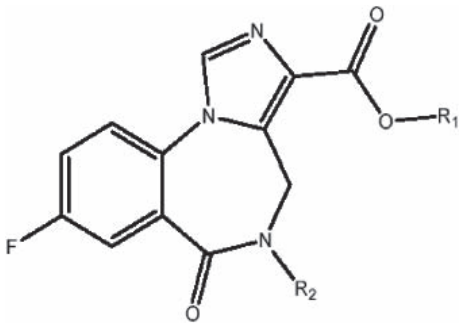

	R1	R2
FMZ	Ethyl-	Methyl-
FEFMZ	Ethyl-	2-Fluoroethyl
FE@FMZ	2-Fluoroethyl-	Methyl-
N-desmethyl FFMZ	2-Fluoroethyl-	H-
Precursor	H-	Methyl-

FIG. 7. Structures of various analogues of FMZ.

receptors with an IC_{50} value (3.5nM) comparable to that of flumazenil (2.8nM). The presented data confirm the potential of [^{18}F]FFMZ for PET imaging of the GABA-ergic system (Figs 8–10).

6.4. [^{18}F]FE@ETO

The proposed synthesis of [^{18}F]FE@ETO allows the production of sufficient amounts of this new PET tracer to serve 1–2 patients with an overall synthesis time below 80 min.

The 11β-hydroxylase (CYP11B1, $P450_{11\beta}$) plays an important role in the biosynthesis of cortisol and aldosterone and has been shown to be a good target for the in vivo imaging of adrenocortical incidentalomas in nuclear medicine. [^{11}C]metomidate (MTO), a potent inhibitor of this enzyme, is used for routine PET imaging of adrenocortical pathology [58–60]. [^{18}F]FE@ETO, (the [^{18}F]fluoroethyl ester of etomidate, (R)-1-(1-phenylethyl)-1H-imidazole-5-carboxylic acid, 2'-[^{18}F]fluoroethyl ester), an analogue of [^{11}C]MTO and [^{11}C]ETO, was chosen due to the suspected similarity of the pharmacokinetic and pharmacodynamic properties and was prepared in a two step procedure. In

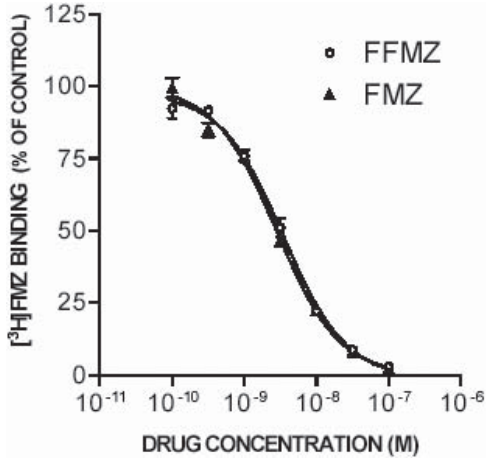

FIG. 8. Competitive binding curves: displacement of [^{3}H]FMZ binding by FFMZ and FMZ. Membranes of rat forebrains were incubated with 2nM [^{3}H]FMZ in the absence or presence of 100μM diazepam (to calculate the 100% control value) or various concentrations of drugs as indicated. Data were analysed by non-linear regression with a curve fitting computer software package (GraphPad Prism 3.0, San Diego; mean values ± SD from three different experiments each performed in triplicate).

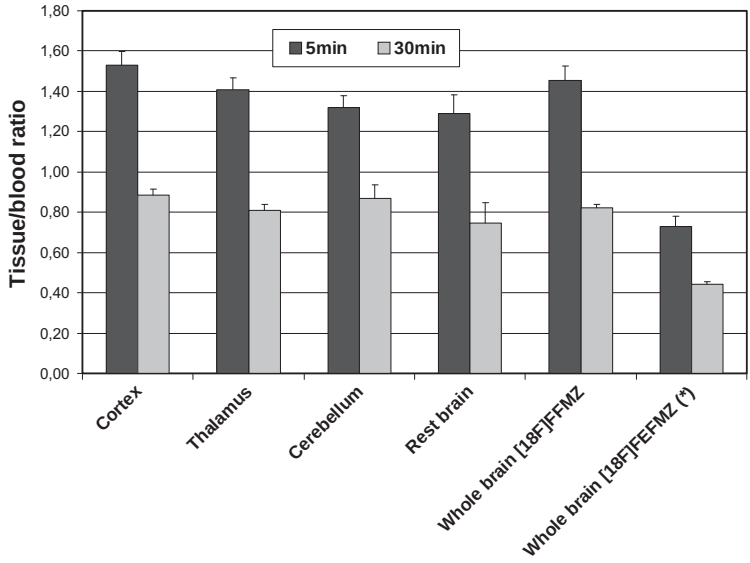

FIG. 9. Showing tissue to blood ratios of brain regions: cerebellum, cortex, thalamus, whole brain and rest of brain (data taken from Ref. [55]).*

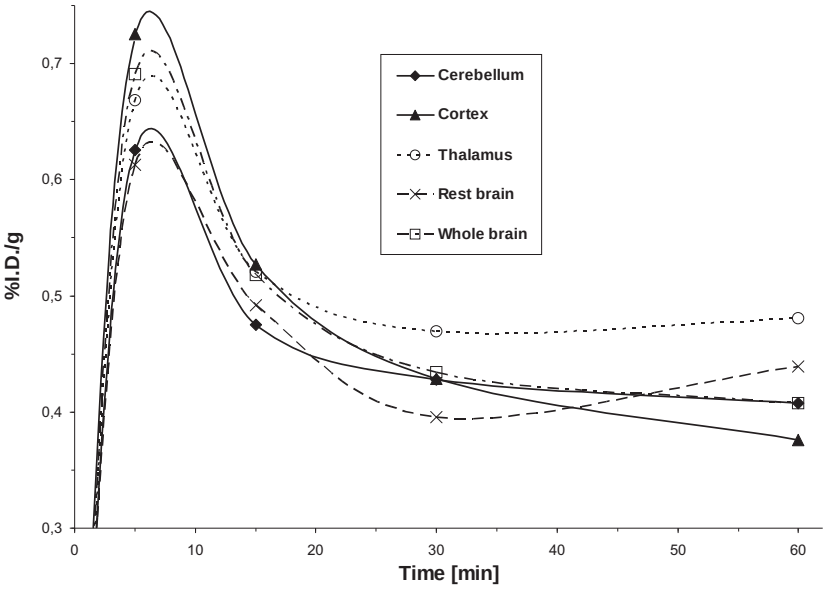

FIG. 10. Showing time–activity curves of FFMZ for various brain regions.

the first step, [^{18}F]fluoride was reacted with 2-bromoethyl triflate using the kryptofix/acetonitrile method to yield 2-bromo-[^{18}F]fluoroethane ([^{18}F]BFE) (Fig. 11). In the second step, [^{18}F]BFE was reacted with the tetrabutylammonium salt of (R)-1-(1-phenylethyl)-1H-imidazole-5-carboxylic acid to yield [^{18}F]FE@ETO, a novel inhibitor of the 11b-hydroxylase.

Male Sprague-Dawley rats were injected with 1.73–3.06 MBq of FE@ETO into a tail vein after venodilatation in a 40°C water bath. Eighteen rats were sacrificed by exsanguination from the abdominal aorta in deep ether anaesthesia after 10 (n = 6), 30 (n = 6) and 60 min (n = 6) and the organs removed, weighed and counted. For binding experiments, rat cerebellar membranes were incubated for 90 min at 4°C in TC-50 buffer, 150mM NaCl, and 2nM of [^{3}H]flunitrazepam in the absence or presence of 10μM diazepam or various concentrations of ETO, MTO and FE@ETO.

In vivo evaluation evinced very high uptake in the adrenal glands (7.52 ± 1.19% ID/g at 30 min), followed by lung (1.18 ± 0.19% ID/g, 10 min), liver (0.59 ± 0.13% ID/g, 10 min) and duodenum (0.7 ± 0.29% ID/g, 60 min) (Figs 12–14). No defluorination or fluoroethyl-ester cleavage was observed. As etomidate-analogues have been used as anesthetics for a long time and the way of action is explained GABA-ergic [61, 62], the authors in addition evaluated binding parameters on GABA receptors.

Brain regions have been compared and showed highest relative uptake in the cortex (2.34) followed by rest brain (2.13), cerebellum (1.96) and thalamus (1.0, reference value). FE@ETO and ETO were able to increase the binding of [^{3}H]flunitrazepam with similar potencies and to a comparable extent (Fig. 15).

FE@ETO shows characteristics suitable for the imaging of adrenocortical pathology with PET. Binding experiments on GABA receptors demonstrate a comparable effect of FE@ETO and ETO (Fig. 16). Hence, FE@ETO possibly

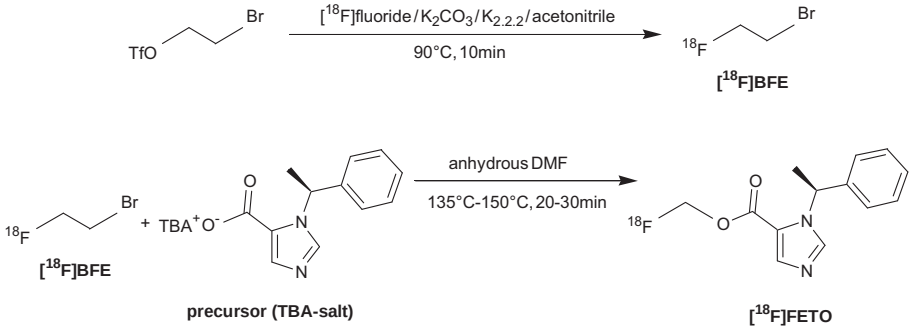

FIG. 11. The reaction scheme for the preparation of [^{18}F]FE@ETO.

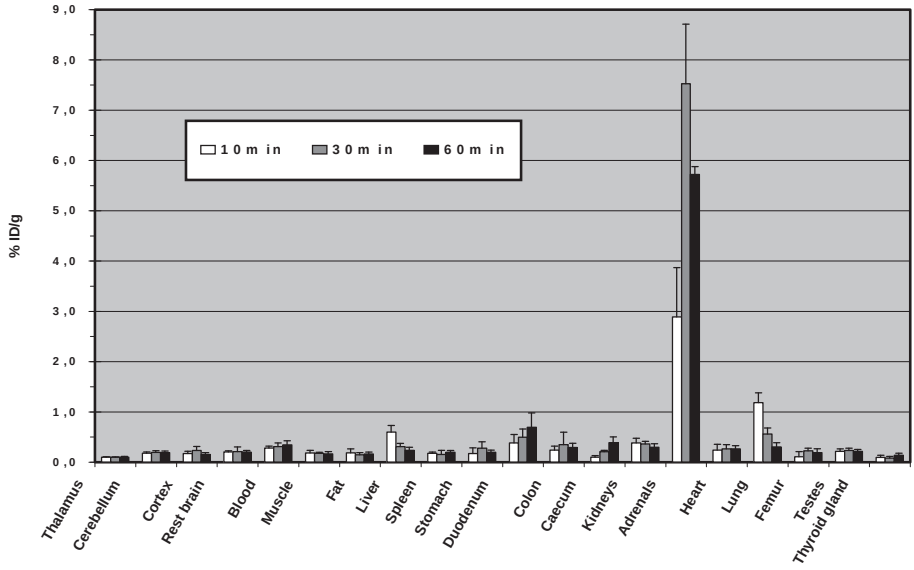

FIG. 12. The values counted in various organs at different time points after application of 1.73–3.06 MBq FE@ETO. Bars express values as per cent injected dose per gram organ (%ID/g).

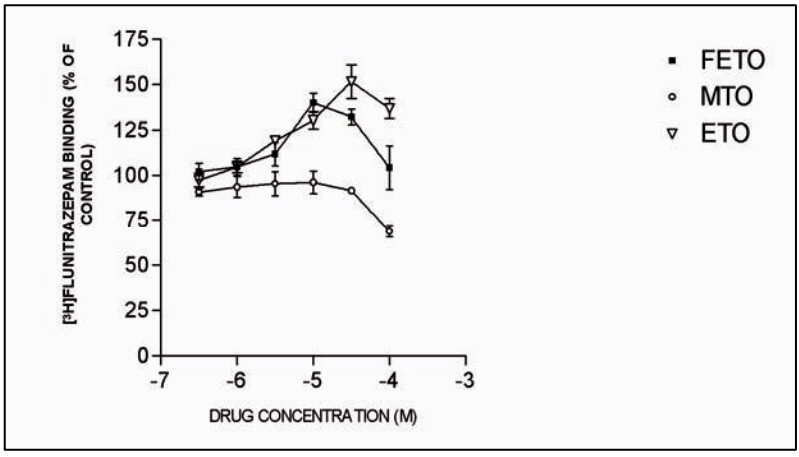

FIG. 13. Effects of ETO, MTO and FE@ETO on [^{3}H]flunitrazepam binding to membranes from rat cerebellum. Membranes were incubated with 2nM [^{3}H]flunitrazepam in the absence or presence of 10μM diazepam or various concentrations of drugs as indicated. Data represent mean values ± SD from three different experiments each performed in triplicate.

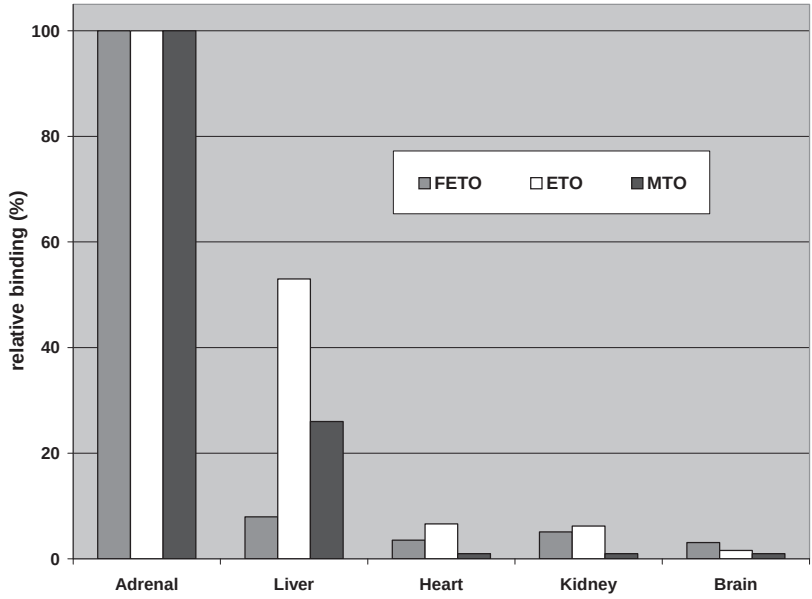

FIG. 14. Relative binding of FE@ETO, ETO and MTO to various rat tissues; normalized to adrenal binding (100%).

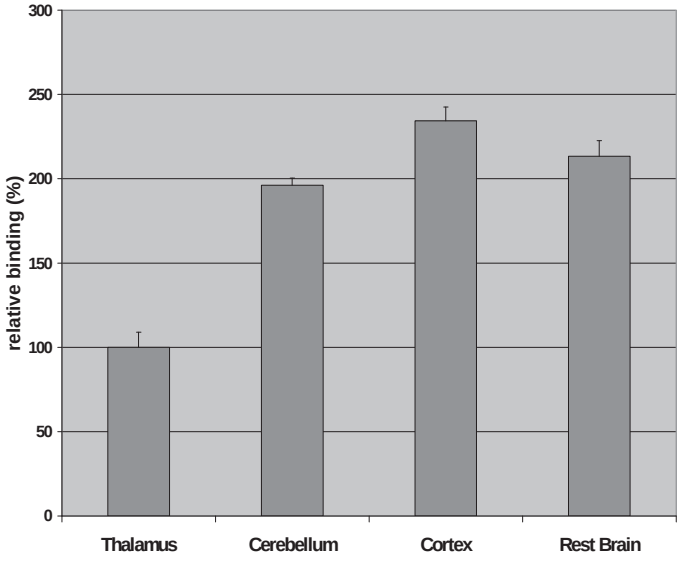

FIG. 15. Calculated ratios of brain regions: cerebellum, cortex and rest brain calculated as per cent of thalamic uptake.

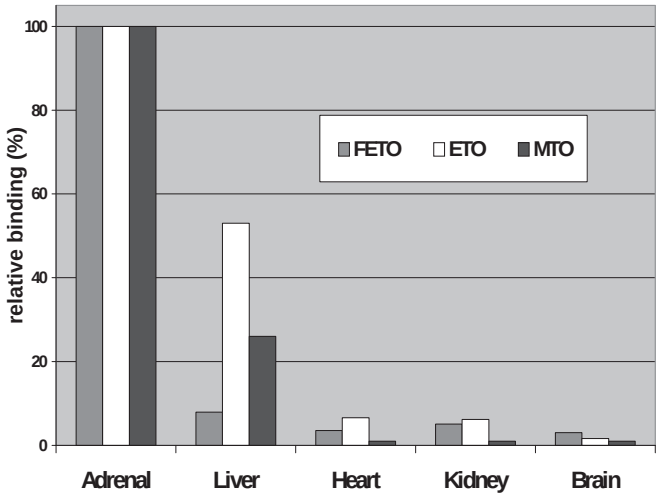

FIG. 16. Organs with the highest uptake. Ratios are expressed as %ID/g organ/blood at the time of highest uptake (lung, liver 10 min; adrenals 30 min; duodenum 60 min).

could also be used to elucidate the function, dynamics and kinetics of narcotic drugs with PET.

6.5. [^{18}F]FE@CFN

Activation of the μ-opioid receptor (μ-OR) by an agonist such as morphine causes analgesia, sedation, reduced blood pressure, itching, nausea, euphoria, decreased respiration, miosis and decreased bowel motility often even leading to constipation.

Although tolerance to respiratory depression develops relatively quickly, it is the single most adverse side effect of opioid use. In medicine, opioids are widely used as effective analgesics for severe pain (www.opioids.com). PET imaging of the μ-OR is still restricted to [^{11}C]carfentanil ([^{11}C]CFN, [63–65]) and used in areas of alcohol abuse and detoxification, therapeutic effectiveness in heroin addicts, pain activation or temporal lobe epilepsy.

Recent findings demonstrated that μ-OR imaging with PET could, beside its application in the human brain, also become a very useful tool in cardiology, providing a better insight into cardiovascular pathophysiology, especially in the ischemic heart and in arrhythmias. Furthermore, cardiovascular effects of drug abuse and chronic μ-OR stimulation could be evaluated and quantified [66–68]. Therefore, the authors' aim was the reliable radiosynthesis of a [^{18}F]fluorinated CFN derivative and its preliminary bioevaluation in rats. The [^{18}F]fluoroethyl

ester of carfentanil, [^{18}F]FE@CFN (2-[^{18}F]fluoroethyl 4-[N-(1-oxopropyl)-N-phenylamino]-1-(2-phenylethyl)-4-piperidinecarboxylate), and its corresponding inactive standard compound were prepared by fluoroethylation of desmethyl-CFN acid (4-[N-(1-oxopropyl)-N-phenylamino]-1-(2-phenylethyl)-piperidine-4-carboxylic acid) with 2-bromo-[$^{18/19}$F]fluoroethane in dimethylformamide (Figs 17 and 18).

Purification of [^{18}F]FE@CFN was achieved via solid phase extraction. Whole body biodistribution was investigated in rats and specific binding was measured autoradiographically in brain slices (Table 3).

[^{18}F]FE@CFN was prepared with excellent purity (>98%) and yields sufficient for routine PET imaging. In rats, considerable uptake was observed in ileum, lung, kidney and heart. Uptake in the rat brain peaked at 5 min (0.21% ID/g). On autoradiographic slices, the highest uptake was seen in the olfactory bulb and cerebral cortex whereas almost no uptake was observed in the cerebellum (Fig. 18).

7. CONCLUSION

The presented considerations are meant to be a basis for discussions on the value of newly developed methods. Originally, the presented method was established for the preparation of [^{18}F]FET. Since fluoroethylations become increasingly used in PET routine diagnosis and research, the method has to be

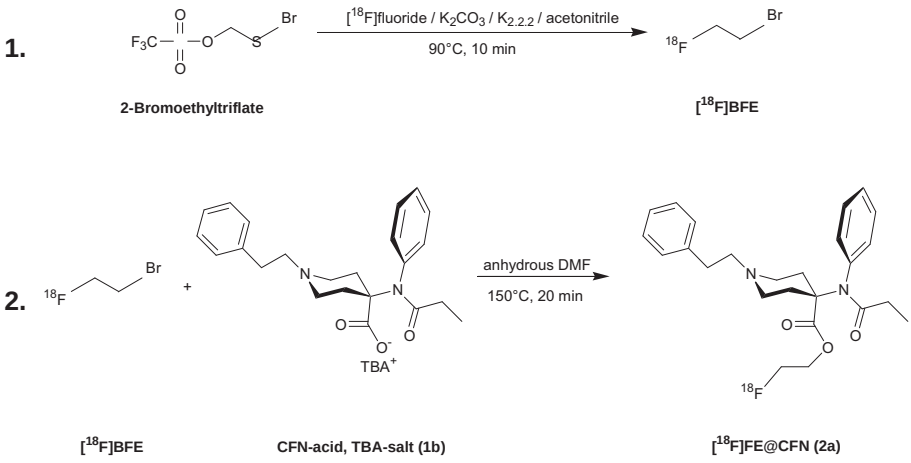

FIG. 17. The reaction scheme for the production of [^{18}F]FE@CFN.

TABLE 3. VALUES IN VARIOUS ORGANS AT DIFFERENT TIME POINTS AFTER ADMINISTRATION OF 0.5–1.5 MBq [^{18}F]FE@CFN AS PER CENT INJECTED DOSE PER GRAM ORGAN
(%ID/g; mean values ± SD; n = 5)

Tissue	5 min	15 min	30 min	60 min
Blood	0.30 ± 0.05	0.18 ± 0.03	0.17 ± 0.02	0.14 ± 0.02
Brain	0.21 ± 0.03	0.17 ± 0.06	0.11 ± 0.04	0.14 ± 0.10
Carcass	0.18 ± 0.05	0.21 ± 0.04	0.25 ± 0.03	0.25 ± 0.02
Colon	0.33 ± 0.10	0.26 ± 0.07	0.43 ± 0.12	0.37 ± 0.05
Fat	0.07 ± 0.04	0.28 ± 0.12	0.62 ± 0.19	0.60 ± 0.11
Femur	0.31 ± 0.03	0.28 ± 0.05	0.26 ± 0.02	0.26 ± 0.04
Heart	0.66 ± 0.06	0.37 ± 0.08	0.29 ± 0.04	0.19 ± 0.01
Ileum	0.95 ± 0.29	3.43 ± 0.50	3.16 ± 0.50	1.14 ± 0.20
Kidney	2.22 ± 0.51	1.10 ± 0.20	1.04 ± 0.07	0.61 ± 0.04
Liver	0.98 ± 0.34	1.71 ± 0.47	1.85 ± 0.18	1.72 ± 0.38
Lung	2.34 ± 0.43	0.96 ± 0.23	0.67 ± 0.07	0.39 ± 0.03
Muscle	0.27 ± 0.04	0.23 ± 0.04	0.16 ± 0.02	0.13 ± 0.01
Pituitary gland	2.40 ± 0.39	3.16 ± 0.70	3.15 ± 0.60	2.66 ± 1.10
Tail	0.46 ± 0.20	0.65 ± 0.15	0.44 ± 0.12	0.40 ± 0.13

integrated in the standard repertoire of radiopharmaceutical preparations. Table 2 was drawn up with special reference to tracers that may serve as templates for future fluoroethylations. As a matter of fact, the concept of a 'me too' generation of analogous radiotracers opens a new perspective for PET centres without on-site radiochemistry units. The derived fluoroethylated compounds normally provide comparable characteristics with respect to their kinetic and dynamic behaviour, but it always has to be taken into account that there is a significant chemical difference to the parent compounds. Therefore, even minor structural changes may cause significant changes in their in vivo behaviour. Some fluoroethyl esters are described as similar tools for PET imaging as compared to their methylated relatives, e.g. FE@ETO [31, 33], some others completely change the biological profile such as FE@FMZ [32, 34]. Nevertheless, the concept of fluoroethylations is a valuable tool for the rising demand of innovative radiotracers in satellite PET centres.

Since there are a variety of methods described for the preparation of fluoroethylated radiopharmaceuticals (vide supra), the method of choice for a

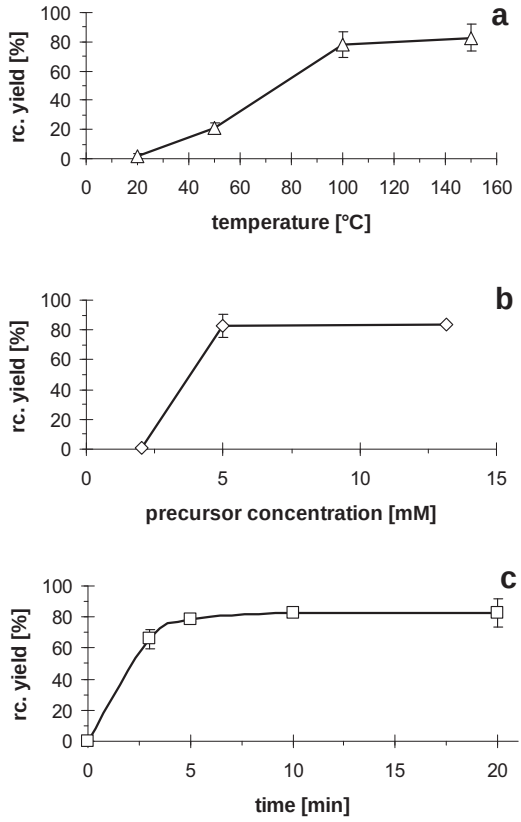

FIG. 18. The evaluated reaction conditions for the preparation of [^{18}F]FE@CFN.

specific synthetic demand has to be evaluated separately for each single case. For example, the addition of NaI has been reported to increase the radiolabelling yields [38, 80], but in the authors' experience with fluoroethylated esters, this effect is reversed (a significant reduction of the labelling yield was observed) [32].

In conclusion, fluoroethylations represent an important and valuable strategy to widen the list of available PET radiotracers without the necessity of synthesizing compounds 'from scratch'. A major drawback of the method is hidden in the fact that fluoroethylated compounds do not exist in nature and are rarely evaluated drugs. This fact demands de novo biomedical evaluations prior to their use for human PET applications in routine diagnosis. Fluoroethylation is a method with restrictions but once established it can serve as a valuable tool for the evaluation and development of new and innovative PET tracers.

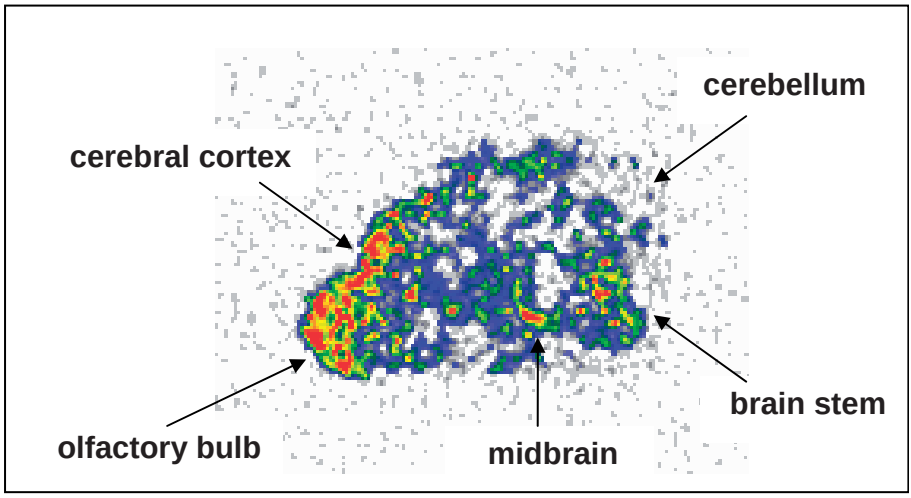

FIG. 19. Showing a typical rat mid-brain slice.

ACKNOWLEDGEMENTS

The authors are indebted to Profs Kletter and Dudczak, Drs Ettlinger, Lanzenberger and Mien, and all the staff at the PET centre Vienna. Parts of the presented work were supported by two research grants from the Austrian National Bank (Jubiläumsfonds der Österreichischen Nationalbank), project numbers 8263 (W. Wadsak) and 11439 (M. Mitterhauser).

REFERENCES

[1] TER-POGOSSIAN, M.M., POWERS, W.E., *Radioisotopes in Scientific Research,* Pergamon Press: London, 1958.
[2] IDO, T., et al., *J Label Compd Radiopharm* 1978; 14:175-184.
[3] HAMACHER, K., COENEN, H.H., STÖCKLIN, G., *J Nucl Med* 1986; 27: 235-238.
[4] ROWE, C., KEEFE, G.O., SCOTT, A.M., TOCHON-DANGUY, H.T., *Medicamundi* 2005; 49/1: 9-16.
[5] COENEN, H.H., COLOSIMO, M., SCHÜLLER, M., STÖCKLIN, G., *J Label Compd Radiopharm,* 1986; 23:587.
[6] BERGMAN, J., ESKOLA, O., LEHIKOINEN, P., SOLIN, O., *Appl Rad Isot,* 2001; 54: 927-933.
[7] ZHENG, L., BERRIDGE, M.S., *Appl Rad Isot.* 2000; 52: 55-61.

[8] ELSINGA, P.H., et al., *J Label Compd Radiopharm,* 2001; 44:S4.
[9] WILSON, A.A., DA SILVA, J.N., HOULE, S., *Nucl Med Biol*, 1996; 23: 487.
[10] BLOCK, D., COENEN, H.H., STÖCKLIN, G., *J Label Compd Radiopharm,* 1987; 24:1029-1042.
[11] SKADDAN, M.B., et al., *J Med Chem*, 2000; 43: 4552.
[12] OH, S.J., et al., *Appl Rad Isot* 1999; 51: 293.
[13] LUNDKVIST, C., HALLDIN, C., GINOVART, N., SWAHN, C.G., FARDE, L., *Nucl Med Biol*, 1997; 24: 621.
[14] CHESIS, P.L., WELSH, M.J., *Appl Rad Isot.* 1990; 41: 259-265.
[15] ZIJLSTRA, S., DE GROOT, T.J., KOK, L.P., VISSER, G.M., VAALBURG, W., *J Org Chem*, 2000; 43: 4552.
[16] DE GROOT, T.J., ELSINGA, P.H., VISSER, G.M., VAALBURG, W., *Appl Rad Isot* 1992; 43: 1335-1339.
[17] WESTER, H.J., HERZ, M., WEBER, W., HEISS, P., SENEKOWITSCH-SCHMIDTKE, R., *J Nucl Med*, 1999; 40: 205-212.
[18] CHALY, T., et al., *Nucl Med Biol*, 1996; 23: 999.
[19] KAZUMATA, K., et al., *J Nucl Med*, 1998; 39: 1521.
[20] GOODMAN, M.M., et al., *Nucl Med Biol* 2000; 27: 1-12.
[21] GRÜNDER, G., et al., *Eur J Nucl Med*, 2001; 28: 1463-1470.
[22] SATYAMURTHY, N., et al., *Appl Radiat Isot*, 1990; 41: 113-129.
[23] SATYAMURTHY, N., et al., *Nucl Med Biol (Int J Radiat Appl Intrum Part B)* 1986; 13: 617-624.
[24] CHI, D.Y., KILBOURN, M.R., KATZENELLENBOGEN, J.A., BRODACK, J.W., WELSH, M.J., *Int J Rad Appl Instr Part A* 1986; 37: 1173-1180.
[25] ZIJLSTRA, S., VISSER, G.M., KORF, J., VAALBURG, W., *Appl Radiat Isot*, 1993; 44: 651-658.
[26] WESTER, H.J., et al., *J Nucl Med* 2000; 41: 1279-1286.
[27] HAMACHER, K., COENEN, H.H., *Appl Radiat Isot* 2002; 57: 853-856.
[28] SUEHIRO, M., et al., *Nucl Med Biol* 1996; 23: 407-412.
[29] TANG, G., WANG, M., TANG, X., LUO, L., GAN, M., *Appl Radiat Isot*, 2003; 58: 219-225.
[30] WILSON, A.A., DA SILVA, J.N., HOULE, S., *Appl Radiat Isot*, 1993; 46: 765-770.
[31] WADSAK, W., MITTERHAUSER, M., *J Label Comp Radiopharm* 2003; 46: 379-388.
[32] WADSAK, W., et al., *J Label Compd Radiopharm* 2003; 46: 1229-1240.
[33] MITTERHAUSER, M., et al., *Eur J Nucl Med Mol Imaging* 2003; 30: 1398-1401.
[34] MITTERHAUSER, M., et al., *Nucl Med Biol* 2004; 31: 291-295.
[35] MITTERHAUSER, M., et al., *Synapse* 2005; 55: 73-79.
[36] CHIN, F.T., MUSACHIO, J.L., CAI, L., PIKE, V.W., *J Label Compd Radiopharm* 2003; 46: S172.
[37] SKADDAN, M.B., et al., *J Med Chem* 2000; 43: 4552-4562.
[38] ZHANG, M.R., FURUTSUKA, K., YOSHIDA, A., SUZUKI, K., *J Label Comp Radiopharm* 2003; 46: 587-598.

[39] SCHIRRMACHER, R., MATHIASCH, B., SCHIRRMACHER, E., RADNIC, D., RÖSCH, F., *J Label Compd Radiopharm* 2003; 46: 959-977.
[40] LU, S.Y., CHIN, F.T., MCCARRON, J.A., PIKE, V.W., *J Label Compd Radiopharm* 2004; 47: 289-297.
[41] COMAGIC, S., PIEL, M., SCHIRRMACHER, R., HÖHNEMANNT, S., RÖSCH, F., *Appl Radiat Isot*, 2002; 56: 847-851.
[42] ZHANG, M.R., et al., *Appl Radiat Isot*, 2002; 57: 335-342.
[43] SCHONBACHLER, R., AMETAMEY, S.M., SCHUBIGER, P.A., *J Label Cpd Radiopharm* 1999; 42: 447-456.
[44] LARSEN, P., ULIN, J., DAHLSTROM, K., JENSEN, M., *Appl Radiat Isot* 1997; 48: 153-157.
[45] VAN DORT, M.E., TLUCZEK, L., *J Label Cpd Radiopharm* 2000; 43(6): 603-612.
[46] SANDELL, J., et al., *J Label Cpd Radiopharm* 2000; 43(4): 331-338.
[47] STEEL, C.J., et al., *J Nucl Med* 1998; 39(5): 237p.
[48] GU, X.-H., ZONG, R., KULA, N.S., BALDESSARINI, R.J., NEUMEYER, J.L., *Bioorganic & Medicinal Chemistry Letters* 2001; 11:3049-3053.
[49] GÜNTHER, I., et al., *Nucl Med Biol* 1997; 24:629-634.
[50] KULA, N.S., et al., *Eur J Pharmacol.* 1999; 385:291-4.
[51] LAVALAYE, J., et al., *Eur J Nucl Med.* 2000; 27:346-349.
[52] NUTT, D.J., MALIZIA, A.L., *Br J Psychiatry* 2001; 179:390-6.
[53] DUNCAN, J., *Adv Neurol* 1999;79:893-9.
[54] MAZIERE, M., HANTRAYE, P., PRENANT, C., SASTRE, J., COMAR, D., *Int J Appl Radiat Isot* 1984 ; 35:973–976.
[55] LEVEQUE, P., LABAR, D., GALLEZ, B., *Nucl Med Biol* 2001; 28:809-14.
[56] MOERLEIN, S.M., PERLMUTTER, J.S., *Eur J Pharmacol* 1992; 218:109-15.
[57] YOON, Y.H., et al., *Nucl Med Biol.* 2003; 30:521-527.
[58] BERGSTRÖM, M., et al., *J Nucl Med* 2000; 41:275-282.
[59] BERGSTRÖM, M., et al., *J Nucl Med* 1998; 39:982-989.
[60] KHAN, T., et al., *Eur J Nucl Med* 2003;
[61] BELLELI, D., PISTIS, M., PETERS, J.A., LAMNERT, J.J., *Neurochemistry International* 1999; 34:447-452.
[62] MOODY, E.J., KNAUER, C.S., GRANJA, R., STRAKHOVAUA, M., SKOLNICK, P., *Toxicology Letters* 1998; **100-101**:209-215.
[63] FOWLER, C.J., FRASER, G.L., *Neurochemistry International* 1994; 24:401–426.
[64] FROST, J.J., et al., *Journal of Computer Assisted Tomography* 1985; 9:231-236.
[65] HEINZ, A., et al., *Arch Gen Psychiatry.* 2005; 62:57-64.
[66] VILLEMAGNE, P.S., DANNALS, R.F., RAVERT, H.T., FROST, J.J., *Eur J Nucl Med Mol Imaging* 2002; 29:1385-1388.
[67] KIENBAUM, P., et al., *Circulation* 2001; 103:850-855.
[68] KIENBAUM, P., HEUTER, T., SCHERBAUM, N., GASTPAR, M., PETERS, J., *J Cardiovasc Pharmacol.* 2002; 40:363-369.
[69] COMAR, D., CARTRON, J., MAZIERE, M., MARAZANO, C., *Eur. J. Nucl. Med.* 1976; 1:11-14.

[70] SCHMITZ, F., et al., *Appl. Radiat. Isot.* 1995;*46*:893-897.
[71] CAMSONNE, R., et al., *J Labelled Compd Radiopharm* 1984; 21:985-991.
[72] HASHIMOTO, K.I., INOUE, O., SUZUKI, K., YAMASAKI, T., KOJIMA, M., *Ann Nucl Med* 1989; 3:63-71.
[73] DOLLE, F., et al., *J Labelled Compd Radiopharm* 2000; 43:997-1004.
[74] FARDE, L., HALL, H., EHRIN, E., SEDVALL, G., *Science* 1986; 231: 258-261.
[75] HALLDIN, C., et al., *J Nucl Med* 1995;36:1275-81.
[76] HOGBERG, T., *Drug Des Discov* 1993; 9:333-50.
[77] HOULE, S., GINOVART, N., HUSSEY, D., MEYER, J.H., WILSON, A.A., *Eur J Nucl Med* 2000; 27:1719-22.
[78] WILSON, A.A., GINOVART, N., HUSSEY, D., MEYER, J., HOULE, S., *Nucl Med Biol* 2002; 29:509-15.
[79] KLUNK, W.E., et al., *Life Sci* 2001; 69:1471-84.
[80] HENRIKSEN, G., HERZ, M., SCHWAIGER, M., WESTER, H.-J., *J Label Compd Radiopharm* 2005; 48:771-779.

A NOVEL FINDING: ANTI-ANDROGEN FLUTAMIDE KILLS ANDROGEN INDEPENDENT PC-3 CELLS
A radiolabelled methyl-choline incorporation into tumour cells

F. AL-SAEEDI
Nuclear Medicine Department, Faculty of Medicine,
Kuwait University (Health Sciences Center),
Safat, Kuwait
Email: Fatimas@hsc.edu.kw

Abstract

[Methyl-^{11}C]-choline was introduced to image many types of cancer, especially prostate cancer. Al-Saeedi et al. reported that the incorporation of [Methyl-^{3}H]-choline into breast tumour (MCF-7) cells correlated strongly with proliferation as determined by [Methyl-^{14}C]-thymidine uptake. Also, Al-Saeedi et al. showed that the chemotherapy using MCF-7 cells treated with 5-Fluorouracil (5-FU) induced modulation in [Methyl-^{3}H]-choline incorporation and certain mechanisms for this modulation were reported. In this study, the androgen dependent prostate tumour (LNCaP) cells were treated with the well known pure anti-androgen drug, flutamide, for 3 d. The cells were then incubated with [Methyl-^{3}H]-choline for 10 min to detect the effect of flutamide on both cell proliferation and choline incorporation. At the same time, a preliminary work was established using androgen independent PC-3 cells treated with flutamide as controls in this study. PC-3 cells were treated with a range of doses of flutamide, inhibiting growth by 20–70%. Treated and control cells were incubated with [Methyl-^{3}H]-choline for 10 min, then in non-radioactive medium to simulate the rapid blood clearance of [Methyl-^{11}C]-choline tracer in control and treated PC-3 cells, and then extracted with organic and aqueous solvents to determine its effect on the intracellular distribution of this tracer. The results were interesting in that they showed that flutamide killed the androgen independent prostate cancer cells, PC-3, and the mechanisms responsible for flutamide induced modulation on [Methyl-^{3}H]-choline incorporation are reported. The PC-3 cell proliferation was inhibited by flutamide. In addition, treatment of PC-3 cells with flutamide for 3 d resulted in a buildup of cells in the S phase and [Methyl-^{3}H]-choline incorporation per a cell was found to be decreased in treated as opposed to untreated cells. In conclusion, flutamide inhibits PC-3 cell proliferation by a certain mechanism (unknown) other than the well-known androgen receptor mechanism, which accordingly induced modulation in [Methyl-^{3}H]-choline incorporation into the PC-3 cells.

1. INTRODUCTION

Many studies suggest that changes in the uptake of PET tracers [1–3] such as ^{18}F-2-fluoro-2-deoxy-D-glucose (^{18}F-FDG) and ^{18}F-fluorothymidine (^{18}F-FLT) after chemotherapy (4, 5), and radiotherapy (6, 7), compared with pretreatment uptake can reflect the efficacy of the drug and the tumour responses to chemotherapy treatment [8]. ^{18}F-FDG-PET has been widely used to investigate many types of cancer such as breast cancer and colorectal cancer after chemotherapy [9]. However, ^{18}F-FDG imaging was found to be limited in the detection of localized prostate cancer because of excessive excretion of the radionuclide into the urine, masking any lower pelvic region lesions [10]. The evaluation of the efficacy of the treatment of men with prostate cancer is mainly based on post-treatment levels of the prostate specific antigen. In addition, digital rectal examination and conventional imaging techniques are used but they are not sensitive enough to detect a local recurrence. [Methyl-^{11}C]-choline PET scan provides a sensitive metabolic and non-invasive imaging, which is not dependent on anatomical distortions. Recently, [Methyl-^{11}C]-choline was introduced to image prostate cancer [1], and in addition to evaluate the post-treatment of the localized prostate cancer [11]. Flutamide is often used as part of the initial treatment of prostate cancer. In this study, the questions of whether flutamide treatment inhibits cell proliferation and whether modulation of [Methyl-^{3}H]-choline incorporation is induced or not in PC-3 cells were investigated.

2. MATERIALS AND METHODS

2.1. Materials

2.1.1. Cell culture and media

The human prostate cancer cells (PC-3 cells) were obtained from the American Type Culture Collection (ATCC).

2.1.2. Radiolabelled compounds

[Methyl-^{3}H]-choline chloride (specific activity: 2.92 TBq/mmol) was obtained from Amersham Pharmacia Biotech UK Ltd (Buckinghamshire, United Kingdom).

2.1.3. Chemicals and reagents

All chemical reagents used were supplied by Sigma-Aldrich (UK) unless otherwise specified. Ultima Gold scintillant fluid was obtained from Meridian. Culture flasks and 96 well plates were obtained from Nunc (Denmark).

2.2. Methods

2.2.1. Cell culture and cell media

PC-3 drug sensitive/wild type cells were grown in Dulbecco's Modified Eagles medium (DMEM) supplemented with 20 U/mL penicillin, 20 μg/mL streptomycin and 10% foetal calf serum. All cells were cultured in monolayers in 25 cm^2 flasks in triplicate, incubated at 37°C (in 5% CO_2:95% air), and allowed to grow exponentially to 70% confluency.

2.2.2. Drug dose and choline incorporation

PC-3 cells were treated with flutamide drug added in concentrations of 0, 5 and 10nM in triplicate in 25 cm^2 flasks and incubated for 3 d.

2.2.3. Cell viability assays

Cell viability was assessed using both the MTT assay and the trypan blue exclusion methods. For MTT assay, cells were seeded in flat bottomed 96 well tissue culture plates at a concentration of 1×10^5 cells/mL medium in a volume of 200 μL per well and were allowed to grow to 70% confluency before adding drugs. The plates were set up for controls and different drug concentrations, then incubated in a humidified atmosphere with 5% CO_2:95% air at 37°C. After reaching 70% confluency, different concentrations of flutamide were added separately into triplicate plates of PC-3 cells and were incubated for 3 d, after which the medium was pipetted out and new medium was added in a final volume of 170 μL per well. Then, 30 μL of MTT (5 mg/mL in phosphate buffered saline (PBS)) was added to each well and incubation of the cells continued. After 4 h, the medium was carefully pipetted out, leaving the adherent cells and precipitate in the wells. A volume of 200 μL of DMSO was then added to each well with gentle mixing for 20 min to dissolve the precipitate and the appearance of crystals was checked under the microscope. Then plates were read in a 96 well plate scanner (ELISA plate reader) at dual filter wavelengths of 540 and 690 nm.

2.2.4. Trypan blue exclusion method

In another set of experiments, cells were grown to 70% confluency in 25 cm^2 flasks in triplicate, followed by addition of 0, 5 and 10nM flutamide to PC-3 cells for 3 d. Dilution was made just prior to counting to prevent viable cells from absorbing the stain and so appearing non-viable. Cells were harvested by trypsinization, neutralized with medium, and washed with PBS. Trypan blue was added to suspended cells at a concentration of 0.4% weight/volume (w/v) for 3–5 min. Live cell numbers were determined by counting with a haemocytometer and expressed as a percentage of their controls. These viability tests were used to determine the optimum treatment concentration and the 50% inhibitory concentration (IC_{50}) for flutamide drug to be used in the subsequent choline incorporation experiments. PC-3 cells were incubated in triplicate in 25 cm^2 flasks with 37 kBq/mL medium/flask [Methyl-^{3}H]-choline for 10 min at 37°C, then the pulse chase and efflux method and flow cytometry were carried out as described below.

2.2.5. [Methyl-^{3}H]-choline pulse chase and efflux

Cells were incubated in triplicate for 10 min at 37°C with 37 kBq [Methyl-^{3}H]-choline/mL of DMEM medium in 25 cm^2 flasks, washed 6 times with ice cold PBS, then incubated with non-radioactive DMEM medium for 10 min. The cells were washed once with ice cold PBS, trypsinized with 0.5 mL trypsin, neutralized with 0.5 mL medium and centrifuged at 10 000g for 5 min at 4°C. Activity in the media was counted using a liquid scintillation counting analyser (LSC-1900CA; Tri-CARB; Packard). Cell pellets were washed once with PBS to remove extracellular protein and the intracellular location of [Methyl-^{3}H]-choline determined by extraction with buffer and organic solvents.

2.2.6. Extraction of radiolabelled metabolites and lipids

Metabolites were extracted from cells using a chloroform/methanol Tris buffer solvent system [12]. Cells were pelleted in eppendorf tubes to which was added 1 mL of methanol and 0.5 mL of chloroform, which was then left at 4°C for 60 min, after which 0.5 mL chloroform was added to the suspension followed by 0.5 mL Tris buffer (10mM, pH7.0) with thorough mixing. After centrifugation at 1000g for 15 min at 4°C, the upper (aqueous) and lower (lipid) phases separated and a sample of each counted for radioactivity. Protein assay content was determined on the cell debris located at the interface of the two phases using standards prepared from a solution of 1.4 mg/mL BSA after solubilization with 1M NaOH and neutralization with HCl.

2.2.7. Flow cytometry

Cells harvested by trypsinization were washed twice in ice cold PBS then resuspended in 100 µL PBS. A volume of 1 mL of ice cold 70% ethanol was added to the cell suspension whilst vortexing and the cells left overnight at -20°C for flow cytometry. For flow cytometry analysis, cell number was adjusted to 1×10^6 cells/sample. A volume of 1 mL of PI/RNAse and triton x-100 staining buffer was added to the cells and the suspension incubated for 20 min, protected from light at room temperature. Flow cytometry was performed using a 488 nm laser on a FACSCalibur flow cytometer (Becton Dickinson) and CELLQuest software (Becton Dickinson) equipped for fluorescence detection, forward, 90° angle light scatter and doublet discrimination.

3. RESULTS

3.1. Cell viability assays

Figure 1 shows the treatment effect, viability and IC_{50} for flutamide on PC-3 cells using MTT (%MTT, n = 12) and trypan blue (%TB, n = 3) tests compared to controls. The IC_{50} for flutamide on PC-3 cells was 10nM. Therefore, PC-3 cells were treated with 10nM flutamide for 3 d in the subsequent experiments.

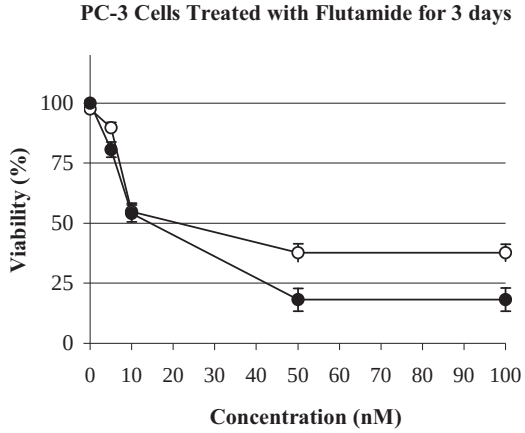

FIG. 1. The viability tests using MTT and trypan blue after 3 d exposure to flutamide of PC-3 cells. Cell viability is expressed as the mean ± SD of the values obtained from three independent experiments of TB (open circles) and from 12 replicates of MTT 96 well plates (closed circles).

3.2. Drug dose and choline incorporation

Figure 2 shows DNA histograms of PC-3 cells incubated with flutamide for 3 d. The IC_{50} for flutamide, 10nM, induced accumulation of DNA in the S phase of PC-3 cells.

[Methyl-^{3}H]-choline incorporation and DNA synthesis (S phase) in PC-3 cells treated with 0, 5 and 10nM flutamide for 3 d (Table 1) demonstrated that whilst treatment of PC-3 cells with flutamide showed a significant cell accumulation in the S phase compared to their controls, [Methyl-^{3}H]-choline uptake declined significantly ($P < 0.0001$) at 10nM concentrations compared with control levels.

4. DISCUSSION

[Methyl-^{11}C]-choline has been recently introduced as a novel tumour seeking PET tracer [1, 13], especially to image and stage prostate cancer [11, 14, 15]. This study demonstrates a decrease in cell viability, as well as an accumulation of cells in the S phase of the cell cycle after the treatment of PC-3 cells with flutamide. Here, some possible mechanisms of flutamide in relation to cell proliferation will be discussed.

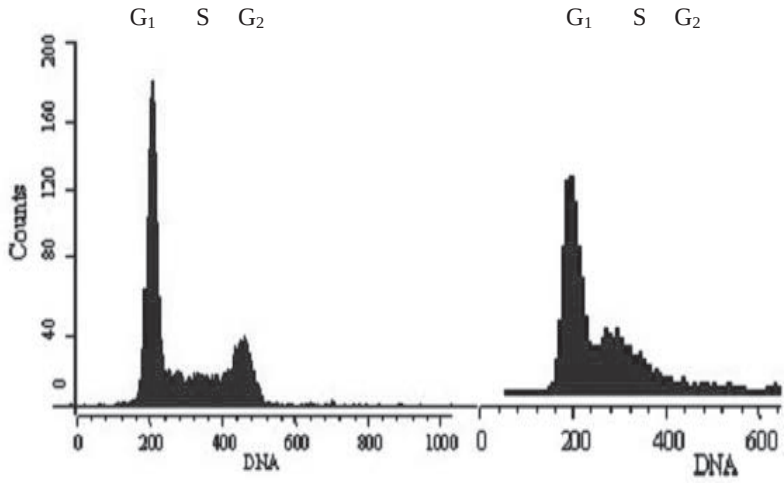

FIG. 2. DNA histograms of PC-3 cells alone (left) and when incubated with 10nM flutamide for 3 d (right).

TABLE 1. [METHYL-^{3}H]-CHOLINE INCORPORATION (n = 6) AND CORRESPONDING S PHASES (n = 3) OF PC-3 CELLS AFTER EXPOSURE TO 0, 5 AND 10nM FLUTAMIDE

*(the data are expressed as the mean dpm/μg protein ± SD (*P < 0.0001 compared with controls))*

Flutamide (nM)	Choline uptake	S phase
0	114.21 ± 0.57 (n = 6)	30.03 ± 0.58 (n = 3)
5	93.98 ± 0.97 (n = 6)	30.54 ± 0.30 (n = 3)
10	65.95 ± 0.72 (n = 6)*	61.81 ± 1.33 (n = 3)*

Prostatic cancer consists of cells that are sensitive to or dependent on hormones, androgen sensitive, such as the human prostate cancer LNCaP cell lines, and others that are hormone independent, androgen insensitive, PC-3 cells. The latter cells express low levels of androgen receptors. Accordingly, PC-3 cells do not respond to either androgens or anti-androgens and have been used extensively as a model for androgen independent and hormone non-responsive prostate cancer [16–19]. In this study, the effect of flutamide was investigated using PC-3 cells as controls. Control and treated cells were incubated with [Methyl-^{3}H]-choline incorporation for 10 min. Studying choline incorporation in PC-3 cells is useful particularly if condsideration is given to the fact that the onset of cancer progression results in the primary tumours being composed predominantly of androgen insensitive cells that are no longer affected by anti-androgens or androgen deprivation [20]. The preliminary study showed that PC-3 cells were killed by flutamide. Flutamide is a well-known anti-androgen drug. Its mechanism of action includes a competitive inhibitor of testosterone and dihydrotestosterone for the AR, interfering with the androgen action [21], and in the author's study its mechanism may involve other unknown mechanisms.

The present study demonstrates a novel finding that flutamide inhibits PC-3 cell proliferation, which was associated with a build-up of cells in the S phase and a dose dependent decrease of [Methyl-^{3}H]-choline incorporation. From the two viability tests (cytotoxic analysis), the IC_{50} for flutamide after 3 d in PC-3 cells was found to be 10nM. A reduction in choline uptake following therapy has been reported in several studies [5, 22]. DeGrado et al. [23] reported that fluorocholine PET uptake, which closely mimics choline uptake by normal tissues and prostate cancer was markedly reduced in patients rescanned during androgen deprivation therapy. Here, PC-3 cells plus flutamide suggests that flutamide acts by another mechanism other than the well-known one that prevents the interaction of testosterone and dihydrotestosterone with

the AR in the prostate. Inaloz et al. [24] have shown that the administration of flutamide in rats inhibits skin growth and proliferation in parallel with a decrease in the epidermal growth factor, a key hormone for skin development, and is known to stimulate cell proliferation and differentiation in a wide range of tissues. Flutamide may result in the inhibition of epidermal growth factor action in PC-3 cells, leading to the inhibition of the cells proliferation and their DNA synthesis, and result in the subsequent alteration to their cellular phospholipid metabolism, especially choline incorporation after the treatment with flutamide, and this is may involve the inhibition of phospholipase D activity.

Another possibility could be mediated through oestrogen receptors. For example, Kawashima et al. [25] reported that in PC-3 cells both the cell growth and the AR activity were remarkably inhibited by tamoxifen (TAM) at 50μM and flutamide at 5–50μM. They reported that anti-oestrogens modulate the transactivation activity of the AR in prostate cancer cells. Although the most prominent characteristic of prostate cancer is its androgen dependence, oestrogen seems to be involved. In the human prostate, ERα is localized in the stromal tissue of the prostate and associated with the progression, metastasis and the hormone refractory phenomenon of the prostate cancer [26, 27]. It was reported that both ERα and ERβ were expressed in PC-3 cells [28]. The activation of ERβ by its putative ligands 5α, androstane-3β and 17β-diol was reported to suppress the growth of the ventral prostate [29]. Activation of such a receptor may be involved in inhibition of cell proliferation and subsequently reduced choline incorporation in PC-3 cells treated with flutamide.

Flutamide may act through similar mechanisms to those involved in the inhibitory effect of TAM, the widely used anti-oestrogen therapy for breast cancer, which are unclear at present. Flutamide may act through caspase activation. Some studies reported that anti-oestrogen, raloxifen induces apoptosis in androgen independent prostate cancer cells through caspase activation [30] and TAM inhibits prostate cancer by inhibiting protein kinase C followed by the induction of p21(waf1/cip1) [31]. Kiss and Crilly [32] reported that in an ER deficient multidrug resistant subline of MCF-7 human breast carcinoma cells, clinically relevant concentrations of TAM inhibited the uptake and phosphorylation of choline and, as a result, the synthesis of corresponding phospholipids. Here, PC-3 cells treated with flutamide showed dose dependent reduced [Methyl-^{3}H]-choline uptake, reflecting a decrease in phospholipid synthesis. Moreover, flutamide can induce apoptosis in PC-3 cells through the formation of free radicals [33], which will inhibit the ability of cells to synthesize new DNA and ultimately reduce its choline uptake. In this study flutamide inhibited cell growth and proliferation as well as [Methyl-^{3}H]-choline incorporation in the AR negative PC-3 cells in vitro. Currently, the study is

extended to investigate many different concentrations of flutamide in both LNCaP cell lines and PC-3 cell lines. Moreover, since the in vitro system differs from the in vivo systems owing to the presence of non-tumour tissue, hypoxic regions, other androgenic, oestrogenic, or any other hormonal or anti-hormonal activities, and other factors, the extrapolation of these findings to the in vivo systems has to be carried out with caution.

REFERENCES

[1] HARA, T., KOSAKA, N., KISHI, H., PET imaging of prostate cancer using carbon-11-choline, J. Nucl. Med. 39(6) (1998) 990-5.

[2] AL-SAEEDI, F., WELCH, A.E., SMITH, T.A.D., [Methyl-^{3}H]-Choline Incorporation Into MCF-7 Tumour Cells: Correlation with Proliferation, Eur. J. Nucl. Med. Mol. Imaging (2005) (in press).

[3] AL-SAEEDI, F., WELCH, A.E., SMITH, T.A.D., Radiolabelled Methyl-Choline Incorporation Into Tumour Cells. Relationship with Proliferation and Chemotherapy-Induced Modulation. 12th European Symposium on Radiopharmacy and Radiopharmaceuticals ESRR'04. September 9-12, 2004 Gdansk/Poland.

[4] ALLAL, A.S., et al., Standardized uptake value of 2-[(18)F] fluoro-2-deoxy-D-glucose in predicting outcome in head and neck carcinomas treated by radiotherapy with or without chemotherapy, J. Clin. Oncol. 20(5) (2002)1398-404.

[5] LICHY, M.P., et al., Monitoring individual response to brain-tumour chemotherapy: proton MR spectroscopy in a patient with recurrent glioma after stereotactic radiotherapy, Neuroradiology 46(2) (2004)126-9.

[6] HIGASHI, K., CLAVO, A.C., WAHL, R.L., In vitro assessment of 2-fluoro-2-deoxy-D-glucose, L-methionine and thymidine as agents to monitor the early response of a human adenocarcinoma cell line to radiotherapy, J. Nucl. Med. 34(5) (1993) 773-9.

[7] KUBOTA, K., et al., Tracer feasibility for monitoring tumor radiotherapy: a quadruple tracer study with fluorine-18-fluorodeoxyglucose or fluorine-18-fluorodeoxyuridine, L-[methyl-14C]methionine, [6-3H]thymidine, and gallium-67, J. Nucl. Med. 32(11) (1991) 2118-23.

[8] HABERKORN, U., et al., Metabolic design of combination therapy: use of enhanced fluorodeoxyglucose uptake caused by chemotherapy, J. Nucl. Med. 33(11) (1992) 1981-7.

[9] KRAK, N.C., HOEKSTRA, O.S., LAMMERTSMA, A.A., Measuring response to chemotherapy in locally advanced breast cancer: methodological considerations, Eur. J. Nucl. Med. Mol. Imaging 31 (2004) Suppl 1:S103-11.

[10] LIU, I.J., ZAFAR, M.B., LAI, Y.H., SEGALL, G.M., TERRIS, M.K., Fluorodeoxyglucose positron emission tomography studies in diagnosis and staging of clinically organ-confined prostate cancer, Urology 57(1) (2001)108-11.

[11] DE JONG, I.J., PRUIM, J., ELSINGA, P.H., VAALBURG, W., MENSINK, H.J., 11C-choline positron emission tomography for the evaluation after treatment of localized prostate cancer, Eur Urol 44(1) (2003a) 32-8; discussion 38-9.
[12] BLIGH, E.G., DYER, W.J., A rapid method of total lipid extraction and purification, Can J Med Sci 37(8) (1959) 911-7.
[13] HOBSON, R.S., BEYNON, A.D., Preliminary quantitative microradiography study into the distribution of bone mineralization within the basal bone of the human edentulous mandible, Arch Oral Biol 42(7) (1997) 497-503.
[14] KOTZERKE, J., et al., Experience with carbon-11 choline positron emission tomography in prostate carcinoma, Eur. J. Nucl. Med. 27(9) (2000) 1415-9.
[15] ZHENG, Q.H., et al., [11C]Choline as a PET biomarker for assessment of prostate cancer tumor models, Bioorg Med Chem 12(11) (2004) 2887-93.
[16] KAIGHN, M.E., NARAYAN, K.S., OHNUKI, Y., LECHNER, J.F., JONES, L.W., Establishment and characterization of a human prostatic carcinoma cell line (PC-3), Invest Urol 17(1) (1979) 16-23.
[17] WARE, J.L., PAULSON, D.F., MICKEY, G.H., WEBB, K.S., Spontaneous metastasis of cells of the human prostate carcinoma cell line PC-3 in athymic nude mice, J Urol 128(5) (1982) 1064-7.
[18] KOZLOWSKI, J.M., et al., Metastatic behavior of human tumor cell lines grown in the nude mouse, Cancer Res 44(8) (1984) 3522-9.
[19] PIZZI, H., et al., Androgen regulation of parathyroid hormone-related peptide production in human prostate cancer cells, Endocrinology 144(3) (2003) 858-67.
[20] CATALONA, W.J., Management of cancer of the prostate, N Engl J Med 331(15) (1994) 996-1004.
[21] BRUFSKY, A., et al., Finasteride and flutamide as potency-sparing androgen-ablative therapy for advanced adenocarcinoma of the prostate, Urology 49(6) (1997) 913-20.
[22] FULHAM, M.J., et al., Mapping of brain tumor metabolites with proton MR spectroscopic imaging: clinical relevance, Radiology 185(3) (1992) 675-86.
[23] DeGRADO, T.R., et al., Synthesis and evaluation of 18F-labeled choline as an oncologic tracer for positron emission tomography: initial findings in prostate cancer, Cancer Res 61(1) (2000) 110-7.
[24] INALOZ, H.S., KETANI, M.A., INALOZ, S.S., YILMAZ, F., KETANI, S., The effects of sialoadenectomy & flutamide on skin development, Clin Exp Obstet Gynecol 27(3-4) (2000) 231-4.
[25] KAWASHIMA, H., et al., Effect of anti-estrogens on the androgen receptor activity and cell proliferation in prostate cancer cells, Urol Res. (2004).
[26] GRIFFITHS, K., Estrogens and prostatic disease. International Prostate Health Council Study Group, Prostate 45(2) (2000) 87-100.
[27] BONKHOFF, H., FIXEMER, T., HUNSICKER, I., REMBERGER, K., Estrogen receptor expression in prostate cancer and premalignant prostatic lesions, Am J Pathol 155(2) (1999)641-7.

[28] LAU, K.M., LaSPINA, M., LONG, J., HO, S.M., Expression of estrogen receptor (ER)-alpha and ER-beta in normal and malignant prostatic epithelial cells: regulation by methylation and involvement in growth regulation, Cancer Res 60(12): (2000) 3175-82.

[29] WEIHUA, Z., et al., A role for estrogen receptor beta in the regulation of growth of the ventral prostate, Proc Natl Acad Sci U S A 98(11) (2001) 6330-5.

[30] KIM, I.Y., et al., Raloxifene, a mixed estrogen agonist/antagonist, induces apoptosis in androgen-independent human prostate cancer cell lines, Cancer Res 62(18) (2002) 5365-9.

[31] ROHLFF, C., et al., Prostate cancer cell growth inhibition by tamoxifen is associated with inhibition of protein kinase C and induction of p21(waf1/cip1), Prostate 37(1) (1998) 51-9.

[32] KISS, Z., CRILLY, K.S., Tamoxifen inhibits uptake and metabolism of ethanolamine and choline in multidrug-resistant, but not in drug-sensitive, MCF-7 human breast carcinoma cells, FEBS Lett 360(2) (1995) 165-8.

[33] NUNEZ-VERGARA, L.J., FARIAS, D., BOLLO, S., SQUELLA, J.A., An electrochemical evidence of free radicals formation from flutamide and its reactivity with endo/xenobiotics of pharmacological relevance, Bioelectrochemistry 53(1) (2001) 103-10.

A SEMI-AUTOMATED [^{13}N]NH_3 PRODUCTION MODULE: DESIGN, QUALITY CONTROL AND OPTIMIZATION

A.R. JALILIAN*, P. ROWSHANFARZAD*, M. SABET**, M. MIRZAII*, A. ZIAEE***, D. SARDARI***

*Cyclotron and Nuclear Medicine Department
Email: ajalilian@nrcan.org

**SSDL and Health Physics Department

Nuclear Research Center for Agriculture and Medicine,
Atomic Energy Organization of Iran,
Karaj

***Science and Research Branch, Azad Islamic University,
Tehran

Islamic Republic of Iran

Abstract

The compound [^{13}N] NH_3 was prepared using a home-made, cost effective prototype module meeting pharmaceutical criteria. The $^{16}O(p,\alpha)^{13}N$ nuclear reaction was chosen as the best method of ^{13}N production. High purity natural water was bombarded by 18 MeV protons with a current intensity of 8 μA. A production yield of 13.5 $mCi \cdot \mu A^{-1} \cdot h^{-1}$ was obtained. Chemical modification of [^{13}N]nitrogen oxides into [^{13}N]NH_3 was accomplished using in-house made De Varda's catalyst. Chemical, radiochemical and radionuclide purity controls performed on the final product showed high radiopharmaceutical purity in the form of [^{13}N]NH_3 produced by a prototype production module. [^{13}N]NH_3 was formulated in normal saline media under appropriate pH and sterile conditions. Microbial and LAL tests were performed on the final product in order to assure its safety for administration to experimental subjects.

1. INTRODUCTION

Improvements in positron emission tomography (PET) have encouraged many research groups to prepare different radiopharmaceuticals following

administration to humans. $[^{13}N]NH_3$ is probably the only clinically used ^{13}N radiotracer (positron energy = 1.19 MeV, tissue range = 5.4 mm, half-life = 9.965 min). Its short half-life can be an advantage, allowing the possibility of performing repeated experiments on the same patient.

No matter what the target is, the chemical process should afford the reduced form of nitrogen atom, i.e. NH_3. The most abundant form of this radiotracer in the biological environment is NH_4^+ which can be used in the wall motion studies of the heart [1], local cardial perfusion [2], study of revascularization after heart transplants [3] and viability tests after myocardial infarction [4]. The authors have been interested in the domestic preparation and quality control of PET radiopharmaceuticals for ultimate use in clinics [5–7]. In this study, one of the simplest routes of production, i.e. irradiation of natural high purity water by protons, has been targeted as well as manufacturing of a prototype $[^{13}N]NH_3$ production module.

Regarding the irradiation of natural water for the production of $[^{13}N]NH_3$, there are some possible chemical reactions. In the first step, oxgen is turned into a nitrogen radical that can scavenge protons from water, producing peroxide. In the next step, the peroxides attack $[^{13}N]NH_3$ and finally nitroxides will be produced:

$$^{13}N + H\text{-}OH \rightarrow {}^{13}NH_3$$

$$^{13}NH_3 + HOH \rightarrow {}^{13}NH_4^+ + OH^-$$

$$^{13}NH_4^+ \ldots\ldots_{\rightarrow} {}^{13}NO_3^- + {}^{13}NO_2^-$$

Using anion retardation resins, the anions can be removed from the target solution. Therefore, by the addition of various radical scavengers such as ethanol or acetic acid, the $[^{13}N]NH_3$ compound will be the major product. The use of reducing agents such as De Varda's catalyst or Ti salts [8] may be the alternative.

2. EXPERIMENTAL

The chemicals were purchased from Aldrich Chemical Company, Germany. All chemicals were recrystallized repeatedly before use. Radio thin layer chromatography (RTLC) was run on polymer backed silica gel (F 1500/LS 254, 20 cm × 20 cm, TLC Ready Foils Schleicher & Schuell). A mixture of acetone–propionic acid–saturated brine (1:2:4) was used as eluent. The radiochromatogram scanner was coupled to a HPGe detector (Canberra germanium

detector; model GC1020-7500SL). The step motor was installed to count a 0.4 cm section each 30 s through the slot of a shielded chamber.

2.1. Preparation of De Varda's catalyst for routine production

Aluminium or copper turnings (50 g) were washed in a 2% solution of SDS (3 × 100 mL), followed by rinsing with double distilled H_2O (3 × 500 mL). The washed turnings were heated separately in a vacuum chamber at 200ºC for 2 h. The turnings were then dispersed in acetone (200 mL) and irradiated in an ultrasound water bath for 1 h and were finally washed by a mixture of acetone:water (1:1) in order to remove organic impurities (3 × 250 mL) and were dried at 200ºC for 4 h. A mixture of both of the above turnings and commercially available zinc powder (Al:Zn:Cu; 9:1:10) were mixed in a rotary motor under reduced pressure at 50–70ºC and the final mixture was dispensed in 5 g portions and to each was added 2 ± 0.1 g of NaOH. The portions were capped carefully under N_2 gas and kept for the production process. De Varda's catalyst containing vials were capped and autoclaved for routine use.

2.2. Production of carrier NH_3 in the production module

A solution of 1% KNO_3 (2 mL) was injected carefully into a De Varda's batch using a flow of He gas. The evolution of gases (NH_3, H_2O vapour) started rapidly after treatment due to the reduction of the NO_3^- anion to NH_3 exothermically. The vapour was finally trapped in a sterile normal saline vial (5 mL) and placed in an ice water bath. An outlet was placed over the last vial in order to control the pressure and this is connected to an exhaust equipped with a charcoal filter. The final solution was checked using colorimetric assay to detect the presence of the NH_4^+ cation using freshly prepared Nessler's reagent ($K_2[HgI_4]$). A concentration of about 1000 ± 10 ppm was produced in a single run starting from the carrier NO_3 anion.

2.3. Selection of the production parameters

In this research, $^{16}O(p,\alpha)^{13}N$ was selected as the best nuclear reaction for the production of ^{13}N, using natural water as the target material, owing to the small amount of produced ^{18}O resulting in ^{18}F, that could be easily separated by physical methods and also for cost effectiveness. Other metal impurities such as ^{51}Cr, ^{52}Mn, ^{55}Co, ^{56}Co, ^{57}Co,^{58}Co and ^{57}Ni radioisotopes were also produced as a result of proton irradiation of the windows and target body, but they could be easily removed in the radiochemical or physical separation process. The optimum proton beam energy was calculated and types of possible impurities

were predicted using previous experimental data given in the literature which showed that the maximum production yield can be achieved with the lowest level of radioactive impurities at 18 MeV proton energy.

2.4. Preparation of [^{13}N]-nitrate/nitrite anions

Nitroxy anions were prepared by 18 MeV proton bombardment of a double distilled H_2O sample (1.7 mL) prepared by passing a distilled sample through the ion retardation resins, followed by a reverse osmosis step that finally reached a maximum conductivity of 0.05 ± 0.001 μsiemens. The sample was irradiated for 15–20 min by 18 MeV protons in an all-silver target in a 30 MeV cyclotron at NRCAM. Cooling was performed using a pressurized flow of He gas.

2.5. Control of radionuclide purity

Gamma spectroscopy of the irradiated target before radiochemical processing was carried out by a HPGe detector coupled with a Canberra™ multichannel analyser. The peaks were observed and the area under the curve was counted for 1000 s. After the reduction and purification steps in the module, the final injectable solution was checked for radionuclide purity as shown in Fig 1.

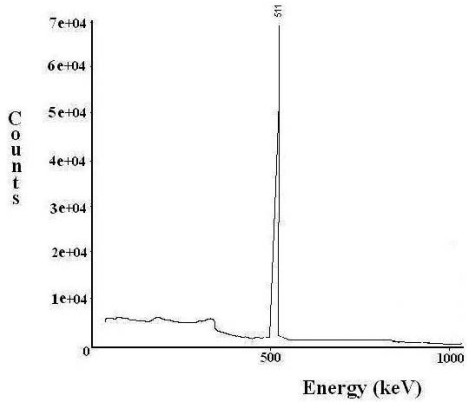

FIG. 1. Gamma spectroscopy of the final injectable solution.

2.6. Chemical purity control

The presence of zinc cation was checked by visible colorimetric assay. Even at 5 ppm of standard zinc concentration, the pinkish complex is visible to the naked eye, while the author's test sample remained similar to the blank. The amount of copper cation was checked in the final solution using colour formation of acidic dithizone reagent reacting with gold dilutions based on a previously reported colorimetric method.

2.7. Radiochemical purity of $[^{13}N]NH_3$

RTLC was performed using a mixture of acetone–propionic acid–saturated brine (1:2:4) as the mobile phase for both the target liquid and final solutions (Fig. 2). The radiochromatogram showed a major and distinct radiopeak at R_f = 0.80, using an in-house made radiochromatogram scanner coupled to a HPGe detector. The step motor was installed to count a 0.4 cm section each 30 s through the slot of a shielded chamber. The NO_3 and NO_2 anions were eluted at R_f = 0.45. The radiochemical yields (higher than 98% in each case, n = 9) were determined by the comparison of NO_3 and NO_2 anions with the major radiopeak at R_f = 0.80 for ^{13}N–NH_3.

TABLE 1. AMOUNTS OF CATION IMPURITIES CHECKED IN THE FINAL SAMPLE

Cation	Origin	Reagent	Present work (ppm)	USP (ppm)	EP (ppm)
Ag^+	Target body	Dithizone	3	3	5
Al^{3+}	De Varda	Dithizone	6	5	8
Zn^{2+}	De Varda	Dithizone	1.5	5	10
Cu^{2+}	De Varda	Dithizone	0.5	5	6
NH_4^+	Impurities	Nessler's	5	2	4
Ni^{2+}	Havar	Dimethylglyoxime	2	4	6
Fe^{2+}	Havar	Bi-pyridyl	5	5	5
Cr^{3+}	Havar	8-Hydroxy-quinoline	3	4	8
Co^{3+}	Havar	8-Hydroxy-quinoline	4	5	10

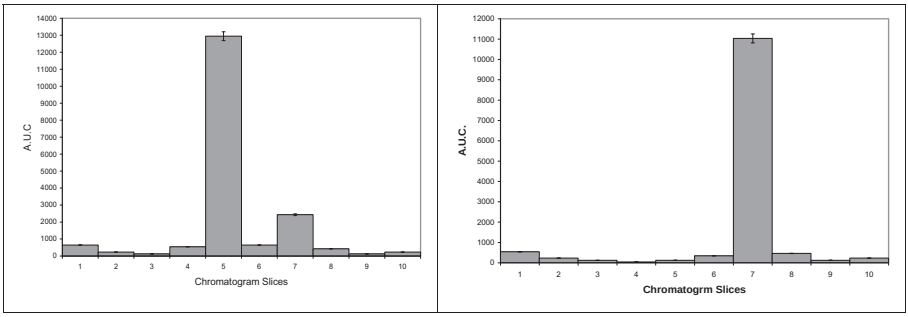

FIG. 2. RTLC of target solution in acetone–propionic acid–saturated brine (1:2:4) as the mobile phase for both the target liquid (left) and final solution (right).

2.8. Half-life measurement

In order to ensure the presence of ^{13}N in the final solution and the absence of other PET radionuclides, activity measurements were performed on radiopharmaceutical samples (3.2 ± 0.1 mCi) and the activities were plotted versus time (Fig. 3).

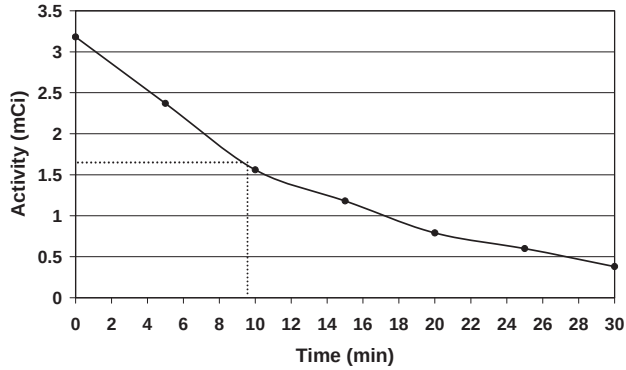

FIG. 3. Decay curve of the final NH_3 sample.

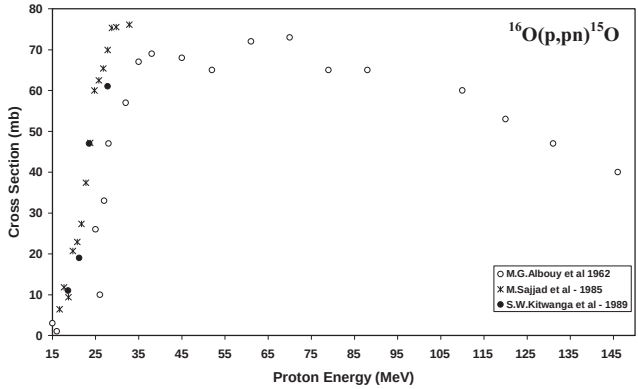

FIG. 4. Comparison of the experimental data for the $^{16}O(p,\alpha)^{13}N$ reaction.

3. RESULTS AND DISCUSSION

The experimental data given in the literature for the $^{16}O(p,\alpha)^{13}N$ nuclear reaction were compared in order to select the optimum proton beam energy (Fig. 4) [9]. It is clearly obvious that all the results with the exception of one report are in good agreement.

The best proton energy for this reaction is 18 MeV. At this energy, the $^{16}O(p,pn)^{15}O$ nuclear reaction which also takes place has been reported by many reseach groups [10–12] (Fig. 5). The probability of ^{15}O production is

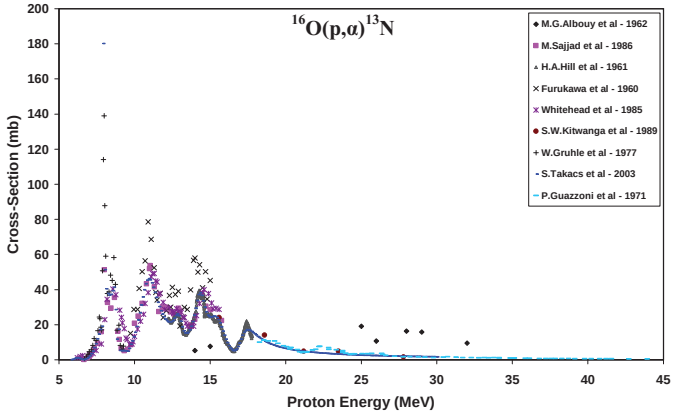

FIG. 5. Comparison of the experimental data for the $^{16}O(p,pn)^{15}O$ reaction.

higher at energies above 18 MeV. The SRIM nuclear code was used for target thickness determination [13].

$[^{13}N]NH_3$ was prepared by 18 MeV proton bombardment of the $^{nat}H_2O$ target. The target was bombarded with a current intensity of 8 μA for 20 min. The chemical separation process was based on a distillation method. The resulting activity of $[^{13}N]NH_3$ was 36 mCi at the end of bombardment and the production yield was 13.5 $mCi \cdot \mu A^{-1} \cdot h^{-1}$ (Fig. 6).

The production yield obtained in this study was comparable to other published data. The yield was calculated in the hot cell, at 10 m distance from the target room using a long PE hose that imposed a percentage of activity loss through the line. The ion exchange chromatography method proposed in some previous publications was rather time consuming. Radiochemical separation was performed by a one step reduction of nitroxy anions in a sealed disposable chamber containing in-house made De Varda's catalyst.

The reaction took place as soon as the target aqueous content was added to the catalyst chamber equipped with a small stirrer rod and in less than 40–60 s the maximum formation of NH_3 took place with a yield of more than 95%. Quality control of the product was performed in two steps. Radionuclide control

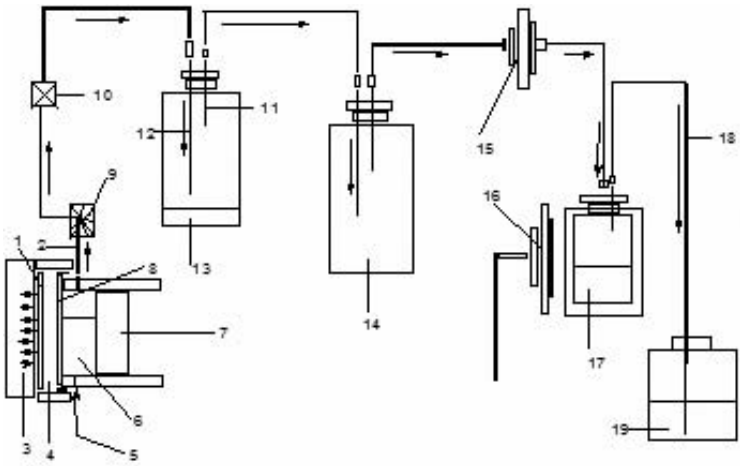

FIG. 6. $[^{13}N]NH_3$ production module details: (1) aluminium window, (2) target outlet, (3) proton beam, (4) cooling gas, (5) target inlet, (6) irradiated liquid, (7) silver body target, (8) Havar window, (9) 6-wedge valve, (10) module inlet valve, (11) catalytic reduction unit outlet, (12) catalytic reduction unit inlet, (13) De Varda's catalyst, (14) gas buffer chamber, (15) 0.22 μm microbial filter, (16) dose calibrator, (17) final sterile solution, (18) over pressure outlet, (19) excess ammonia chemical trap.

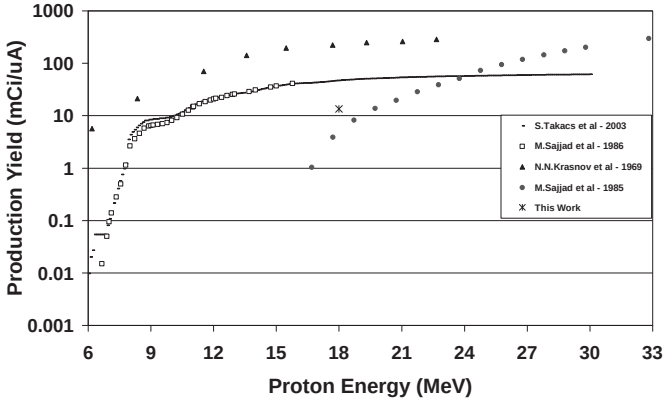

FIG. 7. Comparison of the literature data with the production yield in the present work.

showed the presence of 511 keV gamma energy, originating from ^{13}N, and purity was higher than 99%.

3.1. Chemical control

Owing to the exposure of target material's constituent metals, the possibilty of any chemical impurities must be considered. Since the target body contained the Havar window (mostly containing Fe, Co, Cr, Ni) and silver, the colorimetric assay for the detection of these elements was checked according to USP and EP limitations.

As a result of the use of De Varda's catalyst, the possibility of vaporization of the catalyst elements and contamination of the final solution must be taken into account. Finally, the amount of carrier ammonia in the final preparations due to the presence of nitrate salt impurities was checked using Nessler's test.

3.2. Radiochemical purity

Owing to the formation of nitrite/nitrate anions in the target liquid and consequent formation of ammonium ion after the reduction step, the amounts of each of these components was checked by RTLC before and after the reduction step. A mixture of acetone–propionic acid–saturated brine (1:2:4) was used as the eluent. The ammonium cation migrated to $R_f = 0.8$ while the anions stayed at a lower R_f of 0.45 [14].

3.3. Radionuclide purity

As a result of the interaction of protons with the target material (target body and windows), the possibilty of other nuclear reactions was also considered.

3.4. Rival nuclear reactions of natural water and proton beam

As a result of the use of a high purity natural water sample, the presence of ^{18}O nuclide in natural oxygen (0.038%) could lead to the formation of ^{18}F via the $^{18}O(p,n)^{18}F$ nuclear reaction. By selection of the best proton energy, this possiblity was minimized, but the possibilty of forming ^{18}F ionic forms in the target still remained. It was shown that if the De Varda alloy pretreatment were not performed properly, the presence of impurities in the starting materials, such as organic traces, etc., could produce amounts of volatile ^{18}F-fluorinated wastes that could be distilled from the reaction vessel and lead to the contamination of the final product. By carefully taking into account the probabilities in a normal run, the half-life determination of the final sample could be an important criterion for the presence of long half-life PET radionuclides such as ^{18}F that could not be identified by gamma spectroscopy. A half-life determination diagram is illustrated in Fig. 3.

3.5. Biological controls

The Pyrogen test was performed using a commercial LAL kit (sensitivity 0.125 EU/mL, Charles River Endosafe Co., United States of America). Microbial/fungal tests showed suitable pharmaceutical sterility.

4. CONCLUSION

The method used in this research for the production and chemical separation of $[^{13}N]NH_3$ was quite simple and cost effective, while previous studies given in the literature have reported a production yield similar to the author's work (Fig. 7). Total labelling and formulation of $[^{13}N]NH_3$ took about 2 min, with a yield of 98%. A significant specific activity (≈1200 Ci/mmol) was formed via production of $[^{13}N]$nitroxy anions. No unlabelled and/or labelled by-products were observed upon RTLC analysis of the final preparations by chemical determination tests. The radiopharmaceutical was usable in aqueous solution for at least 25 min and no significant amounts of other radioactive species were detected by RTLC. Trace amounts of other PET radionuclides

(≈1%) were detected by RTLC showing a radiochemical purity of higher than 99% for $[^{13}N]NH_3$. In contrast to other $[^{13}N]NH_3$ production methods, the authors' module represents an easy, rapid, cost effective and fully automated method meeting the suitable quality requirements for a radiopharmaceutical production system. Disposable units, hose lines and filters represent a GMP directed production module for ultimate use of this tracer in the country.

REFERENCES

[1] MASUDA, D., et al., Improvement of regional myocardial and coronary blood flow reserve in a patient treated with enhanced external counterpulsation: evaluation by nitrogen-13 ammonia PET. Jpn Circ J 1999 May; 63(5): 407-411.

[2] PHELPS, M.E., HOFFMAN, E.J., RAYBOUND, C., Factors with affect cerebral uptake and retention of N-13 NH3. Stroke 1977; 8: 694-702.

[3] KITSIOU, A.N., et al., 13N-ammonia myocardial blood flow and uptake: relation to functional outcome of asynergic regions after revascularization, J Am Coll Cardiol 1999 Mar; 33(3): 678-686.

[4] SAWADA, S., et al., Interobserver and interstudy variability of myocardial blood flow and flow-reserve measurements with nitrogen 13 ammonia-labeled positron emission tomography. J Nucl Cardiol 1995 Sep-Oct; 2(5): 413-422.

[5] JALILIAN, A.R., et al., Production Iranian Journal of Nulear Medicine, 12, 13-24, 1998.

[6] JALILIAN, A.R., J. Pharmacy & Pharmaceutical Sciences, 3(1) January-April, 2000. 114-124.

[7] JALILIAN, A.R., et al., Iranian Journal of Nulear Medicine, 21, 49-62, 2004.

[8] AKUTSU, Y., et al., Jpn Circ J 1997 Aug; 61(8): 665-672.

[9] SAJJAD, M., et al., Radiochimica Acta 1986; 39: 165-168.

[10] ALBOUY, M.G., et al., Spallation of oxygen by protons with 20 to 150 MeV, J Phys Lett 1962; 2:306.

[11] KITAWANGA, S.W., LeLEUX, P., LIPNIK, P., VANHORENBEECK, J., Production of N-13 radioactive nuclei from 13C(p,n) or 16O(p,α) reactions, J Phys Rev/C 1989 ; 40: 35.

[12] SAJJAD, M., LAMBRECHT, R.M., WOLF, A.P., Cyclotron isotopes and radiopharmaceuticals, Investigation of some excitation functions for the preparation of 15O, 13N, 11C, J Radiochimica Acta 1985; 38: 57.

[13] ZIEGLER, J., The code of SRIM- the Stopping and Range of Ions in Matter, Version 2000.XX, (2000).

[14] GATLEY, S.J., et al., Int J Rad Appl Instrum [A], 1991; 42(9): 793-796.

RADIOIODINE RADIOPHARMACEUTICALS

(Session 11)

Chairpersons

H.S. BALTER
Uruguay

G.-J. BEYER
Switzerland

PRODUCTION OF RADIOIODINES WITH MEDICAL PET CYCLOTRONS

J.J. ČOMOR*, G.-J. BEYER**, G. PIMENTEL-GONZALES***

*Laboratory of Physics, Vinča Institute of Nuclear Sciences, Belgrade, Serbia

**Division of Nuclear Medicine, University Hospital of Geneva, Geneva, Switzerland

***National Institute of Oncology & Radiobiology, Bedado, Havana, Cuba

Abstract

The authors discuss the possibility of producing radioiodine with mass numbers 120, 123 and 124 via proton reactions on enriched TeO_2 targets with medical PET cyclotrons under three aspects: yield and impurity considerations, technical feasibility and radiopharmaceutical chemistry. The thick target yield for the $^{XXX}TeO_2(p,n)^{XXX}I$ process is of the order of 2.5×10^9 atoms and relatively independent of the mass number. Consequently, the (p,n) process could be a suitable alternative to the well-known $^{124}Xe(p,x)$ method — large scale production technology for ^{123}I. Concerns regarding radionuclide impurities do not play a role any longer, because of availability of the target material with an enrichment close to 100% without increased costs. The standard medical PET cyclotrons and a standardized separation technique can be used for the production of all three isotopes: ^{120}I, ^{123}I and ^{124}I in high purity via the (p,n) reaction. A suitable target consists of a platinum disc carrying about 200–300 mg of TeO_2. A dedicated COmpact Solid Target Irradiation System (COSTIS) has been developed, which is now available commercially. Irradiation conditions are: 13–15 MeV protons, 20 $\mu A/cm^2$ beam intensity. Thus, 10 GBq or 1.5 GBq batches of ^{123}I or ^{124}I, respectively, are practically available using a PET cyclotron. The radioiodine is separated from irradiated TeO_2 targets using a thermochromatographic process. The TeO_2 targets cycled in this way can be reused immediately for the next production run without further treatment. A corresponding good manufacturing practice conform separation module has now been developed (TERIMO = TEllurium based RadioIodine production MOdule) and is available commercially. The losses of target material for one cycle is negligible (<0.2 mg/cycle). Local in-house production of radioiodine has the advantage of obtaining an iodinated radiopharmaceutical compound. Preliminary examples along this line will be presented. The technology described is identical for all three mentioned iodine isotopes with the mass numbers 120, 123 and 124.

1. INTRODUCTION

Positron emission tomography (PET) has become the technique of choice in modern nuclear medical diagnostics. The vast majority of PET diagnostic procedures are currently carried out by radiopharmaceuticals based on the radionuclide ^{18}F and to a much lesser extent by ^{11}C, ^{13}N and ^{15}O. The short half-lives of these radionuclides is limiting the applicability of PET to procedures that are based on tracer molecules with rapid biodistribution and metabolism. However, there are a number of alternative positron emitting radionuclides with significantly longer half-lives which might be used for PET provided that they are produced on-site as they are not yet widely available from commercial suppliers. Among them, the most promising radionuclides, which can be produced by a compact medical cyclotron delivering typically 13–20 MeV proton beams (i.e. by (p,n) nuclear reactions) are: ^{64}Cu, ^{76}Br, ^{86}Y, ^{94m}Tc, ^{120g}I, and ^{124}I [1].

According to current trends in radiopharmacy and nuclear medicine the positron emitting radionuclides ^{120g}I and ^{124}I are of utmost interest [2]. The long half-life of ^{124}I (4.18 d) allows for timely quantitative biodistribution and metabolic studies. It has been shown that PET with ^{124}I labelled tracers is particularly useful in oncology [3]. In addition to common functional visualization, quantitative PET imaging of ^{124}I tracer analogues of ^{131}I labelled therapeutic radiopharmaceuticals can be used for patient specific dosimetric calculations for ^{131}I radiotherapy planning. On the other hand, the ^{120g}I gained attention due to the similarity of its half-life to that of ^{18}F and its usefulness in quantifying the biodistribution of ^{123}I radiopharmaceuticals.

Taking into account the growing interest in the application of ^{120g}I and ^{124}I, every effort made to improve their production technologies is justified. Owing to the identical radiochemical behaviour of isotopes, the technologies developed for these two radioiodines are also suitable for the production of ^{123}I, an important radionuclide for single photon emission computed tomography (SPECT), which is still not widely used in the developing countries owing to logistical problems and its high price. The local production of ^{123}I in PET centres operating small medical cyclotrons could boost the application of this invaluable radionuclide in nuclear medicine.

Even though a number of papers have already been published discussing various aspects of radioiodine production paths by small medical cyclotrons [2, 5–21], there is no consensus yet as to what technology would be the most suitable, particularly if one considers the current good manufacturing practices (GMP) applicable to the production of radiopharmaceuticals. In the case of production of radioiodines, radiation safety is another significant issue, due to the high volatility of certain iodinated species. The paper presents a detailed

description of a GMP compliant technology for the production of ^{120g}I, ^{123}I and ^{124}I, based on a COmpact Solid Target Irradiation System (COSTIS) and on a TEllurium oxide based RadioIodine separation MOdule (TERIMO).

2. NUCLEAR REACTIONS SUITABLE FOR RADIOIODINE PRODUCTION

Taking into account the performances of common compact cyclotrons for medical radionuclide production (13–20 MeV protons and 6–10 MeV deuterons), the only suitable nuclear reactions for radioiodine production are the (p,n) reactions on enriched tellurium isotopes. Figure 1 shows the excitation functions of nuclear reactions leading to the three most important radioiodines. One can easily see that the cross-sections of all three reactions, and consequently their production rates (in terms of atoms per second and μA of beam current), are very similar, meaning that their production technology might be essentially the same concerning the irradiation conditions. The optimal conditions that would give the highest radionuclidic purity and still sufficiently high yields for all three radioiodines are indicated in Figs 1 and 2. It is important to note that most of the compact medical cyclotrons can provide proton beams of sufficient energy (14.9 MeV) for the optimal production of the radioiodines.

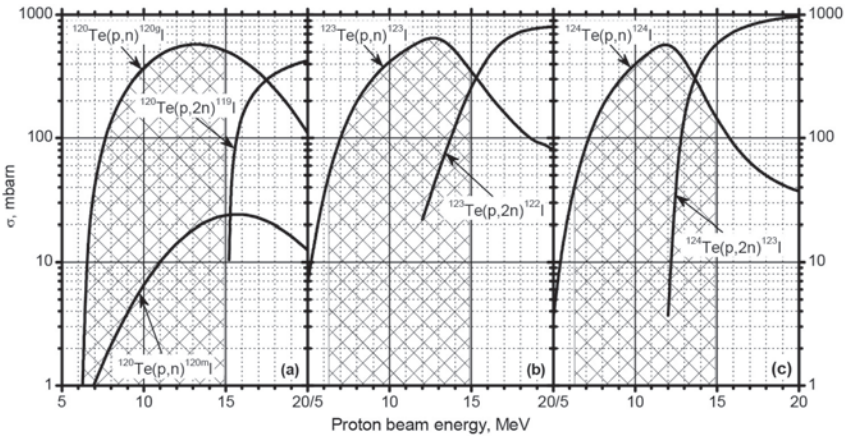

FIG. 1. Excitation functions of proton induced nuclear reactions on tellurium isotopes [14, 22]. The shaded regions represent the most suitable energy range for radioiodine production.

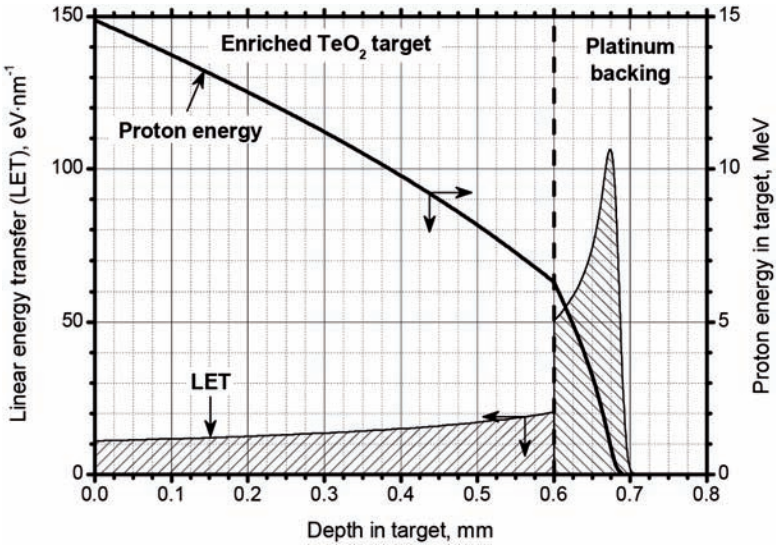

FIG. 2. Stopping of protons in the target disc used for radioiodine production. The thickness of the TeO_2 layer is 0.6 mm; after passing this layer the protons are stopped in the platinum backing.

The radionuclidic purity of radioiodines used for nuclear medical applications is an important aspect for the selection of the appropriate production technology. In general, pure γ emitting impurities do not significantly disturb the PET images (they slightly decrease the signal to noise ratio), provided that the energies of the most prominent lines are below 511 keV. However, in the case of ^{123}I, the other radioiodines increase the radiation dose received by the patient and the high energy γ lines decrease the resolution of the SPECT images.

The most critical radionuclidic impurities for ^{123}I are ^{124}I, ^{126}I and, surprisingly, ^{130}I. These impurities can be produced via (p,n) reactions from the ^{124}Te, ^{126}Te and ^{130}Te impurities in the enriched ^{123}Te target material. The levels of these target impurities were still relatively high in the 1980s. The composition of a typical, close to 70% enriched $^{123}TeO_2$ material and the obtained composition of an ^{123}I product after bombardment with 15 MeV protons is shown in Table 1 [10].

The ^{130}I contamination causes deterioration in the SPECT image due to the five intense and highly energetic gamma transitions of this radionuclide. Since its half-life is similar to that of ^{123}I, the ^{130}I content does not change with time, whereas those of ^{124}I and ^{126}I increase with time due to the decay of ^{123}I. Consequently, the most critical impurity in the target material is the ^{124}Te isotope as it is hard to separate from ^{123}Te. Thus, the absolute isotopic purity of

TABLE 1. COMPOSITION OF NATURAL TELLURIUM AND TYPICALLY ENRICHED $^{123}TeO_2$ IN THE 1980s AND THE COMPOSITION OF AN ^{123}I PREPARATION OBTAINED IN BOMBARDMENT WITH 15 MeV PROTONS
(data taken from Ref. [10])

Mass number	120	122	123	124	125	126	128	130
Natural abundance	0.096	2.60	0.908	4.816	7.14	18.95	31.69	33.80
Target material composition	0.01	2.3	67.3	11.7	3.9	5.7	5.0	4.1
Radionuclide composition			100	2.3	0.04	0.26		2.1

the enriched ^{123}Te is not the most important quality parameter of a target material; it is much more important to have a very small $^{124}Te/^{123}Te$ ratio [23]. Nowadays, the manufacturer of enriched isotopes can provide a ^{123}Te target material with a $^{124}Te/^{123}Te$ ratio of 6×10^{-4} [24]. With such a high purity target material and compact PET cyclotrons, it is possible to produce, via the (p,n) process, ^{123}I having all the quality parameters (radionuclidic purity as well as radionuclide concentration) comparable to the high purity ^{123}I product obtained in the well-known large scale $^{124}Xe(p,x)^{123}I$ production process. The (p,n) process, however, cannot compete with respect to the productivity.

The chemical form of the target material is another important factor for the design of the radioiodine production technology. In general, metallic targets are preferred due to their better heat conduction and mechanical stability. However, in the case of tellurium, targets in the form of TeO_2 are the most suited chemical form for two reasons: first, the vapour pressure of tellurium oxide is lower than that of metallic tellurium at the same temperature, thus less expensive target material is lost during irradiation and thermal processing; second, tellurium oxide targets might be reused immediately after thermochromatographic separation of the produced radioiodines, without troublesome wet chemical processing of the irradiated targets.

3. COST EFFECTIVE TECHNOLOGY FOR RADIOIODINE PRODUCTION WITH MEDICAL CYCLOTRONS

Even though compact medical cyclotrons can deliver rather high currents of proton beams (50–100 μA are common), the large scale production of radioiodines with them is not feasible as the beam power acceptance of the tellurium oxide targets is limited. Practical experiences have shown that a p-beam density

of 20 μA·cm^{-2} seems to be about the limit. If one distributes the p-beam over a larger area, aiming to increase the productivity, one creates the problem of inconvenience in the following separation process. Nonetheless, batches of the order of 3.7 GBq ^{124}I have already been obtained on a routine basis using the technology described in this paper. The investment needed for such a small scale production is reasonably low, i.e. the usage of sophisticated target stations and an automated rabbit target transport system is not really needed and not justified. However, the automation of the post-irradiation target processing is justified, as automation can provide reproducibility, repeatability and reliability required by current GMP for the production of radiopharmaceuticals.

3.1. Targetry

As a result of the specific requirements for local production of radioiodines by compact medical cyclotrons, a COmpact Solid Target Irradiation System (COSTIS) has recently been developed [18]. The target station has been designed in such a way that it can be connected to virtually any existing cyclotron using internal beams for irradiation. Using custom made flanges it can also be connected to any external beam line as well. The principal scheme of COSTIS is presented in Fig. 3, while Fig. 4 shows two typical installations on

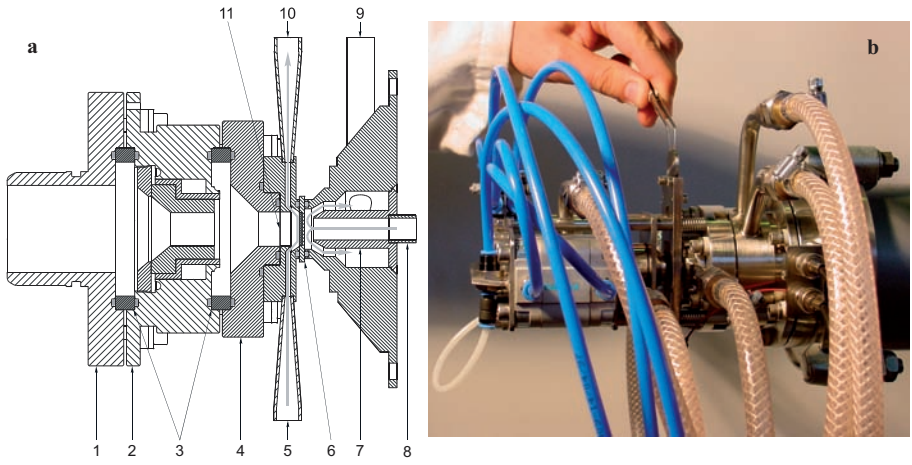

FIG. 3. (a) Simplified cross-sectional view of COSTIS: (1) quick connection flange; (2) water cooled collimator with graphite insert; (3) insulating alumina rings; (4) helium cooling cavity; (5) helium inlet; (6) platinum target disc with TeO_2 in its central groove; (7) water jet; (8) cooling water inlet; (9) cooling water outlet; (10) helium outlet; (11) window foil. (b) Loading of the target coin into COSTIS.

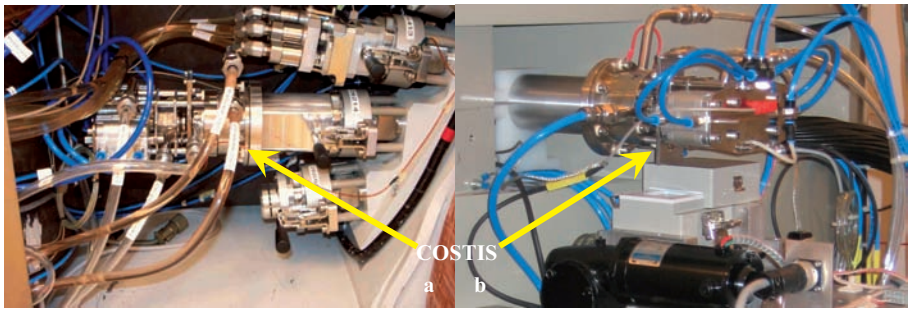

FIG. 4. COSTIS installed on a GE PETrace (a) and IBA Cyclone 18/9 (b) cyclotrons (courtesy of IBA Molecular Imaging).

common compact medical cyclotrons. The beam passes through a water cooled graphite collimator, which forms a circular beam 12 mm in diameter. The next element is a window foil separating the helium cooling loop from the vacuum. The helium stream in this loop cools the window foil as well as the front face of the target disc. Finally, a water jet cools the back face of the target disc.

The target is a 2 mm thick platinum disc, 24 mm in diameter with a circular groove, 12 mm in diameter, in its centre. This groove is filled with the target material, for instance with isotopically enriched TeO_2, which is melted into the groove. Platinum is selected as a metal with a sufficiently high thermal conductivity, which is also chemically inert and not heavily activated by the beam.

The target disc is loaded manually before the irradiation. It is locked in position by two pneumatic actuators during the irradiation. By reversing the action of these actuators, the irradiated target disc is released into a shielded transport container conveniently placed below COSTIS before the irradiation.

COSTIS has been designed as a compromise between high power metallic Te targets, which require troublesome post-irradiation radiochemical processing, and compact low power TeO_2 targets, which allow for easy separation of the produced radioiodine by thermal chromatography. After dry distillation of iodine from the melted oxide and cooling down of the target disc, it can be immediately reused for the next production cycle without any further preparation. This makes the production process simple and cost effective, even though the yields are limited by the beam power that such an oxide target may withstand, which is typically of the order of 350 W. Since January 2005, COSTIS is commercially available from IBA S.A., Louvain-la-Neuve, Belgium.

3.2. Thermochromatographic apparatus

The simplest way of releasing radioiodine from the irradiated TeO_2 targets is by thermochromatography, since after this process the targets can be immediately reused for a new production cycle [2]. Assuming that the diffusion process is the time determining step for the overall release of radioiodine from TeO_2 melts, the release kinetics of radioiodine may be described by the following relation [16]:

$$t_{1/2} = \frac{\ln \frac{\pi^2}{16}}{\pi^2 D} h^2$$

where $t_{1/2}$ is the release half-life, D is the diffusion coefficient and h is the thickness of the TeO_2 layer. However, if convection inside the liquid phase is the time determining step, one can use the following simple equation for describing the relation between fractional release (F) and the release time (t) [16]:

$$F(t) = e^{-\mu_1 t}$$

where the empirical factor μ_1 describes the desorption process from the surface. The radioiodine release kinetics from TeO_2 targets have been extensively studied [16] and it became evident that the release rate is proportional to the target thickness to diameter ratio, provided that circular targets are employed. From the dependence of the release half-time on this ratio one can easily determine that the release half-time for targets designed to be irradiated on COSTIS is 26.3 s (see Fig. 5); thus 97% of the produced radioiodine will be released within just 2 min. This is of utmost importance, as the vapour pressure of molten TeO_2 is not negligible, thus the faster the radioiodine release is, the shorter the time the target has to be kept in a molten state and the lower the losses of expensive enriched target material. The loss of target material during the thermochromatographic process has to be taken into account as a potential source of contamination of the final product as well.

The apparatus for thermochromatographic separation of radioiodine from the irradiated TeO_2 is shown schematically in Fig. 6. It has a quartz target holder for positioning of the target discs, a fast electric heater, a thermocouple for temperature measurements, an alumina trap for adsorbing tellurium oxide vapours and a quartz bulb containing the trapping solution. The iodine vapours

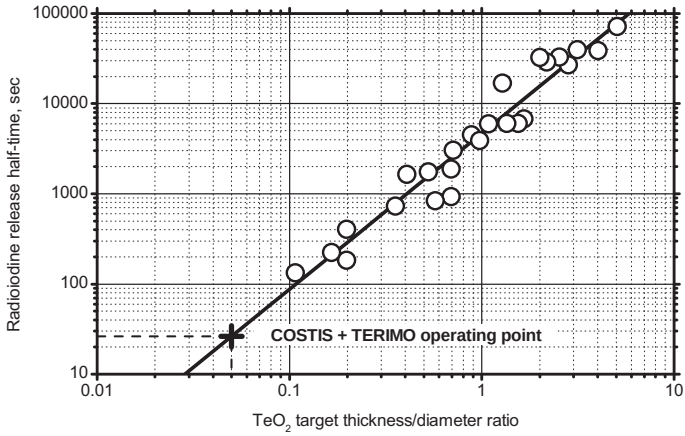

FIG. 5. Release half-time of radioiodine from molten TeO_2 at 800°C as a function of target thickness to diameter ratio. o denotes experimental data from [16], + denotes the operating point of targets designed for irradiation in COSTIS (0.6 mm thick TeO_2 layer, 12 mm in diameter).

are carried through the apparatus via sterile filtered air. The quartz apparatus is shown in Fig. 7.

The quartz oven is integrated into a GMP compliant module for carrying out the whole procedure of radioiodine separation. The scheme of the module is presented in Fig. 8. The operation of the module starts with loading the target coin onto the quartz target holder and closing the quartz apparatus. The rest of the process is carried out fully automatically, controlled by an industrial PLC based control system and monitored on a notebook computer.

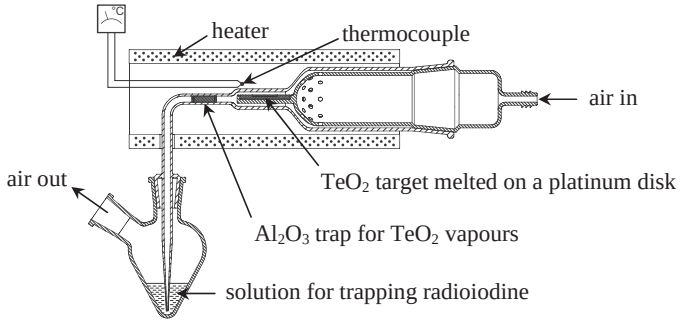

FIG. 6. Schematic view of quartz apparatus for thermochromatographic separation of radioiodine from the irradiated TeO_2 targets.

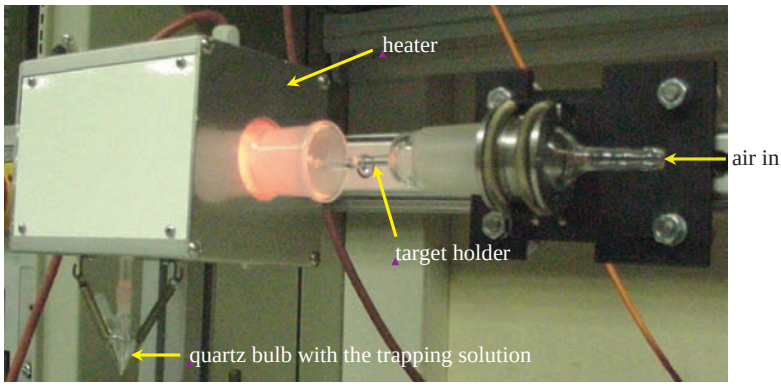

FIG. 7. Quartz apparatus for thermochromatographic separation of radioiodine.

First, the quartz bulb is loaded with a pre-adsorption solution from reservoir B1, then the target is heated up to 550°C in order to clean the target of any volatile contamination it might have picked up during its irradiation and transport (the quartz apparatus is purged by a stream of air during the whole thermochromatographic separation process). Then, the pre-adsorption solution which trapped the impurities is transferred to the waste container, the quartz bulb is washed with the content of reservoir B2 and then the absorption solution from reservoir B3 is transferred to the quartz bulb. The target is then heated up until it melts and the radioiodine is released and becomes trapped in the absorption solution whose volume can be less than 1 mL. After the short period during which the target's temperature is above the melting point (2 min), the system is purged further with the carrier gas (air) for a few more minutes at a lower temperature that is safe for the target material, in order to

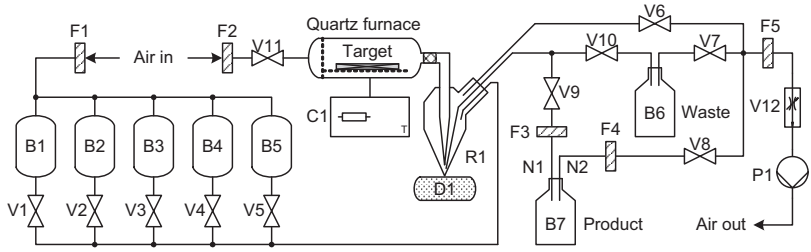

FIG. 8. Technological scheme of TERIMO: (F1–F4) sterile filters; (F5) iodine trap; (B1–B6) process reservoirs; (B7) sterile vial for the product; (N1, N2) sterile needles; (V1–V11) solenoid operated valves; (V12) air flow regulator; (P1) vacuum pump; (R1) trapping vessel; (C1) programmable temperature controller; and (D1) radioactivity detector.

trap the iodine that is still adsorbed at different surfaces inside the furnace and on the alumina filter that retains TeO_2 traces. The trapping solution containing the radioiodine in the form of iodide is then transferred to the sterile product vial passing through a 0.2 μm sterile filter. Finally, the quartz bulb is washed twice with the content of the reservoirs B4 and B5 in order to prepare it for the next run.

The operation of all of the elements of the module are logged into a file that can be visualized on the screen of the computer (see Fig. 9) and it can be printed out as well and attached to the production protocol.

Instead of an alkaline iodine trapping solution, one may load the quartz bulb with a solution containing certain precursors. This way, one may directly produce certain radiopharmaceuticals during the release of the radioiodine from the target. This is possible owing to the fact that the radioiodine carried by the air from the hot target to the quartz bulb is in the form of a highly reactive iodine radical (I^*) with clear electrophylic properties. The possibility of producing o-iodo-hippuric acid and m-iodo-benzylguanidine directly during the thermochromatographic process has already been reported [16].

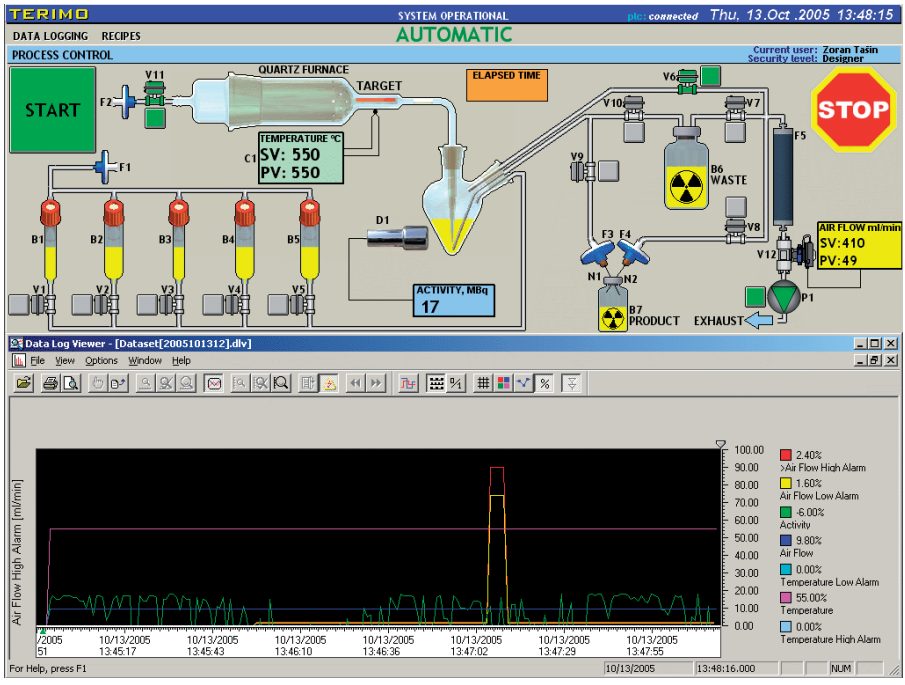

FIG. 9. Synoptic view of the graphical user interface running on a notebook computer while the PLC controls the operation of the module.

The technology described (irradiation of enriched TeO_2 targets using COSTIS installed on common medical cyclotrons and performing the thermochromatographic separation of produced radioiodine using the automated module TERIMO) provides batches of over 10 GBq or 1.5 GBq for ^{123}I and ^{124}I, respectively. Iodine-124 batches of 3.7 GBq are already routinely produced using this technology. By carefully performing the thermochromatographic separation process, the loss of target material during one production cycle (batch) is negligible (<0.2 mg/cycle).

The module is of compact design and consists of three main parts: (1) the module itself that fits into a mini-cell for handling open radioactive materials; (2) the control system that can be installed below the common hot cells; and (3) the notebook computer providing the user interface that communicates with the control system using the TCP/IP protocol.

4. CONCLUSION

Despite the fact that the production of radioiodines by cyclotrons has a long history, there is still no technology available that would allow for cost effective small and medium scale production of radioiodines by compact medical PET cyclotrons following the GMP requirements. The technology described in this paper, which is based on a compact target station (COSTIS) that can be installed on virtually any cyclotron and on a GMP compliant module for radioiodine separation from the irradiated TeO_2 targets (TERIMO) is so far the closest approach to the ideal situation. With a relatively small investment one may produce ^{123}I and ^{124}I in quantities exceeding the in-house needs of a nuclear medical centre for routine applications, not to speak of clinical research. The quality of ^{123}I produced by this technology is comparable to the quality of ^{123}I produced by the well-known ^{124}Xe based technology.

ACKNOWLEDGEMENTS

This work was partially supported by the Ministry of Science and Environmental Protection of Serbia through the realization of the TESLA Project (project code 101247).

REFERENCES

[1] PAGANI, M., STONE-ELANDER, S., LARSSON, S.A., Alternative positron emission tomography with non-conventional positron emitters: effects of their physical properties on image quality and potential clinical applications, Eur. J. Nucl. Med. **24** (1997) 1301.

[2] QAIM, S.M., et al., Some optimisation studies relevant to the production of high-purity ^{124}I and ^{120g}I at a small-sized cyclotron, Appl. Radiat. Isot. **58** (2003) 69.

[3] GLASER, M., LUTHRA, S.K., BRADY, F., Applications of positron-emitting halogens in PET oncology (Review), Int. J. Oncol. **22** (2003) 253.

[4] FREUDENBERG, L.S., et al., Value of ^{124}I-PET/CT in staging of patients with differentiated thyroid cancer, Eur. Radiol. **14** (2004) 2092.

[5] HUPF, H.B., ELDRIDGE, J.S., BEAVER, J.E., Production of Iodine-123 for Medical Applications, Int. J. Appl. Radiat. Isot. **19** (1968) 345.

[6] VAN DEN BOSCH, R., et al., A new approach to target chemistry for the iodine-123 production via the ^{124}Te(p, 2n) reaction, Int. J. Appl. Radiat. Isot., **28** (1977) 255.

[7] BEYER, G.J., DAM, C., ODRICH, H., PIMENTEL, G., Production of ^{123}I at the Rossendorf U-120 cyclotron, Radiochem. Radioanal. Letters **47** (1981) 151.

[8] MICHAEL, H., ROSEZIN, H., APELT, H., BLESSING, G., KNIEPER, J., QAIM, S.M., Some technical improvements in the production of ^{123}I via the ^{124}Te(p,2n)^{123}I reaction at a compact cyclotron, Appl. Radiat. Isot. **32** (1981) 581.

[9] ZAIDI, J.H., QAIM, S.M., STOECKLIN, G., Excitation Functions of Deuteron Induced Nuclear Reactions On Natural Tellurium and Enriched ^{122}Te: Production of ^{123}I via the ^{122}Te(d,n)^{123}I-Process, Int. J. Appl. Radiat. Isot. **34** (1983) 1425.

[10] BEYER, G.J., et al., Production of ^{123}I for Medical Use with Small Accelerators, Isotopenpraxis **24** (1988) 297.

[11] LAMBRECHT, R.M., SAJJAD, M., QURESHI, M.A., AL-YANBAWI, S.J., Production of ^{124}I, J. Radioanal. Nucl. Chem. Lett. **127** (1988) 143.

[12] SHARMA, H.L., ZWEIT, J., DOWNEY, S., SMITH, A.M., SMITH, A.G., Production of ^{124}I for positron emission tomography, J. Lab. Comp. Radiopharm. **26** (1988) 165.

[13] CLEM, R.G., LAMBRECHT, R.M., Enriched ^{124}Te targets for production of ^{123}I and ^{124}I, Nucl. Inst. Meth. Phys. Res. A **303** (1991) 115.

[14] HOHN, A., COENEN, H.H., QAIM, S.M., "Nuclear Data Relevant to the Production of ^{120g}I via the ^{120}Te(p,n)-Process at a Small-Sized Cyclotron", Appl. Radiat. Isot. **49** (1998) 1493.

[15] SHEH, Y., et al., Low energy cyclotron production and chemical separation of "no carrier added" iodine-124 from a reusable, enriched tellurium-124 dioxide/aluminum oxide solid solution target, Radiochim. Acta **88** (2000) 169.

[16] BEYER, G.-J., PIMENTEL-GONZALES, G., Physicochemical and radiochemical aspects of separation of radioiodine from TeO_2-targets, Radiochim. Acta **88** (2000) 175.

[17] KUDELIN, B.K., GROMOVA, E.A., GAVRILINA, L.V., SOLIN, L.M., Purification of recovered tellurium dioxide for re-use in iodine radioisotope production, Appl. Radiat. Isot. **54** (2001) 383.

[18] ČOMOR, J.J., et al., "COSTIS: Compact Solid Target Irradiation System", Proceedings of the Ninth International Workshop on Targetry and Target Chemistry, Turku, Finland, May 23-25 (2002) 46.

[19] ČOMOR, J.J., STEVANOVIĆ, Ž., RAJČEVIĆ, M., KOŠUTIĆ, Đ., "Modeling of thermal properties of a TeO_2 target for radioiodine production", Nucl. Instrum. Meth. A **521** (2004) 161.

[20] GLASER, M., et al., Improved targetry and production of iodine-124 for PET studies, Radiochim. Acta **92** (2004) 951.

[21] YLIMAKI, R.J., KISELEV, M.Y., ČOMOR, J.J., BEYER, G.-J., "Development of Target Delivery and Recovery System for Commercial Production of High Purity Iodine-124", Proceedings of the Tenth International Workshop on Targetry and Target Chemistry, Madison, Wisconsin, USA, August 13-15 (2004) 40.

[22] INTERNATIONAL ATOMIC ENERGY AGENCY, Charged Particle Cross-section Database for Medical Radioisotope Production: Diagnostic Radioisotopes and Monitor Reactions, IAEA-TECDOC-1211, IAEA, Vienna (2001).

[23] TIKHOMIROV, A.V., "Enriched stable isotopes for ^{123}I production: Pathways and prospects", J. Radioanal. Nucl. Chem. **257** (2003) 157.

[24] KUDELIN, B.K., SOLIN, L.M., JAKOVLEV, V.A., "Experience in iodine-123 production via p,n reaction. Synthesis and Applications of Isotopically Labeled Compounds", Vol. 7, Proc. 7th Intern. Symp., Dresden, Germany 18-22 June 2000, PLEISS, U., VOGES, R. (Eds), J.Wiley & Sons Ltd., p. 37.

NEW DEVELOPMENT IN RADIOIODINATED RADIOPHARMACEUTICALS FOR SPECT AND RADIONUCLIDE THERAPY: [^{123}I]/[^{131}I] LABELLED L- AND D-PHENYLALANINE ANALOGUES

M. BAUWENS, J.J.R. MERTENS, T. LAHOUTTE, K. KERSEMANS, C. GALLEZ, A. BOSSUYT
ICMID/BEFY, Vrije Universiteit Brussel,
Brussels, Belgium
Email: jjmerten@vub.ac.be

Abstract

[$^{123/125}$I]-2-Iodo-L-phenylalanine and [$^{123/125}$I]-2-Iodo-D-phenylalanine, with the radioiodine atom in the 2 position of the aromatic ring, were evaluated as potential specific tumour tracers for SPECT. The tracers were obtained with an overall radiochemical yield of at least 98% and a purity of >99% in one pot kit conditions. The tracers were evaluated in vitro using R1M rhabdomyosarcoma cells as the cancer cell model. The initial uptake of [^{125}I]-2-Iodo-D-phenylalanine is slower than that of the L-analogue but from 20 min the uptake as a function of time is the same. The uptake of the D- analogue is proven to occur by the same LAT transport system used by L amino acid and to be satiable, resulting in a Km value of 32μM comparable with the L- analogue. Although both compounds showed an apparent accumulation over 24 h, no incorporation was noticed. In vivo, the biodistribution of [$^{123/125}$I]-2-Iodo-L- and D-phenylalanine in R1M rhabdomyosarcoma bearing rats was measured by dynamic planar imaging. [^{99m}Tc]-PP planar imaging was performed to correct for blood pool activity. [^{123}I]-2-Iodo-D-phenylalanine showed a DUR value of 2.9 at 30 min p.i., while for [^{123}I]-2-Iodo-L-phenylalanine, the DUR value reached 3.2. Blood clearance of the tracers occurred through the kidneys to the bladder, resulting in low tracer activity in the abdomen. The activity in the brain was also low. Specific tumour uptake was confirmed using [^{99m}Tc]-PP and by displacement with L-phenylalanine. In rats, both tracers showed a high in vivo stability up to 2 h p.i., almost no free radioiodide and no other labelled metabolites were observed. The characteristics of the biodistribution make [^{123}I]-2-Iodo-L- and D-phenylalanine promising tumour specific tracers for SPECT. The long term retention of the activity in the tumours coupled to a profound clearance from blood and tissue make these tracers candidates for radionuclide therapy with ^{131}I.

1. INTRODUCTION

Nuclear medicine became molecular imaging. The use of 'smart' radiopharmaceuticals for the imaging of the biochemical changes that come with any disease has allowed a worldwide recognition of the usefulness of scintigraphic imaging in medicine and biology. The latter requires molecules of biological interest, especially for functional imaging of metabolism, tumours and neurotransmission functions using single photon emission computed tomography (SPECT). An effective labelling of compounds of biological interest is required for the preparation of these radiopharmaceuticals and therefore the radiolabelling methodology is considered to be one of the pillars on which nuclear medicine rests. Often, labelling with ^{123}I is preferred as the introduction of ^{99m}Tc multidentate complexing groups (Tc I, III or V) into small molecules can dramatically change the biological activity.

As ^{123}I is currently still rather expensive, 'almost quantitative yields' are required. Daily routine preparations in clinic of ^{123}I radiopharmaceuticals require one pot kit synthesis, as simple as the routine ^{99m}Tc kits (mix and heat), or an automated system with a fast mini-column purification system. For the first, the Cu^{+} assisted nucleophilic exchange in reducing aqueous conditions is well suited, while for the second, the eletrophilic substitution with the highly lipophilic tri-Butyl-Sn as the leaving group offers a good alternative.

Radiopharmaceutical research is matching a new development by designing targeted radiotracers that allow non-invasive imaging of specific gene expression, gene products or protein function in vivo. This approach makes it possible to monitor changes non-invasively at the molecular level, during the natural history of disease and/or after therapy.

There is an increasing interest in tumour specific SPECT tracers for follow-up of tumours after surgery and irradiation and/or chemotherapy, but not in FDG-mimics as [^{18}F]-FDG is not specific enough as it shows high uptake in inflamed tissue. Moreover, when the compound is highly retained in the tumour, the ^{131}I analogues are an alternative for coupled radionuclide therapy.

MIBG, developed in the 1980s and still in use, is such an example as when labelled with ^{123}I it is used as a receptor based (adrenergic receptors) myocardial and tumour tracer, and when labelled with ^{131}I it is used for radionuclide therapy of neuroblastoma, pheochromocytoma and other tumours.

Within the broad spectra of diagnostics and coupled radionuclide therapy, radiolabelled amino acid analogues can fulfil an important role. Amino acid transporters are proteins that mediate amino acid influx and efflux across cell membranes [1]. Their functions are to supply the cells with amino acids, to transport amino acids across barriers (intestine, kidney, blood–brain barrier, placenta, etc.) and to terminate synaptic transmission through reuptake of

excitatory amino acids. Initially, the amino acid transporters were classified on the basis of their functional and pharmacological characteristics. They differ in substrate selectivity and Na^+ dependency of the transport, and also in tissue expression and subcellular localization according to their specific role. Furthermore, the physiological role type can also vary according to the cell or tissue where it is expressed.

The L transporter is a major nutrient transport system responsible for Na^+ independent transport of large neutral amino acids including synthetic amino acids by an obligatory exchange mechanism coupled to an anti-port system [6]. The heterodimeric LAT transport system contains 2 subunits, a heavy chain 4F2/CD98 and a light chain named LAT1 or LAT2.

LAT1 expression was scarcely detected in non-tumour areas [7–9] but highly expressed (up-regulated) in proliferating tissues, in particular malignant tumours, as it plays a critical role in cell growth and proliferation [9]. A remarkable characteristic of system L and the hLAT-1 amino acid uptake is its broad substrate selectivity, which enables the transport system to accept amino acid related compounds, such as D-amino acids and cancer drugs like Melphalan [10]. LAT2 on the other hand has a high level of expression in the small intestine, kidney, placenta and brain and in the epithelia and blood–tissue barriers [11]. It transports all of the isomers of neutral alpha amino acids by facilitated diffusion; however it does not transport D-amino acids. Previously, it was supposed that the amino acid tracers had to be incorporated into the tumour cell proteins [21]. More recently, Langen et al. [22] and Lahoutte et al. [24] showed that it is the increased L mediated transport of amino acid analogues into tumour cells and not necessarily the incorporation that is needed for efficient tumour imaging and follow-up. Langen et al. [25], moreover, have demonstrated that the expression of L transporters and related reversible uptake depend on the proliferation rate of human glioma cells. The authors' group recently developed 2-I-L-tyrosine [31], which shows a very high tumour selectivity, better than [^{18}F]-FDG which is taken up considerably in the brain and inflammatory tissue, and is not retained in the kidney as shown by Tamemasa, Goto et al. and Takeda et al. [32–34]. They showed uptake of [^{14}C] labelled D-Leucine, D-Alanine and D-Tryptophane in mice tumour and human tumour derived tumour cells induced in nude mice, without being able to explain this phenomenon at that time. They suggested that D-Leucine was transported by the same transporter as L-Leucine, but that the isomers were supposed to bind to different parts of the transporter. This transporter was later defined as the L transporter. In 1985, Meyer et al. [1] showed that both the L and D forms of the [^{11}C]-methionine could accumulate in human brain tumours. Since then all the development of, and studies with, radioactively

labelled amino acids for tumour diagnosis with PET and SPECT were focused on the L-enantiomeric form.

The knowledge of the molecular biology of the LAT transporter system drove the authors to explore the D-analogues of tyrosine and phenylalanine, having also noticed that [^{14}C]-D-phenylalanine and D-phenylalanine were taken up in R1M cells by the LAT1 transport system [35]. This paper describes the evaluation of two new tracers L- and D-[^{123}I]-2-I-phenylalanine in R1M tumour bearing rats by scintigraphic imaging.

2. EXPERIMENTAL

2.1. Materials and methods

All the conventional products mentioned were at least analytical or clinical grade and obtained from Sigma-Aldrich. The solvents were of HPLC quality (VWR, Belgium).

2.1.1. Synthesis and radiosynthesis

The synthesis of 2-I-D-phenylalanine/2-I-L-phenylalanine was achieved as already described [27].

Radioiodination with $^{123}I^-$, $^{125}I^-$ or $^{131}I^-$ (10–30 µL) on 1.0 mg 2-iodo-L-phenylalanine or 2-iodo-D-phenylalanine was performed by Cu^+ assisted isotopic exchange under acidic and reducing conditions (0.2 mg $CuSO_4$, 2.5 mg citric acid, 0.5 mg $SnSO_4$, 1.3 mg gentisic acid in 565 µL; 60 min at 100°C) [17]. The reaction mixture was drawn up in a syringe containing the appropriate amount of 'make-up solution' (tri-sodium citrate dihydrate, 71mM) to render the solution isotonic and to adjust the pH to at least 4. The reaction mixture was filtered through a 0.22 µm Ag filter (Millipore, Belgium) to remove the free $^{123}I^-/^{125}I^-$ and through a sterile 0.22 µm filter (Millipore, Belgium) into a sterile vacuum vial. Quality control was achieved by HPLC and Sep-pak C18 (Waters, Belgium). Radiolabelling of both tracers with $^{123}I^-$ or $^{125}I^-$ resulted in a radiochemical purity of >99% and a specific activity of 65 GBq/mmol [^{123}I] labelling and 11 GBq/mmol [^{125}I] labelling.

2.1.2. [^{99m}Tc]-Pyrophosphate

Technescan PYP (Mallinckrodt Medical) ([^{99m}Tc]-PP) was prepared according to producer guidelines. [^{99m}Tc] was obtained from Mallinckrodt.

2.1.3. Quality control

Quality control was achieved by HPLC, using a C8-column (LichrosPher 100RP8 (5 µm), Lichrocart 125-4) and 10/90 MeOH/H_2O containing 1mM NH_4Ac as the mobile phase at 1.0 mL/min while monitoring UV absorption (Hitachi UV detector, 254 nm) and radioactivity (NaI(Tl) detector (Harshaw chemie)).

Chiral chromatography was performed on a chiral column (5 µm Chirobiotic T (Astec) column (150 mm × 4.6 mm)) using 80/20 v/v% methanol/H_2O containing 20mM NH_4Ac at a flow of 1 mL/min. In these conditions a complete separation of the chiral isomers was obtained. The capacity values (K') of L-2-I-Phe and D-2-I-Phe were 2.7 min and 3.8 min, respectively. No transformation of the chirality was observed.

2.2. Reverse transcriptase PCR

Reverse transcriptase PCR was performed using BioTaq RED (Bioline) according to manufacturer's guidelines. The amplification of the cDNA strands was performed using the following conditions: (1) pre-cycle: 94°C for 3 min, 60°C for 1 min, 72°C for 2 min; (2) 26 cycles of 94°C for 1 min, 60°C for 1 min, 72°C for 2 min; (3) hold: 72°C for 10 min. Gel electrophoresis was performed on a 1.5% agarose/EtBr gel at 250 V and 250 mA for 15 min. The entire PCR product was loaded onto the gel; Hyperladder IV (Bioline) was used as a marker. Actin was used as a positive control of the method.

2.3. In vitro experiments

2.3.1. Cell cultures

R1M rhabdomyosarcoma cells (VUB) were cultivated as described [27].

2.3.2. Experimental procedure

All in vitro experiments were carried out in 6-well plates (VWR), using at least three wells for each data point. Cells were counted by means of a Bürker counting chamber. Influx and efflux were studied both in a Na^+ containing buffer (HEPES+: pH7.4; 100mM NaCl (VWR), 2mM KCl (Sigma), 1mM $MgCl_2$ (VWR), 1mM $CaCl_2$ (VWR), 10mM Hepes (Sigma), 5mM Tris (VWR), 1 g/L glucose (VWR) and 1 g/L bovine serum albumin (Sigma)), a Na^+ free buffer (HEPES-: pH7.4; 100mM choline-Cl (Sigma), 2mM KCl, 1mM $MgCl_2$, 1mM $CaCl_2$, 10mM Hepes, 5mM Tris, 1 g/L glucose and 1 g/L bovine serum

albumin) and MEM buffer (pH7.2, containing essential and non-essential amino acids of which 1.2mM of amino acids known to be transported by the L transport system). The process was terminated by physical withdrawal of the buffer and washing three times with ice cold phosphate buffered saline (PBS). Subsequently, the cells were detached from the well with 2 mL of 0.1M NaOH (VWR). The radioactivity of the samples was counted using a gamma counting system (Cobra-inspector 5003, Canberra Packard, Meriden, CT, United States of America).

Time and concentration dependency: For the kinetic studies, the cells were incubated for periods ranging from 1 min to 24 h in 1 mL of MEM under constant partial CO_2 pressure (5%) containing 37 kBq [^{125}I]-2-I-D-Phe or [^{125}I]-2-I-L-Phe. Throughout the 24 h period the viability of the cells was checked using the trypan blue method and also the 15 min uptake of ^{3}H-L-Phe was measured to indicate whether the number of transporters remained constant during the 24 h cell growth.

For concentration dependency, uptake was measured at 1 min uptake with concentrations varying from 0.01 to 0.2mM. The data were fitted to the Michaelis-Menten relation and the apparent Km, Vmax and Ki values were calculated from Eady-Hofstee and Hanes-Woolf and Lineweaver-Burk (LWB) plots. 'Apparent Km' is calculated from Vo conditions, i.e. uptake after 1 min where for the larger part only influx has to be considered.

Using [^{3}H]-L-Phe/L-Phe (Amersham Biosciences/Sigma) as a reference molecule, the type of competition and Ki value of 2-I-D-Phe and 2-I-L-Phe were determined using a double reciprocal LWB plot. The concentration of the inhibitors was 0.1 mM.

Inhibition of [^{125}I]-2-I-D-Phe influx: The cells were incubated with 37 kBq [^{125}I]-2-I-D-Phe for 1 min in HEPES+ and HEPES- buffer supplemented with 8mM L-Phe, 8mM BCH (2-amino-2-norbornane-carboxylic acid, a LAT transport system specific inhibitor) or 8mM MeAIB (methyl amino isobutyric acid, an A/ASC transport system specific inhibitor).

Trans-stimulation of [^{3}H]-L-Phe and [^{125}I]-2-I-D-Phe efflux: The cells were incubated with 37 kBq [^{3}H]-L-Phe or 37 kBq [^{125}I]-2-I-D-Phe for 15 min in HEPES- buffer. The incubation medium was removed and the cells were washed three times with ice cold PBS. Subsequently, HEPES- buffer containing 0.1mM L-Phe or 2-I-D-Phe was added. The efflux medium was removed after 1 min, after which the cells were washed three times with ice cold PBS, detached with 0.1M NaOH, suspended and counted.

Incorporation into cell proteins: The cells were incubated with the radioactive amino acid (37 kBq [^{125}I]-2-I-D-Phe) for a period ranging from 15 min up to 24 h in MEM under constant CO_2 partial pressure (5%) using the GENBOX system. After removal of the radioactive solution, precipitation of

proteins was performed by adding 2 mL of 20% trichloroacetic acid, intense mixing (vortex) followed by cooling for 30 min at 0°C. After two sessions of repeated centrifugation and washing, 2 mL of 0.1M NaOH was added and the radioactivity counted.

2.4. In vivo experiments

2.4.1. Laboratory animals

Water and food was ad libidum during the experimental period. For the tumour model, male Wag/Rij rats (n = 6) (Bioservices, Netherlands) were injected subcutaneously in the right flank (armpit region) with 15×10^6 R1M rhabdomyosarcoma cells.

Imaging experiments with [^{123}I]-2-Iodo-D-phenylalanine, [^{123}I]-2-Iodo-L-phenylalanine and [^{99m}Tc]-PP were performed 6 h p.i. of the R1M cells.

During all imaging experiments, the animals were anaesthetized intraperitoneal with 350 μL (21 mg) of a solution containing 60 mg pentobarbital per mL (Nembutal, 60 mg/mL, Ceva Santé Animale, Belgium). For the biodistribution experiments by dissection, the animals were killed without sedation by cervical dislocation and the organs of interest were dissected.

All tracers were injected intravenously into the penis vein. The study protocol was approved by the ethical committee for animal studies at the authors' institution. Guidelines of the National Institute of Health principles of laboratory animal care (NIH publication 86-23, revised 1985) were followed.

2.4.2. Dynamic planar imaging (DPI).

Imaging was performed using a gamma camera (Philips) in planar mode equipped with a high resolution parallel hole collimator. All images were acquired into 128 × 128 matrices (3.2 zoom factor, pixel size 1.5 mm) and with a photopeak window set at 15% around 159 keV. The injected activity was also calculated as the amount of radioactivity in the syringe before and after injection (Capintec CRC-15R, Ramsey, NJ, USA). To allow semi-quantification of the results of the ROI analysis, the activity in the total body (counts) 20 min p.i. was regarded as the injected amount of radioactivity. ROIs were drawn around the tumour, the contra-lateral background area, both kidneys, heart, brain, bladder, thyroid and total body. The ROI of the heart was used as a measure of blood pool activity. Owing to partial volume effects, the data can be overestimated [18]. The tracer uptake was expressed as DUR (differential uptake ratio; average counts per pixel of the region of interest divided by the average counts per pixel inside the total body).

Imaging was performed for crossed (two by two) experiments with a 2 d interval using four R1M bearing Wag/Rij rats. DPI was started immediately after injection of 18.5 MBq [^{123}I]-2-Iodo-D-phenylalanine or [^{123}I]-2-Iodo-L-Phe and continued up to 90 min for all rats. To test the tumour retention of the compounds, a static image of 10 min was acquired at 0.5, 24 and 48 h p.i. Tumour retention was calculated relative to the time point 0.5 h p.i. as (counts/pixel$_{24h\ or\ 48h}$ / counts/pixel$_{0.5h}$) (decay corrected).

In a separate experiment 2 rats were injected with 200 µL of a 20mM L-Phe solution (2.2 mg/kg) 60 min after the administration of the D-isomer.

[^{99m}Tc]-Pyrophosphate was used to measure the relative blood pool distribution in order to correct the uptake of radioactivity in the tumour as well as the rest of the animal for blood pool activity. In this experiment, all rats were injected with 37 MBq [^{99m}Tc]-PP. Planar images of 10 min were acquired 15 min p.i. The ratios tumour to heart and organ to heart were calculated to correct for blood pool activity in the tumour or organ.

2.4.3. Detection of metabolites

Blood was collected in an EDTA coated vial at different time points; 1 mL of blood was centrifuged at 3000g for 1 min for quantitative plasma separation. To 75 µL of plasma successively 125 µL of 9‰ NaCl solution and 200 µL of 20% trichloroacetic acid were added. After 5 min of centrifugation at 3000g, the supernatant was collected and filtered through a 0.22 µm filter. In a final step, 125 µL of 1M NaAc and 325 µL 20/80 MeOH/H_2O containing 1mM NH4Ac was added. The samples were analysed on RP-HPLC (C8-column (LichrosPher 100RP8 (5 µm), Lichrocart 125-4, λ = 254 nm) (Alltech, Belgium) with 20/80 MeOH/H2O containing 1mM NH4Ac as mobile phase at 1.0 mL/min while monitoring UV absorption (Hitachi UV detector, 254 nm) and radioactivity (NaI(Tl) detector (Harshaw Chemie)).

3. RESULTS

3.1. Synthesis and radiolabelling of 2-I-D-phenylalanine/2-I-L-phenylalanine

2-I-D-Phe and 2-I-L-Phe purity was at least 99%. Radiolabelling of both tracers with $^{123}I^-$ or $^{125}I^-$ resulted in a radiochemical purity of >99% and a specific activity of 65 GBq/mmol ([^{123}I] labelling) and 11 GBq/mmol ([^{125}I] labelling). Chiral chromatography showed that no chiral modification occurred during the labelling. The sterile and isotonic [^{123}I]-2-I-D-Phe solution was injected in the rats within 2–4 h after the preparation. The [^{125}I] labelled

compound was stored at 4°C. HPLC analysis during the long duration of the experiments revealed the quality of the preparation to be stable for at least a month. After that period, a small amount of free radioiodide was observed (2–3%). This was quantitatively removed by filtering the solution through a sterile 0.22 μm Ag membrane filter.

3.2. In vitro results

The in vitro evaluation of 2-I-L-Phe has been described in detail in Ref. [27].

3.2.1. Time and concentration depend on kinetics and affinity

The initial uptake of [^{125}]-2-I-D-phenylalanine in R1M cells in MEM buffer is slower than that of [^{125}I]-2-I-L-Phe (Fig. 1). The uptake of both compounds at longer times, up to 24 h, shows a slight accumulation which is not due either to incorporation (the iodinated phenylalanine analogues are not incorporated into the cell proteins) or to the increase in cell numbers (the results are expressed per million cells or amount of transporters (^{3}H-L-Phe uptake check)).

The Ki calculated from the LWB plot representing the inhibition of the uptake of [^{3}H]-L-PHE/L-PHE in R1M cells in HEPES- medium (Fig. 2) resulted in a value of 50 ± 10μM. In the same conditions, 2-I-L-Phe showed a Ki value of 35 ± 10μM.

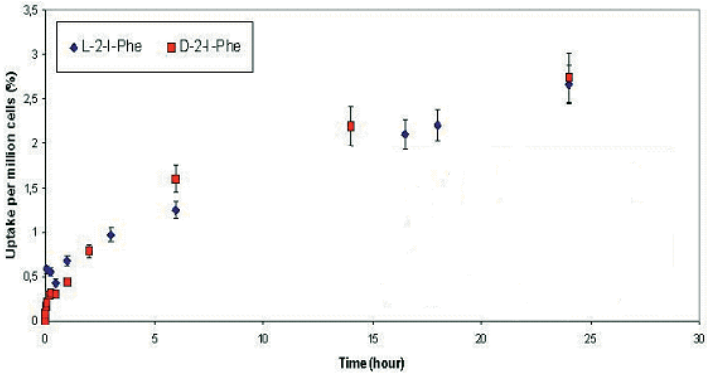

FIG. 1. [^{125}]-2-I-D-Phe and [^{125}]-2-I-L-Phe uptake time kinetics in R1M cells in MEM buffer: mean ± SD (n = 9).

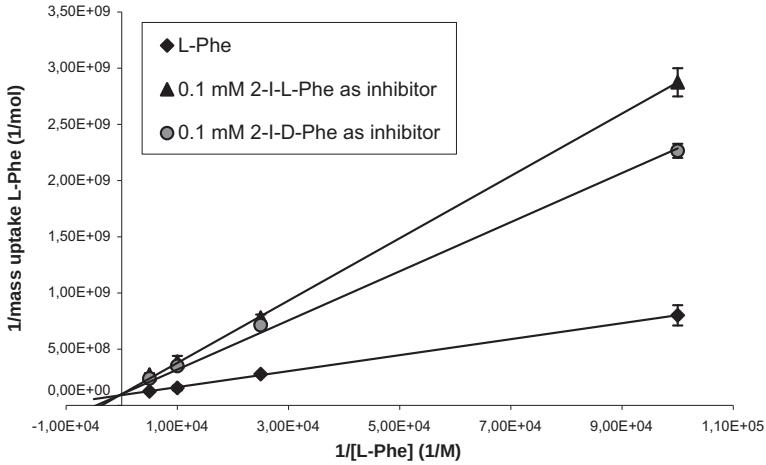

FIG. 2. Inhibition of [^{3}H]-L-Phe/L-Phe uptake by D-2-I-Phe, D-Phe and 2-I-L-Phe: LWB plot data: mean ± SD (n = 3).

3.2.2. Transporter type characterization

The PCR coupled gel electrophoresis of the R1M cell line is depicted in Fig. 3 and clearly shows the presence of potentially functional LAT1 and LAT2 transport systems proven by the presence of the bands for hLAT1, hLAT2 and light chain 4F2hc. The actin band is used for positive control.

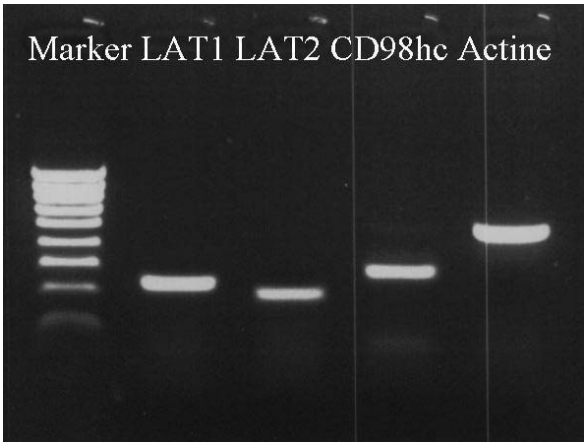

FIG. 3. Gel electrophoresis of LAT1 light chain (LAT1), LAT2 light chain (LAT2), CD98 heavy chain (CD98hc) and actine (Actine).

The uptake of [^{125}I]-2-I-D-Phe in HEPES+ (Na^+ presence) and HEPES- (Na^+ absence) was not significantly different and the uptake was almost quantitatively reduced (2% of the original value) by the presence of 8mM BCH, a specific inhibitor of the L transport system, and also by 8mM of L-phenylalanine. Moreover, 8mM MeAIB (a specific inhibitor of the Na^+ dependent A/ASC transport system) had no influence on the uptake. Figure 3, representing a double reciprocal LWB plot, reveals that the inhibition of [^{3}H]-L-Phe by D-2-I-Phe is competitive and also by 2-I-L-Phe and D-phenylalanine (which were earlier proven to be LAT transported amino acids). The 0.1mM 2-I-D-Phe caused a net efflux of 26% of the initial uptake of [^{3}H]-L-Phe within 1 min while the efflux of [^{125}I]-2-I-D-Phe can be stimulated by BCH and L-Phe.

3.3. In vivo results

3.3.1. In vivo stability

HPLC analysis of the blood plasma showed that within the first 2 h p.i. of [^{123}I]-2-I-D-Phe, neither metabolites nor free radioiodide could be significantly detected. For [^{123}I]-2-I-L-Phe in the same conditions, about 4% free radioiodide and no metabolites were found.

3.3.2. DPI

3.3.2.1. Tumour uptake and biodistribution

The biodistribution of [^{123}I]-2-Iodo-D-Phe and [^{123}I]-2-Iodo-L-Phe was compared with that of the blood flow tracer [^{99m}Tc]-PP. The tumour/heart ratio values for both radioiodinated phenylalanine analogues showed a value of about 2.0 at 15 min whereas it only reached a value of 0.2 for [^{99m}Tc]-PP. Figure 4 shows a composite image of the biodistribution of [^{123}I]-2-I-D-Phe and [^{123}I]-2-I-L-Phe in a R1M tumour rat at 20–30 min p.i. Table 1 depicts the corresponding average DUR values of the tumours and different organs. The uptake in the pancreas zone is not calculated as with DPI the pancreas could not be accurately distinguished from the liver or lower stomach region.

The uptake in the tumours in periods up to 40 min for both [^{123}I]-2-Iodo-D-Phe and [^{123}I]-2-Iodo-L-Phe is shown in Fig. 5. At the maximum uptake, DUR values of 3.01 ± 0.40 and 3.40 ± 0.40 are obtained for [^{123}I]-2-Iodo-L-Phe and [^{123}I]-2-Iodo-D-Phe, respectively. The apparent difference between the time activity curves is not statistically significant ($p = 0.20$, Wilcoxon Signed Rank Test on average values of 30 min).

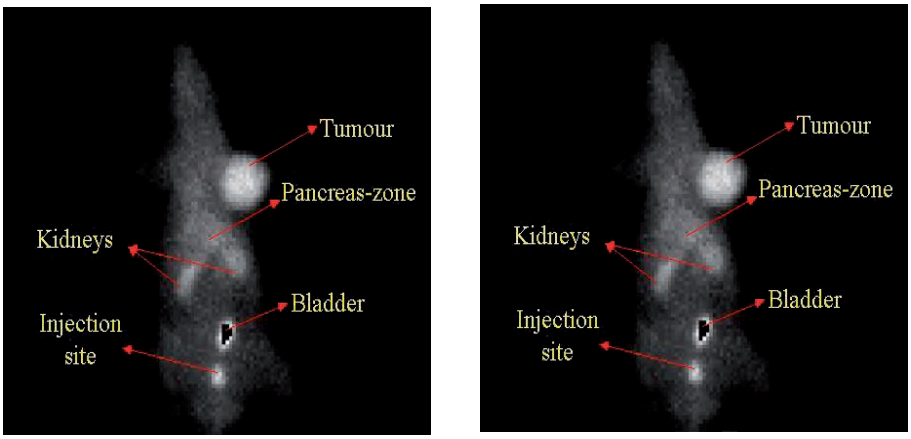

FIG. 4. Composite image (20–30 min) of a R1M rhabdomyosarcoma tumour bearing rat p.i. of 18.5 MBq [^{123}I]-2-I-D-Phe (left) and [^{123}I]-2-I-L-Phe (right). Image: gray scale gamma 1.0, the scale is set to the maximum in the tumour.

Figure 6 shows that the injection of 200 µL of a 20mM L-Phe solution (2.2 mg L-Phe per kg at 60 min) displaces about 25% of [^{123}I]-2-I-D-phenylalanine activity from the tumour. A re-accumulation occurs after displacement as shown by the positive slope up from 65 min.

TABLE 1. AVERAGE DUR VALUES AT 20–30 min p.i. OF [^{123}I]-2-Iodo-D-Phe AND [^{123}I]-2-Iodo-L-Phe
(data = mean ± SD (n = 4))

DUR value	[^{123}I]-2-Iodo-D-phenylalanine	[^{123}I]-2-Iodo-L-phenylalanine
Tumour	2.9 ± 0.4	3.2 ± 0.4
Left kidney	1.9 ± 0.1	1.5 ± 0.1
Heart	1.5 ± 0.1	1.6 ± 0.1
Muscle	0.6 ± 0.1	0.7 ± 0.1
Bladder	3.7 ± 0.3	2.1 ± 0.3
Thryoid	Not detectable	Not detectable
Brain	1.0 ± 0.1	1.2 ± 0.1

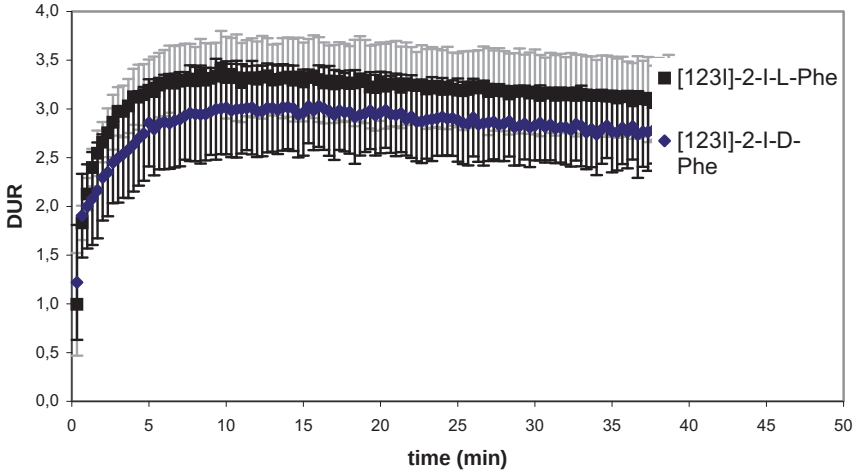

FIG. 5. DUR tumour values of [^{123}I]-2-I-D-Phe and [^{123}I]-2-I-L-Phe as a function of time. Data = mean ± SD (n = 4).

3.3.2.2. Clearance

Figure 7 shows that the clearance of [^{123}I]-2-Iodo-D-phenylalanine from the blood through the kidneys to the bladder is faster than that of [^{123}I]-2-Iodo-L-phenylalanine. In the early time-frames, the increase of activity in the

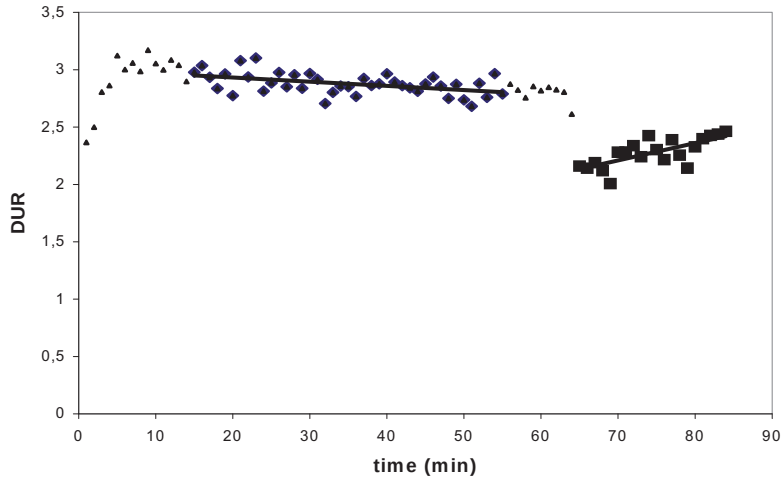

FIG. 6. DUR values of [^{123}I]-2-I-D-Phe as a function of time. At 60 min p.i., a high concentration of L-Phe was injected. Data = mean (n = 2).

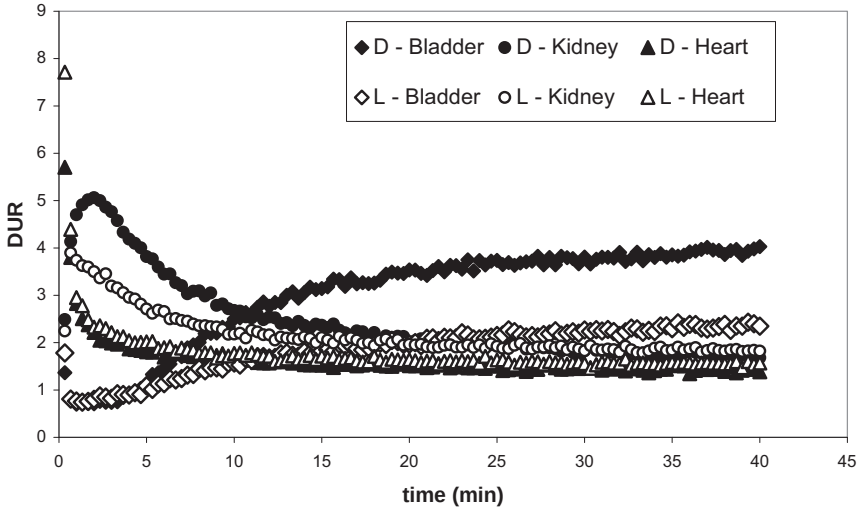

FIG. 7. Uptake (DUR) of [^{123}I]-2-I-D-Phe and [^{123}I]-2-I-L-Phe as a function of time in kidney, heart and bladder. Data = mean ± SD (n = 4).

bladder as a function of time is much higher for the D-isomer than for the L-isomer (the slope of the curve at 5–10 min is 0.27 DUR values/min for the D-isomer and 0.096 DUR values/min for the L-isomer), resulting in a twofold amount of activity in the bladder for the D analogue compared with 2-I-L-Phe at the end of imaging.

3.3.3. Long term biodistribution and retention

Interestingly, for both tracers there is a retention in the tumour over a long time period (48 h). Table 2 shows that a high amount of radioactivity remains in the tumour for a longer time while the DUR values show an apparent increase. Figure 8 shows the biodistribution at 48 h with a clear contrast of the tumour vis a vis the background activity.

4. DISCUSSION

Reverse transcriptase PCR gel electrophoresis (Fig. 3) clearly shows the presence of the mRNA of hCD98hc, hLAT1 and hLAT2 in the R1M cell line, allowing a functional LAT1 and LAT2 transport system. The band width and

TABLE 2. DUR VALUES AND PER CENT RETENTION OF [^{123}I]-2-I-D-Phe AND [^{123}I]-2-I-L-Phe AT 30 min AND 24 AND 48 h p.i. *(data = mean ± SD (n = 4))*

DUR	Tumour (30 min)		Tumour (24 h)		Tumour (48 h)	
	DUR	% Retention	DUR	% Retention	DUR	% Retention
[^{123}I]-2-I-D-Phe	2.9 ± 0.4		3.5 ± 0.3	92 ± 10	3.7 ± 0.3	77 ± 3
[^{123}I]-2-I-L-Phe	3.2 ± 0.4		3.5 ± 0.5	91 ± 10	3.7 ± 0.3	73 ± 7

brightness indicate a greater presence of the LAT1 transport system compared with the LAT2 transport system.

The same intercept of the different lines in the LWB plot (Fig. 2) obtained for L-Phe, 2-I-D-Phe and 2-I-L-Phe reveals that all these compounds enter the R1M cells in vitro by the same transport system(s).

No Na^+ dependence was found, while the influx of [^{125}I]-D-2-I-Phe was completely inhibited by 8mM BCH. The influx of 0.1mM D-2-I-Phe caused an efflux of 26% of the initial [^{3}H]-L-Phe uptake while [^{125}I]-D-2-I-Phe efflux, although a smaller amount, was stimulated by 0.1mM L-Phe and BCH. These characteristics are compliant with the exclusive utilization of the LAT system as an obligatory 1/1 antiport system.

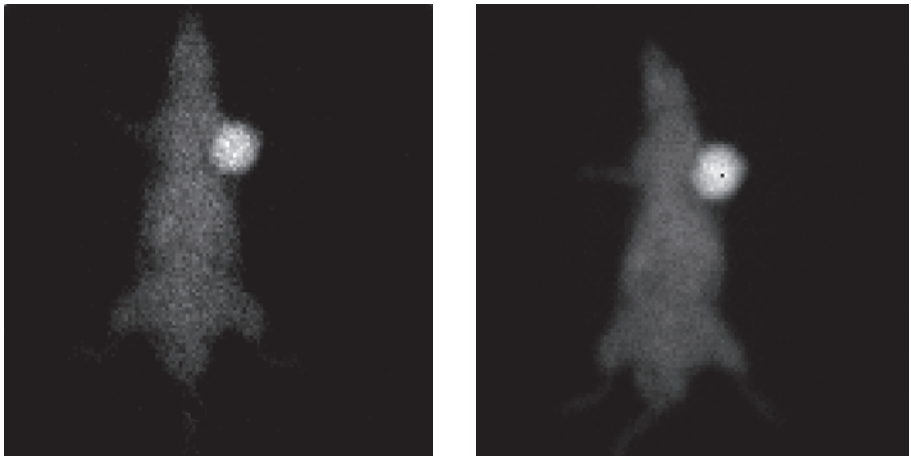

FIG. 8. Composite images of a R1M rhabdomyosarcoma tumour bearing rat p.i. of 18.5 MBq [^{123}I]-2-I-D-Phe (left) and [^{123}I]-2-I-L-Phe (right) at 48 h p.i. Image: gray scale gamma 1.0, the scale is set to the maximum in the tumour.

The difference in initial uptake kinetics (Fig. 2) between 2-I-D-Phe and 2-I-L-Phe might be due to the fact that the D form only shows a high affinity for the LAT1 system and not for LAT2. This is supported by the finding that in cell types expressing only LAT1, no difference in uptake is found between 2-I-D-Phe and 2-I-L-Phe (V. Kersemans, unpublished).

The increase in non-incorporated uptake and apparent retention during stimulated efflux of the radioiodinated phenylalanine analogues can be due to a significant difference in affinity of the intracellular part of the transport protein for the iodinated compounds compared with the natural amino acids present. It is known that the LAT systems show a relatively symmetrical broad selectivity but strongly asymmetrical substrate affinity, such that the intracellular amino acid pool controls their exchange activity [22, 23]. The increase in non-incorporated uptake in vitro as well as a less stimulated efflux than L-Phe can be due to a significant difference in affinity between the radioiodinated D analogue and the natural L amino acid present in the tumour cells.

The in vivo short time kinetics (0–40 min) of tumour uptake show no significant difference for [^{123}I]-2-I-L-Phe and [^{123}I]-2-I-D-Phe (about 10% higher for the L-enantiomer). The tumour uptake was considerably higher than blood flow, measured with [^{99m}Tc]-PP. The high tumour specific uptake could be displaced for 25% by injection of a high dose of natural L-Phe, pointing at the involvement of the LAT transport system. There is a re-accumulation of [^{123}I]-2-I-D-Phe in the tumour after displacement (Fig. 6) indicated by the positive slope up from 65 min.

Over longer time periods (24 and 48 h), a high retention of radioactivity in the tumour is noticed. This retention can be compared with the ‘apparent accumulation’ discussed in the in vitro part as the uptake in vivo occurs by the same transporter type and mechanism.

5. CONCLUSION

The uptake of [$^{123/125}$I]-2-I-D-Phenylalanine and [^{123}I]-2-I-L-Phenylalanine occurs in vitro as well as in vivo exclusively and with a high affinity via the LAT1 system which is overexpressed in many tumour cell lines. Imaging of R1M tumour bearing rats shows specific and fast tumour uptake and an appropriate biodistribution, fast clearance from blood and abdomen and low brain uptake, making [^{123}I]-2-I-D-Phenylalanine and [^{123}I]-2-I-L-Phenylalanine promising tracers for specific tumour imaging within and outside the brain using SPECT. The long term retention of the activity in the tumours coupled to a profound clearance from blood and tissue make these tracers candidates for radionuclide therapy with ^{131}I.

ACKNOWLEDGEMENTS

The authors thank the FWO Vlaanderen and GOA-VUB for their financial support.

REFERENCES

[1] MEYER, G.J., SCHOBER, O., HUNDESHAGEN, H., "Uptake of 11C-L- and D-methionine in brain tumours Eur. J. Nucl Med (1985);10(7-8):373-6.

[2] OHKAME, H., MASUDA, H., ISHII, Y., KANAI, Y., Expression of L-type amino acid transporter 1 (LAT1) and 4F2 heavy chain in liver tumour lesions of rat models, Journal of Surgical oncology, (2001), Vol. 78, p. 265-272.

[3] MEIER, C., RISTIC, Z., KLAUSER, S., VERREY, F., Activation of system L heterodimeric amino acid exchangers by intracellular substrates, The EMBO Journal, Vol. 21 Nr. 4, (2002), p. 580-589.

[4] LAHOUTTE, T., et al., SPECT and PET amino acid tracer influx via system L (h4F2hc-hLAT1) and its transstimulation, J Nucl Med. (2004), Vol 45 N° 9, p.1591-1596.

[5] YANAGIDA, O., KANAI, Y., Human L-Type amino acid transport system 1 (LAT1) : characterisation of function and expression in tumour cell lines, Biochim Biophys Acta, Vol. 1514, (2001), p. 291-302.

[6] SEGAWA, H., et al., Identification and functional characterisation of a Na+-independent neutral L-amino acid transporter with broad substrate selectivity, *The Journal of Biological Chemistry,* Vol. 274, (1999), p. 19745-19751.

[7] KANAI, Y., et al., "Expression cloning and characterisation of a transporters for large neutral amino acids activated by heavy chain 4F2 antigen (CD98)" *J. Biol. Chem.* (1998) 273,23629-23632.

[8] CAMPBELL, W.A., THOMPSON, N.L., " Overexpression of LAT1/CD98 light chain is sufficient to increase system L-amino acid transport activity in mouse hepatocytes but not fibroblasts J. Biol. Chem (2001) 276,16877-16884.

[9] KIM DO, K., et al., " Characterization of the L amino acid transporter in T24 human bladder carcinoma cells Biochem Biophys Acta (2002) Sep 20; 1565(1): 112.

[10] YANAGIDA, O., KANAI, Y., Human L-Type amino acid transport system 1 (LAT1) :characterisation of function and expression in tumour cell lines, Biochim Biophys Acta, Vol. 1514, (2001), p. 291-302.

[11] RAJAN, D.P., et al., Cloning and functional characterisation of a Na(+)-independent, broad-specific neutral amino acid transporter from mammalian intestine, Biochim BioPhys Acta 2000, Jan 15, 1463(1):6-14.

[12] BERGSTROM, M., et al., The normal pipituary examined with positron emission tomography and (methyl-11C)-L-Methionine and (methyl-11C)-D-Methionine, Neuroradiol. (1987), 29, 221-225.

[13] COENEN, H.H., KLING, P., STÖCKLIN, G., "Cerebral metabolism of L-2-^{18}F-fluorotyrosine, a new PET tracer for protein synthesis" J. Nucl. Med., (1989), 30:1376.

[14] BIERSACK, H.J., et al., "Imaging of brain tumours with L-3-^{123}I-iodo-alpha-methyltyrosine and SPECT" J. Nucl. Med. (1989), 30:110.

[15] JAGER, P.L., DE VRIES, E.G., PIERS, D.A., TIMMER-BOSSCHA, H., "Uptake mechanism of L-3-^{125}I-iodo-alpha-methyl-tyrosine and SPECT" Nucl. Med. Comm. (2001), 22(1):87.

[16] HEISS, P., et al., Investigation of transport mechanism and uptake kinetics of O-2- [18F]fluoroethyl-L-tyrosine in vitro and in vivo" J. Nucl Med (1999), 40:1367.

[17] VEKEMAN, M., JOOS, C., MERTENS, J., "L-[2-radioiodo]Tyrosine, a new potential protein synthesis and tumour tracer for SPECT: radiosynthesis and biodistribution in rodent". Eur. J. Nucl. Med., 26(9) (1999), 971.

[18] MERTENS, J., et al., "Uptake study of L-2-^{125}I-o-tyrosine, a new tracer in human colon carcinoma WiDr cells". Eur. J. Nucl. Med. (2000)27:1063.

[19] MERTENS, J., et al., "In Vitro and in Vivo Evaluation of L-2-radioiodo-tyrosine as a new potential tumour tracer for SPECT" J. Labelled Cmp Radiopharm (2001).

[20] LAHOUTTE, T., et al., "Biodistribution of iodinated amino acids: Selection of the optimal analog for oncologic imaging outside the brain". J. Nucl Med (2002).

[21] RAU, F.C., et al., O-(2-[(18)F]fluoroethyl)-L-Tyrosine (FET): a tracer for differentiation of tumour from inflammation in murine lymph nodes, Eur J Nucl Med, (2002), Vol. 29, p. 1039-1046.

[22] LANGEN, K.J., PAULEIT, D., COENEN, H.H., "3-123I-Iodod-alpha-methyl-L-tyrosine:uptake mechanisms and clinical applications. Nucl Med Biol 29(2002) 625-631.

[23] LAHOUTTE, T., et al., In vitro characterisation of the influx of 3-[^{125}I]-iodo-L-Tyrosine and 2-[^{125}I]-iodo-L-Tyrosine into U266 human myeloma cells : Evidence for system T transport, Nucl Med Biol , Vol 28, Issue 2, (2001), p. 129-134.

[24] LAHOUTTE, T., et al., Increase tumour uptake of 3-[^{123}I]-Iodo-L-alpha-methyl-tyrosine after preloading with amino acids, an in vivo animal imaging study, J Nucl Med, Vol 43(9), (2002), p. 1201-1206.

[25] LANGEN, K.J., et al., 3-[^{123}I]Iodo-alpha-methyltyrosine and [methyl-11C]-methionine uptake in cerebral gliomas: a comparative study using SPECT and PET, J Nucl Med, (1997), Vol. 38, p. 517-522.

[26] LAHOUTTE, T., et al., Comparative biodistribution of iodinated amino acids in rats: selection of the optimal analog for oncologic imaging outside the brain, Nucl Med. (2003), Vol 44 N° 9, 1489-1494.

[27] MERTENS, J., et al., Synthesis, radiosynthesis and in vitro characterisation of [125I]-2-iodo-L-phenylalanine in a R1M rhabdomyosarcoma cell model as a new potential tumour tracer for SPECT, Nucl Med Biol, Vol 31, (2004), p. 739-746.

[28] MERTENS, J., et al., "In Vitro and in Vivo Evaluation of L-2-radioiodo-tyrosine as a new potential tumour tracer for SPECT" J. Labelled Cmp Radiopharm (2001).

[29] KERSEMANS, V., et al., In vivo characterization of 123/125I-2-iodo-L-phenylalanine in an R1M rhabdomyosarcoma athymic mouse model as a potential tumour tracer for SPECT., J Nucl Med. (2005) Mar;46(3):532-9.

[30] MERTENS, J., et al., " In Vivo Evaluation of 2-123I-Tyr and 2-123I-Phe as Tumour Specific Tracers for SPECT". Eur. J. Nucl Med (2002) 29:August, Suppl.1, S76.

[31] MERTENS, J., et al., " New Approach of Cell Uptake Kinetics of L-123I-Tyr and L-123I-Phe, New Potential Tumour tracers for SPECT". Eur. J. Nucl Med (2002) 29: August, Suppl.1, P722.

[32] TAMEMASA, O., GOTO, R., SUZUKI, T., Preferential incorporation of some 14C-labeled D-amino acids into tumour-bearing animals, Gann, Vol. 69, August (1978), p. 517-523.

[33] GOTO, R., SUZUKI, T., TAMEMASA, O., Charateristics of D-Leucine uptake by Mouse Ehrlich cells ascites tumour cells, J. Biochem., Vol. 86, (1979), p. 363-369.

[34] TAKEDA, A., GOTO, R., TAMEMASA, O., CHANEY, J.E., DIGENIS, G.A., Biological evaluation of radiolabelled D-Methionine as a parent compound in potential Nuclear imaging, Radioisotopes, Vol. 33, (1984), p. 213-217.

[35] MERTENS, J., et al., Radioactive labelled D-amino acid analogues, a new perspective for tumour therapy and diagnosis: an in vitro evaluation model, Eur J Nucl Med, Vol 30, supplement 2, august (2003), P530.

[36] KUPCZYK-SUBOTKOWSKA, L., et al., " Derivatives of melphalan designed to enhance drug accumulation in cancer cells" J Drug Target (1997); 4(6):359-70.

COMPARISON OF ^{131}I-TYR^3-OCTREOTATE AND ^{131}I-DOTA-TYR^3-OCTREOTATE: THE EFFECT OF DOTA ON PHARMACOKINETICS AND STABILITY

E.B. DE ARAÚJO, E. MURAMOTO, L.T. NAGAMATI,
J.S. CALDEIRA FILHO, R.M. COUTO, C.P.G. SILVA
Institute of Energetic and Nuclear Research, IPEN-CNEN,
São Paulo, Brazil
Email: ebaraujo@ipen.br

Abstract

The authors compared the biodistribution, and in vivo and in vitro stabilities of ^{131}I-Tyr^3-octreotate and ^{131}I-DOTA-Tyr^3-octreotate. The peptides were radioiodinated by the chloramine T method and high radiochemical yields were obtained (greater than 97%). Both labelled compounds showed high stability when incubated in human plasma at 37°C. The ^{131}I-Tyr^3-octreotate showed significant hepatic uptake and biliary excretion. The biodistribution of ^{131}I-DOTA-Tyr^3-octreotate, however, can be compared with the distribution of radiometal labelled octreotide analogues.

1. INTRODUCTION

The introduction of radiolabelled somatostatin analogues for peptide recetor imaging and peptide receptor radiotherapy of neuroendocrine cancer has provided a primary focus of interest in nuclear medicine. The ^{111}In-DTPA-D-Phe^1-octreotide (OctreoScan) became the first radiopeptide to be routinely used for scintigraphy of somatostatin receptor positive tumours [1].

The introduction of the metal chelator DOTA (1,4,7,10-tetraazacyclododecane-1,4,7,10-tetraacetic acid) initiated a marked improvement in the stability of the radioconjugates, allowing the incorporation of a variety of radionuclides, such as ^{90}Y and ^{177}Lu, for receptor mediated therapy and ^{68}Ga and ^{64}Cu for positron emission tomography [2].

^{90}Y-DOTA-octreotide was tested in several clinical studies for use in treatment [3, 4]. One of the most recent developments is the introduction of ^{177}Lu-DOTA-Tyr^3-octreotate, in which the carboxy terminal threoninol has been replaced with the natural amino acid threonine, yielding a very high SSTR2 affinity [5].

For sst-target diagnosis and radiotherapy, radiohalogens offer a broad spectrum of suitable isotopes for single photon emission tomography (^{123}I),

positron emission tomography (^{18}F) and peptide receptor therapy (^{131}I, ^{125}I and ^{211}At). Consequently, ^{123}I labelled Tyr^3-octreotide was the first compound to be used for the imaging of somatostatine receptor positive tumours [6].

However, the experience gained with radioiodinated sst ligands showed that the diagnostic and therapeutic usefulness of these ligands was limited by their unfavourable biokinetics, in vivo deiodination and resulting dosimetry. Owing to fast hepatic uptake and biliary clearance, most of the tracers showed high abdominal background acitivity and fast blood clearance, leading to low tumour uptake. Additionally, they exhibited low tumour retention, which was often attributed to fast intracellular degradation of the tracers and subsequent extracellularization [7].

In this paper, the authors prepared radioiodinated octreotates, ^{131}I-Tyr^3-octreotate and ^{131}I-DOTA-Tyr^3-octreotate, with high radiochemical yield. Although the DOTA chelating group was not necessary to the radioiodination procedure, the authors evaluated the influence of the chelating group on biodistribution, particularly on hepatic uptake, biliary excretion and renal clearance. Tumour uptake was evaluated in nude mice bearing AR42J tumour.

2. MATERIALS AND METHODS

2.1. Reagents

DOTA-Tyr^3-octreotate was provided from piChem by the IAEA and the Tyr^3-octreotate was purchased from Anaspec (EUA). All other reagents were purchased from Sigma-Aldrich. [^{131}I]NaI was obtained from Nordion (Canada).

2.2. Radiolabelling

Radiolabelling of Tyr^3-octreotate and DOTA-Tyr^3-octreotate with ^{131}I- was performed using the chloramine T method. A solution of 10 μg of peptide in 40 μL of PBS (0.05M phosphate buffered saline, pH7.5) was transferred to the reaction vial. After addition of 10 μL (74–111 MBq) of radioiodine solution and 5 μL of chloramine T solution (1 mg/mL PBS), the cap was carefully stirred and the labelling reaction was allowed to proceed for 3 min at room temperature. To the reaction mixture, 5 μL of sodium metabisulphite solution (2 mg/mL PBS) was introduced as a reducing agent. Different molar peptide to radionuclide ratios were applied to the labelling of DOTA-Tyr^3-octreotate with ^{131}I.

2.3. Quality control

Radiochemical purity was determined by HPLC (Waters) using an RP C18 column (4.2 mm × 50 mm, 5 μm, Waters) with UV (230 nm) and radioactivity (Packard Canberra) detection, flow rate of 0.5 mL/min with a linear gradient of 40–80% (v/v) methanol in 50mM sodium acetate buffer (pH5.5) for 20 min, maintained for another 25 min. Free radioiodine was also determined by horizontal zone electrophoresis (Amersham Pharmacia) on Whatman 1 paper, 0.05M barbital buffer, pH8.6, 300 V, 40 min.

2.4. In vitro stability

The in vitro stabilities of ^{131}I-Tyr^3-octreotate and ^{131}I-DOTA-Tyr^3-octreotate were evaluated after incubation in human plasma at 37°C. Radiochemical purity was determined 1, 4 and 24 h after incubation using the electrophoresis procedure.

2.5. Animal studies

Biodistribution studies of ^{131}I-Tyr^3-octreotate and ^{131}I-DOTA-Tyr^3-octreotate were performed on normal Swiss mice and nude mice bearing AR42J rat pancreatic tumours. About 540 kBq/0.1 mL of the respective radiopharmaceutical were injected into the tail vein. The animals were sacrificed at different time points post-injection and the organs of interest were dissected. Tissue samples were weighed and the radioactivity was measured using a gamma counter (Packard). All experiments were carried out following the principles of laboratory animal care.

3. RESULTS AND DISCUSSION

3.1. Radioiodination

Labelled peptides were obtained with radiochemical purities exceeding 95%, as determined by the electrophoresis method.

The authors investigated different molar peptide to radionuclide ratios in order to obtain mono-iodinated peptides to be applied in the biodistribution studies, considering that the di-iodinated peptide no longer binds to the somatostatin receptor, as previously reported [8].

The HPLC profile of the ^{131}I-DOTA-Tyr^3-octreotate obtained when using a molar peptide to radionuclide ratio of 2.73 (7.4 MBq ^{131}I/μg peptide)

produced only one radiochemical species with a retention time of 22.73 min (Fig.1). When using a molar peptide to radionuclide ratio of 0.54 (37 MBq ^{131}I/μg peptide), a second radiochemical species can be observed in the HPLC profile (Fig. 2), with a retention time of 24.9 min, probably related to the di-iodinated form of the peptide.

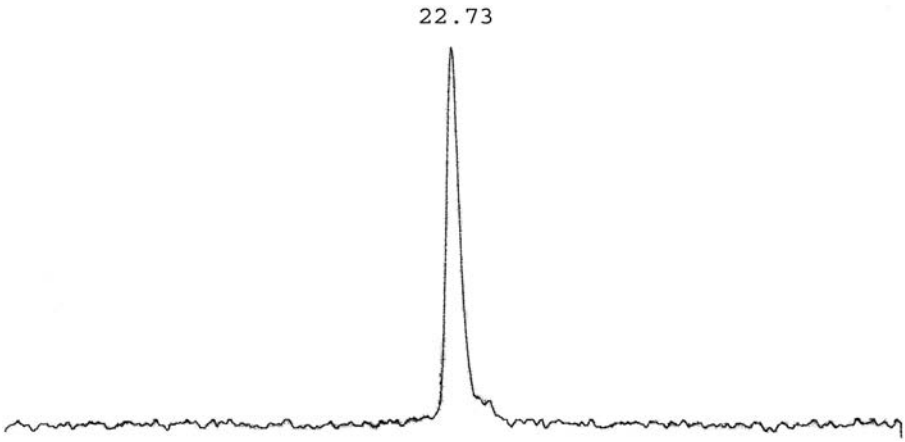

FIG. 1. HPLC profile of ^{131}I –DOTA-Tyr^3-octreotate molar peptide to radionuclide ratio of 2.73 (7.4 MBq/μg).

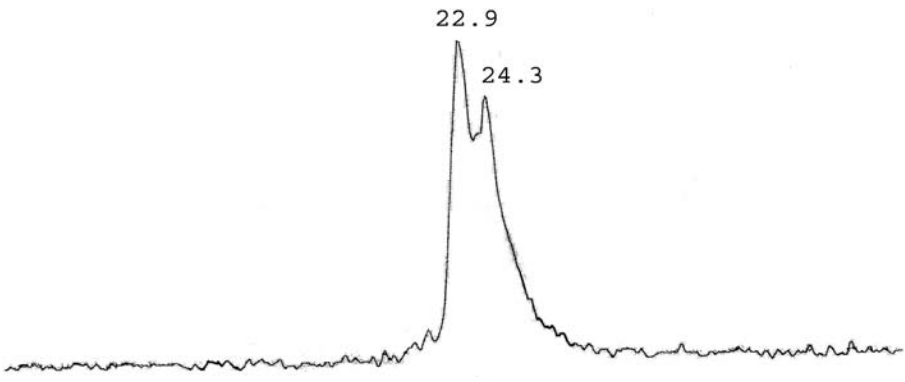

FIG. 2. HPLC profile of ^{131}I-DOTA-Tyr^3-octreotate molar peptide to radionuclide ratio of 0.54 (37 MBq/μg).

3.2. In vitro studies

In vitro studies show clearly the high level of stability of the iodinated ligands even after 24 h of incubation in human plasma (Table 1).

3.3. Biodistribution studies

Biological distribution studies were performed with radiolabelled peptides obtained in a peptide to radionuclide ratio of 2.73 with radiochemical purity exceeding 97%, which obviated the need to undertake the SepPak purification procedure. However, as with other radioiodinated peptides and proteins labelled on constituent tyrosine residues, it was important to study the possibility of dehalogenation in vivo.

The biodistribution data for ^{131}I-Tyr^3-octreotate (Table 2) was similar to that reported for ^{123}I-Tyr^3-octreotide in rats [9] and for ^{125}I-Tyr^3-octreotide and ^{125}I-Tyr^3-octreotate in nude mice [7]. The ^{131}I-Tyr^3-octreotate (Table 2) was extracted rapidly from the blood via hepatobiliary excretion, resulting in high liver uptake (2.28 ± 0.78%ID/g 1 h p.i.) and increasing intestinal uptake to 1 and 4 h p.i. (12.30 ± 4.36%ID/g for the small intestine and 14.85 ± 0.83%ID/g for the large intestine). The ^{131}I-DOTA-Tyr^3-octreotate was predominantly excreted via the kidneys. Nevertheless, renal activity accumulation for this compound was similar to that of ^{131}I-Tyr^3-octreotate.

TABLE 1. IN VITRO STABILITY OF ^{131}I-Tyr^3-OCTREOTATE AND ^{131}I-DOTA-Tyr^3-OCTREOTATE IN HUMAN PLASMA AT 37°C

Labelled peptide	Radiochemical purity (%)			
	Immediately	1 h	4 h	24 h
^{131}I-Tyr^3-octreotate	98.42 ± 0.32	98.43 ± 0.53	96.79 ± 1.01	95.76 ± 0.10
^{131}I-DOTA-Tyr^3-octreotate	95.41 ± 0.51	93.80 ± 0.80	92.40 ± 0.55	91.05 ± 0.55

TABLE 2. BIODISTRIBUTION OF ^{131}I-Tyr^3-OCTREOTATE AND ^{131}I-DOTA-Tyr^3-OCTREOTATE IN NORMAL SWISS MICE

Tissue	^{131}I-Tyr^3-octreotate Dose/g (%)			^{131}I-DOTA-Tyr^3-octreotate Dose/g (%)		
	1 h	4 h	24 h	1 h	4 h	24 h
Total blood	3.17 ± 0.32	0.81 ± 0.12	0.103 ± 0.006	2.56 ± 0.27	1.19 ± 0.13	0.020 ± 0.004
Liver	2.28 ± 0.78	0.42 ± 0.06	0.161 ± 0.034	0.70 ± 0.05	0.36 ± 0.05	0.088 ± 0.018
Spleen	0.76 ± 0.25	0.37 ± 0.11	0.114 ± 0.044	0.57 ± 0.06	0.27 ± 0.04	0.057 ± 0.018
Stomach	3.51 ± 1.67	1.94 ± 1.02	0.093 ± 0.032	3.32 ± 0.45	2.02 ± 0.59	0.19 ± 0.05
Int. (small)	12.30 ± 4.36	1.33 ± 0.96	0.045 ± 0.015	1.48 ± 0.13	0.57 ± 0.12	0.41 ± 0.19
Int. (large)	0.96 ± 0.58	14.85 ± 0.83	0.103 ± 0.032	0.44 ± 0.08	2.18 ± 0.25	1.90 ± 0.82
Kidney	12.54 ± 0.51	9.77 ± 3.46	3.752 ± 1.183	12.18 ± 0.86	9.86 ± 1.00	1.60 ± 0.22
Muscle	0.47 ± 0.24	0.13 ± 0.06	0.022 ± 0.002	0.26 ± 0.02	0.13 ± 0.03	0.03 ± 0.01
Brain	0.08 ± 0.01	0.024 ± 0.003	0.007 ± 0.001	0.08 ± 0.03	0.04 ± 0.010	0.006 ± 0.003
Heart	0.66 ± 0.11	0.20 ± 0.08	0.049 ± 0.020	0.50 ± 0.10	0.20 ± 0.05	0.019 ± 0.003
Lung	1.59 ± 0.40	0.45 ± 0.14	0.013 ± 0.021	0.80 ± 0.42	0.49 ± 0.22	0.052 ± 0.005
Thyroid *	0.49 ± 0.07	1.04 ± 0.20	0.878 ± 0.304	0.55 ± 0.10	1.23 ± 0.17	0.29 ± 0.06
Adrenals*	0.020 ± 0.007	0.007 ± 0.004	0.002 ± 0.0002	0.012 ± 0.003	0.008 ± 0.001	0.0014 ± 0.0005
Pancreas	0.87 ± 0.17	0.23 ± 0.05	0.023 ± 0.008	1.11 ± 0.52	0.79 ± 0.12	0.030 ± 0.010

* % dose organ; values are mean ± SD (n = 6).

Tracer uptake in the pancreas, tumour and adrenal were similar for both compounds ($p = 0.01$) after 1 h p.i. (Table 3). Tumour to blood ratios at 1 h p.i. were similar for both compounds but tumour to liver and tumour to intestine ratios were superior to ^{131}I-DOTA-Tyr^3-octreotate (Table 4).

Both labelled peptides presented low uptake in thyroid, which suggests low in vivo dehalogenation of the compounds.

The distribution pattern of ^{131}I-Tyr^3-octreotate was similar to that reported for ^{123}I-Tyr^3-octreotide in rats [9], with relatively high activity levels in liver and intestine. The biodistribution of ^{131}I-DOTA-Tyr^3-octreotate, however, can be compared with the distribution of radiometal labelled octreotide analogues in mice [10, 11].

TABLE 3. BIODISTRIBUTION OF ^{131}I-Tyr^3-OCTREOTATE AND ^{131}I-DOTA-Tyr^3-OCTREOTATE IN NUDE MICE BEARING AR42J RAT PANCREATIC TUMOURS

Tissue	^{131}I-Tyr^3-octreotate Dose/g (%)		^{131}I-DOTA-Tyr^3-octreotate Dose/g (%)	
	1 h	24 h	1 h	24 h
Total blood	2.12 ± 0.49	0.085 ± 0.035	2.93 ± 0.32	0.124 ± 0.006
Liver	2.07 ± 0.73	0.17 ± 0.03	1.34 ± 0.09	0.149 ± 0.009
Int. (small)	8.75 ± 1.87	0.061 ± 0.001	2.78 ± 0.60	0.067 ± 0.022
Muscle	0.37 ± 0.12	0.024 ± 0.009	0.42 ± 0.21	0.039 ± 0.013
Thyroid *	0.28 ± 0.13	0.516 ± 0.031	0.54 ± 0.17	1.19 ± 0.31
Adrenals*	0.021 ± 0.010	0.002 ± 0.001	0.018 ± 0.004	0.003 ± 0.001
Pancreas	0.78 ± 0.05	0.038 ± 0.001	1.15 ± 0.29	0.047 ± 0.013
Tumour	1.10 ± 0.45	0.18 ± 0.08	1.73 ± 0.01	0.13 ± 0.01

* % dose organ; values are mean ± SD (n = 3).

TABLE 4. TUMOUR TO TISSUE RATIOS AT 1 h p.i. OF ^{131}I-Tyr^3-OCTREOTATE AND ^{131}I-DOTA-Tyr^3-OCTREOTATE IN NUDE MICE BEARING AR42J RAT PANCREATIC TUMOURS

Ratio	^{131}I-Tyr^3-octreotate	^{131}I-DOTA-Tyr^3-octreotate
Tumour to blood	0.51	0.59
Tumour to liver	0.53	1.29
Tumour to intestine (small)	0.13	0.62
Tumour to muscle	2.97	4.12

Although DOTA is not necessary for the radioiodination procedure, the chelating group seems to decrease the lipophilicity as evidenced by the low uptake in liver and intestines of ^{131}I-DOTA-Tyr^3-octreotate. In contrast to ^{131}I-Tyr^3-octreotate, which was eliminated via the hepatobiliary route, the DOTA analogue was predominantly cleared by the kidneys. The ^{131}I-DOTA-Tyr^3-octreotate also presented better tumour to non-tumour ratios, especially for liver and intestine, which are well known to be critical organs for scintigraphy (Table 4).

Radiometal labelled somatostatin derivatives often show longer tumour retention, compared to radioiodinated somatostatin analogues, due to intracellular trapping of the radionuclide or radiolabelled metabolites [7]. Despite this, the results obtained in this study with the ^{131}I-DOTA-Tyr^3-octreotate were promising and suggest the applicability of the compound for SPECT imaging or therapy using, respectively, ^{123}I or ^{131}I in labelling procedures.

ACKNOWLEDGEMENTS

This work was supported by IPEN-CNEN and IAEA.

REFERENCES

[1] KRENNING, E.P., et al., Somatostatin receptor scintigraphy with [^{111}In-DTPA-D-Phe^1]-octreotide in man: metabolism, dosimetry and comparison with [^{123}I-Tyr^3]-octreotide, J. Nucl. Med., **33** (1992) 652-658.

[2] CARSTEN, G., BERTRAN, W., Somatostatin receptor targeting for tumor imaging and therapy, Ann. N.Y. Acad. Sci., **1014** (2004) 258-264.

[3] WALDER, C., et al., Tumor response and clinical benefit in neuroendocrine tumors after 7.4 GBq ^{90}Y-DOTATOC, J. Nucl. Med., **43** (2002) 610-616.

[4] BODEI, L., et al., Receptor-mediated radionuclide therapy with ^{90}Y-DOTATOC in association with amino acid infusion: a phase I study, Eur. J. Nucl. Med., **30** (2003) 207-216.

[5] KWEKKEBOOM, D.J., et al., Treatment of patients with gastro-entero-pancreatic (GEP) tumours with the novel radiolabelled somatostatin analogue [^{177}Lu-DOTA0,Tyr^3]octreotate, Eur. J. Nucl. Med., **30** (2003) 417-422.

[6] KRENNING, E.P., et al., Localisation of endocrine-related tumours with radioiodinated analogue os somatostatin, Lancet, **1** (1989) 242-244.

[7] WESTER, H.J., et al., Comparison of radioiodinated TOC, TOCA and Mtr-TOCA: the effect of carbohidration on the pharmacokinetics, Eur. J. Nucl. Med., **29** (2002) 28-338.

[8] BAKKER, W.H., et al., Iodine-131 labelled octreotide:not an option for somatostatin receptor therapy, Eur. J. Nucl. Med., **23** (1996) 775-781.

[9] BAKKER, W.H., et al., Receptor scintigraphy with a radioiodinated somatostatin analogue: Radiolabeling, purification, biologic activity, and *in vivo* application in animals, J. Nucl. Med., **31** (1990) 1501-1509.

[10] AKIZAWA, H., et al., Renal metabolism of ^{111}In-DTPA-D-Phe^{1}-octreotide *in vivo*, Bioconjugate Chem., **9** (1998) 662-670.

[11] LEWIS, J.S., et al., *In vitro* and *in vivo* evaluation of ^{64}Cu-TETA-Tyr^{3}-octreotate. A new somatostatin analog with improved target tissue uptake, Nucl. Med. Biol., **26** (1999) 267-273.

IODINE LABELLED DIETHYLSTILBESTROL (DES) OF HIGH SPECIFIC ACTIVITY: A POTENTIAL RADIOPHARMACEUTICAL FOR THERAPY OF ESTROGEN RECEPTOR POSITIVE TUMOURS AND THEIR METASTASES?

T. FISCHER, H. SCHICHA, K. SCHOMÄCKER
Department of Nuclear Medicine,
University of Cologne,
Germany
Email: thomas.fischer@uk-koeln.de

Abstract

Diethylstilbestrol (DES) is a well-known, non-steroidal estrogen with higher affinity to the estrogen receptor (ER) than the natural hormone estradiol itself. Radioactively labelled DES would be a useful tool for therapy of ER positive mamma carcinomas and their metastases. Particularly with Auger electron emitters, high cytotoxic potential combined with only slight side effects can be expected. In the present work, DES was labelled by a new method, which allows the synthesis of *I-DES with a higher yield and higher specific activity than achievable with former methods. Binding affinity and cytotoxic effects on MCF-7 mamma carcinoma cells, depending on radioactivity concentration applied and location of decay (nucleus or cell surface), were tested. Different iodine isotopes (^{123}I, ^{125}I, ^{131}I) bound to DES or in the form of iodide were compared with regard to apoptosis, necrosis and viability. Also, the radiation protective effects of the radical scavenger vitamin C were tested. In animal experiments with tumour bearing mice the biodistribution of ^{123}I-DES was investigated. Results showed significantly lower viability of cells exposed to the Auger electron emitters ^{123}I and ^{125}I than those tested in the presence of the ß emitter ^{131}I. All radionuclides induced apoptosis. The amount of apoptosis was different for all nuclides: ^{131}I-DES < ^{125}I-DES < ^{123}I-DES. In the form of iodide, no increase of apoptosis could be detected. Necrosis did not occur in the radioactivity concentration range observed, only secondary necrosis — a late phase of apoptosis — was found. In the presence of vitamin C, a significant reduction of apoptosis was observed, which points to an induction mechanism mainly via free radicals. The ^{123}I-DES showed a high tumour uptake of 42% ID/g in mice, which could be blocked by co-application of 'cold' estrogens. Tumour/background ratios were excellent (tumour/blood = 16.5, tumour/liver = 7.8). *I-DES, in connection with Auger electron emitting radionuclides, seems to be a favourable candidate with a high cytotoxic potential for therapy of ER positive tumours and their metastases.

1. INTRODUCTION

The most common methods for therapy of mamma carcinomas involve the surgical removal of the tumour and/or hormone therapy. If these treatments are not possible (e.g. small metastases), proliferation inhibiting therapy forms such as chemotherapy and radiation, which cause several unpleasant side effects, are used. Therefore, it would be very advantageous to find other, more specific therapy options.

Radioactive labelled estrogens, especially in connection with Auger electron emitters, which have only a very short range (1–10 nm) of radiation, are excellent candidates with which to achieve high specific cytotoxicity, in combination with a low degree of side effects [1–5]. Until the 1970s, the use of Auger electron emitters in cancer therapy was discussed [6] and their impressive cytotoxic potential could be demonstrated [7–22].

Diethylstilbestrol (3,4-Di-(4'-hydroxyphenyl)-hexene-3) (DES) is a well-known, non-steroidal estrogen [23] with higher affinity to estrogen receptor (ER) than the natural hormone estradiol itself [24, 25]. Therefore, radioactively labelled DES would be a promising compound for therapy of ER positive mamma carcinomas and their metastases. Certainly, DES was radioiodinated years ago and its biodistribution was investigated [26–32]. Because of the low specific activity, biodistribution data were disappointing. Recently, however, a modified radioiodination method for DES has been published [33], which allows synthesis of *I-DES with much higher specific activity and radiochemical purity than achievable with former methods. Its affinity for ER remained high after labelling [33].

For testing its cytotoxic effects on MCF-7 mamma carcinoma cells, different iodine isotopes bound to DES or in the form of iodide were compared with regard to apoptosis, necrosis and viability. Last but not the least, the first animal experiments with tumour bearing mice were carried out.

2. MATERIALS AND METHODS

DES was iodinated by chloramin T in methanolic solution according to the literature [33]. Purification and quality control were carried out with reversed phase HPLC (column: Hypersil ODS, 250 mm × 4 mm, 10 µm, eluent A: methanol G, eluent B: water G, gradient: 20% A to 70% A within 5 min, flow: 1 mL/min, UV detection: 254 nm).

MCF-7 tumour cells (DKFZ, Heidelberg, Germany) were cultivated in Dulbecco's Modified Eagle Medium (GIBCO, Grand Island, New York), as

well as Dulbecco's Medium without Phenol Red. The cells' ER status was evaluated with the ER-ICA test from ABBOTT.

For investigation of cell viability, the cells were incubated with a tetrazolium salt (cell proliferation reagent WST-1, Roche Diagnostics), which was cleaved by succinat tetrazolium reductase, an enzyme of the respiratory chain in the membrane of mitochondria. The reaction product was a coloured formazan, which could be measured by optical methods. For the experiments, 100 µL Dulbecco's Modified Eagle Medium containing 1×10^4 MCF-7-cells was transferred to each well of a microtitre plate (MTP) with a flat bottom. One row was kept empty. The cells were incubated in the MTP for 24 h at 37°C and under the above mentioned atmospheric conditions. Then to each well, 100 µL *I-DES or *I-iodide of different concentrations between 0.1 MBq/mL and 5 MBq/mL was added. One row of eight wells was only filled with 100 µL of medium for control. The row that was kept without cells was now filled with 200 µL medium in each well. All set-ups were made fourfold to eightfold. The cells were now incubated for 18 h under the mentioned conditions and then mixed with 20 µL WST-1-reagent. After 2 h incubation at 37°C, the extinction of the samples was determined with the ELISA reader at 450 nm (reference filter: 620 nm).

For determination of apoptosis or necrosis, the Cell Death Detection ELISA from Roche Diagnostics was used. The amount of apoptotic cells in comparison to a control group can be measured by detection of DNA fragments by special antibodies included in the kit. According to whether detection of those fragments occurs before or after cell lysis, it will be possible to distinguish between necrosis and apoptosis. Measured DNA fragments in the supernatant before cell lysis were due to apoptosis, detected DNA fragments after lysis indicated necrosis. In the experiment, 100 µL DMEM containing 1×10^4 MCF-7 cells was transferred to each well of a flat bottomed MTP. The cells were incubated in the MTP for 24 h at 37°C and under the above mentioned atmospheric conditions. Samples, that should be tested in the presence of vitamin C, were mixed with 20 µL of ascorbic acid solution (0.01 mg/mL or 0.1 mg/mL giving 0.001 mg/mL or 0.01 mg/mL in the well). Then, to each well (in the presence or absence of vitamin C) 100 µL *I-DES or *I-iodide in concentrations of between 0.1 and 5 MBq/mL was added. Eight wells were filled with 100 µL of medium instead of radioactive material. All other samples were carried out fourfold to eightfold.

The MTPs were incubated for 18 h under the usual conditions and then centrifuged at 200g. A 20 µL sample of each liquid was transferred for measurement of the amount of necrosis to another streptavidine coated MTP from the Cell Death Detection ELISA^{PLUS} kit. Now, the residual liquid in the first MTP was carefully removed and 200 µL of lysis buffer placed instead in

every well. After 30 min incubation at room temperature, the plate was centrifuged again at 200g and then 20 µL of the liquid was transferred to a second streptavidine coated MTP for determination of apoptosis. For background measurement, some wells were filled with 20 µL of incubation buffer. In addition, some positive controls were also carried out.

Animal experiments were carried out with male tumour bearing DBA/2 mice (Charles River). Three groups of animals (n = 5 in each group) were injected with: (a) 1.5 MBq ^{123}I-DES, (b) 7 µmol DES-2-P + 2 MBq ^{123}I-DES, (c) 7 µmol Estradiol + 2 MBq ^{123}I-DES. Three hours after IV injection, the animals were sacrificed and organs, tissues and blood were measured in a well counter.

3. RESULTS

In Figs 1–3, the relative metabolic activity of succinat tetrazolium reductase (an enzyme of the respiratory chain in mitochondria membrane) is presented, depending on the applied *I-DES or *I-iodide concentration. For all three nuclides, a significant difference can be observed between *I-DES and *I-iodide in the declining cell viability at increasing radioactivity concentrations. When *I-DES labelled with the Auger electron emitters is used, the viability of MCF-7 cells decreases very rapidly according to increasing radioactivity

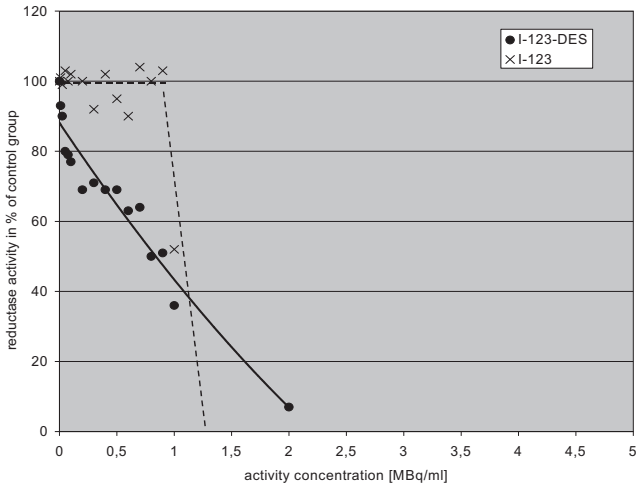

FIG. 1. Relative metabolic succinat tetrazolium reductase activity in MCF-7 cells after 18 h incubation with ^{123}I-DES or ^{123}I^{-} in per cent enzyme activity in control group not exposed to radioactivity (n = 8 per point, SD = ±15–20%).

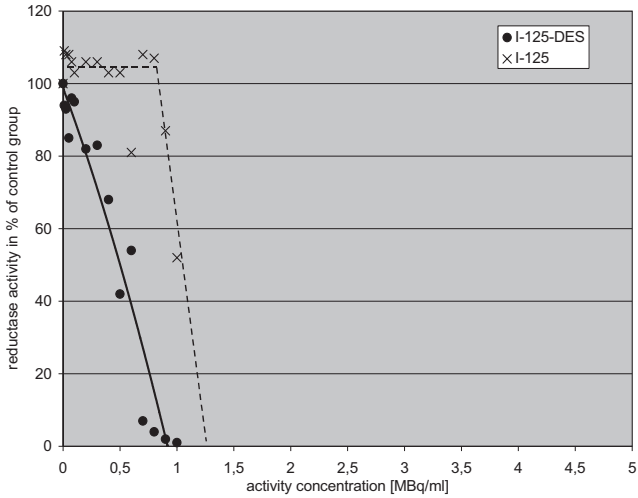

FIG. 2. Relative metabolic succinat tetrazolium reductase activity in MCF-7 cells after 18 h incubation with ^{125}I-DES or ^{125}I$^-$ in percent enzyme activity in control group not exposed to radioactivity (n = 8 per point, SD = ±15 – 20%).

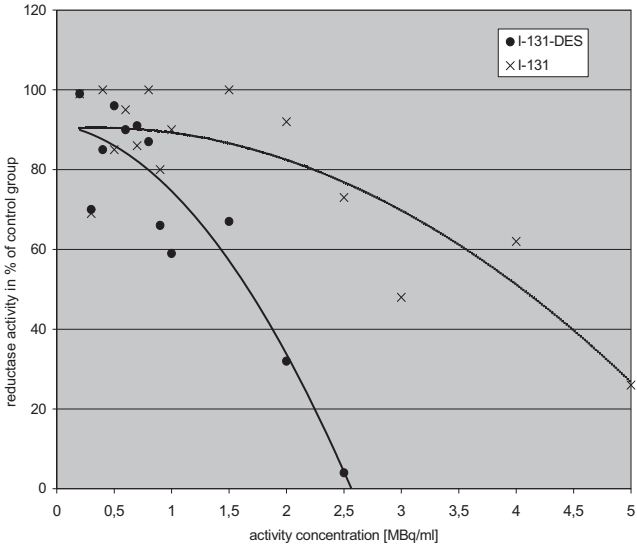

FIG. 3. Relative metabolic succinat tetrazolium reductase activity in MCF-7 cells after 18 h incubation with ^{131}I-DES or ^{131}I$^-$ in per cent enzyme activity in control group not exposed to radioactivity (n = 8 per point, SD = ±15–20%).

concentration. To compare these different gradients of viability decrease, the value V_{50} can be introduced. It is the activity concentration at which the viability decreases to 50% of the initial viability in the control group. The V_{50} values for the Auger electron emitters bound to DES were $V_{50}(^{123}\text{I-DES}) = 0.8$ MBq/mL and $V_{50}(^{125}\text{I-DES}) = 0.5$ MBq/mL. A little less effective is the ß emitter with $V_{50}(^{131}\text{I-DES}) = 1.7$ MBq/mL and the highest concentrations are needed for comparable effects with the nuclides applied in the form of iodide ($V_{50}(^{123}\text{I-iodide}) \approx 1$ MBq/mL, $V_{50}(^{125}\text{I-iodide}) \approx 1$ MBq/mL, and $V_{50}(^{131}\text{I-iodide}) \approx 4$ MBq/mL.

Apoptosis increased (see Figs 4–6) with rising activity concentrations up to 35-fold for ^{123}I-DES, 10-fold for ^{125}I-DES and threefold for ^{131}I-DES compared with a control group. Necrosis increased parallel to apoptosis (results not shown). Presumably this was not really necrosis, but a late phase of apoptosis.

Animal experiments (Fig. 7) showed high specific uptake in prostate and tumour, which could be blocked by estrogen or Honvan (DES-2-P).

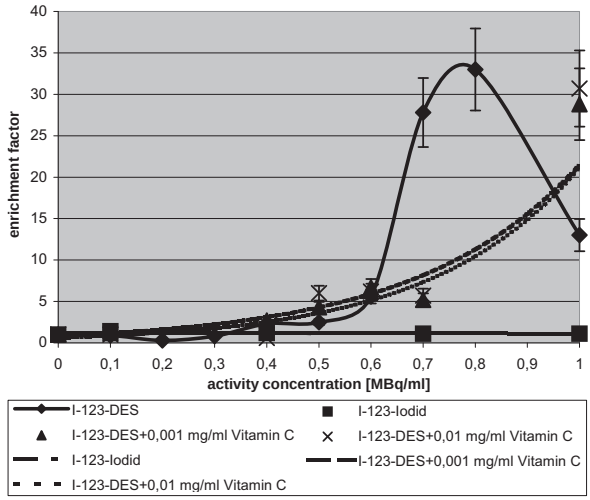

FIG. 4. Apoptosis accumulation factors of MCF-7 cells incubated with different radioactivity concentrations of ^{123}I-DES or ^{123}I-iodide in comparison to cells of an untreated control group (n = 4–8 per point, incubation time: 18 h, SD = ±15%).

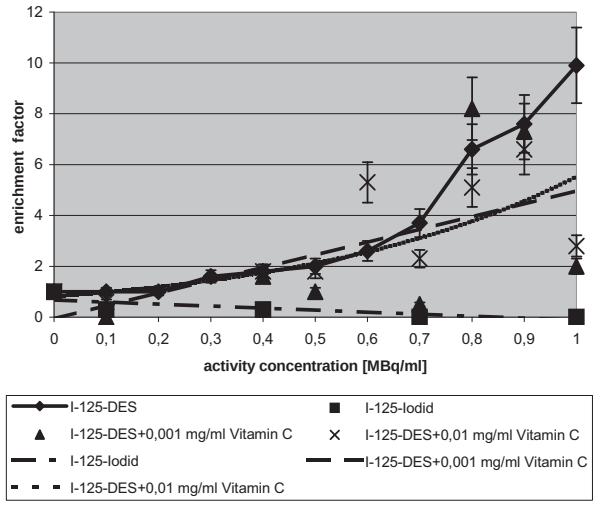

FIG. 5. Apoptosis accumulation factors of MCF-7 cells incubated with different radioactivity concentrations of ^{125}I-DES or ^{125}I-iodide in comparison to cells of an untreated control group (n = 4–8 per point, incubation time: 18 h, SD = ±15%).

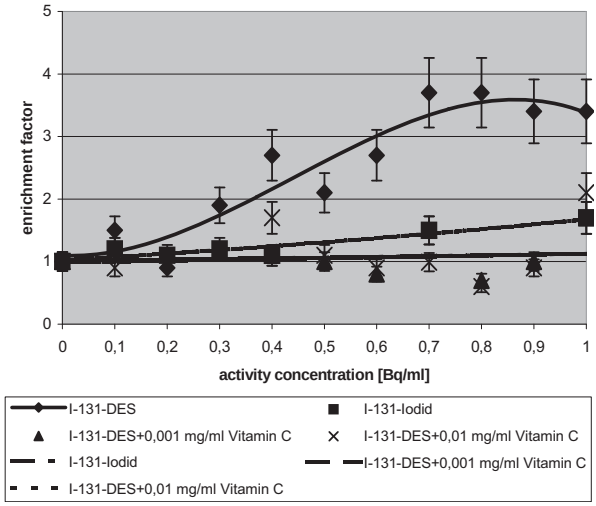

FIG. 6. Apoptosis accumulation factors of MCF-7 cells incubated with different radioactivity concentrations of ^{131}I-DES or ^{131}I-iodide in comparison to cells of an untreated control group (n = 4–8 per point, incubation time: 18 h, SD = ±15%).

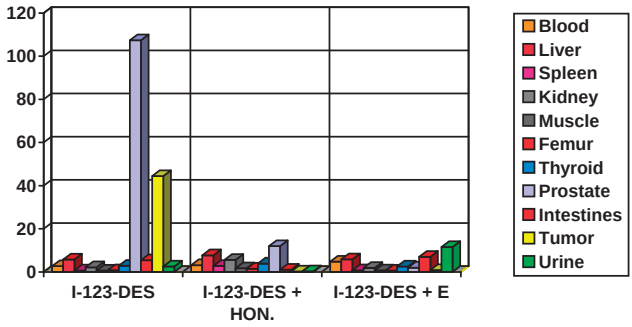

FIG. 7. Biodistribution (in %ID/g) of ^{123}I-DES in tumour bearing male mice with and without co-application of HONVAN™ (DES-2P) or estradiol.

4. CONCLUSIONS

Radioactively labelled DES is a promising compound for therapy of ER positive mamma carcinomas and their metastases. This compound showed, in vitro, a high cytotoxic potential to destroy ER positive tumour cells very specifically. Biodistribution experiments were also very encouraging.

REFERENCES

[1] BURKI, H.J., et al., Inactivation of mammalian cells after disintegrations of ^{3}H or ^{125}I in cell DNA at –196°C, Int. J. Radiat. Biol. **24** (1973) 363.

[2] CHAN, P.C., et al., The radiotoxicity of iodine-125 in mammalian cells. II. A comparative study on cell survival and cytogenetic response to I-125-UdR, I-131-UdR and H-3-TdR, Radiat. Res. **67** (1976) 332.

[3] ADELSTEIN, S.J., The Auger process: a therapeutic promise? Am. J. Roentgen **160** (1993) 707.

[4] SCHARL, A., et al., Rezeptor-vermittelte Anreicherung des intravenös applizierten radiotoxischen Östrogens 16alpha-[^{125}J]Jod-Östradiol-17beta im Rattenuterus, TumorDiagnostik&Therapie **15** (1994) 240.

[5] O'DONOGHUE, J.A., et al., Targeted radiotherapy using Auger electron emitters, Phys. Med. Biol. **41** (1996) 1973.

[6] FEINENDEGEN, L.E., Biological damage from the Auger effect, possible benefits, Radiat. Environ. Biophys. **12** (1975) 85.

[7] AHNSTRÖM, G., et al., On the killing and mutagenic action in E. coli associated with Auger effect during ^{125}I decay, Mutat. Res. **10** (1970) 247.

[8] BLOOMER, W.D., et al., 5-(I-125)-iododeoxyuridine as prototype for radionuclide therapy with Auger emitters, Nature (London) **265** (1977) 620.
[9] BLOOMER, W.D., et al., 5-(I-125)-iododeoxyuridine and the Auger effect: biological consequences and implications for therapy, Pathobio. Annu. **8** (1978) 407.
[10] BLOOMER, W.D., et al., Iodine-125-labelled tamoxifen is differentially cytotoxic to cells containing estrogen receptors, Int. J. Radiat. Biol. **38** (1980) 197.
[11] BLOOMER, W.D., et al., The role of subcellular localization in assessing the cytotoxicity of labeled iododeoxyuridine, iodotamoxifen, and iodoantipyrine, J. Radioanal. Chem. **65** (1981) 209.
[12] BLOOMER, W.D., et al., Iodine-125 cytotoxicity: implications for therapy and estimation of radiation risk, Int. J. Nucl. Med. Biol. **8** (1981) 171.
[13] BLOOMER, W.D., et al., Therapeutic implications of iodine-125 cytotoxicity, Int. J. Radiat. Oncol. Biol. Phys. **8** (1982) 1903.
[14] BLOOMER, W.D., et al., Estrogen receptor-mediated cytotoxicity using I-125, J. Cell Biochem. **21** (1983) 39.
[15] BRADLEY, E.W., et al., The radiotoxicity of iodine-125 in mammalian cells. I. Effects on the survival curve of radioiodine incorporated into DNA, Radiat. Res. **4** (1975) 555.
[16] FEINENDEGEN, L.E., et al., DNA strand breakage and repair in human kidney cells after exposure to incorporated iodine-125 and cobalt-60 ?-rays, Curr. Top. Radiat. Res. **12** (1977) 436.
[17] DESOMBRE, E.R., et al., Therapy of estrogen receptor-positive micrometastases in the peritoneal cavity with Auger-electron-emitting estrogens - theoretical and practical considerations, Acta Oncol. **39** (2000) 659.
[18] KASSIS, A.I., et al., Kinetics of uptake, retention, and radiocytotoxicity of I-125 IUdR in mammalian cells: implication of localized energy deposition by Auger processes, Radiat. Res. **109** (1987) 78.
[19] KRISCH, R.E., Lethal effects of I-125 decay by electron capture in Escherichia coli and bacteriophage T1, Int. J. Radiat. Biol. **21** (1972) 167.
[20] KRISCH, R.E., et al., Further studies of DNA damage and lethality from the decay of iodine-125 in bacteriophages, Int. J. Radiat. Biol. **27** (1975) 553.
[21] SASTRY, K.S.R., Biological effects of the Auger emitter iodine-125: a review. Report No 1 of AAPM Nuclear Task Group No 6, Med. Phys. **19** (1992) 1361.
[22] SCHOMÄCKER, K., et al., Die Kinetik von rezeptorvermittelter Radiotoxizität des 16?-[^{125}I]-Iodöstradiol-3,17?, Nuklearmedizin **37** (1998), 134.
[23] DODDS, E.C., et al., Estrogenic activity of certain synthetic compounds, Nature (London) **141** (1938) 247.
[24] LIEBERMAN, M.E., et al., An estrogen receptor model to describe the regulation of prolactin synthesis by antiestrogens *in vitro*, J. Biol. Chem. **258** (1983) 4741.
[25] KORACH, K.S., et al., Estrogen receptor stereochemistry: ligand binding and hormonal responsiveness, Steroids **56** (1991) 263.
[26] TUBIS, M., et al., The preparation of ^{131}I labeled diethylstilbestrol diphosphate and its potential use in nuclear medicine, Nucl. Med. **5** (1967) 1.

[27] TUBIS, M., et al., The distribution of ^{131}I labeled diethylstilbestrol diphosphate in animals and men with observations on its potential use as a scanning agent of the prostate, Nucl. Med. **5** (1967) 184.

[28] MENDE, T., et al., Experimentelle Untersuchungen über die Verteilung von intravenös injiziertem jodmarkiertem Cytonal (Diäthylstilböstroldiphosphat), Z. Urol. u. Nephrol. **71** (1978) 529.

[29] MENDE, T., et al., Verteilung von Jod-markiertem Diäthylstilböstroldiphosphat nach intravenöser Injektion, Gynäk. Rdsch. **19** (1979) 30.

[30] MELLER-REHBEIN, B., et al., ^{123}I-Diethystilbestrolphophate-a potential tracer for receptorimaging and therapy ? Eur. J. Nucl. Med. **21** (1994) 878 (abstract).

[31] SCHOMÄCKER, K., et al., "Investigations into biokinetics of I-123 Diethylstilbestrol phosphate in tumour-bearing mice", Radioactive Isotopes in Clinical Medicine and Research (Bergmann H, Sinzinger H, eds). Birkhäuser Verlag, Basel (1997) 333-342.

[32] SCHOMÄCKER, K., et al., Biokinetics of I-123-Diethylstilbestrol (DES) in mamma-carcinoma bearing mice. J. Nucl. Med. **40** (1999) 100P (abstract).

[33] FISCHER, T., et al., Labelling, purification, and receptor affinity of radioactive iododiethylstilbestrol (*I-DES) with high specific activity and first structure analysis with ^{nat}I-DES, J. Labelled Compd. Radiopharm. **47** (2004) 669.

^{18}F RADIOPHARMACEUTICALS AND AUTOMATION OF SYNTHESIS

(Session 12)

Chairpersons

V.W. PIKE
United States of America

D. SOLOVIEV
Switzerland

^{18}F BASED RADIOPHARMACEUTICALS AND AUTOMATION OF SYNTHESIS
New ^{18}F radiopharmaceuticals

P.K. GARG, S. GARG
Department of Radiological Sciences,
Wake Forest University Medical Center,
Winston Salem, North Carolina,
United States of America
Email: pgarg@wfubmc.edu

Abstract

Fluorine-18 is one of the most commonly used positron emitting isotopes for clinical and research needs with a physical half-life of 110 min. PET isotopes deposit higher radiation absorbed dose than nuclear medicine isotopes. Because of their relatively short half-life, larger quantities of these isotopes are used at the start of synthesis. Therefore, increased shielding and remote automated synthesis are essential for their safe handling. Unlike other radiopharmaceuticals, it is not practical to produce PET radiopharmaceuticals at a central location for subsequent distribution to clinical and research facilities around the country. This limitation compels various academic and research facilities to manufacture their own PET radiopharmaceuticals for in-house use. For multiple reasons, ^{18}F fluorodeoxyglucose ([^{18}F]FDG) is one of the most commonly used radiopharmaceuticals. The synthesis of [^{18}F]FDG has been optimized and automated, thus allowing independent laboratories to produce this radiopharmaceutical safely. Nonetheless, these laboratories should acquire resources and expertise to fulfil ever increasing regulatory requirements for the safe production and usage of PET radiopharmaceuticals. In addition to [^{18}F]FDG, a wide array of new and novel radiotracers is being developed to explore various biological processes. This paper emphasizes the fact that it is possible to accomplish research and fulfil clinical needs within an academic setting with modest resources. A careful assessment of the need for due diligence in radiation safety issues is very important for the longevity of any PET research endeavour.

Among various positron emitting isotopes, ^{18}F has gained wider popularity. This is largely because of its favourable physical half-life (110 min), allowing multistep synthesis and the capability to transport labelled radiotracer to sites remote from the synthesis laboratory and cyclotron facilities. Continued efforts in developing novel and innovative isotope production targetry now allow production of large quantitites of ^{18}F fluoride, which in turn makes it practical to produce multicurie quantities of ^{18}F fluorodeoxyglucose ([^{18}F]FDG). This advancement eased the work load and beam time on the

cyclotron while meeting the increased clinical demands. Production of larger batches of [^{18}F]FDG also helped in reducing the overall cost of producing this radiopharmaceutical.

Despite a large inventory of radiopharmaceuticals for positron emission tomography (PET), [^{18}F]FDG remains the leading radiopharmaceutical for oncology, and cardiac and neurological applications. Although demand for [^{18}F]FDG depends on the patient load and clinical practices, an average busy PET scanning facility may require ~5–15 doses of [^{18}F]FDG. Because of the short half-life of ^{18}F ($T_{1/2}$ = 110 min), it is not practical to cover the clinical needs for an entire day from one production batch of [^{18}F]FDG. Therefore, production of multiple batches per day may be essential. Currently, a typical [^{18}F]FDG production laboratory may utilize in excess of 3000 mCi of ^{18}F fluoride, whereas laboratories with smaller [^{18}F]FDG consumption may use 200–1000 mCi of ^{18}F fluoride isotope. Safe and effective handling of such large amounts of radioisotopes mandates careful design of the laboratory and procurement of necessary equipment and accessories. The automated synthesis of [^{18}F]FDG is well described and several automated synthesis modules are now available on the market. Nonethelesss, a careful assessment of compatibility of these modules with local expertise and needs is important.

Currently, [^{18}F]FDG plays a significant role in PET imaging. The future of PET depends on the availability of additional radiopharmaceuticals with higher specificity and selectivity to various diseases. Numerous neuroreceptor ligands are labelled with C-11, a significant number of ligands are also labelled with ^{18}F for neuroimaging, and oncological and cardiac applications. In this paper, the major emphasis is on the ^{18}F labelled radiopharmaceuticals and their safe and effective handling options.

The last five years have been a boom for the advancement in PET technology and its applications. During this period, PET scanners have improved in terms of their spatial resolution and subsequently advanced to a CT–PET fusion technology. This advancement not only helped improve image quality but also provided efficient and high throughput screening to handle increased patient volumes. While these advancements are helpful for an improved and effective diagnosis, they underscore the need for newer and improved PET ligand agents. Although, additional inventory of PET imaging agents would not necessarily increase the quantities of ^{18}F handled by radiochemistry personnel, it does provide a challenge to accommodate multiple synthesis protocols with varying chemistries within the constraints of a typical PET research and clinical facility. Although the synthesis of [^{18}F]FDG is now routine and well standardized, the synthesis of other radiotracers could be more complex and involved. For the last several years, the authors' research group has been engaged in the development of PET tracers for a variety of

applications. One of the approaches pursued was to design newer PET imaging molecules using templates for exisiting drugs. To that end, the authors developed ^{18}F labelled *p*-fluorobenzylguanidine [1, 2], ^{18}F labelled monoclonal antibodies and their fragments [3, 4] and peptides [5], and ^{18}F labelled androgens [6] and various other neuroimaging agents The authors derived these newer molecules from templates that have been tested and used in clinical or preclinical studies using other imaging modalities. The other benefit of this approach was that the biological properties of the parent analogues were known. Therefore, successful translation of these molecules for PET imaging was straightforward. Some of the molecules that were produced and evaluated over the last few years are briefly described.

Meta-iodobenzylguanidine (MIBG; Fig. 1) was first developed as a norepinephrine (NE) mimic to detect and treat neuroendocrine tumours. Successful use of MIBG in the detection of neural crest tumours and cardiac sympathetic innervations led the authors to develop the ^{18}F labelled analogue, i.e. ^{18}F *p*-fluorobenzylguanidine ([^{18}F]PFBG, Fig. 1) for PET imaging. The structures of PFBG, MIBG and NE are shown in Fig. 1 for comparison and to highlight the similarity in their structures.

The synthesis of [^{18}F]PFBG and their initial in vitro and in vivo results have already been reported [2, 7, 8]. In small animals, [^{18}F]PFBG shows higher specificity for the target tissues compared to that with MIBG [1, 8]. Encouraged by these studies, the authors explored the potential of [^{18}F]PFBG in detecting myocardial infarct in a dog model. As shown in Fig. 2, [^{18}F]PFBG images acquired 16 d post-infarction lack ^{18}F accumulation in the area of infarction despite reperfusion of the myocardium from newly formed collateral

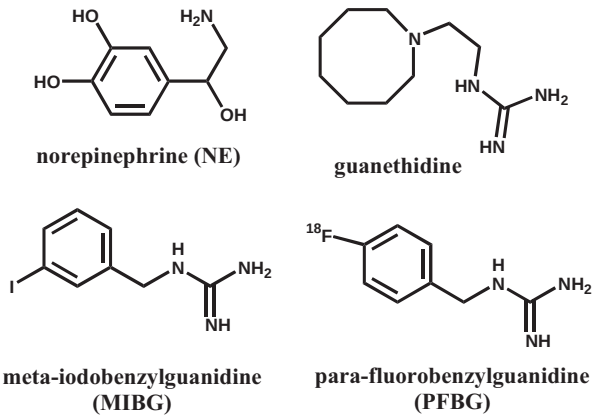

FIG. 1. Structure of MIBG and PFBG, and their resemblance to NE.

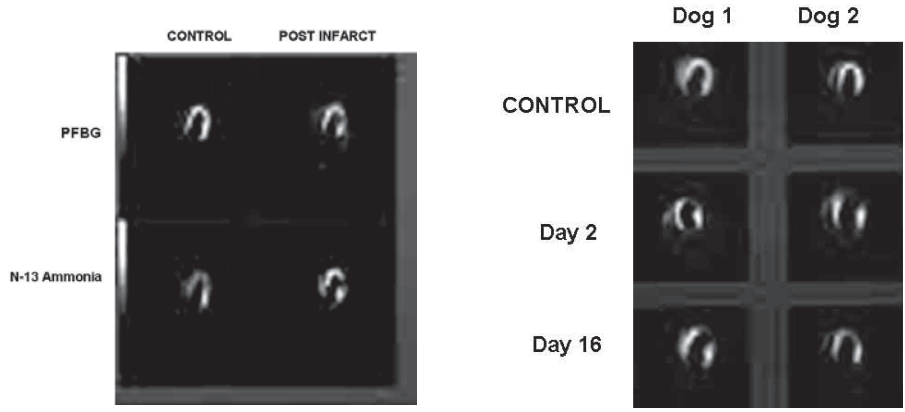

FIG. 2. PET images using [^{18}F]PFBG (innervation tracer) and ^{13}N ammonia (perfusion tracer) in dog heart. Left panel shows well perfused heart prior to surgery and a distinct tracer uptake deficit 2 d post-surgery scans. The right panel shows continued [^{18}F]PFBG uptake deficit 16 d post-surgery.

blood vessels [9]. As shown in the left hand graphic of Fig. 2, [^{18}F]PFBG and ^{13}N ammonia both showed an area of marked decrease in accumulating both radiotracers 2 d post-surgery compared with control (pre-surgery scans). The [^{18}F]PFBG accumulation deficit persisted even 16 d post-surgery as shown for two dogs in Fig. 2, right hand panel. These observations suggest that blood vessel ligation not only leads to perfusion deficit, but may have caused damage to the myocardium that was not detectable from blood perfusion scans, but which was quite evident on [^{18}F]PFBG scans.

A graphical representation of these results is shown in Fig. 3. The graph presents radioactivity uptake in the area of infarction using ^{13}N ammonia for myocardial perfusion and using [^{18}F]PFBG to assess innervation. A sharp decrease in both the tracers' uptake was noticed in the area of infarction when images were acquired 2 d post-surgery: [^{18}F]PFBG 59% of control values; ^{13}N ammonia 61% of control values. Although perfusion deficit resolved 16 d post-surgery as seen from ^{13}N images, [^{18}F]PFBG deficit remained unchanged even 23 d post-surgery (Fig. 3). These observations suggest that the [^{18}F]PFBG accumulates in tissues that were damaged during infarction and the damage existed three weeks after surgery despite recovery of blood perfusion [9, 10].

[^{18}F]PFBG also shows promise for its applications in oncology. When tested on dogs with spontaneous pheochromocytoma, [^{18}F]PFBG showed a rapid and high uptake at tumour sites. PFBG accumulation peaked within minutes of injection [11] and remained constant for the duration of the study.

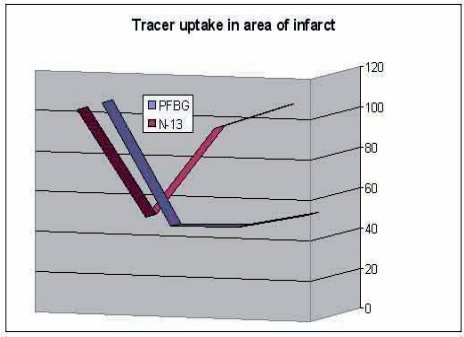

FIG. 3. Graphic representation of normalized uptake of ^{13}N ammonia and [^{18}F]PFBG in the area of myocardial infarction for pre-infarct, 2, 16 and 23 d post-infarction studies.

A coronal view of the PET scan from one of the dogs with pheochromocytoma acquired after injecting with [^{18}F]PFBG is shown in Fig. 4. The [^{18}F]PFBG localized in the right adrenal gland mass within the first few minutes and remained constant. A rapid clearance of radioactivity from the blood pool and a persistent retention of tracer within the area of the adrenal mass were observed from time activity curves generated from region of interest analysis. PET images of dogs with spontaneous pheochromocytomas utilizing [^{18}F]PFBG showed an SUV of 20–45 [11].

The authors further evaluated [^{18}F]PFBG utility in a diabetic rat heart model. Diabetes was induced by injecting streptozotocine (55 mg/kg i.p.) in male Sprague Dawley rats. One week later, blood glucose levels were

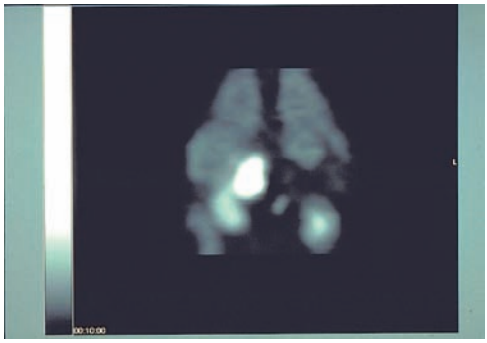

FIG. 4. [^{18}F]PFBG accumulation in the area of adrenal mass of a dog with suspected pheochromocytoma at 20–30 min post-injection of [^{18}F]PFBG.

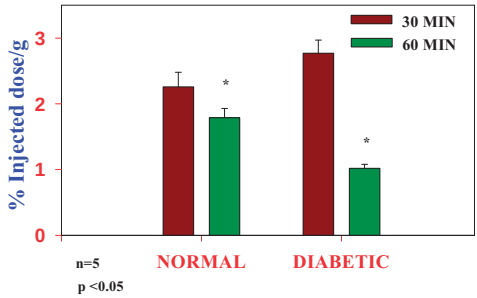

FIG. 5. [^{18}F]PFBG uptake in diabetic and normal rat hearts at 30 and 60 min p.i.

monitored and rats with glucose levels of >200 mg/dL were used for the study. A separate group of rats with no diabetes was used as control. As shown in Fig. 5, a higher [^{18}F]PFBG accumulation was observed in diabetic rat hearts at 30 min followed by rapid and significant washout of activity from the heart by 60 min. In comparison, [^{18}F]PFBG uptake and washout was less dramatic in normal rat hearts. These observations indicate a reduced retention of [^{18}F]PFBG in the vesicles, perhaps due to reduced NE transporter acitivy in diabetic rat heart. These observations are similar to those reported earlier using MIBG in the same model [12].

One of the probable causes of failed or ineffective radiation therapy is the presence of hypoxia in tumours. These hypoxic areas are radioresistant and also respond poorly to chemotherapy and other therapeutic interventions. 2-nitroimidazoles have been shown to possess excellent radiosensitization properties. These compounds are taken up by the tumours and under hypoxic conditions they are metabolized via a 2 electron reduction pathway. The reduced species remains trapped within the hypoxic areas. If developed, 2-nitroimidazole compounds could help in the assessment of the tumour hypoxia fraction. Therefore, misonidazole, a first generation radiation sensitizer was one of the first 2-nitroimidazoles to be labelled with ^{18}F for its use as a hypoxia imaging agent [13, 14]. Although the high lipophilicity of this molecule causes low target tissue to blood ratios (<1.6), imaging experiments showed promise [15]. Encouraged from these studies, newer ^{18}F labelled 2-nitroimidazoles are being developed to obtain a hypoxia imaging agent with better imaging characterisitics and pharmacokinetics. Some of the recently developed compounds include ^{18}F FAZA [16], ^{18}F EF [17, 18] and ^{18}F PK 110 [19]. Unfortunately, most of these compounds continue to possess high lipophilicity, leading to slow clearance from the blood pool and confounding image analysis.

Recently, the authors' group designed a water soluble 2-nitroimidazole analogue using the pimonidazole template. A microPET image of a mouse with human colorectal carcinoma tumour xenograft using ^{18}F PIMO is shown in Fig. 6. As evident from such microPET images, radioactivity is cleared rapidly via urinary excretion from the body and the tumour showed high retention of the radiotracer throughout the study. A general lack of radioactivity from most normal organs signifies the potential of this compound as a useful hypoxia imaging agent with improved imaging characteristics.

Prostate cancer represents a significant health problem worldwide for the male population. Early diagnosis and detection of this disease ensures effective treatment. Nonetheless, besides the PSA test, no advance imaging modality exists that can provide early detection and localization of this disease to aid in selecting appropriate treatment regimens for better therapeutic outcome. [^{18}F]FDG has been ineffective in the detection and localization of this disease. Recently, ^{18}F choline [20], ^{18}F FDHT [21] and ^{18}F FMDHT [6] have been developed. In mice bearing prostate tumour xenografts, the tumour uptake of ^{18}F choline was similar to that of [^{18}F]FDG, whereas in patients with prostate cancer, ^{18}F choline detected more lesions and showed higher SUVs than did [^{18}F]FDG. Use of [^{18}F]FDHT in prostate cancer patients showed an avid uptake in tumour areas on PET images [22]. Nonetheless, a rapid metabolic degradation of this compound was seen in humans.

The authors recently developed a metabolically stable ^{18}F androgen (FMDHT) that exhibits a high affinity for tumours expressing androgen receptors [6]. In their preliminary studies, the authors observed a selective

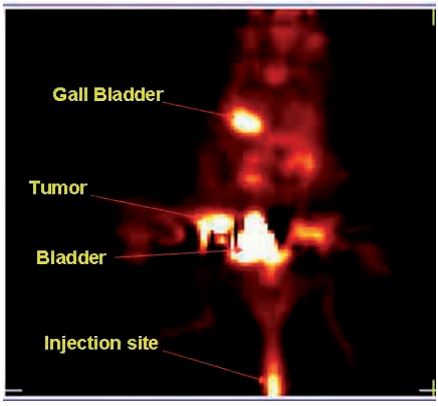

FIG. 6. MicroPET image of a mouse bearing HT-29 human colorectal tumour xenograft. A 30 min frame image acquired 90–120 min after injecting with ^{18}F pimonidazole.

uptake and distribution pattern of this tracer in mice and rats. As with most steroidal compounds, including [^{18}F]FDHT, the clearance of [^{18}F]FMDHT occurred via the GI track in mice and rats.

The authors further assessed the potential of [^{18}F]FMDHT as a prostate imaging agent using microPET. The imaging characteristics of [^{18}F]FMDHT were assessed using microPET imaging of an androgen dependent LnCAP tumour xenograft in mice. As shown in Fig. 7, the tumour was clearly visible on the microPET image. Additional studies were carried out using [^{18}F]FMDHT and comparing its imaging characteristics with other currently available PET imaging agents. Figure 8 shows a head-on comparison of [^{18}F]FMDHT images with [^{18}F]choline and [^{18}F]FDG in the same mice bearing the LnCAP tumour xenograft. As evident from these images, a better visualization of tumour was

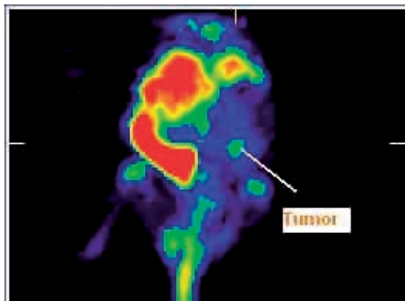

FIG. 7. MicroPET image of a mouse bearing the LnCAP tumour xenograft

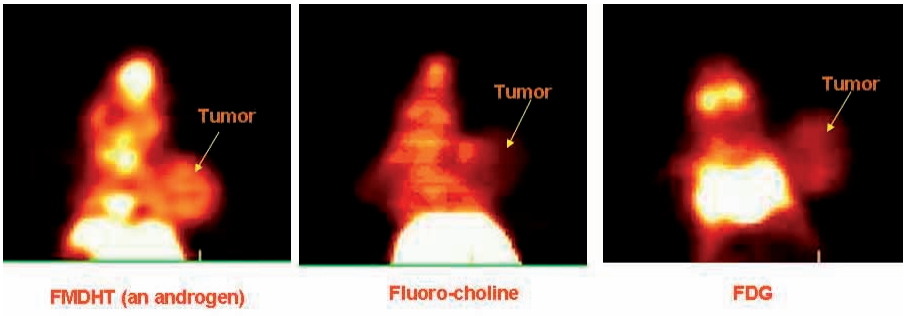

FIG. 8. MicroPET image of a mouse bearing the LnCAP tumour xenograft. Among the three ligands used, more intense uptake of radioactivity was evident with [^{18}F]FMDHT compared with [^{18}F]choline or [^{18}F]FDG.

observed using [^{18}F]FMDHT. Imaging characristics of [^{18}F]FMDHT as assessed from these studies were far superior to those of other imaging agents.

The other area of significance for PET imaging is to diagnose breast cancer and to follow the therapy outcome in those patients. Although [^{18}F]FDG has been successful in imaging breast tumours and their recurrence, development of receptor based ligand, for example [^{18}F]fluoroestradiol, would provide information on the hormonal status of the tumours. Therefore, developing this tracer offers advantages over [^{18}F]FDG which include localizing breast cancer sites, predicting the response to tumour therapy and assessing the estrogen blocking effect of hormonal therapies such as the tamoxifen and aromatase inhibitors. Several research groups are involved in developing such PET imaging agents with clinical potential. Some of the initial clinical studies performed using these tracers show encouraging results [23, 24].

In addition, several ^{18}F labelled amino acids have been developed as PET imaging probes that utilize the active amino acid transport mechanism for their accumulation in target sites. Several ^{18}F PET imaging agents are under investigation by various researchers. An ^{18}F labelled fluoromethyl tyrosine has shown a higher SUV in brain tumours than that seen with [^{18}F]FDG [25].

Because of the relatively short half-life of ^{18}F, its role in utilizing the monoclonal antibodies (MAb) and other bioactive molecular probes has been ignored for a long time. Continuing their work on developing novel radiohalogenation methods, the authors explored the possibility of labelling MAbs with ^{18}F [4]. Using their newly developed labelling technique, they successfully labelled MAbs with ^{18}F in good radioconjugation yields and within time-frames compatible with a short half-life isotope while retaining the immunoreactivity of the labelled MAb [4, 26]. In tumour bearing mice, ^{18}F labelled MAb showed a significant uptake in the tumours within 2–4 h p.i. [3]. The authors further assessed the utility of ^{18}F labelled MAb to detect tumours in dogs with radiolabelled MAbs and MAb fragments. A PET scan using a ^{18}F labelled TP-3 Fab antibody fragment was successful in detecting spontaneous osteosarcoma in dogs [4, 27].

Besides its role in oncology, PET imaging plays a significant role in the detection and monitoring of various neurological disorders. In their continued efforts to develop novel nortropane analogues for brain receptor imaging studies, the authors developed a ^{18}F labelled *N*-(3-fluoropropyl)-2-β-carbomethoxy-3-β-(4-bromophenyl)nortropane (FPCBT) as a potentially useful ligand for dopamine transporter (DAT) imaging. This compound has a binding affinity (K_i) of 3.3nM, 36.4nM, and 196nM for the DAT, SERT and NET, respectively. The in vivo properties assessed in non-human primates showed preferential uptake of this tracer in DAT rich areas of the brain (Fig. 9).

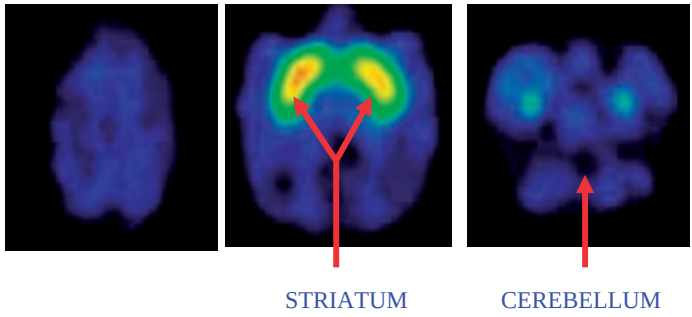

FIG. 9. PET image of a babboon brain after injecting ^{18}F FPCBT. An intense uptake in striatal area and minimal to negligible uptake in cerebellum are evident.

A rapid uptake of this tracer in the brain with highest accumulation in the striatum was observed. Despite excellent accumulation in the striatum, a modest striatum to cerebellum ratio (St:Cb = 3.3) observed for this ligand reduced the enthusiasm to pursue it. A large collection of ^{18}F labelled radiotracers exist for neuroreceptor imaging. Recently developed tracers include ^{18}F ACF and ^{18}F AFM for the SERT [28], ^{18}F reboxitine analogue to image NET [29] and ^{18}F Fallypride for D2 dopamine receptor imaging [30].

While ^{18}F compounds and molecular imaging probes are being developed at a fierce pace, their handling and usage in radiochemical synthesis requires particular care. In general, a positron emitting isotope imparts 2–10 fold higher radiation doses to personnel than those received from the isotopes commonly used for nuclear medicine imaging. For example, a 1 mCi unshielded gamma emitting nuclear medicine isotope produces an exposure of 0.2–2.2 R/h at 1 cm from the surface (depending on gamma energies) while exposure to a 1 mCi PET isotope at 1 cm would be ~5.8 R/h, signifying a need for more careful and cautious handling of PET isotopes. Because of a short physical half-life, larger quantities of these isotopes are routinely used for radiochemical synthesis, thus further increasing the risk of higher exposure. Therefore, it is important to use extra caution and to develop safe handling practices in the laboratories. An automated or remote handling procedure for the delivery of the radioisotopes and for the synthesis of PET radiopharmaceuticals is essential to minimize personnel exposure. Although several manufacturers are developing automated synthesis boxes, their application is mainly limited to carrying out synthesis of ligands that are fully evaluated and closer to routine use. It is important to highlight that a number of PET tracers with somewhat complicated chemistries are still synthesized manually with limited or no

automation. Once evaluated and the synthesis optimized, it is likely that the synthesis of those molecules can be adapted to the existing modules.

There are several synthesis modules that are now commercially available for [^{18}F]FDG production. One can now produce multiple batches of [^{18}F]FDG with one set-up routine in the beginning. Although multiple radiotracers utilizing similar chemistries can be produced using an [^{18}F]FDG box, it would be difficult to adapt new ligand synthesis to these modules without the help of experienced radiochemistry personnel. Therefore, there is a growing need for more flexible automation sytems.

Because of the different chemistries involved, it is difficult to develop an automated synthesis module for each individual ligand. Therefore, a large number of research groups design their own semi-automated synthesis modules that are either operated by remote electric valves or by programmable logic controllers. The complicated aspect of this option is that these modules are custom tailored for individual needs and are often prone to failure. Since these modules are highly individualized, it is difficult for others to adapt and use them with any reproducibility and reliability. One of the low cost automated synthesis boxes commercially available is shown in Fig. 10. Although all the synthesis functions are automated and streamlined, they are customized for the synthesis of a particular radiotracer. Several manufacturers have commercial modules that are now available to perform simple to complex radiochemical syntheses. Most of these modules are computer controlled and adapt well to a

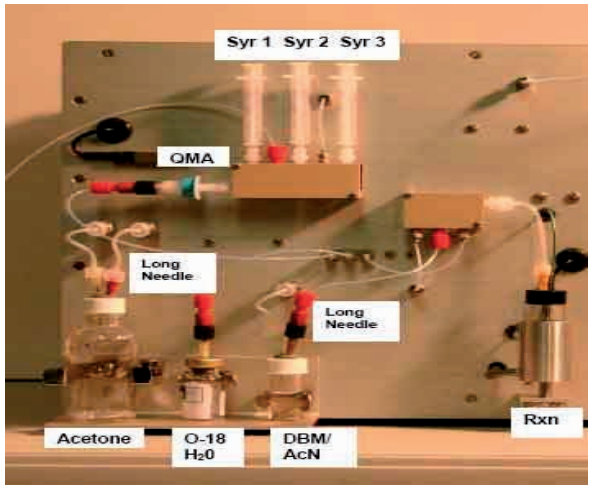

FIG. 10. An automated synthesis module for producing ^{18}F fluorobromo methane from ^{18}F fluoride.

FIG. 11. A fully automated synthesis module housed in a hot cell for producing ^{11}C labelled radiopharmaceuticals.

hot cell, cave, or even mini-cells. One of the examples is shown in Fig. 11. This particular unit is used for the synthesis of ^{11}C labelled molecules. A large number of neuroreceptor ligands and other ^{11}C radiopharmaceuticals use ^{11}C methyl iodide as a common synthone. Therefore, a number of molecules can be synthesized using this module. There are several advantages of these commercial modules; the user does not need to learn the mechanics behind the module and the procedures are mostly standardized by the manufacturers. The three major categories of modules that are available in the market are: a ^{11}C methyl iodide production and methylation module; ^{18}F nucleophilic fluorination modules and ^{18}F electrophilic fluorination modules. Although not all synthesis can be accomplished using one of the available modules, they are optimized for the production of most commonly used radiopharmaceuticals. It is important to remember that some of the fully automated modules are quite expensive and could cost well above US $100 000. Nonetheless, it does provide an option to establish reliable and regulatory compliant production of radiopharmaceuticals. Using automated synthesis modules is by far the most effective, safe and practical approach to manufacture radiopharmaceuticals.

The production of PET radiopharmaceuticals is becoming increasingly valuable and indispensable. Unlike a decade ago, at present, one has multiple choices for the safe and effective handling of PET isotopes. It is imperative that radiopharmaceutical laboratory design should consider addressing requirements of their local regulatory agencies and personnel safety. All PET research radiopharmaceutical laboratories should require a properly shielded

workplace. The level of shielding and automation need depends on workload, resources and expertise. There are several options available to minimize personnel exposure in a PET radiochemistry laboratory. The most primitive but practical option is the lead lined fume hood or a lead cave. A typical lead cave is shown in Fig. 12. The work area is covered with lead bricks and radiochemistry synthesis apparatus lies inside the lead lined area. The operator can see the inside operations through lead glass windows. The reagents are added from outside using syringes and slider valves that are located outside the lead lined area and which are easily accessible without entering the radiation field. The lead glass windows allow monitoring of the reactions without having to lean over the lead wall. These lead caves are suitable to house a computer controlled synthesis box or a remotely controlled procedure where minimal or no operator interventions are necessary inside the work area. The use of these lead lined hoods is not well suited for developmental work since access is difficult and the potential for exposure is quite high. In addition, allowable quantities of radioactivity usage in one of these lead caves should be restricted if lacking ceiling shielding.

The next option is the use of hot cells (Fig. 13). The hot cell concept is similar to that described for the lead cave. The hot cells are primarily lead caves but provide front and side panels for easy access. In addition, these cells are

FIG. 12. Fume hood converted to lead lined cave for remote handling of radioisotopes. The reagents are added from outside using syringes and slider valves (located on upper right hand corner of lead wall) and push buttons (on right side sash) to the reaction vessel located behind the lead wall.

FIG. 13. A typical hot cell fitted with robotic arms (manipulators). The front door is closed for radiochemistry operations. The front panel provides easy access to various valves or other optional procedures.

shielded at the top and the bottom ends which significantly reduces the radiation exposure in and around the radiochemistry laboratory. The hot cells provide easy access to inside work space for preparatory work before the synthesis and for easy cleanup after use. During the synthesis, all doors and side panels are closed to minimize radiation exposure to laboratory personnel. These hot cells are ideal to house synthesis boxes and automated procedures. Depending on the option purchased, the final product can be delivered either to a lead lined side drawer or accessed from a side panel without opening the hot cell doors. It is advisable to wait for the radioactivity to decay before opening the hot cell doors for cleanup or for setting up for reuse. There are several manufacturers that sell hot cells internationally. Since this is a large investment, it is advisable to match the options that a particular vendor supplies and the site requirements for safe and effective operation before finalizing a hot cell vendor. It should not be assumed that all hot cell vendors will provide the same options, designs and accessories.

A large number of laboratories acquire robotic arms (manipulators) to help with remote handling of radioactivity within the hot cell (Fig. 14). If semi-automated synthesis or manual interventions are anticipated during the radio-synthesis, it is strongly advised to have manipulators installed in the hot cells (Figs 14 and 15). As shown in Figs 14 and 15, the operator works with the manipulator arms from outside the hot cell. The arms aid in moving and transfering radioactivity from one place to another and activating or proceeding with the next process as needed, similar to that performed during manual processing. Once the skill to operate these manipulators is mastered,

FIG. 14. Operation of robotic arms (manipulators) from outside for safe and effective radiochemical handling.

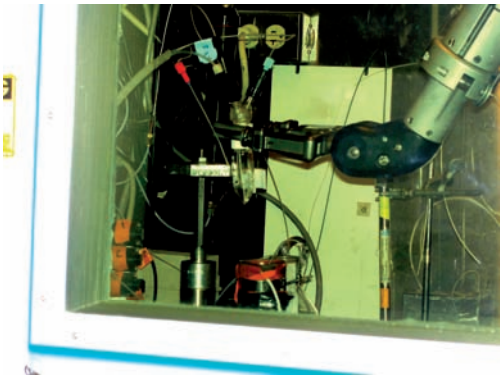

FIG. 15. Inside view of the hot cell while operator is working with the manipulators from outside the hot cell.

they are helpful in accomplishing manual synthesis steps remotely and safely. In addition, this option facilitates safe handling of multicurie quantities of radioactivity while maintaining safety. These manipulators provide convenient work access within the hot cell area while the doors are closed (Fig. 15). There are several vendors manufacturing manipulators that work in hot cells and most of them ship these items internationally. Most hot cell vendors can retrofit these manipulators if not purchased during the hot cell acquisition or installation.

If deferring the manipulator purchase at the time of hot cell purchase, it is advisable to opt for manipulator hole cut-out plugs. The manufacturer will make the housing insert for manipulators and will cover these with lead plugs to retain their integrity while providing the flexibility to install manipulators by removing these plugs as needed at a later date.

Hot cell manufacturers have responded to the ever increasing regulatory requirements for the production of safe and effective radiopharmaceuticals. Stringent pharmaceutical quality control criteria can now be met with HEPA filter options available with some hot cells. Once the radiopharmaceutical is prepared, it is collected in a sterile vial under a totally sterile environment and further doses can be taken using dose drawing options available from certain hot cell manufacturers.

It is important to develop newer and novel radiotracers to advance the field of radiopharmaceutical chemistry. The descriptive path is to explore the potential of various radiotracers while the goal is to develop radiotracers with clinical relevance. To achieve that goal, one would need to combine expertise in medicinal chemistry, organic chemistry, radiochemistry, radiation safety and regulatory compliance with a good understanding of clinical issues. It is important to bridge the gap between preclinical testing of the newly developed radiotracers and carefully and cautiously testing and using these new imaging agents in humans.

In conclusion, production of new and novel radiopharmaceuticals is simpler and reproducible now, depite increased demands requiring manufacture of larger and multiple batches of these radiopharmaceuticals.

REFERENCES

[1] GARG, P.K., GARG, S., ZALUTSKY, M.R., Fluorine-18 labelled analogs of meta-iodobenzyl guanidine. J. Labelled Compd. and Radiopharm., *32:* 544-546, 1993.

[2] GARG, P.K., GARG, S., ZALUTSKY, M.R., Synthesis and preliminary evaluation of *para*- and *meta*-[^{18}F]fluorobenzylguanidine. Nuc. Med. Biol., *21:* 97-103, 1994.

[3] GARG, P.K., GARG, S., BIGNER, D.D., ZALUTSKY, M.R., Selective localization of an ^{18}F-labeled Mel-14 monoclonal antibody F(ab')$_2$ fragment in a subcutaneous human glioma xenograft model. Cancer Res., *52:* 5054-5064, 1992.

[4] GARG, P.K., GARG, S., ZALUTSKY, M.R., Fluorine-18 labeling of monoclonal antibodies and fragments with preservation of immunoreactivity. Bioconj. Chem., *2:* 44-49, 1991.

[5] GARG, S., GARG, P.K., ZALUTSKY, M.R., Acylation reagents for the radiohalogenation of peptides. J. Labelled Compd. and Radiopharm., *32:* 212-213, 1993.

[6] GARG, P.K., LABAREE, D.C., HOYTE, R.M., HOCHBERG, R.B., [7α-^{18}F]Fluoro-17α-methyl-5α-dihydrotestosterone: a ligand for androgen receptor-mediated imaging of prostate cancer. Nucl. Med. Biol., *28:* 85-90, 2001.

[7] GARG, P.K., NG, C.K., SOUFER, R., Synthesis and biodistribution of meta-[^{18}F]fluorobenzylguanidine in the presence and absence of desimipramine (DMI, an uptake 1 blocker) using rats. J. Labelled Compd. and Radiopharm., *40*, 1997.

[8] GARG, P.K., GARG, S., WELSH, P., ZALUTSKY, M.R., Fluorine-18 labeled analog of metaiodobenzylguanidine. J. Labelled Compd. and Radiopharm., *22:* 544-546, 1999.

[9] BERRY, C.R., et al., Para-[18F]fluorobenzylguanidine kinetics in a canine coronary artery occlusion model. J Nucl Cardiol, *3:* 119-129, 1996.

[10] BERRY, C.R., GARG, P.K., ZALUTSKY, M.R., COLEMAN, R.E., DeGRADO, T.R., Uptake and retention kinetics of para-fluorine-18-fluorobenzylguanidine in isolated rat heart. J Nucl Med, *37:* 2011-2016, 1996.

[11] BERRY, C.R., et al., Imaging of pheochromocytoma in 2 dogs using p-[18F] fluorobenzylguanidine. Vet Radiol Ultrasound, *43:* 183-186, 2002.

[12] KIYONO, Y., KAJIYAMA, S., FUJIWARA, H., KANEGAWA, N., SAJI, H., Influence of the polyol pathway on norepinephrine transporter reduction in diabetic cardiac sympathetic nerves: implications for heterogeneous accumulation of MIBG. Eur J Nucl Med Mol Imaging, *32:* 438-442, 2005.

[13] VALK, P.E., MATHIS, C.A., PRADOS, M.D., GILBERT, J.C., BUDINGER, T.F., Hypoxia in human gliomas: demonstration by PET with fluorine-18-fluoromisonidazole. J Nucl Med, *33:* 2133-2137, 1992.

[14] MARTIN, G.V., et al., Noninvasive detection of hypoxic myocardium using fluorine-18-fluoromisonidazole and positron emission tomography. J. Nucl. Med., *33:* 2202-2208, 1992.

[15] RAJENDRAN, J.G., et al., Hypoxia and glucose metabolism in malignant tumors: evaluation by [18F]fluoromisonidazole and [18F]fluorodeoxyglucose positron emission tomography imaging. Clin Cancer Res, *10:* 2245-2252, 2004.

[16] SORGER, D., et al., [18F]Fluoroazomycinarabinofuranoside (18FAZA) and [18F]Fluoromisonidazole (18FMISO): a comparative study of their selective uptake in hypoxic cells and PET imaging in experimental rat tumors. Nucl Med Biol, *30:* 317-326, 2003.

[17] MAHY, P., et al., Preclinical validation of the hypoxia tracer 2-(2-nitroimidazol-1-yl)- N-(3,3,3-[(18)F]trifluoropropyl)acetamide, [(18)F]EF3. Eur J Nucl Med Mol Imaging, *31:* 1263-1272, 2004.

[18] JOSSE, O., LABAR, D., GEORGES, B., GREGOIRE, V., MARCHAND-BRYNAERT, J., Synthesis of [18F]-labeled EF3 [2-(2-nitroimidazol-1-yl)-N-(3,3,3-trifluoropropyl)-acetamide], a marker for PET detection of hypoxia. Bioorg Med Chem, *9:* 665-675, 2001.

[19] GARG, P.K., DeGRAFF, W., GARG, S., ZALUTSKY, M.R., MITCHELL, J.B., 4-Fluorobenzyl amine and phenylalanine methyl ester conjugates of 2-nitroimidazole: Synthesis and evaluation as hypoxic cell radiosensitizers. Int. J. Radiat. Oncol. Biol. Phys., *23:* 593-596, 1992.

[20] DeGRADO, T.R., et al., Synthesis and evaluation of (18)F-labeled choline analogs as oncologic PET tracers. J Nucl Med, *42:* 1805-1814, 2001.
[21] BONASERA, T.A., et al., Preclinical evaluation of fluorine-18-labeled androgen receptor ligands in baboons. J Nucl Med, *37:* 1009-1015, 1996.
[22] LARSON, S.M., et al., Tumor localization of 16beta-18F-fluoro-5alpha-dihydrotestosterone versus 18F-FDG in patients with progressive, metastatic prostate cancer. J Nucl Med, *45:* 366-373, 2004.
[23] MORTIMER, J.E., et al., Positron emission tomography with 2-[18F]Fluoro-2-deoxy-D-glucose and 16alpha-[18F]fluoro-17beta-estradiol in breast cancer: correlation with estrogen receptor status and response to systemic therapy. Clin Cancer Res, *2:* 933-939, 1996.
[24] MANKOFF, D.A., et al., [18F]fluoroestradiol radiation dosimetry in human PET studies. J Nucl Med, *42:* 679-684, 2001.
[25] INOUE, T., et al., 18F alpha-methyl tyrosine PET studies in patients with brain tumors. J Nucl Med, *40:* 399-405, 1999.
[26] ZALUTSKY, M.R., GARG, P.K., JOHNSON, S.H., COLEMAN, R.E., Fluorine-18 antimyosin monoclonal antibody fragments: preliminary investigation in a canine myocardial infarct model. J. Nucl. Med., *33*, 1992.
[27] PAGE, R.L., et al., Positron emission tomographic images of osteosarcoma in dogs using an ^{18}F-labeled monoclonal antibody Fab fragment. J. Nucl. Med, *35:* 1506-1513, 1994.
[28] HUANG, Y., et al., A new positron emission tomography imaging agent for the serotonin transporter: synthesis, pharmacological characterization, and kinetic analysis of [11C]2-[2-(dimethylaminomethyl)phenylthio]-5-fluoromethylphenylamine ([11C]AFM). Nucl Med Biol, *31:* 543-556, 2004.
[29] LIN, K.S., DING, Y.S., KIM, S.W., KIL, K.E., Synthesis, enantiomeric resolution, F-18 labeling and biodistribution of reboxetine analogs: promising radioligands for imaging the norepinephrine transporter with positron emission tomography. Nucl Med Biol, *32:* 415-422, 2005.
[30] RICCARDI, P., et al., Amphetamine-induced displacement of [(18)f] fallypride in striatum and extrastriatal regions in humans. Neuropsychopharmacology, *31:* 1016-1026, 2006.

RAPID METHOD FOR RADIOFLUORINATION OF PYRIDINE DERIVATIVES: PROSTHETIC GROUPS FOR LABELLING BIOACTIVE MOLECULES

I. AL JAMMAZ*, B. AL OTAIBI*, H. RAVERT**, J. AMARTEY*

*Cyclotron and Radiopharmaceuticals Department,
King Faisal Specialist Hospital and Research Centre,
Riyadh, Saudi Arabia
Email: jammaz@kfshrc.edu.sa

** Division of Nuclear Medicine and Radiation Health Sciences,
The Johns Hopkins Medical Institutions,
Baltimore, Maryland,
United States of America

Abstract

Ethyl 2-[^{18}F]fluoro-4-pyridine and ethyl 6-[^{18}F]fluoro-3-pyridine carboxylates were synthesized by catalyzed nucleophlic no-carrier-added radiofluorination. Treatment of the ethyl-2-(N,N,N-trimethylammonium)-4-pyridine- and ethyl-6-(N,N,N-trimethylammonium)-3-pyridine carboxylate.treflate precursors with radiofluoride and Kryptofix 2.2.2 in anhydrous acetonitrile at 95°C provided these radiofluorinated intermediates with a greater than 90% radiochemical yield within 2 min reaction time. These intermediates served as precursors to obtain the activated N-succinimidyl 2-[^{18}F]fluoro-4-pyridine and 6-[^{18}F]fluoro-3-pyridine carboxylate esters for efficient coupling to amine functions in bioactive molecules. This technique was used to radiofluorinate a model chemotactic peptide (N-Formyl-Nle-Leu-Phe-Nle-Tyr-Lys). Biodistribution studies in normal CBA/J mice revealed very rapid clearance through the renal system.

1. INTRODUCTION

Synthesis of fluorinated aromatic compounds has been achieved by one of three main routes: (1) fluorination by molecular F_2, (2) fluorination by the Schiemann reaction and (3) nucleophilic substitution on a precursor with a good leaving group. The first two methods suffer from several drawbacks that have led to limited success [1–3]. Another method of limited utilization has been halogen–halogen exchange. The main drawbacks of this method are the elevated temperature and long reaction time which preclude its use on many

molecules [4, 5]. Furthermore, the short half-life of ^{18}F imposes an additional time constraint on the application of such a method. The efficiency and simplicity of the nucleophilic fluoride substitution has been accepted and applied for the production of several radiopharmaceuticals from precursor substrates bearing a good leaving group [6, 7]. As part of their on-going research effort to develop prosthetic precursors for the radiohalogenation of bioactive molecules such as peptides, the authors have synthesized N-succinimidyl activated esters of the 2-[^{18}F]fluoro-4-pyridine and 6-[^{18}F]fluoro-3-pyridine carboxylates. These intermediates were then used to label a potent chemotactic peptide [N-Formyl-Nle-Leu-Phe-Nle-Tyr-Lys] and a biodistribution study in normal CBA/J mice was investigated.

2. EXPERIMENTAL

The chemicals used in the study were all analytical reagent grade purchased from Aldrich (St. Louis, United States of America) and were used without further purification unless stated. Acetonitrile was kept over molecular sieves. Sep-Pak cartridges were purchased from Waters-Millipore (USA). Thin layer chromatographic (TLC) sheets were purchased from Gelman Sciences Inc. (Ann Arbor, USA). High performance liquid chromatography (HPLC) analysis was carried out on Econosil C-18 reversed phase columns (semi-preparative, 250 mm × 10 mm or analytical, 250 mm × 4.6 mm). The solvent system used for the latter was non-linear gradient (eluant A, water with 0.1 TFA; eluant B, acetonitrile/water, 3/1 v/v with 0.1% TFA; gradient, 0–90% B, 90–0% B and 90–10% B over 10 min each at a flow rate of 1.5 mL/min). A Jasco (Tokyo, Japan) chromatographic system equipped with a variable wavelength ultraviolet monitor and in tandem with a Canberra flow through radioactivity detector was used. Ultraviolet absorption was monitored at 254 nm. Chromatograms were acquired and analysed using BORWIN software. Melting points were determined on a Thomas Hoover Unimelt capillary melting point apparatus. Mass spectroscopy was run on a Quattra electrospray mass spectrometer (ES-MS).

2.1. Ethyl-6-(N,N,N-trimethylammonium)-3-pyridine carboxylate.treflate (6b)

Compounds (2a,b), (3a,b), (4a,b), (5a,b), (6a), (7a) and (8a) in Figs 1 and 2 were all synthesized utilizing the methods reported by Stöcklin et al. [8] and Amartey et al. [9, 10]. Compound (5b), (250 mg, 1.25 mmol) was dissolved in dry dichloromethane (3 mL) and was purged with nitrogen for 5 min. Methyl-trifluoromethane sulphonate (150 uL, 1.25 mmol) was added through a rubber

septum. The mixture was stirred at ambient temperature overnight. The reaction mixture was then concentrated under reduced pressure to obtain a yellowish paste. Upon treatment with cold ether, white crystals of the triflate (6b) separated out. The crystals were filtered and washed with cold ether and dried in a desiccator.

2.2. 6-fluoro-3-methylpyridine (7b)

In a plastic flask kept at ice–salt bath temperature, Olah's reagent [11] (4 mL, pyridine:HF 30:70% w/w) was used to dissolve compound (1b) (1.0 g, 9.25 mmol). To control the rise in temperature, sodium nitrite (0.7 g, 10.1 mmol) was added in small portions while stirring. The mixture was continuously stirred at ambient temperature overnight followed by quenching in crushed ice. The excess acid was carefully neutralized with sodium hydroxide (5.0M). The product was then extracted with ether (2 × 50 mL) and dried over anhydrous sodium sulphate. Evaporation of the ether yielded an oily material, which was used immediately.

2.3. 6-fluoro-3-pyridine carboxylic acid (8b)

Compound (7b), (0.25 g, 2.25 mmol) was added to a solution of potassium permanganate (1.5 g, 4.5 mmol) in water (10 mL). The mixture was made alkaline by adding few drops of sodium hydroxide (5M) and was then heated to reflux for 5 h. The unreacted permanganate was reduced with sodium thiosulphate. The solid manganese dioxide formed was filtered off and the filtrate was then concentrated to approximately 50 mL. Acidification with concentrated hydrochloric acid precipitated the fluorinated nicotinic acid. The product was filtered, washed with cold water and dried to obtain a white solid material.

2.4. Ethyl 2-fluoropyridine-4-carboxylate (9a) and ethyl 6-fluoropyridine-3-carboxylate (9b)

Compound (8a), (50 mg, 0.35 mmol) was dissolved in absolute ethanol (2 mL) followed by the addition of concentrated sulphuric acid (100 μL). The mixture was heated in a sealed vial overnight at 60°C. The reaction mixture was carefully basified using ammonium hydroxide while cold. The product was then extracted with ether (2 × 10 mL) and dried over anhydrous sodium sulphate. Evaporation of the ether yielded an oily greenish material, which was solidified by cooling. The same procedure was used to produce ethyl 6-fluoropyridine-3-carboxylate (9b) starting from 6-fluoropyridine-3-carboxylic acid (8b).

2.5. N-succinimidyl 2-fluoropyridine-4-carboxylate (SFPa, 10a) and N-succinimidyl 6-fluoropyridine-3-carboxylate (SFPb, 10b)

To a mixture of 2-fluoropyridine-4-carboxylic acid (8a) (50 mg, 0.35 mmol) and TEA (100 μL, 0.71 mmol) dissolved in acetonitrile (300 μL), O-(N-succinimidyl)-tetramethyluronium tetrafluoroborate (TSTU) (128 mg, 0.43 mmol) was added and heated in a heating block for 1 h at 90°C. The reaction mixture was diluted with hexane/ethyl acetate 7/3 v/v (1 mL) and passed though a Sep-Pak silica cartridge. Then the product was eluted by hexane/ethyl acetate 7/3 v/v (5 mL). After the solvent was evaporated to dryness, white crystals separated and were dried under vacuum. The same procedure was used to produce N-succinimidyl 6-fluoropyridine-3-carboxylate (SFPa, 10b) starting from 6-fluoropyridine-3-carboxylic acid (8b).

2.6. Chemotactic peptide-2-fluoropyridine-4-carboxylate conjugate (peptide-SFPa, 11a) and chemotactic peptide-6-fluoropyridine-3-carboxylate conjugate (peptide-SFPb, 11b)

Chemotactic peptide, (4.15 mg, 5 μmol) was dissolved in 9:1 acetonitrile: DMF (100 μL). This was followed by the addition of compound (10a) (2.0 mg, 8.4 μmol). Enough triethylamine (TEA) solution in acetonitrile was added to attain pH9. The reaction mixture was heated in a heating block for 20 min at 95°C. The reaction mixture was diluted with water (1 mL) and mixed well. The solution was then loaded onto a Sep-Pak C-18 cartridge, washed with water (5 mL), blow dried with air and the conjugate (11a) eluted with ethanol (1 mL). After the solvent was evaporated to dryness, white crystals separated, which were dried under vacuum. The same procedure was used to produce chemotactic peptide-6-fluoropyridine-3-carboxylate conjugate (peptide-SFPb, 11b) starting from N-succinimidyl 6-fluoropyridine-3-carboxylate (10b).

2.7. Radiosynthesis

Aqueous [18F]-fluoride was produced by the 18O (p,n) 18F reaction. The fluoride activity (5–20 mCi, 185–740 MBq) was trapped in Kryptofix 2.2.2 (5 mg) and potassium carbonate (1 mg) in acetonitrile/water solution (950 μL/50 μL), then dried by azeotropic distillation with aliquots of acetonitrile. The solid residue was resolubilized in 0.2 mL of CH_3CN containing the required amount of precursor ethyl-2-(N,N,N-trimethylammonium)-4-pyridine carboxylate.triflate (6a) or ethyl-6-(N,N,N-trimethylammonium)-3-pyridine carboxylate.triflate (6b). The reaction mixtures were heated in a capped 2 mL reaction vial at 95°C and fractions were taken for chromatographic analysis at 2, 5, 8 and 10 min. The

intermediates ethyl 2-[^{18}F]fluoro-4-pyridine and 6-[^{18}F]fluoro-3-pyridine carboxylates (12a,b) were extracted with ether (2 × 1 mL) and passed through a Sep-Pak silica cartridge. Each layer was dried with a steady stream of nitrogen. For subsequent hydrolysis, residues were resolubilized with acetonitrile (500 μL) followed by the addition of sodium hydroxide (100 μL, 1M) and heated at 95°C for 5 min. After acidification with hydrochloric acid (100 uL, 1M), reaction mixtures were dried by azeotropic distillation with aliquots of acetonitrile in the presence of TEA (10 μL). For activation, solutions of O-(N-succinimidyl)-tetramethyluronium tetrafluoroborate (TSTU, 5 mg) in acetonitrile (100 μL) were added and heated for 15 min at 95°C. Reaction mixtures were diluted with hexane (3 mL) before passing through a Sep-Pak cyano cartridge. Finally, N-succinimidyl 2-fluoropyridine-4-carboxylate ([^{18}F]SFPa) (14a) and N-succinimidyl 6-fluoropyridine-3-carboxylate ([^{18}F]SFPb) (14b) were eluted from the cartridge with hexane/ethyl acetate (8/2, v/v).

The $SFP_{a,b}$ solutions which contain TEA were dried and the chemotactic peptide (50 μg) in acetonitrile:DMF (9:1) was added and then heated for 15 min at 95°C. The peptide reaction mixtures were diluted with water (1 mL) and passed through a Sep-Pak C-18 cartridge. Finally, peptide-[^{18}F]$SFP_{a,b}$ conjugates (15a,b) were eluted with absolute ethanol (1 mL). For the determination of stability in plasma, peptide-[^{18}F]$SFP_{a,b}$ conjugates (100 μL, 20 μCi) were incubated with human plasma (500 μL) in duplicate at 37°C for 2 h. This was followed by precipitation using a mixture of acetonitrile/ethanol (1:1 v/v) and centrifuging at 5000 rpm for 5 min. The supernatant layer was then analysed by HPLC to determine the stability in plasma.

2.8. In vivo biodistribution

The biodistribution was performed in normal female mice to ascertain the in vivo distribution profile of the radiotracer peptide-[^{18}F]SFPa (15a). Mice (CBA/J, 25–30 g) were injected via the tail vein with 0.1 mL of the radiotracer formulated in saline containing 2% absolute ethanol. Each dose contained 20 μCi (740 kBq) of radioactivity. Animals were sacrificed at 5, 30 and 120 min post-injection and organs and tissues of interest were dissected, weighed and assayed for radioactivity. The percentage injected dose per gram was then calculated for all tissues using a stored sample of the injection solution to estimate the total dose injected per mouse. The animal biodistribution experiments were performed in accordance with institutional, national and international regulations governing the safe and humane use of laboratory animals in research.

3. RESULTS AND DISCUSSION

3.1. Organic chemistry

The synthesis of the precursor triflates (6a and 6b) needed for the radiofluorination reactions is outlined in Fig. 1, whereas the scheme shown in Fig. 2 was used to synthesize the reference compounds (8a,b, 9a,b, 10a,b and

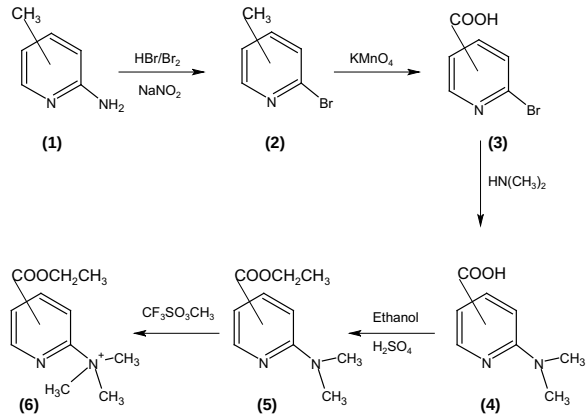

FIG. 1. Synthesis of ethyl-2-(trimethylammonium)-4-carboxylate (6a) and ethyl-6-(trimethylammonium)-3-carboxylate (6b) triflates.

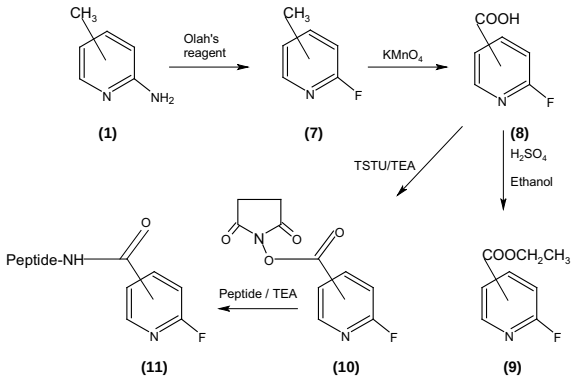

FIG. 2. Synthesis of the reference compounds 2-fluoro-4-pyridine carboxylate (a) and 6-fluoro-3-pyridine carboxylate (b).

11a,b). These compounds were characterized by physical, chromatographic and spectral data and were in agreement with the anticipated structures.

Methyltrifluoromethane sulphonate was used to convert compound (5b) to the precursor ammonium.triflate (6b) as white crystals with a 35% yield; melting point = 139–141°C. The calculated molecular mass of $C_{11}H_{17}N_2O_2$ (the cationic portion of the molecule) was 209.26. This was in agreement with the found ES-MS $[M + 1]^+ = 210$. The ^{1}Hnmr spectroscopic data obtained for this precursor (400 MHz, CD_3CN, with TMS as the reference) is as follows: δ1.40 (t, 3H, -O-CH_2CH_3), δ 3.55 (s, 9H, N-$(CH_3)_3$), δ 3.46 (q, 2H, -O-CH_2CH_3), δ 8.11 (d, 1H, H5), δ 8.27 (d, 1H, H5) and δ 8.77 (s, 1H, H2). Compound (7b) was obtained as an oily material with a very good yield (83%) by diazotization of the starting material (1b) with Olah's reagent. Permanganate oxidation of this oily intermediate furnished the corresponding acid (8b) also with an excellent yield (94%) as a white solid, melting point = 150–152°C. The molecular mass calculated for $C_6H_4FNO_2$ was 141 and the ES-MS found was $[M + 1]^+ = 142$. ^{1}Hnmr spectroscopic data for the acid 8b is as follows: (DMSO) δ 7.33 (d, 1H, H5), δ 8.44 (d, 1H, H4), δ 8.77 (s, 1H, H2). Compounds 8a and 8b were converted to their corresponding ethyl esters using the classical esterification method to give compounds 9a and 9b with good yields (55% and 50%, respectively) as oily materials which solidified upon cooling. The calculated molecular mass of $C_8H_8FNO_2$ was 168 and the ES-MS found was $[M + 1]^+ = 169$ for both compounds 9a and 9b. ^{1}Hnmr spectroscopic data for 9a and 9b are as follows: ($CDCl_3$) (9a) δ1.15 (t, 3H, -O-CH_2CH_3), δ 3.34 (q, 2H, -O-CH_2CH_3), δ 9.23 (s, 1H, H2), δ 9.34 (d, 1H, H5), δ 10.2 (d, 1H, H5), and (9b) δ1.20 (t, 3H, -O-CH_2CH_3), δ 3.46 (q, 2H, -O-CH_2CH_3), δ 6.75 (d, 1H, H4), δ 8.17 (d, 1H, H5), δ 8.82 (s, 1H, H2). The activated ester intermediates 10a and 10b were obtained as white crystals by the activation of the corresponding acids (8a and 8b) using TSTU as described above. Chemical yields for 10a and 10b were 47% and 45%, respectively. Both activated esters decomposed when the temperature reached 121–123°C. The calculated molecular mass of $C_{10}H_7FN_2O_4$ was 238.17. This was in agreement with the found ES-MS $[M + 1]^+ = 239$ for both esters. The amide linked targeted fluorinated chemotactic peptides were obtained as white solids by conjugation of compounds 10a and 10b with chemotactic peptide. The overall yields were greater than 80%. Chemical purity was found to be greater than 98% without HPLC purification as confirmed by analytical HPLC. Both fluoropyridine-peptide conjugates showed molecular ion at 948, corresponding to the $[M + 1]^+$ ion as expected.

3.2. Radiochemistry

The synthetic approaches for preparation of the chemotactic peptide-[^{18}F]SFPa,b conjugates (15a,b) (Fig. 3) entailed several reaction sequences. The key precursors ethyl-2-(N,N,N-trimethylammonium)-4-pyridine carboxylate.triflate (6a) or ethyl-6-(N,N,N-trimethylammonium)-3-pyridine carboxylate.triflate (6b) were treated using classical catalyzed nucleophlic substitution on an ammonium leaving group with no-carrier-added radiofluoride reported earlier [9, 10]. The radiochemical yields of the intermediates ethyl 2-[^{18}F]-fluoropyridine and 6-[^{18}F]-fluoro-3-pyridine carboxylates (12a,b) were found to be greater than 90% at all reaction times ranging from 2 to 10 min as determined by HPLC and confirmed by TLC-SG developed with the ethyl acetate:methanol 8:2 (v/v) solvent system. It was observed that between 2 and 10 min reaction time there was no significant change in the radiochemical yield (Table 1). Similarly, increasing the amount of the triflate precursors from 2 to 10 mg was not advantageous. In order to eliminate or reduce the concentration of most polar impurities, both ester intermediates were extracted by ether and followed by passing through a Sep-Pak silica cartridge prior to the conversion to the corresponding acids. It was also necessary to convert both ethyl ester intermediates to the corresponding acid prior to activation with TSTU. This led to a quantitative conversion of the ester intermediates to the corresponding [^{18}F]SFP$_{a,b}$ esters (14a,b) in a short period of time and at relatively lower

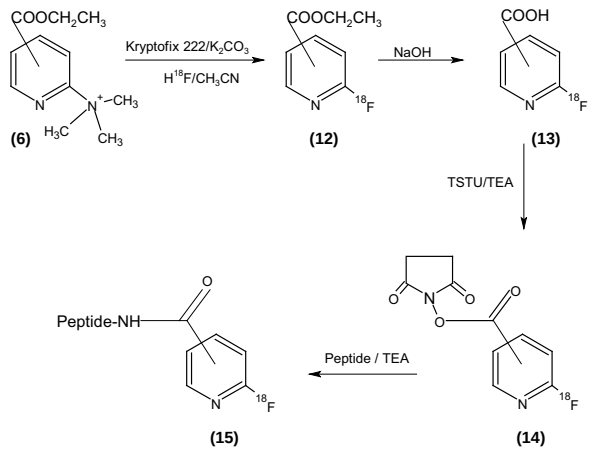

FIG. 3. Radiosynthesis of 2-[^{18}F]fluoro-4-pyridne carboxylate (a) and 6-[^{18}F]fluoro-3-pyridine carboxylate (b) compounds.

TABLE 1. RADIOCHEMICAL YIELDS OF THE INTERMEDIATES ETHYL 2-[^{18}F]FLUORO-4-PYRIDINE AND 6-[^{18}F]FLUORO-3-PYRIDINE CARBOXYLATES

Time (min) 5 mg	Ethyl 2-[^{18}F]fluoro-4-pyridine carboxylates	Ethyl 6-[^{18}F]fluoro-3-pyridine carboxylates
2	91.9 ± 1.2	93.5 ± 1.8
5	91.0 ± 3.1	91.4 ± 2.6
8	92.8 ± 1.9	95.4 ± 0.5
10	92.1 ± 4.3	93.0 ± 2.1
Precursor (mg) 5 min.		
2	91.5 ± 2.2	91.5 ± 0.8
5	92.0 ± 1.9	93.8 ± 1.4
8	92.3 ± 2.9	94.3 ± 3.4
10	89.0 ± 3.1	90.1 ± 4.1

temperature. Because of the ionic character of TSTU, the authors have been able to purify [^{18}F]SFPa,b esters (14a,b) by adsorption on Sep-Pak cyano cartridge, followed by elution with hexane/ethyl acetate (8/2, v/v) and replacing the laborious HPLC purification. The radiochemical yields ranged between 60 and 70% (decay corrected) with a preparation time of about 60 min. Radiochemical purities of both [^{18}F]SFP$_{a,b}$ esters (14a,b) were always greater than 98% as determined by HPLC and confirmed by TLC-SG using ethyl acetate:methanol (8:2) as a mobile phase. The retention times and Rf values for all intermediates and the final product are shown in Table 1. The dry residues of [^{18}F]SFP$_{a,b}$ (14a,b) were reacted with the chemotactic peptide in DMF and acetonitrile in the presence of TEA for 15 min at 95°C. The difference between the unlabelled peptide and the conjugates permitted the isolation of the peptide-[^{18}F]SFP$_{a,b}$ conjugates (15a,b) by passing through a Sep-Pak C-18 cartridge and eluting with absolute ethanol (1 mL). Hence, the Sep-Pak purification technique is amenable to automation and holds considerable promise as a rapid and simple method for the radiofluorination of bioactive molecules with high specific activity, a prerequisite for studying low capacity and saturable sites. The overall radiochemical yields ranged between 40 and 50% (decay corrected) with a preparation time of about 80 min. Radiochemical purities of both peptide-[^{18}F]SFP$_{a,b}$ conjugates (15a,b) were greater than 98% as determined by HPLC and confirmed by TLC-SG.

TABLE 2. RETENTION TIME OF THE INVESTIGATED SPECIES

Compound	Retention time (min)	Rf values
Ethyl 2-[^{18}F]fluoro-4-pyridine carboxylate	9.45	0.7–0.8
Ethyl 2-[^{18}F]fluoro-4-pyridine carboxylate	9.37	0.7–0.8
2-[^{18}F]fluoro-4-pyridine carboxylic acid	7.27	0.0–0.2
6-[^{18}F]fluoro-3-pyridine carboxylic acid	7.27	0.0–0.2
[^{18}F]-N-succinimidyl-2-fluoro-4-pyridine carboxylate	7.20	0.4–0.5
[^{18}F]-N-succinimidyl-6-fluoro-3-pyridine carboxylate	7.10	0.4–0.5
2-[^{18}F]fluoro-4-pyridine carboxylate chemotactic peptide conjugate	10.90	0.0
6-[^{18}F]fluoro-3-pyridine carboxylate chemotactic peptide conjugate	10.92	0.0

3.3. Biodistribution studies

The biodistribution data in normal CBA/J mice are shown in Table 3. Generally, the peptide-[^{18}F]SFPa (15a) appears to clear fast from most of the tissues. This trend is similar to that seen with the same chemotactic peptide when coupled with [^{18}F]fluorinatedbenzene [12]. However, the initial uptake of peptide-[^{18}F]SFPa in the liver and the kidney was fivefold lower for the former and almost twice as high for the latter than reported for the [^{18}F]fluorinated-benzene-peptide. These differences are mainly attributed to the higher hydrophilicity of the peptide-[^{18}F]SFPa in comparison with [^{18}F]fluorinated-benzene-peptide. In addition, the lower bone activity for peptide-[^{18}F]SFPa can be due to the high stability of the carbon–fluorine bond.

4. CONCLUSION

The authors have developed a ‘synthetic’ figure leading to the procurement of key precursors needed for radiofluorination of the hydrophilic pyridine carboxylic acids. The radiofluorination reactions proceeded in very

TABLE 3. BIODISTRIBUTION OF THE CHEMOTACTIC PEPTIDE-2-[^{18}F]FLUOROPYRIDINE-4-CARBOXYLATE CONJUGATE IN NORMAL MICE

Organ/tissue	5 min	30 min	120 min
Blood	3.1 ± 1.2	0.4 ± 0.3	0.2 ± 0.1
	5.0 ±0.1	*0.9 ±0.1*	*0.1 ±0.1*
Liver	2.6 ± 1.2	0.4 ± 0.3	0.1 ± 0.1
	14.2 ±1.3	*1.6 ±0.3*	*0.4 ±0.2*
Lung	2.1 ± 1.8	0.3 ± 0.2	0.2 ± 0.1
	4.5 ±0.4	*0.9 ±0.1*	*0.6 ±0.2*
Kidney	39.2 ± 2.3	18.0 ± 1.9	4.9 ± 2.5
	26.0 ±1.3	*10.9 ±0.7*	*0.9 ±0.2*
Intestine	2.5 ± 1.8	0.4 ± 0.3	0.13 ± 0.1
	4.5 ±0.3	*6.9 ±0.6*	*0.7 ±0.2*
Heart	2.4 ± 1.4	0.2 ± 0.04	0.2 ± 0.03
	2.7 ±0.3	*0.4 ±0.04*	*0.11 ±0.1*
Muscle	2.7 ± 2.2	0.5 ± 0.2	0.3 ± 0.2
	1.4 ±0.1	*0.3 ±0.1*	*0.1 ±0.1*
Bone	0.7 ± 0.4	0.6 ± 0.2	0.8 ± 0.3
	3.9 ±1.1	*1.4 ±0.6*	*0.4 ±0.2*
Spleen	2.8 ± 2.1	0.6 ± 0.3	0.2 ± 0.1
	3.0 ±0.2	*0.6 ±0.1*	*0.4 ±0.5*

The values are average of %dose/g ± standard deviation for n = 4. Italicized results reported by Vaidyanathan and Zalutsky [12].

high yields (>90%) and in a relatively short 'synthetic' time (2 min). These acids were subsequently converted to their N-succinimidyl activated esters followed by conjugation with chemotactic peptide as a model through their lysine moieties. Sep-Pak purifications make this technique amenable to automation and hold considerable promise as a rapid and simple method for the radiofluorination of bioactive molecules. Tissue distribution in normal CBA/J mice showed that the peptide-[^{18}F]SFPa was excreted predominantly (as expected) through the renal system.

ACKNOWLEDGEMENTS

The authors wish to thank M. Al-Amoudi for the MS analysis. This project was supported by the Research Centre of the King Faisal Specialist Hospital & Research Centre (RAC # 2040027).

REFERENCES

[1] WILKINSON, J., Recent advances in the selective formation of C-F bond, Chem. Rev. 92 (1992) 505.

[2] BUTLER, R., The diazotization of heterocyclic primery amines, Chem. Rev. 75 (1975) 241.

[3] CAMPBELL, A., CHAN, E., CHOOI, S., DEADLY, L., SHANKS, R., The synthesis of some substituted methyl pyridinecarboxylates, Aust. J. Chem. 2 (1971) 377.

[4] DOLL, F., et al., Synthesis and nicotinic acetylcholine receptor in-vivo binding, J Med. Chem. 42 (1999) 2251.

[5] HORTI, A., RAVERT, H., LONDON, E., DANNALS, R., Synthesis of radiotracer for studying nicotinic acetylcholine receptors (+/-)-exo-2-(2-[18F]fluor-5-pyridyl)-7-azabicyclic[2.2.0] heptane, J. Labelled compd. Radiopharm. 38 (1996) 356.

[6] BERRIDGE, M., TEWSON, T., Chemistry of fluorine-18 radiopharmaceuticals, J. Appl. Radiat. Iso., 37, 8, 685.

[7] HAKA, M., KILBOURN, M., WATKINS, D., TOORONGIAN, S., Aryltrimethylammonium trifluoromethanesulfonates as precursors to aryl [^{18}F]fluorides: improved synthesis of [^{18}F]GRB-13119, J. Label. Compds. Radiopharm. 27 (1989) 833.

[8] WESTER, H., HAMACHER, K., STÖCKLIN, G., A comparative study of n.c.a. fluorine-18 labeling of proteins via acylation and photochemical conjugation, Nucl. Med. Biol. 23 (1996) 365.

[9] AL JAMMAZ, I., AL OTAIBI, B., AMARTEY, J., Synthesis of 2-[^{18}F]-fluoroisonicotinic acid hydrazide: Potential radiotracers for tuberculosis, J. of Labeled Compounds and Radiopharm. 44 (2001) 451.

[10] AMARTEY, J., AL JAMMAZ, I., AL OTAIBI, B., Synthesis of 2-[^{18}F]-fluoroisonicotinic acid hydrazide and initial biological evaluation, J. of Nucl. Med. Biol. 29/8 (2002) 801.

[11] OLAH, G., et al., Synthetic methods and reactions. 63. Pyridinium poly (hydrogen fluoride) (30% pyridine-70% hydrogen fluoride): a convenient reagent for organic fluorination reactions, J. Org. Chem. 44 (1979) 3872.

[12] VAIDYANATHAN, G., ZALUTSKY, M., Fluorine-18 labeled chemotactic peptides: A potential approach for the PET imaging of bacterial infection, J Nucl. Med. Biol. 22, 6 (1995) 759.

1-[^{18}F]FLUOROETHYLENEGLYCOL-2-NITROIMIDAZOLES: A NOVEL CLASS OF POTENTIAL HYPOXIA PET MARKERS

R.J. ABDEL-JALIL*, M. ÜBELE**, W. EHRLICHMANN**, W. VOELTER***, H.-J. MACHULLA**

*Chemistry Department,
Faculty of Science,
Hashemite University,
Zarka, Jordan
Email: jalil@hu.edu.jo

** Radiopharmazie,
PET-Zentrum,
Universitätsklinikum Tübingen

***Abteilung für Physikalische Biochemie des
Physiologisch-chemischen Instituts der Universität Tübingen

Tübingen, Germany

Several hypoxia markers contain a nitroimidazole moiety as the reactive chemical species, e.g. ^{18}FNIM [1], ^{18}FETNIM [2], ^{18}FMISO [3] or ^{18}FAZA [4]. It is believed that these imaging agents primarily enter tissue by diffusion and are trapped due to radical formation and subsequent intracellular reaction in the case of decreased oxygen concentration [5]. In particular, the blood brain barrier permeability is thought to play a crucial role in the cerebral uptake of the marker within hypoxia tissues [6].

Recently, new hypoxia PET markers [7] have been developed with higher lipophilicity compared to ^{18}FMISO to enhance the blood brain barrier permeability while avoiding excess non-specific biodistribution. However, none of the developed markers offered improved biological properties over ^{18}FMISO, a well-accepted hypoxic agent. This unsuccesful enhancement of trapping may be due to the lack of an oxygen atom in the β-position to the 2-nitroimidazole ring in these markers [6].

In an attempt to develop new hypoxia markers exhibiting rapid localization in hypoxic tissue, the authors present the synthesis of new hypoxia PET markers with higher lipophilicity than ^{18}FMISO and the required β-oxygen atom (Fig. 1).

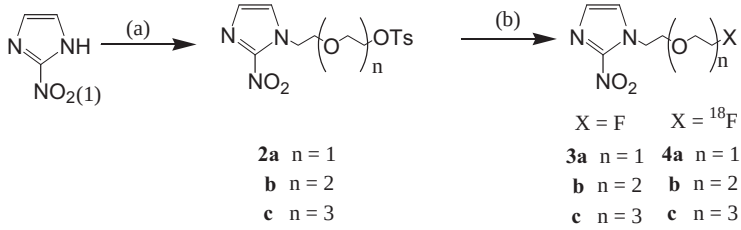

a) TsO-$(CH_2CH_2O)_{n = 2, 3, 4}$-Ts, Et_3N, DMF, rt, 4 d; b) (i) CsF, [bmim][BF_4], CH_3CN, 100 °C, 1h or (ii) *n*-Bu_4NF, THF, rt, 5d; ^{18}F-radiolabeling: (iii) $K^{18}F$/Kryptofix 2.2.2., CH_3CN, 80 °C, 10 min.

FIG. 1. Synthetic scheme for 2-nitroimidazole derivatives.

REFERENCES

[1] LIM, J.L., BERRIDGE, M.S., Appl. Radiat. Isot. 44 (1993) 1085-1091.
[2] TOLVANEN, T., et al., J. Nucl. Med. 43 (2002) 1674-1680.
[3] KAEMAERAEINEN, E.-L., KYLLOENEN, T., NIHTILAE, O., BJOERK, H., SOLIN, O., J. Label. Compd. Radiopharm. 47 (2004) 37-45.
[4] REISCHL, G., et al., J. Nucl. Med. 43 (2002) 364.
[5] MACHULLA, H.-J., Imaging of Hypoxia, Kluwer Acad. Publishers, Netherlands, 1999.
[6] MATHIAS, C.J., et al., Life Sci. 41 (1987) 199-206.

RADIOSYNTHESIS AND IN VIVO EVALUATION IN MELANOMA-BEARING MICE OF *O*-(2-[^{18}F]FLUOROETHYL)-L-TYROSINE AS A TUMOUR TRACER

MINGWEI WANG, DUANZHI YIN, YONGXIAN WANG
Radiopharmaceutical Centre,
Shanghai Institute of Applied Physics, CAS,
Shanghai, China
Email: wmwnuclear@163.com

Abstract

Radiolabelled amino acid *O*-(2-[^{18}F]fluoroethyl)-L-tyrosine ([^{18}F]FET), a clinical potential PET tracer for metabolic imaging of tumour, was synthesized from direct nucleophilic displacement reaction of the precursor *N*-BOC-(*O*-2-tosyloxyethyl)-L-tyrosine methyl ester with the activated [^{18}F]fluoride ion, followed by acidic and basic hydrolysis of the protective groups. The biological evaluation of [^{18}F]FET was investigated with biodistribution studies and qualitative autoradiography (QARG) in B16 melanoma-bearing mice and its activity–time curve was investigated in normal mice. The total synthesis time was within 60 min and the radiochemical yield was about 45% (not decay corrected) and a radiochemical purity of more than 95% after simplified solid phase extraction. [^{18}F]FET showed rapid and high uptake and long retention in tumour as well as low uptake in the brain. The ratios of tumour to brain, tumour to muscle, tumour to blood and tumour to skin of [^{18}F]FET were 4.13 ± 0.38, 2.01 ± 0.20, 2.03 ± 0.12 and 3.40 ± 0.14, respectively at 30 min post-injection and 3.63 ± 0.44, 2.85 ± 0.32, 2.80 ± 0.76 and 4.26 ± 0.63, respectively at 60 min post-injection. The QARGs demonstrated remarkable accumulation of [^{18}F]FET in melanoma with high contrast. In conclusion, [^{18}F]FET was synthesized via a convenient route and it could be a very practical PET tracer for brain tumour imaging and a probable alternative for peripheral tumour imaging.

1. INTRODUCTION

2-[^{18}F]fluoro-2-deoxy-D-glucose ([^{18}F]FDG) is the most important ^{18}F labelled radiopharmaceutical used worldwide as a positron emission tomography (PET) tracer for tumour diagnosis [1, 2]. However, its inherent limitations for brain tumour diagnosis are also well known, such as the false positive findings due to the uptake of the normal brain tissues and inflammatory and infectious lesions [3–5] and low imaging contrast for brain tumour

diagnosis [6, 7]. During the search for new PET tracers, radiolabelled amino acids were widely studied and their powerful clinical potential as tumour PET tracers in neuro-oncology and for peripheral tumours such as lymphoma demonstrated [8]. More attention has been paid to the positron emitter ^{18}F labelled amino acids owing to its advantages over ^{11}C for PET and ^{123}I for SPECT [9], of which the most typical example is *O*-(2-[^{18}F]fluoroethyl)-L-tyrosine ([^{18}F]FET), an analogue of tyrosine developed recently [3, 10]. It was synthesized by a nucleophilic displacement reaction with much higher radiochemical yield than L-[^{18}F]FT [11, 12] and [^{18}F]FMT [13, 14], which were both derived from an electrophilic substitution reaction. Originally, [^{18}F]FET was prepared by a two-step reaction consisting of fluorination of 1,2-bis(tosyloxy)ethane and fluoroethylation of unprotected L-tyrosine, then using HPLC [10] or simple solid phase extraction [15] to separate the final product. However, the existing two-step synthesis of [^{18}F]FET appears cumbersome because of the two separate purifications involved in the process. Later, one-step syntheses of [^{18}F]FET via direct nucleophilic radiofluorination of corresponding precursors were developed by Hamacher and Coenen [16] and Wanga et al. [17].

In this paper, the authors present a novel synthesis method of [^{18}F]FET that they have developed from easily available precursor to improve the radiochemical yield and to simplify the purification procedure. The feasibility of [^{18}F]FET as a PET tracer for brain and probably peripheral tumour imaging was evaluated in B16 melanoma-bearing mice via biodistribution and autoradiography.

2. MATERIALS AND METHODS

2.1. General

Aminopolyether Kryptofix 222 (4,7,13,16,21,24 hexaoxa-1,10-diazabicyclo [8.8.8]hexacosan, $K_{2.2.2.}$) and dry acetonitrile were purchased from Acros, tetrabutylammonium fluoride trihydrate (TBAF·$3H_2O$) from Fluka, *N*-BOC-L-tyrosine methyl ester (*N*-BOC-L-Tyr-OMe) from GL Biochem (Shanghai) Ltd, trifluoroacetic acid from Merck and 1,2-bis(tosyloxy)ethane from TCI. Other chemicals, including sodium hydroxide, potassium carbonate, ammonium chloride, ethyl acetate, acetonitrile and chloroform were of spectral analysis grade or HPLC grade and obtained from the Shanghai Chemical Company (China). All of the chemicals and solvents were used directly without further purification. Sep-Pak Silica Plus cartridge for solid phase extraction and mini-vials were purchased from Waters Corporation, United States of America and

Alltech Associates, Inc., USA, respectively. GF_{254} silica gel plate based on glass came from the Huiyou Silica Development Co. Ltd, Yantai, Shangdong, China.

^{1}H NMR assays were performed on an AVANCE 500 NMR spectrometer (BRUKER). Mass spectra were recorded on a MicroMass GCT CA 055 mass spectrometer (Agilent LCMSD-SL, Agilent Technologies, Palo Alto, USA). Autoradiography was performed on a Packaged Cyclone Storage Phosphor System with storage phosphor scanner and screen (Perkin Elmer, USA). Radioactivity was measured with either a radioactivity counter (FJ-391A2, Beijing Nuclear Instruments, Beijing, China) or radioimmune gamma counter (SN-697, Rihuan Photoelectric Instruments Co. Ltd, Shanghai, China). Thin layer chromatography (TLC) was performed using an imaging scanner (AR-2000, Bioscan, USA) or visualized by UV lamp (Anting Electronic Instruments, Shanghai, China). HPLC was carried out on a Dionex summit system equipped with a P680 HPLC pump (Dionex, USA), PDA-100 photodiode array detector, flow count detector (Bioscan, USA), analytical Vydac C18 column (10 μm, 2.5 mm × 250 mm, Shimadzu Corporation, Japan).

No-carrier-added aqueous [^{18}F]fluoride ion was supplied by Amersham Kexing Pharmaceuticals Co. Ltd.

2.2. Synthesis of [^{18}F]FET

2.2.1. Preparation of the radiofluorinated precursor

To a solution of *N*-BOC-L-tyrosine methyl ester (366 mg) in dry MeCN (10 mL) was added a solution of 1,2-bis(tosyloxy)ethane (580 mg) in dry MeCN (15 mL) and K_2CO_3 (30 mg) and the reaction mixture was stirred under reflux. After 3 h, the solvent was removed under reduced pressure and the residue redissolved in saturated aqueous NH_4Cl solution and extracted with AcOEt. The organic phase was dried over $MgSO_4$, filtered and solvent removed under reduced pressure. The residue was purified by chromatography on silica gel eluted with CH_2Cl_2 and $CHCl_3/Et_2O$ (2:1, vol/vol) to afford *N*-BOC-(*O*-2-tosyloxyethyl)-L-tyrosine methyl ester as yellow oil. MS-EI (m/z,%) : 493 (M^+, 0.8), 437 (0.6), 420 (1.1), 392 (0.3), 377 (1.1), 376 (4.3), 360 (0.5), 332 (0.2), 305 (59), 264 (0.2), 248 (1.1), 219 (0.2), 199 (100), 188 (1.0), 155 (17), 134 (2.2), 117 (1.4), 107 (6.4), 91 (35), 90 (6.0), 88 (5.3), 77 (0.5), 65 (3.4), 59 (3.4), 57 (9.7), 41 (1.6) ; ^{1}H-NMR ($CDCl_3$/TMS) : δ = 7.83–7.81 (d, *J* = 8Hz, 2H), 7.36–7.34 (d, *J* = 8Hz, 2H), 7.01–7.00 (d, *J* = 8Hz, 2H), 6.73–6.71 (d, *J* = 8Hz, 2H), 4.55–4.52 (t, *J* = 6Hz, 1H), 4.36–4.35 (m, 2H), 4.13–4.11 (m, 2H), 3.71 (s, 3H), 3.06–2.97 (m, 2H), 2.46 (s, 3H), 1.42 (s, 9H).

2.2.2. Direct nucleophilic radiofluorination

No-carrier-added aqueous [^{18}F]fluoride ion was treated as previously described [18, 19] to afford the activated $^{18}F^-$–$K_{2.2.2.}$–K_2CO_3 complex. The synthesis route of [^{18}F]FET was determined as in Fig. 1, with slight modifications made according to the literature [16, 17].

To the above complex was added a solution of *N*-BOC-(*O*-2-tosyloxyethyl)-L-tyrosine methyl ester (5 mg) in anhydrous acetonitrile (0.7 mL) and the mixture was heated to 130°C for 30 min. The reaction mixture was dried by evaporation under reduced pressure with a stream of N_2 gas.

2.2.3. Solid phase extraction and removal of protective groups

After cooling to room temperature with a cold nitrogen stream, the dry residue was redissolved in dichloromethane (1.5 mL). The solution was passed through a Sep-Pak Silica Plus cartridge preconditioned with diethyl ether and then eluted with diethyl ether (3 mL). The eluate was dried again with a stream of N_2 gas. Trifluoroacetic acid (0.5 mL) was added to the dry residue and maintained at room temperature for 5 min. Afterwards, the solvent was evaporated under a continuous N_2 flow. To the residue was added 1 mol/L aqueous NaOH solution (0.5 mL), followed by heating for 10 min at 80°C to conduct hydrolysis. The reaction mixture was neutralized with a 1 mol/L solution of HCl (0.5 mL). After adding a certain volume of phosphate buffer saline (PBS, pH7.4), the solution was passed through a sterile 0.22 μm membrane filter to afford the isotonic [^{18}F]FET injection solution.

2.2.4. Quality analyses

The radiochemical purity of [^{18}F]FET was determined using TLC and HPLC. TLC was performed on gel plate based on glass, using CH_3CN/H_2O (95/5, vol/vol) as the developing agent. The mobile phase of HPLC was

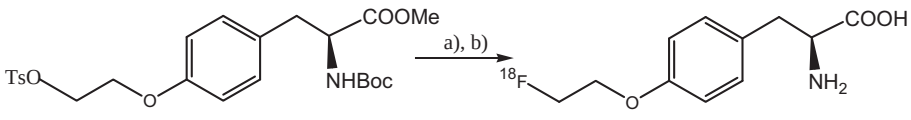

FIG. 1. Reaction conditions: (a) $^{18}F^-$–$K_{2.2.2.}$–K_2CO_3, CH_3CN, 130°C, 30 min; (b) Sep-Pak Silica Plus cartridge; TFA, RT, 3 min; NaOH/H_2O, 90°C, 5 min.

ethanol/water/acetic acid/ammonium acetate (10/87.5/2.25/0.25, by volume) at a flow rate of 1 mL/min.

2.3. Animal experiments

The animal experiments were performed according to the guidelines of the Shanghai Institute of Pharmaceutical Industry (SIPI). The female C57BL/6 mice bearing B16 melanoma (weighing 20–22 g) and normal mice were also supplied by SIPI. All the animals were kept in cages with standardized conditions of light, asepsis and free access to water and food. Mice were inoculated with B16 melanoma cell in the front right armpit. Experiments were performed 8–10 d after inoculation of the tumour cells. At this time, the tumours weighed 300–800 mg and a tumour diameter was about 0.5–1.0 cm.

2.3.1. Biodistribution studies

The tumour-bearing mice were injected with 2.90–3.70 MBq (80–100 μCi) of [^{18}F]FET in 100 μL of PBS through the tail vein. Three mice were sacrificed at each time point by extirpation of eyeball at 5, 10, 30, 60, 90 and 120 min post-injection. After, the dissection was carried out and the tissue samples of interest, including tumour, brain, liver, heart, lung, spleen, kidney, stomach, small intestine, pancreas, muscle, bone, skin and blood, were collected. All samples were weighed and the radioactivity was measured using a SN-697 type radioimmune gamma counter, applying a decay correction. Counts were compared with those of standards and the results were expressed as a percentage of injected radioactivity dose per gram of tissue (%ID/g).

2.3.2. Qualitative autoradiography (QARG)

Another three groups of model mice (n = 3 in each group) were also injected with 2.90–3.70 MBq (80–100 μCi) of [^{18}F]FET in 100 μL of PBS into the tail vein and sacrified at 10, 30 and 60 min post-injection for QARG. QARG was performed using non-sectioned whole body autoradiography. In other words, the intact, completely bleeding carcases of each group were placed directly onto the multisensitive storage phosphor screen for exposure of 5 min in the imaging cassette at room temperature, without cutting into micron thick sections. Then, the storage phosphor screens were read by the storage phosphor scanner with the resolution of 300 DPI to acquire the phosphor image for the qualitative observation of tumour uptake of [^{18}F]FET.

2.3.3. Activity–time correlation of blood

Before the above animal experiments, three normal mice were injected in the tail vein with [^{18}F]FET for the investigation of activity–time correlation of blood. 5 μL of blood was collected by cutting the tail at 1, 3, 5, 10, 15, 30, 45, 60, 90, 120, 150 and 180 min post-injection followed by measurement of the radioactivity of blood at each time point. The activity–time correlation of blood was expressed as a function of time with radioactivity per μL of blood and analysed with DAS 1.0 drug analysis software.

3. RESULTS AND DISCUSSION

3.1. Synthesis of [^{18}F]FET

Originally, [^{18}F]FET was prepared by a two-step reaction consisting of fluorination of 1,2-bis(tosyloxy)ethane and fluoroethylation of unprotected L-tyrosine, then using HPLC [10] or simple solid phase extraction [15] to separate the final product. However, the existing two-step synthesis of [^{18}F]FET appeared cumbersome because of the two separate purifications involved in the process. Later, one-step syntheses of [^{18}F]FET via direct nucleophilic radiofluorination of corresponding precursors were developed by Hamacher et al. [16] and Wanga et al. [17].

In this paper, [^{18}F]FET has been prepared from the nucleophilic substitution of the above tosylated precursor with [^{18}F]fluoride ion in CH_3CN at 130°C for 30 min followed by acidic and basic hydrolysis as shown in Fig. 1. The total synthesis time was about 50 min and a high radiochemical yield was recorded (45% on average, no decay corrected) and high radiochemical purity (more than 95%). Purification via a Sep-Pak Silica Plus cartridge prior to hydrolysis was used instead of HPLC after hydrolysis, which resulted in the simplification of the preparation and the shortening of the whole synthesis time.

3.2. Biodistribution studies

The biodistribution results of [^{18}F]FET in B16 melanoma-bearing mice are summarized in Table 1. [^{18}F]FET showed very fast accumulation into the whole body with a peak occurring at 10 min after IV administration. The radioactivity in the blood of [^{18}F]FET injected mice decreased from 12.6 ± 3.8 at 10 min post-injection to 2.0 ± 0.3 at 180 min post-injection. The uptakes of [^{18}F]FET in all organs decreased with time from 10 min post-injection, e.g.

TABLE 1. BIODISTRIBUTION OF [^{18}F]FET IN ORGANS OF B16 MELANOMA-BEARING MICE
(n = 3, mean ± SD)

	Uptake (%ID/g)							
	5 min	10 min	30 min	60 min	90 min	120 min	150 min	180 min
Tumour	12.7 ± 6.6	19.4 ± 5.6	16.3 ± 5.7	14.6 ± 0.7	12.9 ± 2.0	8.2 ± 3.8	2.4 ± 0.1	2.0 ± 0.1
Skin	5.0 ± 3.6	7.5 ± 1.8	4.8 ± 0.2	3.4 ± 1.4	2.5 ± 1.2	1.9 ± 0.0	1.0 ± 0.1	1.3 ± 0.2
Brain	2.4 ± 1.3	4.3 ± 0.7	3.9 ± 0.6	4.0 ± 0.0	3.5 ± 0.3	3.4 ± 1.8	2.5 ± 0.3	2.0 ± 0.1
Liver	11.3 ± 4.4	14.2 ± 1.5	7.5 ± 0.5	4.8 ± 0.4	4.2 ± 0.3	2.9 ± 0.6	1.8 ± 0.7	1.5 ± 0.7
Heart	12.5 ± 4.5	14.3 ± 2.6	8.1 ± 0.6	5.3 ± 0.4	4.7 ± 0.5	3.0 ± 0.8	2.4 ± 0.4	1.8 ± 0.5
Lung	10.9 ± 3.9	14.4 ± 2.6	8.6 ± 0.6	5.6 ± 0.6	4.7 ± 0.6	3.3 ± 1.0	2.7 ± 0.2	1.8 ± 0.7
Spleen	9.3 ± 5.1	15.0 ± 1.7	8.4 ± 0.8	6.0 ± 0.5	5.8 ± 0.6	3.5 ± 0.9	3.4 ± 0.9	2.0 ± 0.7
Kidney	15.4 ± 6.5	14.9 ± 1.8	9.3 ± 0.1	6.6 ± 0.6	5.7 ± 0.9	3.7 ± 0.7	3.3 ± 0.7	2.1 ± 0.2
Intestine	9.7 ± 4.3	12.8 ± 1.6	7.3 ± 0.8	5.0 ± 1.0	5.0 ± 0.6	5.0 ± 0.3	2.5 ± 0.6	2.0 ± 0.2
Pancreas	27.5 ± 3.7	59.8 ± 9.1	41.1 ± 8.1	32.9 ± 8.6	26.4 ± 9.2	21.1 ± 7.0	15.8 ± 7.8	11.1 ± 1.5
Muscle	9.5 ± 4.9	12.2 ± 2.4	8.1 ± 0.6	5.1 ± 0.5	4.6 ± 0.5	3.0 ± 0.6	2.8 ± 0.4	1.9 ± 0.0
Bone	10.0 ± 4.1	17.7 ± 1.7	14.6 ± 3.3	11.9 ± 1.1	11.3 ± 1.0	10.9 ± 3.8	9.6 ± 0.8	8.2 ± 1.2
Stomach	10.3 ± 5.8	10.7 ± 1.3	6.0 ± 1.2	5.9 ± 0.8	5.8 ± 1.8	4.4 ± 1.3	3.3 ± 0.5	2.5 ± 0.2
Blood	12.0 ± 3.8	12.6 ± 3.8	8.0 ± 0.6	5.2 ± 0.2	5.0 ± 1.4	2.8 ±0.6	2.7 ± 0.3	2.0 ± 0.3

19.4 ± 5.6, 4.3 ± 0.7 and 59.8 ± 9.1 at 10 min post-injection to 2.0 ± 0.1, 2.0 ± 0.1 and 11.1 ± 1.5 at 180 min post-injection in the tumour, brain and pancreas, respectively. [^{18}F]FET showed a certain volume of bone uptake and retention of [^{18}F]FET in the pancreas was higher than that in the other organs as previously reported [10, 17].

The ratios of T/B, T/M, T/Bd and T/S of [^{18}F]FET were 4.13 ± 0.38, 2.01 ± 0.20, 2.03 ± 0.12 and 3.40 ± 0.14 at 30 min post-injection and 3.63 ± 0.44, 2.85 ± 0.32, 2.80 ± 0.76 and 4.26 ± 0.63 at 60 min post-injection. The higher T/B ratios indicated the usefulness of [^{18}F]FET as a PET tracer for brain tumour imaging. Moreover, [^{18}F]FET was also shown to be a promising PET tracer for peripheral tumour imaging with great potential due to the relatively high ratios of T/M, T/Bd and T/S.

3.3. QARG

The accumulation of [^{18}F]FET in the tumour was further confirmed by in vivo QARGs as shown in Fig. 2. The uptake of [^{18}F]FET in B16 melanoma was

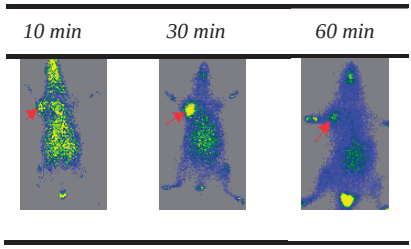

FIG. 2. QARG via non-sectioned whole body autoradiography in the B16 melanoma-bearing mice after intravenous injection of [^{18}F]FET. The arrow indicates the location of the tumour.

visualized vividly at 30 min post-injection and maintained enough contrast of tumour-to-counterparts up to 60 min post-injection. These observations were highly consistent with the results obstained from the biodistribution studies. QARGs showed that the biodistribution patterns of [^{18}F]FET correlated with the implantation positions of the tumours.

Actually, [^{18}F]FET has been investigated to diagnose peripheral tumour by PET imaging [20]. Here, QARG was performed using the non-sectioned whole body autoradiography method which has not, to the authors' knowledge, been used to characterize in vivo biological behaviour of radiolabelled substances to date. Generally, conventional autoradiographs are carried out by frozen section autoradiography using a freeze microtome to cut the tissues of interest, such as the brain or whole body, into sections of thickness ~10–30 μm [21]. The whole procedure is very cumbersome and time consuming, which is a disadvantage for short lived positron emitters such as ^{18}F and ^{11}C. It is necessary to acquire quantitative information regarding the distribution of the receptor in the brain or the accumulation of each organ in the whole body for related tracers. However, when qualitative visualization of accumulation of tracers in tumour tissue is the main purpose, QARG should be taken as a selective method. Qualitative evaluation of tumour uptake could be achieved rapidly by QARGs within about 30 min of acquisition of carcases injected with tracers. Certainly, its limitations are also obvious compared with conventional autoradiographs and small animal PET (microPET), availability of which is rather restricted at present [22].

3.4. Blood activity–time correlation

The blood radioactivity curve of [^{18}F]FET is depicted in Fig. 3. The analysis of the results implied that the activity–time correlation of blood in mice was consistent with a two-component model with a short distribution

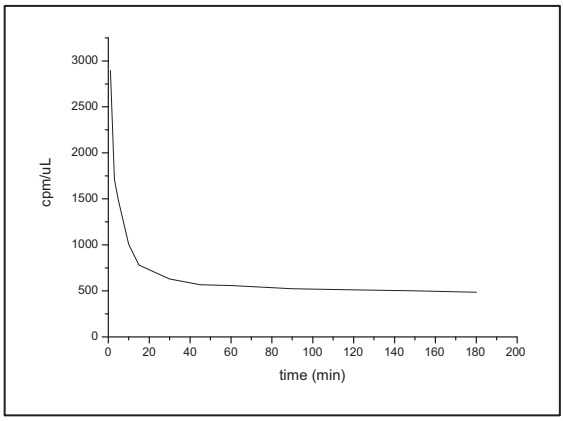

FIG. 3. Blood activity–time correlation of [^{18}F]FET in mice.

phase ($T_{1/2\alpha}$ = 3.7 min) and long clearance phase ($T_{1/2\beta}$ = 448.0 min). Combined with the above results of biodistribution and QARGs, this suggested that [^{18}F]FET might be a rapid PET imaging agent for tumour diagnosis.

4. CONCLUSION

[^{18}F]FET was directly synthesized from the tosylated precursor of *N*-BOC-(*O*-2-tosyloxyethyl)-L-tyrosine methyl ester within 60 min with a good radiochemical yield (45% on average, not decay corrected) and radiochemical purity (more than 95%). Biological evaluation of [^{18}F]FET in B16 melanoma-bearing mice showed significantly high ratios of T/B, T/M, T/Bd and T/S. The results demonstrated that [^{18}F]FET could be used as a useful PET tracer for brain tumour imaging and probably for peripheral tumour imaging.

ACKNOWLEDGEMENTS

The authors are very grateful to Amersham Kexing Pharmaceuticals Co. Ltd for the supply of no-carrier-added aqueous [^{18}F]fluoride ion. Furthermore, they appreciate the excellent technical support in the animal experiments provided by the technologists at their institution.

REFERENCES

[1] HUSTINX, R., BENARD, F., ALAVI, A., Whole-body FDG-PET imaging in the management of patients with cancer, Semin Nucl Med 32 (2002) 35-46.

[2] GAMBHIR, S.S., et al., A tabulated summary of the FDG PET literature, J Nucl Med (2001) 42(Suppl):1S-93S.

[3] HEISS, P., et al., Investigation of transport mechanism and uptake kineticsof O-(2-[^{18}F]fluoroethyl)-L-tyrosine in vitro and in vivo, J Nucl Med 40 (1999) 1367-1373.

[4] KUBOTA, R., et al., Microautoradiographic study for the differentiation of intratumoral macrophages, granulation tissues and cancer cells by the dynamics of fluorine-18-fluorodeoxyglucose uptake, J Nucl Med 35 (1994) 104-112.

[5] SHREVE, P.D., ANZAI, Y., WAHL, R.L., Pitfalls in oncologic diagnosis with FDG PET imaging: physiologic and benign variants, Radiographics 19 (1999) 61-77.

[6] BROWN, R.S., et al., Glucose transporters and FDG uptake in untreated primary human non-small cell lung cancer, J Nucl Med 40 (1999) 556-565.

[7] MAROM, E.M., et al., Correlation of FDG-PET imaging with Glut-1 and Glut-3 expression in early-stage non-small cell lung cancer, Lung Cancer 33 (2001) 99-107.

[8] JAGER, P.L., et al., Radiolabeled amino acids: basic aspects and clinical applications in oncology, J Nucl Med 42 (2001) 432- 45.

[9] LAVERMAN, P., BOERMAN, O.C., CORSTENS, F.H.M., OYEN, W.J.G., Fluorinated amino acids for tumour imaging with positron emission tomography, Eur J Nucl Med 29 (2002) 681-690.

[10] WESTER, H.J., Synthesis and radiopharmacology of O-(2-[^{18}F]fluoroethyl)-L-tyrosine for tumor imaging, J Nucl Med 40 (1999) 205-212.

[11] COENEN, H.H., KLING, P., STÖCKLIN, G., Cerebral metabolism of L-[2-^{18}F]fluorotyrosine, a new PET tracer of protein synthesis, J Nucl Med 30 (1989) 1367–1372.

[12] WIENHARD, K., et al., Increased amino acid transport into brain tumors measured by PET of L-(2-^{18}F)fluorotyrosine, J Nucl Med 32 (1991) 1338-1346.

[13] INOUE, T., et al., Biodistribution studies on L-3-[fluorine-18]fluoro-alpha-methyl tyrosine: a potential tumor-detecting agent, J Nucl Med 39 (1998) 663-667.

[14] INOUE, T., et al., ^{18}F alpha-methyl tyrosine PET studies in patients with brain tumors, J Nucl Med 40 (1999) 399-405.

[15] TANG, G.H., WANG, M.F., TANG, X.L., LUO, L., GAN, M.Q., Fully automated synthesis of O-(2-[^{18}F]fluoroethyl)-L-tyrosine, Journal of Nuclear and Radiochemistry 25 (2003) 44-48 (in Chinese).

[16] HAMACHER, K., COENEN, H.H., Efficient routine production of the ^{18}F-labelled amino acid O-(2-[^{18}F]fluoroethyl)-L-tyrosine, Appl Radiat Isot 57 (2002) 853-856.

[17] WANGA, H.E., et al., Evaluation of F-18-labeled amino acid derivatives and [^{18}F]FDG as PET probes in a brain tumor-bearing animal model, Nucl Med Biol 32 (2005) 367-375.

[18] BLOCK, D., COENEN, H.H., STÖCKLIN, G., Nucleophilic ^{18}F-Fluorination of 1,n-disubstituted alkanes as fluoroalkylated agents, J Label Compd Radiopharm 24 (1987) 1029–1042.

[19] BLOCK, D., COENEN, H.H., STÖCKLIN, G., ^{18}F-Fluorination of H-acidic compounds, J Label Compd Radiopharm 25 (1988) 200-216.

[20] PAULEIT, D., et al., PET with *O*-(2-^{18}F-Fluoroethyl)-L-Tyrosine in Peripheral Tumors: First Clinical Results, J Nucl Med 46 (2005) 411-416.

[21] BERGSTRÖM, M., et al., Autoradiography with Positron Emitting Isotopes in Positron Emission Tomography Tracer Discovery, Mol Imag Biol 5 (2003) 390–396.

[22] BAUER, A., et al., Evaluation of ^{18}F-CPFPX, a Novel Adenosine A1 Receptor Ligand: In Vitro Autoradiography and High-Resolution Small Animal PET, J Nucl Med 44 (2003) 1682-1689.

CYCLOTRON BASED RADIONUCLIDES AND GENERATORS

(Session 13)

Chairpersons

M.M. VORA
Saudi Arabia

M. HAJI-SAEID
IAEA

PRODUCTION OF RADIONUCLIDES WITH A CYCLOTRON

D.J. SCHLYER
Department of Chemistry,
Brookhaven National Laboratory,
Upton, New York,
United States of America
Email: schlyer@bnl.gov

Abstract

The production of radioisotopes for use in biomedical procedures such as diagnostic imaging and/or therapeutic treatments may be achieved through nuclear reactions from charged particle bombardment using an accelerator. The goal is to get the target material into the beam, keep it there during the irradiation and then remove the product radionuclide from the target material efficiently and quickly. The specific design of the cyclotron target is what allows one to achieve this goal. For every radionuclide, there are usually nearly as many target designs as there are people producing the isotope. The design and use of cyclotron targets can be a very complex problem and involves the use of physics, chemistry and engineering in order to produce a target which is reliable and efficient. This paper addresses how basic principles of physics, engineering and chemistry apply to radionuclide production with an accelerator. The concept of power density applied to cyclotron targets, various means of heat removal from the target, and the efficient extraction and separation of the desired product radionuclide from both the target material and the other radioisotopes present is discussed.

1. INTRODUCTION

Nuclear medicine offers one of the safest ways to diagnose and/or treat a number of serious, life threatening diseases including cancer. It does so without adverse effects on normal organs and without the debilitating side effects of some of the more common treatments and extended hospital stays. Each day, thousands of patients with cancer, heart disease and other illnesses receive a radioisotope injection either for diagnosis or for treatment. Radioisotopes and radiopharmaceuticals, which are at the heart of nuclear medicine, are used in the United States of America alone in almost 40 000 procedures every day, and in more than 100 million laboratory tests each year [1–4]. Radioisotopes for these uses are produced either by neutron bombardment of a target material in nuclear reactors or from charged particle bombardment in particle accelerators.

In accelerators, the typical charged particle reactions utilize protons, deuterons and helium nuclei ($^{3}He^{++}$ and α particles) [5].

One clear advantage that accelerators possess is the fact that, in general, the target and product are different chemical elements. This makes it possible to find a suitable chemical or physical means of separation and to achieve high specific activities. The ability to control the energy of the bombarding particle can also lead to fewer radioisotopic impurities by selecting the optimum energy window for irradiation.

The availability of accelerators fits into several categories. First there are university based cyclotrons that are typically multiparticle machines with energies around 30–50 MeV. Then there are the hospital based machines, which are generally dedicated to the production of the standard PET radioisotopes (^{11}C, ^{13}N, ^{15}O and ^{18}F). These cyclotrons accelerate protons in the 10–19 MeV range, and some also produce deuterons with an energy of about half that of the proton (5–9 MeV). The cyclotrons used by industry for large scale production are typically 30 MeV proton only machines, although there are some using lower energies for dedicated production of some radioisotopes [6].

2. NUCLEAR REACTIONS

2.1. Compound nucleus

There is a wide variety of nuclear reactions which are used in an accelerator to produce the artificial radioactivity. The energies of the bombarding particles which are used range from a few MeV to hundreds of MeV [7]. One of the most useful models for nuclear reactions is the compound nucleus model original introduced by Bohr in 1936. In this model, the incident particle is absorbed into the nucleus of the target materials and the energy is distributed throughout the compound nucleus. In essence, the nucleus comes to some form of equilibrium before decomposing with the emission of particles. These two steps are considered to be independent of one another. It doesn't matter how the compound nucleus got to the high energy state, the evaporation of the particles will be independent of the way in which it was formed. The total amount of excitation energy contained in the nucleus will be given by the equation:

$$U = \frac{M_A}{M_A + M_a} T_a + S_a$$

where: U = excitation energy

M_A = mass of the target nucleus

M_a = mass of the incident particle

T_a = kinetic energy of the incident particle

S_a = binding energy of the incident particle in the compound nucleus

The nucleus can decompose along several channels as shown in Fig. 1.

2.2. Q values

There is a minimum energy below which a nuclear reaction will not occur except by tunnelling effects. When the compound nucleus decomposes, the kinetic energy of all the products may be either greater or less than the total kinetic energy of all the reactants. If the energy of the products is greater, then the reaction is said to be exoergic. If the kinetic energy of the products is less than the reactants, then the reaction is endoergic. The magnitude of this difference is called the Q value. If the reaction is exoergic, Q values are positive.

$$Q = \sum \Delta(\text{react}) - \sum \Delta(\text{prod})$$

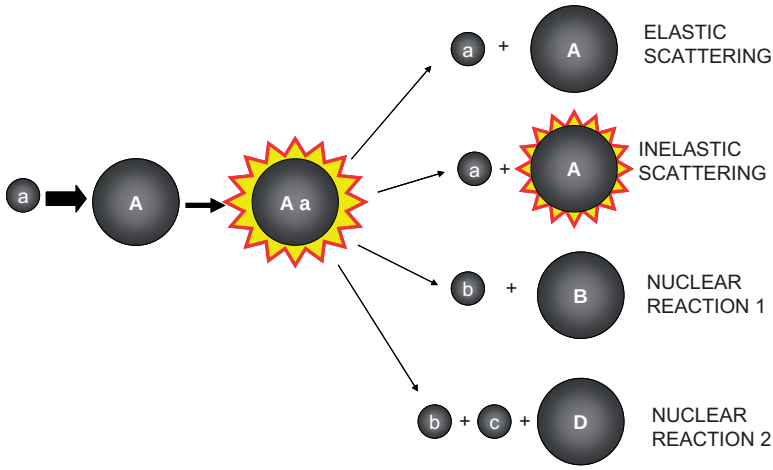

FIG. 1. Compound nucleus and reaction pathways.

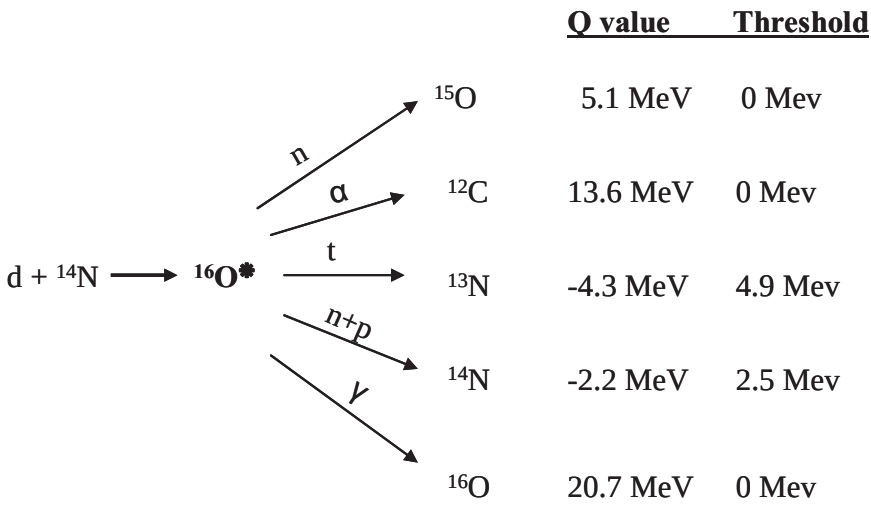

FIG. 2. Diagram of the reactions channels and their associated Q values and threshold energies for the reaction of a deuteron with a ^{14}N nucleus.

An example of the possible reaction pathways is shown in Fig. 2 along with their corresponding Q values and reaction thresholds. The energy changes in a nuclear reaction are large enough that changes in the mass of the reactants and products are observable.

The threshold energy is defined as the minimum projectile energy necessary to satisfy mass energy and momentum conservation. The incident particle energy must be sufficient to overcome the Coulomb barrier and to overcome a negative Q of the reaction. Particles with energies below this barrier have a very low probability of reacting.

2.3. Coulomb barrier

The Coulomb barrier is a measure of the nucleus–nucleus charge repulsion. The Coulomb barrier is given by the relationship.

$$V_{coul} = \frac{(Z_p e)(Z_T e)}{d} = \frac{Z_p Z_T e^2}{R_p + R_T} \approx \frac{0.90 Z_p Z_T}{(A_p^{1/3} + A_T^{1/3})} \text{MeV}$$

where: V_{coul} = Coulomb barrier

Z_p = atomic number of the particle

Z_T = atomic number of the target

R_p = atomic radius of the particle

R_T = atomic radius of the target

A_p = atomic mass of the particle

A_T = atomic mass of the target

Since the compound nucleus must carry off some kinetic energy, the Coulomb barrier measured in the laboratory will be corrected by the amount:

$$V_{coul}^{lab} = \left[\frac{A_{CN}}{A_T} \right] V_{coul}$$

where A_{CN} is the mass of the compound nucleus and A_T is the mass of the target.

Thus, the energy required to induce a nuclear reaction increases as the Z of the target material increases and as the Z of the incident particle increases. For many low Z materials it is possible to use a low energy accelerator, but for high Z materials, it is necessary to increase the particle energy [8].

2.4. Nuclear reaction cross-section

The nuclear reaction cross-section represents the total probability that a compound nucleus will be formed and that it will decompose in a particular channel. This parameter is often symbolized by the Greek letter σ and has the units of barns (10^{-24} cm^2). The number of reactions occurring in one second is given by the relation [8]:

$$dn = I_0 N_A ds \sigma_{AB}$$

where: dn = number of reactions occurring in one second

I_0 = number of particles incident on the target in one second

N_A = number of target nuclei per gram

ds = thickness of the material in grams per cm^2

σ_{ab} = cross-section expressed in units of cm^2

In practical applications, the thickness ds of the material can be represented by a slab of thickness s, thin enough that the cross-section can be considered constant. $N_A ds$ is then the number of target atoms in a 1 cm^2 area of thickness s. If the target material is a compound rather than a pure element, then the number of nuclei per unit area is given by the expression:

$$N_A = \frac{F_A C \Im}{A_A}$$

where: N_A = number of target nuclei per gram

F_A = fractional isotopic abundance

C = concentration in weight

$\Im$ = Avogadro's number

A_A = atomic mass number of nucleus A

3. PRACTICAL PRODUCTION OF RADIOISOTOPES

3.1. Thick target yields

The cross-section is always a function of energy and therefore the yield of the reaction y(E) is also a function of energy. When the cross-sections σ(E) of all reactions concerned are known, the thick target yield Y(E, ΔE) for each radionuclide can be calculated by either numerical or analytical integration of y(E), as a function of both incident projectile energy E and energy loss ΔE of beam in the target itself.

$$Y(E,\Delta E) = \int_{E-\Delta E}^{E} y(E)dx$$

where: Y(E,ΔE) = yield between the energy E and E-ΔE

ΔE = energy lost as the beam passes through a distance x of the target

y(E) = yield of a particular radionuclide at a particular energy E

This definition holds in the raw approximation of a monochromatic beam of energy E, in which the integrand y(x) represents the thin target excitation function.

3.2. Saturation factors

The rate of production is of course affected by the fact that the resulting nuclide is radioactive and is thus undergoing radioactive decay. For short lived nuclides, the competition between formation and decay will come to equilibrium after sufficiently long bombardment times. This point is called saturation, meaning that no matter how much longer the irradiation occurs the production rate is equal to the rate of decay and no more product will be formed.

The rate of formation in this case is given by:

$$R = N\lambda/(1-e^{-\lambda t})$$

where: R = rate of formation of nuclei

N = number target nuclei present at the end

λ = decay constant

The term in the denominator is often referred to as the saturation factor and accounts for the competition of the production of nuclei due to the particle reaction and the radioactive decay of the nuclei which have been produced. It is clear why the assumption had to be made that the beam current was nearly constant since a variation in the beam current would affect the relative number of nuclei being created versus the number being destroyed by decay.

If this relation is substituted back into the cross-section equation then the result is:

$$\sigma_i = 2.678 \times 10^{-10} \left[\frac{A\lambda \ N_i}{I\rho x(1-e^{-\lambda t})} \right]$$

where: σ_i = cross-section for process (mb)

A = atomic mass of the target (amu)

λ = decay constant for species i (sec^{-1})

ρ = density of the target material (g/cm^3)

t = time of irradiation (sec)

x = thickness of the target (cm)

I = beam current (μA)

It should be noted that the time of irradiation and the decay constant are both given in the seconds. This is due to the fact that the beam current is defined in microamperes (μA) which is 6.2×10^{12} charges/second.

3.3. Practical production times

At shorter irradiation times, the fraction of product generated is related to the saturation factor given by $(1\text{-}e^{-\lambda t})$, where λ is the decay constant for the decaying nuclide and t the bombardment time. It is evident that an irradiation equivalent to one half-life would result in 50% saturation. The practical production limit of a given radionuclide is then in most part determined by the half-life of the isotope. It is relatively easy to come near saturation for the production of ^{15}O with a 2 min half-life, but it is not reasonable to irradiate a target for the production of ^{18}F to near the point of saturation because of the times involved.

3.4. Radionuclidic purity

One of the basic facts of life in radioisotope production is that it is not always possible to eliminate the radionuclidic impurities even with the highest isotopic enrichment and the widest energy selection. An example of this is given in Fig. 3 for the production of ^{123}I with a minimum of ^{124}I impurity [9–12].

As can be seen from Fig. 3, it is not possible to eliminate the ^{124}I impurity from the ^{123}I using a proton on ^{124}Te reaction because the ^{124}I is being made at the same energy. All that can be done is to minimize the ^{124}I impurity by choosing an energy interval where the production of ^{124}I is near a minimum. In this case, proton energies higher than about 20 MeV will give a minimum of ^{124}I impurity.

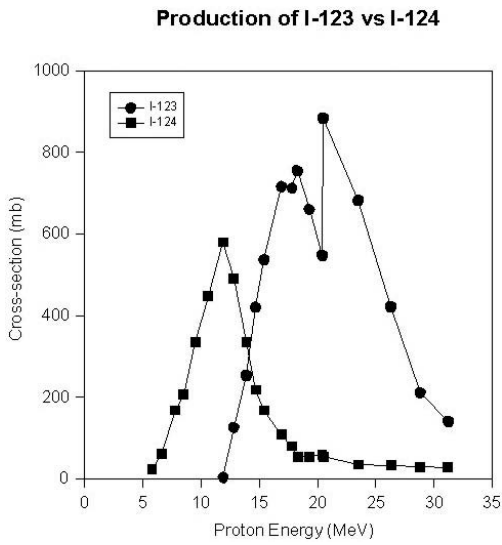

FIG. 3. Cross-sections for the production of ^{123}I and ^{124}I from ^{124}Te using the $^{124}Te(p,n)^{124}I$ and $^{124}Te(p,2n)^{123}I$ nuclear reactions.

3.5. Specific activity

Specific activity is the fraction of radiolabelled molecules relative to the total number of molecules and is usually expressed as a unit of radioactivity per mole of compound. Specific activity is a critically important property in the preparation of radiotracers. It is particularly important in PET, where the radionuclide is incorporated into a radiotracer that is used to probe some physiological process in which very small amounts of the native biomolecule are used. When carrying out these studies, such as probing the number of receptors or the concentration of an enzyme, considerations of the total mass of compound injected become even more important [13, 14]. There is, of course, an ultimate limit to specific activity when nothing but the radioactive atoms or radiolabelled molecules are present. The characteristics of the same radioisotopes are shown in Table 1.

There is a clear need to reach reliable production of high specific activity radiopharmaceuticals, as present day tracers and certainly future tracers include receptor/transporter ligands that are potent. In order for PET to be a true tracer technique, receptor occupancy with the radiolabelled tracer should be kept below 5% in order to avoid pharmacological or pharmacodynamic effects.

TABLE 1. CHARACTERISTICS OF SOME RADIOISOTOPES

Nuclide	Half-life (min)	Decay mode	Maximum specific activity (theoretical)
C-11	20.4	100%$^+$	9220 Ci/μmole (341 TBq/μmole)
N-13	9.98	100%$^+$	18 900 Ci/μmole (700 TBq/μmole)
O-15	2.03	100%$^+$	91 730 Ci/μmole (3394 TBq/μmole)
F-18	109.8	97%$^+$	1710 Ci/μmole (63.4 TBq/μmole)
Cu-62	9.74	99.7%$^+$	19 310 Ci/μmole (714 TBq/μmole)
Ga-68	68.0	89%$^+$	2766 Ci/μmole (102 TBq/μmole)
Br-75	96.0	75.5%$^+$	1960 Ci/μmole (73 TBq/μmole)
Rb-82	1.25	95.5%$^+$	150 400 Ci/μmole (5565 TBq/μmole)
I-122	3.62	75.8%$^+$	51 950 Ci/μmole (1922 TBq/μmole)
I-124	6019.2	23.3%$^+$	31 Ci/μmole (1.15 TBq/μmole)

4. CYCLOTRON TARGETS

4.1. Types of target

The goal of a cyclotron target is to get the target material into the beam, keep it there during the irradiation and then remove the product radionuclide from the target material efficiently and quickly. The specific design of the cyclotron target is what allows one to achieve this goal. Unless care is taken in the design and fabrication of the target, the production of the radioisotope can be far from optimal and may even be impossible. Although the underlying nuclear phenomena are very well known, target behaviour in the form of yield, maximum beam current and obtainable specific activity varies within and across different users. Much of this variation can be attributed to less than optimal matching of the targets and their operating conditions to the actual cyclotrons used. There is a close interplay between beam parameters (size, intensity, emittance, orientation and energy) and the performance of a given target. This variation is seen even within the range of commercial target/cyclotron combinations. A great deal of useful information about targets and target chemistry can be found in the proceedings of the International Workshop on Targets and Target Chemistry. These proceedings are available on-line by courtesy of TRIUMF at http://www.triumf.ca/wttc/proceedings.html This is a very valuable resource for all who are concerned with the production of radioisotopes.

Targets can be made for solids, liquids and gases. There are some advantages and disadvantages to each of these states of matter. The gases are usually easy to get in and out of the target and the separation of the radioactive product from the target material is often simple when compared to solids or liquids. However, gas targets suffer from such effects as beam density reduction and in-target chemistry. Liquid targets often boil and solid targets may vaporize and the radioisotopes may be difficult to separate from the target material after irradiation. Many of these problems are a direct result of the heating of the target by the beam.

4.2. Power deposition

One of the main concerns in targets is the deposition of power in the material during irradiation. If the power deposited exceeds the ability of the target to remove the heat, the target will eventually be destroyed or the target material will be melted, volatilized or reduced in density to the point where the yield will be drastically reduced. In liquid targets, the material may boil and thereby reduce the average density. In gaseous targets, the density of the gas is reduced in the beam strike area. All these effects are a result of the increased temperature in the beam strike area and this in turn is a result of the power deposited by the beam as it passes through matter.

Power (W) = 1 mAΔE (MeV)

The power deposited in the material is the beam current in microamps multiplied by the energy loss in MeV and the result is the number of watts deposited.

The exact position of the heat deposition will depend on the dE/dx (stopping power) of the beam in the target material with most of the heat being deposited near the end of the particle range in the Bragg peak. A simple approximation for the stopping power is given by the relation:

$$\frac{-dE}{dx} = \frac{4\pi z^2 e^4}{m_0 V^2} \frac{\Im Z}{A} \ln \frac{2m_0 V^2}{I}$$

where: dE/dx = energy loss per unit length

z = atomic number of the projectile

e = elementary charge 4.803×10^{-10} $(erg\text{-}cm)^{1/2}$

m_0 = electron rest mass (g)

V = relativistic projectile velocity (cm-sec^{-1})

$\Im$ = Avogadro's number

Z = atomic number of the target material

I = adjusted ionization potential of the target material (eV)

Some additional helpful approximations are that the relativistic velocity is given by the relation:

$$V = 1.384\sqrt{\frac{E}{m}}10^9 \text{ cm/s}$$

where: E = particle energy in MeV

m = particle atomic mass number

The other useful approximations for the adjusted ionization potential are:

$I = 13\ Z$ (eV) if $Z \leq 13$

$I = 9.76\ Z + 58.8\ Z^{-0.19}$ (eV) if $Z > 13$

The stopping power of particles other than protons is given by the relationships:

deuterons $S_d(E) = S_p(E/2)$

tritons $S_t(E) = S_p(E/3)$

^{3}He $S_{\square}(E) = 4S_p(E/3)$

^{4}He $S(E) = 4S_p(E/4)$

4.3. Heat transfer

In order to have a useful accelerator target for the production of a radionuclide, it is necessary to remove the heat generated by the passage of the

beam. There are three modes of heat transfer which are active in targets — conduction, convection and radiation. Radiation is only a significant mode of heat loss at high temperatures (>500ºC). Gases and liquids can transfer heat via convection and conduction. Heat transfer in solids is somewhat simpler than in other media since the heat usually flows through the target matrix mainly by conduction.

Once the heat has been transferred to the cooled surface of the target, it will usually be removed by a fluid such as water flowing against the back of the target. Most of the problems arise at the interfaces, where there are discontinuities in the heat transfer, such as where the target material meets the backing material or where the backing material meets the cooling water. The more efficient the transfer design at these interfaces, the better the heat transfer will be and the less likely one is to have problems with loss of target material or damage to the target during the irradiation.

In cyclotron targetry, it is usual to have both free convection and forced convection. In a gas or liquid target during irradiation, the heating of the fluid inside the target body will cause free convection currents to be set up which will aid in removing heat from the fluid and decrease the effects of density reduction. It is also usual to have some forced convective flow of gas over the front entrance window to the target. For many reasons, this gas is often helium. Since this gas has very low viscosity, it is very efficient in cooling the front window.

There are several factors which contribute to the maximum beam currents which may be run with a solid target. Just as is the case with gas and liquid targets, the beam density is a determining factor. If there are 'hot' spots in the beam, the highest current at which the target may be run will be much lower than if the beam has a uniform profile.

As a simple example of heat transfer in a solid target, use can be made of a thallium target which can be considered as a three layer system facing the accelerator vacuum on one side and the coolant fluid on the other as shown in Fig. 4 [15].

Layer 1: The ^{203}Tl deposit has a physical thickness of 80×10^{-4} cm and is denoted by 'a' in the diagram. In this layer, ^{201}Pb is produced by the ^{203}Tl(p,3n)^{201}Pb nuclear reaction using 30 MeV protons hitting the target at a θ° beam–target angle. Owing to excitation, ionization and bremstrahlung, protons lose kinetic energy in this layer which is converted into heat. Assuming the current density ($\mu A/mm^2$) is constant over the whole surface area, the total heat production rate q_{Tl} (J/s) and the heat production rate per unit of volume q'''_{Tl} ($J \cdot cm^{-3} \cdot s^{-1}$) in this layer are related as:

$$q_{Tl} = q'''_{Tl} aS$$

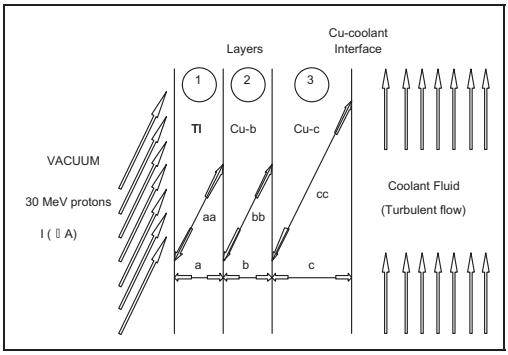

FIG. 4. The three layer system showing the target material on the far left with the coolant on the far right.

Layer 2: The Cu–b layer has a physical thickness of b cm. In this layer protons emerging from the Tl layer are stopped completely. The heat production rate q_{Cu} and the heat production rate per unit volume q'''_{Cu} in this layer are linked by:

$$q_{Cu} = q'''_{Cu} bS$$

Layer 3: The Cu–c layer has a physical dimension of c cm and merely serves as a mechanical support for the Tl layer. The total heat (q_T) produced in the layers is transferred to the coolant fluid through this layer by conduction.

$$q_T = q_{Tl} + q_{Cu}$$

At the Cu–c/coolant interface, the heat is transferred to the coolant only by convection, i.e. no subcooled nucleate boiling occurs and the bulk temperature of the coolant is a constant (T_w).

In steady state conditions, the heat and heat transfers result in a temperature profile represented in Fig. 5, where:

T = temperature

T_m = maximum temperature at the vacuum/Tl interface

T_i = temperature at the Tl/Cu–b interface

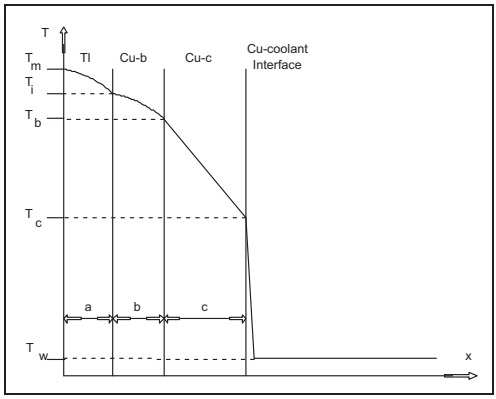

FIG. 5. Temperature profile through the target during irradiation.

T_b = temperature at the Cu–b/Cu–c interface

T_c = temperature at the Cu–c/coolant interface

T_w = temperature of the coolant

The exact temperatures can be calculated if the heat transfer parameters are known. The integrity of the thallium layer is extremely important since this will dramatically affect the transfer of heat through the layer as well as the stopping power of the layer.

4.4. In target chemistry

The chemistry occurring inside a cyclotron target is the basis for the chemical products which are produced during irradiation. The reaction of the highly excited nucleogenic atom with the surroundings during the de-excitation is the determining factor by which radiolabelled molecules will be formed. Many of the chemical reactions occurring were first studied using hot atom chemistry. However, the conditions inside the production target are quite different from a typical hot atom experiment. In the case of a hot atom experiment, the beam current is usually less than 1 μA and the gas is at a pressure of much less than 100 kPa. In a normal production gas target, the beam current may be 20 or 30 μA (or higher with the newer targets) and the pressure up to 7×10^6 Pa. However, in many cases the results from hot atom experiments have been very successful in explaining the product distributions from production gas targets. The state of the matter inside a cyclotron target of course depends on the state of the matter

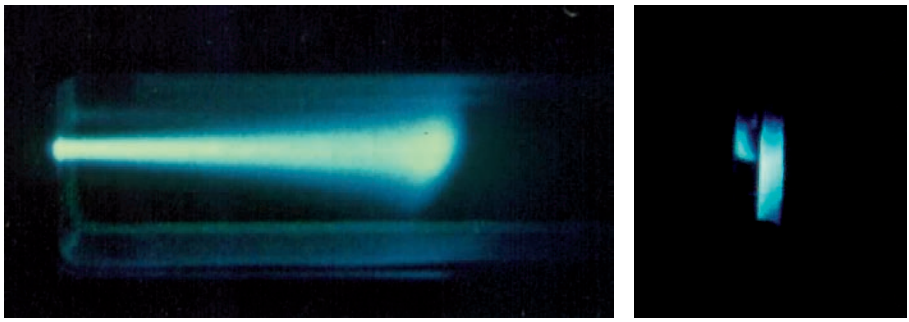

FIG. 6. View inside a gas target (left) during irradiation where the highly excited and ionized gas molecules emit light and heat. Water target (right) shows light emission from the highly excited molecules (with perhaps a small contribution from Cherenkov radiation) as the beam slows in the water. The effects of boiling can also be observed in the picture in the second band of light near the top of the target as the beam passes through the water vapour and is stopped in the water behind the bubble. Gas target picture courtesy of S.-J. Heselius.

being bombarded. In a gas target, the gas is highly ionized and ion–molecule, as well as highly endothermic, reactions are occurring. A view inside the target during irradiation is shown in Fig. 6 [16–18].

Nearly any chemical species can be formed in this ionic soup. When other gases are present, either as contaminants or as additives, the situation becomes very complex. In most cases the final product distribution will be determined by the thermodynamics of the situation since there is more than enough energy to overcome the kinetic activation barriers which would place constraints on the product distribution at lower temperatures.

5. SEPARATION OF RADIOISOTOPES FROM TARGETS

5.1. Gas and liquid targets

The separation of the radioisotope from the target material in gas and liquid targets is usually a simple matter of trapping the desired compound. In the case of a liquid target, this can be a resin or a solid support such as the trapping of fluoride ion on a resin column after irradiation of ^{18}O water [19]. In the gas target, the desired radioisotope can be reacted with some other compound while still in the gas stream, as is the case with carbon dioxide produced in a nitrogen gas target where the $[^{11}C]CO_2$ can be transformed into $[^{11}C]$methanol in lithium aluminium hydride [20, 21].

5.2. Solid targets

Many of the radionuclides used in the modern practice of nuclear medicine can be produced in available cyclotrons using solid targets. Further material on some radioisotopes can be found in Ref. [22].

For most solid targets, electroplating is the best method for producing targets that will withstand high beam currents and yet can be easily processed, although pressed powder targets and salt targets are in common usage. Good thermal contact between the target material and the cooling plate allows beam currents to be higher and by using electrochemical processing and recovery of the material, the processing is greatly simplified.

There are several prerequisites for the successful preparation of a solid target. The following is a list of the physiochemical requirements for a solid target [23]:

- The layer must be homogeneous over the entire surface area;
- The layer must adhere strongly to the carrier at the temperatures typical of those achieved during irradiation;
- The layer must be smooth (not spongy), dense (no occlusions nor vacuoles) and stress free;
- The layer must be free of any organic plating additives (complexing agents or surfactants).

6. CONCLUSION

Development of new and clinically useful radioisotopes and radiopharmaceuticals (tagged compounds) is the single most important contributor to the progress and growth of the field of nuclear medicine. Diagnostic imaging, using techniques such as single photon emission tomography and positron emission tomography (PET), and the measurement of in vivo organ function, physiology, or biochemistry, have become indispensable tools in both clinical research and in patient work-up and management and in drug research and development [24]. Nuclear medicine provides patients with the chance of early diagnosis and a more tailored course of treatment. Effective treatment of disease, in particular cancer, using appropriate radioisotopes, is becoming a reality. The speciality is expanding, with specific PET and single photon emission tomography radiopharmaceuticals allowing for an extension from functional process imaging in tissue to pathological processes and nuclide directed treatments. PET is an example of a technique that has been shown to

yield the physiological information necessary for clinical oncology diagnoses based upon altered tissue metabolism [25].

Most PET drugs are currently produced using a cyclotron at locations that are in close proximity to the hospital or academic centre at which the radiopharmaceutical will be administered. The evolution of PET radiopharmaceuticals has introduced a new class of 'drugs' requiring production facilities and product formulations that must be closely aligned with the scheduled clinical utilization. The production of the radionuclide in the appropriate synthetic form is but one critical component in the manufacture of the finished radiopharmaceutical.

ACKNOWLEDGEMENTS

This research was carried out at Brookhaven National Laboratory under contract DE-AC02-98CH10886 with the US Department of Energy.

REFERENCES

[1] ADELSTEIN, S.J., MANNING, F.J., Isotopes for Medicine and the Life Sciences, National Academy Press, Washington, D.C., (1995).

[2] UNITED STATES DEPARTMENT OF ENERGY, Health and Environmental Research Advisory Committee, Subcommittee on Nuclear Medicine. *Review of the Office of Health and Environmental Research Program: Nuclear Medicine.* Washington, D.C., U.S. Department of Energy, August (1989).

[3] SRIVASTAVA, S.C., Is there life after technetium: What is the potential of developing new broad-based radionuclides. Semin. Nucl. Med. 26, 119-131 (1996).

[4] HOLMES, R.A., "National Biomedical Tracer Facility: Planning and Feasibility Study", U.S. Department of Energy, Society of Nuclear Medicine, New York, New York (1991).

[5] HELUS, F., COLOMBETTI, L.G., (ed) (1983) Radionuclide Production, CRC Press Inc. Boca Raton, Florida.

[6] SCHLYER, D.J., (1987) Production of Short-lived Radiopharmaceuticals for PET. Nuclear Instruments and Methods in Physics Research B24/25 925-927.

[7] GANDARIAS-CRUZ, D., OKAMOTO, K., (1988) Status on the Compilation of Nuclear Data for Medical Radioisotopes Produced by Accelerators, IAEA Report INDC(NDS)-209/GZ.

[8] DECONNINCK, G., (1978) Introduction to Radioanalytical Physics, Nuclear Methods Monographs No.1 Elsevier Scientific Publishing Co. Amsterdam.

[9] GUILLAUME, M., LAMBRECHT, R.M., WOLF, A.P., (1975) Cyclotron production of ^{123}Xe and high purity ^{123}I: A comparison of tellurium targets. *International Journal of Applied Radiation and Isotopes* **26**, 703-707.

[10] LAMBRECHT, R.M., WOLF, A.P., "Cyclotron and short-lived halogen isotopes for radiopharmaceutical applications", Radiopharmaceuticals and Labelled Compounds (Proc. Int. Conf. Copenhagen, 1973), Vol. 1, IAEA, Vienna (1973) 275–290.

[11] QAIM, S.M., STÖCKLIN, G., (1983) Production of some medically important short-lived neutron deficient radioisotopes of halogens. *Radiochimica Acta*, **34**, 25-40.

[12] CLEM, R.G., LAMBRECHT, R.M., (1991) Enriched ^{124}Te targets for production of ^{123}I and ^{124}I. *Nuclear Instruments and Methods* **A303**, 115-118.

[13] FOWLER, J.S., WOLF, A.P., Working against time. Rapid radiotracer synthesis and imaging the human brain. Accounts of Chem Res 1997; 30:181-8.

[14] DANNALS, R., RAVERT, H.T., WILSON, A.A., WAGNER, H.N., Special problems associated with the synthesis of high specific activity carbon-11 labeled radiotracers. In: Emran AM, editor. New Trends in Radiopharmaceutical Synthesis, Quality Assurance and Regulatory Control. New York: Plenum Press, 1991:21-30.

[15] VAN DEN WINKEL, P., Private communication 2004.

[16] HESELIUS, S.-J., LINDBLOM, P., SOLIN, O., (1982) Optical studies of the influence of an intense ion beam on high pressure gas targets. International Journal of Applied Radiation Isotopes 33, 653-659.

[17] HESELIUS, S.-J., SCHLYER, D.J., WOLF, A.P., (1989) A Diagnostic Study of Proton-beam Irradiated Water Targets, Appl. Radiat. Isot., Int. J. Radiat. Appl. Instrum. Part A, 40 663-669.

[18] WIELAND, B.W., SCHLYER, D.J., WOLF, A.P., (1984). Charged Particle Penetration in Gas Targets Designed for Accelerator Production of Radionuclides Used in Nuclear Medicine. Int. J. Appl. Radiat. Isot. 35, 387-396.

[19] SCHLYER, D.J., BASTOS, M.A., ALEXOFF, D., WOLF, A.P., Separation of [^{18}F]fluoride from [O-18] water using anion exchange resin. Int J Appl Radiat Isot [A] 1990; 41:531-3.

[20] LANGSTROM, B., LUNDQVIST, H., The preparation of [^{11}C]methyl iodide and its use in the synthesis of [^{11}C]methyl-L-methionine. Int J Appl Radiat Isot 1976; 27:357-63.

[21] LANGSTROM, B., et al., Synthesis of compounds of interest for positron emission tomography with particular reference to synthetic strategies for ^{11}C labeling. Acta Radiol Suppl 1990; 374:147-51.

[22] INTERNATIONAL ATOMIC ENERGY AGENCY, Standardized High Current Solid Targets for Cyclotron Production of Diagnostic and Therapeutic Radionuclides, Technical Reports Series No. 432, IAEA, Vienna (2004).

[23] VAN DEN BOSSCHE, B., FLORIDOR, G., DECONINCK, J., VAN DEN WINKEL, P., HUBIN, A., Steady-state and pulsed current multi-ion simulations for a thallium electrodeposition process, Journal of Electroanalytical Chemistry 531 (1) p.61-70 (2002).

[24] WAHL, R., editor, Principles and Practice of Positron Emission Tomography, Lippincott Williams & Wilkens, Philadelphia, 2002.

[25] WELCH, M.J., REDVANLY, C.S., editors. Handbook of Radiopharmaceuticals. Sussex: John Wiley & Sons, 2003.

PERSPECTIVES FOR THE LARGE SCALE PRODUCTION OF RADIOLANTHANIDES WITH MEDICAL POTENTIAL

G.-J. BEYER*, H.L. RAVN**, U. KÖSTER**

*Cyclotron Unit, Division of Nuclear Medicine,
University Hospital of Geneva

**CERN ISOLDE

Geneva, Switzerland
Email: gerd.beyer@hcuge.ch

Abstract

The new developments in systemic radionuclide therapy based on chelated peptides calls for metallic radioisotopes with new characteristics. Especially important for new applications is the high specific activity of radiotracers and their availability in therapeutic amounts. The rare earth radionuclides play a dominant role in this context, because of their diversity of radiation properties and half-lives. Presently used methods in production of isotopes of interest have reached their technical limitations, and the progress in systemic radionuclide therapy is limited by availability of radionuclides with the desired characteristics. These radionuclides are either only or best produced in high energy spallation and fragmentation reactions. This paper discusses the opportunity for industrial scale production of such new radioisotopes for future medical use in a fully parasitic or prime user mode. The target and ion source techniques developed for producing high purity mass separated radioactive ion beams at CERN ISOLDE is a well-documented new type of rapid, efficient, continuous and automatic radiochemical separation. Its key element, the electromagnetic isotope separator on-line (ISOL), allows the efficient production of very pure samples of almost all radioactive isotopes with the highest possible specific activity, i.e. the carrier free form. Until now these techniques have exclusively been used to make radioactive ion beams of short lived species for scientific purposes. It is now generally recognized that simplified variants of these techniques will also allow harvesting samples of longer lived, high purity and carrier free radionuclides as byproducts from the spent target material, spent beam absorbers or, eventually, from dedicated on-line target stations. Although current emphasis tends to be limited to producing 'exotic' radioisotopes, the authors believe that the time has come to prepare for more rational and large scale industrial radioisotope production methods using the ISOL target techniques. The future production sites should be put in synergy with either the planned upgrade of CERN ISOLDE and/or one of the major new physics research facilities planned for using GeV proton beams of MW power such

as EURISOL, neutrino factories, spallation neutron sources or accelerator driven systems where the production rates will be orders of magnitude higher than those at current facilities.

1. INTRODUCTION

New achievements in the development of biospecific tracer molecules, such as bioconjugated monoclonal antibodies and peptides, call for metallic radionuclides showing suitable radiation properties for different aspects of therapy. Depending on the tissue to be targeted, there is a need for metallic radionuclides of suitable half-life and with a large variety of different decay properties. The group of the rare earth elements (lanthanides and the other elements of the Group IIIB: Sc and Y) is particularly interesting since it contains more than 700 radionuclides amongst which can be found all the kinds of decay properties desirable. For the following reasons, the entire group of rare earth elements plays and will continue to play an important role in the R&D of radiopharmaceuticals for therapy as well as in their future clinical application [1]:

(i) Owing to the chemical similarity of the rare earth elements we are practically allowed to handle, the radionuclides of this group serve as 'homologues' in a standard protocol for the therapy.
(ii) The chemical similarity of the lanthanides provides a unique possibility to study relationships between physicochemical molecule parameters and the biological response *without changing the basic tracer molecule.* A large number of suitable radionuclides may be used simultaneously in a most efficient way for this kind of R&D work.
(iii) The radionuclides of the rare earth elements provide an almost universal variety of half-life and form of radiation such as single photon emitters for single photon emission tomography (SPECT), beta emitters for therapy with a large range of beta energies, positron emitters for positron emission tomography (PET), an alpha emitter (^{149}Tb), as well as several interesting Auger electron emitters.

With regard to the first aspect, it has already been shown that ^{90}Y and ^{177}Lu are used with the same peptide conjugate without changes in the protocol. As regards the second aspect, mixtures (cocktails) of several radiolanthanides allow a form of 'fine tuning' in tracer development, especially for therapy, as reported, for example, in Ref. [2]. Finally, the third aspect opens the door to individual in vivo dosimetry using PET based on the homologues positron emitter available in the group.

A selection of radionuclides of the rare earth elements is shown in Table 1, including their main potential for an application in diagnosis, for

TABLE 1. SELECTION OF SUITABLE RADIONUCLIDES OF THE RARE EARTH ELEMENTS WITH POTENTIAL USE IN NUCLEAR MEDICINE AND RELATED R&D

Diagnosis		R&D	Therapy		
SPECT	PET		β^-	α	e
^{87g}Y	^{44}Sc	^{88}Y	^{47}Sc*	^{149}Tb	^{165}Er
^{147}Eu	^{85}Y	^{173m}Ce	**^{90}Y**	^{225}Ac/ progeny	
^{147}Gd	**^{86}Y**	^{139}Ce	^{142}Pm		
^{149}Gd	^{134}Ce/La	^{141}Ce	^{143}Pm		
^{155}Tb	^{138}Nd/Pr	^{143}Pm	^{149}Pm*		
^{157}Dy	^{140}Nd/Pr	^{144}Ce/Pr	^{153}Sm*		
^{167}Tm	^{142}Sm/Pm	^{144}Pm	^{156}Eu		
^{169}Yb	^{152}Tb	^{145}Sm	^{159}Gd		
		^{145}Eu	^{161}Tb		
		^{146}Gd/Eu	**^{166}Ho***		
		^{147}Nd	^{169}Er		
		^{148}Gd	**^{177}Lu***		
		^{149}Eu			
		^{152}Eu			
		^{153}Gd			
		^{159}Dy			
		^{168}Tm			
		^{170}Tm			
		^{171}Lu			
		^{172}Hf/Lu			
		^{173}Lu			
		^{174}Lu			

Note: The generator–parent nuclides listed under the PET isotopes are also pure Auger electron emitters if one neglects the positrons of the short lived progeny nuclides. The β^- nuclides for therapy labelled with an asterisk (*) show gamma transitions suitable for SPECT. The nuclides highlighted in bold are those that are already routinely used in the nuclear medical practice.

therapy or for certain R&D work. The following criteria were used in selecting the isotopes:

(a) Nuclear medical imaging using gamma cameras or SPECT requires from the radionuclide proper single photon radiation in the energy range of about 100–300 keV (the ideal would be 140 keV, the photon energy of ^{99m}Tc, the most widely used radionuclide in classical nuclear medical imaging with SPECT). The half-life should be between several hours and about a month.
(b) PET requires the positron decay mode, with positron branching, as high as possible and with a gamma contribution as low as possible.
(c) For therapeutic application it is desirable to have three types of radionuclide. For treatment of manifested solid tumour nodes, beta emitting radionuclides are useful, without gamma radiation, that could contribute to uncontrolled whole body dose of the patient. However, an accompanied gamma radiation suitable for SPECT imaging (100–300 keV) is an advantage. The half-life of the beta emitting isotopes should preferably be between two days and about two weeks. Alpha emitting nuclides are useful for treatment of single cancer cells in circulation (targeted alpha therapy). Fortunately, there is one suitable isotope (^{149}Tb) in this class of elements. Owing to their chemical similarity, ^{225}Ac has also been included into the discussion. Finally, Auger electron emitters are demanded for targeting the DNA inside a cancer cell directly. In principle, all radionuclides that decay via EC mode are Auger electron emitters. The criteria for the nuclides of this group are the half-life (<1 month), available purity of the isotope (specific activity) and the absence of accompanying gamma radiation.
(d) Radionuclides for research distinguish themselves from others by having a suitable half-life of between a week and a year; they must also have very suitable characteristic gamma lines that allow them to be detected easily in a mixture of several isotopes and beta radiation should be absent for easier handling. Essentially, all the SPECT isotopes are suitable for R&D as well.

The nuclear medical community is well aware of the technical difficulties in meeting the fast growth in this demand. Consequently, alternative production routes, ways of cooperation in new large basic physics facilities and new techniques such as mass separation are presently under discussion in order to benefit from the potential of upcoming advanced nuclear centres with their powerful accelerator installations [3].

2. STATUS OF COMMERICAL PRODUCTION OF RADIOLANTHANIDES

As can be seen from Table 1, there are only a few radionuclides of the rare earth elements that are commercially available today. A review on the general production of radiolanthanides has recently been given by Roesch [1]. There are, in principle, three main production routes: (i) radioactive decay (^{90}Y), (ii) neutron induced reactions performed in reactors, leading to the neutron rich nuclides, and (iii) charged particle induced reactions, leading mainly to the neutron deficient nuclides.

The ^{90}Y may be seen as an exception, because this isotope is generated in the decay from the long lived fission product ^{90}Sr, that is, one of the more dangerous fission products. A high degree of technical effort and a correspondingly high level of investment was needed in order to set up a GMP conform production technology that is absolutely safe from the point of view of radioprotection and that meets the high requirements of radionuclidic purity.

The other nuclides highlighted in Table 1, ^{153}Sm, ^{166}Ho and ^{177}Lu, are generally produced in reactors via the (n,γ) process, leading to preparations that are primarily not carrier free. According to Culter et al. [4], the contents of required nuclides in the irradiated target are 1.4%, 0.43% and 18% for ^{153}Sm, ^{166}Ho and ^{177}Lu, respectively (conditions: MURR Reactor, n flux density = 3×10^{14} $cm^{-2} \cdot sec^{-1}$, 155 h irradiation time, using highly enriched target materials). In a few cases one can nevertheless obtain non-carrier added (n.c.a.) preparations in the (n,γ) process, if the required product is generated from the radioactive decay of the primary (n,γ) product. Examples are ^{149}Pm, ^{151}Pm, ^{161}Tb, ^{166}Ho (after double neutron capture) and ^{177}Lu [5]. The high specific activity ^{177}Lu is produced from irradiated Yb targets according to Lebedev et al. [6]. The double neutron capture process in combination with the beta decay provides some possibilities for making a few radiolanthanides in n.c.a. quality. Examples are ^{166}Ho or ^{156}Eu. The latter isotope can be made in reasonable quantities from ^{154}Sm according to:

$$^{154}\text{Sm (n,}\gamma\text{) } ^{155}\text{Sm} \rightarrow ^{155}\text{Eu (4.96 a) (n,}\gamma\text{) } ^{156}\text{Eu. } (\sigma_1 = 5.5 \text{ b}) \quad (\sigma_2 = 4040 \text{ b})$$

Owing to the high formation cross-section, the long lived intermediate product is burned down efficiently to the required ^{156}Eu. These examples should simply illustrate that radiochemistry provides certain possibilities for making rare earth isotope products in higher qualities. Nevertheless, we are confronted with the problem that it only allows deriving one product from each target.

A similar situation occurs in accelerator based production routes [1]. Cyclotrons provide increased possibilities for making radiolanthanides. Generally, carrier free products can be obtained since the production process is generally combined with a change in the nuclear charge of the target element. Usually, the amount of target material needed is larger, mainly because of smaller formation cross-sections in the charged particle induced reactions. The larger quantities of target material require greater effort in their radiochemical separation, since usually a carrier free product has to be separated from a neighbouring 'macro' amount of target material. Even if this separation can be carried out in an efficient way, the problem of 'one target, one product' remains.

A more rational approach would be to separate the radiolanthanides from fission products. At least the $ß^-$ emitting rare earth nuclides for the lanthanides up to Eu/Gd and for Y may be considered as products. Yttrium-91 has been routinely produced from fission in the Department of Radioisotopes in the Rossendorf Research Centre [7]. Praseodymium-143 has been separated at high quality and used as a DTPA complex to measure local blood flow in eye surgery using mini-Si-detector probes. Even ^{153}Sm has clearly been obtained in the Sm fraction of fission produced radiolanthanides. However, consideration needs to be given to the significant dilution of the product nuclei resulting from the presence of other isotopes of the same element produced simultaneously, including the stable isotopes. In the case of Sm these isotopes would be ^{154}Sm (stable), ^{152}Sm (stable), ^{151}Sm (91a) and ^{149}Sm (stable). The isotope ^{150}Sm is shielded by ^{150}Nd. This gives the advantage that from one target it would be possible to harvest several elements. However, a mass separation step would be needed if the production of high quality preparations was required.

3. HIGH ENERGY PROTON INDUCED REACTIONS

Nowadays, the discovery, production and study of new and existing radioactive isotopes are done by means of radioactive ion beam (RIB) facilities as shown in Fig. 1. In particular, those based on the isotope separator on-line (ISOL) attached to an intense accelerator beam are of interest here. They are very efficient and their use of thick targets (mole/cm^2) results in extremely high production rates of nuclei with half-lives ranging from minutes to weeks. These radionuclides are less interesting for nuclear physics studies, but of potential interest for medical applications. Such facilities are optimized for the production of the most short lived nuclei far from the line of stability for nuclear physics studies and need nuclear reactions with high energy particles

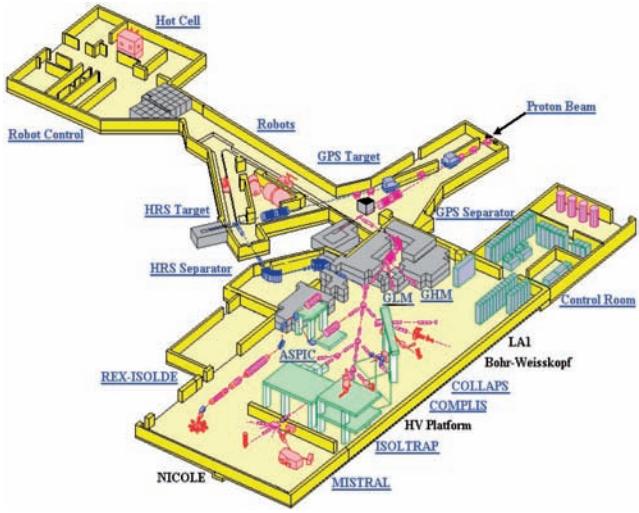

FIG. 1. Layout of the world leading ISOL facility CERN ISOLDE.

for their production. Apart from the cost, this has important technical consequences. The reactions have many exit channels so that the resulting product mixture is very complex both chemically and isotopically. In order to make continuously pure samples of interesting short lived exotic species, a number of particular fast procedures for their purification has been developed especially for the rare earth elements.

These new isotope production techniques are centred on an electromagnetic mass separation that, in conjunction with a chemically selective release from the target and/or the ion source, allows production of mono-isotopic ion beams with high efficiency. By collection of the continuous ion beam of long lived nuclei, the strength of the high purity radioisotopes obtained for medical research has been thoroughly demonstrated and reviewed, in particular with respect to the biomedical research done with carrier free lanthanides, mainly performed within the experimental programme at ISOLDE [8–12]. In this paper, emphasis is made of the virtues of the ISOL production and separation methods that have been developed in conjunction with electromagnetic mass separation and the possibility for their general use in the large scale production of almost any existing radionuclide of interest.

These procedures are now ripe for application in the commercial radioisotope production process where they could rapidly be introduced as an additional purification step in the existing production lines for making carrier free variants of currently used medical isotopes. For production of more

uncommon isotopes of similar high quality, the present ISOL facilities only allow supplying the samples needed for biomedical research. In future, they may become widely available as by-products of a number of planned new large basic physics research facilities on-line to GeV proton accelerators in the MW class, such as EURISOL [13, 14]. Cooperation with one of these constitutes an opportunity for their large scale industrial production. This may be done either in an off-line mode, independent of the physics programme where the radionuclides are harvested from the spent targets, or ultimately from dedicated on-line target stations optimized for the longer lived medical radioisotopes.

The onset of the spallation reaction at proton or light ions at energies >100 MeV opens up a vast range of neutron deficient nuclei while the almost full range of neutron rich nuclei may be produced by the same particles or by fast neutron induced fission of ^{232}Th or ^{238}U. For years this has been exploited in the RIB facilities for production and study of the most short lived species [15]. As shown in Fig. 2 these scientifically interesting nuclei located at the extremes of the production curve are accompanied by a huge amount of longer lived nuclei found at the top of the yield curve. It can be seen that production rates of up to 10^{13} atoms/s may be reached in the future facilities. They result from the tens of millibarn formation cross-sections in conjunction with the use of very thick targets (moles/cm^2).

These production methods have only rarely been used for supplying nuclear medicine research and not at all for commercial production. The reason is not only the difficult access to the energetic particle beams and their

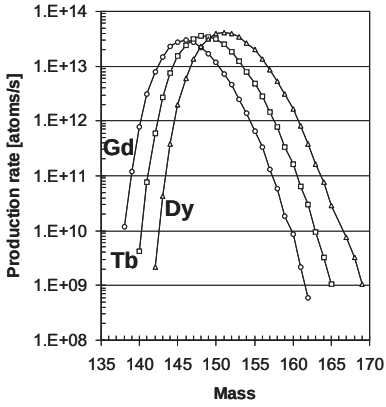

FIG. 2. Production rates at EURISOL for some rare earth isotopes which could be retrieved from the 30 cm long Hg converter target irradiated with a 5 mA, 1 GeV proton beam.

present modest intensities but also a lack of suitable radiochemical methods. The many exit channels of these reactions result in very complex reaction mixtures both chemically and isotopically as seen in the example shown in Fig. 2. To separate an isotope of interest out of this large amount of target material requires a very high chemical selectivity in conjunction with a mass separation.

The authors believe that the time has come to establish more rational and larger scale industrial radioisotope production using these reactions since the long lived residues may in the future become available for free as a by-product from the MW targets needed for production of short lived species in a number of planned facilities.

4. NEW PRODUCTION METHODS DERIVED FROM ISOL TECHNIQUES

It has been a major challenge to transfer rapidly and continuously the reaction products brought to rest in a thick target into an accelerated ion beam of short lived nuclei as illustrated in Fig. 3. The sensitivity to impurities, the 10^{-8} mol/s low throughput of many ISOL ion sources and the short delay requirement does not allow using conventional aqueous phase chemistry to separate the radioactive element from the target material. Instead, new physico-chemical methods based on high temperature targets were developed (see for example Ref. [16]). They allow the mass transfer to the ion source of the wanted species to be effected via diffusion in the solid state and vacuum sublimation. Production of a very broad range of radioactive ion beams is currently

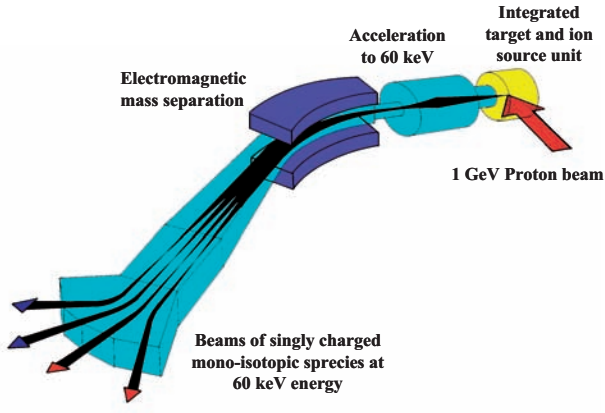

FIG. 3. The principle of the on-line mass separator.

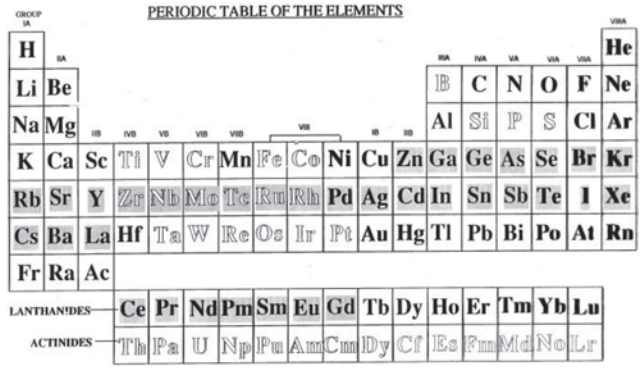

FIG. 4. Elements for which radioisotopes can be produced in carrier free form using the ISOL technique [15].

available for the elements shown in Fig. 4 by combining the release of the products from refractory compounds kept at high temperature with an ion source of a mass separator [15].

A typical combined target and ion source unit [17] developed for each element or group thereof is shown in Fig. 5. The mass separation assures a purification from any other produced isotope of the same element of $>10^3$, i.e

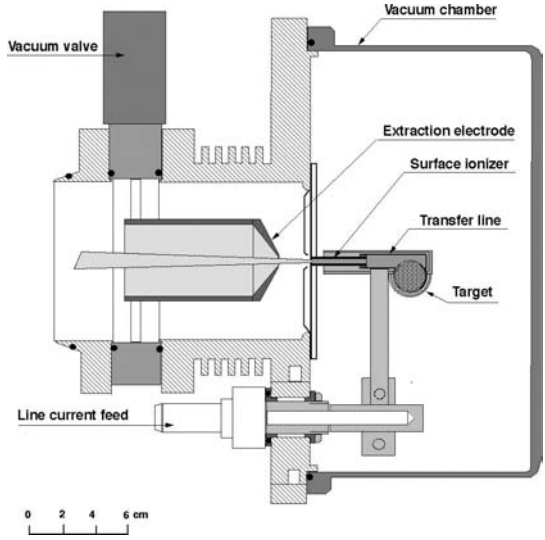

FIG. 5. A typical ISOLDE target and ion source unit as used for production of the rare earth elements.

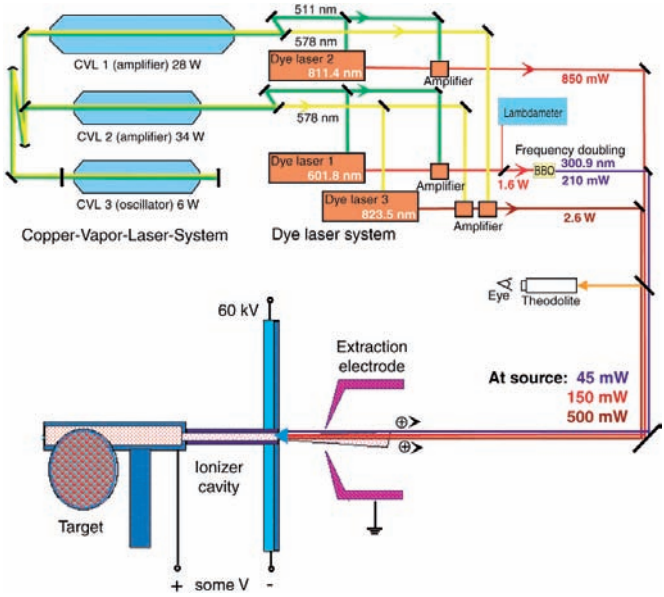

FIG. 6. Schematic layout of the RILIS at ISOLDE [6].

the typical achievable mass separation enhancement factor. The chemical separation factor from any produced isobar can reach the same order of magnitude. This is particularly true for the recently developed resonance ionization laser ion sources (RILIS) [18] of which the principle is shown in Fig. 6 [13]. Combined with the high temperature target, it allows the conversion of the order of 10% of the nuclei produced in the target into particularly pure beams of the elements shown in Fig. 7.

Since there is no need for a high speed of release as in the nuclear research application, the extreme temperatures that shorten the lifetime of the target oven and ion source can be avoided. Cost effective variants of these new radiochemical techniques developed for the ISOL RIB facilities are already available and ready to be transferred to the industry for production of the above mentioned high quality radioisotopes.

Although operating specialized target units on-line may become the ultimate solution for continuous production of selected radionuclides, use of the ISOL methods in an off-line mode seems to be the most appropriate.

In this way, the irradiated reaction material charged into the target and ion source unit may be obtained from a variety of sources ranging from conventional (n,γ) reaction products to samples abundantly available in a high energy accelerator laboratory. These range from target units or samples of refractory

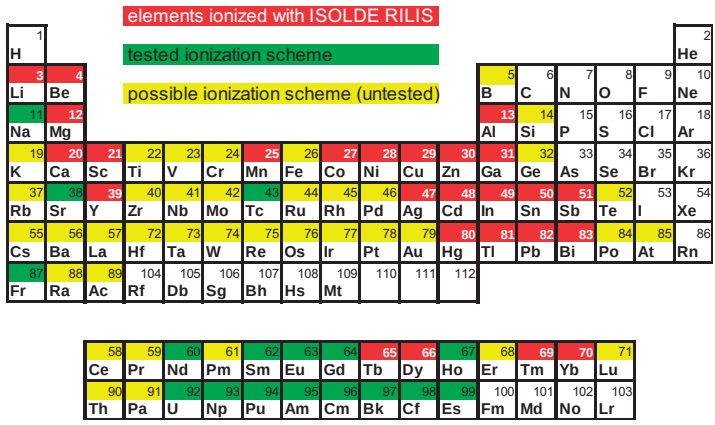

FIG. 7. Elements for which the RILIS ionization scheme has been tested at ISOLDE or other RILIS facilities using copper vapour pump lasers.

target materials irradiated in the spent beam absorbers to samples separated from any other radioactive waste and brought into an ion source friendly form. An overview of radiochemical techniques related to the separation of lanthanides is given in Ref. [19]. The idea of processing materials that are normally considered to be radioactive waste in order to separate 'high tech' isotope products for research and medical application has already been demonstrated [20]. A typical example of a new, highly desirable product that such a facility could mass produce is the often discussed $^{82}Sr/^{82}Rb$ generator which has extremely high isotopic purity. It is presently not available since it needs off-line Sr isotope separation, the feasibility of which has already been demonstrated at ISOLDE [21, 22].

The use of the described ISOL methods brings a number of other advantages. The non-destructive high temperature separation allows the targets or the target materials to be used for many irradiations. This reduces the waste flow and makes it almost free of liquids. The carrier free radioactive isotopes are delivered as an ion beam which conveniently allows their collection by implantation in any substrate optimized for the efficient labelling of the pharmaceutical product [11] or production of very compact (mm^3) isotope generators [23].

The broad product spectrum, in combination with the mass separation, allows the simultaneous collection of a large number of interesting radionuclei with these high quality parameters. This is a powerful tool to support systematic research activities in radiopharmaceutical development [8].

5. MEDICAL ISOTOPES FROM FUTURE HIGH POWER ACCELERATOR DRIVEN PROJECTS

Modern accelerators with GeV proton beams in the multi-MW power class are today on our horizon to serve as drivers for a number of planned research and energy producing purposes. They range from various neutrino sources over RIB facilities to accelerator driven systems for nuclear waste management. Common to them all is the need to convert the energy of the beam into a flux of various types of short lived particle by stopping it in a converter target consisting of an element with high Z. As a by-product, the spallation reaction yields a vast spectrum of useful radionuclides. Accumulated in the converter target they all represent an interesting production opportunity if they are harvested by means of the above mentioned methods.

Since the project group of the recently finished EURISOL Report [24] has decided to make provisions for associating industrial isotope production with its operation, examples taken from this project are discussed below. With its 'proton to neutron converter' target and several target stations connected to mass separators, it represents perhaps the most elegant source for providing the raw material needed to produce these 'high tech' medical isotope products. An associated laboratory described in Ref. [13] would constitute a unique potential for industrial production of essentially all existing radioisotopes of interest.

The main source of radioisotopes could be the spallation neutron source needed to decouple the high power deposited by a proton beam from the target and the ion source for production of fission fragment beams. As shown in Fig. 8 [25], such a target may consist of a mercury flow that serves both as neutron source and heat transfer medium. Samples extracted from the Hg target and cooling loop allow parasitic harvesting to the physics experiments' mixed spallation products well suited for subsequent refinement in an off-line mass separator.

In Table 2, the calculated production rates in the EURISOL converter target of a number of interesting radionuclides are given. These are only a few cases representative of different applications that serve to illustrate the potential of the proposed isotope production mode using the Hg target. They compare very favourably with other technologies, where any exist for producing sufficient quantities of the radioisotopes concerned. (Included for comparison is the production rate of the most important fission product, ^{99}Mo, extensively used as a generator for ^{99m}Tc, of which the production is not optimal with the Hg target undergoing mainly spallation reactions). There are a number of radionuclides (especially from the lanthanides) with great potential for therapeutic application [8].

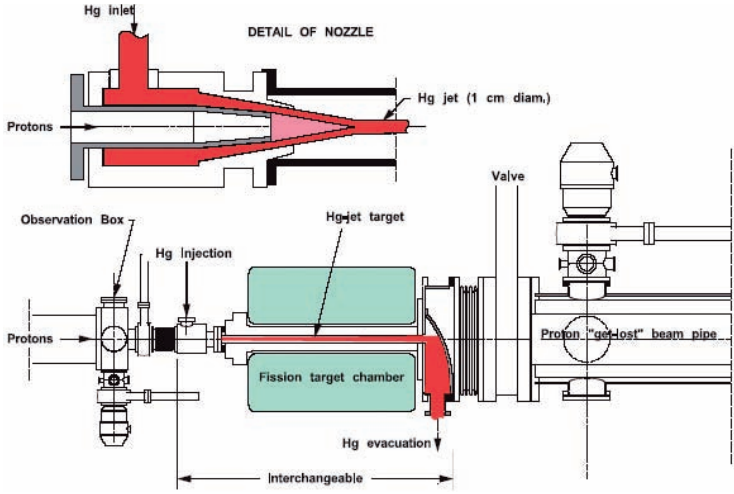

FIG. 8. Schematic layout of a high power target module. A jet of mercury is injected via an annular nozzle that allows coaxial injection of the multi-MW, 1 GeV proton beam. Neutrons from the (p,xnyp) reaction in the Hg then interact with the surrounding hot UC_x fission target matrix, from which the radioactive atoms produced emerge for ionization and subsequent acceleration.

A number of long lived isotopes were included that are suitable for use in generators, thus making short lived isotopes available on-site in a hospital without running facilities for direct production. Examples are ^{188}W, ^{82}Sr, ^{68}Ge and ^{44}Ti, but this list is not exhaustive. Finally, the authors have included some radioisotopes of the light elements needed for various applications in industry and research. These radionuclides are usually difficult to obtain (^{32}Si, ^{26}Al and ^{28}Mg), but could be produced with relative ease in connection with the EURISOL facility.

In addition, the possibility of access to samples collected from the radioactive beam spectrum, spent targets, as well as material activated in the spent beam absorbers, would give free access to an unlimited variety of both conventional and new radioisotopes.

6. CONCLUSION AND OUTLOOK

The mass separation technology derived from the RIB-ISOL facilities constitutes a technically very attractive new operational step ready to be integrated into large scale medical isotope production. It makes available

TABLE 2. ESTIMATED PRODUCTION RATES AT EURISOL FOR A NUMBER OF INTERESTING NUCLIDES WHICH COULD BE RETRIEVED FROM THE Hg TARGET [13]

Radio-isotope	Half-life $T_{1/2}$	X-section σ (mb)[‡]	Production rate[§] (per s)	Alternative production processes		Applications
192-Ir	74 d	2.58E+00	**1.0E+14**	(n,γ)	reactor	Sealed sources for industry and cancer therapy
188-W/Re	69 d	6.90E-02	**2.7E+12**	(2n,γ)	HFR**	Radio-immunotherapy with 188-Re
178-W/Ta	22 d	8.08E+00	**3.1E+14**	(p,4n)	accelerator	Generator with potential in PET[†]
177-Lu	6.7 d	6.31E-02	**2.4E+12**	(n,γ)	reactor	Therapy with labelled antibodies and peptides
166-Ho	25.8 h	5.30E-03	**2.0E+11**	(n,γ)	reactor	Therapy with labelled antibodies and peptides
149-Tb	4.12 h	9.21E-01	**3.5E+13**			Targeted alpha therapy, single cancer cell targeting
148-Gd	74.6a	5.31E-01	**2.1E+13**	spallation	accelerator	Low energy alpha sources
153-Sm	46.75 h	1.41E-03	**0.6E+11**	(n,γ)	reactor	Therapy of bone metastases
127-Xe	76.4 d	9.22E-02	**3.5E+12**	(p,x...)	accelerator	SPECT*, lung ventilation and brain perfusion
117m-Sn	13.6 d	1.78E-01	**0.7E+13**	(n,γ)	HFR	Systemic radionuclide therapy
99-Mo/ 99m-Tc	66 h	2.78E-01	**0.6E+13**	(n,f)	reactor	Most important radionuclide for nuclear medical imaging
89-Sr	50.5 d	5.39E-01	**2.1E+13**	(n,γ), (n,p)	reactor	Palliative therapy of bone metastases
82-Sr/Rb	25.5 d	1.36E-01	**0.5E+13**	(p,4n)	accelerator	Generator, PET, myocardial perfusion
68-Ge/Ga	288 d	9.38E-02	**3.6E+12**	(p,2n), spall.	accelerator	Different PET imaging procedures, calibration of PET
67-Cu	61.9 h	3.83E-01	**1.5E+13**	(p,α)	accelerator	Therapy with labelled antibodies and peptides
44-Ti/Sc	47.3 y	1.77E-03	**0.7E+11**	spallation	accelerator	Generator, great potential for PET
32-Si	101 y	3.03E-02	**1.2E+12**			Important isotope for R&D and technical application
26-Al	7.16e5 y	6.05E-03	**2.3E+11**	(p,n)	cyclotron	Important isotope for R&D and technical application
28-Mg	20.9 h	1.45E-02	**0.6E+12**			Important isotope for R&D

* SPECT: Single photon emission computerized tomography, most common nuclear medical functional imaging technology, based on gamma emitting radionuclides

† PET: Positron emission tomography, modern and most recent functional imaging technology in nuclear medicine, based on the positron annihilation and coincidence detection and localization of the two 511 keV annihilation photons

‡ σ: Cumulative cross-sections for formation in an Hg-target irradiated by 1 GeV protons.

§ rate: Production rates per s for a 5-mA 1-GeV proton beam in a 30 cm long Hg-target. The Hg inventory is expected to be 500 L. Assuming that after saturation has been achieved we would distil 5 L/h: this would then produce 4 Ci of 99-Mo per hour, for example. For smaller proton beam currents, the numbers would have to be scaled accordingly

* HFR: High flux reactor.

another dimension in terms of the quality of isotopes prepared, namely, the highest possible specific activity and isotopic purity.

Used either on-line or off-line to modern accelerator beams, it opens up in addition a vast range of other useful isotopes presently in demand, but so far not available for medical application. By applying these techniques to the abundant long lived residues that will become available as by-products from the targets of future high power accelerator driven physics projects, they may be made available on an industrial production scale.

The delivery of these high quality radioisotopes in the form of an energetic ion beam has opened up a number of new techniques for production of radiopharmaceutical products by means of ion implantation.

REFERENCES

[1] ROESCH, F., FORSSELL-ANDERSON, E., Radiolanthanides in Nuclear medicine, Metal Ions in Biological Systems, Volume 42: Metal Complexes in Tumor Diagnosis and as Anticancer Agents, A.Siegel and H.Siegel (eds.), Marcel Decker, Inc., New York - Basel 2004, pp.77-108.

[2] BEYER, G.J., et al., The influence of EDTMP-concentration on the biodistribution of radio-lanthanides and ^{225}Ac in tumor bearing mice, Nuclear Medicine and Biology **24** (1997) 367.

[3] RIVARD, M.J., et al., The US national isotope program: Current status and strategy for future success, Appl- Rad. And Isotopes **63** (2) (2005) 157-178.

[4] CULTER, C.S., et al., Cancer Biotherapy & Radiopharmaceuticals **15** (6) (2000) 531.

[5] MIKOLAJCZAK, R., PARUS, J., Prospects for carrier-free lanthanide production in the nuclear reactor, COST D18/0004/Working group Meeting, Athens (Greece), May 20-22 (2004).

[6] LEBEDEV, N.A., NOVGORODOV, A.F., MISIAK, R., BROCKMANN, J., ROESCH, F., Radiochemical separation of no-carrier-added ^{177}Lu as product via the ^{176}Yb(n,γ)^{177}Yb ◊ ^{177}Lu process, Appl.Radiat.Isotopes. **53** (2000) 421.

[7] JANTSCH, K., et al., 30 Jahre Radioaktive Präparate Rossendorf, ROTOB & ISOCOMMERZ Booklet, D.Dörr, H.Schmidtke and I.Hein (eds.) Rossendorf 1988.

[8] BEYER, G.J., Radioactive Ion Beams for Biomedical Research and Application, Hyperfine Interaction **129** (2000) 529-553.

[9] BEYER, G.J., Radioactive ion beams for biomedical research and nuclear medical application, in: Advanced Technology and Particle Physics (ICATPP-7), Villa Olmo, Como (Italy), Oct.15-19, 2001, World-Scientific, New York, pp.504-511.

[10] BEYER, G.J., et al., Spallation produced ^{167}Tm for medical application, in:Medical Radionuclide Imaging 1980, IAEA Vienna, IAEA-SM-247/60 (1981) Vol.1, pp.587-598.

[11] BEYER, G.J., RUTH, T.J., The Role of Electromagnetic Isotope Separators in the Production of Radiotracers for Bio-Medical Research and Nucler Medical Applications, Nucl. Instr. and Meth. B204 (2003) 694-700.

[12] BEYER, G.J., et al., Targeted Alpha Therqapy (TAT) in vivo – direct evidence for single cancer cell kill using ^{149}Tb-Rituximab, Eur.J. of Nuclear Medicine and Molecular Imaging **33** (4) (2004) 547-554.

[13] RAVN, H.L., et al., Appendix C in [24] http://www.ganil.fr/eurisol/Final_Report/APPENDIX-C.pdf

[14] BEYER, G.J., KOESTER, U., RAVN, H.L., Medical Isotope Program at a Multi-MW proton Driver, Proc. Workshop on Physics with a Multi-MW Proton Source, May 25-27, 2004, CERN (Switzerland).
[15] RAVN, H.L., ALLARDYCE, B.W., On-line mass separators, in Treatise on Hevy Ion Science, Vol.8, D.A.Bromley (ed.), Plenum Press, New York 1988.
[16] BEYER, G.J., NOVGORODOV, A.F., ROESCH, F., RAVN, H., Spallation Produced Radioisotopes for Nuclear Medical Applicatioon, in Data Requirement for Medical Radio-Isotope production, Tokyo (Japan) April 20-24, IAEA Vienna, (1987), Isotopenpraxis **25** (1) (1989) 2-10.
[17] KÖSTER, U., ISOLDE target and ion source chemistry, Radiochimica Acta **89** (2001) 749-756.
[18] KÖSTER, U., Resonance ionization laser ion sources, Nucl. Phys. **A701** (2002) 441c-451c.
[19] BEYER, G.J., HERRMANN, E., TYRROFF, H., Gewinnung tragerfreier Radionuklide der Lanthaniden (Production of carrier-free radionuclides of the lanthanides), Isotopenpraxis **13** (6) (1977) 193-203.
[20] NOVGORODOV, N.A., et al., Isolation of lanthanide and hafnium radioisotopes from a massive Ta-target irradiated with 1 GeV protons, Mid-Term Evaluation Workshop on LanthanideChemistry for Diagnosis and Therapy, F.Roesch (ed.), COST Chemistry Action D 18, Heidelberg (Germany), 22-25 July 2002, p.29.
[21] BEYER, G.J., ROESCH, F., RAVN, H.L., A high purity $^{82}Sr/^{82}Rb$ generator, CERN-Report, CERN-EP/90-91 (1990)
[22] YUSHKEVICH, Y.V., et al., A high efficient ion source with surface ionization for the determination of micro-traces of radioactive Sr isotopes, Report JINR Dubna P13-94-213 (1994), Annual Report, Inst.Nuclear Chemistry, University Mainz 1993/1994.
[23] BEYER, G.J., RAVN, H.L., A new type of $^{81}Rb/^{81m}Kr$ generator made by ion implantation, Appl. Radiat. Isot. **35** (1984) 1075.
[24] The EURISOL Report, A feasibility study for a European Isotope-Separation-On-Line Radioactive Ion Beam Facility, http://www.ganil.fr/eurisol/Final_Report.html
[25] RAVN, H.L., Advanced target concepts for production of radioactive ions and neutrino beams, Nucl. Instr. and Meth. **B204** (2003) 197-204.

PRODUCTION OF ^{123}I-MIBG AT IPEN-CNEN/SP

M.F. DE BARBOZA, V. SCIANI, R. HERRERIAS,
M.M.N. MATSUDA, N.T.O. FUKUMORI, L.C.A. SUMIYA,
H. MATSUDA, A.A. SOUZA, M.M. GOES, J.T. PIRES,
J. MENGATTI, C.P. GOMEZ DA SILVA
Instituto de Pesquisas Energéticas e Nucleares IPEN-CNEN,
São Paulo, Brazil
Email: mbarboza@ipen.br

Sodium [^{123}I]iodide is obtained in a Cyclone 30 (IBA) at IPEN-CNEN/SP. The production process uses the following nuclear reaction: ^{124}Xe (p,2n)$\rightarrow^{123}$Cs$\rightarrow^{123}$Xe$\rightarrow^{123}$I. The ^{124}Xe gas is highly enriched (>99.8%) which results in ultra pure ^{123}I end product. The water cooled target (internal volume = 75 mL) is machined from aluminium alloy. In front of the target there are two helium cooled molybdenum windows and an alignment system consisting of a pair of four sector collimators. The irradiation is performed with protons of 30 MeV energy and an effective beam current on target of 60–70 μA. The ^{124}Xe transference from the storage bottle to the target and the recovery of the gas after irradiation and return to the bottle is made cryogenically with liquid nitrogen through stainless steel pipes. The [^{123}I] activity on the wall of the target is rinsed with sterile water and the [^{123}I] active solution (60–70 mL) is transferred to the hot cell. With a ^{124}Xe gas pressure (without proton beam) of 2 bars, about 220 MBq/μA of ^{123}I at end of bombardment was obtained.

The labelling process is based on the copper(I) assisted exchange radioiodination methods using MIBG sulphate, $(NH_4)_2SO_4$ and $CuSO_4$ at 165–170ºC for 30 min. Some groups have reported that radiochemical purity after the exchange radioiodination was sufficient and that no further purification was needed. From these data, the preliminary conclusion is that 1% benzyl alcohol and a low temperature (–10ºC) are effective stabilizers of ^{123}I-MIBG solutions over 24 h. Addition of 1% benzyl alcohol and storage at 4ºC resulted in a fourfold reduction of the formation rate of free [*I]. Amartey [1] concluded that temperature and benzyl alcohol had a slight cumulative effect in retarding decomposition and the product remained above 90% for over 7 d at the lower specific activities [2, 3].

After the reaction time has elapsed, the vial is cooled to room temperature and a sterile saline–benzyl alcohol 1% solution is added. The volume is adusted until a desirable radioactive concentration is achieved. The active solution is sterilized through a 0.22 μm Millipore filter. After quality control aproval, the final product is delivered to nuclear medicine centres.

The radiochemical and radionuclide tests of ^{123}I are determined with Whatmann 3MM paper (1.5 cm × 12 cm) in 85% MeOH (R_f $*I^-$ = 0.75 and R_f $*IO_3^-$ = 0.40) and by γ ray spectroscopy using a HPGe detector, before the labelling procedure. The radiochemical impurity of ^{123}I–MIBG is evaluated in a fast paper chromatographic system: Whatman 3MM (1 cm × 8 cm), in n-butanol, acetic acid and water (5:2:1) as a solvent.

The values are: R_f ^{123}I–MIBG = 1.0 and free [^{123}I] iodide = 0.0 [4, 5]. The retention of ^{123}I solution in a strong anionic resin is greater than 99% and the recovery of ^{123}I–Na is more than 97% of total activity in 3 mL of 0.02N NaOH. The radionuclide purity of ^{123}I–Na and the radiochemical purity of ^{123}I–MIBG are >98% and >97%, respectively, in 90% of all routine production during a 24 h period at low temperature, without any purification step (Tables 1 and 2). The SD is less than 1.0%.

The microbiological analysis is determined in a different culture medium which is incubated both at room temperature and at 33 ± 2ºC. The apirogenicity is evaluated using the 'in vitro' Limulus test. The method was developed, validated and simplified to extend it to large scale productions at the IPEN-CNEN/SP radiopharmacy centre.

During 2004, 129.5 GBq of ^{123}I–Na and 48 GBq of ^{123}I–MIBG in 37 batches, respectively, were distributed to approximately 28 hospitals and nuclear medicine centres in Brazil.

TABLE 1. RADIOCHEMICAL PURITY OF ^{123}I –Na AND ^{123}I –MIBG IN PAPER CHROMATOGRAPHIC SYSTEM

Batch (n = 37)	^{123}I–Na	^{123}I–MIBG
M	98.89	97.68
SD	0.26	0.35

TABLE 2. STABILITY OF ^{123}I –MIBG KEPT AT LOW TEMPERATURE

Batch (n = 37)	1 h	24 h
M	98.81	97.72
SD	0.30	0.58

REFERENCES

[1] AMARTEY, J.K., AL-JAMMAZ, I., LAMBRECHT, R.M., An efficient batch preparation of high specific activity [^{123}I] and [^{124}I] mBGI., Appl. Radiat. Isot. **54** (2001) 711–714.

[2] MERTENS, J., GYSEMANS, M., "Cu^{1+} assisted nucleophilic exchange radiohalogenation: application and mechanistic approach", New Trends in Radiopharmaceutical Synthesis, Quality Assurance, and Regulatory Control (EMRA, A.M., Ed.), Plenum Press, New York (1991) 53.

[3] NEVES, M., PAULO, A., PATRICIO, L., A kit formulation of [^{123}I]-metaiobenzylguanidine (MIBG) using Cu (I) generated "in-situ" by sodium disulphide, Appl. Radiat. Isot. **43** (1992) 737.

[4] ALMEIDA, M.A., DE BARBOZA, M.F., COLTURATO, M.T., The synthesis of ^{131}I-MIBG. In Cox, P.H. & Touya, E. News Perspectives in Nuclear Medicine. Pt 2, p.185, Gordon & Breach Science Publishers (1985).

[5] ROSSOUW, D.T., Routine Production and Quality Control of ^{123}I-labeled mBGI at NAC, Appl. Radiat. Isot. **43** (1992) 1301-1302.

A NEW ^{82}Sr–^{82}Rb GENERATOR

A. BILEWICZ, B. BARTOŚ
Institute of Nuclear Chemistry and Technology,
Warsaw
Email: abilewicz@ichtj.wew.pl

R. MISIAK, B. PETELENZ
Institute of Nuclear Physics,
Cracow

Poland

Owing to the similarity of rubidium and potassium cations, the radionuclide ^{82}Rb, a positron emitter, has been used in nuclear medicine to characterize myocardial perfusion with high sensitivity and specificity [1–3]. The advantage of ^{82}Rb PET versus classical SPECT with ^{201}Tl is the short half-life of ^{82}Rb ($T_{1/2}$ = 75 s) which allows one to scan patients every 10 min and to reduce the exposure of patients to radiation. Additionally, ^{82}Rb is a generator produced from the longer lived parent radionuclide ^{82}Sr ($T_{1/2}$ = 25.55 d), which also permits clinical PET studies in hospitals which do not have expensive on-site cyclotrons. Numerous methods for the manufacture of ^{82}Sr–^{82}Rb generator have already been described [4, 5]. All these procedures, however, suffer from various limitations, e.g. complicated multistep separation of ^{82}Sr from the rubidium target and insignificant radiation resistance of the organic extractans and ion exchange resins. To get around these disadvantages the authors used an inorganic ion exchanger — cryptomelane MnO_2 which has a tunnel framed structure with exchangeable alkali or alkali earth cations. The average tunnel diameter is 280 pm, therefore the sorbent is selective for those cations with crystal ionic radii of 130–150 pm, e.g. K^+, Rb^+, Ba^{2+} and Ra^{2+}. To find the optimum conditions for Rb^+–Sr^{2+} separations, the distribution coefficients (K_d) of Rb^+ and Sr^{2+} on cryptomelane MnO_2 were determined as a function of HNO_3 concentration. The influence of the HNO_3 concentration on the K_d for Sr^{2+} and Rb^+ on cryptomelane MnO_2 was studied. It was observed that K_d for Rb^+ even at 1M HNO_3 is very high. This confirms the high affinity of cryptomelane MnO_2 for cations with ionic radii close to 150 pm. For Sr^{2+}, whose ionic radius is lower (118 pm), K_d decreases with increasing concentration of H^+ ions. For the efficient separation of the Rb^+–Sr^{2+} pair, 0.5 mol/dm^3 HNO_3 was chosen as the optimal solution, wherein the K_d for Rb^+ on cryptomelane MnO_2 is greater than 10^4, while for Sr^{2+} it is close to 1. This allows one to perform a simple and quantitative separation of ^{82}Sr from the irradiated rubidium target.

The ^{82}Sr isotope was produced in the AIC-144 cyclotron located in the Institute of Nuclear Physics, Cracow. In the pilot experiment, a target of 0.133 g RbCl of natural isotopic abundance (72.17% ^{85}Rb, 27.83% ^{87}Rb) was irradiated for 4 h with the internal proton beam of 48 MeV and 0.5 μA. At this energy, proton activation of the natural rubidium target leads to direct or indirect formation of ^{82,83,85}Sr and ^{82,83,84,86}Rb isotopes. The radionuclides detected by gamma spectrometry in the irradiated target are presented in Table 1. After the 8 d waiting period, which is enough to allow decay of ^{83}Sr, the RbCl target was dissolved in 0.5M HNO_3 solution. Next, the solution was passed through the cryptomelane MnO_2 column bed. The inactive rubidium (target material) and ^{83,84,86}Rb were quantitatively adsorbed on the cryptomelane MnO_2. The effluent from the column was made alkaline with 1M NaOH to pH6–8. Afterwards, the strontium radionuclides from the neutralized solution were loaded on top of the SnO_2(aq) bed. The inorganic ion exchanger (tin oxide) was prepared by acidification of sodium stannate solution according to the procedure described in Ref. [6]. The ^{82}Rb formed from decay of ^{82}Sr was eluted from the column by 0.9% NaCl (physiological saline). The elution was performed every 10 min. The radionuclide purity of the effluent was measured by gamma spectroscopy after the decay of ^{82}Rb. Additionally, the decay curves of the effluent fractions were also measured. The ^{82}Sr and ^{85}Sr breakthroughs measured by gamma spectroscopy were lower than the established limits. After passing 1 L of 0.9% NaCl through the column, no significant breakthrough was observed either by gamma spectrometry or by analysis of the decay curves. The half-life of the eluted ^{82}Rb determined from the decay curve measured for more than 6 expected half-lives, is identical with the value reported in the literature.

TABLE 1. RADIONUCLIDES DETECTED IN THE ^{nat}RbCl TARGET AFTER IRRADIATION WITH A 48 MeV PROTON BEAM

Radionuclide	$T_{1/2}$ (d)	Activity (MBq)	Nuclear reaction
^{82}Sr	25.5	6.49	^{85}Rb(p,4n) ^{82}Sr
^{83}Sr	1.35	4.45	^{85}Rb(p,3n) ^{83}Sr
^{85}Sr	64.8	8.55	^{85}Rb(p,n) ^{85}Sr ^{87}Rb(p,3n) ^{85}Sr
^{83}Rb	86.2	18.60	^{83}Sr(EC, β^+)$\rightarrow$^{83}Rb
^{84}Rb	32.9	14.29	^{85}Rb(p,pn) ^{84}Rb
^{86}Rb	18.7	18.66	^{85}Rb(n,γ) ^{86}Rb

REFERENCES

[1] ANDERSON, C.J., WELCH, M.J., Chem. Rev. **99** (1999) 2219.
[2] PARKASH, R., DEKEMP, R.A., RUDDY, T.D., J. Nucl. Card. **11** (2004) 440.
[3] EPSTEIN, N.J., et al., Appl. Radiat. Isotop. **60** (2004) 921.
[4] BRIHAYE, C., GUILLAUME, M., COGNEAU, M., J. Biophys. Med. Nucl. **6** (1982) 151.
[5] VALLABHAJOSULA, S., et al., J. Nucl. Med. **22** (1981) 76.
[6] CLEARFIELD, A., Inorganic Ion Exchange Materials, CRC Press Inc., Boca Raton, Florida (1982) p.144.

CYCLOTRON PRODUCTION OF ^{103}Pd VIA PROTON INDUCED REACTIONS ON A ^{103}Rh TARGET

M. SADEGHI, H. AFARIDEH, G. RAISALI
Cyclotron Department, Nuclear Research Centre
for Agriculture & Medicine,
P.O. Box 31585-4395,
Karaj, Islamic Republic of Iran
Email: msadeghi@nrcam.org

M. HAJI-SAEID
International Atomic Energy Agency,
Vienna

Abstract

Electroplated rhodium was employed as the target for cyclotron production of ^{103}Pd. The electrodeposition of rhodium metal on a copper backing experiments were performed in acidic sulphate media using $RhCl_3 \cdot 3H_2O$, $Rh_2(SO_4)_3$ (recovered from hydrochloric acid solution) and also the commercially available Rhodex plating baths. The paper discusses development of a high current density (2.4 A/cm^2) electrodissolution system that allows solubilization of rhodium fragments, powder, and pieces of foil and wire in the presence of hydrochloric acid and chlorine gas. An electrodissolution apparatus was found better than other dissolution methods in terms of personnel shielding and ^{103}Pd yield. The ion exchange column chromatography method was simple and effective for the purification of ^{103}Pd.

1. INTRODUCTION

Prostate cancer is a common malignancy in men in the Western world. In recent years, improvement in biochemical diagnostic methods and the availability of a wide range of treatment options have increased the number of patients surviving free of disease. It has been noted that the proportion of patients treated by permanent brachytherapy is rapidly increasing (more than 40 000 in 1998 in the United States of America) and reached 50% in 2006 [1]. The favourable results of permanent implants may, however, not be reproducible if strict treatment procedures and patient selection guidelines are not followed. For this reason, regular updates on recommendations are published

by the American Brachytherapy Society [1], which also reports on the large number of clinical studies and dosimetry problems [2–12]. Essentially, two radionuclides, namely ^{125}I and ^{103}Pd, are used for this technique. As early as 1958, ^{103}Pd was proposed by Harper et al. [13] for interstitial implantation. It was not until 1987 that encapsulated ^{103}Pd sources became commercially available in the USA, where a company now operates more than 10 dedicated accelerators to produce this nuclide [14]. Recently, a manufacturer in Europe also brought its patented type of ^{103}Pd seed implants to the world market.

The accelerator production method for ^{103}Pd used nowadays is based on the irradiation of rhodium metal with rather low energy protons via the reaction ^{103}Rh (p,n)^{103}Pd, followed by a default chemical separation of the radionuclide from the expensive target material. Harper et al. [15] and Lagunas-Solar et al. [16] described some early procedures.

An alternative production and purification route for ^{103}Pd employing silver targets has been proposed by Fassbender et al. [17].

Irradiated rhodium metal targets (plated layers, foils and wires) have been frequently dissolved by sodium bisulphate fusion (time consuming, complex medium), by gold tetrachloroaurate oxidation (very expensive, time consuming) and by alternating current electrodissolution in hydrochloric acid. Up to now the latter method has been recommended for the solubility of foils (not applicable for rhodium powder, wires or fragments) [18, 19]. A new, high current density electrodissolution technique resulting in quantitative solubility of the target material in acid has been developed.

Since rhodium is a precious metal, it is, therefore, essential that it be recovered from the processed solution of the radiochemical separation and reused for preparation of the electrodeposition bath. The electrodeposition of Rh using Rhodex baths gives quite acceptable quality for irradiation purposes. However, after electrodissolution and radiochemical separation, rhodium is present as chloride complexes in about 6M HCl solutions and not suitable for direct use in the Rhodex bath. The investigations were, therefore, conducted to evaluate the cycle of recovery/electrodissolution/electrodeposition for routine production of ^{103}Pd.

2. EXPERIMENTAL

The production of ^{103}Pd is mainly achieved via the nuclear reaction ^{103}Rh (p, n)^{103}Pd, which is well suited to low energy cyclotrons [20]. The production of this radionuclide in the Islamic Republic of Iran is highly important, therefore the Cyclone-30 cyclotron (IBA, Belgium) at NRCAM was employed. This work was also partially supported by the IAEA. The solid targetry system in

this cyclotron is made up of a pure copper backing on which the target materials are electrodeposited. To take full benefit of the excitation function and to avoid the formation of the radionuclide impurity ^{101}Pd, the proton entrance energy should be 18 MeV [20]. The physical thickness of the rhodium layer is chosen in such way that for a given beam/target angle geometry the particle exit energy should be 6 MeV. According to the SRIM code, the thickness has to be 475 μm for 90° geometry. To minimize the thickness of the rhodium layer (and hence lowering the cost price per target), a 6° geometry is preferred, in which case a 48 μm layer is recommended. Identification and assay of gamma ray emitting radionuclides were carried out using gamma spectroscopy with a high purity germanium (HPGe) detector (Canberra™ model GC1020-7500SL).

2.1. Target fabrication

Rh target preparation from sulphate plating baths

To prepare the sulphate baths, the hydrated rhodium oxide (Rh_2O_3(aq)) was used which in turn had been recovered from hydrochloride acid solution containing rhodium chloride complexes. Therefore, the procedure included two parts:

(1) Recovery of Rh as rhodium oxide from chloride solution

The hydrochloric acid solution containing Rh was primarily obtained from the electrodissolution of the irradiated rhodium target on which a radiochemical separation of ^{103}Pd had been performed. This solution was passed through a 0.45 μm filter (HVLP, Millipore), the filtrate evaporated to near dryness, 300 mL water added to the residue and the pH of the solution adjusted to 10–10.5 with 10M NaOH until a yellow, colloidal solution of Rh_2O_3(aq) was formed.

To improve the filterability of the yellow Rh_2O_3(aq) precipitate, the solution was allowed to digest for 24 h at 50°C under gentle stirring and then passed through a Bleu Band filter paper (Schleich & Scheull 589). The precipitate on the filter was washed several times with water to remove most of the adsorbed Cl^- ions. Since some of the yellow precipitate had gone through the filter paper, the filtrate was passed through a second 0.45 μm filter. The Rh_2O_3(aq) on the filters was left in air for 24 h to dry, followed by grinding into a fine powder, then dried for 48 h under vacuum at room temperature and finally weighed.

(2) Electrodeposition of Rh on the Cu backings

To prepare the plating solution, 5.7 g of the recovered hydrated rhodium oxide (for 4 targets with a thickness of about 48 μm) was transferred into a 100 mL beaker with a magnetic stirring bar and 10 mL of 95% sulphuric acid was then carefully introduced into the beaker. The beaker was covered with a watch glass. The solution was heated to 350°C under gentle stirring until SO_2 fumes evolved and thereafter heating continued for 15 min. A brownish yellow solution was then obtained. The solution was added to 300 mL of water in a 600 mL beaker, passed through a 0.45 μm filter paper and the pH adjusted to 1.0–2.0. Five grams of sulphamic acid was then added to the solution and diluted to 450 mL with water. The electrolyte solution was transferred into the plating vessel and a direct current applied to the electrodes. The electrodeposition was carried out at 60°C under bi-directional stirring (1000 rpm, 8s/8s) for 24 h using a current density of 8.55 mA/cm^2.

2.2. Electrodissolution

The electrodissolution system consists of a cylindrical upper body (diameter 70 mm, height 120 mm) and a conical lower part (height 30 mm) ending in a 12 mm diameter circular window allowing the attachment of the filter combination. The latter consists of a classical G-4 glass frit fitted with an end glass tube allowing removal and recirculation of the solution by means of a high flow rate (1 L/min) peristaltic pump. This loop contains water coolant (glycol) to allow removal of heat produced during the electrochemical dissolution of the Rh. The G-4 supports a home-made graphite fibre (diameter 100 mm, 360 holes of 0.5 mm) clamped in a ring of copper (to ensure electrical contact) and a Perspex ring. Above the filter combination, a supply compartment allows introduction of reagents that is also done by means of peristaltic pumps. The upper graphite ring electrode (thickness 2 mm, external diameter 100 mm, window diameter 20 mm) is also mounted in a copper/Perspex ring combination 30 mm above the graphite filter. Sealing of the system is obtained by means of O-rings and by clamping different parts. The upper window of the unit is closed by means of a Perspex cover fitted with nipples that allow the escape of nitrogen oxide and excess chlorine. The latter are absorbed in sodium hydroxide solution to avoid contamination of the environment (Fig. 1).

The main problem in the ^{103}Pd radiochemical stage is dissolution of target material due to extremely low chemical reactivity of rhodium metal towards acids, alkalis and other corrosive reagents. The Cu carrier was dissolved by flow rate controlled introduction of nitric acid into the vessel holding the vertically

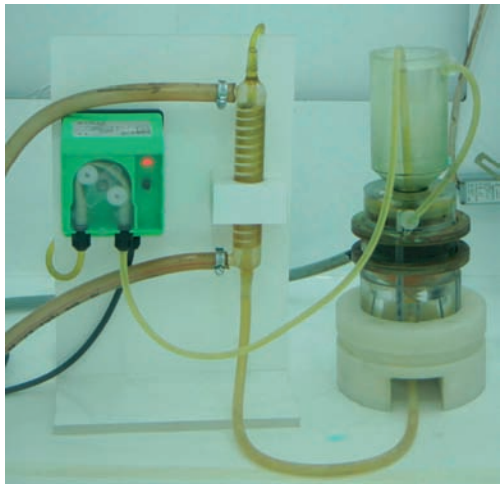

FIG. 1. Electrodissolution set-up.

mounted target and the Rh layer was not dissolved. The resulting $Cu(NO_3)_2$/HNO_3 solution was removed by filtration through a glass/graphite filter combination whereby the Rh fragments are collected on the filter and the vessel walls. Rhodium fragments were washed with water and removed. A mixture of 12M hydrochloric acid and chlorine gas was introduced into the vessel. Electrochemical dissolution of the Rh was done by applying a high AC density (2.4 A/cm^2) between the electrographite filter and a perforated circular upper graphite electrode mounted at an appropriate distance from the carbon filter.

2.3. Separation of carrier free ^{103}Pd

The Cu/Rh/Pd separation was achieved using a Dowex1X8 (Cl^-)/100–200 mesh column (1.5 cm × 10 cm). Copper was eluted with 0.03M HCl, rhodium with 6M HCl and palladium with a 1:1 mixture of 0.5M NH_3/NH_4Cl [21].

3. RESULTS AND DISCUSSION

Electroplated rhodium targets can be prepared from home-made or commercially available sulphate or chloride baths containing appropriate plating additives. When home-made plating solutions are used, the addition of 1% sulphamic acid is recommended. As a plating technique, constant current (DC

or AC) electrolysis at elevated temperature (40–60°C) can be applied. As the plating current efficiency is less than 100%, plating to depletion (>98% rhodium deposition) is recommended. To estimate the quality of the electroplated rhodium targets, some criteria had to be taken into account such as homogeneity, morphology, visual appearance of the rhodium layer and thermal shock.

The homogeneity of the rhodium layer is important as it may seriously affect the production rate of ^{103}Pd. This was determined by measuring the thickness of several parts of the layer by micrometer and calculating the standard deviation of the data.

All electrodeposited Rh target layers were examined in morphology by a scanning electron microscopy (using a Joel model JSM 6400 at an accelerating voltage of 20 kV). The photomicrographs were then compared with each other and also with the ones obtained from the Rhodex solution. The evaluation of the quality of the layers was achieved by comparison of the photomicrographs in terms of size and form of the Rh nuclei and the extent to which they overlapped each other; the smaller, more spherical and the more overlapped nuclei were considered to be good plating qualities.

The thermal shock tests involved heating the target up to 500°C (the temperature that the Rh layer can experience during a high current irradiation) for 1 h followed by submersion in cold (15°C) water. The absence of crack formation and peeling of the rhodium layers indicated good adhesion.

To increase the Rh dissolution rate and to avoid boiling of solution, closed loop circulation through a water (glycol) cooler is introduced. To increase the dissolution rate, chlorine gas was introduced between two graphite fibres.

Experimental data of dissolutions are summarized in Table 1. The experiments were done up to 30 A current and with hydrochloric acid concentrations of 6M and 12M.

TABLE 1. DISSOLUTION TRIALS WITH FRAGMENTED RHODIUM AND PIECES OF FOIL AND WIRE
(effective area of electrographite = 16.5 cm^2)

W(Rh) (g)	J (A/cm^2)	Acidity (N)	t (min)	T (°C)	Residual Rh (g)	Dissolved Rh (%)	Chlorine gas
0.4901	1.5	6	180	95	0.1102	77.5	no
0.4903	1.8	6	180	75	0.0978	80.0	no
0.4922	1.8	12	210	85	0.0580	88.2	no
0.4935	1.8	6	210	75	0.0076	98.46	yes
0.4907	1.8	12	210	75	0.0052	98.93	yes
0.7310	2.4	12	240	85	0.0072	99.01	yes

There are impurities such as $^{102m,102,101m}Rh$ in this solution. On the basis of differences in the affinity of doubly charged $PdCl_4^{2-}$ and triply charged $RhCl_6^{3-}$, the anion exchange method was used for the separation of palladium from rhodium. After eluting with 100 mL 0.03M HCl, which is intended to remove Cu^{2+} and other metal ions, such as $Zn^{2+}$and Fe^{3+}, which adhere to the resin; the resin was eluted 120 mL 6M HCl at a 4 mL/min flow rate. The elution was continued for a total volume of 120 mL and 30 mL of distilled water was then used to remove the HCl remaining in the column. The mixed NH_3+NH_4Cl(1:1) eluant (100 mL) was used to release ^{103}Pd from the resin. After anion exchange with Dowex1X8 (Cl^-)/100–200 mesh and taking a gamma ray spectrum by HPGe detector, the ^{103}Pd purity obtained was more than 99% (Figs 2 and 3).

4. CONCLUSIONS

The rhodium target for production of ^{103}Pd can be prepared by the electrodeposition technique. For the purpose, either a chloride electroplating bath through $RhCl_3$(aq) or sulphate bath through Rh_2O_3(aq) (recovered from hydrochloric acid solution), H_2SO_4 and sulphamic acid can be used. The former

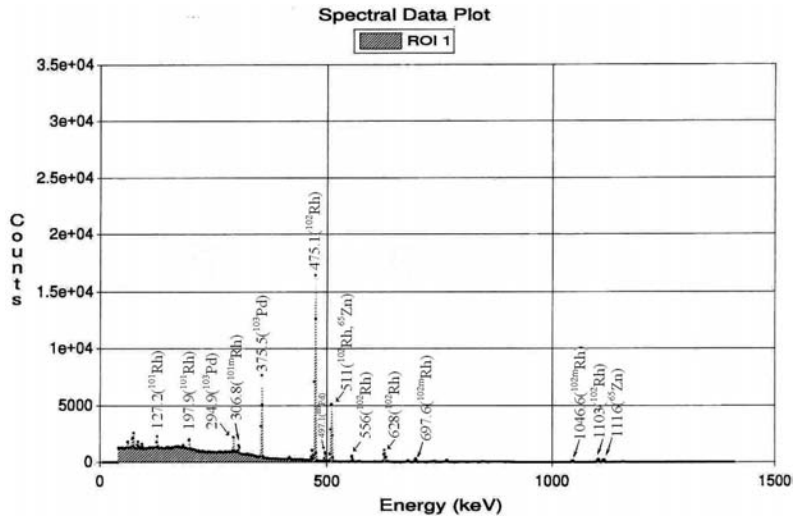

FIG. 2. Gamma ray spectrum of an irradiated ^{103}Rh target after electrodissolution, other peaks include the Pb detector shielding fluorescence X rays.

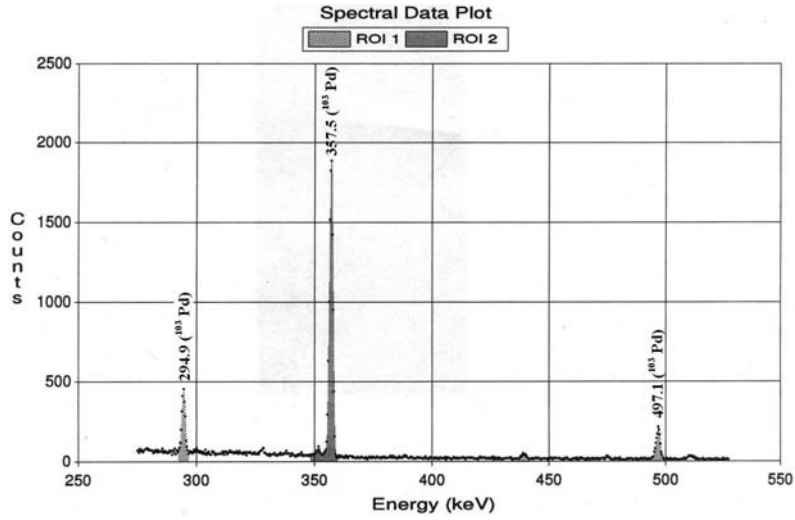

FIG. 3. HPGe spectrum of radiochemically separated ^{103}Pd. No other peaks have been detected in the γ spectrum.

bath is recommended for low current beam irradiation (up to 200 μA) and the latter for current beam irradiation of higher than 200 μA.

The high current density results in a high production rate of the electroactive chlorine species that rapidly dissolves the rhodium present at the working electrode. The dissolution rate depends on parameters such as current, concentration of HCl and weight of rhodium. In general, the magnitude of these parameters is time dependent. The optimum conditions of the electrodissolution were as follows: 12N HCl solution, AC density higher than 2.4 A/cm^2, temperature 85°C and bubbling chlorine gas, in which case the dissolution rate was greater than 99%.

Recovery of ^{103}Pd from rhodium solution was achieved by ion exchange column with Dowex1X8 resin and NH_3+NH_4Cl (1:1) as eluant; the obtained ^{103}Pd purity was more than 99%.

REFERENCES

[1] NAG, S., BEYER, D., FRIEDLAND, J., GRIMM, P., NATH, R., Int. J. Radiat. Oncol. Biol. Phys. 44 (1999) 789.

[2] MERRICK, G.S., BUTLER, M.W., DORSEY, A.T., LIEF, J.H., Int. J. Radiat. Oncol. Biol. Phys. 44 (1999) 1111.

[3] PRETE, J.J., et al., Int. J. Radiat. Oncol. Biol. Phys. 40 (1998) 1001.
[4] LING, C.C., Int. J. Radiat. Oncol. Biol. Phys. 23 (1992) 81.
[5] MESSING, E., et al., Int. J. Radiat. Oncol. Biol. Phys. 44 (1999) 801.
[6] BLASKO, J.C., WALLNER, K., GRIMM, P.D., J. Urol. 154 (1995) 1096.
[7] BLASKO, J.C., et al., Urol. Clin. North Am. 23 (1996) 633.
[8] PORTER, A.T., BLASKO, J.C., GRIMM, P.D., REDDY, S.M., RAGDE, H., Californian Cancer J. Clin. 45 (1995) 165.
[9] DATTOLI, M., WALLNER, K., SORACE, R., J. Brachyther. Int. 13 (1997) 347.
[10] RAGDE, H., et al., Semin. Surg. Oncol. 13 (1997) 438.
[11] STOCK, R.G., STONE, N.N., TARBERT, A., Int. J. Radiat. Oncol. Biol. Phys. 41 (1998) 101.
[12] WHITTINGTON, R., et al., Int. J. Radiat. Oncol. Biol. Phys. 44 (1999) 1107.
[13] HARPER, P., LATHROP, K., BALDWIN, L., Ann. Surg. 148 (1958) 606.
[14] PORAZZO, M.S., et al., Int. J. Radiat. Oncol. Biol. Phys. 23 (1992) 1033.
[15] HARPER, P.V., LATHROP, K., NEED, J.L., ORNL-LR-DWG 51564 (1961) 124.
[16] LAGUNAS-SOLAR, M.C., AVILA, M.J., JOHNSON, P.C., Appl. Radiat. Isot. 38 (1987) 151.
[17] FASSBENDER, M., NORTIER, F.M., SCHROEDER, I.W., VAN DER WALT, T.N., Radiochimica Acta 87 (1999) 87.
[18] BOX, W.D., In ORNL-3802 UC-23-Isotopes-Industrial Technology TID-450.39th, (1964), p.29.
[19] LAGUNAS-SOLAR, M.C., AVILA, M.J., JOHNSON, P.C., Int. J. Appl. Radiat. Isot. 38(2) (1987) 151.
[20] HERMANNE, A., SONCK, M., FENYVESI, A., DARABAN, L., Nucl. Inst. & Meth. In Phys. Res. B, 170**,** (2000) 281.
[21] ZHANG, C., WANG, Y., ZHANG, Y., ZHANG, X., Applied Radiation & Isotopes, **55,** 441 (2001).

THE STATUS AND POTENTIAL OF NEW RADIONUCLIDE GENERATORS PROVIDING POSITRON EMITTERS TO SYNTHESIZE NEW TARGETING VECTORS FOR PET

F. ROESCH*, K.P. ZHERNOSEKOV*, D.V. FILOSOFOV**, M. JAHN*, M. JENNEWEIN*

*Institute of Nuclear Chemistry, University of Mainz, Mainz, Germany
Email: frank.roesch@uni-mainz.de

**Joint Institute of Nuclear Research, LNP, Dubna, Russian Federation

Abstract

The ^{68}Ge/Ga generator (^{68}Ge, $T_{½}$ = 270.8 d) provides a cyclotron independent source of positron emitting ^{68}Ga ($T_{½}$ = 68 min, β^{+}_{β} branching = 89%), which can be used for coordinative labelling. Recently, tumour imaging using ^{68}Ga labelled DOTA conjugated peptides became one of the most exciting approaches to diagnose neuroendocrine and other tumours and metastases because (i) octreotide derivatives with high affinity and selectivity to somatostatin receptor expressing tumour cells are available, (ii) syntheses of DOTA conjugated targeting vectors are straightforward due to the kit type labelling, and (iii) PET/CT scanners perfectly correlate morphological and functional parameters. However, for labelling of biomolecules via bifunctional chelators, ^{68}Ga(III) as eluted initially needs to be preconcentrated and purified from ^{68}Ge(IV), Zn(II), Ti(IV) and Fe(III). The paper describes a system for the simple and efficient handling of the ^{68}Ge/^{68}Ga generator eluates with a microchromatography column filled with about 50 mg of a cation exchange resin. Chemical purification and volume concentration of ^{68}Ga are carried out in an 80% acetone/0.15M HCl solution. Finally, more than 97% of ^{68}Ga is obtained in 400 µL of a 98% acetone/0.05M HCl solution. The initial ^{68}Ge contamination of the eluate was reduced by a factor of 1000. Contents of Zn(II), Fe(III) and Ti(IV) were reduced significantly. Consequently, the processed fraction can be used directly for the synthesis of radiopharmaceuticals. The developed system represents a simple and efficient way of labelling DOTA conjugated biomolecules with generator produced ^{68}Ga(III). [^{68}Ga]DOTATOC and [^{68}Ga]DOTANOC were successfully used in a series of human somatostatin receptor expressing tumour diagnoses with PET/CT.

1. INTRODUCTION

Radionuclide generator systems continue to play a key role in providing both diagnostic and therapeutic radionuclides for various applications in nuclear medicine, oncology and interventional cardiology. Key advantages of the use of radionuclide generators include reasonable cost, the convenience of obtaining the desired radionuclide progeny on demand and the availability of the radionuclide progeny in high specific activity, no carrier added form. Although many parent/progeny pairs have been evaluated as radionuclide generator systems, in particular for the application of labelled PET radiopharmaceuticals (Table 1), there are only a relatively small number of generators which are currently in routine clinical and research use [1].

Those generators can be categorized according to the half-life of the progeny nuclide. The short lived progeny cover half-lives of a few minutes. As the short half-lives do not allow radiochemical synthesis, these systems are relevant for perfusion imaging exclusively. The longer lived progeny, on the other hand, provide the potential for development of labelled radiopharmaceuticals. Recently, the ^{68}Ge/Ga and ^{72}Se/As systems have found impressive application, but also the ^{44}Ti/^{44}Sc generator represents a promising system.

The ^{68}Ge/Ga generator (^{68}Ge, $T_{½}$ = 270.8 d) provides a cyclotron independent source of positron emitting ^{68}Ga ($T_{½}$ = 68 min, β^{+}_{β} branching = 89%), which can be used for coordinative labelling. Recently, tumour imaging using ^{68}Ga labelled DOTA conjugated peptides became one of the most exciting approaches with which to diagnose neuroendocrine and other tumours and metastases because (i) octreotide derivatives with high affinity and selectivity to somatostatin receptor expressing tumour cells are available, (ii) syntheses of DOTA conjugated targeting vectors are straightforward due to the kit type labelling, and (iii) PET/CT scanners perfectly correlate morphological and functional parameters. Radiolabelled peptides designed for tumour receptor targeting are of great interest for diagnostic imaging and/or radionuclide therapy [2]. Somatostatin analogues such as DOTA-DPhe^{1}-Tyr^{3}-octreotide (DOTATOC) and DOTA-DPhe^{1}-Nal^{3}-octreotide (DOTANOC) labelled with radiogallium (^{66,67,68}Ga) show high potential for diagnosis of somatostatin receptor expressing tumours, improved binding affinity and very promising properties in vivo [3, 4]. In particular, if PET/CT is used, a highly accurate diagnosis is provided.

TABLE 1. RADIONUCLIDE GENERATORS WITH POTENTIAL FOR PET

Generator system		Parent	Progeny			
		$T_{½}$	$T_{½}$	β^{+}_{branch} (%)	E^{+}_{β} (MeV)	Application
^{82}Sr	^{82}Rb	25.6 d	1.27 min	95.0	1.41	Perfusion
^{140}Nd	^{140}Pr	3.37 d	3.39 min	51.0	0.544	Perfusion
^{118}Te	^{118}Sb	6.00 d	3.6 min	74.0	0.882	Perfusion
^{122}Xe	^{122}I	20.1 h	3.6 min	77.0	1.09	(Labelling)
^{128}Ba	^{128}Cs	2.43 d	3.62 min	69.0	0.869	Perfusion
^{134}Ce	^{134}La	3.16 d	6.4 min	63.0	0.756	Perfusion
^{62}Zn	^{62}Cu	9.26 h	9.74 min	97.0	1.28	Labelling, perfusion
^{52}Fe	^{52m}Mn	8.28 d	21.1 min	97.0	1.13	Perfusion
^{68}Ge	^{68}Ga	270.8 d	1.135 h	89.0	0.74	Labelling, perfusion
^{110}Sn	^{110m}In	4.1 h	1.15 h	62.0	0.623	Labelling
^{44}Ti	^{44}Sc	47.3 a	3.927 h	94.0	0.597	Labelling
^{72}Se	^{72}As	8.4 d	1.083 d	88.0	1.02	Labelling

2. AIM

The commercially available $^{68}Ge/^{68}Ga$ radionuclide generator (Fig. 1) based on a TiO_2 phase (Cyclotron Co., Obninsk, Russian Federation) recently became an object for evaluation and can be successfully used for $^{68}Ga^{3+}$ recovery. This type of generator allows the elution of more than 50% of the activity of ^{68}Ge generated in the first year with 5–7 mL of 0.1M HCl. However, the eluate contains long lived ^{68}Ge (10^{-2}%, increasing with time or frequency of generator use), small amounts of Zn(II) as generated from the decay of ^{68}Ga, Ti(IV) and Fe(III), and can contain radiolysis products. It thus should not be used for labelling directly.

One approach to overcome these problems (i.e. of processing ^{68}Ga(III) eluate) was described recently [3, 5] using an anion exchanger. The initial 0.1M HCl eluate must be mixed with concentrated HCl in order to achieve a 20 mL solution of an overall HCl concentration of 5.5M. Under these conditions, Ga(III) can be adsorbed on an anion exchanger such as $[GaCl_4]^-$ and eluted with H_2O in low volumes (>0.5 mL). However, this strategy does not allow direct loading of the ^{68}Ga(III) activity on the resin from 0.1M HCl and thus

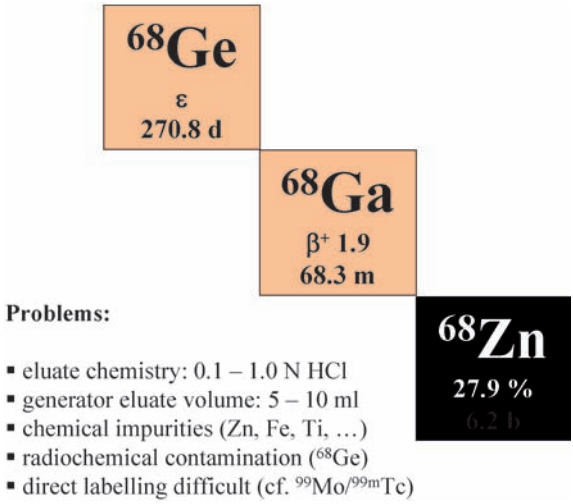

FIG. 1. Scheme of the $^{68}Ge/^{68}Ga$ radionuclide generator system and problems related to the direct use of the generator eluate for medical directions.

adds an additional step. Moreover, it does not provide purification of Ga(III) from Zn(II) and Fe(III). Finally, residual acid amounts might lead to an uncontrollable low pH value of the final fraction. Further approaches include microwave supported labelling [6] or fractionation of the eluates [7].

The aim of authors' work is to develop an efficient and simplified system for processing of generator produced $^{68}Ga^{3+}$ adequate for clinical requirements. It involves (i) preconcentration of the eluted ^{68}Ga, (ii) purification of the eluted ^{68}Ga, (iii) isolation of the purified ^{68}Ga in a form useful for labelling (acceptable pH and volume), (iv) labelling and preparation of an injectable ^{68}Ga labelled radiopharmaceutical and (v) construction of a corresponding apparatus with a capability in the design for an automated 'module'.

The key step is in the direct transfer of the initial 0.1M HCl $^{68}Ga(III)$ eluate on a cation exchanger. Analysis of cation exchanger distribution coefficients with Bio-Rad AG 50W-X8 in hydrochloric acid–acetone medium [8] shows that Ga(III) can be eluted from the resin with minimum volume and low acid amount, with Ga(III) purified from Ge(IV), Zn(II), Ti(IV) and even Fe(III). This approach was used to develop a processing of generator produced $^{68}Ga^{3+}$ for labelling of biomolecules containing appropriate bifunctional chelators.

3. MATERIALS AND METHODS

3.1. ^{68}Ge/^{68}Ga radionuclide generator

Commercial generators based on a TiO_2 phase adsorbing ^{68}Ge(IV) were obtained from the Cyclotron Co., Obninsk, Russian Federation. In the present study, 20 and 30 mCi systems were used. According to its technical certification, not less than 50% of ^{68}Ga generated can be eluted with 5 mL 0.1M HCl in the first year of operation, decreasing not less than 25% after 3 years or after 200 elutions. The breakthrough of ^{68}Ge is described as less than 0.01% within three years of operation or during the first 200 elutions.

3.2. Radiometals used for ion exchange distribution measurements

Ga(III): 110 MBq of ^{68}Ga in 7 mL of 0.1M HCl were obtained from a 1 year old 20 mCi generator after more than 200 elutions. The absolute activity of ^{68}Ga was determined using a curie meter. As its ^{18}F position was used, the activity shown was corrected for the different positron branching of ^{18}F and ^{68}Ga (96.9% versus 89%).

Ge(IV): The activity of ^{68}Ge in the ^{68}Ga eluate used was about 170 kBq. The absolute activity of ^{68}Ge was analysed by γ spectrometry using an HPGe detector about 2 d after the corresponding radionuclide generator elution. These samples indicate a constant level of ^{68}Ga as generated by the percentage of co-eluted ^{68}Ge.

Fe(III): ^{59}Fe was produced by a neutron capture reaction on natural iron, whereby 198 mg of iron oxide (Fe_2O_3) was irradiated for 50 d at the HMI neutron source BER II at 1.6×10^{14} n·cm^{-2}·s^{-1}, yielding 440 MBq ^{59}Fe. The iron oxide was dissolved in HNO_3 solution and after evaporation transferred into appropriate solutions. The activity of ^{59}Fe was analysed by γ spectrometry using a HPGe detector.

Mn(II): ^{54}Mn was co-obtained with ^{59}Fe in an activity of 0.25 MBq per 1 MBq of ^{59}Fe. The activity of ^{54}Mn was analysed by γ spectrometry using a HPGe detector.

Zn(II): ^{69}Zn was produced with specific activity of ~700 kBq/mg by irradiation of 380 µg of ^{68}Zn ($Zn(NO_3)_2$, >98% isotopically enriched ^{68}Zn) for 6 h at the TRIGA II reactor Mainz at a neutron flux of 4×10^{12} cm^{-2}·s^{-1}. The target was subsequently dissolved in 0.1M HCl. The activity of ^{69}Zn was analysed by γ spectrometry using a HPGe detector.

3.3. Chemicals and equipment

Analytical reagent grade chemicals and Milli-Q water (18.2 MΩ·cm) were used. A Bio-Rad AG 50W-X8 cation exchanger minus 400 mesh was preferred to prepare a microchromatography column. DOTATOC was kindly provided by Novartis Pharma AG.

For labelling reactions, 11 mL glass vials, Mallinckrodt and reaction vessels PP, Brand were used. A heating block with a 1.5 cm lead thickness for radiation adsorption was built using 24 V PTC heating elements. For processing of the labelling product, C-18 cartridges, Phenomenex Strata-X Tubes, 30 mg were used. Sterile filtration was done on a 0.22 μm MILLEX®GV membrane filter. For quality control, TLC (aluminium sheets, silica gel 60, eluent 0.1M Na_3citrate) and HPLC (Machery Nagel column, Nucleosil 5 C18-AB, 250 mm × 4 mm; eluent, 20% AcCN, 80% TFA 0.01% in H_2O, 1 mL/min) were used.

4. EXPERIMENTS

4.1. Distribution of metallic cations

A microchromatography column was prepared using 53 mg of the resin. The distribution of various cations on this cation exchanger column was investigated. First, ^{68}Ga in 7 mL of 0.1M HCl was loaded dynamically (within 1–2 min) on the chromatography column. In the second step, the column was eluted with acetone–HCl solutions of 80% acetone and HCl concentrations of 0.1M, 0.15M and 0.2M. The volume of these mixtures ranged from 0.6 to 5.0 mL. The remaining solution was removed by air. Thirdly, the ^{68}Ga was eluted in 0.4 mL of a 98% acetone–0.05M HCl solution with a 2 min pause after the column filling. The column was finally reconditioned with 1 mL 4M HCl and 1 mL H_2O.

Thus, 5 fractions were obtained for analysis of their content of the various chemical and radiochemical impurities:

(1) 7 mL 0.1M HCl, (2) 80% acetone–HCl solution, (3) 98% acetone–0.05M HCl solution, (4) 4M HCl (this fraction represents the amounts of metals remaining after the elution with the 98% acetone–0.05M HCl solution), (5) H_2O.

Using the same protocol, the distribution of ^{59}Fe, ^{54}Mn and ^{69}Zn, containing 83 μg and 130 μg of Fe(III) and Zn(II), respectively, was determined. In addition, the distribution of Ti(IV) was investigated in order to estimate the distribution, eventually co-eluted within the ^{68}Ga fraction. Thus, 20 μg Ti(IV) in 5 mL 0.lM HCl was processed the same way. The distribution of Ti(IV) in the different fractions was studied using an Elan 5000 ICP-MS (Perkin-Elmer).

4.2. Labelling

In the case of the new 30 mCi ^{68}Ge/^{68}Ga generator, about 600–750 MBq of ^{68}Ga was obtained with 7 mL of 0.1M HCl. In addition, in order to obtain about 1400 MBq, two 30 mCi generators were combined and eluted with 12 mL of 0.1M HCl in a cascade scheme. These fractions were processed and applied for labelling. After preconcentration and purification of the initial generator eluates on the microchromatography column, ^{68}Ga(III) was eluted with the 400 μL 98% acetone–0.05M HCl solution (2×10^{-5} mol HCl). This fraction was used directly for labelling. For labelling with ^{68}Ga(III), DOTA-octreotides (DOTATOC, DOTANOC) and desferrioxamine-B-succinyl-octreotide (DFOOC) were used. All labelling reactions were carried out at temperatures of ~98°C. Kinetics of the syntheses were recorded up to 15 min by taking aliquots of 1 μL at 1, 2, 5, 10, 15 min.

Two approaches were studied, namely ^{68}Ga labelling with or without additional buffer solutions. The processed activity was added to 4.5 mL pure H_2O in a standard glass reagent vial (11 mL, Mallinckrodt) containing 7–14 nmol DOTATOC. To achieve higher specific activity 0.5–0.7 mL 1 molal HEPES, pH4.0–4.1 (according to Ref. [6]) was added to 2 mL reaction vessels (PP, Brand equipped with a vent) containing 2–5 nmol DOTATOC.

4.3. Purification of primary labelling products

The reaction mixture was passed through a small C-18 cartridge (Phenomenex Strata-X Tubes, 30 mg). After washing the cartridge with H_2O (aqua ad iniectabilia), the ^{68}Ga labelled peptides were recovered with 200–400 μL of pure ethanol.

4.4. Quality control

Quality control was performed using TLC and HPLC. For HPLC, an aliquot was dissolved in TFA 0.1% in H_2O and used for analysis. Acetone content was studied by a gas chromatography HP 6890 series GC system.

4.5. Synthesis for clinical application

Priorities for routine synthesis of ^{68}Ga-DOTATOC were safety and highest overall yield. The following scheme was developed for routine synthesis of ^{68}Ga-DOTATOC (Fig. 2). A microchromatography column with about 50 mg of the cation exchanger was prepared using two three-way valves. The ^{68}Ge/Ga radionuclide generator was connected to the column. PEEK capillary

tubing connected the reagent vials in a heating block. The column could be eluted using a standard single use syringe (3) and was connected to the waste vial (2). Syntheses were performed in pure water as described above using 14 nmol DOTATOC. After purification of the product on the C-18 cartridge, the ethanol eluate containing the pure ^{68}Ga-DOTATOC was dissolved in 5–10 mL 0.9% saline solution and sterilized by filtration through a 0.22 μm membrane filter. Routine quality control was performed rapidly by TLC.

5. RESULTS

5.1. ^{68}Ge/^{68}Ga radionuclide generator performance (^{68}Ga yield, ^{68}Ge breakthrough)

All generator systems utilized provided stable recovery of ^{68}Ga of >50% (up to 80% in the first instance). More than 90% of the activity available can be eluted within the first 5 mL of 0.1M HCl. A ^{68}Ge breakthrough of less than 0.01% of the actual ^{68}Ge activity was detected for all ^{68}Ge/Ga generation within the first year of operation. This reflects the technical characteristics (see Section 3) of the producer. Up to 0.05% of ^{68}Ge could be detected in the eluate of an 'old' generator with >200 elutions.

5.2. Eluate purification: Chemical and radiochemical purities

Relative distribution of ^{68}Ga(III), ^{68}Ge(IV), Zn(II), Ti(IV), Fe(III) and Mn(II) on a microchromatography column (53 mg AG 50 W-X8 200–400 mesh) in hydrochloric acid–acetone media have been evaluated systematically. The cation exchanger provides almost quantitative adsorption of more than 99% of ^{68}Ga(III) from the 0.1M HCl solution. Less than 2% of ^{68}Ga(III) is lost in applying the 80% acetone–0.05M HCl solution. After all the purification steps, more than 97% of ^{68}Ga(III) could be recovered in the 98% acetone–0.05M HCl solution. The scheme is illustrated in Fig. 2.

^{68}Ge(IV) passes through the column in 0.1M HCl and is additionally washed with 80% acetone–HCl solutions. The processed ^{68}Ga fraction finally contains <0.01% of ^{68}Ge relative to the initial eluate. Thus, a ^{68}Ge decontamination factor of >1000 was achieved.

The purification step with 80% acetone–0.15M HCl allows the significant reduction of the amount of Zn(II) to less than 10^{-3}% and Fe(III) up to 11% (see Fig. 3). Both Ti(IV) and Mn(II) could be eluted from the resin mainly in 4M HCl and only 0.1% of Ti(IV) and 10% of Mn(II) were detected in the processed ^{68}Ga fraction.

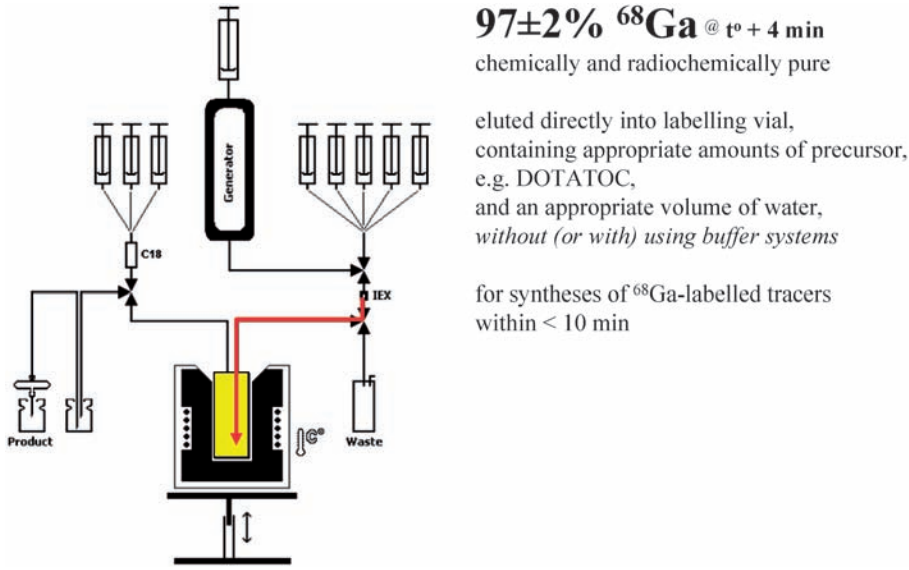

FIG. 2. Scheme of the generator associated post-processing resulting in a ^{68}Ga labelling unit.

5.3. Volume

Finally, the volume of the isolated, chemically and radiochemically purified ^{68}Ga fraction is 400 µL with HCl amounts of 2×10^{-5} mol.

5.4. Time

With application of the scheme described above (Fig. 2), processing of the eluate requires only 4 min.

5.5. Labelling

The preconcentrated and purified ^{68}Ga(III) eluted from the resin with 400 µL of the 97.6% acetone–0.05M HCl mixture was used for labelling reactions. For labelling in pure water, up to 700 MBq ^{68}Ga(III) was added to 4–4.5 mL (preheated) H_2O in standard reagent vials containing 7–14 nmol DOTATOC. The amount of HCl contained in the final eluate solution (400 µL 98% acetone–0.05M HCl = 2×10^{-5} mol H^+) provided an overall pH of 2.30 (±0.05). No incorporation was achieved at higher or lower pH. At ~98°C, the radiolabelling yield was over 95% within 10 min. Variable radiochemical yield

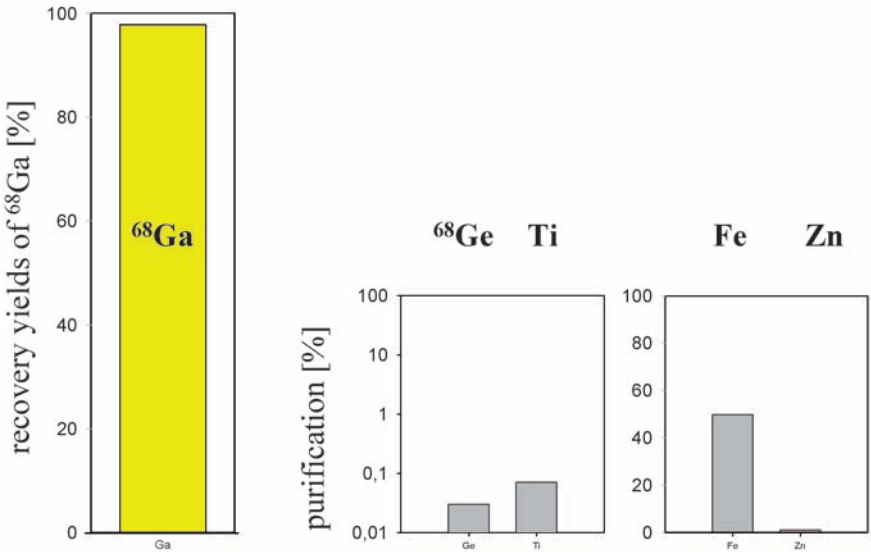

FIG. 3. Purification factors achieved within the generator associated post-processing (cf. FIG. 2).

and increased adsorption on the glass surface were detected if less than 14 nmol of peptide was used. Incorporation also dropped with decreasing reaction temperature.

5.6. Specific activity

Specific activities of up to 40 MBq/nmol could be achieved using pure water as the solvent of DOTATOC. In this case, the processed ^{68}Ga eluate (2×10^{-5} mol HCl, up to 1400 MBq) was added to 0.5–0.7 mL 1 molal HEPES solutions of pH4.0–4.1 in 2 mL reaction vessels containing 2–4 nmol DOTATOC, the radiochemical yield was up to 88% and the specific activity up to 450 MBq/nmol at ~99°C within 10 min.

5.7. Purification

Radiochemical purity over 99% was achieved by processing the labelling fraction on small C-18 cartridges independent of the initial labelling yield (cf. Fig. 4). However, essential losses of the peptide on the RP phase occurred if less than 4 nmol of DOTATOC was used. After incubation of the reaction mixture at ~98°C for 10 min, the overall acetone content was about 5 µg. The

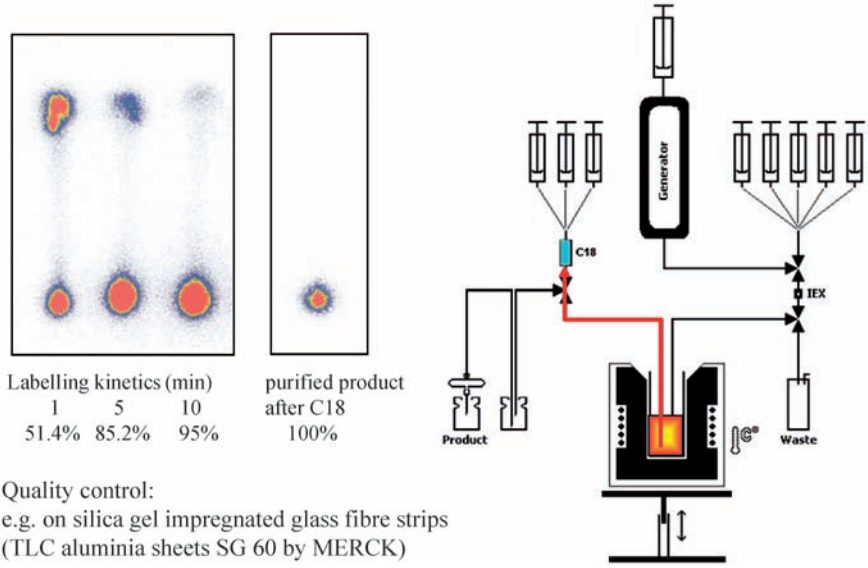

FIG. 4. Purification and pre- and post-purification quality control of ^{68}Ga radiopharmaceuticals associated to the post-processing and synthesis scheme.

final product after processing on C-18 contained not more than 0.15 µg of acetone.

6. DISCUSSION

For labelling of biomolecules via bifunctional chelators, ^{68}Ga(III) as eluted initially needs to be preconcentrated and purified from ^{68}Ge(IV), Zn(II), Ti(IV) and Fe(III). The authors describe a system for simple and efficient handling of the ^{68}Ge/^{68}Ga generator eluates with a microchromatography column filled with about 50 mg of a cation exchange resin (Bio-Rad AG 50W-X8) as the main component. Chemical purification and volume concentration of ^{68}Ga are carried out in an 80% acetone–0.15M HCl solution. Finally, more than 97% of ^{68}Ga are obtained in 400 µL of a 97.6% acetone–0.05M HCl solution. The initial ^{68}Ge contamination of the eluate was reduced by a factor of 1000. Contents of Zn(II), Fe(III) and Ti(IV) were reduced significantly. Consequently, the processed fraction can be used directly for the synthesis of radiopharmaceuticals.

Simple labelling protocols were used for routine preparation of ^{68}Ga-DOTATOC as a prototype of a ^{68}Ga labelled PET radiopharmaceutical. The

reaction was carried out in pure water using 14 nmol of DOTATOC and resulted in high incorporation and high overall yield. Up to 400 MBq of DOTATOC with specific activity up to 40 MBq/nmol could be obtained after processing on C-18 with a new 30 mCi generator.

Within 20 min, an injectable radiopharmaceutical such as ^{68}Ga-DOTATOC can be prepared with specific activities of up to 450 MBq/nmol. While standard specific activities of 40 MBq/nmol are quite acceptable for clinical diagnosis using ^{68}Ga-DOTATOC, increased specific activities can be required for clinical application of DOTA-peptides with potential pharmacological side effects [7].

The application of C-18 cartridges for final purification seems to be an essential step which provides high radiochemical purity independent of labelling yield. Furthermore, additional quality control might be avoided.

Thus, a rapid, simple and chemically efficient processing of generator produced ^{68}Ga(III) was developed. The process guarantees safe preparation of injectable ^{68}Ga-DOTATOC (or other ^{68}Ga labelled radiopharmaceuticals) for routine application and can be successfully used in the clinical environment. Simple equipment for routine preparation of injectable ^{68}Ga-DOTATOC was installed in various nuclear medicine departments equipped with a PET/CT. More than 1000 patients with known neuroendocrine tumours were involved in initial systematic studies to establish and evaluate a clinical protocol. Both [^{68}Ga]DOTATOC and [^{68}Ga]DOTANOC were successfully used in a series of human somatostatin receptor expressing tumour diagnoses with PET/CT. The developed system represents a simple and efficient way for the labelling of DOTA conjugated biomolecules with generator produced ^{68}Ga(III). Moreover, a variety of other ^{68}Ga labelled compounds might be synthesized for many other applications. The current level of radiochemical development and radiopharmaceutical investigation clearly indicates a significant potential for the ^{68}Ge/Ga generators, for applications in basic research and for routine application in state of the art nuclear medicine. In particular, for countries or medical centres not yet running medical cyclotrons and/or not yet owning a sophisticated organic radiopharmaceutical production infrastructure, the availability of the ^{68}Ge/Ga generator might help to initiate PET chemistry developments and patient diagnoses using PET.

As the developed scheme guarantees safe preparation of injectable ^{68}Ga labelled DOTA conjugates for routine application (easy to automate) it has been successfully used in clinical environments. Using the authors' system, over the last year several German clinical centres have been involved in establishing clinical protocols for application of ^{68}Ga-DOTATOC and similar compounds in more than 500 patients. The clinical impact is extraordinarily high. Using PET and in particular PET/CT, the diagnosis of neuroendocrine tumours and

metastases is significantly superior to the current state of the art approaches using ^{111}In-DTPA-octreotide and SPECT.

Owing to the low costs of the ^{68}Ge/Ga generators and to the simple kit type of labelling, this approach is straightforward and to be adopted in clinical centres not owning a cyclotron for in-house productions of ^{11}C and ^{18}F, and/or not owning a rather complicated and expensive organic labelling chemistry facility in conjunction with the required hot cell and automated synthesis modules. Some other features of the generator system are of additional importance:

Diagnosis:

- Per generator elution, up to three patients can be diagnosed.
- The generator can be eluted every 3 or 4 h at almost 100% yield, allowing clinical applications of up to 4 or 5 elutions per day with up to 20 patient studies per day.
- A generator once installed can work one year or more and more than 500 PET studies might be performed.
- The price per patient study thus will be very low.
- Owing to the 68 min half-life of ^{68}Ga, patients do not need to stay in the hospital at all.

Therapy:

- As many of the therapeutic targeting vectors today are designed for labelling with trivalent metallic cations (^{90}Y, ^{153}Sm, ^{177}Lu, etc.), ^{68}Ga PET scans could become a standard approach for pre-and post-therapeutic screening.

Furthermore, supposing that the biomedical targeting approach will require longer lived positron emitters, there are two other PET radionuclide generators.

One is the ^{44}Ti ($T_{½}$ = 47 a)/^{44}Sc ($T_{½}$ = 3.927 h) radionuclide generator which provides a very similar chemical system. The longer lived progeny ^{44}Sc, however, presents a physical half-life adequate to biological investigations, where the 68 min half-life of ^{68}Ga appears to be too short. Similar to ^{68}Ga(III), the ^{44}Sc(III) action needs to be adequate to label many of the already existing targeting vectors containing bifunctional chelators for trivalent cations. Last year, the authors started a programme on the development of this system.

The second is the ^{72}Se/As system which provides a 26 h positron emitter with 88% positron branching. The authors recently developed the basic

radiochemistry for this generator and have shown the potential of longer lived radioarsenic to image the targeting parameters of monoclonal antibodies.

In addition, in particular if targeting vectors such as monoclonal antibodies are used instead of small peptides, the authors recently proposed the radioarsenic isotopes ^{72}As ($T_{½}$ = 26 h, 88% β^+_β branching) and ^{74}As ($T_{½}$ = 17.78 d, 29% β^+_β branching). As a proof of principle, they successfully tested the hypothesis that a new chimeric IgG3 monoclonal antibody ch3G4 (Tarvacin®) directed against anionic phospholipids and labelled with radioactive arsenic isotopes can be used for the vascular targeting and molecular imaging of solid tumours in rats in vivo. For generators using no carrier added ^{72}Se, the authors described the distillation of $AsCl_3$, while Se remains in non-volatile compounds in the residue, and developed a solid phase extraction system with ^{72}Se fixed as metallic Se. Systematic chemical investigations on the labelling chemistry of no carrier added radioarsenic are currently being developed prior to the application of ^{72}As labelled compounds [9–12].

Thus, the potential of PET radionuclide generator systems seems to fit excellently with the strategy of the IAEA in facilitating the development of modern medical imaging technologies in the developing countries.

REFERENCES

[1] RÖSCH, F., KNAPP, F.F., "Radionuclide generators", Handbook of Nuclear Chemistry, Vol. 4 (VÉRTES, A., NAGY, S., KLENCSÁR, Z., RÖSCH, F., Eds), Kluwer Academic Publishers, The Netherlands (2003) 81-118.

[2] MÄCKE, H.R., GOOD, S., "Radiometals (non-Tc, non-Re) and bifunctional labeling chemistry", Handbook of Nuclear Chemistry, Vol. 4 (VÉRTES, A., NAGY, S., KLENCSÁR, Z., RÖSCH, F., Eds), Kluwer Academic Publishers, The Netherlands (2003) 279-314.

[3] HOFMANN, M., et al., Biokinetics and imaging with the somatostatin receptor PET radioligand ^{68}Ga-DOTATOC: preliminary data, Eur. J. Nucl. Med. (2001) 28:1751–1757.

[4] WILD, D., et al., DOTA-NOC, a high-affinity ligand of somatostatin receptor subtypes 2, 3 and 5 for labelling with various radiometals, Eur. J. Nucl. Med. (2003) 30: 1751–1757.

[5] MEYER, G.-J., MÄCKE, H.R., SCHUHMACHER, J., KNAPP, W.H., HOFMANN, M., ^{68}Ga-labelled DOTA-derivatised peptide ligands, Eur. J. Nucl. Med. (2004) 31: 1097–1104.

[6] VELIKYAN, I., BEYER, G.J., LÅNGSTRÖM, B., Microwave-Supported Preparation of ^{68}Ga Bioconjugates with High Specific Radioactivity, Bioconjugate Chem. (2004) 15: 554-560.

[7] BREEMAN, W.A.P., et al., Radiolabelling DOTA-peptides with ^{68}Ga, Eur. J. Nucl. Med. (2004) 32: 478–1104.
[8] STERLOW, F.W.E., VICTOR, A.H., VAN ZYL, C.R., ELOFF, C., Distribution coefficient and cation exchange behavior of elements in hydrochloric acid-acetone, Anal. Chem. 1971; 43: 870-876.
[9] JENNEWEIN, M., SCHMIDT, A., NOVGORODOV, A.F., QAIM, S.M., RÖSCH, F., A no-carrier-added ^{72}Se/^{72}As radionuclide generator based on distillation, Radiochim Acta 92 (2004) 245-249.
[10] JENNEWEIN, M., et al., A new method for radiochemical separation of arsenic from irradiated germanium oxide, Appl Radiat Isot 63 (2005) 343–351.
[11] JENNEWEIN, M., et al., A no-carrier-added ^{72}Se/^{72}As radionuclide generator based on solid phase extraction, Radiochim Acta 93 (2005) 579-583.
[12] JENNEWEIN, M., HERMANNE, A., MASON, R.P., THORPE, P.E., RÖSCH, F., A new method for the labelling of proteins with radioactive arsenic isotopes, Nucl Instr Methods B, 2006, in press.

RADIOPHARMACY

(Session 14)

Chairpersons

N.G. HARTMAN
United Kingdom

E. JANEVIK-IVANOVSKA
The Former Yugoslav Republic of Macedonia

NUCLEAR PHARMACY PRACTICES IN THE UNITED STATES OF AMERICA

K. OZKER
Medical College of Wisconsin,
Milwaukee, Wisconsin,
United States of America
Email: ozker@mcw.edu

Abstract

There are more than 450 nuclear pharmacies in the United States of America. Approximately 80% of these are centralized nuclear pharmacies operated by three major companies: Cardinal Health, Tyco Healthcare/Mallinckrodt and GE Healthcare. There are 88 independent facilities and two additional companies specialized in PET radiopharmaceuticals: CTI/PETNET and Eastern Isotopes. Institutional nuclear pharmacies, representing 20% of the radiopharmacies in the USA, prepare multidose radiopharmaceuticals in university or hospital settings. All commercial nuclear pharmacies are licensed by a state board of pharmacy and operate under the supervision of an authorized nuclear pharmacist. The Nuclear Regulatory Commission requires that all nuclear pharmacists be certified pharmacists, completing an approved programme consisting of 200 h of didactic and 500 h of practical training. Recently, requirements for aseptic compounding and dispensing of radiopharmaceuticals have been developed by the United States Pharmacopoeia (USP <797>). The Society of Nuclear Medicine communicated with the USP in late 2004 regarding unique situations specific to the preparation of radioactive compounds (such as radiation exposure, shielding requirements and contamination risks) that would make it difficult to comply fully with the new USP regulations. The USP <797> Sterile Compounding Committee subsequently approved revisions and exemptions for radiopharmaceutical compounding.

Currently, radiopharmaceutical preparation in the United States of America is mostly performed by centralized radiopharmacies (CRPh). CRPh provide single patient unit doses in shielded containers to their customers. The advantages of this practice to nuclear medicine providers are: minimization of radiation exposure; simplification of regulatory requirements including paperwork; and reduction of risk to staff, patients and the public. In general, procurement, preparation and dispensing of radiopharmaceuticals is provided by CRPh, which makes a wide variety of products available for immediate delivery. Dose preparation, labelling, quality control, record keeping and radioactive waste retrieval are all performed by the CRPh. These services

reduce the responsibilities of the nuclear medicine facility, including those involving risk management, quality assurance and regulatory standards in an efficient and cost effective manner. The capability to acquire agents on the same day from CRPh eliminates the necessity of having certain expensive supplies available at the imaging location, particularly a $^{99}Mo/^{99m}Tc$ generator [1].

In a high volume nuclear medicine facility, a hospital radiopharmacy (HRPh) may be more cost effective compared to purchasing unit doses from a CRPh. Preparation of radiopharmaceuticals in-house can save money since a large number of patient doses may be obtained from a single multidose vial. The number of studies performed each day (and thus the number of injected doses) must be high enough to justify the cost of staffing, supplies and quality assurance procedures. Currently, there are more than 450 radiopharmacies in the USA of which CRPh represent about 80% of these, operated by three major companies: Cardinal Health, Tyco Healthcare/Mallinckrodt and GE Healthcare. Cardinal Health (formerly Syncor) has the largest network of facilities following its merger with Geodax Imaging (19 pharmacies) in July 2005 [2]. There are two other CRPh companies dedicated solely to PET radiopharmaceuticals: CTI/PETNET (39 pharmacies) and Eastern Isotopes (9 pharmacies). There are 88 independent commercial CRPh laboratories and about 70 institutional radiopharmacies located in hospitals or universities [1, 2].

All commercial CRPh are licensed by a state board of pharmacy and operated under the supervision of an authorized nuclear pharmacist. The possession, handling, dispensing and waste management of radiopharmaceuticals are regulated by the Nuclear Regulatory Commission (NRC) or an agreement state regulatory agency such as the State Board of Radiation Protection. The NRC requires that all nuclear pharmacists be certified pharmacists, completing an approved programme consisting of 200 h of didactic and 500 h of practical training involving radiopharmaceuticals [3]. Various programmes offer either on-site classroom training or remote education. The first graduate level radiopharmacy programme was taught at the University of Southern California, from which graduated 210 students between 1968 and 1986. The Purdue University programme has been in operation since 1972. The University of New Mexico and the University of Arkansas jointly developed a remote learning programme which is currently available on the internet. A syllabus for nuclear pharmacy training published by the American Pharmaceutical Association in 1995 as a guide for educational institutions and educators (faculty/preceptors) is based on the NRC requirements for authorized nuclear pharmacist training. The NRC requirement for authorized nuclear pharmacy programmes contains 200 class room hours covering the following topics:

radiation physics and instrumentation, radiation protection, mathematics related to radioactivity, radiation biology and radiopharmaceutical chemistry.

Some 500 h of practical training in a radiopharmacy under the supervision of an authorized nuclear pharmacist is also required. Nuclear pharmacy certificate programmes are currently offered at The University of Arkansas, The Massachusetts College of Pharmacy, Mercer University, The University of New Mexico, The University of North Carolina, The Medical University of South Carolina, The University of Oklahoma, Purdue University and Temple University [1]. Several nuclear pharmacy companies, such as Cardinal Health, have established their own training programmes [2].

NRC requirements for radiopharmacies are based on radiation safety principles to minimize patient, occupational and public radiation exposure. Additionally, guidelines for aseptic compounding and dispensing of radiopharmaceuticals developed by the United States Pharmacopoeia (USP) have recently become enforceable by the Food and Drug Administration (USP Chapter <797> regulations effective 1 January 2004). All healthcare facilities that prepare sterile products for medical use, including biological agents, diagnostic agents, drugs, nutrients and radiopharmaceuticals, must comply with these regulations. USP <797> describes pharmacies as having one of three risk levels: low, medium or high [4].

(1) Low risk conditions are where all compounding with aseptic manipulations occur entirely with ISO Class 5 (old class 100) or better air quality using only sterile ingredients, products, components and devices.
(2) Medium risk conditions include multiple individual or small doses of sterile products that are compounded or pooled to prepare a compounded sterile product that will be administered either to multiple patients or to one patient on multiple occasions. USP <797> implies that medium risk compounding must also take place in an ISO Class 5 or better air environment.
(3) High risk conditions include the use of non-sterile ingredients, components or devices and sterile ingredients, components or devices which are exposed to air quality inferior to ISO Class 5. In this case, the compound must subsequently be sterilized in an ISO Class 5 environment.

Radiopharmaceuticals are considered compounded sterile products according to USP <797>. All sterile compounding is to be performed in an ISO Class 5 environment using a laminar airflow workbench. The area surrounding the location where the compounding and/or sterilization occur is called the buffer zone (clean room). Buffer zones should meet at least an ISO Class 7

level (old class 10 000) of cleanliness. Buffer zone surfaces must be smooth, impermeable, readily cleanable and capable of sanitization. Low and medium risk environments must have controlled ISO level Class 5 cleanliness as well as a buffer zone and an additional ante area (where gowning and hand washing are carried out) which does not necessarily need to be separated by a physical wall. High risk environments must have the same features as the low and medium risk sites but the additional ante area must be separated from the buffer zone by a physical barrier [4, 5].

USP <797> regulations are currently enforceable by the Food and Drug Administration and the State Board of Pharmacy, Medicine and Nursing. Healthcare institutions must begin to comply with the requirements of USP <797> over a specific timeline. The Society of Nuclear Medicine communicated with the USP in late 2004 about unique situations specific to the preparation of radioactive compounds (such as radiation exposure, shielding requirements and contamination risks) that would make it difficult to comply fully with the USP regulations. The USP Sterile Compounding Committee met in October 2004 and approved the following revisions to USP <797> [6]:

(1) Currently official <797> requires positive pressure for all sterile compounding, but that is wrong for radioactive and other hazardous drugs.
(2) Direct visual inspection of highly radioactive CSPs is not required.
(3) The $^{99m}Tc/^{99}Mo$ generator systems shall be stored and eluted (operated) under conditions recommended by their manufacturers and applicable state and federal regulations.
(4) Three or fewer sterile products may be prepared in lower than ISO Class 5 air when there is no direct contact contamination and administration begins within 1 h and is completed within 12 h of preparation.

The Sterile Compounding Committee reviews received comments, then determines whether additional revision is necessary before the next version is published in the Pharmacopeial Forum as an Interim Revision Announcement which bears a date for official USP adoption. The next <797> will appear either in an annual USP revision, e.g. USP 29 in 2006 or in one of the two semi-annual supplements to each annual USP revision [6].

On the basis of the latest approved revisions of USP <797>, there are still several uncertainties regarding exemptions for radiopharmaceutical compounding that can affect the design of a nuclear pharmacy.

The Joint Commission on Accreditation of Healthcare Organizations (JCAHO) has begun to survey hospitals for compliance with USP <797>. JCAHO expects healthcare organizations to have performed a risk assessment/

gap analysis and established an action plan for achieving compliance by January 2005, and to have implemented interim steps to mitigate the impact of non-compliance, assure sterility in compounding by July 2005 and to have completed action plans and achieved full compliance by January 2008 [7].

REFERENCES

[1] AMERICAN PHARMACIST ASSOCIATION, Radiopharmaceuticals, Nuclear Medicine and Nuclear Pharmacy: An Overview. In: Kowalsky RJ, and Falen SW. Radiopharmaceuticals in Nuclear Pharmacy and Nuclear Medicine 2nd ed. American Pharmacist Association, (2004) 1-15.

[2] CARDINAL HEALTH NUCLEAR PHARMACY SERVICES, www.nps.cardinal.com/NPS/content/nucpharm/index.asp. Accessed on September 19, 2005.

[3] BOARD OF PHARMACEUTICAL SPECIALTIES, Nuclear Pharmacy Practice Guidelines. Website Available at: www.bpsweb.org. Accessed on September 19, 2005.

[4] US PHARMACOPEIA, The United States Pharmacopeial Convention, Inc. U.S. Pharmacopeia 27. Chapter <797>, Pharmaceutical Compounding – Sterile Preparations, Rockville, MD: U.S. Pharmacopeial Convention, Inc., (2003).

[5] US PHARMACOPEIA, The United States Pharmacopeial Convention, Inc. U.S. Pharmacopeia 28, Chapter <797> Pharmaceutical Compounding – Sterile Preparations, Rockville, MD: U.S. Pharmacopeial Convention, Inc., (2004).

[6] US PHARMACOPEIA, The United States Pharmacopeial Convention, Inc. Website Available at: www.usp.org/standards/proposed 797 revisions.html. Accessed on June 24, 2005.

[7] AMERICAN HOSPITAL ASSOCIATION, JCAHO clarifies expectations and timelines in compliance with USP <797> Website Available at: www.aha.org/ashe/codes/jcaho/clarify_usp797.html. Accessed on July 25, 2005.

REGULATORY ASPECTS OF HOSPITAL RADIOPHARMACY AND CLINICAL TRIALS

A.A. SOYLU
Nuclear Medicine Department,
Faculty of Medicine, Ankara University

Monrol Radiopharmaceutical Company

Ankara, Turkey
Email: ayfersoylu@yahoo.com

Abstract

The number of clinical research studies is increasing as scientists concentrate their efforts on diagnosing, treating and preventing diseases by increasing knowledge about human health. The progress of nuclear medicine is heavily dependent on development of new radiopharmaceuticals. Many research studies exist relating to new radiopharmaceuticals, but it is a known fact that the number of studies involving human application of these investigated products is comparatively low. While the main problem is financial, owing to the insufficiency of the market, overregulation of clinical studies on humans and uncertainties on how these regulations should apply to radiopharmaceuticals compared to regular pharmaceutical products has always been another issue. The purpose of this paper is to discuss the main regulations on clinical trials in general and to evaluate certain points specific to clinical studies involving radiopharmaceuticals, and at the same time assess the existing radiopharmacy legislation.

1. INTRODUCTION

The Declaration of Helsinki, published in 1964 [1] by the World Medical Association and entitled Ethical Principles for Medical Research Involving Human Subjects, and its revised forms (1975, 1983, 1989, 1996, 2000 and 2004) and clarification notes (2002, 2004), should constitute the basis for all medical research on human beings with a set of recommendations that guide responsible physicians all over the world. Special caution should also be given to the welfare of animals used for research and to the environment in which the trial is conducted .

2. CLINICAL TRIAL

A clinical trial may be defined as: "Any investigation in human subjects intended to discover or verify the clinical, pharmacological or pharmacodynamic effects of a drug, identify any adverse reactions related to a drug, study the absorption, distribution, metabolism and excretion of the drug with the object of ascertaining its safety and/or efficacy" [2]. Clinical trials may either be commercially funded or non-commercial. Studies set up for commercial goals are usually sponsored by industrial companies for the purpose of drug development and registration. It takes years for a new drug to be put on the market and results obtained only by authorized clinical trials can be relied on for marketing authorization of an investigational medicinal product (IMP). Non-commercial clinical trials are generally conducted by academia and use existing medicinal products to optimize treatment regimes or establish new techniques with the same products. But there are occasions where a new pharmaceutical product is tried on patients by non-commercial investigators. Many studies involving the use of radiopharmaceuticals on human beings fall into this category. Investigators who are authorized health professionals conducting non-commercial trials must be responsible for all administrative, financial and legal obligations and must assume the human subject protection requirements completely, just as with commercial sponsors. The regulations apply equally to commercial and non-commercial trials.

3. IMP

A general definition of IMP would be: "A pharmaceutical form of an active substance or placebo being tested, or to be tested, or to be used, as a reference in a clinical trial, including a medicinal product which has a marketing authorization but is, for the purposes of the trial, used or assembled (formulated or packaged) in a way different from the authorized form, or used for an indication not included in the summary of product characteristics under the authorization for that product, or used to gain further information about the authorized form" [2].

4. RADIOPHARMACEUTICALS

Radiopharmaceuticals may be argued to be different from classical drug products in being radioactive and carrying a small amount of material in a small volume of injection. A radiopharmaceutical is applied to a patient usually only

once or a few times in their lifetime. In general, these products spend a short time in the body and no biological effect is expected to occur by the introduction of a radiopharmaceutical to a human being. On-site preparation and immediate use may be other aspects of radiopharmaceuticals differing from regular drug products. In spite of these arguments, radiopharmaceuticals are considered as medicinal products [3] and any radiopharmaceutical used in a clinical trial is therefore subject to all the legislation regarding IMP.

The radioactive nature of radiopharmaceuticals also makes it necessary to follow the regulations related to ionizing radiation. Euratom Directive 97/43, entitled Protection of Individuals Against the Dangers of Ionizing Radiation in Relation to Medical Exposure applies to exposure of healthy individuals or patients voluntarily participating in medical or biological, diagnostic or therapeutic, research programmes [4].

5. GOOD CLINICAL PRACTICE (GCP)

The European Directive on Good Clinical Practice in Clinical Trials — 2001/20/EC [2] together with its supplements [5] constitute the main regulations in Europe which apply to all IMP, including radiopharmaceuticals. This directive, which became fully operational on 1 May 2004, has many implications covering various issues on trials such as the suitability of investigators and facilities, the quality of the IMP, informed consent from the subjects, ethics committees and the European Clinical Trials Database. The main purpose of the Directive on clinical trials is to guide the EU Member States on the implementation of good clinical practice in the conduct of clinical trials on medicinal products for human use by adopting laws, regulations and administrative provisions.

The European Commission Directive 2005/28/EC [5] is one of the recent supplements of Directive 2001/20/EC strengthening the legal basis and establishing more specific terms for GCP. This new directive clarified some questions regarding the use of unauthorized products in clinical trials and was to be implemented by the Member States by 29 January 2006.

GCP is a set of minimum standards for clinical trials which ensure the protection of the rights, welfare and safety of human subjects and the validity of collected data and reported results. It also covers issues related to the design, conduct, performance, auditing, recording and reporting of clinical trials. An individual who participates in a clinical trial either as a recipient of the IMP or as a control is the ‘subject’ of this trial. The subjects can be healthy volunteers or patients. The rights, safety and well-being of the trial subjects are the most

important considerations and should prevail over the interests of science and society.

6. CLINICAL TRIALS

All clinical research studies involving humans must be designed according to a 'protocol', which is a document describing the objectives, design, methodology, statistical considerations and organization of that specific trial and must have been approved by the related regulatory bodies before the trial commences. Detailed preclinical studies should have been carried out, covering both clinical and non-clinical aspects of the IMP. In studies with classical pharmaceutical products, the preclinical work is followed by phase I clinical studies if the available information is found to be satisfactory. The studies are usually carried out on a small number (50–100) of healthy volunteers, starting with a dose as low as possible and then increasing the dose until the desired effect is reached. During phase II, the investigational product is given to 200–400 patients with the indicated disorder. In general, a larger number of patients are involved in phase III of the project, some receiving a placebo, for a valid statistical evaluation of the results. The situation may be different for clinical trials involving the use of radiopharmaceuticals; studies on healthy volunteers may be omitted in order to avoid unnecessary radiation exposure to the public and the trial may continue with a small number of patients after adequate preclinical evidence has been obtained.

The Directive 2001/83/EC [3], which is also related to medicinal products for human use and was implemented on 1 May 2004, does not directly regulate clinical trials but clearly states that any application for market authorization of a medicinal product in the EU should be accompanied by a complete dossier containing the documents related to the results of the clinical trials carried out on that product. 2004/27/EC [6] is an amendment of this directive and gives more details on clinical trial file preparation, documentation and similar issues.

7. GOOD MANUFACTURING PRACTICE (GMP)

Directives 2001/20/EC, 2001/83/EC and 2003/94/EC [7], which is an extension of GMP to IMP, clearly require that IMP activities for human use be carried out in licensed premises in accordance with GMP and the competent authorities are required to inspect these activities. A 'qualified person' must be assigned to ensure that the GMP requirements are met for the IMPs released. The qualified person must be the holder of a diploma, certificate or other

evidence of formal qualification in pharmacy, chemistry, medicine, biology or related life science and must have gained experience in similar work and acquired the necessary skills [3].

Many non-EU countries have their national regulations set similarly and they are being harmonized by the efforts of the International Conference on Harmonization (ICH). Guideline CPMP/ICH/135/95 [8], entitled Good Clinical Practice has been adopted by the Committee for Medicinal Products for Human Use. It is decided that results of clinical trials which have been carried out in accordance with this guideline should be accepted by Australia, Canada, the EU, Japan, the Nordic countries and the United States of America.

8. CONCLUSION

The above discussion should make it clear that use of unauthorized radiopharmaceuticals on human beings is certainly subject to permission being granted by the competent authorities. This covers home-made radiopharmaceuticals and any changes in the method of preparation of a licensed radiopharmaceutical including dividing up and packaging or presentation. Even the use of an authorized radiopharmaceutical for a different indication or given at a different dosage or use of a different route of administration other than that registered on the authorization are considered as cases which need permission. The only exception are the clinical studies which involve standard application of approved radiopharmaceuticals to assess the efficacy of a treatment (e.g. bone scan used for monitoring in a chemotherapy trial), which are not considered as clinical trials and thus there is no need to go through the procedures for gaining clinical trial permission for such projects.

The recent amendments on the other hand, state that authorization will not be required for a process involving reconstitution prior to administration of the product or packaging if these are done in hospitals, health centres or clinics by pharmacists or qualified persons and if the IMP is intended to be used exclusively in that institution. The procedures for importing IMPs from other countries are also simplified. Trials with products having marketing authorizations and manufactured or imported in accordance with EU rules are permitted to be carried out if they are conducted on patients with the same indication specified in the marketing authorization. However, guidance is needed which specifies how to protect the subjects in such applications.

Owing to the unique nature of radiopharmaceuticals, various organizations have been working on defining a set of current GMP conditions, specifically developed for radiopharmaceuticals. The Radiopharmacy Group of the European Association of Nuclear Medicine has prepared Draft Guidelines on

Current Good Radiopharmacy Practices for Radiopharmaceuticals in Nuclear Medicine-GRPP and Draft Guidelines on Current Good Manufacturing Practices for Positron Emission Tomography and Other Locally Produced Radiopharmaceuticals-PET GMP [9].

Similar efforts follow in the USA where the Food and Drug Administration (FDA) has recently announced a proposed rule for the production of PET drugs [10] and also draft guidance providing additional information about the proposed regulation when it becomes a final rule [11]. The proposed rule is intended to set the minimum standards for the production and testing of PET radiopharmaceuticals and guide the producers on achieving these requirements. Although these current GMP conditions differ greatly from those of non-PET drugs, the aim is, of course, to ensure that the best quality PET radiopharmaceutical was available for the patient regardless of the purpose and place of production and the person who carried out the production.

The finalization of the rule and the guidance by the FDA may be expected to help speed up the international harmonization procedures.

REFERENCES

[1] WORLD MEDICAL ASSOCIATION DECLARATION OF HELSINKI, Ethical Principles for Medical Research Involving Human Subjects, Helsinki, Finland, June 1964.

[2] EUROPEAN COMMISSION, Directive 2001/20/EC of the European Parliament and of the Council of 4 April 2001 on the approximation of the laws, regulations and administrative provisions of the Member States relating to the implementation of good clinical practice in the conduct of clinical trials on medicinal products for human use (*Official Journal L 121, 1/5/2001 p. 34 – 44).*

[3] EUROPEAN COMMISSION, Directive 2001/83/EC of the European Parliament and of the Council of 6 November 2001 on the Community code relating to medicinal products for human use *(Official Journal L 311, 28/11/2001 p. 67 - 128)*.

[4] EUROPEAN COMMISSION, Council Directive 97/43 Euratom, Health Protection of Individuals Against the Dangers of Ionizing Radiation in Relation to Medical Exposure ,The Council of the European Union (*Official Journal L 180, 09/07/1997 p. 22 – 27)*.

[4] EUROPEAN COMMISSION, Commission Directive 2005/28/EC of 8 April 2005 laying down principles and detailed guidelines for good clinical practice as regards investigational medicinal products for human use, as well as the requirements for authorisation of the manufacturing or importation of such products *(Official Journal L 91, 09/04/2005 p. 13 - 19*).

[6] EUROPEAN COMMISSION, Amended by Directive 2004/27/EC of the European Parliament and of the Council of 31 March 2004 amending Directive 2001/83/EC on the Community code relating to medicinal products for human use (*Official Journal L 136, 30/4/2004 p. 34 - 57*).

[7] EUROPEAN COMMISSION, Commission Directive 2003/94/EC of 8 October 2003 laying down the principles and guidelines of good manufacturing practice in respect of medicinal products for human use and investigational medicinal products for human use (*Official Journal L 262, 14/10/2003 p. 22 - 26*).

[8] INTERNATIONAL CONFERENCE ON HARMONIZATION, Note for Guidance on Good Clinical Practice, ICH/135/95, Committee for Medicinal Products for Human Use , July 1996 .

[5] EUROPEAN JOURNAL OF NUCLEAR MEDICINE, The Draft Guidelines on Good Radiopharmacy practices for Radiopharmaceuticals (GRPhP) in Nuclear Medicine and the Draft Guidelines on Good Manufacturing Practices for Positron Emission Tomography (PET) Radiopharmaceuticals, EJNM (2003) 30:BP63-BP72.

[6] UNITED STATES FOOD AND DRUG ADMINISTRATION, Current good Manufacturing Practice for Positron Emission Tomography Drugs : draft for proposed rule by USFDA ; 21 CFR Parts 210,211,212 (*Fed Reg V 70, no 181, Sept 20 2005 p 55038-55062).*

[7] UNITED STATES FOOD AND DRUG ADMINISTRATION, PET Drug Products-Current Good Manufacturing Practice-Draft Guidance, Sept 2005, USFDA (CDER).

STANDARDIZATION AND QUALITY CONTROL OF AN IN-HOUSE FORMULATION OF ^{99m}Tc(V)-DMSA IN TUMOUR IMAGING AND ASSESSMENT OF TUMOUR BIOLOGY: WORK IN PROGRESS

P.S. CHOUDHURY*, N.C. GOOMER**, A. GUPTA*,
D.C. DOVAL***, T. KATARIA+, A.K. VAID***, P.K. SHARMA*

* Department of Nuclear Medicine
Email: pschoudhury@rgci.org

** Department of Medical Oncology

*** Department of Radiation Oncology
Rajiv Gandhi Cancer Institute and Research Centre

+Regional Centre for Radiopharmaceuticals (BRIT)

New Delhi, India

Abstract

Various in-house formulated radiopharmaceuticals have been used for tumour imaging with varied success. In order to achieve clinically reproducible results, the purity and stability of the formulation needs to be standardized. The objective of the present study was to reproduce a simple but optimum method for in-house formulation of ^{99m}Tc(V)-DMSA from the commercially available DMSA(III) kits for its use as an agent for assessing tumour biology. The authors used two commercially available kits of DMSA(III): one from the Board of Radiation & Isotope Technology (BRIT) and the other from Amersham. Both kits were formulated as per the manufacturer's protocol. The authors determined the radiochemical purity using TLC (T-6145 TLC precoated plated silica gel with a 24 nm fluorescent indicator on polyester supplied by Sigma/ Merck) with a solvent containing n-butanol acetic acid water (3:2:3 v/v). Free pertechnetate levels were measured using TLC-SG in saline. Per cent labelling of DMSA and free pertechnetate was calculated and the ratios of DMSA(III) and DMSA(V) were estimated. These were carried out for a period of 3 h. Observations showed that the radiochemical purity of DMSA(V) for the Amersham kit was optimum at about 1 h post-labelling. The same effect was observed in 15 min in the kit that was supplied by BRIT. The time of optimum radiochemical purity was reduced to 15 min by bubbling oxygen through the preparation for 20 min and attributed to oxidation of tin. Human

biodistribution studies showed predominantly renal pelvicalyceal excretion in a radiochemically pure preparation with physiological concentration in the bladder. The cardiac blood pool showed significant tracer washout in 3–4 h. A pilot study carried out has so far shown a maximum tumour concentration with adequate target to non-target ratio occurring by 3 h post-injection in patients with histologically proven lung carcinoma.

1. INTRODUCTION

Malignant transformation leads to major biochemical changes within a cell. These include modifications of the energy metabolism of the cell such as glucose and other substrate utilization, protein synthesis and expression of receptor and antigens. These biochemical changes are difficult to map by conventional morphological imaging studies and require the use of tracers which can assess tumour viability. Standardization of a particular method of formulation is important to achieve the highest radiochemical purity and stability over an optimum time duration and thereby achieve the desired clinical results. The paper reports on the standardization, quality control and initial clinical results of one such radiopharmaceutical — ^{99m}Tc(V)-DMSA.

2. MATERIALS AND METHODS

2.1. Kits used

The authors formulated ^{99m}Tc(V)-DMSA from two commercially available kits of DMSA(III). One of the kits was procured from the Board of Radiation & Isotope Technology (BRIT) India (kit 1) and the other was from Amersham Inc., United Kingdom (kit 2).

2.2. Kit preparation

Formulation of the BRIT kit was done by adding 7 mg of $NaHCO_3$ in 0.2 mL of water for injection and $^{99m}TcO_4^-$ simultaneously to the reaction vial. The kit contains 1 mg of DMSA and 0.3 mg of $SnCl_2 \cdot 2H_2O$. An equal volume of air was withdrawn from the reaction vial. Mixing followed by incubation was done for 15 min.

Formulation of the Amersham kit (1 mg DMSA, 0.42 mg of $SnCl_2 \cdot 2H_2O$, 0.7 mg ascorbic acid, 2.9 mg sodium chloride and 50 mg inositol) was done by

adding 0.2 mL 7.5% w/v $NaHCO_3$ + $^{99m}TcO_4^-$. Mixing, followed by incubation, was done for 15 min.

2.3. Analysis of the preparation

Radiochemical purity was determined by a combination of two chromatographic systems using TLC (T-6145 TLC precoated plated silica gel with 254 nm fluorescent indicator on polyester supplied by Sigma, silica gel 60F 254 TLC aluminium strip supplied by Merck) with a solvent containing n-butanol:acetic acid:water (3:2:3 v/v). Free pertechnetate levels were measured using TLC–SG in saline. Test samples were applied by 1 mL syringe 2 cm from the bottom of the chromatography strips. The length of the strip was 15 cm and the width was 0.5 cm. The strips were marked every 1 cm and placed in prepared ascending chromatography development jars. The strips were removed after 10 cm elution and dried. Strips were cut every 1 cm for the butanol–acetic acid–water system. The strip from the saline system was cut into two equal portions. Both the systems were then counted in a well counter. Per cent labelling of DMSA and free pertechnetate was calculated and the ratios of DMSA(III) and DMSA(V) were calculated. These were carried out for over 3 h. The same procedure was repeated on multiple occasions and the reproducibility was verified. On the basis of the authors' observations, the oxygen bubbling method was tried with the Amersham kit where pure hospital grade oxygen was bubbled through the preparation for 20 min. Chromatographic methods to assess radiochemical purity were performed as above. The above chromatographic procedures were reproduced on multiple occasions with kits from different batches.

2.4. Biodistribution studies and clinical trials

Limited clinical trials in the form of a pilot study were carried out in the patients of biopsy proven lung carcinoma during staging workup to evaluate the tumour concentrating capability of the radiopharmaceutical and the in vivo kinetics of the tumour. Whole body imaging was performed with a gamma camera. 740 MBq of the prepared ^{99m}Tc(V)-DMSA was injected intravenously and images were aquired immediately, at 1, 2 and 3 h. SPECT of the region of primary malignancy was performed. The radiochemical purity was assessed by chromatography concomitantly.

3. RESULTS

3.1. Analysis of the kits

Different batches of both the kits were used for chromatographic studies. It was observed that the unbound (free) $^{99m}TcO_4$ (technetium pertechnetate) in both kits was less than 5%. This was also substantiated in the imaging studies. Biodistribution and initial clinical studies showed predominantly renal pelvicalyceal excretion and bladder concentration. No tracer concentration was seen in the salivary glands, thyroid gland or stomach, suggesting the absence of significant unbound $^{99m}TcO_4$ in the preparation. Radiochemical purity in both the kits was more than 90% with the method of formulation used. However, the incubation time taken to achieve this purity was variable in both the kits. The kit supplied by BRIT (India) took 15 min of incubation time (Fig. 1), whereas the Amersham kit required about 1 h of incubation time (Fig. 2) to achieve the same purity. Significant amounts of DMSA(III) were found in the latter preparation after 15 min of incubation (Fig. 3). On bubbling with hospital grade oxygen for 20 min, the desired radiochemical purity was achieved in 15 min (Fig. 4). Both kits were stable for at least 3 h (Figs 5–7 and Tables 1–3).

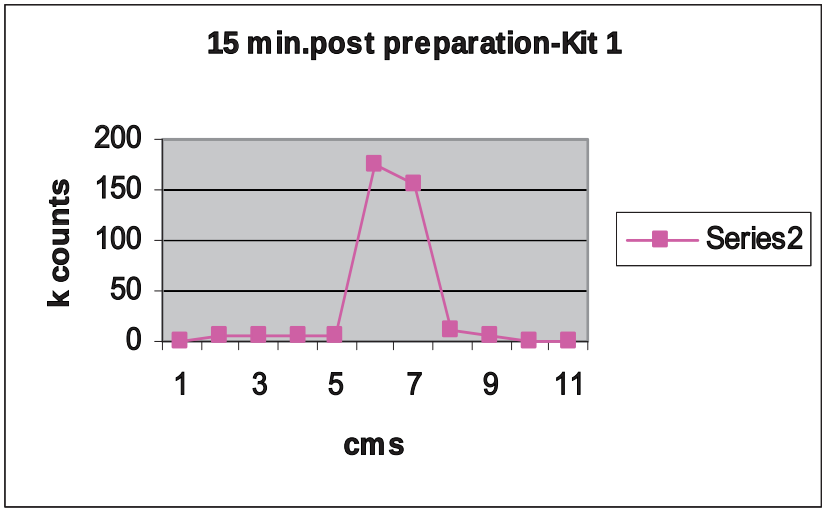

FIG. 1. Radiochemical purity 92.34%.

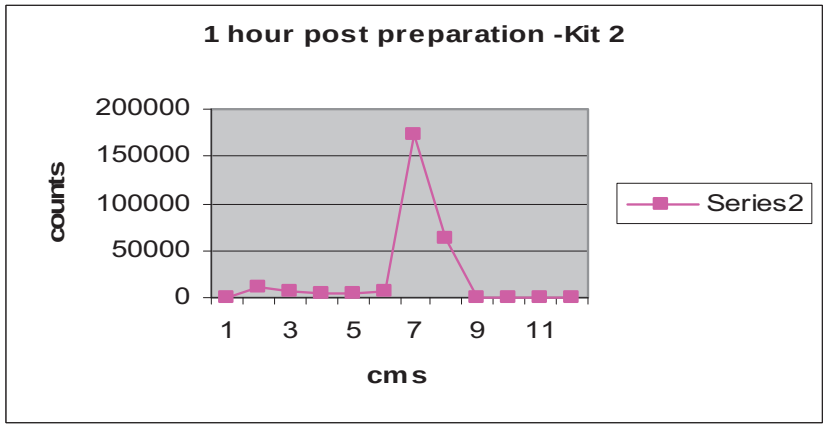

FIG. 2. Radiochemical purity 91%.

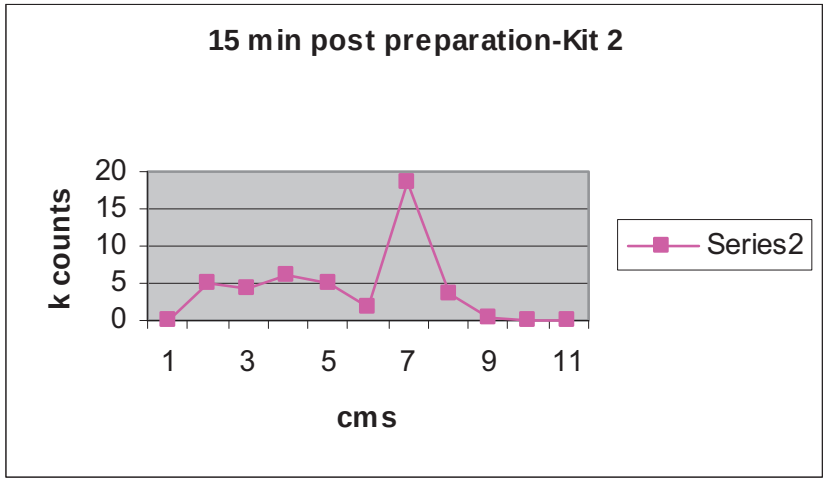

FIG. 3. Radiochemical purity 50.36%.

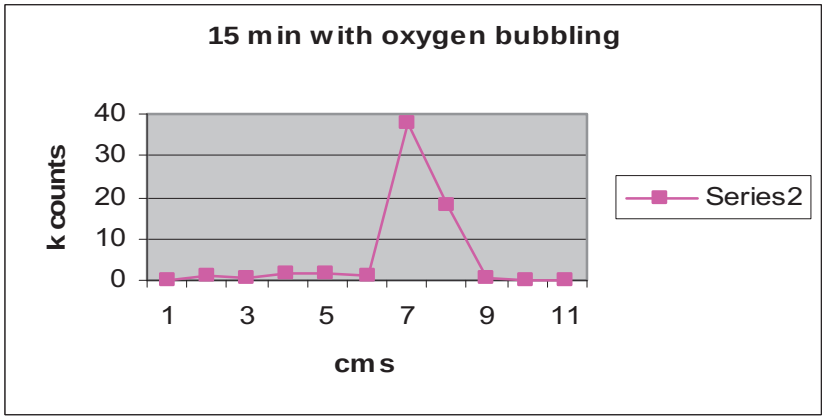

FIG. 4. Radiochemical purity 90%.

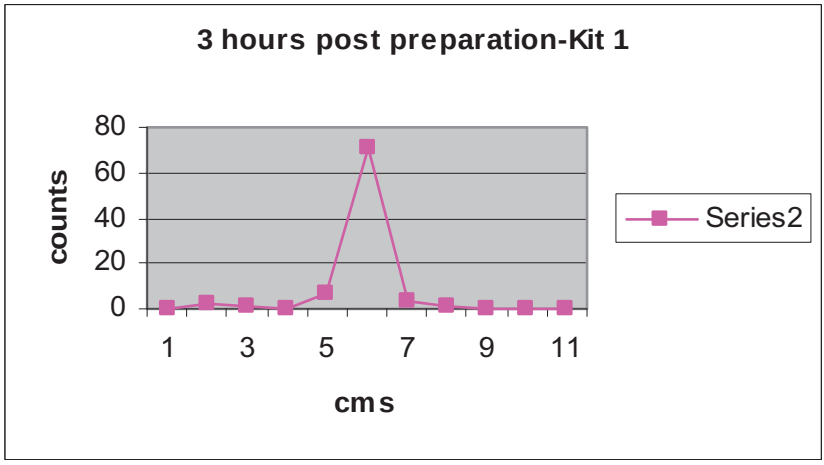

FIG. 5. Radiochemical purity 92%.

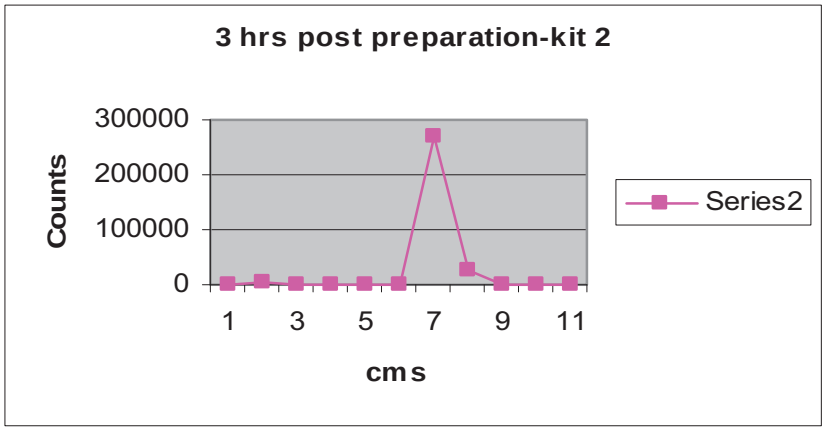

FIG. 6. Radiochemical purity 93%.

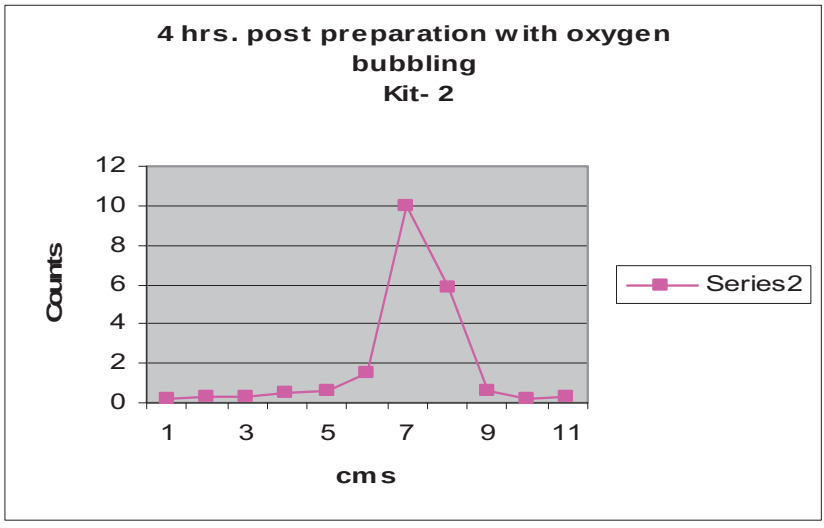

FIG. 7. Radiochemical purity 93%.

TABLE 1. CHROMATOGRAPHIC ANALYSIS OF THE KITS*
(*15 min incubation, no oxygen bubbling)*

Kit	$^{99m}TcO_4^-$	Reduced/hydrolysed $^{99m}TcO_2$	DMSA(III)	DMSA(V)
1	<5%	<5%	<5%	90–98%
2	<5%	<5%	Approx 50%	Approx 50%

* The above results reflect the overall performance of a number of samples of both the kits from different batches. The pH of the preparations was 8.5–9.0. The Rf values for ^{99m}Tc(III)-DMSA and ^{99m}Tc(V)-DMSA were 0.3 and 0.6–0.7, respectively.

TABLE 2. CHROMATOGRAPHIC ANALYSIS OF THE KITS*
(*1 h incubation, no oxygen bubbling)*

Kit	$^{99m}TcO_4^-$	Reduced/hydrolysed $^{99m}TcO_2$	DMSA(III)	DMSA(V)
1	<5%	<5%	<5%	90–98%
2	<5%	<5%	<5%	>90%

* The above results reflect the overall performance of a number of samples of both the kits from different batches. The pH of the preparations was 8.5–9.0. The Rf values for ^{99m}Tc(III)-DMSA and ^{99m}Tc(V)-DMSA were 0.3 and 0.6–0.7, respectively.

TABLE 3. CHROMATOGRAPHIC ANALYSIS OF THE KITS*
(*15 min incubation, no oxygen bubbling)*

Kit	$^{99m}TcO_4^-$	Reduced/hydrolysed $^{99m}TcO_2$	DMSA(III)	DMSA(V)
1		Not performed		
2	<5%	<5%	<5%	>90%

* The above results reflect the overall performance of a number of samples of both the kits from different batches. The pH of the preparations was 8.5–9.0. The Rf values for ^{99m}Tc(III)-DMSA and ^{99m}Tc(V)-DMSA were 0.3 and 0.6–0.7, respectively.

3.2. Biodistribution and clinical studies

An initial clinical trial (pilot study) in 10 diagnosed cases of lung carcinoma showed adequate concentration in the tumour and coexistent bone metastasis in 3 cases. Imaging at 3 h post-injection appears to be the optimum point at which to achieve a good target to non-target ratio for interpretation of the images.

Evaluation of in vivo tumour biology in the above cases was done post-treatment (Figs 8–10). The clinical and morphological response correlated well with the corresponding scintigraphy findings.

4. DISCUSSION

In routine clinical practice the authors have been preparing ^{99m}Tc(V)-DMSA simply by adding 0.2 mL of 7.5% w/v $NaHCO_3$ + $^{99m}TcO_4^-$ simultaneously to the commercially available DMSA(III) kits. This method has been described in the literature, with slight modifications between different studies, and a radiochemical purity of >95% has been achieved [1–5]. However, similar

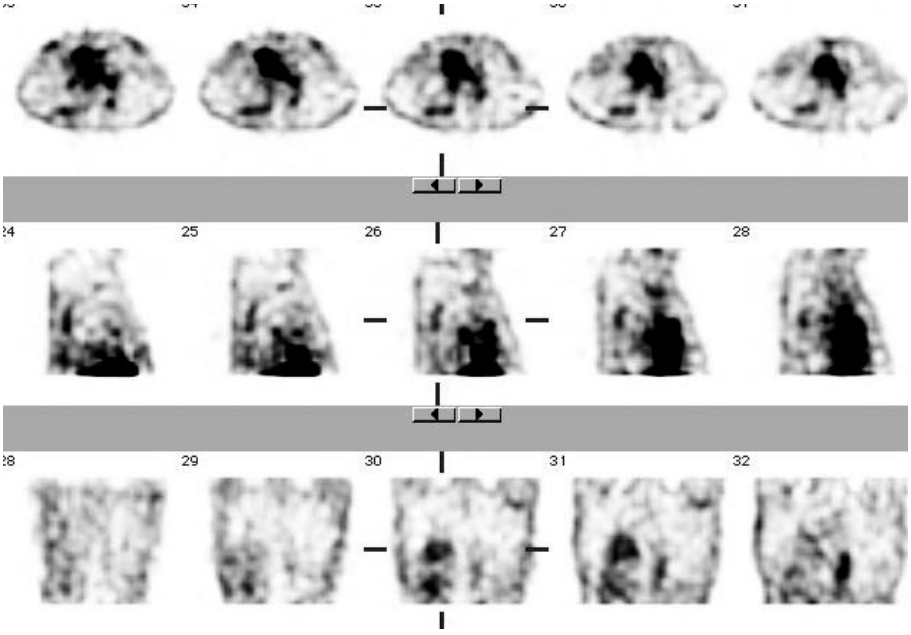

FIG. 8. Pretreatment ^{99m}Tc(V)-DMSA scan in a 63 year-old male showing tumour concentration in a case of lung carcinoma involving right lower lobe.

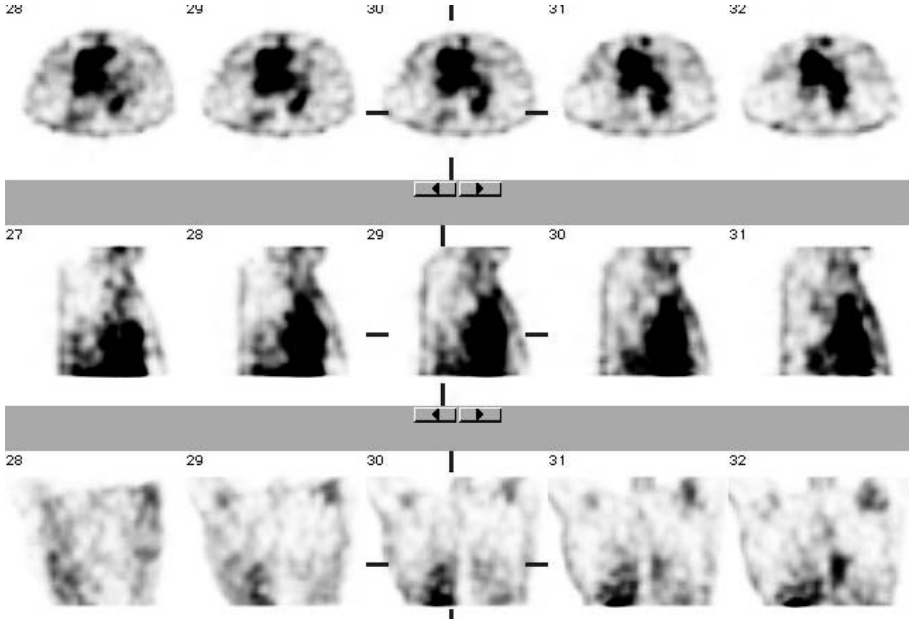

FIG. 9. ^{99m}*Tc(V)-DMSA scan in the same patient post-treatment (concurrent chemotherapy and external radiation) showing residual disease.*

radiochemical purity could not be reproduced by Washburn et al., who reported a radiochemical purity of <77% with this method. Although the authors have not undertaken prior chromatographic studies, their clinical results and biodistribution of the formulated radiopharmaceutical, by this method, have been inconsistent (unpublished data). It has been stated that the stannous concentration of the renal DMSA kit can play a role in the radiochemical purity of the ^{99m}Tc(V)-DMSA preparation. The kit supplied by BRIT contains 0.3 mg of $SnCl_2 \cdot 2H_2O$ and it would be possible to achieve >95% purity by adding only $NaHCO_3$ in 15 min. On the other hand, the kit supplied by Amersham contained 0.42 mg of $SnCl_2 \cdot 2H_2O$ and 0.7 mg ascorbic acid in addition. With the same method of formulation, the authors could achieve the same level of radiochemical purity but with an extended incubation time. The reason for this could be attributed to the presence of ascorbic acid which stops tin from being oxidized. It has been stated that oxidation of tin is responsible for the conversion of DMSA(III) to DMSA(V). Kumar [7] aimed to improve the radiochemical purity to 100% and also determine whether stannous oxidation plays an important role in the process of conversion of DMSA(III) to DMSA(V). He studied the change in radiochemical purity in response to

FIG. 10. Post-treatment CT scan of the chest in the same patient showing residual disease corresponding to the scintigraphic abnormality.

varying amounts of tin and oxygenation time. On bubbling compressed oxygen for 5 min he could achieve 100% purity in 20 min. Increasing the bubbling time resulted in a corresponding decrease in the time needed to achieve the same purity. In the study, the authors could also achieve the same purity by adding the oxygen bubbling method to their protocol in kit 2. This enabled the oxidation of excess tin and facilitated the conversion by countering the effect of the added ascorbic acid in this process.

It has been reported that the pH of the preparation could also be a determining factor in achieving a high radiochemical purity for DMSA(V). Oh et al. obtained a radiochemical yield of 95 ± 1.2% within 10 min and a preparation which was stable for 7 h. The radiochemical purity was 92 ± 1.5% at pH9. However, at a lower pH the yield was below 90% and a higher reaction time was required to achieve a purity of >90%. In the study, the measured pH after formulation was in the range 8.5–9. Biodistribution studies (Fig. 11) showed predominantly renal pelvicalyceal excretion in a radiochemically pure preparation with physiological concentration in the bladder. Cardiac blood pool concentration showed significant washout over time. Clinical studies reported in the literature have predominantly focused on tumour detection,

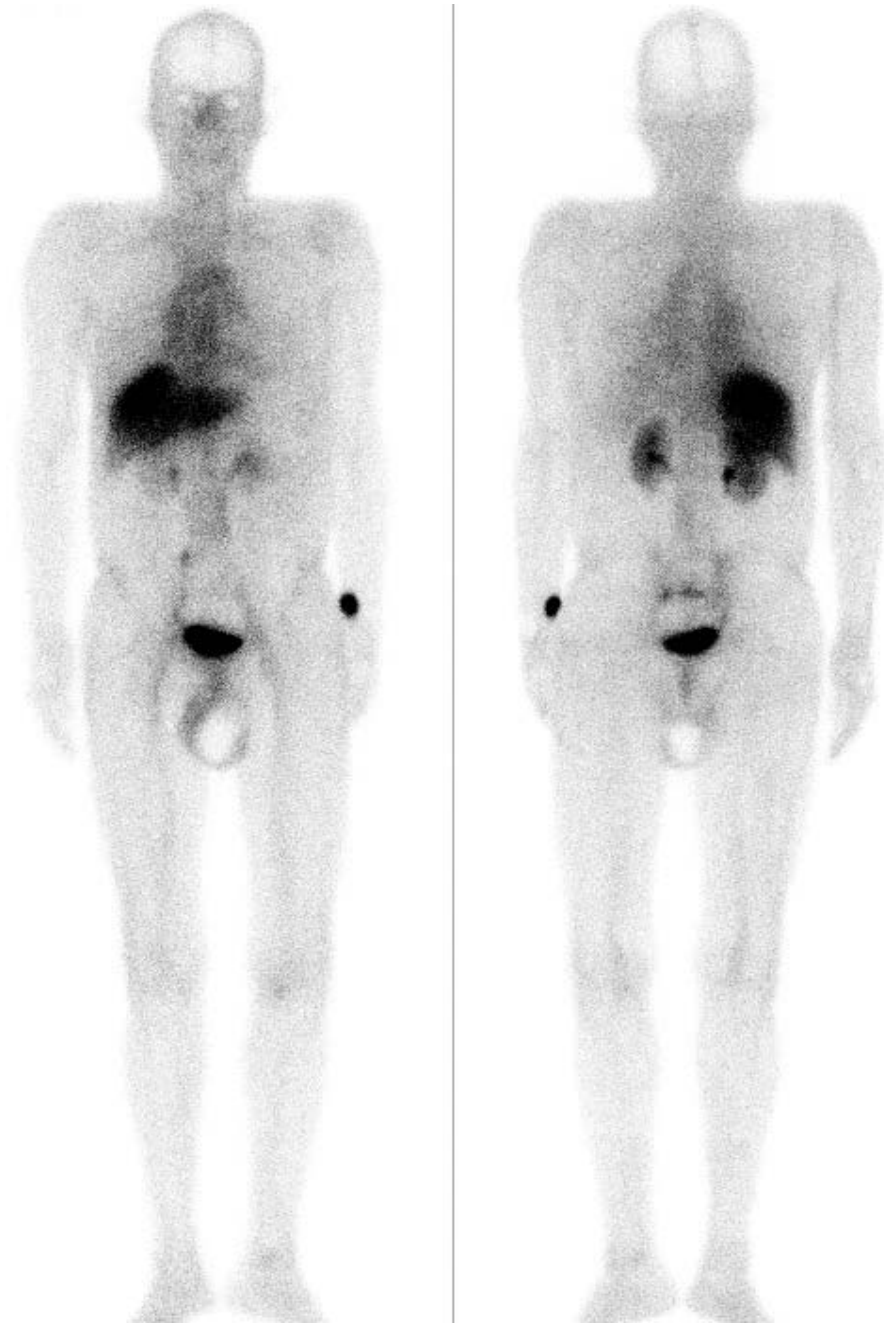

FIG. 11. Normal biodistribution of ^{99m}Tc(V)-DMSA in a radiochemically pure preparation.

mostly in medullary carcinoma thyroid and bone metastasis [9–12]. The authors are attempting to study tumour biology with an emphasis on detection, response to treatment and follow-up. Initial clinical results have been encouraging.

5. CONCLUSION

The authors have so far been able to standardize and reproduce an optimum radiochemically pure formulation of ^{99m}Tc(V)-DMSA. The BRIT kit formulation achieves a faster conversion to DMSA(V) and achieves good tumour concentration in a radiochemically pure preparation. The Amersham kit formulation without oxygen bubbling requires a longer incubation time for the same process. The radiochemical yield and stability of both kits were found to be the same. This formulation has been shown to concentrate in the active tumour and the current study suggest 3 h post-injection as being the optimum imaging time to achieve a good target to non-target ratio in the lesions.

ACKNOWLEDGEMENT

This study was supported by a grant (IAEA E1.30.28) from the IAEA in the framework of the coordinated research project entitled Standardization and Quality Control of In-house Prepared Radiopharmaceuticals in Nuclear Oncology.

REFERENCES

[1] OHTA, H., et al., A new imaging agent for medullary carcinoma of the thyroid, *J Nucl Med 25 (1984) 323-325.*

[2] WESTERA, G., GADZE, A., HORST, W., A convenient method for the preparation of ^{99m}Tc(V)-dimercaptosuccinic acid [^{99m}Tc(V)-DMSA], *J Appl Radiat Isot 36 (1985) 311-312.*

[3] CHAUHAN, U.P.S., et al., Evaluation of a DMSA kit for instant preparation of ^{99m}Tc(V)-DMSA for tumour and metastasis scintigraphy, *Nucl Med Biol 19 (1992) 825-830.*

[4] BABBAR, A., KASHYAP, R., CHAUHAN, U.P.S., A convenient method for the preparation of ^{99m}Tc labelled pentavalent DMSA and its evaluation as a tumour imaging agent, *J Nucl Med Biol 35 (1991) 100-104.*

[5] RAMAMOORTHY, N., et al., Preparation and evaluation of ^{99m}Tc(V)-DMSA complex: Studies in medullary carcinoma of thyroid, *Eur J Nucl Med 12 (1987) 623-628.*

[6] WASHBURN, L.C., BINIAKIEWICZ, D.S., MAXON, H.R., Possible preparation of ^{99m}Tc(V)-DMSA by a simple modified method using a commercial kit for ^{99m}Tc(III)-DMSA, *Nucl Med Biol 22 (1995) 689-691.*

[7] KUMAR, V., Evaluation of stannous oxidation in the preparation of ultra-high purity ^{99m}Tc(V)-DMSA, *Nucl Med Commun 22 (2001) 1261-1266.*

[8] OH, S.J., et al., Simple and reliable preparation of pentavalent ^{99m}Tc m-dimeraptosuccinic acid at alkaline pH without oxygen bubbling, *Nucl Med Commun 22 (6) (2001) 613-616.*

[9] SAHIN, M., et al., Evaluation of metastatic bone disease with pentavalent ^{99m}Tc dimercaptosuccinic acid: a comparison with whole body scanning and 4/24 hour quantitation of vertebral lesions, *Nucl Med Commun 21(3) (2000) 251-258.*

[10] LAM, A.S., et al., Pentavalent ^{99m}Tc DMSA imaging in patients with bone metastasis, *Nucl Med Commun 18(10) (1997) 907-914.*

[11] AMBRUS, E., et al., Value of ^{99m}Tc MIBI & ^{99m}Tc(V)DMSA scintigraphy in evaluation of breast mass lesions, *Anticancer Res 17 (1997) 1599-1605.*

[12] HIRANO, T., et al., Preparation & clinical evaluation of technetium-^{99m} dimercaptosuccinic acid for tumour scintigraphy, *Eur J Nucl Med 21(1) (1994) 82-85.*

DEVELOPMENT OF CENTRALIZED RADIOPHARMACIES IN SPAIN: A SUCCESSFUL EXPERIENCE IN EUROPE

I. OYARZÁBAL, R. JIMÉNEZ-SHAW
Molypharma, S.A.,
Madrid, Spain
Email: rjs@molypharma.es

Abstract

Good manufacturing practice requirements applied to radiopharmaceuticals compounding and unit dose preparation were seen as an opportunity when they were made compulsory by law in Spain during the mid-1990s. An innovative company was set up to develop centralized radiopharmacies or 'nuclear pharmacies', as they are known in the United States of America, with units designed for a safe and efficient operation with respect to product and personnel and which fulfil radioactive and pharmaceutical criteria. A quality management system has been implanted and a computerized management system supports the operation of each unit, helping the operator in their work, preventing mistakes and human error, and keeping control of record and traceability. An e-business system based upon the internet allows customers to place an order for their needs and provides additional information.

1. INTRODUCTION

In Spain, 650 000 nuclear medicine procedures are performed every year in more than 120 nuclear medicine departments in public and private hospitals.

The doses to be administered to patients were traditionally prepared by hospital personnel in small hot laboratories in the departments. However, during the 1990s new legislation was developed that triggered the need for a change in the model. The change from radiotracers to the new concept of radiopharmaceuticals led to pharmaceutical requirements for the development, fabrication, commercialization and preparation of radioactive compounds and their administration to patients. Additionally, regulatory authorities imposed quality assurance rules in nuclear medicine practices.

As regards dose preparation and administration, those legal requirements established new specific criteria derived from compliance with good manufacturing practices (GMPs) in several areas such as the following:

— Premises and equipment;
— Qualification of personnel;
— Quality systems with procedures, records and documentation control;
— Traceability.

Implementation of all these changes not only meant significant investments in terms of time and resources but also important modifications in habits and practices developed over many years. Several initiatives were launched to cope with the need for change, the concept of centralized radiopharmacies being among them, particularly in regions with a high density of nuclear medicine departments where scale economies make these pharmacies efficient.

Currently, a completely new system governs the preparation of unit doses of radiopharmaceuticals in the country:

— 45% of the unit doses are prepared and supplied from 6 centralized radiopharmacies;
— 20% of the unit doses are prepared in hospital radiopharmacies but managed and operated by an external contractor;
— 35% of the unit doses are prepared in hospital radiopharmacies managed by hospital personnel.

The significant penetration of centralized radiopharmacies should be stressed. This makes Spain the European country in which the pharmacies have progressed the most, in spite of its different population density rates. They are owned and operated by private companies that have taken the initiative to bring this preparation and distribution system to the Spanish radiopharmaceutical sector.

2. INNOVATIVE CONCEPT

Spanish centralized radiopharmacies can be considered as an innovative sector in Europe, as they offer hospitals the possibility of outsourcing their compounding needs to an external contractor in order to save costs and focus on their patients.

Molypharma's innovation in this field can be seen in three features:

(1) *Common system of radiopharmacies*: In order to provide a better service and obtain synergies, the company has developed several radiopharmacies with a central administrative hub that provides software and other

support. Design, systems and operation of each unit are practically identical.

(2) *E-business*: The company has developed an e-business system in order to provide customers with an easy method to set up error free orders and to guarantee traceability. This e-business system is composed of:
   — Software that processes orders, issues invoices and offers information through the internet located at the company's headquarters; and
   — Other software that manages every step of the pharmacy production located at each unit.

   Both softwares are interconnected via the internet.

(3) *Quality*: In order to focus all the activities on their customer's needs and complying with the strictest regulations, the company established an ISO 9001 certified quality management system and designed their units and operations according to GMP standards.

Operation of the first centralized radiopharmacy started in 2000. There were three operating units as of 2005.

3. UNIT DESIGN AND LAYOUT

Each unit has been designed to meet both GMPs and radioactive regulations. These are conflicting regulations, as GMPs call for the protection of the product, requiring positive pressure to avoid possible contamination of the product, while radioactive regulations establish protection for the operator and the environment, requiring negative pressure. This apparent contradiction is solved in the company's units through having a pressure cascade, the laminar air flow open cabins being in negative pressure in relation to the clean room where they are located. The clean room is in positive pressure over the reception and expedition rooms in order to avoid any possible contamination.

The laminar airflow open cabins are shielded to protect the operator and include a dose calibrator activimeter connected to the computer system. Labelling and unit dispensing is done within the cabins. Operators are comfortably seated. Generators are eluted in a special cabinet.

The unit also has conventional laboratory equipment and rooms, quality control, air conditioning and filters, as required by pharmaceutical and radioactive regulations.

4. QUALITY MANAGEMENT SYSTEM

Quality is of paramount importance to Molypharma in all its activities in such a way that:

— The quality of all its products and services is controlled. Molypharma controls the quality of its product with the maximum efficacy and safety and under conditions for continued improvement.
— The client's needs and expectations are always met satisfactorily.
— The operations at its facilities are always carried out under optimum radiological safety and protection conditions.

To carry out its activities, the company has adopted a quality management system based on processes in accordance with the standard UNE-EN-ISO 9001:2000 requirements. The quality management system has been certified by AENOR, the Spanish Association of Standardization and Certification. The company also holds a licence for use of the 'Madrid Excelente' seal of guarantee, issued by the regional government of Madrid and based on the EFQM model of management.

The quality management system has the same quality manual and standard operating procedures for each unit. These standard operating procedures include reception, inventory and registry of materials, compounding and quality control of each radiopharmaceutical, expedition of materials, and maintenance, verification and calibration of equipment. There are also general standard operating procedures for audits, customers and process flow management, etc.

Quality assurance performance is measured regularly by a set of indexes. One of the most important indexes is punctuality. It measures the percentage of on-time deliveries. This index is measured every month and it is compared with the goal of achieving a 99% success rate. In some units, the average punctuality index is better than 98%.

5. E-BUSINESS SYSTEM

Customers can place their orders easily through the internet. The only software needed is an internet navigator, either Netscape or Explorer. Each hospital can have several users with their own user name and password. The access is made through a secure connection.

The order web page is user friendly. The only field that must be typed in is the name of the doctor making the prescription. Scroll bars manage all the

other fields. Once the product is selected from a different list for each customer, it is only necessary to set activity at the calibration time and delivery time and date. The system automatically proposes the agreed delivery time. Each order can have different lines, each line being a different product.

Filling in the name in the patient field is an option for the customer. The database is designed to comply with the confidentiality required for these types of data. Some of Molypharma's customers leave it blank and others put in either the real name of the patient or another kind of patient identification, such as a clinical history number. Each order is automatically downloaded to the computer system located in each radiopharmacy, avoiding possible human errors.

In addition to order management, this e-business system (known as Molysic) can handle a lot of valuable information for the customer. Customers can check the status of pending orders and orders already delivered and have access to a set of predesigned queries such as a list of products and a list of delivered activity by date and isotope, etc. This query is very useful for complying with the requirements of radioactive regulatory authorities.

Customers can rapidly have access to the identity of each unit dose. Just by typing the identification number of a single dose, the system delivers the following information: order number, container identification, delivery note number, worker identification (who prepared the dose), identification of eluted and labelled vials, expiry date, volume, patient identification, etc. The system provides all this information in an error free way, as a bar code reader controls every step of preparation.

Molyfact is the invoicing side of the e-business system. It gets all the information from Molysic and allows the company to invoice each hospital with their own requests. It can invoice for each delivery or over some defined period, such as a week, a month, and so on. It also provides each customer with statistics about its consumption in euros, not in units.

6. RADIOPHARMACY MANAGEMENT SYSTEM

The management system of Molypharma's radiopharmacies, Udemon, is automated from receipt of on-line orders to the issuing of the final product, and covers all the intermediate steps of the compounding of radiopharmaceuticals. Udemon also generates the documentation required for transport and delivery and:

— Ensures complete traceability of the product, from the supplier's details to those of the dosage delivered to the client.

— Identifies each single dose via bar coded labels and all the data required by current legislation.
— Minimizes the possibility of human error, owing to the extensive use of bar codes on vials, containers, processes and operators.

Udemon has three main modules: (i) administrative, (ii) compounding and (iii) communication.

The administrative module deals with personnel identification, customer specifications, supplier identification and product portfolio. Other important submodules are orders to suppliers, orders from customers, inventory control and production control.

The compounding module makes it possible to operate the central radiopharmacy very efficiently from a personnel point of view as every minor step is automated. The main submodules are elution, which controls each generator, vial labelling, quality control, syringe dispensing, and label and documentation printing. Each excursion, which can involve several deliveries to different hospitals, has its computer generated consignment note. Each delivery has a delivery note, a list of unit doses per container and an optional second set of labels to be added to the clinical history.

Every step of the production process is controlled by bar codes. Bar codes are applied to each vial and generator that arrives at the pharmacy, to each worker involved in every step and to each intermediate vial of the elution or labelled product. Bar codes are also applied to unit doses and containers, avoiding the possibility of sending a dose to another customer in error.

The communication submodule exchanges information with the central Molysic e-business system. It downloads customers orders and uploads suppliers orders and other information required for traceability and invoicing.

7. HUMAN RESOURCES

Each unit has two specialists in radiopharmacy. To obtain this qualification in Spain, the person must be either a chemist or a pharmacist and to have completed a two year residency in a hospital. The company provides additional education in quality, GMPs, customer relations, software and management.

Each unit has several technicians that have taken a two year course after high school. They also receive further education in the company. The number of technicians per unit depends on the number of doses to be prepared per day and on the opening hours.

Internal communication is facilitated by an intranet application accessible through a virtual private network that is available to all personnel. It contains information on quality and production indices, quality systems and procedures, practical company information and additional features. It also permits exchange of opinions through a discussion forum. A satisfaction personnel survey is performed every year, its results being published on the intranet.

8. DISTRIBUTION

Unit dose syringes are conditioned inside a sterilized envelope with their label. Several unit doses can be delivered in a type 'A' certified package. The company has designed and certified that the package contains a 4 mm lead shield covered by a stainless steel container (127 mm × 127 mm × 270 mm), with handle, reinforced hinges and closure system, two-piece expanded polystyrene padding, plastic drum, metallic lid, closure ring and safety strapping.

The pharmacy also manages the waste of some hospitals. Hospital personnel dispose of used syringes in a biohazard plastic container. This container is situated within a protective shield. After the container is closed and measured as an exempt radioactive package, it is sent to the pharmacy's waste room. Once it is considered non-radioactive, it is disposed of as conventional biohazard waste by a specialized company.

In order to focus on the radiopharmacy business and to provide the best possible service to the customer, physical distribution is subcontracted to a specialized multimodal transport company that operates in several dangerous goods sectors. The transport company has its own vans and drivers. This scheme requires very close collaboration between the radiopharmacy company and the transport company, and several common procedures have been developed and implemented.

A hospital representative, usually a nuclear medicine technician, signs delivery notes, indicating the actual time of receipt. This time is introduced subsequently into the system to obtain the punctuality index.

9. CONCLUSION

Development of a GMP standard network of centralized radiopharmacies in Spain has been an achievement based on the innovative implementation of an e-business system with extensive use of internet and computer software and hardware, as well as a quality management system. These systems

are interconnected with an instructed staff and a customer focused strategy, making for a well-balanced organization.

Hundreds of radiopharmaceutical unit doses are efficiently compounded outside of the hospital every day. These unit doses are delivered on time, error free, and with high quality and assured traceability, providing a smooth and valuable hospital radiopharmacy relationship.

CHAIRPERSONS OF SESSIONS

Session 1	S. GOMEZ DE CASTIGLIA F.F. KNAPP, Jr.	Argentina United States of America
Session 2	A. DUATTI J. KÖRNYEI	Italy Hungary
Session 3	I. CARRIO E.K.J. PAUWELS	Spain Netherlands
Session 4	R. ALBERTO M. VENKATESH	Switzerland India
Session 5	R.S. KAMEL N. RAMAMOORTHY	IAEA IAEA
Session 6	M. JEHANGIR R. MIKOLAJCZAK	Pakistan Poland
Session 7	A. VERBRUGGEN M.R.A. PILLAI	Belgium IAEA
Session 8	C. DECRISTOFORO K.K. SOLANKI	Austria IAEA
Session 9	J. HARVEY TURNER M. DONDI	Australia IAEA
Session 10	H.-J. MACHULLA M.C. LEE	Germany Republic of Korea
Session 11	H.S. BALTER G.-J. BEYER	Uruguay Switzerland
Session 12	V.W. PIKE D. SOLOVIEV	United States of America Switzerland
Session 13	M.M. VORA M. HAJI-SAEID	Saudi Arabia IAEA
Session 14	N.G. HARTMAN E. JANEVIK-IVANOVSKA	United Kingdom The Former Yugoslav Republic of Macedonia

SECRETARIAT OF THE SYMPOSIUM

M.R.A. PILLAI	Scientific Secretary
K.K. SOLANKI	Scientific Co-Secretary
R. PERRICOS	Conference Services
L. BARRIOS	Conference Assistance
R.J. BENBOW	Proceedings Editor

PROGRAMME COMMITTEE

M. DONDI
M. HAJI-SAEID
R.S. KAMEL
M.R.A. PILLAI
N. RAMAMOORTHY (*Chairperson*)
K.K. SOLANKI

LIST OF PARTICIPANTS

Abdel-Jalil, R.J.
Chemistry Department,
Faculty of Sciences and Arts,
Hashemite University,
P.O. Box 330127,
13133 Zarka, Jordan
Fax: +96253403333
Email: jalil@hu.edu.jo

Abdul Rahman, A.
Technical Service Division,
Malaysian Institute for Nuclear,
Technology Research (MINT),
Bangi, 43000 Kajang,
Selangor Darul Ehsan, Malaysia
Fax: +60389282992
Email: anwar@mint.gov.my

Abedin, M.Z.
Institute of Nuclear Science
& Technology,
Atomic Energy Research
Establishment,
Ganakbari, P.O. DEPZ,
Savar, Dhaka, Bangladesh
Fax: +88028613051
Email: ripd_inst@yahoo.com

Afroz, S.
Centre for Nuclear Medicine
and Ultrasound,
Dhaka Medical College Hospital,
Bangladesh Atomic Energy
Commission (BAEC),
Dhaka-1000, Bangladesh
Email: nmcdhaka@agni.com

Al Rayyes, A.H.
Cyclotron and Medical
Radioisotopes Division,
Atomic Energy Commission,
P.O. Box 6091,
Damascus, Syrian Arab Republic
Fax: +963116112289
Email: aalraies@aec.org.sy

Al-Azzawi, H.M.
Directorate of Chemistry and Petrochemical Industry,
Ministry of Science and Technology,
P.O. Box 0765, Al-Jadrya,
Baghdad, Iraq
Email: hisham_alazzawi@yahoo.com

Alberto, R.
Institute of Inorganic Chemistry,
University of Zurich,
Winterthurerstrasse 190,
8057 Zurich, Switzerland
Fax: +41446356802
Email: ariel@aci.unizh.ch

Ali, O.I.
National Agency for Food and Drug Administration and Control,
NAFDAC Headquarters,
Plot 2032 Olusegun Obasanjo Way,
Wuse Zone 7,
Abuja, Nigeria
Fax: +23495241461
Email: aliotib@yahoo.com

Al-Jammaz, I.
Cyclotron & Radiopharmaceutical,
MBC-03,
King Faisal Specialist Hospital and Research Centre,
P.O. Box 3354,
Riyadh 1211, Saudi Arabia
Fax: +96614424743
Email: jammaz@kfshrc.edu.sa

Al-Nuzal, S.M.D.
Directorate of Chemistry and Petrochemical Industry,
Ministry of Science and Technology,
P.O. Box 0765, Al-Jadrya,
Baghdad, Iraq
Email: saadidhaher@yahoo.com

Al-Saeedi, F.J.	Nuclear Medicine Department, Faculty of Medicine, Kuwait University, P.O. Box 24923, 13110 Safat, Jabria, Kuwait Fax: +9655338936 Email: fatimas@hsc.edu.kw
Alwan, I.F.	Directorate of Chemistry and Petrochemical Industry, Ministry of Science and Technology, P.O. Box 0765, Al-Jadrya, Baghdad, Iraq Email: rchpimost@most-Iraq.com
Andráskó, M.	Institute of Isotopes Co. Ltd, Konkoly Thege M. Str. 29–33, 1121 Budapest, Hungary Fax: +3613959070 Email: andrasko@izotop.hu
Andreae, F.	piCHEM Research & Development, Kahngasse 20, 8045 Graz, Austria Fax: +43316681711/4 Email: andreae@pichem.at
Antalffy, M.	Institute of Isotopes Co. Ltd, Konkoly Thege M. Str. 29–33, 1121 Budapest, Hungary Fax: +3613959070 Email: antalffy@izotop.hu
Aras, G.	Department of Nuclear Medicine, Faculty of Medicine, Ankara University, 06100 Ankara, Turkey Fax: +903123620897 Email: okucuk@medicine.ankara.edu.tr

Arrechedera Mejias, L.I.
Facultad de Farmacia,
Universidad Central de Venezuela,
Los Chaguaramos,
Apartado Postal 47008,
Caracas 1041-A, Venezuela
Fax: +582126052707; +582126052701
Email: arrechel@camelot.rect.ucv.ve

Artl, A.
piCHEM Research & Development,
Kahngasse 20,
8045 Graz, Austria
Fax: +43316681711/4
Email: artl@pichem.at

Asikoglu, M.
Department of Radiopharmacy,
Faculty of Pharmacy,
Ege University,
35100 Izmir, Turkey
Fax: +902323885258
Email: asikoglum@pharm.ege.edu.tr

Avila Sobarzo, M.J.
Chilean Nuclear Energy Commission,
Amunátegui 95,
P.O.Box 188-D,
6500687 Santiago, Chile
Fax: +5623646277
Email: mavila@cchen.cl

Balter, H.S.
Centro de Investigaciones
Nucleares,
Facultad de Ciencias,
Igua 4225,
11400 Montevideo, Uruguay
Fax: +59825250895
Email: jbalter@cin.edu.uy

Banerjee, S.
Radiopharmaceuticals Division,
RLG Building,
Bhabha Atomic Research Centre,
Trombay, Mumbai 400 085, India
Fax: +912225505151
Email: sharmila@apsara.barc.ernet.in

Baranyai, L.
Institute of Isotopes Co. Ltd,
Konkoly Thege M. Str. 29–33,
1121 Budapest, Hungary
Fax: +3613959070
Email: barlajos@izotop.hu

Bayomy, T.
Nuclear Medicine Department,
Arab Contractors Medical Centre (ACMC),
Gabal Al Akhdar,
P.O. Box 9033,
Nasr City, 11765 Cairo, Eqypt
Fax: +2026821624
Email: tamerbayomy@hotmail.com

Benz, L.M.
Hans Wälischmiller GmbH,
Schießstattweg 16,
88677 Markdorf, Germany
Fax: +497544951499
Email: lb@hwm.com

Beran, M.
Nuclear Physics Institute,
Academy of Sciences,
250 68 Rez, Prague,
Czech Republic
Fax: +420220940151
Email: beran@ujf.cas.cz

Bercik, I.
BIONT a.s.,
Karloveska 63,
84229 Bratislava, Slovakia
Fax: +421220670748
Email: bercik@biont.sk

Beyer, G.-J.
Cyclotron Unit,
University Hospital of Geneva,
24 rue Micheli-du-Crest,
1211 Geneva-14, Switzerland
Fax: +41223727585
Email: gerd.beyer@hcuge.ch

Bilewicz, A.
Institute of Nuclear Chemistry and Technology,
Dorodna 16,
03-195 Warsaw, Poland
Fax: +48228111532
Email: abilewicz@ichtj.wew.pl

Bortoleti de Araújo, E.
Instituto de Pesquisas,
Energéticas e Nucleares,
Av. Prof. Lineu Prestes 2242,
Cidade Universitária,
BR-05508-000 Sao Paulo, SP,
Brazil
Fax: +551138120253
Email: ebaraujo@ipen.br

Boucekkine, N.
Department of Nuclear Medicine,
CHU Bab El Oued,
Boulvard Said Touati,
16000 Bab El Oued,
Algiers, Algeria
Fax: +21321965101
Email: nadiaboucekkine@yahoo.fr

Bozóky, Z.
"Fodor József" National Centre of Public Health,
National Research Institute for Radiobiology and Radiohygiene,
Anna Utca 5,
1221 Budapest, Hungary
Fax: +3614822012
Email: bozoky@hp.osski.hu

Bruskin, A.
SSC Institute of Biophysics,
Ministry of Health,
Zhivopisnaya Street 46,
123182 Moscow,
Russian Federation
Fax: +70951903590
Email: a_bruskin@mail.ru

Bucher, C.	THP Medical Products, Vertriebs GmbH, Shuttleworthstrasse 19, 1210 Vienna, Austria Fax: +4312928280-88 Email: ch.bucher@thp.at
Burkart, W.	Department of Nuclear Sciences and Applications, International Atomic Energy Agency, Wagramer Strasse 5, P.O. Box 100, 1400 Vienna, Austria Fax: +43126007 Email: w.burkart@iaea.org
Cabral Gonzalez, P.	Catedra de Radioquimica, Facultad de Quimica, Universidad de la República, General Flores 2124, P.O. Box 1157, 11800 Montevideo, Uruguay Fax: +59829241906 Email: pcabral@fq.edu.uy
Cañellas, C.O.	Tecnonuclear S.A., Arias 4149, 1430, Buenos Aires, Argentina Fax: +541145456005 Email: canellas@tecnonuclear.com.ar
Carrio, I.	Nuclear Medicine Department, Hospital Sant Pau, Avenida Padre Claret 167, 08025 Barcelona, Spain Fax: +34932919409 Email: icarrio@santpau.es
Cepelová, Z.	BIONT a.s., Karloveska 63, 84229 Bratislava, Slovakia Fax: +421220670686 Email: capelova@biont.sk

Cetto, A.M.
Department of Technical Cooperation,
International Atomic Energy Agency,
Wagramer Strasse 5, P.O. Box 100,
A-1400 Vienna, Austria
Fax: +43126007
Email: a.cetto@iaea.org

Chakraborty, M.
Laboratory Nuclear Medicine Section,
c/o Tata Memorial Hospital,
Bhabha Atomic Research Centre,
Annex Building, Jerbai Wadia Road,
Parel, Mumbai 400 012, India
Fax: +912224171872
Email: mayukh29@rediffmail.com

Cheng, Zuoyong
Nuclear Power Institute of China,
P.O. Box 436,
Chengdu 610041, China
Fax: +862885868504
Email: mrchengzy@yahoo.com.cn

Choudhury, P.S.
Department of Nuclear Medicine,
Rajiv Gandhi Cancer Institute & Research Centre — Sector 5,
New Delhi 110085, India
Fax: +911127051037
Email: pschoudhury@rgci.org

Cojocaru-Toma, M.
Ministry of Health,
Institute of Pharmacy,
Post Code MD 2028,
2/1 Korolenko str.
Chisinau, Moldova
Fax: +37322737448
Email: inf_isf@rambler.ru

Comor, J.J.
Laboratory of Physics (010),
Vinca Institute of Nuclear Sciences,
P.O. Box 522,
11001 Belgrade, Serbia
Fax: +381114447963
Email: jcomor@vin.bg.ac.yu

Cortes-Blanco, A.
Spanish Agency for Medicines and Healthcare Products,
C/Alcala 56,
28071 Madrid, Spain
Fax: +34918225161
Email: acortesb@agemed.es

Crudo, J.L.
Division Radiofármacos,
Centro Atomico Ezeiza,
Presb. Gonzalez y Aragon 15,
(B1802AYA) Ezeiza,
Buenos Aires, Argentina
Fax: +541167798288
Email: jlcrudo@cae.cnea.gov.ar

Çuçi, T.
Institute of Nuclear Physics,
P.O. Box 85,
Tirana, Albania
Email: triumfcuci@yahoo.com

Das, T.
Radiopharmaceuticals Division,
Bhabha Atomic Research Centre,
Trombay, Mumbai 400 085, India
Fax: +912225505345
Email: tdas@apsara.barc.ernet.in

de Jong, M.H.
Department of Nuclear Medicine,
Erasmus MC,
Rotterdam, Netherlands
Email: m.hendriks-dejong@erasmusmc.nl

Decristoforo, C.
Clinical Department of Nuclear Medicine,
Medical University Innsbruck,
Anichstrasse 35,
6020 Innsbruck, Austria
Fax: +4351250422659
Email: clemens.decristoforo@uibk.ac.at

Djokic, D.
Laboratory for Radioisotopes,
Vinca Institute of Nuclear Sciences,
P.O. Box 522,
11001 Belgrade, Serbia
Fax: +381112438134
Email: djokici@vin.bg.ac.yu

Dondi, M.
Department of Nuclear Sciences and Applications,
International Atomic Energy Agency,
Wagramer Strasse 5, P.O. Box 100,
1400 Vienna, Austria
Fax: +43126007
Email: m.dondi@iaea.org

Duatti, A.
Laboratory of Nuclear Medicine,
Department of Radiology,
University of Ferrara,
Via L. Borsari 46,
44100 Ferrara, Italy
Fax: +39532236589
Email: dta@unife.it

Ebrahimi-Fakhari, F.
Chemistry Department,
Philipps University Marburg,
Hans-Meerwein Strasse,
35032 Marburg, Germany
Fax: +4964212863427
Email: ebrahimi@staff.uni-marburg.de

El Haouzi, M.
Laboratoire National du Contrôle des Médicaments,
Ministère de la Santé,
B.P. 6206,
Rabat, Morocco
Fax: +21237681931
Email: melhaouzi@sante.gov.mo

Esiashvili, S.
National Cancer Centre,
Sairme Street B/L 6, Apt.15,
0194 Tbilisi, Georgia
Email: sesiash@yahoo.com

Faintuch, B.L.
Radiopharmacy Centre,
Institute of Energetic and Nuclear Research (IPEN/CNEN),
Av. Professor Lineu Prestes 2242,
Cidade Universitária,
BR-05508-900 Sao Paulo, SP,
Brazil
Fax: +551138169257
Email: faintuch@ipen.br

Farstad, B.
Isotope Laboratories,
Institute for Energy Technology,
P.O. Box 40,
2027 Kjeller, Norway
Fax: +4763803021
Email: brit.farstad@ife.no

Ferro-Flores, G.
Instituto Nacional de Investigaciones Nucleares (ININ),
Kilometro 36.5,
Carretera Mexico-Toluca,
52045 Municipio de Ocoyoacac,
Mexico
Fax: +525553297306
Email: gff@nuclear.inin.mx

Figols de Barboza, M.
Instituto de Pesquisas Energéticas e Nucleares,
Avenida Professor Prestes 2242,
Cidade Universitária,
BR-05508-000 Sao Paulo, SP,
Brazil
Fax: +551138169257
Email: mbarboza@ipen.br

Fischer, T.
Department of Nuclear Medicine,
University of Cologne,
Kerpener Strasse 62,
50924 Cologne, Germany
Fax: +492214786777
Email: thomas.fischer@uk-koeln.de

Flores de la Torre, J.A.
Universidad Autonoma de Zacatecas,
Unidad Academica de Estudios Nucleares,
Cipres # 10 FRACC La Penuela,
98068 Zacatecas, Mexico
Fax: +525553297322
Email: arman_do19@hotmail.com

Fresvig, M.
GE Healthcare,
Amersham Health,
P.O. Box 4220 Nydalen,
0401 Oslo, Norway
Fax: +4723186025
Email: marianne.fresvig@ge.com

Freud, A.
Nuclear Research Centre NEGEV,
Israel AEC,
P.O. Box 9001,
Beer-Sheva 84190, Israel
Fax: +97286567015
Email: freud@netvision.net.il

Gandomkar, M.
Radioisotope Deparment,
Nuclear Research Centre,
Atomic Energy Organization of Iran,
P.O. Box 11365-3486,
Tehran, Islamic Republic of Iran
Fax: +98218020887
Email: msgandomkar@yahoo.com

Garg, P.K.
PET Center,
Center for Biomolecular Imaging,
Wake Forest University Medical Center,
Medical Center Blvd,
Winston-Salem, NC 27157,
United States of America
Email: pgarg@wfubmc.edu

Geets, J.-M.
Ion Beam Applications s.a.,
Chemin du Cyclotron 3,
1348 Louvain-la-Neuve, Belgium
Fax: +3210475958
Email: geets@iba.be or piccoli@iba.be

Gibson, P.N.
Institute for Health and
Consumer Protection,
Joint Research Centre,
Via E. Fermi 1,
21020 Ispra (VA), Italy
Fax: +390332785388
Email: neil.gibson@jrc.it

Giubbini, R.M.T.
Spedali Civili di Brescia,
Medicina Nucleare,
Piazza Spedali Civili 1,
25100 Brescia, Italy
Email: giubbini@spedalicivili.brescia.it

Gjerde, H.
Amersham Health,
P.O. Box 4220 Nydalen,
0401 Oslo, Norway
Fax: +4723186024
Email: hallvard.gjerde@ge.com

Gniazdowska, E.
Institute of Nuclear Chemistry
and Technology,
Dorodna 16,
03-195 Warsaw, Poland
Fax: +48228111532
Email: egniazdo@ichtj.waw.pl

Gomez de Castiglia, S.I.
Centro Atómico Ezeiza,
Comisión Nacional de Energía Atómica,
Avenida Del Libertador 8250,
1429 Buenos Aires, Argentina
Fax: +541167798288
Email: silgomez@cae.cnea.gov.ar

Gourni, E.
National Centre for Scientific
Research (NCSR) “Demokritos”,
P.O. Box 60228,
15310 Aghia Paraskevi,
Athens, Greece
Fax: +302106522661
Email: egourni@yahoo.gr

Gunawardana, C.
Lady Ridgeway Hospital for
Children,
Dr. Danister de Silva Mawatha,
Colombo 08, Sri Lanka
Fax: +9412691521
Email: chamly2000@yahoo.com

Haji-Saeid, S.M.
Department of Nuclear Sciences and Applications,
International Atomic Energy Agency,
Wagramer Strasse 5, P.O. Box 100,
1400 Vienna, Austria
Fax: +43126007
Email: m.haji-saeid@iaea.org

Hansson, L.K.
Medical Products Agency,
P.O. Box 26,
751-03 Uppsala, Sweden
Fax: +4618548566
Email: lena.hansson@mpa.se

Harbo, B.T.
Isotope Laboratories,
Institute for Energy Technology,
P.O. Box 40,
2027 Kjeller, Norway
Fax: +4763803021
Email: bente.tange.harbo@ife.no

Hartman, N.G.
Addenbrooke's Hospital,
Hills Road,
Cambridge CB2 2QQ,
United Kingdom
Email: nh289@cam.ac.uk

Hawerkamp, A.
Eurotope GmbH,
Robert-Rössle-Strasse 10,
13125 Berlin, Germany
Fax: +4930941084160
Email: andrea.hawerkamp@eurotope.de

Hazra, D.K.
Nuclear Medicine Unit,
S.N. Medical College Agra,
Soami Bagh,
Agra 282003, India
Fax: +91562226524
Email: hazra@sancharnet.in

Hong, Seong-Seok
KIRAMS,
Korea Cancer Centre Hospital,
215 Gongneung Dong, Nowon-ku,
Seoul, Republic of Korea
Email: mkh@kcchsun.kcch.re.kr

Husbyn, M.
GE Healthcare,
Amersham Health,
P.O. Box 4220 Nydalen,
0401 Oslo, Norway
Fax: +4723186025
Email: mette.husbyn@ge.com

Iller, E.
Radioisotope Centre,
POLATOM,
05-400 Otwock-Swierk, Poland
Fax: +48227180351
Email: e.iller@polatom.pl

Ishfaq, M.M.
Isotope Production Division,
Pakistan Institute of Nuclear Science
and Technology (PINSTECH),
P.O.Box 1482,
Islamabad, Pakistan
Fax: +92519290275
Email: mishfaq@pinstech.org.pk

Jahren, G.
GE Healthcare,
Amersham Health,
P.O. Box 4220 Nydalen,
0401 Oslo, Norway
Fax: +4732186026
Email: grete.jahren@ge.com

Jalilian, A.R.
Cyclotron Department,
Nuclear Research Centre for
Agriculture & Medicine,
P.O. Box 31585-4395,
Karaj, Islamic Republic of Iran
Fax: +982624411106
Email: ajalilian@nrcam.org

Janevik-Ivanovska, E.
Medical Faculty,
Institute of Pathophysiology
and Nuclear Medicine,
Vodnjanska 17,
1000 Skopje,
The Former Yugoslav Republic of Macedonia
Fax: +38923147203
Email: janevik@yahoo.com

Janoki, Gy.A.
Frederic Joliot-Curie National Institute for Radiobiology and Radiohygiene,
Anna Utca 5,
1221 Budapest, Hungary
Email: janoki@hp.osski.hu

Janota, B.
Radioisotope Centre,
POLATOM,
05-400 Otwock-Swierk, Poland
Fax: +48227180351
Email: b.janota@polatom.pl

Jehangir, M.
Isotope Production Division,
Pakistan Institute of Nuclear Science and Technology (PINSTECH),
P.O.Box 1482,
Islamabad, Pakistan
Fax: +92519290275
Email: mustansar@pinstech.org.pk

Jiménez-Shaw, R.
Molypharma,
Dr. Severo Ochoa 37-4-1,
28100 Alcobendas,
Madrid, Spain
Fax: +34914905740
Email: rjs@molypharma.es

Jovanovic, S.
Faculty of Sciences,
University of Montenegro,
P.O. Box 211,
81000 Podgorica, Serbia
Fax: +38181244608
Email: bobo_jovanovic@yahoo.co.uk

Jurina, V.
Public Health Authority of the Slovak Republic,
Trnavska cesta 52,
82645 Bratislava, Slovakia
Fax: +421244372619
Email: jurina@uvzsr.sk

Moghaddam, K.K.	Cyclotron Department, Nuclear Research Centre for Agriculture & Medicine, Rajaee Shahr, P.O. Box 31585-4395, Karaj, Islamic Republic of Iran Fax: +982624411106 Email: kkamali@nrcam.org
Kamel, R.	Department of Technical Cooperation, International Atomic Energy Agency, Wagramer Strasse 5, P.O. Box 100, 1400 Vienna, Austria Fax: +43126007 Email: r.kamel@iaea.org
Kassai, Z.	BIONT a.s., Karloveska 63, 84229 Bratislava, Slovakia Fax: +421220670748 Email: kassai@biont.sk
Khanna-Hazra, P.	S.N. Medical College, Soami Bagh, Agra 282003, India Fax: +915622226524 Email: hazra@sancharnet.in
Kibwage, I.O.	Faculty of Pharmacy, College of Health Sciences, University of Nairobi, P.O. Box 19676, Nairobi 00202, Kenya Fax: +254202711132 Email: okibwage@uonbi.ac.ke
Kim, Yu-Seok	KIRAMS, Korea Cancer Centre Hospital, 215 Gongneung Dong, Nowon-ku, Seoul, Republic of Korea Email: mkh@kcchsun.kcch.re.kr

Kiondo, P.M.
Nuclear Medicine Unit,
Mulago Hospital,
P.O.Box 7051,
Kampala, Uganda
Fax: +25641532591
Email: pmkiondo@med.mak.ac.ug

Knapp, F.F.
Nuclear Medicine Program,
Oak Ridge National Laboratory,
Building 4501, MS 6229,
P.O. Box 2008,
Bethel Valley Road,
Oak Ridge, TN 37831-6229,
United States of America
Fax: +18655746226
Email: knappffjr@ornl.gov

Knopp, R.
Eurotope GmbH,
Robert-Rössle-Strasse 10,
13125 Berlin, Germany
Fax: +4930941084160
Email: roger.knopp@eurotope.de

Környei, J.
Institute of Isotopes Co. Ltd,
Konkoly Thege M. Str. 29–33,
1121 Budapest, Hungary
Fax: +3613959070
Email: kornyei@izotop.hu

Környeiné Kovács, G.
"Uzsoki" Hospital,
Department of Nuclear Medicine,
Uzsoki str. 29,
1145 Budapest, Hungary
Fax: +3614673772
Email: kornyei@uzsoki.hu

Korsak, A.
Radioisotope Centre,
POLATOM,
05-400 Otwock-Swierk, Poland
Fax: +48227180351
Email: a.korsak@polatom.pl

Kovac, P.	BIONT a.s., Karloveska 63, 84229 Bratislava, Slovakia Fax: +421220670748 Email: kovac@biont.sk
Kudelin, B.K.	V.G. Khlopin Radium Institute, 28, 2nd Murinski Avenue, 194021 St. Petersburg, Russian Federation Fax: +78122476181 Email: kudelin@atom.nw.ru
Kuecuek, N.O.	Department of Nuclear Medicine, Faculty of Medicine, Ankara University, 06100 Ankara, Turkey Fax: +903123620897 Email: n.ozlem.kucuk@medicine.ankara.edu.tr
Kugel, D.J.	St. Luke's Hospital, 801 Ostrum St., Bethlehem, PA 18015, United States of America Fax: +16109237224 Email: debikugel@aol.com
Laznicek, M.	Faculty of Pharmacy, Charles University, Heyrovskeko 1203, 500 05 Hradec Kralove, Czech Republic Fax: +420495514373 Email: laznicek@faf.cuni.cz
Laznickova, A.	Faculty of Pharmacy, Charles University, Heyrovskeho 1203, 500 05 Hradec Kralove, Czech Republic Fax: 420495518002 Email: laznicko@faf.cuni.cz

Lee, Myuna-Chul
Department of Nuclear Medicine,
Seoul National University Hospital,
28 Yongon-dong, Chongno-gu,
Seoul 110-744, Republic of Korea
Fax: +8227457690
Email: mychlee@yahoo.com

Leyva Montaña, R.
Centro de Isotopos,
AENTA, CITMA,
Ave. Monumental y Carr. La Rada km 3½,
San José de Las Lajas,
Apartado Postal 3415,
Havana, Cuba
Fax: +5378661821
Email: rene@centis.edu.cu

Lipka, R.J.
OBRI POLATOM,
Woj Mazowieckie,
05-400 Otwock-Swierk, Poland
Email: treborl_pl@yahoo.com

Lungu, V.
Institute of Physics and Nuclear
Engineering "Horia Hulubei",
Str. Atomistilor 407,
P.O. Box MG 6,
76900 Bucharest, Magurele, Romania
Fax: +4014231701
Email: vlungu2000@yahoo.com

Luo, Zhifu
China Institute of Atomic Energy,
P.O. Box 275 ext. 12,
Beijing 102413, China
Fax: +861069358952
Email: lzhf@iris.ciae.ac.cn

Macásek, F.
BIONT, a.s.,
Karloveska 63,
84229 Bratislava, Slovakia
Fax: +421220670748
Email: macasek@biont.sk

Machulla, H.-J.
Radiopharmacy PET Centre,
University of Tübingen,
Röntgenweg 15,
72076 Tübingen, Germany
Fax: +497071295264
Email: machulla@uni-tuebingen.de

Malhotra, A.
Department of Nuclear Medicine,
All India Institute of Medical Sciences,
New Delhi 110029, India
Fax: +911126588663
Email: arun190@hotmail.com

Malja, S.
Institute of Nuclear Physics,
P.O. Box 85,
Tirana, Albania
Fax: +3554362596
Email: smalja@albmail.com

Marujo Marques, F.
Instituto Tecnológico e Nuclear,
Estrada nacional 10,
Apartado 21,
2686-953 Sacavém, Portugal
Fax: +351219941455
Email: fmarujo@itn.pt

Mat Ail, N.
Pharmacy Division,
Kuala Lumpur Hospital,
Jalan Pahang,
50386 Kuala Lumpur, Malaysia
Fax: +60320930293
Email: mhh@cimb.com.my

Máthé, D.
"Fodor József" National Centre
of Public Health,
National Research Institute for
Radiobiology and Radiohygiene,
Anna utca 5,
1221 Budapest, Hungary
Fax: +3614822012
Email: mdomokos@hp.osski.hu

Mather, S.J.
Imperial Cancer Research Fund,
Department of Nuclear Medicine,
St. Bartolomew's Hospital,
51–53 Bartholomew Close,
London EC1 7BE, United Kingdom
Fax: 441717963907
Email: stephen.mather@cancer.org.uk

Melichar, F.
Nuclear Physics Institute,
Academy of Sciences,
250 68 Rez, Prague,
Czech Republic
Fax: +42026875481
Email: melichar@ujf.cas.cz

Mertens, J.J.
Radiopharmaceutical Chemistry/BEFY,
Vrije Universiteit Brussel,
Cyclotron Building,
Laarbeeklaan 103,
1090 Brussels, Belgium
Fax: +3223053131
Email: jjmertens@vub.ac.be

Mesa Dueñas, N.
Instituto de Nefrología (INEF)
"Dr. Aberlardo Buch Lopez",
Ave. 26 y Rancho Boyeros Cerro,
10600 Havana, Cuba
Fax: +5378812413 or +5372041188
Email: mninef@infomed.sld.cu

Miceva Ristevska, S.
Institute of Pathophysiology
and Nuclear Medicine,
Medical Faculty,
Vodnjanska 17,
1000 Skopje,
The Former Yugoslav Republic of Macedonia
Email: svetlana@ukim.edu.mk

Mikolajczak, R.
Radioisotope Centre,
POLATOM,
05-400 Otwock-Swierk, Poland
Fax: +48227180350
Email: r.mikolajczak@polatom.pl

Mishra, A.K.
Division of Cyclotron and
Radiopharmaceutical Sciences,
Institute of Nuclear Medicine
and Allied Sciences,
Brig. S.K. Mazumdar Road,
Timarpur, New Delhi 110054, India
Fax: ++911123919509
Email: akmishra@inmas.org

Mititelu, M.R.
Central Clinical Emergency
Military Hospital,
Cal Plevnei 134, Sector 6,
010242 Bucharest, Romania
Fax: +4022223670
Email: ralunuclear@yahoo.com

Mitterhauser, M.
Department of Nuclear Medicine,
Allgemeines Krankenhaus Universitätskliniken,
Währinger Gürtel 18-20,
1090 Vienna, Austria
Fax: +431404001559
Email: markus.mitterhauser@meduniwien.ac.at

Naidoo, C.
Radionuclide Production Group,
IThemba Labs,
P.O. Box 722,
Somerset West 7129, South Africa
Fax: +27218433901
Email: clive@tlabs.ac.za

Nano, G.
Dompe SpA,
Via Campo di Pile SNC,
Z.1. Pile,
67100 L'Aquila, Italy
Fax: +390862338219
Email: nano@dompe.it

Napaporn, T.
Department of Radiology,
Division of Nuclear Medicine,
Siriraj Hospital Medical School,
Bangkok 10700, Thailand
Fax: +6624127165
Email: sintj@mahidol.ac.th

Niculae, D.
National Institute for Physics and Nuclear Engineering "Horia Hulubei",
Atomistilor Street 407,
P.O. Box MG-6,
76900 Bucharest – Magurele, Romania
Fax: +4021454440
Email: radphy@ifin.nipne.ro

Novotny, D.
Hans Wälischmiller GmbH,
Rossendorfer Ring 42,
01328 Dresden, Germany
Fax: +493512663410
Email: waelischmiller_dresden@t-online.de

Ocak, M.
Department of Pharmaceutical Technology,
Faculty of Pharmacy,
Istanbul University,
34116 Istanbul, Turkey
Fax: +902125306734
Email: melocak@yahoo.com

Oliver, Y.P.
Centro de Investigaciones Nucleares,
Facultad de Ciencias,
Igua 4225,
11400 Montevideo, Uruguay
Fax: +59825250895
Email: poliver@cin.edu.uy

Narbutt, J.
Institute of Nuclear Chemistry and Technology,
Dorodna 16,
03-195 Warsaw, Poland
Fax: +48228111532
Email: jnarbut@ichtj.waw.pl

Özer, A.Y.
Department of Radiopharmacy,
Faculty of Pharmacy,
Hacettepe University,
06100 Ankara, Turkey
Fax: +903123114777
Email: ayozer@hacettepe-edu.tr

Ozker, K.
Medical College of Wisconsin,
9200 W. Wisconsin Avenue,
Milwaukee, WI 53226,
United States of America
Fax: +14147713460
Email: ozker@mcw.edu

Pasquali, M.
Laboratory of Nuclear Medicine,
Department of Radiology,
University of Ferrara,
Via L. Borsari 46,
44100 Ferrara, Italy
Fax: +39532236589
Email: dta@unife.it

Pauwels, E.K.J.
Department of Nuclear Medicine,
Leiden University Medical Centre,
C4-075,
Albinusdreef 2,
2333 ZA Leiden, Netherlands
Fax: +31715266751
Email: ernestpauwels@gmail.com

Pawlak, D.
Radioisotope Centre,
POLATOM,
05-400 Otwock-Swierk, Poland
Fax: +48227180351
Email: d.pawlak@polatom.pl

Pedersen, B.
Danish Medicines Agency,
Axel Heidesgade 1,
2300 København, Denmark
Email: bp@dkma.dk

Perewusnyk, G.
Swiss Federal Office of Public Health,
Division of Radiation Protection,
3003 Bern, Switzerland
Fax: +41313228383
Email: gloria.perewusnyk@bag.admin.ch

Pereyra Molina, V.E.
Nuclear Medicine National Institute,
C. Mayor Rafael Zubieta #1555,
Miraflores, La Paz, Bolivia
Fax: +59122112784
Email: inamen@entelnet.bo

Persson, B.E.
Medical Products Agency,
P.O. Box 26,
751-03 Uppsala, Sweden
Fax: +4618548566
Email: bengt.persson@mpa.se

Pike, V.W.
Molecular Imaging Branch,
National Institute of Mental Health,
Building 101 RM B3 C346A,
10 Center Drive,
Bethesda, MD 20892-1003,
United States of America
Fax: +13014805112
Email: pikev@mail.nih.gov

Pillai, M.R.
Department of Nuclear
Sciences and Applications,
International Atomic Energy Agency,
Wagramer Strasse 5, P.O. Box 100,
1400 Vienna, Austria
Fax: +43126007
Email: M.R.A.Pillai@iaea.org

Pimentel, G.J.
National Institute of Oncology
and Radiobiology,
Calle 29 E y 29,
Vedado Plaza,
10400 Havana, Cuba
Email: gilmara@infomed.sld.cu

Pirmettis, I.
Institute of Radioisotopes,
NCSR “Demokritos”,
Patriarchou Grigoriou and Napoeleos,
15310 Aghia Paraskevi,
Athens, Greece
Fax: +302106524480
Email: ipirme@rrp.demokritos.gr

Poramatikul, N.
Radioisotope Production Programme,
Office of Atoms for Peace (OAP),
16 Vibhavadee Rangsit Road,
Chatujak,
Bangkok 10900, Thailand
Fax: +6625620127
Email: nipavan@oaep.go.th

Prats Capote, A.	Centre for Clinical Research, 34 Street no. 4501e/ 45 y 47, Kholy, Playa, 11300 Havana, Cuba Fax: +5372043298 Email: anais.prats@infomed.sld.cu
Pruszynski, M.	Institute of Nuclear Chemistry and Technology, Dorodna 16, 03-195 Warsaw, Poland Fax: +48228111532 Email: mprusz@ichtj.waw.pl
Rajec, P.	BIONT a.s., Karloveska 63, 84229 Bratislava, Slovakia Fax: +421220670748 Email: rajec@biont.sk
Rakiás, F.	National Institute of Pharmacy, P.O. Box 450, 1372 Budapest, Hungary Fax: +3612663245 Email: rakias.ferenc@ogyi.hu
Ramamoorthy, N.	Department of Nuclear Sciences and Applications, International Atomic Energy Agency, Wagramer Strasse 5, P.O. Box 100, 1400 Vienna, Austria Fax: +43126007 Email: n.ramamoorthy@iaea.org
Razbash, A.A.	Cyclotron Co. Ltd, 1, Bondarenko Square, Obninsk, Kaluga Region 249033, Russian Federation Fax: +70843997048 Email: razbash_isotop@obninsk.com

Rey Rios, A.M.
Catedra de Radioquimica,
Facultad de Quimica,
Universidad de la República,
General Flores 2124,
P.O. Box 1157,
11800 Montevideo, Uruguay
Fax: +59829241906
Email: arey@fq.edu.uy

Robles, A.M.
Centro de Investigaciones Nucleares,
Facultad de Ciencias,
Igua 4225,
11400 Montevideo, Uruguay
Fax: +59825250895
Email: anamar@cin.edu.uy

Rodriguez, G.
Centro de Investigaciones Nucleares,
Facultad de Ciencias,
Igua 4225,
11400 Montevideo, Uruguay
Fax: +59825250895
Email: grodri@cin.edu.uy

Roesch, F.
Institut für Kernchemie,
Johannes Gutenberg Universität,
Fritz-Strassmann-Weg 2,
55128 Mainz, Germany
Fax: +4961313924692
Email: frank.roesch@uni-mainz.de

Rossbach, M.
Department of Nuclear
Sciences and Applications,
International Atomic Energy Agency,
Wagramer Strasse 5, P.O. Box 100,
1400 Vienna, Austria
Fax: +43126007
Email: m.rossbach@iaea.org

Rossi, G.
ENEA UTS FIS-ION,
C.R. Casaccia,
S.P. Anguillarese 301,
00060 Rome, Italy
Fax: +3930484874
Email: rossig@casaccia.enea.it

Rossouw, D.D.
IThemba Labs,
P.O. Box 722,
7129 Somerset West,
South Africa
Fax: +27218433901
Email: niel@tlabs.ac.za

Sadeghi, M.
Cyclotron Department,
Nuclear Research Centre for
Agriculture & Medicine,
P.O. Box 31585-4395,
Karaj, Islamic Republic of Iran
Fax: +982614411106
Email: msadeghi@nrcam.org

Salouti, M.
Radioisotope Department,
Nuclear Research Centre,
P.O. Box 11365-3486,
Tehran, Islamic Republic of Iran
Fax: +98218020887
Email: saloutim@yahoo.com

Santos, R.G.
Centre for Development of
Nuclear Technology (CDTN),
Av. Prof. Mario Werneck s.n.,
CP 941,
BR-30123-970 Belo Horizonte,
Minas Gerais, Brazil
Fax: +553134993380
Email: santosr@cdtn.br

Satpati, D.
Radiopharmaceuticals Division,
Bhabha Atomic Research Centre,
Mumbai 400085, India
Fax: +912225595371
Email: drishtys@apsara.barc.ernet.in

Saw, M.M.
Department of Nuclear Medicine
and PET Centre,
Block 2, Basement 1,
Singapore General Hospital,
Outram Road,
169608 Singapore
Fax: +6563230735
Email: maungmaungsaw@hotmail.com

Sawe, S.F.	Tanzania Atomic Energy Commission (TAEC), P.O. Box 743, Arusha, United Republic of Tanzania Fax: +255272509709 Email: shovisawe@hotmail.com
Schlyer, D.	Department of Chemistry, Brookhaven National Laboratory, Upton, NY 11973-5000, United States of America Email: schlyer@bnl.gov
Sedda, A.F.	ENEA UTS FIS-ION, C.R. Casaccia, S.P. Anguillarese 301, 00060 Rome, Italy Fax: +3930484874 Email: anqioco.sedda@casaccia.enea.it
Sergieva, S.	Sofia Cancer Centre, Kv. “Mladost” 1, Blvd. Andrey Saharov 1, P.O. Box 54, Sofia 1756, Bulgaria Fax: +3592761530 Email: sergieva_s@yahoo.com
Sevastyanov, Yu.G.	Cyclotron Co. Ltd, 1, Bondarenko Square, Obninsk, Kaluga Region 249033, Russian Federation Fax: +70843997048 Email: cyclotron@obninsk.com
Siddig, S.M.A.	Institute of Nuclear Medicine, Molecular Biology and Oncology (INMO), University of Gezira, P.O. Box 20, Wad Medani, Sudan Fax: +249511843862 Email: siddig@Email.com

Singh, N.
Institute of Nuclear Medicine and Allied Sciences,
Brig. S.K. Mazumdar Road,
Timarpur, Delhi 110054, India
Email: namsingh1@yahoo.com

Sirandoni Riquelme, G.
Regional Hospital of Temuco,
Guillermo MacDonald 02551,
Barrio Ingles,
Temuco, IX Region, Chile
Fax: +5624296660
Email: gsirandoni@araucaniasur.cl

Sobreira, A.C.
Rem Indústria e Comércio Ltda,
Rua Columbus 282,
05304-010 Sâo Paulo, SP,
Brazil
Fax: +551138316922
Email: anacelia@rem.ind.br

Solanki, K.K.
Department of Nuclear Sciences and Applications,
International Atomic Energy Agency,
Wagramer Strasse 5, P.O. Box 100,
1400 Vienna, Austria
Fax: +43126007
Email: k.solanki@iaea.org

Solodyannikova, O.I.
Department of Nuclear Medicine,
Institute of Oncology,
Lomonosov Str. 33/43,
Kiev-22, Ukraine
Fax: +380442590182
Email: oko@mail.ru

Soloviev, D.
Cyclotron Unit,
University Hospital of Geneva,
24 rue Micheli-du-Crest,
Geneva-14, Switzerland
Fax: +41223727585
Email: dmitri.soloviev@hcuge.ch

Soroa, V.E.
Radiobiology — Centro de Medicina Nuclear,
Comisión Nacional de Energía Atómica,
Avenida Del Libertador 8250,
1429 Buenos Aires, Argentina
Fax: +541148052123
Email: tate@cnea.gov.ar

Soylu, A.A.
Department of Nuclear Medicine,
Faculty of Medicine,
Ankara University,
06100 Cebeci Ankara, Turkey
Fax: +903123620897
Email: ayfersoylu@yahoo.com

Suzuki, K.
Department of Medical Imaging,
Research Centre for Charged
Particle Therapy,
National Institute of Radiological
Sciences (NIRS),
9-1, Anagawa 4-chome,
Inage-ku, Chiba-shi 263,
Japan
Fax: +81432063261
Email: kazutosi@nirs.go.jp

Tandon, P.
Radiological Physics & Advisory Division,
Bhabha Atomic Research Centre,
CT&CRS Building,
Anushaktinagar,
Mumbai 400 094, India
Fax: +912225519209
Email: ptandon_barc@rediffmail.com

Tendilla del Pozo, J.I.
Instituto Nacional
de Investigaciones Nucleares (ININ),
Kilometro 36.5,
Carretera Mexico-Toluca,
52045 Municipio de Ocoyoacac,
Mexico
Fax: +5553297316
Email: jtp@nuclear.inin.mx

Thakur, M.L.
Radiopharmaceutical Research,
Thomas Jefferson University,
1020 Locust Street, Suite 359,
Philadelphia, PA 19107,
United States of America
Fax: 215-923-9245
Email: mathew.thakur@jefferson.edu

Tiskevicius, S.
Nuclear Medicine Department,
Vilnius University Institute of Oncology,
Santariskiu 1,
2021 Vilnius, Lithuania
Fax: +37052720164
Email: sigitas.tiskevicius@delfi.lt

Trabelsi, M.
Centre national des sciences et technologies nucléaires,
Pôle technologique,
Sidi Thabet,
2020 Ariana, Tunisia
Fax: +21671537555
Email: moez.trabelsi@cnstn.rnrt.tn

Tran Van Quy
Vietnam Atomic Energy Commission,
59 Ly Thuong Kiet Street,
Hanoi, Vietnam
Fax: +84494234133
Email: tranquyru@yahoo.com

Trtic-Petrovic, T.
Laboratory of Physics (010),
Vinca Institute of Nuclear Sciences,
P.O. Box 522,
11001 Belgrade, Serbia
Fax: +381114447963
Email: ttrtic@vin.bg.ac.yu

Turner, J.H.
Fremantle Hospital,
University of Western Australia,
Alma Street,
Fremantle WA 6160, Australia
Fax: +61894312889
Email: harvey.turner@health.wa.gov.au

Tzanopoulou, S.	Institute of Biology, National Centre for Scientific Research (NCSR) “Demokritos”, P.O. Box 60228, 15310 Aghia Paraskevi, Athens, Greece Fax: +302106511767 Email: tina@bio.demokritos.gr
Vallabhajosula, S.	Nuclear Medicine, New York Presbyterian Hospital and Weill Medical College of Cornell University, 525 East 68th Street, STARR 2-21 New York, NY 10021, United States of America Fax: +2127469010 Email: svallabh@med.cornell.edu
Vandecapelle, M.	Federal Agency for Nuclear Control (FANC), Ravenstein Street 36, 1000 Brussels, Belgium Fax: +3222892112 Email: marleen.vandecapelle@fanc.fgov.be
Venkatesh, M.	Radiopharmaceuticals Division, Bhabha Atomic Research Centre, Mumbai 400085, India Fax: +912225505151 or +91225505345 Email: meerav@apsara.barc.ernet.in
Verbruggen, A.M.	Laboratory of Radiopharmaceutical Chemistry, University Hospital, Gasthuisberg-Radiopharmacy, Herestraat 49, B-3000 Leuven, Belgium Email: alfons.verbruggen@farm.kuleuven.ac.be
Verdera Presto, E.S.	TECHI S.A., Bulevar Espana 2729, Apartamento 701, Montevideo, Uruguay Fax: +59822008060 Email: sverdera@hotmail.com

Verk, T.
Department of Radiophysics,
Institute of Oncology,
Zaloska 2,
1000 Ljubljana, Slovenia
Fax: +38614319108
Email: tverk@onko-i.si

Volkova, O.N.
"Techsnabexport",
Staromonetny per. 26,
119180 Moscow, Russian Federation
Fax: +70952302638
Email: tenex@online.ru

von Wenzel-Obholzer, K.S.
Department of Nuclear Medicine,
Dr. A. Bernard May Cancer Care Centre,
P.O. Box 8650,
Windhoek, Namibia
Fax: +264612033263
Email: kvwo@iafrica.com.na

Vora, M.M.
Cyclotron and Radiopharmaceuticals Department,
King Faisal Specialist Hospital and Research Centre,
MBC-03, P.O. Box 3354,
Riyadh 11211, Saudi Arabia
Fax: +9664424743
Email: vora@kfshrc.edu.sa

Wang, Mingwei
Radiopharmaceutical Centre,
Shanghai Institute of Applied Physics, CAS,
2019 Jialuo Road,
Jiading,
Shanghai 201800, China
Fax: +862159554696
Email: wmwnuclear@163.com

Wang, Yongxian
Radiopharmaceutical Centre,
Shanghai Institute of Applied Physics, CAS,
2019 Jialuo Road,
Jiading,
Shanghai 201800, China
Fax: +862159556884
Email: yongxianw@163.com

Wastiel, C.
Institut Universitaire Radiophysique,
Grand Pré 1,
1007 Lausanne, Switzerland
Fax: +41216233435
Email: claude.wastiel@chuv.ch

Westera, G.
Nuclear Medicine,
Centre for Radiopharmaceutical Science,
University Hospital Zürich,
8091 Zürich, Switzerland
Fax: +41442554428
Email: gerrit.westera@dmr.usz.ch

Xie, Wucheng
China Atomic Energy Authority (CAEA),
8A Fucheng Road,
Haidian District,
Beijing 100037, China
Fax: +861088581511
Email: xiewch@caea.gov.cn

Yassine, T.
Radioisotope Division,
Department of Chemistry,
Atomic Energy Commission,
P.O. Box 6091,
Damascus, Syrian Arab Republic
Fax: +963116112289
Email: tyassin@aec.org.sy

Zaknun, J.
Department of Nuclear
Sciences and Applications,
International Atomic Energy Agency,
Wagramer Strasse 5, P.O. Box 100,
1400 Vienna, Austria
Fax: +43126007
Email: j.zaknun@iaea.org

Zalutsky, M.R.
Department of Radiology,
Duke University Medical Center,
P.O. Box 3808,
Durham, NC 27710,
United States of America
Fax: +19196847121
Email: zalut001@mc.duke.edu

Zasepa, M.	Institute of Nuclear Chemistry and Technology, Dorodna 16, 03-195 Warsaw, Poland Fax: +48228111532 Email: mkz@ichtj.waw.pl
Zhang, Jianfeng	National Institute for Radiological Protection, CDC, 2 Xinkang Street, Deshengmenwai, Beijing 100088, China Fax: +861062012501 Email: zhangjianfengbj@hotmail.com
Zitko-Krhin, M.	Department for Nuclear Medicine, University Medical Centre, Zaloska 7, 1525 Ljubljana, Slovenia Fax: +38615222237 Email: mojca.zitko@kclj.si
Zolle, I.	Ludwig-Boltzmann Institute of Nuclear Medicine, Zimmermanngasse 22/8, 1090 Vienna, Austria Fax: +4314057198 Email: ilse.zolle@univie.ac.at
Zuvic, M.	Clinical Hospital Centre, Department of Nuclear Medicine and Radiation Protection, Kispaticeva 12, 10000 Zagreb, Croatia Fax: +38512421874 Email: mzuvic@kbc-zagreb.hr
Zyuzin, A.	Advanced Cyclotron Systems Inc. (ACSI), 7851 Alderbridge Way, Richmond, BC V6X 2A4, Canada Fax: +16042761495 Email: azyuzin@advancedcyclotron.com

AUTHOR INDEX

The International Symposium on Trends in Radiopharmaceuticals (ISTR-2005) covered developments across the entire spectrum of radiopharmaceutical science, including radionuclide production and radiochemical processing; manufacture and quality control; advances in radiopharmaceuticals research; good manufacturing practices and regulatory aspects. Volume 1 covers technetium radiopharmaceuticals and radioisotope production in research reactors. Volume 2 covers cyclotron based isotopes, therapeutic and PET radiopharmaceuticals and radiopharmacy.

INTERNATIONAL ATOMIC ENERGY AGENCY
VIENNA
ISBN 92–0–101707–3
ISSN 0074–1884